NASA CP-2001

ADVANCES IN ENGINEERING SCIENCE

Volume 2

13th Annual Meeting
Society of Engineering Science
Sponsored by JIAFS
Hampton, VA, November 1–3, 1976

NASA
National
Aeronautics and
Space
Administration

Society of
Engineering Science

NASA Conference Publications (CP Series) contain compilations of scientific and technical papers or transcripts arising from conferences, workshops, symposia, seminars, and other professional meetings that NASA elects to publish.

The text of these proceedings was reproduced directly from author-supplied manuscripts for distribution prior to opening of the meeting. NASA has performed no editorial review of the papers other than those contributed by its employees or contractors.

NASA CP-2001

Advances In Engineering Science

Volume 2

13th Annual Meeting
Society of Engineering Science
Hampton, VA, November 1–3, 1976

Sponsored by Joint Institute for Advancement of Flight Sciences
NASA Langley Research Center
and
George Washington University

NASA
National
Aeronautics and
Space
Administration

Society of
Engineering Science

For sale by the National Technical Information Service
Springfield, Virginia 22161
Price – $11.50

DISCLAIMER NOTICE

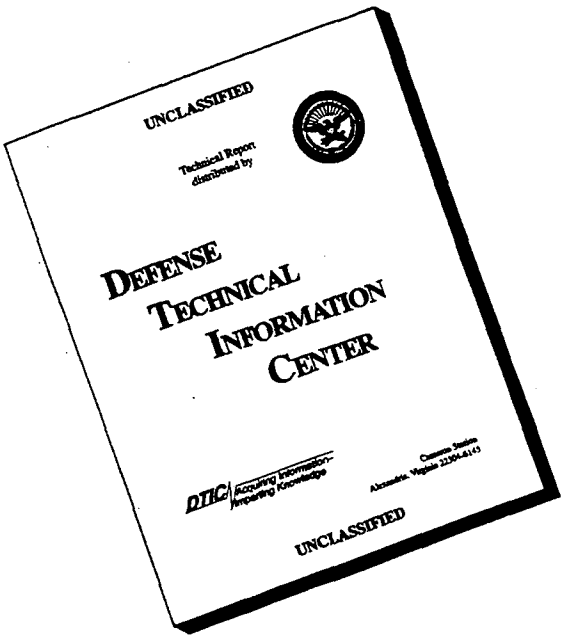

THIS DOCUMENT IS BEST QUALITY AVAILABLE. THE COPY FURNISHED TO DTIC CONTAINED A SIGNIFICANT NUMBER OF PAGES WHICH DO NOT REPRODUCE LEGIBLY.

PREFACE

The technical program of the 13th Annual Meeting of the Society of Engineering Science, Inc., consisted of 159 invited and contributed papers covering a wide variety of research topics, a plenary session, and the Annual Society of Engineering Science Lecture. Thirty-three of the technical sessions contained invited and/or contributed papers while two of the sessions were conducted as panel discussions with audience participation.

These Proceedings, which contain the technical program of the meeting, are presented in four volumes arranged by subject material. Papers in materials science are contained in Volume I. Volume II contains the structures, dynamics, applied mathematics, and computer science papers. Volume III contains papers in the areas of acoustics, environmental modeling, and energy. Papers in the area of flight sciences are contained in Volume IV. A complete Table of Contents and an Author Index are included in each volume.

We would like to express particular appreciation to the members of the Steering Committee and the Technical Organizing Committee for arranging an excellent technical program. Our thanks are given to all faculty and staff of the Joint Institute for Advancement of Flight Sciences (both NASA Langley Research Center and The George Washington University) who contributed to the organization of the Meeting. The assistance in preparation for the meeting and this document of Sandra Jones, Virginia Lazenby, and Mary Torian is gratefully acknowledged. Our gratitude to the Scientific and Technical Information Prgrams Division of the NASA Langley Research Center for publishing these Proceedings is sincerely extended.

Hampton, Virginia 1976

J. E. Duberg

J. L. Whitesides

Co-Chairmen

J. E. Duberg
NASA Langley Research Center

J. L. Whitesides
The George Washington University

Steering Committee

W. D. Erickson, NASA Langley Research Center
P. J. Bobbitt, NASA Langley Research Center
H. F. Hardrath, NASA Langley Research Center
D. J. Martin, NASA Langley Research Center
M. K. Myers, The George Washington University
A. K. Noor, The George Washington University
J. E. Duberg, NASA Langley Research Center, Ex-officio
J. L. Whitesides, The George Washington University, Ex-officio

Technical Organizing Committee

C. L. Bauer, Carnegie-Mellon University
L. B. Callis, NASA Langley Research Center
J. R. Elliott, NASA Langley Research Center
K. Karamcheti, Stanford University
P. Leehey, Massachusetts Institute of Technology
J. S. Levine, NASA Langley Research Center
R. E. Little, University of Michigan-Dearborn
J. M. Ortega, Institute for Computer Applications in Science and Engineering
E. M. Pearce, Polytechnic Institute of New York
A. D. Pierce, Georgia Institute of Technology
E. Y. Rodin, Washington University
L. A. Schmit, University of California at Los Angeles
G. C. Sih, Lehigh University
E. M. Wu, Washington University

SOCIETY OF ENGINEERING SCIENCE, INC.

The purpose of the Society, as stated in its incorporation document, is "to foster and promote the interchange of ideas and information among the various fields of engineering science and between engineering science and the fields of theoretical and applied physics, chemistry, and mathematics, and, to that end, to provide forums and meetings for the presentation and dissemination of such ideas and information, and to publish such information and ideas among its members and other interested persons by way of periodicals and otherwise."

OFFICERS

L. V. Kline, President
IBM Corporation

S. W. Yuan, First Vice President and Director
The George Washington University

C.E. Taylor, Second Vice President and Director
University of Illinois

E. Y. Rodin, Second Vice President and Director
The George Washington University

R. P. McNitt, Secretary
Virginia Polytechnic Institute and State University

J. Peddieson, Treasurer
Tennessee Technological University

DIRECTORS

B. A. Boley, Northwestern University
G. Dvorak, Duke University
T. S. Chang, Massachusetts Institute of Technology
E. Montroll, University of Rochester
J. M. Richardson, North American Rockwell Corp.
E. Saibel, Army Research Office
J. W. Dunkin, Exxon Production Research Co.
J. T. Oden, University of Texas

CORPORATE MEMBERS

Chevron Oil Field Research Company
Exxon Production Research Company
IBM Corporation
OEA Incorporated

CONTENTS

PREFACE iii

VOLUME I

ANNUAL SOCIETY OF ENGINEERING SCIENCE LECTURE

CONTINUUM MECHANICS AT THE ATOMIC SCALE 1
A. Cemal Eringen

MATERIALS SCIENCE I
Chairmen: C. L. Bauer and E. Pearce

MICROSCOPIC ASPECTS OF INTERFACIAL REACTIONS IN DIFFUSION BONDING PROCESSES 3
Michael P. Shearer and Charles L. Bauer

MACROSCOPIC ASPECTS OF INTERFACIAL REACTIONS IN DIFFUSION BONDING PROCESSES 15
R. W. Heckel

FRACTURE IN MACRO-MOLECULES 27
K. L. DeVries

STRUCTURE-PROPERTY RELATIONSHIPS IN BLOCK COPOLYMERS 37
James E. McGrath

MATERIALS SCIENCE II
Chairman: R. E. Little

A CRITICAL REVIEW OF THE EFFECTS OF MEAN AND COMBINED STRESSES ON THE FATIGUE LIMIT OF METALS 51
R. E. Little

INFLUENCE OF ACOUSTICS IN SEPARATION PROCESSES 61
Harold V. Fairbanks

MICROMECHANICS OF SLIP BANDS ON FREE SURFACE 67
S. R. Lin and T. H. Lin

ON ONSAGER'S PRINCIPLE, DISLOCATION MOTION AND HYDROGEN EMBRITTLEMENT . . 77
M. R. Louthan, Jr., and R. P. McNitt

MATERIALS SCIENCE III
Chairman: J. H. Crews, Jr.

WAVE SPEEDS AND SLOWNESS SURFACE IN ELASTIC-PLASTIC MEDIA OBEYING TRESCA'S YIELD CONDITION 85
T. C. T. Ting

MATHEMATICAL MODELLING OF UNDRAINED CLAY BEHAVIOR 95
Jean-Hervé Prévost and Kaare Høeg

THEORY OF ORTHODONTIC MOTIONS 103
Susan Pepe, W. Dennis Pepe, and Alvin M. Strauss

NONLINEAR EFFECTS IN THERMAL STRESS ANALYSIS OF A SOLID PROPELLANT ROCKET MOTOR 111
E. C. Francis, R. L. Peeters, and S. A. Murch

COMPUTER SIMULATION OF SCREW DISLOCATION IN ALUMINUM 137
Donald M. Esterling

COMPOSITE MATERIALS
Chairman: E. M. Wu

MOISTURE TRANSPORT IN COMPOSITES 147
George S. Springer

A HIGH ORDER THEORY FOR UNIFORM AND LAMINATED PLATES 157
King H. Lo, Richard M. Christensen, and Edward M. Wu

STOCHASTIC MODELS FOR THE TENSILE STRENGTH, FATIGUE AND STRESS-RUPTURE OF FIBER BUNDLES 167
S. Leigh Phoenix

PROGRESSIVE FAILURE OF NOTCHED COMPOSITE LAMINATES USING FINITE ELEMENTS 183
Ralph J. Nuismer and Gary E. Brown

RESIDUAL STRESSES IN POLYMER MATRIX COMPOSITE LAMINATES 193
H. Thomas Hahn

DYNAMIC FRACTURE MECHANICS
Chairman: G. C. Sih

INFLUENCE OF SPECIMEN BOUNDARY ON THE DYNAMIC STRESS INTENSITY FACTOR . . 205
E. P. Chen and G. C. Sih

FINITE-ELEMENT ANALYSIS OF DYNAMIC FRACTURE 215
J. A. Aberson, J. M. Anderson, and W. W. King

APPLICATION OF A NOVEL FINITE DIFFERENCE METHOD TO DYNAMIC CRACK PROBLEMS 227
Yung M. Chen and Mark L. Wilkins

RAPID INTERFACE FLAW EXTENSION WITH FRICTION 239
L. M. Brock

FRACTURE MECHANICS
Chairman: H. F. Hardrath

DYNAMIC DUCTILE FRACTURE OF A CENTRAL CRACK 247
Y. M. Tsai

A STUDY OF THE EFFECT OF SUBCRITICAL CRACK GROWTH ON THE GEOMETRY DEPENDENCE OF NONLINEAR FRACTURE TOUGHNESS PARAMETERS 257
D. L. Jones, P. K. Poulose, and H. Liebowitz

ON A 3-D "SINGULARITY-ELEMENT" FOR COMPUTATION OF COMBINED MODE STRESS INTENSITIES 267
Satya N. Atluri and K. Kathiresan

INFLUENCE OF A CIRCULAR HOLE UNDER UNIFORM NORMAL PRESSURE ON THE STRESSES AROUND A LINE CRACK IN AN INFINITE PLATE 275
Ram Narayan and R. S. Mishra

THE EFFECT OF SEVERAL INTACT OR BROKEN STRINGERS ON THE STRESS INTENSITY FACTOR IN A CRACKED SHEET 283
K. Arin

ON THE PROBLEM OF STRESS SINGULARITIES IN BONDED ORTHOTROPIC MATERIALS 291
F. Erdogan and F. Delale

IMPACT AND VIBRATION
Chairman: H. L. Runyan, Jr.

HIGHER-ORDER EFFECTS OF INITIAL DEFORMATION ON THE VIBRATIONS OF CRYSTAL PLATES 301
Xanthippi Markenscoff

BIODYNAMICS OF DEFORMABLE HUMAN BODY MOTION 309
Alvin M. Strauss and Ronald L. Huston

IMPACT TENSILE TESTING OF WIRES 319
T. H. Dawson

NUMERICAL DETERMINATION OF THE TRANSMISSIBILITY CHARACTERISTICS OF A SQUEEZE FILM DAMPED FORCED VIBRATION SYSTEM 327
Michael A. Sutton and Philip K. Davis

A MODEL STUDY OF LANDING MAT SUBJECTED TO C-5A LOADINGS 339
P. T. Blotter, F. W. Kiefer, and V. T. Christiansen

ROCK FAILURE ANALYSIS BY COMBINED THERMAL WEAKENING AND WATER JET IMPACT 349
A. H. Nayfeh

VOLUME II

PANEL: COMPUTERIZED STRUCTURAL ANALYSIS AND DESIGN - FUTURE AND PROSPECTS 361

Moderator: L. A. Schmit, Jr.

Panel Members: Laszlo Berke
Michael F. Card
Richard F. Hartung
Edward L. Stanton
Edward L. Wilson

STRUCTURAL DYNAMICS I
Chairman: L. D. Pinson

ON THE STABILITY OF A CLASS OF IMPLICIT ALGORITHMS FOR NONLINEAR STRUCTURAL DYNAMICS 385
Ted Belytschko

A REVIEW OF SUBSTRUCTURE COUPLING METHODS FOR DYNAMIC ANALYSIS 393
Roy R. Craig, Jr., and Ching-Jone Chang

CORIOLIS EFFECTS ON NONLINEAR OSCILLATIONS OF ROTATING CYLINDERS AND RINGS 409
Joseph Padovan

ON THE EXPLICIT FINITE ELEMENT FORMULATION OF THE DYNAMIC CONTACT PROBLEM OF HYPERELASTIC MEMBRANES 417
J. O. Hallquist and W. W. Feng

FREE VIBRATIONS OF COMPOSITE ELLIPTIC PLATES 425
C. M. Andersen and Ahmed K. Noor

STRUCTURAL DYNAMICS II
Chairman: S. Utku

SOME DYNAMIC PROBLEMS OF ROTATING WINDMILL SYSTEMS 439
J. Dugundji

DYNAMIC INELASTIC RESPONSE OF THICK SHELLS USING ENDOCHRONIC THEORY AND THE METHOD OF NEARCHARACTERISTICS 449
Hsuan-Chi Lin

VIBRATIONS AND STRESSES IN LAYERED ANISOTROPIC CYLINDERS 459
G. P. Mulholland and B. P. Gupta

INCREMENTAL ANALYSIS OF LARGE ELASTIC DEFORMATION OF A ROTATING CYLINDER 473
George R. Buchanan

VARIATIONAL THEOREMS FOR SUPERPOSED MOTIONS IN ELASTICITY, WITH APPLICATION TO BEAMS 481
M. Cengiz Dökmeci

RESPONSE OF LONG-FLEXIBLE CANTILEVER BEAMS TO APPLIED ROOT MOTIONS . . . 491
Robert W. Fralich

STRUCTURAL SYNTHESIS
Chairman: F. Barton

OPTIMAL DESIGN AGAINST COLLAPSE AFTER BUCKLING 501
E. F. Masur

OPTIMUM VIBRATING BEAMS WITH STRESS AND DEFLECTION CONSTRAINTS 509
Manohar P. Kamat

AN OPTIMAL STRUCTURAL DESIGN ALGORITHM USING OPTIMALITY CRITERIA 521
John E. Taylor and Mark P. Rossow

A RAYLEIGH-RITZ APPROACH TO THE SYNTHESIS OF LARGE STRUCTURES WITH ROTATING FLEXIBLE COMPONENTS 531
L. Meirovitch and A. L. Hale

THE STAGING SYSTEM: DISPLAY AND EDIT MODULE 543
Ed Edwards and Leo Bernier

NONLINEAR ANALYSIS OF STRUCTURES
Chairman: M. S. Anderson

SOME CONVERGENCE PROPERTIES OF FINITE ELEMENT APPROXIMATIONS OF PROBLEMS IN NONLINEAR ELASTICITY WITH MULTI-VALUED SOLUTIONS 555
J. T. Oden

ELASTO-PLASTIC IMPACT OF HEMISPHERICAL SHELL IMPACTING ON HARD RIGID SPHERE 563
D. D. Raftopoulos and A. L. Spicer

LARGE DEFLECTIONS OF A SHALLOW CONICAL MEMBRANE 575
Wen-Hu Chang and John Peddieson, Jr.

A PLANE STRAIN ANALYSIS OF THE BLUNTED CRACK TIP USING SMALL STRAIN DEFORMATION PLASTICITY THEORY 585
J. J. McGowan and C. W. Smith

GAUSSIAN IDEAL IMPULSIVE LOADING OF RIGID VISCOPLASTIC PLATES 595
Robert J. Hayduk

BEAMS, PLATES, AND SHELLS
Chairman: M. Stern

RECENT ADVANCES IN SHELL THEORY 617
James G. Simmonds

FLUID-PLASTICITY OF THIN CYLINDRICAL SHELLS 627
Dusan Krajcinovic, M. G. Srinivasan, and Richard A. Valentin

THERMAL STRESSES IN A SPHERICAL PRESSURE VESSEL HAVING TEMPERATURE-DEPENDENT, TRANSVERSELY ISOTROPIC, ELASTIC PROPERTIES 639
T. R. Tauchert

ANALYSIS OF PANEL DENT RESISTANCE 653
Chi-Mou Ni

NEUTRAL ELASTIC DEFORMATIONS 665
Metin M. Durum

A STUDY OF THE FORCED VIBRATION OF A TIMOSHENKO BEAM 671
Bucur Zainea

COMPOSITE STRUCTURES
Chairman: J. Vinson

ENVIRONMENTAL EFFECTS OF POLYMERIC MATRIX COMPOSITES 687
J. M. Whitney and G. E. Husman

INTERLAYER DELAMINATION IN FIBER REINFORCED COMPOSITES WITH AND WITHOUT SURFACE DAMAGE 697
S. S. Wang

STRESS INTENSITY AT A CRACK BETWEEN BONDED DISSIMILAR MATERIALS 699
Morris Stern and Chen-Chin Hong

STRESS CONCENTRATION FACTORS AROUND A CIRCULAR HOLE IN LAMINATED COMPOSITES 711
C. E. S. Ueng

TRANSFER MATRIX APPROACH TO LAYERED SYSTEMS WITH AXIAL SYMMETRY 721
Leon Y. Bahar

APPLIED MATHEMATICS
Chairman: J. N. Shoosmith

APPLIED GROUP THEORY APPLICATIONS IN THE ENGINEERING (PHYSICAL, CHEMICAL, AND MEDICAL), BIOLOGICAL, SOCIAL, AND BEHAVIORAL SCIENCES AND IN THE FINE ARTS 731
S. F. Borg

RESPONSE OF LINEAR DYNAMIC SYSTEMS WITH RANDOM COEFFICIENTS 741
John Dickerson

APPLICATIONS OF CATASTROPHE THEORY IN MECHANICS 747
Martin Buoncristiani and George R. Webb

STABILITY OF NEUTRAL EQUATIONS WITH CONSTANT TIME DELAYS 757
L. Keith Barker and John L. Whitesides

CUBIC SPLINE REFLECTANCE ESTIMATES USING THE VIKING LANDER CAMERA MULTISPECTRAL DATA 769
Stephen K. Park and Friedrich O. Huck

ADVANCES IN COMPUTER SCIENCE
Chairman: J. M. Ortega

DATA MANAGEMENT IN ENGINEERING 779
J. C. Browne

TOOLS FOR COMPUTER GRAPHICS APPLICATIONS 791
R. L. Phillips

COMPUTER SYSTEMS: WHAT THE FUTURE HOLDS 805
Harold S. Stone

VOLUME III

AEROACOUSTICS I
Chairman: D. L. Lansing

HOW DOES FLUID FLOW GENERATE SOUND? 819
Alan Powell

SOUND PROPAGATION THROUGH NONUNIFORM DUCTS 821
Ali Hasan Nayfeh

EXPERIMENTAL PROBLEMS RELATED TO JET NOISE RESEARCH 835
John Laufer

NONLINEAR PERIODIC WAVES 837
Lu Ting

AEROACOUSTICS II
Chairman: A. Nayfeh

FEATURES OF SOUND PROPAGATION THROUGH AND STABILITY OF A FINITE SHEAR LAYER 851
S. P. Koutsoyannis

EFFECTS OF HIGH SUBSONIC FLOW ON SOUND PROPAGATION IN A VARIABLE-AREA DUCT 861
A. J. Callegari and M. K. Myers

EFFECTS OF MEAN FLOW ON DUCT MODE OPTIMUM SUPPRESSION RATES 873
Robert E. Kraft and William R. Wells

INLET NOISE SUPPRESSOR DESIGN METHOD BASED UPON THE DISTRIBUTION OF ACOUSTIC POWER WITH MODE CUTOFF RATIO 883
Edward J. Rice

ORIFICE RESISTANCE FOR EJECTION INTO A GRAZING FLOW 895
Kenneth J. Baumeister

A SIMPLE SOLUTION OF SOUND TRANSMISSION THROUGH AN ELASTIC WALL TO A RECTANGULAR ENCLOSURE, INCLUDING WALL DAMPING AND AIR VISCOSITY EFFECTS 907
Amir N. Nahavandi, Benedict C. Sun, and W. H. Warren Ball

WAVE PROPAGATION
Chairman: E. Y. Rodin

PARAMETRIC ACOUSTIC ARRAYS - A STATE OF THE ART REVIEW 917
Francis Hugh Fenlon

NON-DIMENSIONAL GROUPS IN THE DESCRIPTION OF FINITE-AMPLITUDE SOUND PROPAGATION THROUGH AEROSOLS 933
David S. Scott

ONE-DIMENSIONAL WAVE PROPAGATION IN PARTICULATE SUSPENSIONS 947
Steve G. Rochelle and John Peddieson, Jr.

A CORRESPONDENCE PRINCIPLE FOR STEADY-STATE WAVE PROBLEMS 955
Lester W. Schmerr

ACOUSTICAL PROBLEMS IN HIGH ENERGY PULSED E-BEAM LASERS 963
T. E. Horton and K. F. Wylie

ATMOSPHERIC SOUND PROPAGATION
Chairman: M. K. Myers

A MICROSCOPIC DESCRIPTION OF SOUND ABSORPTION IN THE ATMOSPHERE 975
H. E. Bass

PROPAGATION OF SOUND IN TURBULENT MEDIA 987
Alan R. Wenzel

NOISE PROPAGATION IN URBAN AND INDUSTRIAL AREAS 997
Huw G. Davies

DIFFRACTION OF SOUND BY NEARLY RIGID BARRIERS 1009
W. James Hadden, Jr., and Allan D. Pierce

THE LEAKING MODE PROBLEM IN ATMOSPHERIC ACOUSTIC-GRAVITY WAVE PROPAGATION 1019
Wayne A. Kinney and Allan D. Pierce

STRUCTURAL RESPONSE TO NOISE
Chairman: L. Maestrello

THE PREDICTION AND MEASUREMENT OF SOUND RADIATED BY STRUCTURES 1031
Richard H. Lyon and J. Daniel Brito

ON THE RADIATION OF SOUND FROM BAFFLED FINITE PANELS 1043
Patrick Leehey

ACOUSTOELASTICITY 1057
Earl H. Dowell

SOUND RADIATION FROM RANDOMLY VIBRATING BEAMS OF FINITE CIRCULAR CROSS-SECTION 1071
M. W. Sutterlin and A. D. Pierce

ENVIRONMENTAL MODELING I
Chairman: L. B. Callis

A PHENOMENOLOGICAL, TIME-DEPENDENT TWO-DIMENSIONAL PHOTOCHEMICAL MODEL OF THE ATMOSPHERE 1083
George F. Widhopf

THE DIFFUSION APPROXIMATION - AN APPLICATION TO RADIATIVE TRANSFER IN CLOUDS 1085
Robert F. Arduini and Bruce R. Barkstrom

CALIBRATION AND VERIFICATION OF ENVIRONMENTAL MODELS 1093
Samuel S. Lee, Subrata Sengupta, Norman Weinberg, and Homer Hiser

ON THE ABSORPTION OF SOLAR RADIATION IN A LAYER OF OIL BENEATH A LAYER OF SNOW 1105
Jack C. Larsen and Bruce R. Barkstrom

THE INFLUENCE OF THE DIABATIC HEATING IN THE TROPOSPHERE ON THE STRATOSPHERE 1115
Richard E. Turner, Kenneth V. Haggard, and Tsing Chang Chen

ENVIRONMENTAL MODELING II
Chairman: M. Halem

USE OF VARIATIONAL METHODS IN THE DETERMINATION OF WIND-DRIVEN OCEAN CIRCULATION 1125
Roberto Gelós and Patricio A. A. Laura

OPTICALLY RELEVANT TURBULENCE PARAMETERS IN THE MARINE BOUNDARY LAYER . . 1137
K. L. Davidson and T. M. Houlihan

THE NUMERICAL PREDICTION OF TORNADIC WINDSTORMS 1153
Douglas A. Paine and Michael L. Kaplan

SIMULATION OF THE ATMOSPHERIC BOUNDARY LAYER IN THE WIND TUNNEL FOR MODELING OF WIND LOADS ON LOW-RISE STRUCTURES 1167
Henry W. Tieleman, Timothy A. Reinhold, and Richard D. Marshall

NUMERICAL SIMULATION OF TORNADO WIND LOADING ON STRUCTURES 1177
Dennis E. Maiden

PLANETARY MODELING
Chairman: J. S. Levine

THE MAKING OF THE ATMOSPHERE 1191
Joel S. Levine

ATMOSPHERIC ENGINEERING OF MARS 1203
R. D. MacElroy and M. M. Averner

CREATION OF AN ARTIFICIAL ATMOSPHERE ON THE MOON 1215
Richard R. Vondrak

A TWO-DIMENSIONAL STRATOSPHERIC MODEL OF THE DISPERSION OF AEROSOLS FROM THE FUEGO VOLCANIC ERUPTION 1225
Ellis E. Remsberg, Carolyn F. Jones, and Joe Park

ENERGY RELATED TOPICS
Chairman: W. D. Erickson

SOLAR ENERGY STORAGE & UTILIZATION 1235
S. W. Yuan and A. M. Bloom

SOLAR HOT WATER SYSTEMS APPLICATION TO THE SOLAR BUILDING TEST FACILITY AND THE TECH HOUSE 1237
R. L. Goble, Ronald N. Jensen, and Robert C. Basford

D. C. ARC CHARACTERISTICS IN SUBSONIC ORIFICE NOZZLE FLOW 1247
Henry T. Nagamatsu and Richard E. Kinsinger

HYDROGEN-FUELED SUBSONIC AIRCRAFT - A PERSPECTIVE 1265
Robert D. Witcofski

VOLUME IV

PANEL: PROSPECTS FOR COMPUTATION IN FLUID DYNAMICS IN THE NEXT DECADE 1279

Moderator: P. J. Bobbitt

Panel Members: J. P. Boris
George J. Fix
R. W. MacCormack
Steven A. Orszag
William C. Reynolds

INVISCID FLOW I
Chairman: F. R. DeJarnette

FLUX-CORRECTED TRANSPORT TECHNIQUES FOR TRANSIENT CALCULATIONS OF STRONGLY SHOCKED FLOWS 1291
J. P. Boris

LIFTING SURFACE THEORY FOR RECTANGULAR WINGS 1301
Fred R. DeJarnette

IMPROVED COMPUTATIONAL TREATMENT OF TRANSONIC FLOW ABOUT SWEPT WINGS . . 1311
W. F. Ballhaus, F. R. Bailey, and J. Frick

APPLICATION OF THE NONLINEAR VORTEX-LATTICE CONCEPT TO AIRCRAFT-INTERFERENCE PROBLEMS 1321
Osama A. Kandil, Dean T. Mook, and Ali H. Nayfeh

AN APPLICATION OF THE SUCTION ANALOGY FOR THE ANALYSIS OF ASYMMETRIC FLOW SITUATIONS 1331
James M. Luckring

INVISCID FLOW II
Chairman: P. J. Bobbitt

TRANSONIC FLOW THEORY OF AIRFOILS AND WINGS 1349
P. R. Garabedian

THE MULTI-GRID METHOD: FAST RELAXATION FOR TRANSONIC FLOWS 1359
Jerry C. South, Jr., and Achi Brandt

APPLICATION OF FINITE ELEMENT APPROACH TO TRANSONIC FLOW PROBLEMS 1371
Mohamed M. Hafez, Earll M. Murman, and London C. Wellford

INVERSE TRANSONIC AIRFOIL DESIGN INCLUDING VISCOUS INTERACTION 1387
Leland A. Carlson

VISCOUS FLOW I
Chairman: S. Rubin

NUMERICAL SOLUTIONS FOR LAMINAR AND TURBULENT VISCOUS FLOW OVER SINGLE AND MULTI-ELEMENT AIRFOILS USING BODY-FITTED COORDINATE SYSTEMS 1397
Joe F. Thompson, Z. U. A. Warsi, and B. B. Amlicke

THREE-DIMENSIONAL BOUNDARY LAYERS APPROACHING SEPARATION 1409
James C. Williams, III

TURBULENT INTERACTION AT TRAILING EDGES 1423
R. E. Melnik and R. Chow

SHOCK WAVE-TURBULENT BOUNDARY LAYER INTERACTIONS IN TRANSONIC FLOW . . . 1425
T. C. Adamson, Jr., and A. F. Messiter

SEPARATED LAMINAR BOUNDARY LAYERS 1437
Odus R. Burggraf

VISCOUS FLOW II
Chairman: D. M. Bushnell

NUMERICAL AND APPROXIMATE SOLUTION OF THE HIGH REYNOLDS NUMBER SMALL SEPARATION PROBLEM 1451
R. T. Davis

THE RELATIVE MERITS OF SEVERAL NUMERICAL TECHNIQUES FOR SOLVING THE COMPRESSIBLE NAVIER-STOKES EQUATIONS 1467
Terry L. Holst

CALCULATION OF A SEPARATED TURBULENT BOUNDARY LAYER 1483
Barrett Baldwin and Ching Mao Hung

THE LIFT FORCE ON A DROP IN UNBOUNDED PLANE POISEUILLE FLOW 1493
Philip R. Wohl

STABILITY OF FLOW OF A THERMOVISCOELASTIC FLUID BETWEEN ROTATING COAXIAL CIRCULAR CYLINDERS 1505
Nabil N. Ghandour and M. N. L. Narasimhan

STABILITY OF A VISCOUS FLUID IN A RECTANGULAR CAVITY IN THE PRESENCE OF A MAGNETIC FIELD 1509
C. Y. Liang and Y. Y. Hung

AIRCRAFT AERODYNAMICS
Chairman: R. E. Kuhn

ADVANCED TRANSONIC AERODYNAMIC TECHNOLOGY 1521
Richard T. Whitcomb

DESIGN CONSIDERATIONS FOR LAMINAR-FLOW-CONTROL AIRCRAFT 1539
R. F. Sturgeon and J. A. Bennett

ON THE STATUS OF V/STOL FLIGHT 1549
Barnes W. McCormick

DEVELOPMENT OF THE YC-14 1563
Theodore C. Nark, Jr.

EXPERIMENTAL FLUID MECHANICS
Chairman: J. Schetz

THE CRYOGENIC WIND TUNNEL 1565
Robert A. Kilgore

DESIGN CONSIDERATIONS OF THE NATIONAL TRANSONIC FACILITY 1583
Donald D. Baals

AERODYNAMIC MEASUREMENT TECHNIQUES USING LASERS 1603
William W. Hunter, Jr.

HYPERSONIC HEAT-TRANSFER AND TRANSITION CORRELATIONS FOR A ROUGHENED SHUTTLE ORBITER 1615
John J. Bertin, Dennis D. Stalmach, Ed S. Idar, Dennis B. Conley, and Winston D. Goodrich

PROPULSION AND COMBUSTION
Chairman: A. J. Baker

HYDROGEN-FUELED SCRAMJETS: POTENTIAL FOR DETAILED COMBUSTOR ANALYSIS . . 1629
H. L. Beach, Jr.

THREE-DIMENSIONAL FINITE ELEMENT ANALYSIS OF ACOUSTIC INSTABILITY OF SOLID PROPELLANT ROCKET MOTORS 1641
Robert M. Hackett and Radwan S. Juruf

ACOUSTIC DISTURBANCES PRODUCED BY AN UNSTEADY SPHERICAL DIFFUSION FLAME 1653
Maurice L. Rasmussen

FLOW FIELD FOR AN UNDEREXPANDED, SUPERSONIC NOZZLE EXHAUSTING INTO AN EXPANSIVE LAUNCH TUBE 1665
Robert R. Morris, John J. Bertin, and James L. Batson

EFFECTS OF PERIODIC UNSTEADINESS OF A ROCKET ENGINE PLUME ON THE PLUME-INDUCED SEPARATION SHOCK WAVE 1673
Julian O. Doughty

FLIGHT DYNAMICS AND CONTROL I
Chairman: A. A. Schy

AERIAL PURSUIT/EVASION 1685
Henry J. Kelley

DESIGN OF ACTIVE CONTROLS FOR THE NASA F-8 DIGITAL FLY-BY-WIRE AIRPLANE 1687
Joseph Gera

PERFORMANCE ANALYSIS OF FLEXIBLE AIRCRAFT WITH ACTIVE CONTROL 1703
Richard B. Noll and Luigi Morino

BEST-RANGE FLIGHT CONDITIONS FOR CRUISE-CLIMB FLIGHT OF A JET AIRCRAFT 1713
Francis J. Hale

FLIGHT DYNAMICS AND CONTROL II
Chairman: M. J. Queijo

EXPERIMENT DESIGN FOR PILOT IDENTIFICATION IN COMPENSATORY TRACKING TASKS 1721
William R. Wells

RESULTS OF RECENT NASA STUDIES ON AUTOMATIC SPIN PREVENTION FOR FIGHTER AIRCRAFT 1733
Joseph R. Chambers and Luat T. Nguyen

HIGH ANGLE-OF-ATTACK STABILITY-AND-CONTROL ANALYSIS 1753
Robert F. Stengel

TERMINAL AREA GUIDANCE ALONG CURVED PATHS - A STOCHASTIC CONTROL APPROACH 1767
J. E. Quaranta and R. H. Foulkes, Jr.

LIST OF PARTICIPANTS 1779

Introductory Remarks For A Panel Discussion Session

on

COMPUTERIZED STRUCTURAL ANALYSIS AND DESIGN - FUTURE AND PROSPECTS

Lucien A. Schmit, Jr.
University of California, Los Angeles

The renowned numerical analyst, Dr. Richard W. Hamming, has written "The Purpose of Computing Is Insight, Not Numbers". As we take a look at the past, present, and future prospects for computerized structural analysis and design, we would do well to keep this charge in mind.

Huge strides have been made in the development of reliable structural analysis methods during the past thirty years. A vast array of powerful structural analysis tools has emerged and found widespread acceptance in engineering practice. The steady growth and availability of large scale general purpose digital computers has facilitated the development of rather general structural analysis capabilities, notably the various finite element programs. Also, as confidence has grown in our ability to predict the behavior of alternative designs, there has been a natural tendency to come to grips with the problems of wider scope that make up the structural design process. As one looks to the future and asks, what are the prospects, it appears that many of the new developments envisioned are characterized by an innate desire to strengthen creative control over the use of computers in structural analysis and design.

The development of computer programs for structural analysis, particularly finite-element methods, has been motivated by the need for economical and reliable prediction of structural behavior. Over the past 15 years, workers in the finite-element field have given attention to improving the theoretical foundations and the numerical techniques used. However, even more emphasis has been placed on increasing problem size, improving generality of configuration and extending finite-element methods to deal with more complex structural behavior. Mature computer programs for linear static and dynamic analysis of a rather general class of structures are generally available and widely used today. Programs capable of handling buckling analysis as well as nonlinear static and dynamic response also exist, although they are somewhat less mature. In his remarks, Professor Wilson observes that "new computer programs with improved accuracy and efficiency will not necessarily be adopted by the profession unless they solve problems that existing programs cannot." As we look ahead, it is likely that the growing use of composite materials as well as the need to treat crack growth and fatigue failure modes will provide impetus for the development of new programs. Also, as Dr. Stanton suggests,

it is anticipated that computational models characterizing real composite materials will become a bridge that helps bring the technology of the materials scientist to the structural engineer. While large pipeline and parallel process computers have not yet had a significant impact on the solution of structural analysis problems, they are expected to find important application in large scale transient response problems, nonlinear analyses, and design optimization studies.

The structural design problem is substantially more involved than the analysis problem, even if attention is restricted to simple proportioning. When configuration, material, and topological changes are considered, the structural design problem becomes very complex and it is not well understood. Dr. Berke traces the history of automated structural design beginning with the early structural index work, followed by: the advent of the general nonlinear programming formulation, the subsequent resurgence of the fully stressed design method, and the emergence of the discretized optimality criteria approach. As pointed out by Dr. Card, recent advances in the mathematical programming approach to structural design have been based on approximation concepts including design variable linking, deletion of redundant constraints, and design oriented structural analysis methods. Nonlinear mathematical programming methods cannot handle thousands of design variables and discretized optimality criteria techniques have difficulty identifying the set of critical constraints that will be active at the final optimum design. It is reasonable to expect that hybrid methods, which synergistically combine nonlinear mathematical programming methods with discretized optimality criteria techniques and design oriented structural analysis will emerge in the near future. Looking further ahead, it is likely that increased attention will be given to configuration, material, and topological design changes. Efforts will be made to gain deeper understanding of the design problems formal structure. Also, as Dr. Berke suggests, it may be possible to bring artificial intelligence to bear on the structural design problem through the use of adaptive learning network ideas.

As we look to the future, many of the developments projected by the panel seem to reflect a deep innate desire to strengthen creative control over the use of computers in structural analysis and design. The growth of easy access computing via simple problem oriented languages used in an interactive mode with graphic displays leads to greater involvement of the computer system user. As Dr. Hartung points out, structural engineers will spend more of their time as software synthesizers who select technical modules from program libraries and they will phase out of the ad hoc programming activities that have been so common during the last fifteen years. Software systems generated by computer specialists, numerical analysts and a few engineers with special training in modern programming techniques will have to be extremely well-documented, so that structural engineers will be able to use them while maintaining creative control. The pressing importance of solving the software dissemination, standardization, and accreditation problem is emphasized by Dr. Hartung and Dr. Card. Integrated procedures for interdisciplinary system design tend to focus attention on the importance of automated data management. It is interesting to note that many of the interdisciplinary system design procedures reflect the current in series design process that is commonplace

in industry today. Emphasizing data management, while minimizing change in the basic design process and the associated organizational structure, tends to preserve whatever creative control currently exists over the system design process. Finally, it would seem that the future prospects for minicomputers and microcomputers in structural analysis, touched on by Professor Wilson, Dr. Hartung and Dr. Stanton, may also enhance the structural engineer's opportunity to exercise more creative control over different analysis tasks, such as nonlinear dynamic response and characterization of actual composite materials. In closing, let me express my confidence that the barriers to computerized structural design, so aptly set forth by Dr. Card, will in time be overcome. As we move forward in the area of computerized structural analysis and design it may be useful for us to ponder the cryptic words of the poet T. S. Eliot, who in a very different context wrote, "Where is the wisdom we have lost in knowledge? Where is the knowledge we have lost in information?"

AUTOMATED STRUCTURAL DESIGN — FUTURE AND PROSPECTS

Laszlo Berke
Air Force Flight Dynamics Laboratory

Structural optimization has been an active area of research for many decades and has aided generations of engineers to find rational solutions to structural design problems of ever increasing complexity. There is now a noticeable lessening of research activity in this field. If this trend persists, it will unfavorably influence the future prospects of optimization. This will occur at a time when needs for optimization capabilities will predicably increase in the wake of ambitious developments in integrated procedures for automated aerospace vehicle design.

It is usually constructive to recall past achievements prior to assessing future prospects. New design challenges and new developments in computing capabilities continually produce new trends which, however, tend to build on past achievements. We can recall the precomputer era when the "in" thing was to perform optimization of compression panels with every conceivable geometry. Most of this work was based on the heuristic optimality criteria of simultaneous failure modes. Redundant structures were analyzed at that time by various approximation methods, and their members were manually sized to attain their respective critical stress levels. Repetitive application of this procedure was later formalized as the "fully stressed design method", FSD for short. These two early optimality criteria methods served the designers well at that time, and in most practical situations continue to do so, even today.

With the early appearance of computers, optimization methodology faced a new challenge. Relying on the emerging computational capabilities, nonlinear mathematical programming was introduced in the late fifties as the proper general framework for all structural optimization problems. Research along these lines became the new "in" thing during the exciting decade of the sixties. Research money was relatively abundant and a proliferation of results followed. One of the most important results was to rethink the basic nature of optimization problems and of the methods which can successfully solve them. It was conclusively shown that, in general, neither the simultaneous failure modes for components, nor FSD for redundant structures, resulted in an optimum design. As computing power increased and the powerful finite element methods became the most popular analysis tool for redundant structures, an unfortunate but basic shortcoming of nonlinear programming methods became apparent. The increasing number of reanalyses required as a function of the number of design variables rendered them impractical to finite element models that, by the mid-sixties, routinely consisted of thousands of elements. The discredited FSD had to be reinstated for strength optimization of large, redundant, finite element systems, and new, "exact", discretized, optimality criteria methods had to be introduced for stiffness constraints. After a slow start in the late sixties, these stiffness-related, discretized, optimality criteria methods provided a new turning point once again. Now they are widely accepted as the latest "in" thing for such diverse constraints as displacements, static stability,

dynamic response, and flutter. Even such exotic new requirements as aeroelastic tailoring and various control characteristics of flexible, advanced-composite aircraft are being considered.

One can briefly assess the current state of the art by saying that efficient mathematical programming methods are available for design problems of virtually any complexity. However, the number of design variables must be kept reasonable, either by appropriate modeling or by the nature of the problem. For final detailed design the problem is not entirely under control. Detailed structural models use thousands of finite elements, each with more or less independent size variables. Current practical capabilities for combined strength and stiffness design are theoretically improper heuristic mixtures of the "incorrect" FSD and the "correct", stiffness-related, optimality-criteria approaches. The recent advocacy of advanced composites tends to further aggravate the situation. While immediate needs for optimization are filled by the design teams with various pragmatic approaches of more or less parochial character, generally acceptable solutions are lacking for many important problems.

The future holds many new additional challenges. Optimization techniques in general, and nonlinear programming in particular, will continue to benefit from increasing computing capabilities which will help them to permeate the design process deeper and deeper. The emergence of integrated and automated vehicle design technology, based on ambitiously defined executive data management systems, will underscore the need for further automation. This automation must relate to both the analysis and the redesign process while relying on efficient optimization techniques.

Integrated analysis and design capabilities, when fully developed, could result in such voluminous information that it would tax the perceptive capabilities of human designers despite great versatility of information display. A higher form of optimization, enhanced with learning capabilities, could be a useful tool to digest the large amounts of analysis information and "suggest" design changes. Within the broad area of artificial intelligence research, considerable practical software and hardware capabilities have been developed in the particular field of adaptive learning networks. Once such a network is "trained" to approximate the behavior of a real system, it can be interrogated in a fraction of the computer time necessary to query the real system. As an experienced engineer acquires a "feel" for a particular problem as it progresses, learning networks are conceived essentially to do the same. Incorporation of such machine intelligence in future automated structural design will enable the engineer of tomorrow to more adequately use his unique human ability — creativity.

BIBLIOGRAPHY

1. Shanley, F. R.: Weight-Strength Analysis of Aircraft Structures. Dover Publication, 1960.

2. Sheu, C. Y.; and Prager, W.: Recent Developments in Optimal Structural Design. Applied Mechanics Reviews, vol. 21, no. 10, Oct. 1968.

3. Schmit, L. A.; and Pope, G. G.: Structural Design Applications of Mathematical Programming Techniques. AGARDograph A6-149, 1970.

4. Berke, L.; and Khot, N. S.: Use of Optimality Criteria Methods for Large Scale Systems. AGARD-LS-70, Oct. 1974.

5. Barron, R. L.: Learning Networks Improve Computer-Aided Prediction and Control. Computer Design, Aug. 1975.

OVERCOMING THE BARRIERS TO

COMPUTERIZED STRUCTURAL DESIGN

Michael F. Card
Langley Research Center

INTRODUCTION

From a research point of view, the prospects for computerized structural analysis and design appear to be excellent. Computerized analysis is now an integral part of all major structural engineering projects. There is considerable ongoing research on advanced design techniques, in both government and industry; recently NASA has taken a significant step towards enhancing the use of computers in design with initiation of the IPAD project (Refs 1 and 2). However, the development of a major thrust to advance the design state of the art by automation has been slow. For example, it has taken about six years for a satisfactory arrangement to be negotiated between government and industry for IPAD. Thus, it would appear that there are some significant barriers to acceptance of computerized design as a national goal.

BARRIERS

Some of the major barriers which I perceive are

- THE ALL KNOWING DESIGNER SYNDROME
- THE COOKBOOK ENGINEER
- MAN'S FASCINATION WITH MACHINES
- COSTS
- STANDARDIZATION/ACCREDITATION

A facetious illustration of the first barrier is shown in figure 1. One of the ghosts of the past has been the perception that most of the really serious design work is done by a clever, experienced designer, a unique individual who through sheer physical insight is able to master all problems. Unfortunately, as structural designs have become more and more complex, the single designer with complete mastery of his structure is a vanishing breed. The size and complexity of major structural projects do not permit any such seat-of-the-pants designer to make a significant contribution, except in the very earliest stage of design. Even in the embryonic stages of design, with only his insight, he is hard pressed to make a convincing technical case for the credibility of his ideas.

A second barrier to the acceptance of computerized design is at an opposite pole from the practical designer. The computer cookbook engineer (see figure 2) can be viewed as a serious threat to any engineering or research organization. The reliance on the computer to do design is a terrible temptation to transfer engineering responsibility and understanding to a machine. Methods to discourage misapplication and lack of proper solution checking are a constant concern of most organizations who perform computerized design activities. To reduce development costs, there are tremendous pressures to rely on computerized analysis and design and to eliminate qualification testing. But, how do we ensure that computations are accurate and appropriate?

A third barrier is man's fascination with machines. As illustrated in figure 3, the exposure of engineers with good structural insight to the computer can be dangerous. The process of transition of the structures engineer to computer software specialist is suggested. While computer science may benefit by cross-fertilization, there must remain a hardcore group of structural specialists who are able to interpret and apply the results of computerized designs and who may conceivably invent new techniques.

A fourth barrier (common to all current advanced technologies) is the unknowns associated with costs. As illustrated in figure 4, the resources to perform structural design in the aircraft industry have been steadily increasing. The hope of automated design is that the computer will reduce manhours expended in design and that computer hour costs will not increase enough to offset the manhour cost reduction. If the computer design process is too complex, however, a net cost reduction will not be realized, even though the depth and accuracy in which real-time design cycles can be executed will be significantly increased.

The cost barrier is complicated by government experiences with computerized analysis development. Recent NASA experience with NASTRAN and FLEXSTAB suggests that the government must modify its future role in the support of major computer code developments. As illustrated in figure 5, the pattern for development costs will include government support of initial development costs including software design, coding, early debugging, testing and maintenance; however, after the code is sufficiently matured, it will be up to a community of users to continue its financial support. Lack of commitments by user groups to assume this financial burden will necessarily slow the pace of advanced computerized capability.

The final barrier is the issue of standardization and accreditation. As a member of the government, I recognize the need for both elements, but I am somewhat sceptical of the process (e.g. fig. 6) by which it can be accomplished. Once it is admitted that such a process is needed, a tremendous power struggle for the right to control the process is created. The protagonists come from industry, university and government. They range from the industrialists who are fighting to retain competitive edges in computer hardware and software systems to the technical societies and government agencies who are struggling to be recognized as the all-powerful certifying agent. The addition of standardization and certification requirements will of necessity retard the development pace of automated design tools.

PROSPECTS

I believe that the barriers to general acceptance of automated structural designs can be overcome. As illustrated in figure 7, significant progress is being made in aerospace applications of computerized sizing with very accurate analysis becoming both feasible and cost effective.

The keys to overcoming the barriers already mentioned are as follows:

FUTURE ATTRACTIONS

- DESIGNERS ON SCOPES RATHER THAN BOARDS
- BRAINWORK RATHER THAN DOGWORK

PREREQUISITES

- DESIGN PROBLEMS OF SUFFICIENT COMPLEXITY
- NEED FOR REDESIGN SPEED

CENTRAL STEPS

- COMPUTERIZED DESIGN TRAINING IN UNIVERSITIES AND INDUSTRY
- SERIES OF STRUCTURAL TESTS TO DEMONSTRATE EFFECTIVENESS OF AUTOMATED DESIGN
- MOBILITY IN TECHNOLOGY TRANSFER THROUGH STANDARDIZATION

To attract young people to the structural design profession, it seems likely that man's fascination with machines can be exploited to eliminate the drafting board. For the existence of such an advanced design capability, however, there are two prerequisites. Foremost is the challenge to design a structure or vehicle of sufficient complexity to warrant such techniques. As an example, development of advanced supersonic cruise aircraft designs have offered a greater stimulus to computerized design development than subsonic transport designs because of greater technical complexities (especially in aeroelastic design) and more demanding payload requirements. A second prerequisite is the urgency for speed in the design cycle. Generally design cycle speed requirements are generated by competition, mission and market targets, and design time costs; however, in economically depressed industries, the tendency is to stretch out vehicle development times.

Finally, I suggest three central steps which might be taken to overcome resistance to computerized structural design. First, to eliminate the cookbook engineer, a serious attempt should be made to properly train engineers in the use of the computer for design. This is particularly important in university training where the ethics of using the computer can be taught. Second, to address the fear of fallibility of computer-generated designs, there should

be a series of design and structural test activities whose purpose is to validate the credibility of computer-generated designs. Finally, the cost-effectiveness of computerized design systems can be achieved with selective use of standardization to permit some technology transfer of structural design techniques to a wider range of industries.

REFERENCES

1. Heldenfels, R. R.: Automating the Design Process: Progress, Problems, Prospects and Potential. Presented at 14th AIAA/ASME/SAE Structural Dynamics & Materials Conference, Williamsburg, VA, March 20-22, 1973. AIAA Paper 73-410.

2. Sobieszczanski, J.; Voigt, S. J.; Fulton, R. E.: On Computer-Aided Design of Aerospace Vehicles. Applied Mech. Div., vol. 7. ASME Structural Optimization Symposium, Winter Annual Meeting New York, Nov. 17-21, 1974.

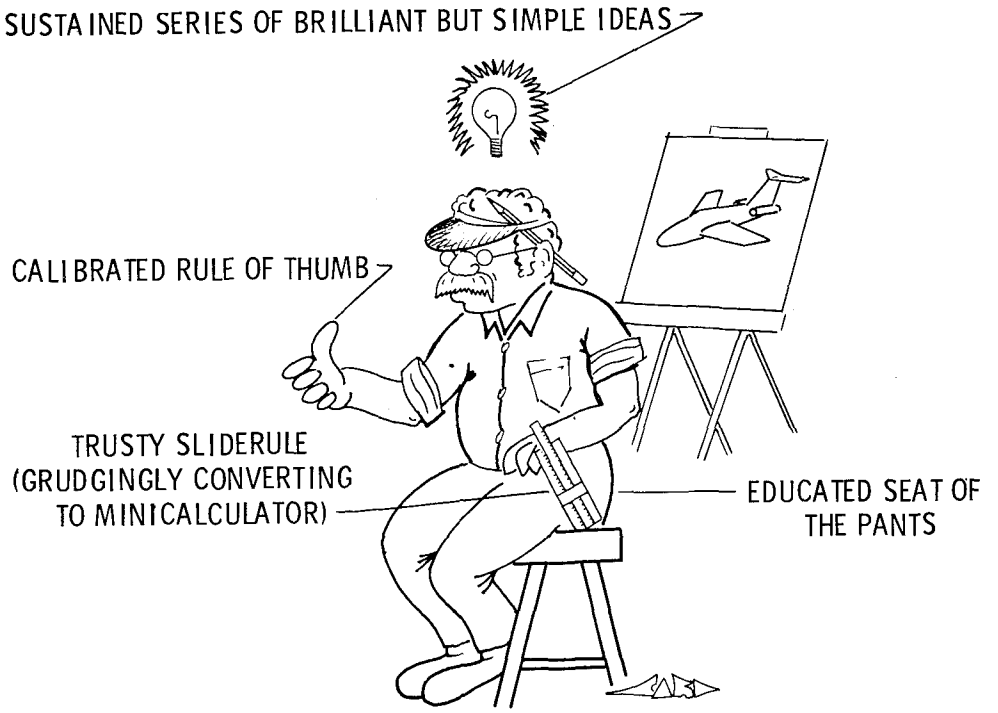

Figure 1.- The all-knowing designer syndrome.

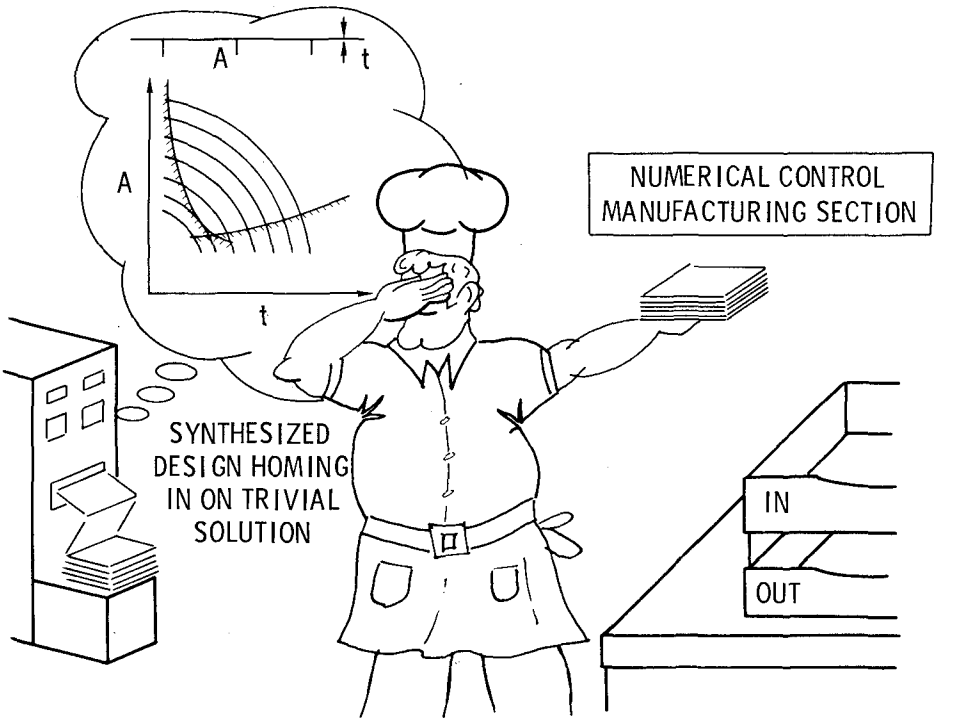

Figure 2.- The computer cookbook engineer.

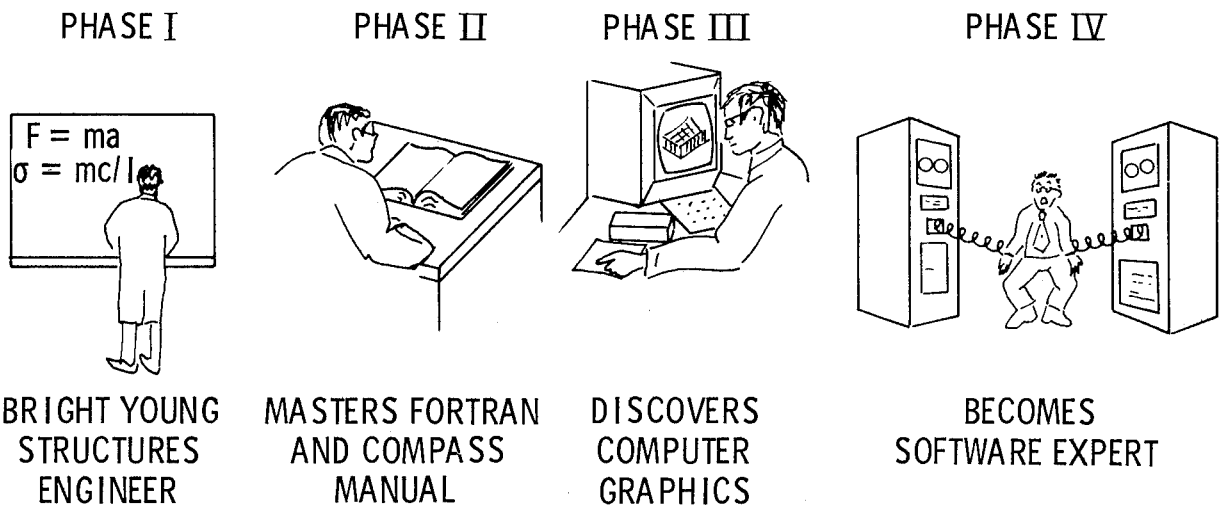

Figure 3.- Man's fascination with machines.

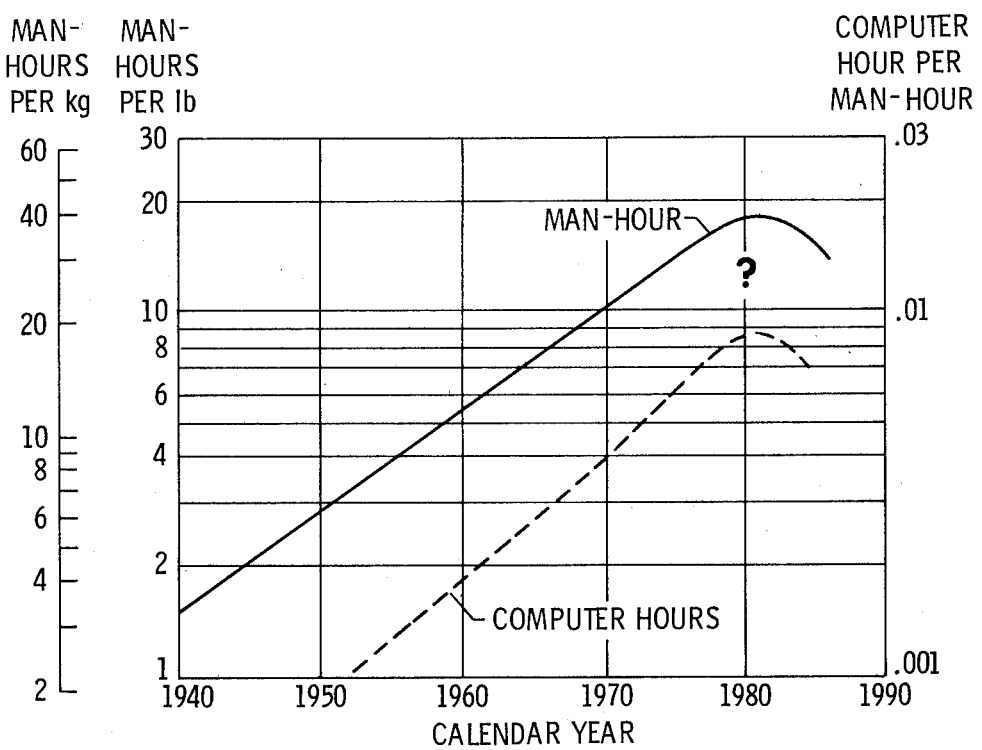

Figure 4.- The increasing costs of aircraft design.

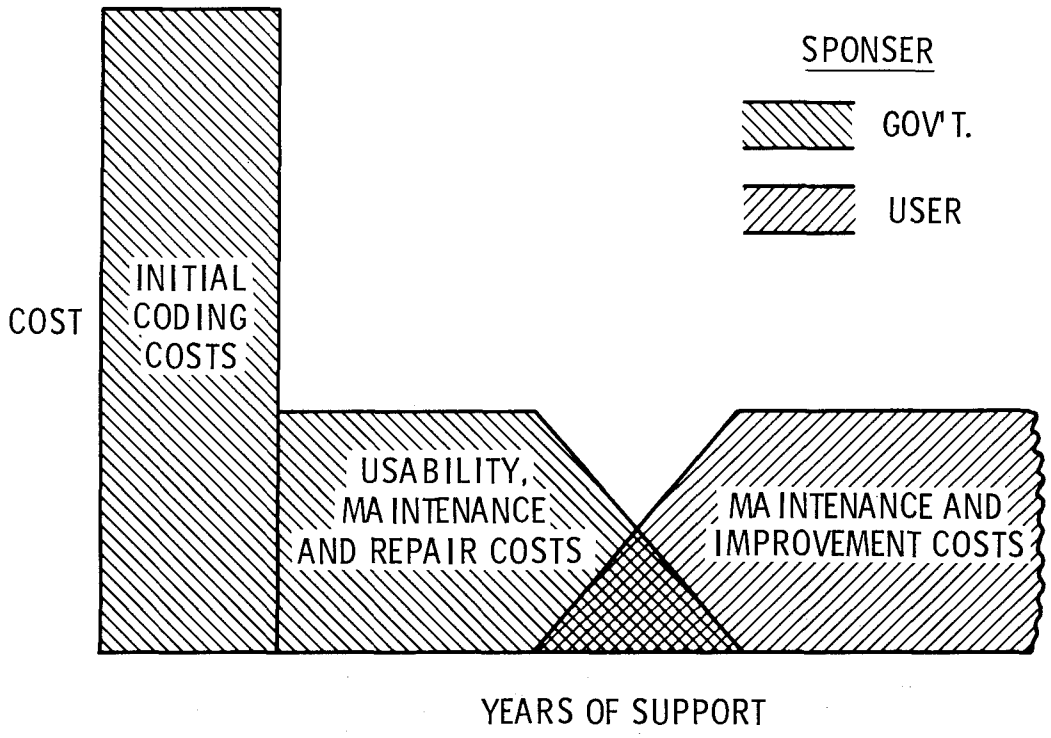

Figure 5.- Computer code development cost sharing.

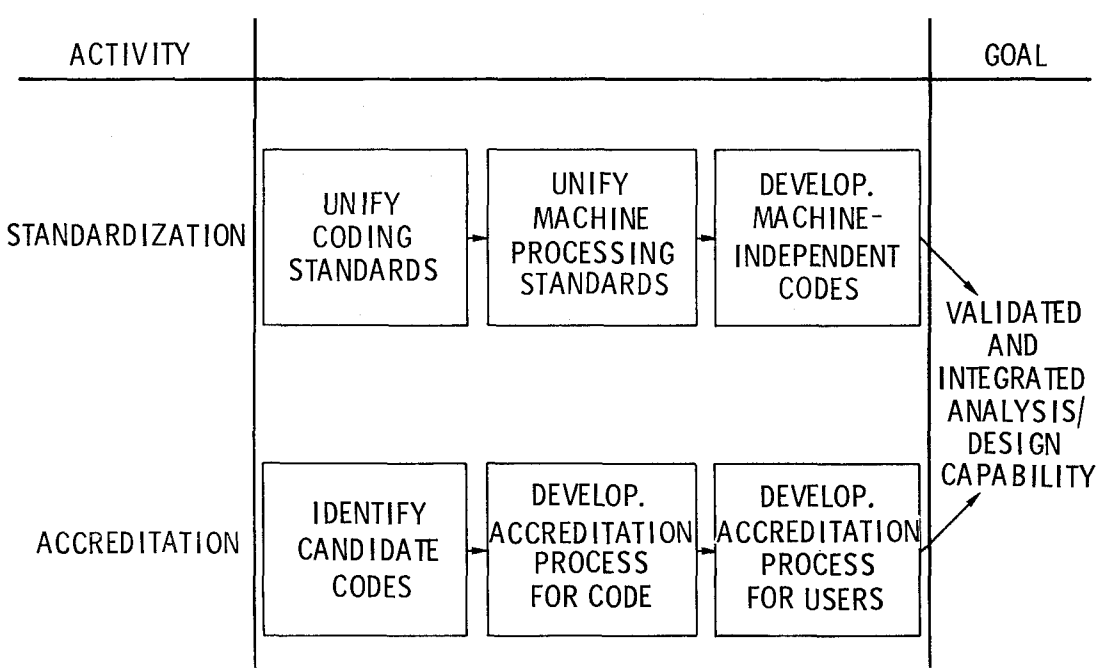

Figure 6.- The process of standardization and accreditation of analysis and design codes.

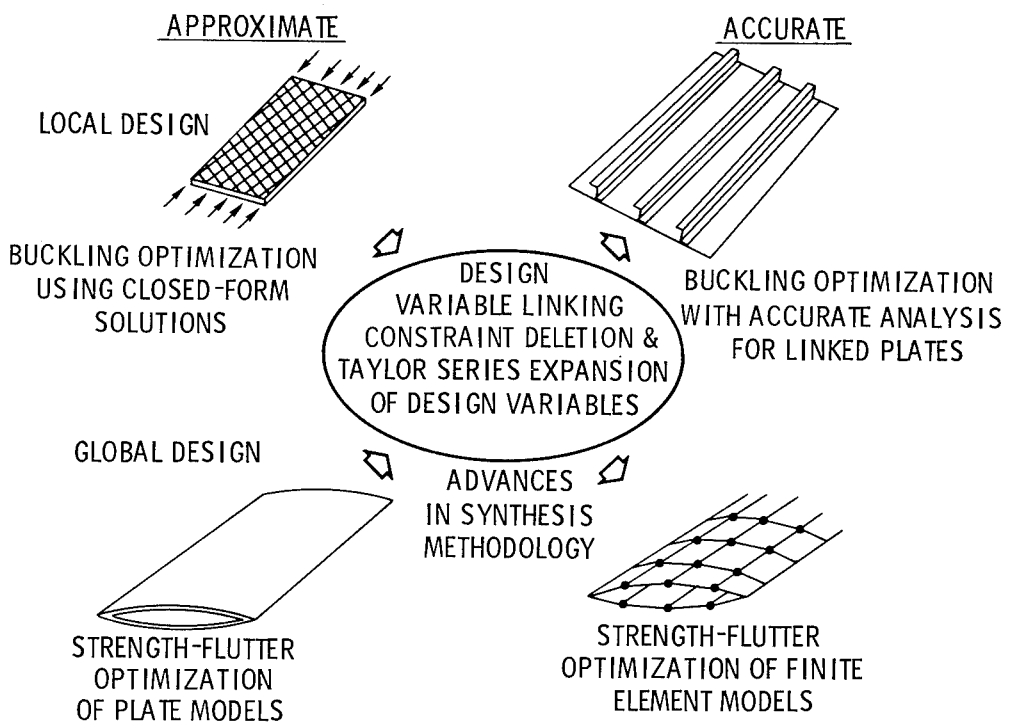

Figure 7.- Progress in automated structural design.

COMPUTERIZED STRUCTURAL ANALYSIS AND DESIGN -- FUTURE AND PROSPECTS

Richard F. Hartung
Lockheed Research Laboratory

OPENING REMARKS

The analysis and design of structures by computer methods will be influenced in the future by new developments in computer hardware and software and by the development of new analysis capability. These developments will tend to relieve the engineer of much of the programming activity in which he now engages and will provide him with a very powerful array of analysis tools that allow him to solve a greater variety of problems. Much of the routine data handling activity that now occupies the engineer's time will be taken care of by data managers or eliminated by compatible interdisciplinary engineering analysis software. In short, engineers will be able to spend more time doing engineering work.

Software technology is changing rapidly. Ad hoc programming techniques that have been used in the development of much of the present-generation, structural-analysis software are no longer satisfactory for this purpose. More formal coding procedures and new programming languages will be used to facilitate program development, checkout, application, and maintenance. Future software will be systems oriented with extensive libraries of technical modules, matrix utilities, and driver programs that communicate via a common data base or a super executive program. Data base management techniques specifically oriented to the large files of numerical data arising in scientific analysis will be in common use. More attention will be given to program documentation and configuration control to insure that software will be perpetuated as personnel changes occur.

Most structural engineers will have neither the inclination nor the necessary training to plan and program good software systems. These tasks will be done by computer specialists, numerical analysts, and engineers with extensive training and experience in the use of modern programming techniques. The structural engineer will no longer have to be a software developer; instead he will be a software synthesizer who selects modules from program libraries and executes them as required to solve the problem at hand. Although he may know very little about computer programming, he will have available to him a very powerful computer capability that he can operate with a simple problem-oriented language. Furthermore, as various engineering organizations begin to share the same analysis system there will be much more interaction between various engineering organizations (e.g., structures, thermo, aero, loads, etc.) during the design process.

The problem of software dissemination has not yet been satisfactorily resolved. While millions of dollars in public funds have been spent in recent years on software development, relatively little of it is readily available to the public. Several questions need to be answered. (1) How can a structural engineer with a problem determine what computer programs are available to solve his problem? (2) How can the appropriate program be obtained or used? (3) Who will provide technical assistance on the use of the program? (4) How will the costs of the dissemination and consultation be handled? New approaches to this problem will be explored in the future. Some of the current structural analysis programs are available from computer utility companies on a surcharge basis. An increasing number of industries, that previously relied on crude approximate techniques or simply ignored structural analysis altogether, are beginning to use these structural analysis programs on a routine basis. For example, one manufacturer of office reproducing machines has begun to use computer programs to perform dynamic analysis of its machines in order to reduce vibrations and thus improve the sharpness of the reproductions produced by the machine. In the future, regulatory agencies may require that structures in which public safety is involved be designed and analyzed using computer programs that have been certified. This could have a significant affect on design procedures.

Minicomputers and microcomputers will continue to become more powerful and less expensive. These machines will assume the role of interactively handling many pre- and post-processing functions that are now done in a batch mode on the macrocomputers. One interesting possibility is that special purpose minicomputers will be developed to execute specific structural analysis programs. Under this scheme, one could obtain a turn-key structural analysis capability including software, hardware, and documentation.

More powerful macrocomputers presently under development will make available to the analyst the low cost, high capacity, high speed computer needed to conduct transient-response and nonlinear analyses or to perform design and optimization studies. Such problems require that the governing equations be solved a large number of times in order to obtain a solution. Currently, the cost of these analyses are prohibitive when applied to large structural models needed to represent real structures.

As the analyst's capability to solve complex problems (e.g., those involving nonlinear phenomena, transient response, or buckling) is increased, so will be the amount of judgment that he is required to exercise. Selection of the various solution parameters, solution strategy, and discretized structural model requires extensive experience. To guide the analyst in this kind of problem, preprocessors could be developed which, when given data that describes the structure and type of analysis to be performed, would provide the analyst with information to guide him in making a mathematical model and selecting an appropriate solution strategy. The preprocessor could even automatically set many of the solution parameters in the computer program in much the same way that an automatic camera selects exposure parameters based on light meter readings. The experienced user could override these settings, of course, if he felt it appropriate. Such capability would enable the analyst to conduct a more accurate analysis in less time and with lower cost.

To be prepared to function effectively in the environment of the future, engineering students will have to be given a balanced curricula that provides both a good background in fundamentals of mechanics and familiarity with concepts such as discrete representation of structures, matrix algebra, and numerical analysis that are fundamental to computer analysis of structures.

In summary, the structural analyst will surrender some autonomy in the area of software development and utilization. More formal programming and data format procedures will be required. However, the analyst will have available to him powerful, system-oriented, engineering analysis programs that will enable him to solve complex interdisciplinary problems and relieve him of much of the routine noncreative work with which he must now contend.

COMPUTER SIMULATION OF COMPOSITE MATERIALS FOR STRUCTURAL DESIGN

Edward L. Stanton
Prototype Development Associates, Inc.

As almost anyone involved in structural design today will tell you, the use of composite materials for primary structure tends to make structural response more difficult to predict. The reasons for this increased difficulty range from problems in material characterization to problems in predicting the complex load interactions that can occur among constituents during failure. This is not to say that simple effective modulus methods should not be used when appropriate, obviously they should. However, even in this situation it may require more than the rule of mixtures to determine the effective moduli for a representative volume element of the material.

The point of this preamble is to indicate yet another role that the computer is assuming in structural design; namely, a bridge that helps bring the technology of the materials scientist to the structural engineer. This is an area of considerable activity at all levels, and it seems clear that the role of the computer will grow as computational models are developed that better characterize real composite materials. The models now available are typically used in a preprocessor mode to characterize statistically homogeneous stress-strain behavior, and in a postprocessor mode to predict margins of safety or survival probabilities. Also, computer data files are becoming the archive source for materials test data as it is developed for many new composites thus replacing the traditional handbook.

The mode in which the computer is used to fill the roles just described will more than likely change with the new minicomputers and other hardware developments. Computational models in the future may use specially designed macroprocessors for digital simulation of constituents. There are several factors that make computer simulations of this type attractive: one, the rapid advances in electronic chip technology make it economically feasible, and two, the triaxial as well as statistical nature of the materials behavior make an all software simulation expensive. To illustrate this point, it currently requires almost as much computer time to calculate survival probabilities for some 3D materials given the state of stress and strain as it does to compute the effective modulus stress-strain solution for the structure. While this may appear excessive, it reflects the computational difficulty that can occur when material behavior is characterized by a complex microstructure.

THE FUTURE OF COMPUTERIZED STRUCTURE ANALYSIS

Edward L. Wilson
University of California, Berkeley

OPENING REMARKS

The solution of problems in the field of computational mechanics has progressed to the point in time where general purpose computer programs are used for the majority of problems. As a result of the large investment in development effort and the familiarization of many users with a particular code, new computer programs for the solution of linear structural mechanics problems have not emerged in the past few years. However, it is reasonable to state that a large portion of every major computer program is obsolete and should be modified if optimum accuracy or efficiency is to be realized. Of course there are several reasons why these general purpose codes are not being modified or significantly extended. First, some codes are operated on a royalty basis; therefore, there is little motivation to increase their efficiency. Second, many codes are so large and have been developed over such a long period of time that it is practically impossible to make basic changes. Third, the basic architecture of the code will not permit a change in the basic numerical approach to a problem. It is my observation that major new numerical techniques will only be used in general purpose programs if a completely new program is developed. It is also my opinion that new programs will not necessarily be adopted immediately by the profession unless they solve problems that existing programs cannot solve. This is because the user, in general, will not risk change to a new, unfamiliar program for the sake of accuracy and efficiency only.

While new capability is presently the only reason for the use of a new computer program, within the next few years the development of new, inexpensive computer hardware may be a compelling reason to change computer programs. The development of parallel and pipeline large expensive computers has not had a significant impact on the solution of problems in computational mechanics. However, minicomputers (less than $50,000 with input, output and low speed storage) are currently being used very effectively for the solution of medium-size problems. In my opinion, the most significant change is yet to come. Within the past year several different types of micro-computers (only 8 to 16 bits) have been developed. The present prices of these small programmable computers, complete with local storage and input-output interfaces, range from $200 to $500. If a system of these micro-computers is specifically designed for the solution of finite element systems, it may be possible to solve large dynamic nonlinear systems at a minimum of cost. In light of the new computer hardware developments the purpose of my present research is to re-examine several traditional numerical methods and to introduce some new numerical approaches for both linear and nonlinear analysis.

ON THE STABILITY OF A CLASS OF IMPLICIT ALGORITHMS FOR NONLINEAR STRUCTURAL DYNAMICS

Ted Belytschko
University of Illinois at Chicago

SUMMARY

Stability in energy for the Newmark β-family of time integration operators for nonlinear material problems is examined. It is shown that the necessary and sufficient conditions for unconditional stability are equivalent to those predicted by Fourier methods for linear problems.

INTRODUCTION

In this paper, stability in energy for the Newmark family (ref. 1) of time integration operators is examined. Stability for these operators was considered in the original paper of Newmark, who used essentially Fourier techniques which are strictly applicable only to linear problems. Belytschko and Schoeberle (ref. 2) have shown the unconditional stability of the particular form of the Newmark β-operator that corresponds to the trapezoidal rule ($\gamma=\frac{1}{2}$, $\beta=\frac{1}{4}$) for nonlinear material problems by energy methods. Hughes (ref. 3) extended this proof to the range of parameters ($\gamma=\frac{1}{2}$, $\beta\geq\frac{1}{4}$). In this paper, it is shown by generalizing the definition of discrete energy, sufficient conditions for unconditional stability in energy on both γ and β can be obtained. These conditions are equivalent to the necessary conditions for the unconditional stability of the Newmark operators in linear problems, so the conditions obtained herein are necessary and sufficient for the unconditional stability for nonlinear material problems.

PRELIMINARY EQUATIONS

The equations will here be presented in the formalism of the finite element method. As indicated in Belytschko, et al (ref. 4), the spatial discretization in finite difference methods is basically identical, so the choice of finite element notation is only a matter of convenience, not a restriction on the proof. The equations will only be outlined; details may be found in Zienkiewicz (ref. 5).

The fundamental step in any spatial discretization, which is often called the semidiscretization, is a separation of variables

in the form

$$\underline{u}(\underline{x},t) = \underline{\phi}(\underline{x})\ \underline{d}^{(e)}(t) \tag{1}$$

where $\underline{x}$ is the Cartesian coordinate, t the time, $\underline{u}$ the displacement field, $\underline{\phi}$ the shape functions, and $\underline{d}^{(e)}$ the nodal displacement of element e. The strains can then be related to the nodal displacements by

$$\underline{\varepsilon} = \underline{B}\,\underline{d}^{(e)} = \underline{B}\,\underline{L}^{(e)}\,\underline{d} \tag{2}$$

where $\underline{B}$ consists of derivatives of the shape functions and $\underline{L}^{(e)}$ is the connectivity matrix. The discrete equations of motion are then

$$\underline{M}\,\underline{a} + \underline{f} = \underline{p} \tag{3}$$

where $\underline{M}$ is the mass matrix, $\underline{a}$ the nodal accelerations (second derivatives of $\underline{d}$ with respect to time), $\underline{p}$ the external nodal forces and $\underline{f}$ the internal nodal forces, which are given by

$$\underline{f} = \sum_e \underline{L}^{(e)T}\underline{f}^{(e)} = \sum_e \underline{L}^{(e)T} \int_{V^{(e)}} \underline{B}^T\underline{\sigma}\ dV \tag{4}$$

Equations (3) and (4) can be derived from the principle of virtual work with the inertial forces included in a d'Alembert sense; see for example Belytschko, et al (ref. 6).

We define a discrete internal energy by

$$U_1 = 0$$

$$U_{I+1} = U_I + \tfrac{1}{2} \sum_e \int_{V^{(e)}} \Delta\underline{\varepsilon}_I^T \left[(1-\mu)\underline{\sigma}_I + \mu\underline{\sigma}_{I+1}\right] dV \tag{5}$$

where upper case subscripts denote the time step and Δ denotes a forward difference

$$\Delta\underline{\varepsilon}_I = \underline{\varepsilon}_{I+1} - \underline{\varepsilon}_I \tag{6a}$$

and

$$0 \le \mu \le 1 \tag{6b}$$

When $\mu=\frac{1}{2}$, eq. (5) represents a trapezoidal integration of the nonlinear stress strain curve, while $\mu=0$ corresponds to Euler integration.

By means of eqs. (2) and (4), eq. (5) can also be written as

$$U_{I+1} = U_I + \tfrac{1}{2} \Delta \underline{d}_I^T [(1-\mu) \underline{f}_I + \mu \underline{f}_{I+1}] \tag{7}$$

We require that the discrete internal energy be positive definite, so that

$$\sum_{J=1}^{I} \Delta \underline{\varepsilon}_J^T [(1-\mu) \underline{\sigma}_J + \mu \underline{\sigma}_{J+1}] \geq 0 \tag{8}$$

The kinetic energy T is given by

$$T_I = \tfrac{1}{2} \underline{v}_I^T \underline{M} \underline{v}_I \tag{9}$$

where $\underline{v}$ are the nodal velocities (first derivative of $\underline{d}$ with respect to time).

The Newmark difference formulas are

$$\underline{v}_{I+1} = \underline{v}_I + \Delta t [(1-\gamma) \underline{a}_I + \gamma \underline{a}_{I+1}] \tag{10}$$

$$\underline{d}_{I+1} = \underline{d}_I + \Delta t \underline{v}_I + \Delta t^2 [(\tfrac{1}{2}-\beta) \underline{a}_I + \beta \underline{a}_{I+1}] \tag{11}$$

When $\beta > 0$, these equations are implicit, and hence for nonlinear materials, the solution of a nonlinear system of equation is necessary. The exact solution of the nonlinear system of equations at each time step is not possible; at each time step there will be an error $\underline{f}_I^{err}$ given by

$$\underline{f}_I^{err} = \underline{p}_I - \underline{f}_I - \underline{M} \underline{a}_I \tag{12}$$

We define an energy error criterion

$$|\Delta \underline{d}_I^T [(1-\mu) \underline{f}_I^{err} + \mu \underline{f}_{I+1}^{err}]| < \varepsilon (U_I + T_I) \tag{13}$$

where ε is a small constant and require that the solution of the nonlinear equations at each time step satisfy this criterion.

PROOF OF UNCONDITIONAL STABILITY

We will now show that the error criterion, eq. (13), is a sufficient condition for the unconditional stability in energy of the Newmark integration formulas for $\gamma \geq \frac{1}{2}$, $\beta \geq \gamma/2$. Stability in energy is described in Richtmyer and Morton (ref. 7) and has previously been used for the derivation of stability conditions for the solution of linear problems by the Newmark β-method by Fujii (ref. 8).

The demonstration of unconditional stability in energy requires that it be shown that a positive definite norm of the solution is bounded regardless of the size of the time step. As pointed out in reference 7, the norm need not be the physical energy, though in many cases it is. For the purposes of this proof, we define the norm by

$$S_I = T_I + U_I + (2\beta-\gamma)\underline{a}_I^T \underline{M}\, \underline{a}_I \tag{14}$$

Because of the requirement of eq. (8), U_I is positive definite, whereas the positive definiteness of the mass matrix $\underline{M}$ assures the positiveness definiteness of the remaining two quantities if

$$2\beta \geq \gamma \tag{15}$$

Stability in energy is then assured if we can show that S_I is always bounded, i.e. that

$$S_{I+1} \leq (1+\varepsilon^*) S_I \tag{16}$$

where ε^* is an arbitrarily small quantity. The interpretation of the condition of eqs. (14) and (16) is as follows. Provided that the discrete internal energy is a monotonically increasing function of the displacements, the boundedness of S_I implies that the velocities and displacements are bounded, which corresponds to the notion of stability.

The proof of stability then consists of deducing eq. (16) from eqs. (7) to (11) and the homogeneous form of eq. (3). From eqs. (9) and (10), it follows that

$$\begin{aligned} T_{I+1} = T_I &+ \Delta t\, \underline{v}_I^T \underline{M}\, [(1-\gamma)\underline{a}_I + \gamma \underline{a}_{I+1}] \\ &+ \frac{\Delta t^2}{2} [(1-\gamma)\underline{a}_I^T + \gamma \underline{a}_{I+1}^T] \underline{M}\, [(1-\gamma)\underline{a}_I + \gamma \underline{a}_{I+1}] \end{aligned} \tag{17}$$

so

$$T_{I+1} = T_I + \left[\Delta \underline{d}_I^T + \Delta t^2(\beta-\tfrac{1}{2}\gamma)\underline{a}_I^T + \Delta t^2(\tfrac{1}{2}\gamma-\beta)\underline{a}_{I+1}^T\right]$$
$$\underline{M}\left[(1-\gamma)\underline{a}_I + \gamma\underline{a}_{I+1}\right] \tag{18}$$

Thus if we let

$$\gamma = \mu \tag{19}$$

then eqs. (7) and (18) yield

$$T_{I+1} + U_{I+1} = T_I + U_I + \Delta \underline{d}_I^T\left[(1-\gamma)(\underline{M}\,\underline{a}_I + \underline{f}_I)\right.$$
$$\left. + \gamma(\underline{M}\,\underline{a}_{I+1} + \underline{f}_{I+1})\right] + \Delta t^2\left[(\beta - \tfrac{\gamma}{2})\underline{a}_I^T + (\tfrac{\gamma}{2}-\beta)\underline{a}_{I+1}^T\right]\underline{M}$$
$$\left[(1-\gamma)\underline{a}_I + \gamma\underline{a}_{I+1}\right] \tag{20}$$

The second term on the right hand side of eq. (20) corresponds to the error in energy as defined by eq. (13), and the last term can be rearranged so that we obtain

$$T_{I+1} + U_{I+1} \leq (1+\varepsilon)(T_I+U_I) + \Delta t^2(\gamma-2\beta)(\underline{a}_{I+1}^T\,\underline{M}\,\underline{a}_{I+1} - \underline{a}_I\,\underline{M}\,\underline{a}_I)$$
$$+ \Delta t^2(\gamma-\tfrac{1}{2})(\gamma-2\beta)(\underline{a}_{I+1}^T - \underline{a}_I^T)\,\underline{M}\,(\underline{a}_{I+1} - \underline{a}_I) \tag{21}$$

The last term on the right hand side of eq. (21) is negative semi-definite if

$$\gamma \geq \tfrac{1}{2} \qquad \text{and} \qquad 2\beta \geq \gamma \tag{22}$$

or if both of the above inequalities are reversed. However, if the inequalities are reversed, as can be seen from eqs. (14) and (15), the norm S_I is not positive definite. Hence, only the conditions given by eq. (22) are pertinent. Under these conditions, the inequality of eq. (21) applies even if the last term is dropped. The remaining terms then yield eq. (16).

DISCUSSION AND CONCLUSIONS

Several remarks should be noted in applying these results to computations. First, the stability hinges on the achievement of a solution in each time step that satisfies eq. (13). The convergence of solution schemes, such as the modified Newton Raphson method, cannot be assured, and is therefore the primary obstacle in obtaining stable solutions. The difficulties are particularly severe in elastic-plastic problems if the tangential stiffness method is used whenever unloading takes place over a large part of the mesh.

It is also not clear whether the form of the error criterion, eq. (13), is suitable for very fine meshes. Numerical experiments indicate that it becomes increasingly difficult to satisy eq. (13) for finer meshes, for although the criterion appears to be mesh-independent in that the right hand side increases with the size of the physical problem, the right hand side does not vary as a mesh is refined. Furthermore, in very large meshes there is a possibility of cancellation of errors, i.e. positive error energy transfer in one portion, with negative error energy transfer in another portion. This can be avoided by placing the absolute value within the summation.

Results have been reported for a special case of this operator ($\gamma=\frac{1}{2}$, $\beta=\frac{1}{4}$) in reference 2. Both material and geometric nonlinearities were included in those problems. However, the proofs given here and in reference 2 require the absence of geometric nonlinearities; if geometric nonlinearities are included, eq. (5) does not imply eq. (7), for in geometrically nonlinear problems $\Delta\underline{B}$ does not vanish. Hence, as shown in reference 9, in geometrically nonlinear problems, energy transfer is associated with the rotation of a stressed member: this effect results in the generation of energy if the stress is tensile and is hence destabilizing under those conditions. In many structural dynamics problems, the total rigid body rotation that takes place is insufficient for this energy generation to be significant. However, test problems have been devised where the energy error is so large that for practical purposes the computation can be considered unstable.

Finally, we comment on some experience with the requirement of eq. (8). This condition requires that the numerical integration of the internal work always yield a positive quantity. In elastic-plastic materials and other strongly dissipative materials, this condition poses no problems. However, when the stress is a single-valued function of the strain, eq. (8) can easily be violated in cyclic load paths. However, numerical experiments do not indicate that violation of eq. (8) results in any catastrophic failure of the computation.

REFERENCES

1. Newmark, N.: A Method of Computation for Structural Dynamics. Journal of the Engineering Mechanics Division, Proceedings of ASCE, 1959, 67-94.

2. Belytschko, T.; and Schoeberle, D.: On The Unconditional Stability of an Implicit Algorithm for Nonlinear Structural Dynamics. Journal of Applied Mechanics 42, 1975, 865-869.

3. Hughes, T.J.R.: A Note on the Stability of Newmark's Algorithm in Nonlinear Structural Dynamics. International Journal of Numerical Methods in Engineering, 1976.

4. Belytschko, T.; Kennedy, J.M.; and Schoeberle, D.F.: On Finite Element and Difference Formulations of Transient Fluid-Structure Problems. Proceedings of Computational Methods in Nuclear Engineering, ANS Mathematics and Computations Division, Charleston, South Carolina, April 1975.

5. Zienkiewicz, O.C.: The Finite Element Method in Engineering Science. McGraw-Hill, London, 1972.

6. Belytschko, T.; Chiapetta, R.L.; and Bartel, H.D.: Efficient Large Scale Nonlinear Transient Analysis by Finite Elements. International Journal for Numerical Methods in Engineering, 10, 1976, 579-596.

7. Richtmyer, R.D.; and Morton, K.W.: Difference Methods for Initial Value Problems. Interscience Publishers, New York, 1967.

8. Fujii, H: Finite-Element Schemes: Stability and Convergence. Advances in Computational Methods in Structural Mechanics and Design, ed. Oden, J.T., et al, UAH Press, Huntsville, Alabama, 1972, 201-218.

9 Belytschko, T.; Holmes, N.; and Mullen, R.: Explicit Integration - Stability, Solution Properties, and Cost. Finite Element Analysis of Transient Structural Behavior, ed. Belytschko, T.B., et al, ASME, New York, 1975.

A REVIEW OF SUBSTRUCTURE COUPLING METHODS FOR DYNAMIC ANALYSIS*

Roy R. Craig, Jr. and Ching-Jone Chang
The University of Texas at Austin

SUMMARY

This paper assesses the state of the art in substructure coupling for dynamic analysis. A general formulation, which permits all previously described methods to be characterized by a few constituent matrices, is developed. Limited results comparing the accuracy of various methods are presented.

INTRODUCTION

Analysis of the response of a complex structure to dynamic excitation is usually accomplished by analyzing a finite element model of the structure. Since the finite element model may contain thousands of degrees of freedom, and since the structure may consist of several substructures which are designed and fabricated by different organizations, it is desirable to have a method of dynamic analysis which permits the number of degrees of freedom of the dynamic model to be reduced and which also allows as much independence as possible in the design and analysis of substructures. The names substructure coupling and component mode synthesis have been applied to the process of partitioning a structure into substructures, or components, and describing the physical displacements of the substructures in terms of generalized coordinates which are the amplitudes of predetermined substructure modes. A number of substructure coupling methods have been proposed. The goal of most of these has been to permit analytical determination of system natural modes and frequencies from given finite element models of the structure. To a lesser extent, the use of experimentally-determined substructure data to synthesize mathematical models of structures has been considered.

One classification of substructure coupling methods is based on the conditions imposed at the interface between one substructure and the adjoining substructures when mode shapes are determined for the substructure. One class is called fixed-interface methods, and a second is called free-interface methods. Related to the latter is a class which may be called loaded-interface methods. Finally, some consideration has been given to permitting arbitrary interface conditions which may be a combination of the above three types. Such a method may be called a hybrid method.

The following classes of modes are used in defining substructure generalized coordinates: normal modes, constraint modes, attachment modes, and rigid-body modes. These are defined in greater detail in a later section of the paper.

*This work was supported by NASA Grant NSG 1268.

SYMBOLS

The principal defining equations are given in parenthesis after the definition of each symbol.

A interface equilibrium matrix (29)
B displacement compatibility matrix (29)
C combination of A and B (33)
$\underline{f}$ substructure force vector (1)
$\bar{F}$ equivalent force vector (15)
G flexibility matrix (19)
k substructure stiffness matrix (1)
K system stiffness matrix (30, 37, 45)
L Lagrangian (26)
m substructure mass matrix (1)
M system mass matrix (30, 37, 45)
p substructure generalized coordinate vector (22, 25)
q system generalized coordinate vector (31)
R inertia relief matrix (14)
T substructure kinetic energy (21)
T_1 substructure transformation matrix (22)
T_2 system transformation matrix (31, 36)
U substructure potential energy (21)
x substructure physical coordinate vector (1)
η Lagrange multiplier vector (26)
Θ free-interface or loaded-interface normal mode matrix (7)
κ substructure generalized stiffness matrix (24, 25)
λ,Λ substructure eigenvalue, eigenvalue matrix (2, 3)
μ substructure generalized mass matrix (24, 25)
ν Lagrange multiplier vector (26)
ξ generalized coordinate (27)
σ Lagrange multiplier vector (38)
Φ fixed-interface normal mode matrix (4)
$\underline{X}$ modified attachment mode matrix (20)
$\bar{X}$ unmodified attachment mode matrix (13, 17)
Ψ constraint mode matrix (11)

Subscripts and Superscripts:

d dependent coordinates (32)
i non-interface (interior) coordinates (1)
j interface (junction) coordinates (1)
k kept coordinates (18)
ℓ linearly-independent coordinates (32)
r rigid-body modes, temporary constraints (14, 15)
u unrestrained coordinates (15)

HISTORICAL REVIEW

The following is a brief review of the development of a number of substructure coupling methods:

Hurty (refs. 1,2) developed the first substructure coupling method capable of analyzing substructures with redundant interface connection. Fixed interface normal modes, rigid-body modes and redundant constraint modes are used to define substructure generalized coordinates.

Bamford (ref. 3) introduced attachment modes, and developed a hybrid substructure coupling method.

Craig and Bampton (ref. 4) and Bajan and Feng (refs. 5,6) modified Hurty's method by pointing out that it is unnecessary to separate the set of constraint modes into rigid-body modes and redundant constraint modes.

Goldman (ref. 7) and Hou (ref. 8) developed methods which employ free-interface substructure normal modes. They differ in the technique used to effect coupling of the substructures, as will be explained in a subsequent section.

Benfield and Hruda (ref. 9) introduced two new concepts: they employed Guyan reduction (ref. 10) to determine interface loading, and they used a coupling strategy which differs slightly from strategies used by previous authors. These features serve as the basis for four methods described by Benfield and Hruda: free-free, constrained, free-free with interface loading, and constrained with interface loading.

MacNeal (ref. 11) developed a hybrid method which allows some substructure interface coordinates to be constrained while others are free. He also suggested the use of statically derived modes to improve the representation of the substructure motion.

Goldenberg and Shapiro (ref. 12) employed a method similar to Hou's, but provided for arbitrary mass loading of interface points.

Rubin (ref. 13) extended MacNeal's method to include second-order residual effects of modes truncated from the final set free-interface substructure normal modes.

Kuhar and Stahle (ref. 14) introduced a dynamic transformation which approximates the effect of modes which are truncated from the final set of system generalized coordinates.

In a recent paper Hintz (ref. 15) describes two statically complete interface mode sets which he calls "the method of attachment modes" and "the method of constraint modes." The former set is combined with both free-interface normal modes and with fixed-interface normal modes to form system coordinates. The latter is combined only with fixed-interface normal modes.

In reference 16 Craig and Chang describe three methods for reducing the

number of interface coordinates in the final system equations obtained by the Hurty method or the Craig-Bampton method. In reference 17 Craig and Chang provide examples of substructure coupling based on the methods of MacNeal and Rubin.

The previous references are primarily concerned with the use of substructure coupling methods in the analytical determination of modes and frequencies of complex structures. Several studies, however, explore the use of experimental data as input to coupling procedures. The following studies are of this nature:

Klosterman's thesis (ref. 18) provides a comprehensive study of the experimental determination of modal representations of structures including the use of these models in substructure coupling. In reference 19 Klosterman treats substructure coupling by two methods which he calls "component mode synthesis" and "general impedance method" respectively. The former closely parallels Bamford's work. In reference 20 Klosterman and McClelland introduce "inertia restraint" and outline a coupling procedure that appears to be especially suited to coupling two substructures where one is represented by modes and the second by a finite-element model.

Kana and Huzar (refs. 21,22) developed a semi-empirical energy approach for predicting the damping of a structure in terms of damping of substructures.

Hasselman (ref. 23) employs a perturbation technique to describe substructure damping and discusses, in a general way, coupling of substructures using either free-interface modes or fixed-interface modes.

Two symposia on the topic of substructure coupling have been held (refs. 24,25). Survey papers of particular importance, which were presented at these symposia, are references 26 and 27.

A GENERAL FORMULATION OF SUBSTRUCTURE COUPLING FOR DYNAMIC ANALYSIS

The substructure coupling methods mentioned in the preceding section may be described by a single comprehensive formulation. Differences in the methods result from the use of different mode sets to describe substructure generalized coordinates and different methods of enforcing compatibility of substructure interfaces. We will first define the mode sets used in representing the substructure physical displacements in terms of substructure generalized coordinates. Then, using the Lagrange multiplier method, we will show how enforcement of compatibility at substructure interfaces leads to system equations of motion. Finally, the vectors and matrices which define the various methods are tabulated.

Definition of Mode Sets

The physical displacements of each substructure are represented in terms of substructure generalized coordinates through the use of various "assumed modes," including normal modes of the substructure and certain static deflec-

tion modes.

The equation of motion of a substructure, when connected to other substructures and executing undamped free vibration, may be written in the form

$$\begin{bmatrix} m_{ii} & m_{ij} \\ m_{ji} & m_{jj} \end{bmatrix}^{\alpha} \begin{Bmatrix} \ddot{x}_i \\ \ddot{x}_j \end{Bmatrix}^{\alpha} + \begin{bmatrix} k_{ii} & k_{ij} \\ k_{ji} & k_{jj} \end{bmatrix}^{\alpha} \begin{Bmatrix} x_i \\ x_j \end{Bmatrix}^{\alpha} = \begin{Bmatrix} 0 \\ f_j \end{Bmatrix}^{\alpha} \tag{1}$$

Fixed-Interface Normal Modes

Fixed-interface normal modes are obtained by setting $x_j \equiv 0$ and solving for the free-vibration modes of the substructure. Equation (1) reduces to the eigenvalue problem

$$(k_{ii} - \lambda^2 m_{ii})\, x_i = 0 \tag{2}$$

The resulting substructure eigenvalues (frequencies) form a diagonal matrix

$$\Lambda \equiv \text{diag}\ (\lambda_1^2\ \lambda_2^2\ \ldots\ \lambda_{N_i}^2) \tag{3}$$

and the corresponding normalized eigenvectors (mode shapes) form the modal matrix

$$\Phi \equiv \begin{bmatrix} \phi_{i1} & \phi_{i2} & \cdots & \phi_{iN_i} \\ 0 & 0 & \cdots & 0 \end{bmatrix} \tag{4}$$

where N_i is the total number of substructure interior coordinates.

Free-Interface Normal Modes; Loaded-Interface Normal Modes

Free-interface normal modes are obtained by setting $f_j \equiv 0$ in equation (1) and solving for the resulting modes and frequencies of the substructure. Thus,

$$(k - \lambda^2 m)\, x = 0 \tag{5}$$

The matrix of eigenvalues is

$$\Lambda \equiv \text{diag}\ (\lambda_1^2\ \lambda_2^2\ \ldots\ \lambda_N^2) \tag{6}$$

where $N = N_i + N_j$ is the total number of substructure degrees of freedom. Since the structure may be unrestrained, there may be N_r rigid-body modes. The normalized eigenvectors form the modal matrix

$$\Theta \equiv \begin{bmatrix} \theta_{i1} & \theta_{i2} & \cdots & \theta_{iN} \\ \theta_{j1} & \theta_{j2} & \cdots & \theta_{jN} \end{bmatrix} \tag{7}$$

Several methods (e.g., refs. 9,12) employ loaded-interface normal modes. These are obtained by augmenting the interface mass and/or stiffness in equation (5) to give

$$\left[\begin{bmatrix} k_{ii} & k_{ij} \\ k_{ji} & (k_{jj} + \bar{k}_{jj}) \end{bmatrix} - \lambda^2 \begin{bmatrix} m_{ii} & m_{ij} \\ m_{ji} & (m_{jj} + \bar{m}_{jj}) \end{bmatrix}\right] \begin{Bmatrix} x_i \\ x_j \end{Bmatrix} = \begin{Bmatrix} 0 \\ 0 \end{Bmatrix} \tag{8}$$

$\bar{k}_{jj}$ and $\bar{m}_{jj}$ are the interface "loading" matrices. The symbol Θ will be used for the modal matrix corresponding to equation (8).

Constraint Modes

To complement fixed-interface substructure normal modes a set of constraint modes may be employed (e.g., refs. 2,4). A constraint mode is defined by imposing a unit displacement on one physical coordinate and zero displacement on the remainder of a specified subset of the substructure physical coordinates. The procedure employed to obtain constraint modes is equivalent to applying a Guyan reduction to all interior coordinates; i.e., the mass is neglected in the top row-partition of equation (1) and unit displacements are imposed successively on all junction coordinates giving

$$[k_{ii} \quad k_{ij}] \begin{bmatrix} \Psi_{ij} \\ I_{jj} \end{bmatrix} = 0 \tag{9}$$

Thus, the N_j constraint modes which form the columns of the constraint mode matrix Ψ are obtained by solving the (multiple) static deflection problem

$$k_{ii} \Psi_{ij} = -k_{ij} \tag{10}$$

Then,

$$\Psi \equiv \begin{bmatrix} \Psi_{ij} \\ I_{jj} \end{bmatrix} \tag{11}$$

If the substructure is unrestrained, Ψ will contain N_r linearly independent rigid-body modes. As noted in reference 4, constraint modes and fixed-interface normal modes are orthogonal with respect to the stiffness matrix k.

Attachment Modes

Attachment modes are "static" modes which may be used to complement free-interface substructure normal modes (e.g., refs. 3,11,15,18). An attachment mode is defined by imposing a unit force on one physical coordinate and zero force on the remainder of a specified subset of substructure physical coordi-

nates. Attachment modes will be described first for restrained structures (for which k is non-singular) and then for unrestrained structures.

Attachment modes for restrained substructures.-Attachment modes for a restrained substructure are obtained by solving the multiple static deflection problem

$$\begin{bmatrix} k_{ii} & k_{ij} \\ k_{ji} & k_{jj} \end{bmatrix} \begin{bmatrix} \bar{X}_{ij} \\ \bar{X}_{jj} \end{bmatrix} = \begin{bmatrix} 0 \\ I_{jj} \end{bmatrix} \tag{12}$$

Then the attachment mode matrix is defined by

$$\bar{X} \equiv \begin{bmatrix} \bar{X}_{ij} \\ \bar{X}_{jj} \end{bmatrix} \tag{13}$$

Attachment modes can be expressed as linear combinations of free-interface normal modes. However, in a later section when the normal mode set is truncated, the attachment modes will be modified so that they are orthogonal to the kept normal modes. The modified attachment mode set will be called X.

Attachment modes for unrestrained substructures.-For an unrestrained substructure, attachment modes may be obtained by using rigid-body inertia forces to equilibrate applied forces and by temporarily imposing a set of N_r nonredundant constraints. Let Θ_r be the set of N_r (normalized) rigid-body modes of the substructure and let

$$R = I - m\Theta_r \Theta_r^T \tag{14}$$

be the inertia relief matrix (ref. 15). Then, the attachment modes may be obtained from

$$\begin{bmatrix} k_{rr} & k_{ru} & k_{rj} \\ k_{ur} & k_{uu} & k_{uj} \\ k_{jr} & k_{ju} & k_{jj} \end{bmatrix} \begin{bmatrix} 0 \\ \bar{X}_{uj} \\ \bar{X}_{jj} \end{bmatrix} = R \begin{bmatrix} 0 \\ 0 \\ I_{jj} \end{bmatrix} \equiv \begin{bmatrix} \bar{F}_{rj} \\ \bar{F}_{uj} \\ \bar{F}_{jj} \end{bmatrix} \tag{15}$$

where r stands for the N_r restrained interior coordinates and u stands for the $N_u = N_i - N_r$ unrestrained interior coordinates. From equation (15)

$$\begin{bmatrix} k_{uu} & k_{uj} \\ k_{ju} & k_{jj} \end{bmatrix} \begin{bmatrix} \bar{X}_{uj} \\ \bar{X}_{jj} \end{bmatrix} = \begin{bmatrix} \bar{F}_{uj} \\ \bar{F}_{jj} \end{bmatrix} \tag{16}$$

Finally,

$$\bar{X} \equiv \begin{bmatrix} 0 \\ \bar{X}_{uj} \\ \bar{X}_{jj} \end{bmatrix} \tag{17}$$

Rigid-body modes may be removed from the $\bar{X}$ matrix by premultiplying it by R^T.

Truncation of Mode Sets

One of the most significant features of substructure coupling techniques is that they permit the number of degrees of freedom of a system to be reduced in a systematic manner through truncation of the mode sets which define the generalized coordinates of the system. Hintz (ref. 15) has provided a comprehensive discussion of truncation of mode sets. Although truncation is usually accomplished by elimination of some coordinates associated with substructure normal modes (e.g., ref. 26), truncation may also be associated with other coordinates such as constraint mode coordinates (e.g., ref. 16). Attention will be confined here to the former, i.e., truncation of normal mode coordinates. The subscript k will be used to denote the columns of Φ or Θ which are kept. For example, the N_k modes which are kept form the columns of Θ_k, where

$$\Theta_k \equiv \begin{bmatrix} \Theta_{ik} \\ \Theta_{jk} \end{bmatrix} \tag{18}$$

The diagonal matrix of corresponding eigenvalues will be denoted by Λ_{kk}.

As noted previously, attachment modes can be expressed as linear combinations of the free-interface normal modes. However, when the normal mode set is truncated, the attachment modes can no longer be represented in terms of Θ_k. On the contrary, it is possible to modify the attachment modes so that they are orthogonal to the modes in Θ_k (e.g., see refs. 13,17). This will be illustrated here for attachment modes of a restrained substructure.

Note, in equation (12), that the columns of $\bar{X}$ correspond to columns of the flexibility matrix k^{-1}. The contribution of the kept normal modes to this flexibility matrix is given by (see ref. 17)

$$G_k = \Theta_k \Lambda_{kk}^{-1} \Theta_k^T \tag{19}$$

The contribution of the modes in Θ_k to $\bar{X}$ can be removed from $\bar{X}$ leaving

$$X = \bar{X} - \Theta_k \Lambda_{kk}^{-1} \Theta_{jk}^T \tag{20}$$

Energy Expressions for Substructures; Coordinate Transformation

The derivation of system equations of motion will be based on Lagrange's equations of motion with undetermined multipliers. Expressions for kinetic energy and strain energy of the substructures are required. These will be given first for substructure physical coordinates and then in terms of substructure generalized coordinates.

The kinetic energy and potential energy of a substructure are given by

$$T = \frac{1}{2} \dot{x}^T m \dot{x} \quad , \quad U = \frac{1}{2} x^T k x \tag{21}$$

respectively. The substructure physical coordinates, x, may be expressed in terms of substructure generalized coordinates, p, by the coordinate transformation

$$x = T_1 p \tag{22}$$

When the above coordinate transformation is inserted into equations (21), the substructure generalized mass and stiffness matrices are obtained. Thus,

$$T = \frac{1}{2} \dot{p}^T \mu \dot{p} \quad , \quad U = \frac{1}{2} p^T \kappa p \tag{23}$$

where

$$\mu = T_1^T m T_1 \quad , \quad \kappa = T_1^T k T_1 \tag{24}$$

Substructure Coupling; System Equations of Motion

To illustrate coupling of substructures to form a system, two substructures, α and β, will be employed. Let

$$p \equiv \begin{Bmatrix} p^\alpha \\ p^\beta \end{Bmatrix} , \quad \mu \equiv \begin{bmatrix} \mu^\alpha & 0 \\ 0 & \mu^\beta \end{bmatrix} , \quad \kappa \equiv \begin{bmatrix} \kappa^\alpha & 0 \\ 0 & \kappa^\beta \end{bmatrix} \tag{25}$$

The substructure generalized coordinates are not all independent but are related by force equilibrium and displacement compatibility at substructure interfaces. These relationships may be expressed by the equations

$$A p = 0 \quad , \quad B p = 0$$

respectively. Then, a Lagrangian may be formed as follows:

$$L = \frac{1}{2}\dot{p}^T \mu \dot{p} - \frac{1}{2} p^T \kappa p + \eta^T A p + \nu^T B p \tag{26}$$

The system equations may be obtained by applying Lagrange's equation in the form

$$\frac{d}{dt}\left(\frac{\partial L}{\partial \xi_n}\right) - \frac{\partial L}{\partial \xi_n} = 0 \tag{27}$$

where ξ_n can refer to p_n, η_n or ν_n. Then equations (26) and (27) may be combined to give

$$\mu \ddot{p} + \kappa p = A^T \eta + B^T \nu \tag{28}$$

together with the constraint equations

$$A p = 0 \quad , \quad B p = 0 \tag{29}$$

In the works cited previously, two basic approaches have been employed for solving the coupled equations contained in equations (28) and (29). Both lead to system equations of the form

$$M \ddot{q} + K q = 0 \tag{30}$$

The method used by most authors will be referred to as the implicit method. It involves the use of a coordinate transformation T_2 to replace the set of dependent coordinates, p, by a set of linearly independent coordinates q. Thus,

$$p = T_2 q \tag{31}$$

Let p be partitioned into dependent coordinates, p_d, and linearly independent coordinates, p_ℓ, as follows:

$$p \equiv \begin{Bmatrix} p_d \\ p_\ell \end{Bmatrix} \tag{32}$$

and let the constraint matrices A and B be combined to form the matrix C, i.e.,

$$C p \equiv \begin{bmatrix} A \\ B \end{bmatrix} p = 0 \tag{33}$$

Since C will have fewer rows than columns, equations (32) and (33) may be combined and written in the form

$$[C_{dd} \; C_{d\ell}] \begin{bmatrix} p_d \\ p_\ell \end{bmatrix} = 0 \tag{34}$$

where C_{dd} is a non-singular square submatrix of C. Then

$$\begin{Bmatrix} p_d \\ p_\ell \end{Bmatrix} = \begin{bmatrix} -C_{dd}^{-1} C_{d\ell} \\ I_{\ell\ell} \end{bmatrix} p_\ell \tag{35}$$

Let $q \equiv p_\ell$. Then equations (31) and (35) give

$$T_2 \equiv \begin{bmatrix} -C_{dd}^{-1} C_{d\ell} \\ I_{\ell\ell} \end{bmatrix} \tag{36}$$

as the general expression for transformation matrix T_2. The matrices M and K in equation (30) are given by

$$M = T_2^T \mu T_2 \quad , \quad K = T_2^T \kappa T_2 \tag{37}$$

Goldman (ref. 7) solved equations (28) and (29) by an approach which will be referred to as the explicit method. Let

$$\sigma \equiv \begin{Bmatrix} \eta \\ \nu \end{Bmatrix} \tag{38}$$

Then equation (28) may be written

$$\mu \ddot{p} + \kappa p = C^T \sigma \tag{39}$$

σ may be related to p by multiplying equation (39) by $C \mu^{-1}$ and incorporating equation (33). Then equation (39) may be written in the form

$$\mu \ddot{p} + [I - C^T (C \mu^{-1} C^T)^{-1} C \mu^{-1}] \kappa p = 0 \tag{40}$$

Goldman's final system equations are obtained by letting

$$p = \kappa^{-1/2} q \tag{41}$$

Then equation (40) can be reduced to the form of equation (30) with

$$M = I \ , \ K = \kappa^{1/2} \mu^{-1} [I - C^T (C \mu^{-1} C^T)^{-1} C \mu^{-1}] \kappa^{1/2} \tag{42}$$

Since equation (41) implies no reduction in number of coordinates, equation (30) leads to some extraneous frequencies and modes in the Goldman method.

Description of Various Coupling Methods

Table I shows the constituent vectors and matrices (i.e., T_1, p, T_2, etc.) of a representative selection of the substructure coupling methods named earlier in the historical review. In all cases the methods fit into the general formulation just described. However, in a few cases the notation has been simplified by employing a partitioning of C (or B) different from that indicated in equations (34) and (36).

CONVERGENCE PROPERTIES

Desirable characteristics for substructure coupling methods include (e.g., see refs. 13,15): computational efficiency, interchangeability, component flexibility, synthesis flexibility, static completeness, and test compatibility. Although it is not within the scope of this paper to make a detailed comparison of coupling techniques on the basis of the above criteria, a few results concerning computational efficiency, i.e., convergence, will be presented. Several authors have previously discussed convergence of system frequencies (e.g., refs. 13,16,26,27). Rubin (ref. 13) also considered convergence of mode shapes and shear and moment in beam elements.

Figure 1 shows frequency and RMS bending moment convergence properties of mode 3 of a clamped-clamped uniform beam.

CONCLUDING REMARKS

A general formulation has been presented which permits substructure coupling methods to be defined in terms of a few constituent matrices. Although a detailed comparison of various substructure coupling methods has not been within the scope of this paper, it is hoped that the presentation of this general formulation will facilitate future studies of substructure coupling methods. At the present time the use of substructure coupling as an analysis tool seems to be a well-developed subject. On the contrary, much remains to be learned about effective ways to use substructure coupling in conjunction with experimental studies. It is hoped that this topic will receive increased attention in the future.

REFERENCES

1. Hurty, W.C.: Vibrations of Structural Systems by Component Mode Synthesis. Proc. ASCE, vol. 85, no. EM4, Aug. 1960, pp. 51-69.

2. Hurty, W.C.: Dynamic Analysis of Structural Systems Using Component Modes. AIAA Journal, vol. 3, no. 4, Apr. 1965, pp. 678-685.

3. Bamford, R.M.: A Modal Combination Program for Dynamic Analysis of Structures. Tech. Memo. 33-290, Jet Propulsion Laboratory, Pasadena, CA, July 1967.

4. Craig, R.R., Jr.and Bampton, M.C.C.: Coupling of Substructures for Dynamic Analyses. AIAA Journal, vol. 6, no. 7, July 1968, pp. 1313-1319.

5. Bajan, R.L. and Feng, C.C.: Free Vibration Analysis by the Modal Substitution Method. American Astronautical Society Paper No. 68-8-1, AAS Symposium on Space Projections from the Rocky Mountain Region, Denver, CO, July 1968.

6. Bajan, R.L.; Feng, C.C.; and Jaszlics, I.J.: Vibration Analysis of Complex Structural Systems by Modal Substitution. Proc. 39th Shock and Vibration Symposium, Monterey, CA, Oct. 1968.

7. Goldman, R.L.: Vibration Analysis by Dynamic Partitioning. AIAA Journal, vol. 7, no. 6, June 1969, pp. 1152-1154.

8. Hou, S.: Review of Modal Synthesis Techniques and a New Approach. The Shock and Vibration Bulletin, no. 40, pt. 4, Naval Research Laboratory, Washington, D.C., Dec. 1969, pp. 25-39.

9. Benfield, W.A. and Hruda, R.F.: Vibration Analysis of Structures by Component Mode Substitution. AIAA Journal, vol. 9, no. 7, July 1971, pp. 1255-1261.

10. Guyan, R.J.: Reduction of Stiffness and Mass Matrices. AIAA Journal, vol. 3, no. 2, Feb. 1965, p. 380.

11. MacNeal, R.H.: A Hybrid Method of Component Mode Synthesis. J. of Computers and Structures, vol. 1, no. 4, Dec. 1971, pp. 581-601.

12. Goldenberg, S. and Shapiro, M.: A Study of Modal Coupling Procedures. (Grumman Aerospace Corp.; NASA Contract No. NAS-10635-8.) NASA CR-112252, 1972.

13. Rubin, S.: An Improved Component-Mode Representation. AIAA Paper No. 74-386, AIAA/ASME/SAE 15th Structures, Structural Dynamics and Materials Conference, Las Vegas, Nevada, April 1974.

14. Kuhar, E.J. and Stahle, C.V.: A Dynamic Transformation Method for Modal Synthesis. AIAA Journal, vol. 12, no. 5, May 1974, pp. 672-678.

15. Hintz, R.M.: Analytical Methods in Component Modal Synthesis. AIAA Journal, vol. 13, no. 8, Aug. 1975, pp. 1007-1016.

16. Craig, R.R., Jr. and Chang, C-J.: Substructure Coupling with Reduction of Interface Coordinates--Fixed-Interface Methods. TICOM Rept. No. 75-1, The University of Texas at Austin, Austin, TX, Jan. 1975.

17. Craig, R.R., Jr. and Chang, C-J.: Free-Interface Methods of Substructure Coupling for Dynamic Analysis. AIAA Journal (accepted for publication).

18. Klosterman, A.L.: On the Experimental Determination and Use of Modal Representations of Dynamic Characteristics. Ph.D. dissertation, University of Cincinnati, 1971.

19. Klosterman, A.L.: A Combined Experimental and Analytical Procedure for Improving Automotive System Dynamics. Paper No. 720093, Society of Automotive Engineers, Automotive Engineering Congress, Detroit, MI, Jan. 1972.

20. Klosterman, A.L. and McClelland, W.A.: Combining Experimental and Analytical Techniques for Dynamic System Analysis. presented at 1973 Tokyo Seminar on Finite Element Analysis, Nov. 1973.

21. Kana, D.D. and Huzar, S.: Synthesis of Shuttle Vehicle Damping Using Substructure Test Results. Interim Report for NASA Contract No. NAS8-27569, Southwest Research Institute, San Antonio, TX, June 1972.

22. Kana, D.D. and Huzar, S.: Synthesis of Shuttle Vehicle Damping Using Substructure Test Results. J. Spacecraft and Rockets, vol. 10, no. 12, Dec. 1973, pp. 790-797.

23. Hasselman, T.K.: Damping Synthesis from Substructure Tests. AIAA Paper No. 74-387, presented at AIAA/ASME/SAE 15th Structures, Structural Dynamics and Materials Conference, Las Vegas, NV, Apr. 1974.

24. Neubert, V.H. and Raney, J.P., eds.: Synthesis of Vibrating Systems. The American Society of Mechanical Engineers, Nov. 1971.

25. Ryan, R.S., ed.: Symposium on Substructure Testing and Synthesis. NASA Marshall Space Flight Center, Aug. 1972.

26. Hurty, W.C.: Introduction to Modal Synthesis Techniques. Synthesis of Vibrating Systems, ASME, Nov. 1971.

27. Benfield, W.A.; Bodley, C.S.; and Morosow, G.: Modal Synthesis Methods. Symposium on Substructure Testing and Synthesis, NASA, Aug. 1972.

TABLE I.-VECTORS AND MATRICES DEFINING SUBSTRUCTURE COUPLING METHODS

Matrix, etc. \ Method (Type)	Goldman (Free-interface, Explicit)	Hou (Free-interface, Implicit)	Goldenberg & Shapiro (Loaded-interface, Implicit)	Craig & Bampton Bajan & Feng* (Fixed-interface, Implicit)	Benfield & Hruda** (Free-interface, Implicit)	Hintz† (Free-interface, Implicit)	Craig & Chang†† (Free-interface, Implicit)
T_1^α	$\begin{bmatrix} \Theta_{ik}^\alpha \\ \Theta_{jk}^\alpha \end{bmatrix}$	$\begin{bmatrix} \Theta_{ik}^\alpha \\ \Theta_{jk}^\alpha \end{bmatrix} \equiv \begin{bmatrix} \Theta_{id}^\alpha & \Theta_{i\ell}^\alpha \\ \Theta_{jd}^\alpha & \Theta_{j\ell}^\alpha \end{bmatrix}$	$\begin{bmatrix} \Theta_{ik}^\alpha \\ \Theta_{jk}^\alpha \end{bmatrix} \equiv \begin{bmatrix} \Theta_{id}^\alpha & \Theta_{i\ell}^\alpha \\ \Theta_{jd}^\alpha & \Theta_{j\ell}^\alpha \end{bmatrix}$	$\begin{bmatrix} \psi_{ij}^\alpha & \phi_{ik}^\alpha \\ I_{jj}^\alpha & 0 \end{bmatrix}$	$\begin{bmatrix} \Theta_{ik}^\alpha \\ \Theta_{jk}^\alpha \end{bmatrix}$	$\begin{bmatrix} X_{ij}^\alpha & \Theta_{ik}^\alpha \\ X_{jj}^\alpha & \Theta_{jk}^\alpha \end{bmatrix}$	$\begin{bmatrix} X_{ij}^\alpha & \Theta_{ik}^\alpha \\ X_{jj}^\alpha & \Theta_{jk}^\alpha \end{bmatrix}$
T_1^β	$\begin{bmatrix} \Theta_{ik}^\beta \\ \Theta_{jk}^\beta \end{bmatrix}$	$\begin{bmatrix} \Theta_{ik}^\beta \\ \Theta_{jk}^\beta \end{bmatrix}$	$\begin{bmatrix} \Theta_{ik}^\beta \\ \Theta_{jk}^\beta \end{bmatrix} \equiv \begin{bmatrix} \Theta_{id}^\beta & \Theta_{i\ell}^\beta \\ \Theta_{jd}^\beta & \Theta_{j\ell}^\beta \end{bmatrix}$	$\begin{bmatrix} \psi_{ij}^\beta & \phi_{ik}^\beta \\ I_{jj}^\beta & 0 \end{bmatrix}$	$\begin{bmatrix} 0 & \Theta_{ik}^\beta \\ I_{jj}^\beta & 0 \end{bmatrix}$	$\begin{bmatrix} X_{ij}^\beta & \Theta_{ik}^\beta \\ X_{jj}^\beta & \Theta_{jk}^\beta \end{bmatrix}$	$\begin{bmatrix} X_{ij}^\beta & \Theta_{ik}^\beta \\ X_{jj}^\beta & \Theta_{jk}^\beta \end{bmatrix}$
p	$\begin{Bmatrix} p_k^\alpha \\ p_k^\beta \end{Bmatrix}$	$\begin{Bmatrix} p_d^\alpha \\ p_\ell^\alpha \\ p_k^\beta \end{Bmatrix}$	$\begin{Bmatrix} p_d \\ p_\ell \end{Bmatrix} \equiv \begin{Bmatrix} p_d^\alpha \\ p_d^\beta \\ p_\ell^\alpha \\ p_\ell^\beta \end{Bmatrix}$	$\begin{Bmatrix} x_j^\alpha \\ p_k^\alpha \\ x_j^\beta \\ p_k^\beta \end{Bmatrix}$	$\begin{Bmatrix} p_k^\alpha \\ x_j^\beta \\ p_k^\beta \end{Bmatrix}$	$\begin{Bmatrix} p_j^\alpha \\ p_k^\alpha \\ p_j^\beta \\ p_k^\beta \end{Bmatrix}$	$\begin{Bmatrix} f_j^\alpha \\ p_k^\alpha \\ f_j^\beta \\ p_k^\beta \end{Bmatrix}$
A	not applicable	not applicable	not applicable	not applicable	not applicable	not applicable	$\begin{bmatrix} I_{jj}^\alpha & 0 & I_{jj}^\beta & 0 \end{bmatrix}$
B	$\begin{bmatrix} \Theta_{jk}^\alpha & -\Theta_{jk}^\beta \end{bmatrix}$	$\begin{bmatrix} \Theta_{jd}^\alpha & \Theta_{j\ell}^\alpha & -\Theta_{jk}^\beta \end{bmatrix}$	$\begin{bmatrix} \Theta_{jd} & \Theta_{j\ell} \end{bmatrix} \equiv \begin{bmatrix} \Theta_{jd}^\alpha & -\Theta_{jd}^\beta & \Theta_{j\ell}^\alpha & -\Theta_{j\ell}^\beta \end{bmatrix}$	$\begin{bmatrix} I_{jj}^\alpha & 0 & -I_{jj}^\beta & 0 \end{bmatrix}$	$\begin{bmatrix} \Theta_{jk}^\alpha & -I_{jj}^\beta & 0 \end{bmatrix}$	$\begin{bmatrix} X_{jj}^\alpha & \Theta_{jk}^\alpha & -X_{jj}^\beta & -\Theta_{jk}^\beta \end{bmatrix}$	$\begin{bmatrix} X_{jj}^\alpha & \Theta_{jk}^\alpha & -X_{jj}^\beta & -\Theta_{jk}^\beta \end{bmatrix}$
T_2	$\kappa^{-1/2}$	$\begin{bmatrix} -[\Theta_{jd}^\alpha]^{-1}\Theta_{j\ell}^\alpha & [\Theta_{jd}^\alpha]^{-1}\Theta_{jk}^\beta \\ I_{\ell\ell}^\alpha & 0 \\ 0 & I_{kk}^\beta \end{bmatrix}$	$\begin{bmatrix} -\Theta_{jd}^{-1}\Theta_{j\ell} \\ I_{\ell\ell} \end{bmatrix}$	$\begin{bmatrix} 0 & 0 & I_{jj}^\alpha \\ I_{kk}^\alpha & 0 & 0 \\ 0 & 0 & I_{jj}^\beta \\ 0 & I_{kk}^\beta & 0 \end{bmatrix}$	$\begin{bmatrix} I_{kk}^\alpha & 0 \\ \Theta_{jk}^\alpha & 0 \\ 0 & I_{kk}^\beta \end{bmatrix}$	$\begin{bmatrix} 0 & 0 & I_{jj}^\alpha \\ I_{kk}^\alpha & 0 & 0 \\ [X_{jj}^\beta]^{-1}\Theta_{jk}^\alpha & -[X_{jj}^\beta]^{-1}\Theta_{jk}^\beta & [X_{jj}^\beta]^{-1}X_{jj}^\alpha \\ 0 & I_{kk}^\beta & 0 \end{bmatrix}$	$\begin{bmatrix} -[X_{jj}^\alpha+X_{jj}^\beta]^{-1}\Theta_{jk}^\alpha & [X_{jj}^\alpha+X_{jj}^\beta]^{-1}\Theta_{jk}^\beta \\ I_{kk}^\alpha & 0 \\ [X_{jj}^\alpha+X_{jj}^\beta]^{-1}\Theta_{jk}^\alpha & -[X_{jj}^\alpha+X_{jj}^\beta]^{-1}\Theta_{jk}^\beta \\ 0 & I_{kk}^\beta \end{bmatrix}$
q	$\begin{Bmatrix} q_k^\alpha \\ q_k^\beta \end{Bmatrix}$	$\begin{Bmatrix} q_\ell^\alpha \\ q_k^\beta \end{Bmatrix} \equiv \begin{Bmatrix} p_\ell^\alpha \\ p_k^\beta \end{Bmatrix}$	$\{q_\ell\} \equiv \{p_\ell\}$	$\begin{Bmatrix} q_k^\alpha \\ q_k^\beta \\ q_j \end{Bmatrix} \equiv \begin{Bmatrix} p_k^\alpha \\ p_k^\beta \\ x_j^\alpha \end{Bmatrix}$	$\begin{Bmatrix} q_k^\alpha \\ q_k^\beta \end{Bmatrix} \equiv \begin{Bmatrix} p_k^\alpha \\ p_k^\beta \end{Bmatrix}$	$\begin{Bmatrix} q_k^\alpha \\ q_k^\beta \\ q_j \end{Bmatrix} \equiv \begin{Bmatrix} p_k^\alpha \\ p_k^\beta \\ p_j^\alpha \end{Bmatrix}$	$\begin{Bmatrix} q_k^\alpha \\ q_k^\beta \end{Bmatrix} \equiv \begin{Bmatrix} p_k^\alpha \\ p_k^\beta \end{Bmatrix}$
N_t = total d.o.f.	$N_k^\alpha + N_k^\beta$	$N_k^\alpha + N_k^\beta - N_j$	$N_k^\alpha + N_k^\beta - N_j$	$N_k^\alpha + N_k^\beta + N_j$	$N_k^\alpha + N_k^\beta$	$N_k^\alpha + N_k^\beta + N_j$	$N_k^\alpha + N_k^\beta$

*Hurty's method is equivalent to this method.
**The other methods of Benfield & Hruda may be similarly described.
†The other methods of Hintz may be similarly described.

††A complete description of this method, together with its relationship to the methods of MacNeal and Rubin, is the subject of a forthcoming paper.

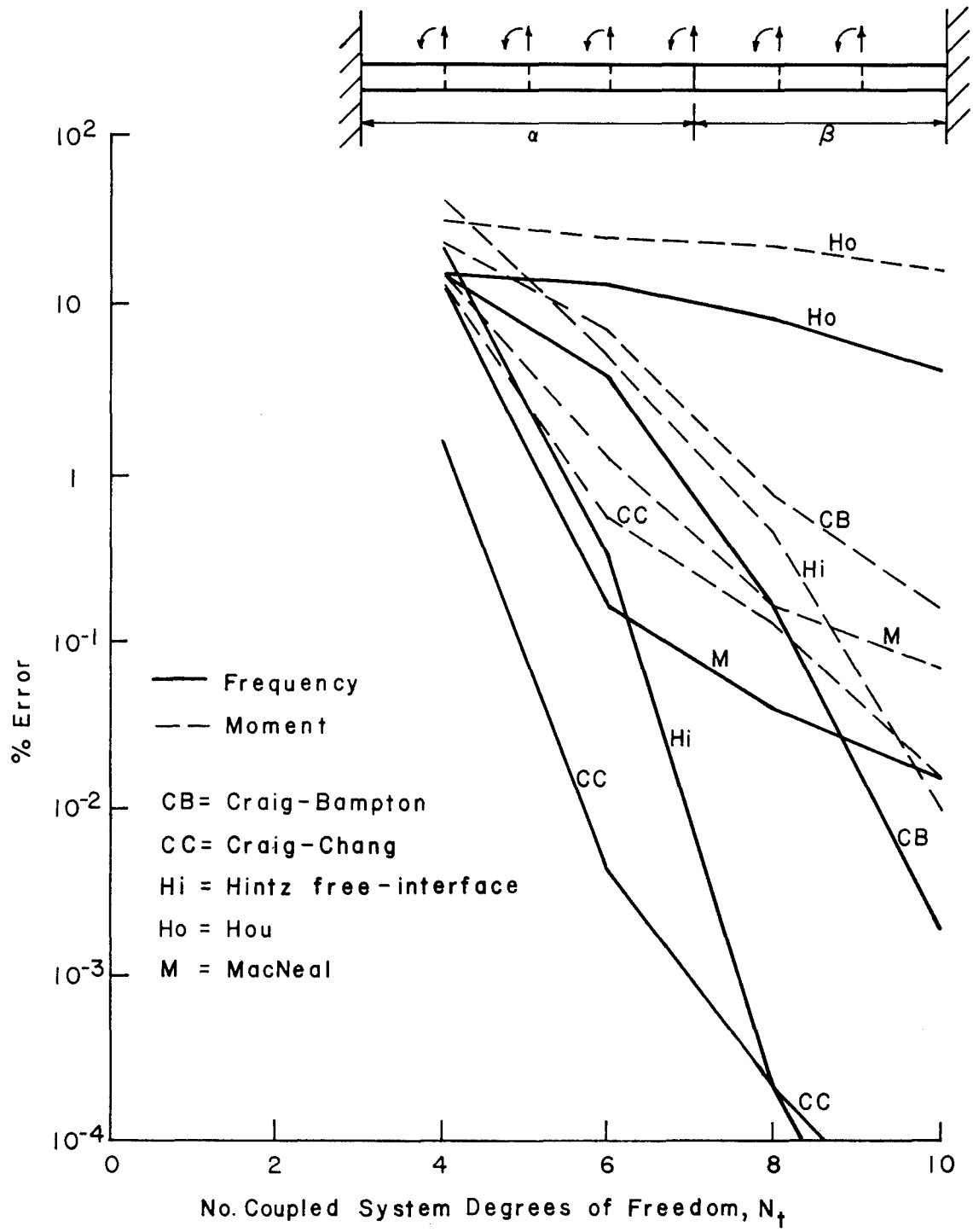

Figure 1.-Frequency and RMS Moment Convergence for Mode 3 of Clamped-Clamped Beam.

CORIOLIS EFFECTS ON NONLINEAR OSCILLATIONS OF ROTATING CYLINDERS AND RINGS

Joseph Padovan
University of Akron

SUMMARY

The effects which moderately large deflections have on the frequency spectrum of rotating rings and cylinders are considered. To develop the requisite solution, a variationally constrained version of the Lindstedt-Poincare procedure is employed. Based on the solution developed, in addition to considering the effects of displacement induced nonlinearity, the role of Coriolis forces is also given special consideration.

INTRODUCTION

Numerous engineering applications (tires, turbines, satellites, etc.) contain rotor systems which are essentially rings or shells of revolution rotating about their axes. Obviously, in order to properly influence their design, a thorough dynamic analysis is necessary. In this regard, numerous papers have been published which deal with the free vibration properties of such systems. Most such work has centered on stationary configurations, as can be seen from the excellent surveys by references 1 and 2. The effects of rotation, in particular Coriolis forces, have been discussed by references 3 to 7. With the exception of references 6 and 7 which treated small dynamic deformations superposed on large static deformations, the previous investigations incorporating Coriolis acceleration forces have been limited to linear shell theories. This is a shortcoming since numerous rotor systems, tires, satellites, and turbines are flexible enough to undergo significant deflections in the form of moderately large rotations.

It is the purpose of this paper to consider the effects which such moderately large rotations have on the frequency spectrum of rotating structures. In particular, the analysis presented will consider the free vibration characteristics of rotating rings and cylinders wherein the deflections involve moderately large rotations. Since the analytical model used to characterize the stated problem involves nonlinear partial differential equations, a modified version of the renormalized perturbation procedure is employed to evaluate the overall solution. This modification was undertaken since the usual renormalized procedure is unwieldy for systems of equations involving a multitude of frequency eigenvalue branches and secondly yields steady state results which are irregular for the linearized case. The modification employed involves prescribing the system energy in advance; hence, a hierarchy of energy states is obtained from which the strained parameter can be evaluated. The resulting solution employing this procedure is regular, and thus, the proper limiting behavior is obtained for the linearized

case. Based on the solution, in addition to considering the global effects of nonlinearity, special emphasis is centered on determining the effects of Coriolis forces in the range of deformations marked by moderately large rotations. Hence the effects on the backward and forward traveling waves will be evaluated.

GOVERNING EQUATIONS

Since the nonlinear oscillations of rotating, elastically supported rings and infinite cylinders undergoing deflections involving moderately large rotations are considered herein, the governing displacement equations of motion employed to model the stated problem are defined by (refs. 2,4,6, and 7)

$$A_1 W,_{\theta\theta\theta\theta}+A_2(V,_\theta+W)+(\kappa+\frac{P}{R})W-\varepsilon A_2(\frac{1}{2}W,_\theta^2+V,_{\theta\theta}W,_\theta+V,_\theta W,_{\theta\theta}+WW,_{\theta\theta}) -$$

$$\frac{3}{2}\varepsilon^2 A_2 W,_\theta^2 W,_{\theta\theta}+f\cos(m\theta)\cos(\omega t)+\rho h(W,_{tt}-2\Omega V,_t-\Omega^2 W) = 0 \qquad (1)$$

$$A_2(V,_{\theta\theta}+W,_\theta+\varepsilon W,_\theta W,_{\theta\theta})-\rho h(V,_{tt}+2\Omega W,_t-\Omega^2 V) = 0 \qquad (2)$$

where

$$A_1 = \frac{EI}{R^4} \quad , \quad A_2 = \frac{Eh}{R^2} \qquad (3)$$

such that $\varepsilon = W_m/R$ and θ, t, $(\ )_{,\theta}$, $(\ )_{,t}$, W, V, W_m, E, I, h, R, ρ, P, κ, ω, and Ω respectively represent circumferential space, time, space and time differentiation, radial and circumferential shell displacements, maximum radial displacement, Young's modulus, moment of inertia, shell thickness, radius and density, internal pressure, foundation elasticity, exciting frequency, and lastly, the rotational speed of the shell. Due to the inherent nature of the circumferential coordinate space and the fact that the steady state response is being sought, it follows that W and V are periodic in both space and time. To round out the requisite field equations, the following potential energy functional is associated with equations (1) and (2), namely

$$\gamma = \int_0^T \int_0^{2\pi} \{A_1 W,_{\theta\theta}^2+A_2(V,_\theta^2+2V,_\theta W+W^2)+\varepsilon A_2(V,_\theta W,_\theta^2+WW,_\theta^2) +$$

$$\frac{1}{4}\varepsilon^2 A_2 W,_\theta^4+(\kappa+\frac{P}{R})W^2+2f\cos(m\theta)\cos(\omega t)W-\rho h[\Omega^2(R^*+W)^2+W,_t^2 +$$

$$\Omega^2 V^2+V,_t^2+2\Omega(R^*+W)V,_t-2\Omega W,_t V]\}d\theta dt \qquad (4)$$

where $T = \frac{1}{2\pi\omega}$ and $R^* = R/W_m$.

SOLUTION

As noted earlier, the standard renormalized perturbation procedure has the twofold difficulty of yielding irregular results as $\varepsilon \to 0$ and secondly, is unwieldy when more than one equation of motion involving several frequency eigenvalue branches is considered. This difficulty is circumvented by prescribing the systems potential energy in advance such that $(W; V) = (W(\theta,t,f,m,\gamma); V(\theta,t,f,m,\gamma))$. Once the solution is obtained, the role of γ and W are reversed to that employed in the traditional version of the renormalized procedure. To initiate the solution, ω is treated as the strained parameter; hence W, V, and ω are expanded in the following perturbation series

$$\langle W; V; \omega \rangle = \sum_{i=0}^{\infty} \langle W_i; V_i; \omega_i \rangle \varepsilon^i \tag{5}$$

such that time is stretched so that $\tau = \omega t$.

In order to obtain the zeroth order equations, ε is set to zero; this yields

$$A_1 W_{o,\theta\theta\theta\theta} + (A_2 + \kappa + \frac{P}{R}) W_o + A_2 V_{o,\theta} + \rho h(\omega_o^2 W_{o,tt} -$$

$$2\omega_o \Omega V_{o,\tau} - \Omega^2 W_o) + f \cos(m\theta) \cos(\tau) = 0 \tag{6}$$

$$A_2 (V_{o,\theta\theta} + W_{o,\theta}) = \rho h(\omega_o^2 V_{o,\tau\tau} + 2\omega_o \Omega W_{o,\tau} - \Omega^2 V_o) \tag{7}$$

$$\Gamma = \int_0^{2\pi} \int_0^{2\pi} \{A_1 W_{o,\theta\theta}^2 + A_2 (V_{o,\theta}^2 + 2V_{o,\theta} W_o + W_o^2) + (\kappa + \frac{P}{R}) W_o^2 +$$

$$2f \cos(m\theta) \cos(\tau) W_o - \rho h[\Omega^2 (R^* + W_o)^2 + \omega_o^2 W_{o,\tau}^2 + \Omega^2 V_o^2 + \omega_o^2 V_{o,\tau}^2 +$$

$$2\omega_o \Omega (R^* + W_o) V_{o,\tau} - 2\omega_o \Omega W_{o,\tau} V_o]\} d\theta d\tau \tag{8}$$

whereas with time, the potential energy space is stretched so that $\Gamma = \gamma/\Omega$. Since the steady state solution is sought,

$$(W_o; V_o) = (W_{co}; V_{co}) \cos(m\theta) + (W_{so}; V_{so}) \sin(m\theta) \tag{9}$$

where $W_{co}, \ldots$ are time dependent. Employing equations (9), (6), and (7) reduce to the following matrix set of ordinary differential equations, namely

$$\omega_o^2 [B_{1m}] \underset{\sim}{Y}_{mo,\tau\tau} + \omega_o [B_{2m}] \underset{\sim}{Y}_{mo,\tau} + [B_{3m}] \underset{\sim}{Y}_{mo} + f \underset{\sim}{\cos}(\tau) = \underset{\sim}{0} \tag{10}$$

such that

$$\underset{\sim}{Y}_{mo} = (W_{co}, V_{so}, W_{so}, V_{co})^T \tag{11}$$

Noting that $[B_{2m}]$ is skew symmetric while $[B_{1m}]$ and $[B_{3m}]$ are purely symmetric, the steady state form of $\underset{\sim}{Y}_{mo}$ is given by

$$\underset{\sim}{Y}_{mo} = \underset{\sim}{Z}_{mc} \cos(\tau) + \underset{\sim}{Z}_{ms} \sin(\tau) \tag{12}$$

where $\underset{\sim}{Z}_{mc}$ and $\underset{\sim}{Z}_{ms}$ satisfy the matrix equation

$$\begin{Bmatrix} f \\ \sim \\ 0 \\ \sim \end{Bmatrix} = \begin{bmatrix} \omega_o^2[B_{1m}]-[B_{3m}] & \omega_o[B_{2m}] \\ \omega_o[B_{2m}] & \omega_o[B_{1m}]-[B_{3m}] \end{bmatrix} \begin{Bmatrix} \underset{\sim}{Z}_{mc} \\ \underset{\sim}{Z}_{ms} \end{Bmatrix} \tag{13}$$

Noting that the pencil of equation (13) yields the characteristic equation of equation (10), equation (12) becomes unbounded for ω_o equal to the natural frequency eigenvalues of the linear case. The properties of such eigenvalues can be ascertained by developing the appropriate Rayleigh quotient. This is possible by inserting $\gamma_m \alpha \underset{\sim}{Z}_m e^{j\tau}$ into equation (10) to yield a complex second order regular polynomial matrix problem. The inner product of this expression and $\underset{\sim}{Z}_m$ yields a bilinear form from which the following modified version of Rayleigh's quotient is obtained, namely

$$\omega_o = j \frac{\bar{\underset{\sim}{Z}}_m^T[B_{2m}]\underset{\sim}{Z}_m}{2\rho h \bar{\underset{\sim}{Z}}_m^T \underset{\sim}{Z}_m} + \left[\frac{\bar{\underset{\sim}{Z}}_m^T[B_{3m}]\underset{\sim}{Z}_m}{\rho h \bar{\underset{\sim}{Z}}_m^T \underset{\sim}{Z}_m} - \left(\frac{\bar{\underset{\sim}{Z}}_m^T[B_{2m}]\underset{\sim}{Z}_m}{4\rho h \bar{\underset{\sim}{Z}}_m^T \underset{\sim}{Z}_m} \right)^2 \right]^{1/2} \tag{14}$$

As can be seen from equation (14), Coriolis forces cause a twofold bifurcation in the number of eigenvalue branches. Following the previous comments, the relationship between Γ and ω_o, W_o, and V_o must be evaluated by inserting equations (9) and (12) into equation (8); this yields

$$\begin{aligned} &[A_1 m^4 + A_2 + \kappa + \frac{P}{R} - \rho h(\Omega^2 + \omega_o^2 m^2)](W_{cco}^2 + W_{cso}^2 + W_{sco}^2 + W_{sso}^2) + \\ &[A_2 m^2 - \rho h(\Omega^2 + m^2\omega_o^2)](V_{cco}^2 + V_{cso}^2 + V_{sco}^2 + V_{sso}^2) + 2mA_2(V_{sco}W_{cco} + \\ &V_{sso}W_{cso} - V_{cco}W_{sco} - V_{cso}W_{sso}) - 2\rho h\omega_o \Omega m(W_{cco}V_{cso} - W_{cso}V_{cco} + \\ &W_{sco}V_{sso} - W_{sso}V_{sco} - V_{cco}W_{cso} + V_{cso}W_{cco} - V_{sco}W_{sso} + \\ &V_{sso}W_{sco})] = \Gamma/\pi^2 \end{aligned} \tag{15}$$

where $W_{cco}, \ldots, V_{sso}$ denote coefficients of the W_o and V_o solution, namely

$$(W_o;V_o) = (W_{cco};V_{cco})\cos(m\theta)\cos(\tau)+\ldots+(W_{sso};V_{sso})\sin(m\theta)\sin(\tau)$$

As can be seen from equations (13) and (15), four potential energy resonances are initiated for $\omega_o \sim O(\omega_{mf})$ wherein ω_{mf} are the frequency eigenvalues of the linear problem. Hence equation (5) is regular for $\varepsilon \to 0$ (the linear case).

The first order set of field equations can be obtained by taking the first derivative of equations (1), (2), and (4) with respect to ε and then setting ε to zero. This yields

$$A_1 W_{1,\theta\theta\theta\theta}+A_2(V_{1,\theta}+W_1)+(\kappa+\frac{P}{R})W_1+\rho h(\omega_o^2 W_{1,\tau\tau}-2\Omega\omega_o V_{1,\tau}-\Omega^2 W_1) =$$

$$A_2(\frac{1}{2}W_{o,\theta}^2-V_{o,\theta\theta}W_{o,\theta}+V_{o,\theta}W_{o,\theta\theta}+W_o W_{o,\theta\theta}) - 2\rho h(\omega_1\omega_o W_{o,\tau\tau}-\Omega\omega_1 V_{o,\tau}) \quad (16)$$

$$A_2(V_{1,\theta\theta}+W_{1,\theta})-\rho h(\omega_o^2 V_{1,\theta\theta}+2\Omega\omega_o W_{1,\tau}-\Omega^2 V_1) =$$

$$-A_2 W_{o,\theta}W_{o,\theta\theta}+2\rho h(\omega_1\omega_o V_{o,\tau\tau}+\Omega\omega_1 W_{o,\tau}) \quad (17)$$

$$\int_0^{2\pi}\int_0^{2\pi}\{2A_1 W_{o,\theta\theta}W_{1,\theta\theta}+2A_2(V_{o,\theta}+W_o)(V_{1,\theta}+W_1)+A_2(V_{o,\theta}+W_o)W_{o,\theta}^2+$$

$$2(\kappa+\frac{P}{R})W_o W_1+2f\cos(m\theta)\cos(\tau)W_1-2\rho h[\Omega^2(R^*+W_o)W_1+$$

$$\omega_o\omega_1 W_{o,\tau}^2+\omega_o^2 W_{o,\tau}W_{1,\tau}+\Omega^2 V_o V_1+\omega_o\omega_1 V_{o,\tau}^2 +$$

$$\omega_o^2 V_{o,\tau}V_{1,\tau}+\Omega\omega_1 R^* V_{o,\tau}+\Omega\omega_o R^* V_{1,\tau}+\Omega\omega_o W_1 V_{o,\tau} +$$

$$\Omega\omega_o W_o V_{1,\tau}+\Omega\omega_1 W_o V_{o,\tau}-\Omega\omega_o W_{1,\tau}V_o-\Omega\omega_o W_{1,\tau}V_1-$$

$$\Omega\omega_1 W_{1,\tau}V_o]\}d\theta d\tau = 0 \quad (18)$$

Noting the form of the inhomogeneities appearing in equations (16) and (17), it follows that W_1 and V_1 can be taken in the form

$$(W_1;V_1) = (W_{c1};V_{c1})\cos(2\tau)+(W_{s1};V_{s1})\sin(2\tau)+$$

$$\ldots+(W_{ss1};V_{ss1})\sin(m\theta)\sin(\tau) \quad (19)$$

where the coefficients $W_{c1},\ldots$ are directly obtained upon inserting equation (19) into equations (16) and (17). Furthermore, employing equation (19) in conjunction with the first order potential energy constraint, equation (18), the following functional relationship is obtained for ω_1, namely

$$\omega_1 = \omega_1 \left(1/D(2\omega_0,0),\ 1/D(0,2m),\ 1/D(2\omega_0,2m)\right) \tag{20}$$

where D is the determinant of the pencil of equation (13). Hence for $\omega_0 \sim 0(\omega_{mf})$, ω_1 is bounded and positive definite. This follows since $1/D(2\omega_0,0),\ldots$etc. remain bounded for $\forall\omega_0\varepsilon(0,\infty)$. Therefore, unlike the zeroth order set, W_1 and V_1 remain bounded for $\forall\omega_0$.

In order to obtain the second order field equations, equations (1), (2), and (4) are differentiated twice and then ε is set to zero. This operation yields

$$A_1 W_{2,\theta\theta\theta\theta} + A_2(V_{2,\theta} + W_2) + (\kappa + \frac{P}{R})W_2 + \rho h[\omega_0^2 W_{2,\tau\tau} - 2\Omega\omega_0 V_{2,\tau} -$$

$$\Omega^2 W_2] = A_2[W_{1,\theta}W_{0,\theta} + V_{1,\theta\theta}W_{0,\theta} + V_{0,\theta\theta}W_{1,\theta} + V_{1,\theta}W_{0,\theta\theta} + V_{0,\theta}W_{1,\theta\theta} +$$

$$W_1 W_{0,\theta} + W_0 W_{1,\theta\theta}] + \frac{1}{2} A_2 W_{0,\theta}^2 W_{0,\theta\theta} - \rho h[2\omega_2\omega_0 W_{0,\tau\tau} +$$

$$\omega_1^2 W_{0,\tau\tau} + 2\omega_1\omega_0 W_{1,\tau\tau} - 2\Omega\omega_2 V_{0,\tau} - 2\Omega\omega_1 V_{1,\tau}] \tag{21}$$

$$A_2(V_{2,\theta\theta} + W_{2,\theta}) - \rho h(\omega_0^2 V_{2,\tau\tau} + 2\Omega\omega_0 W_{2,\tau\tau} - \Omega^2 V_2) =$$

$$-A_2(W_{1,\theta}W_{0,\theta\theta} + W_{0,\theta}W_{1,\theta\theta}) + \rho h(\omega_1^2 V_{0,\tau\tau} + 2\omega_0\omega_2 V_{0,\tau\tau} +$$

$$2\omega_2\Omega W_{0,\tau} + 2\omega_1\Omega W_{1,\tau}) \tag{22}$$

$$0 = \int_0^{2\pi}\int_0^{2\pi} \{A_1 W_{1,\theta\theta}^2 + 2A_1 W_{0,\theta\theta}W_{2,\theta\theta} + A_1(V_{1,\theta} + W_1)^2 +$$

$$2A_2(V_{0,\theta} + W_0)(V_{2,\theta} + W_2) + A_2(2(V_{0,\theta} + W_0)W_{0,\theta}W_{1,\theta} +$$

$$(V_{1,\theta} + W_1)W_{0,\theta}^2) + \frac{1}{4} A_2 W_{0,\theta}^4 + (\kappa + \frac{P}{R})(W_1^2 + 2W_0 W_2) +$$

$$2f\cos(m\theta)\cos(\tau)\, W_2 - \rho h[2\Omega^2(R^* + W_0)W_2 + \Omega^2 W_1^2 +$$

$$\omega_0^2(2W_{2,\tau}W_{0,\tau} + W_{1,\tau}^2) + 4\omega_0\omega_1 W_{0,\tau}W_{1,\tau} + 2\omega_2\omega_0 W_{0,\tau}^2 +$$

$$\Omega^2(2V_0 V_2 + V_1^2) + \omega_0^2(2V_{2,\tau}V_{0,\tau} + V_{1,\tau}^2) + 4\omega_1\omega_0 V_{1,\tau}V_{0,\tau} +$$

$$2\omega_0\omega_2 V_{0,\tau}^2 + 2\Omega\omega_0(R^* + W_0)V_{2,\tau} + 2\Omega\omega_1(R^* + W_0)V_{1,\tau} +$$

$$2\Omega\omega_2(R^* + W_0)V_{0,\tau} + 2\Omega\omega_0 W_1 V_{1,\tau} + 2\Omega\omega_1 W_1 V_{0,\tau} + 2\Omega\omega_0 W_{2,\tau}V_0 -$$

(continued)

$$2\Omega\omega_0 W_{0,\tau} V_2 - 2\Omega\omega_0 W_{2,\tau} V_0 - 2\Omega\omega_1 W_{0,\tau} V_1 - 2\Omega\omega_1 W_{1,\tau} V_0 -$$

$$2\Omega\omega_2 W_{0,\tau} V_0]\}d\theta d\tau \qquad (23)$$

As in the zeroth and first order cases, noting the inhomogeneities of equations (21) and (22), W_2 and V_2 take the form, namely

$$(W_2; V_2) = (W_{c2}; V_{c2}) \cos(2\tau) + \ldots$$

$$+ (W_{ss2}; V_{ss2}) \sin(3m\theta) \cos(3\tau) \qquad (24)$$

Employing equations (24), (21), and (22), it can be shown that the following proportionalities exist, that is

$$(W_2; V_2) \propto (W_2(1/D^3(\omega_0,m)); V_2(1/D^3(\omega_0,m))) \qquad (25)$$

Hence W_2 and V_2 become unbounded for $\omega_0 \sim O(\omega_{mf})$. The requisite form of ω_2 can be obtained by inserting equation (24) into the second order potential energy functional, namely equation (23). After extensive manipulations, this operation yields the following proportionalities for ω_2, that is

$$\omega_2 = \omega_{2NUM}(1/D^4(\omega_0,m))/\omega_{2DEN}(1/D^2(\omega_0,m)) \qquad (26)$$

Thus for $\omega_0 \sim O(\omega_{mf})$, $\omega_2 \sim O(1/D^2(\omega_0,m))$ where, since $D^2(\omega_{mf},m)$ is singular, ω_2 is itself unbounded and negative definite. Additionally W_2 and V_2 are themselves unbounded at such values of ω_0.

DISCUSSION

Stopping the solution at this point, W, V, and ω are given by

$$(W; V; \omega) \sim (W_0; V_0; \omega_0) + (W_1; V_1; \omega_1)\varepsilon +$$

$$(W_2; V_2; \omega_2)\varepsilon^2 + O(\varepsilon^3) \qquad (27)$$

Due to the procedure employed, it follows that W and V are regular in ε, including $\varepsilon \equiv 0$. This result is, in contrast to standard renormalized perturbation procedures which do not yield zeroth order solutions exhibiting the proper unbounded behavior for ω on the order of the linear system frequencies.

The softening behavior of the ring or infinite cylinder can be directly obtained by considering the fundamental relationship between ω and Γ. Before doing this, the nature of the ω_0 dependency of ω must be ascertained. In particular, for $\omega_0 \sim O(\omega_{mf})$,

$$\omega \sim \omega_0 + \varepsilon 0(1) - \varepsilon^2 0 \left(\frac{1}{D^2(\omega_0, m)}\right) + 0(\varepsilon^3) \qquad (28)$$

where since ω_2 is negative definite and unbounded, ω is itself negative definite and unbounded. Such unboundedness occurs at each of the eigenvalues of the pencil of equation (13). Note as Ω is set to zero, the two pairs of eigenvalue branches merge back to the two frequency branches of the stationary state, and hence, the traditional frequencies are obtained.

Eliminating ω_0 from equations (28) and (15), it follows that since ω is unbounded and negative definite for $\omega_0 \sim 0(\omega_{mf})$, the overall steady state harmonic behavior of the ring or infinite cylinder is of the softening type. Hence, as ω is raised or lowered, the usual softening type jump phenomenon is encountered.

In the context of the foregoing, the results can be summarized by the following remarks:

(1) Coriolis forces induce bifurcations in the frequency spectrum;

(2) Such bifurcations extend into the range of deflections marked by moderately large rotations;

(3) All branches exhibit a softening type behavior; this applies to the branches associated with forward as well as backward traveling waves;

(4) Driving frequencies in the neighborhood of the linear system frequency may induce jump phenomena;

(5) Setting $\Omega \to 0$ yields the results for stationary rings and cylinders.

REFERENCES

1. Bert, C.W. and Egle, D.M., Journal of Spacecraft and Rockets, Vol. 6, No. 12, Dec. 1969, pp. 1345-1361.

2. Leissa, A.W., "Vibration of Shells," NASA SP-288, 1973.

3. Srinivasan, A.V. and Lauterbach, G.F., Journal of Engineering for Industry, Vol. 93, 1971, pp. 1229-1231.

4. Penzes, L.E. and Kraus, H., AIAA Jr., Vol. 10, 1972, pp. 1309-1313.

5. Padovan, J., Journal of Sound and Vibration, Vol. 31, No. 4, 1973, pp. 469-482.

6. Padovan, J., Computers and Structures, Vol. 5, 1975, pp. 145-154.

7. Padovan, J., International Journal of Solids and Structures, Vol. 11, 1975, pp. 1367-1380.

ON THE EXPLICIT FINITE ELEMENT FORMULATION OF THE DYNAMIC CONTACT PROBLEM OF HYPERELASTIC MEMBRANES*

J. O. Hallquist and W. W. Feng
Lawrence Livermore Laboratory, University of California
Livermore, California

SUMMARY

Contact-impact problems involving finite deformation axisymmetric membranes are solved by the finite element method with explicit time integration. The formulation of the membrane element and the contact constraint conditions are discussed in this paper. The hyperelastic, compressible Blatz and Ko material is used to model the material properties of the membrane. Two example problems are presented.

INTRODUCTION

The purpose of this paper is to present a method for the dynamic analysis of contact-impact problems involving hyperelastic compressible membranes. A strain energy functional developed by Blatz and Ko (ref. 1) is used to characterize the material of the membrane. This element was added to HONDO (ref. 2), a finite element code that explicitly integrates the equations of motion. The contact-impact algorithm, which was also added to HONDO, was recently developed by Hallquist (ref. 3) and is briefly described here.

Two examples are provided to demonstrate the capability of the method: in the first, a flat circular membrane is inflated by a pressure loading into a thick-walled sphere; and in the second, the sphere is impacted into the membrane.

FORMULATION

Equation of Motion

Since an explicit time integration scheme is being considered, the equation of motion becomes

$$\vec{\vec{M}}\ddot{\vec{u}} = \vec{P} - \vec{F} \tag{1}$$

where $\vec{\vec{M}}$ is the diagonal (lumped) mass matrix, $\ddot{\vec{u}}$ is a global vector of nodal accelerations, $\vec{P}$ is the applied load vector, and $\vec{F}$ is the stress divergence vector. This equation is integrated by the velocity-centered central difference method.

*Work was performed under the auspices of the United States Energy Research and Development Administration under contract No. W-74-05-eng-48.

Material Properties

The strain energy density per unit undeformed volume u_s for a compressible hyperelastic material is expressed as

$$u_s = \mu\left[I_1 - 3 + \frac{1 - 2\nu}{\nu}\left(I_3^{-\frac{\nu}{1-2\nu}} - 1\right)\right] \tag{2}$$

where μ is the shear modulus, ν is Poisson's ratio, and I_i is the ith strain invariant. These invariants can be expressed in terms of the principal stretch ratios λ_1, λ_2, λ_3 in the meridional, circumferential, and transverse directions, respectively, as

$$\begin{aligned} I_1 &= \lambda_1^2 + \lambda_2^2 + \lambda_3^2 \\ I_3 &= \lambda_1^2 \lambda_2^2 \lambda_3^2 \end{aligned} \tag{3}$$

For thin membranes, the stress component normal to the midsurface is assumed to be zero; hence, λ_3 can be expressed in terms of λ_1 and λ_2

$$\lambda_3 = (\lambda_1\lambda_2)^{-\frac{\nu}{1-\nu}} \tag{4}$$

and the strain energy density becomes a function of λ_1 and λ_2.

Membrane Element

An isoparametric axisymmetric membrane element is shown in Figure 1. The R, Z, and meridional coordinates S of the undeformed configuration are related to the natural coordinate L through

$$\begin{aligned} R &= \frac{1}{2}(1 - L)R^i + \frac{1}{2}(1 + L)R^j \\ Z &= \frac{1}{2}(1 - L)Z^i + \frac{1}{2}(1 + L)Z^j \\ S &= \frac{1}{2}(1 - L)S^i + \frac{1}{2}(1 + L)S^j \end{aligned} \tag{5}$$

and similarly for the displacement components u_r and u_z

$$\begin{aligned} u_r &= \frac{1}{2}(1 - L)u_r^i + \frac{1}{2}(1 + L)u_r^j \\ u_z &= \frac{1}{2}(1 - L)u_z^i + \frac{1}{2}(1 + L)u_z^j \end{aligned} \tag{6}$$

In the deformed configuration, the r and z coordinates along the midsurface are given by

$$\begin{aligned} r &= u_r + R \\ z &= u_z + Z \end{aligned} \tag{7}$$

The principal sketch ratios λ_1 and λ_2 can be defined as

$$\lambda_1 = \left[\left(\frac{dr}{dS}\right)^2 + \left(\frac{dz}{dS}\right)^2\right]^{1/2} \qquad \lambda_2 = \frac{r}{R} \tag{8}$$

Substitution of equations (5) and (6) into equation (7), putting the result into equation (8), and applying the chain rule leads to expressions for λ_1 and λ_2 in terms of the nodal point quantities

$$\lambda_1 = \frac{1}{\ell}\left[\left(R^j + u_r^j - R^i - u_r^i\right)^2 + \left(Z^j + u_z^j - Z^i - u_z^i\right)^2\right]^{1/2}$$
$$\lambda_2 = 1 + \frac{(1 - L)u_r^i + (1 - L)u_r^j}{(1 - L)R^i + (1 + L)R^j} \tag{9}$$

where $\ell = S^j - S^i$.

Since λ_1 and λ_2 are now functions of the natural coordinate L, the total strain energy stored within the membrane element during deformation can be expressed as the integral

$$U = \pi h \ell \int_{-1}^{1} u_s \, R dL \tag{10}$$

in which h is the thickness of the undeformed membrane.

The partial derivatives of U with respect to the nodal displacement components yield nodal point forces that are subsequently accumulated into the stress divergence vector. In the problem under consideration these derivatives can be calculated very easily. For example, the nodal point force acting in the r-direction at the ith node is given by

$$\frac{\partial U}{\partial u_r^i} = \pi h \ell \int_{-1}^{1} \left(T_1 \frac{\partial \lambda_1}{\partial u_r^i} + T_2 \frac{\partial \lambda_2}{\partial u_r^i}\right) R dL \tag{11}$$

where T_1 and T_2 are Lagrange stresses in the meridional and circumferential directions, respectively. A two point Gauss quadrature is used to perform the above integrations.

The lumped masses for each element are found by the addition of the off-diagonal terms of the consistent mass matrix to the diagonal term. Each membrane element yields the following contributions to the nodal point mass at nodes i and j, respectively,

$$m_i = 2\pi\rho\ell h \, (R^i/3 + R^j/6)$$
$$m_j = 2\pi\rho\ell h \, (R^j/3 + R^i/6) \tag{12}$$

where ρ is the mass density of the undeformed membrane.

For stability the time step Δt is restricted such that the inequality

$$\Delta t^2 < \frac{4}{\lambda^2} \tag{13}$$

is satisfied where λ^2 is the maximum eigenvalue of $\vec{M}^{-1}\vec{K}$ in which $\vec{K}$ is the stiffness matrix.

A time step Δt is calculated for every element in the mesh and 90 percent of the smallest value is then used. For the membrane element λ^2 is calculated exactly from

$$\lambda^2 = \frac{1}{M_i}\left(\frac{\partial^2 U}{\partial u_r^{i2}} + \frac{\partial^2 U}{\partial u_z^{i2}}\right) + \frac{1}{M_j}\left(\frac{\partial^2 U}{\partial u_r^{j2}} + \frac{\partial^2 U}{\partial u_z^{j2}}\right) \tag{14}$$

Contact-Constraint Conditions

Two elastic bodies occupying regions B^1 and B^2 in the reference configuration at time $t = 0$ are shown in Figure 2. The boundaries of B^1 and B^2 are denoted by ∂S^1 and ∂S^2, respectively. After deformation at time $t \neq 0$, these bodies occupy regions b^1 and b^2. The boundaries of b^1 and b^2 are denoted by ∂s^1 and ∂s^2. Whenever b^1 and b^2 are in contact, the nodal points on ∂s^1 in the contact region are constrained to slide along line segments connected by nodal points lying on ∂s^2. Separation is permitted when the interface pressure is negative. Impact and release conditions are applied whenever nodal points on ∂s^1 come into contact with ∂s^2. These conditions, which are based on the generalization of those given by Hughes, et al. (ref. 4), conserve linear and angular momentum.

Constraint conditions must be imposed into the equations of motion for each node of ∂s^1 in contact with a segment of ∂s^2. These conditions are imposed through a transformation of displacements which is performed at the beginning of each time step. In this transformation the radial and vertical displacement components of the node on ∂s^1 are transformed into a displacement component tangential to the segment and a relative displacement component normal to the segment of ∂s^2 on which it rests. Since no separation is permitted during the time step the displacement, velocity, and acceleration of this latter component are set to zero. A transformation matrix $\vec{T}$ is constructed which relates the vector of global displacements $\vec{u}$ to a vector $\vec{u}'$ containing the transformed components

$$\vec{u} = \vec{T}\,\vec{u}' \tag{15}$$

Letting $\vec{T}$ remain constant throughout the time step and differentiating equation (15) with respect to time yields

$$\ddot{\vec{u}} = \vec{T}\,\ddot{\vec{u}}' \tag{16}$$

Equation (16) is substituted into equation (1) and the resulting equation is premultiplied by $\vec{T}^t$ in order to obtain the modified equations of motion

$$\vec{M}'\,\ddot{\vec{u}}' = \vec{T}^t(\vec{P} - \vec{F}) \tag{17}$$

which contains the contact constraints. Here $\vec{M}' = \vec{T}^t\,\vec{M}\vec{T}$. Although $\vec{M}$ is diagonal $\vec{M}'$ is not. For computational efficiency the appropriate off-diagonal masses are summed to the diagonal.

After equation (17) is solved for $\ddot{\vec{u}}'$, the normal accelerations of the nodes of ∂s^1 on ∂s^2 relative to ∂s^2 are set to zero. The global accelerations then

follow directly from equation (16).

EXAMPLES

In the following examples, all physical quantities are given in nondimensional form. Any consistent units may be assumed without altering the results.

Inflation of a Membrane into a Thick-Walled Sphere

A flat unstretched circular membrane with a thickness of 0.01 and a radius of 2.0 is positioned beneath a thick-walled sphere having an inner radius of 0.40 and an outer radius of 0.60. In the undeformed configuration, the distance measured perpendicularly from the center of the membrane to the center of the sphere is 1.20. The hyperelastic material described by equation (2) is used to model the material of both the membrane and the sphere with ν and μ set to 0.463 and 150. Densities of 1.5 and 0.15 were assumed for the material of the membrane and sphere, respectively.

The membrane is inflated by a pressure p defined by

$$\begin{aligned} 0 \le t \le 0.11 \qquad & p = 1.250 \\ 0.11 < t \le 0.15 \qquad & p = 1.250 - 1.125\left(\frac{t - 0.11}{0.40}\right) \\ t > 0.15 \qquad & p = 0.125 \end{aligned} \tag{18}$$

and is brought into contact with the sphere.

In Figure 3 the deformed shapes at various times throughout the deformation time history are shown. At late times some wrinkling occurs (for example, note the last frame) and the calculation ceases to be meaningful. A total of eighty elements were used in the calculation. Forty elements were of the membrane type.

Thick-Walled Sphere Impacting a Membrane

In this example the thick-walled sphere impacts the flat circular membrane with an initial velocity of 1.0. The dimensions and material properties of the membrane and sphere are identical to those of the preceding example. In Figure 4 the deformed shapes at various times are shown. Maximum deflection occurs at the center of the membrane at approximately t = 0.90 after which rebound begins. Separation of the sphere and membrane occurs at approximately t = 1.94.

In the above examples the stress at the center of the membrane increases significantly after the initial contact thereby providing evidence that a large amount of sliding occurs during contact.

REFERENCES

1. Blatz, P. J.; and Ko, W. L.: Application of Finite Elastic Theory to the Determination of Rubbery Materials. Trans. of the Soc. of Rheology, vol. 6, 1962, pp. 223-251.

2. Key, S. W.: HONDO - A Finite Element Computer Program for the Large Deformation Dynamic Response of Axisymmetric Solids. Sandia Laboratories, SLA-74-39, Albuquerque, New Mexico, 1974.

3. Hallquist, J. O.: A Procedure for the Solution of Finite Deformation Contact-Impact Problems by the Finite Element Method. Lawrence Livermore Laboratory, UCRL-52066, Livermore, California, 1976.

4. Hughes, T. J.; Taylor, R. L.; Sackman, J. L.; Curnier, A.; and Kanoknukulchai, W.: A Finite Element Method for a Class of Contact-Impact Problems. J. of Computer Methods in Applied Mechanics and Engineering. (To be published.)

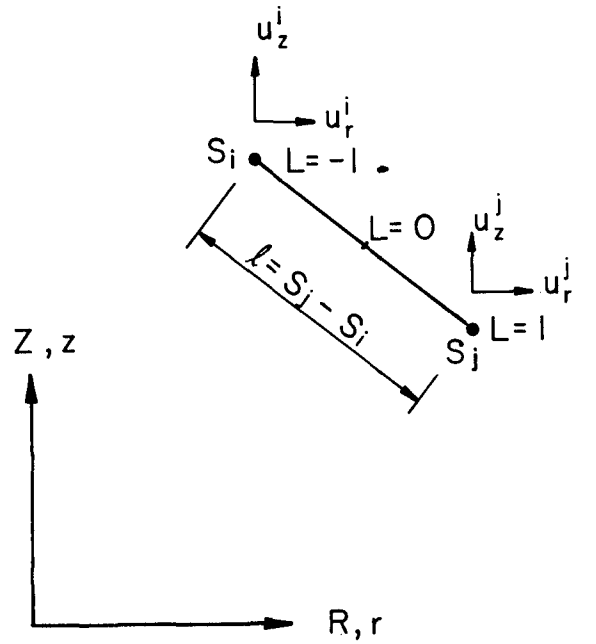

Figure 1.- Definition of membrane element.

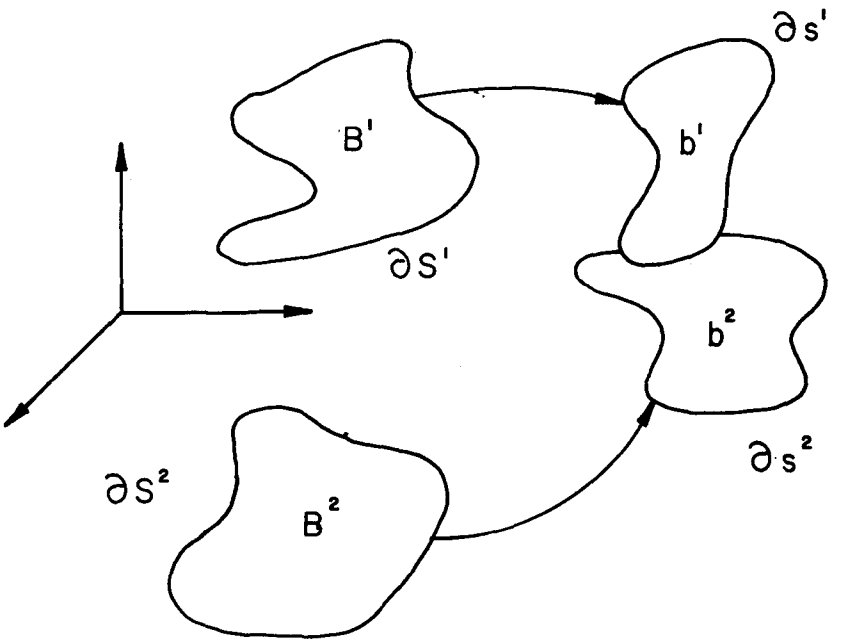

Figure 2.- Two bodies in the reference and deformed-contact configurations.

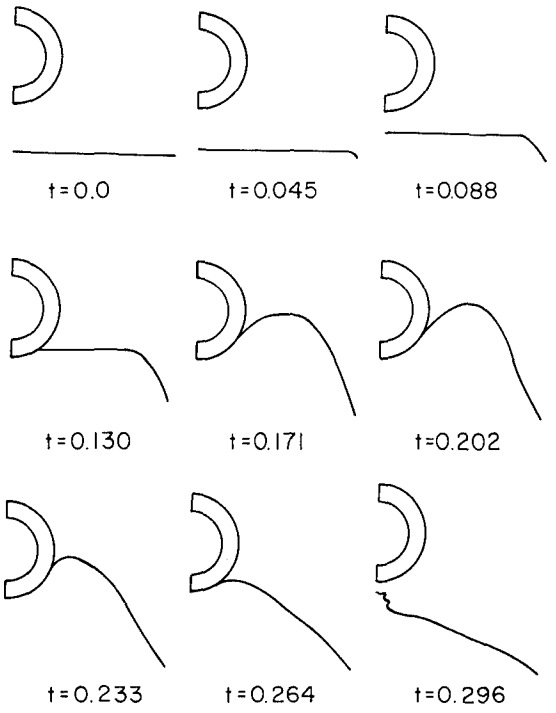

Figure 3.- Inflation of circular membrane into thick-walled sphere.

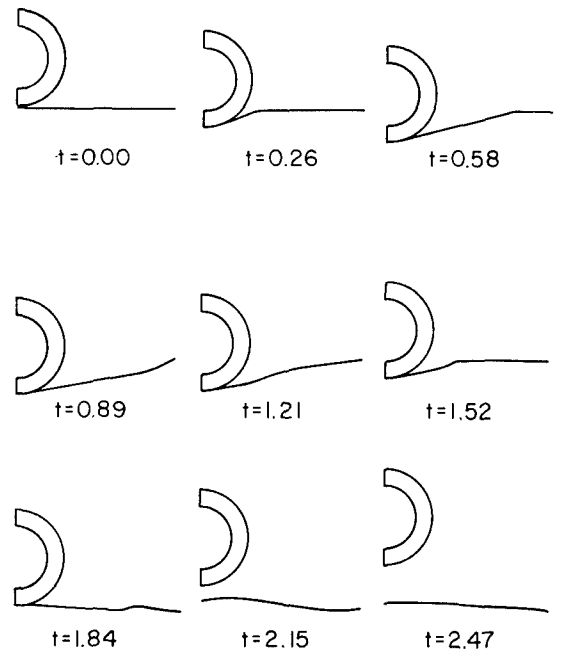

Figure 4.- Impact of thick-walled sphere into circular membrane.

FREE VIBRATIONS OF LAMINATED COMPOSITE ELLIPTIC PLATES

C. M. Andersen
College of William and Mary

Ahmed K. Noor
Joint Institute for Advancement of Flight Sciences
The George Washington University

SUMMARY

A study is made of the free vibrations of laminated anisotropic elliptic plates with clamped edges. The analytical formulation is based on a Mindlin-Reissner type plate theory with the effects of transverse shear deformation, rotary inertia, and bending-extensional coupling included. The frequencies and mode shapes are obtained by using the Rayleigh-Ritz technique in conjunction with Hamilton's principle. A computerized symbolic integration approach is used to develop analytic expressions for the stiffness and mass coefficients and is shown to be particularly useful in evaluating the derivatives of the eigenvalues with respect to certain geometric and material parameters. Numerical results are presented for the case of angle-ply composite plates with skew-symmetric lamination.

INTRODUCTION

Although a number of studies have been devoted to the free-vibration analysis of isotropic elliptic plates (refs. 1 to 4), investigations of orthotropic plates are rather limited in extent (refs. 5 and 6), and to the authors' knowledge, no publications exist dealing with the free vibration of laminated anisotropic elliptic plates. The present study focuses on this problem. More specifically, the objectives of this paper are (1) to present a computational procedure based on the use of computerized symbolic integration in conjunction with the Rayleigh-Ritz technique for the free-vibration analysis of laminated anisotropic elliptic plates and (2) to study the effect of variations in the lamination and geometric parameters of the plate on its vibration characteristics.

The analytical formulation is based on a form of the Mindlin-Reissner plate theory with the effects of transverse shear deformation, anisotropic material behavior, rotary inertia, and bending-extensional coupling included. The frequencies and mode shapes are obtained by using the Rayleigh-Ritz technique in conjunction with Hamilton's principle. The stiffness and mass coefficients are developed using the symbolic and algebraic manipulation language MACSYMA (refs. 7 and 8). Computerized algebraic manipulation, in addition to reducing the tedium of the analysis and the likelihood of errors,

was shown to be particularly useful in evaluating the derivatives of the eigenvalues with respect to certain geometric and material parameters. Other applications of computerized algebraic manipulation in structural mechanics are reported in references 9 and 10.

SYMBOLS

a_1, a_2	semimajor and semiminor axes of elliptic plate
$C_{\alpha\beta\gamma\rho}, C_{\alpha 3 \beta 3}$	extensional and transverse shear stiffnesses of plate, respectively
$D_{\alpha\beta\gamma\rho}$	bending stiffnesses of plate
E_L, E_T	elastic moduli in direction of fibers and normal to fibers, respectively
$F_{\alpha\beta\gamma\rho}$	stiffness interaction coefficients of plate
G_{LT}, G_{TT}	shear moduli in plane of fibers and normal to plane of fibers, respectively
h	plate thickness
[K]	element stiffness matrix
K_{ij}	stiffness coefficients
[M]	mass matrix
M_{ij}	mass coefficients
m_o, m_1, m_2	density parameters of plate
T	kinetic energy of plate
U	strain energy of plate
u_α, w	displacement components in coordinate directions
θ	fiber orientation angle of individual layers
ν_{LT}	Poisson's ratio measuring strain in T-direction due to uniaxial normal stress in the L-direction
$\Pi(u_\alpha, w, \phi_\alpha)$	functional defined in equation (1)
ρ	material density of the plate

ϕ_α rotation components

$\{\psi\}$ vector of undetermined parameters

ψ_i ith component of vector $\{\psi\}$

Ω plate domain

ω circular frequency of vibration of the plate

$\partial_\alpha \equiv \frac{\partial}{\partial x_\alpha}$

MATHEMATICAL FORMULATION

The analytical formulation is based on a form of the Mindlin-Reissner plate theory with the effects of transverse shear deformation, anisotropic material behavior, rotary inertia, and bending-extensional coupling included. A displacement formulation is used with the fundamental unknowns consisting of the displacement and rotation components of the middle plane of the plate u_α, w, and ϕ_α. (See fig. 1 for sign convention.) Throughout this paper, the range of the Greek indices is 1,2 and a term in which any Greek index appears twice is to be summed over that index. The fundamental unknowns are assumed to have a sinusoidal variation in time with angular velocity ω (the circular frequency of vibration of the plate). The functional used in the development of the stiffness and mass matrices is given by

$$\Pi(u_\alpha, w, \phi_\alpha) = T - U \tag{1}$$

where

$$U = \frac{1}{2}\int\Big[C_{\alpha\beta\gamma\rho}\,\partial_\alpha u_\beta\,\partial_\gamma u_\rho + 2F_{\alpha\beta\gamma\rho}\,\partial_\alpha u_\beta\,\partial_\gamma \phi_\rho + D_{\alpha\beta\gamma\rho}\,\partial_\alpha \phi_\beta\,\partial_\gamma \phi_\rho + C_{\alpha 3\beta 3}\,(\partial_\alpha w\,\partial_\beta w + 2\phi_\alpha\,\partial_\beta w + \phi_\alpha\phi_\beta)\Big]\,d\Omega \tag{2}$$

$$T = \frac{1}{2}\omega^2\int\Big[m_o(u_\alpha u_\alpha + ww) + 2m_1 u_\alpha \phi_\alpha + m_2 \phi_\alpha \phi_\alpha\Big]\,d\Omega \tag{3}$$

In equations (2) and (3), $C_{\alpha\beta\gamma\rho}$, $D_{\alpha\beta\gamma\rho}$, and $F_{\alpha\beta\gamma\rho}$ are extensional stiffnesses, bending stiffnesses, and stiffness interaction coefficients of the plate; $C_{\alpha 3\beta 3}$ are transverse shear stiffnesses of the plate; m_o, m_1, and

m_2 are density parameters of the plate; Ω is the plate domain; and

$$\partial_\alpha \equiv \frac{\partial}{\partial x_\alpha} .$$

The displacement and rotation components are approximated by expressions of the form

$$\begin{Bmatrix} u_\alpha \\ w \\ \phi_\alpha \end{Bmatrix} = [N] \{\psi\} \tag{4}$$

where $[N]$ is a matrix of a priori chosen approximation functions and $\{\psi\}$ is a vector of undetermined coefficients. In the present study the functions in the matrix $[N]$ are chosen to be polynomials in x_1 and x_2.

The stiffness and mass matrices of the plate are obtained by first replacing the generalized displacements in equations (2) and (3) by their expressions in terms of the approximation functions and then applying the stationary condition of the functional Π, namely,

$$\delta\Pi = 0 \tag{5}$$

If the undetermined coefficients $\{\psi\}$ are varied independently and simultaneously, one obtains the following set of equations for the plate:

$$[K]\{\psi\} = \omega^2 [M]\{\psi\} \tag{6}$$

where $[K]$ and $[M]$ are the stiffness and mass matrices of the plate, respectively. The matrix $[K]$ is symmetric and positive definite and the matrix $[M]$ is symmetric. The eigenvalues and eigenvectors are obtained by using the technique described in reference 11.

EVALUATION OF STIFFNESS AND MASS COEFFICIENTS

The stiffness and mass coefficients were evaluated using the computerized symbolic and algebraic manipulation system MACSYMA. The MACSYMA program used in evaluating these coefficients is given in the appendix. The major tasks performed on MACSYMA are

(1) Selecting approximation functions for each of the fundamental unknowns with undetermined coefficients $\{\psi\}$ in equation (4) and developing analytic expressions for the strain and kinetic energies as quadratic functions in $\{\psi\}$

(2) Specifying a pattern-matching technique for evaluating the integrals over the elliptic domain (using the function INT(F) (see appendix))

(3) Forming the stiffness and mass coefficients as second derivatives of the strain and kinetic energies with respect to the undetermined coefficients as

$$K_{ij} = \frac{\partial^2 U}{\partial \psi_i \, \partial \psi_j} \qquad \omega^2 M_{ij} = \frac{\partial^2 T}{\partial \psi_i \, \partial \psi_j} \tag{7}$$

In view of the symmetry of K_{ij} and M_{ij}, only the upper triangular portions are formed in a machine readable (LISP) format. These are subsequently converted using the MACSYMA system to a form which closely resembles FORTRAN code (the MACSYMA program used in the conversion is not included in the appendix). Finally, a TECO program (DEC's editor for PDP-10 computers) is executed to produce the final code.

The aforementioned computerized algebraic manipulation approach significantly reduced the tedium of the analysis and the likelihood of errors. Moreover, since analytic exact expressions are obtained for both the stiffness and mass coefficients, the derivatives of the eigenvalues with respect to any of the material or geometric parameters can be readily computed by using the following formula (ref. 12):

$$\frac{\partial \left(\omega_i^2\right)}{\partial d} = \{\psi\}_i^T \left[\left[\frac{\partial K}{\partial d}\right] - \omega_i^2 \left[\frac{\partial M}{\partial d}\right]\right] \{\psi\}_i \tag{8}$$

where d refers to any of the material or geometric parameters of the plate and subscript i refers to the ith eigenvalue and eigenvector. In equation (8), the eigenvectors are assumed to be $[M]$ orthonormal, i.e.,

$$\{\psi\}_i^T \, [M] \, \{\psi\}_i = 1 \tag{9}$$

The two matrices $\left[\frac{\partial K}{\partial d}\right]$ and $\left[\frac{\partial M}{\partial d}\right]$ can be easily evaluated using the MACSYMA system.

Equation (8) shows that the derivatives of the eigenvalues with respect to any of the geometric and material parameters of the plate can be calculated with little extra work. These derivatives can be used to obtain an approximate estimate for the eigenvalues corresponding to a modified (new) value of the parameters without having to resolve the eigenvalue problem, equation (6). To accomplish this, a first-order Taylor's series expansion of the eigenvalues in terms of the problem parameter is used (see ref. 12)

$$(\omega_i^*)^2 \simeq \omega_i^2 + (d^* - d) \frac{\partial (\omega_i^2)}{\partial d} \tag{10}$$

where an asterisk refers to a modified (new) value.

NUMERICAL STUDIES

Numerical studies were conducted to investigate the effects of variations in the plate geometry and lamination parameters on the vibration characteristics of elliptic plates with clamped edges. Angle-ply laminates having antisymmetric lamination with respect to the middle plane are considered. The material characteristics of the individual layers were taken to be those typical of high-modulus graphite-epoxy composites, namely,

$$E_L/E_T=40 \qquad G_{LT}/E_T=0.6 \qquad G_{TT}/E_T=0.5 \qquad \nu_{LT}=0.25$$

where subscript L refers to the direction of the fibers, subscript T refers to the transverse direction, and ν_{LT} is the major Poisson's ratio. The fiber orientation was taken to be $+\theta/-\theta/+\theta/-\theta/\ldots$, $(0<\theta<45)$. All numerical studies were obtained using the Rayleigh-Ritz technique with 10-term approximation functions for each of the fundamental unknowns. The special symmetries exhibited by the free-vibration modes of antisymmetric laminates were utilized in the analysis (see refs. 13 and 14). The four combinations of symmetry and antisymmetry with respect to the x_1- and x_2-axis have been considered. Typical results are presented in figures 2 to 4 showing the effects of variations in each of the following parameters on the vibration frequencies: (1) the aspect ratio of the plate a_1/a_2, (2) the number of layers of the plate NL, and (3) the fiber orientation angle θ of the individual layers.

Figure 2 shows that for elliptic plates having the same h/a_2, the frequencies of free vibration decrease with the increase in the aspect ratio a_1/a_2. The differences between the frequency curves for thick and thin plates in figure 2 are mainly attributed to transverse shear deformation. As expected, these differences are more pronounced for the higher modes. Figure 3 shows that the frequencies increase rapidly as the number of layers increases from 2 to 4. Further increase in the number of layers does not have significant effect on the lower frequencies. Figure 4 shows that the minimum frequency associated with each of the four basic symmetric-antisymmetric modes increases with the increase in the fiber orientation angle θ from 5° to 45°. This is not true, in general, for the higher modes.

CONCLUDING REMARKS

The free-vibration response of anisotropic plates with clamped edges is studied. The analytical formulation is based on Mindlin-Reissner type theory with the effects of transverse shear deformation, rotary inertia, and bending-extensional coupling included. The frequencies and mode shapes are obtained by using the Rayleigh-Ritz technique in conjunction with Hamilton's principle. A computerized symbolic integration approach is used to develop analytic exact expressions for the stiffness and mass coefficients and is

shown to be particularly useful for evaluating the derivatives of the eigenvalues with respect to certain geometric and material parameters. Numerical results are presented showing the effects of variation in the geometric and material parameters on the free-vibration response of composite elliptic plates with clamped edges.

APPENDIX

MACSYMA PROGRAM FOR ANGLE-PLY COMPOSITE ELLIPTIC PLATE

The MACSYMA program used in evaluating the stiffness and mass coefficients of angle-ply elliptic plates is given herein. The definitions of the different symbols in the program are shown on the right.

Approximation Functions (Doubly-Symmetric Vibration Modes)

```
AAA[I]:=AA[I,1]
       +AA[I,2]*X^2+AA[I,3]*Y^2
       +AA[I,4]*X^2*Y^2+AA[I,5]*X^4+AA[I,6]*Y^4
       +AA[I,7]*X^4*Y^2+AA[I,8]*X^2*Y^4+AA[I,9]*X^6+AA[I,10]*Y^6
W:(1-R^2)*AAA[1];
F1:X*(1-R^2)*AAA[2];
F2:Y*(1-R^2)*AAA[3];
U:Y*(1-R^2)*AAA[4];
V:X*(1-R^2)*AAA[5];

GRADEF(R,X,COS(TH)/A)$
GRADEF(R,Y,SIN(TH)/B)$
GRADEF(TH,X,-Y/(A*B*R^2))$
GRADEF(TH,Y,X/(A*B*R^2))$
```

X	≡	x_1
Y	≡	x_2
U	≡	u_1
V	≡	u_2
W	≡	w
F_1	≡	ϕ_1
F_2	≡	ϕ_2
R^2	≡	$(x_1/a_1)^2 + (x_2/a_2)^2$
A	≡	a_1
B	≡	a_2
AA[I,J]	≡	$\{\psi\}$

Plate Stiffness Matrices

```
CCC:MATRIX([CC11,CC12,0],[CC12,CC22,0],[0,0,CC66]);
DDD:MATRIX([DD11,DD12,0],[DD12,DD22,0],[0,0,DD66]);
FFF:MATRIX([0,0,FF16],[0,0,FF26],[FF16,FF26,0]);
CCCC:MATRIX([CC55,0],[0,CC44]);
```

Strain-Displacement Relationships

```
UVDERIV:MATRIX([DIFF(U,X)],[DIFF(V,Y)],[DIFF(U,Y)+DIFF(V,X)])$
PHIDERIV:MATRIX([DIFF(F1,X)],[DIFF(F2,Y)],[DIFF(F1,Y)+DIFF(F2,X)])$
WDERIV:MATRIX([DIFF(W,X)+F1],[DIFF(W,Y)+F2])$
```

Strain Energy

```
UU:(1/2)◆TRANSPOSE(UVDERIV).(CCC.UVDERIV + FFF.PHIDERIV)
   +(1/2)◆TRANSPOSE(PHIDERIV).(FFF.UVDERIV + DDD.PHIDERIV)
   +(1/2)◆TRANSPOSE(WDERIV).CCCC.WDERIV$
```

UU ≡ U

Kinetic Energy

```
T:(1/2)◆(U^2+V^2+W^2+(H^2/12)◆(F1^2+F2^2))$
KILL(U,V,W,F1,F2,CCC,FFF,DDD,CCCC,UVDERIV,PHIDERIV,WDERIV,AAA,LABELS)$
SUB:[X=A◆R◆COS(TH),Y=B◆R◆SIN(TH)];
UU:SUBST(SUB,UU)$
TT:SUBST(SUB,TT)$
```

TT ≡ $T/(\rho h \omega^2)$

Integration Over Elliptic Domain

```
II[0,0]:2$
II[MMM,NNN]:=IF NNN = 0
   THEN (2◆MMM-1)/(2◆MMM)◆II[MMM-1,0]
   ELSE (2◆NNN-1)/(2◆(MMM+NNN))◆II[MMM,NNN-1];
NONZERO(XX):=IS(NOT(XX=0));
CPRED(XXX):=IS(FREEOF(SIN,XXX) AND FREEOF(COS,XXX) AND FREEOF(R,XXX));
MATCHDECLARE(COEF,CPRED)$
MATCHDECLARE([EE1,EE2,EE3],NONZERO)$
DEFRULE(RULE1,COEF◆R^EE1◆COS(TH)^EE2◆SIN(TH)^EE3,
   IF REMAINDER(EE2-1,2)=0 AND REMAINDER(EE3-1,2)=0
      THEN COEF/(EE1+1)◆II[(EE2-1)/2,(EE3-1)/2]
      ELSE 0);
INT(XXX):=APPLY1(EXPAND(R◆COS(TH)◆SIN(TH)◆XXX),RULE1);
```

Formation of Upper Triangular Terms of Stiffness and Mass Matrices

```
ARG(J):=[['ELLIPS,8000+J],'MT,'MU,'TT,'UU,'ARG];
FOR J:50 STEP -1 THRU 1 DO[
   J1:1+REMAINDER(J-1,5),
   J2:ENTIER((J+4)/5),
   GT:DIFF(TT,AA[J1,J2]),
   GU:DIFF(UU,AA[J1,J2]),
   FOR I THRU J DO[
      I1:1+REMAINDER(I-1,5),
      I2:ENTIER((I+4)/5),
      HT:DIFF(GT,AA[I1,I2]),
      HU:DIFF(GU,AA[I1,I2]),
      MT[I,J]:IF HT=0 THEN 0 ELSE INT(HT),
      MU[I,J]:IF HU=0 THEN 0 ELSE INT(HU)  ],
   TT:EV(TT,AA[J1,J2]=0),
   UU:EV(UU,AA[J1,J2]=0),
   IF J=27 OR J=21 OR J=1
      THEN (APPLY(SAVE,ARG(J)),  KILL(MT,MU))   ]$
```

[UU] ≡ [K]

[TT] ≡ [M]/ρh

MACSYMA Functions

$$\text{DIFF}(F,X) = \frac{\partial F}{\partial X}$$

$$\text{INT}(F) = \left[\int_{-\pi}^{\pi}\int_{0}^{1} F(R,\theta)\, R\, dR\, d\theta\right]/\pi\, a_1\, a_2$$

GRADE F functions specify that the derivative of the first argument with respect to the second argument is given by the third argument.

The KILL Command erases from memory expressions which are no longer needed.

REFERENCES

1. Callahan, W. R.: Flexural Vibrations of Elliptical Plates When Transverse Shear and Rotary Inertia Are Considered. J. of the Acoustical Society of America, vol. 36, May 1964, pp. 823-829.

2. Leissa, A. W.: Vibration of a Simply Supported Elliptical Plate. J. of Sound and Vibration, vol. 6, July 1967, pp. 145-148.

3. Sato, K.: Free Flexural Vibrations of an Elliptical Plate With Simply Supported Edge. J. of the Acoustical Society of America, vol. 52, Sept. 1972, pt. 2, pp. 919-922.

4. Sato, K.: Free Flexural Vibrations of an Elliptical Plate With Free Edge. J. of the Acoustical Society of America, vol. 54, Aug. 1973, pp. 547-550.

5. Desiderati, F. W.; and Laura, P. A.: Vibrations of Rib-Stiffened Elliptical and Circular Plates. J. of the Acoustical Society of America, vol. 48, pt. 1, pp. 6-11.

6. Hoppmann, W. H., II: Flexural Vibration of Orthogonally Stiffened Circular and Elliptical Plates. Proceedings 3rd U.S. National Congress on Applied Mechanics, June 1958, pp. 181-187.

7. Moses, J.: MACSYMA - The Fifth Year. ACM Sigsam Bull., vol. 8, no. 3, Aug. 1974, pp. 105-110.

8. Martin, W. A.; and Fateman, R. J.: The MACSYMA System. Proceedings Second Symposium on Symbolic and Algebraic Manipulation, S. R. Petrick, Ed., Association for Computing Machinery, 1971, pp. 59-75.

9. Levi, I. M.: Symbolic Algebra by Computer-Applications to Structural Mechanics. AIAA Paper No. 71-363, Presented at the AIAA/ASME 12th Structures, Struct. Dynamics and Materials Conference, Anaheim, CA, April 19-21, 1971.

10. Wilkins, D. J.: Applications of a Symbolic Algebra Manipulation Language for Composite Structures Analysis. Computers and Structures, vol. 3, pp. 801-807.

11. Martin, R. S.; and Wilkinson, J. H.: Reduction of the Symmetric Eigenproblem, $AX=\lambda BX$ and Related Problems to Standard Form. Numerische Mathematik, Bd. 11, 1968, pp. 99-110.

12. Fox, R. L.; and Kapoor, M. P.: Rates of Change in Eigenvalues and Eigenvectors. AIAA J., vol. 6, no. 12, 1968, pp. 2426-2429.

13. Noor, A. K.: Symmetries in Laminated Composite Plates. Developments in Theoretical and Applied Mechanics, vol. 8, Proceedings of the Eighth Southeastern Conference on Theoretical and Applied Mechanics, 1976, pp. 225-246.

14. Noor, A. K.; Mathers, M. D.; and Anderson, M. D.: Exploiting Symmetries for Efficient Post-Buckling Analysis of Composite Plates. Presented at the AIAA/ASME/SAE 17th Structures, Structural Dynamics, and Materials Conference, Valley Forge, PA, May 5-7, 1976.

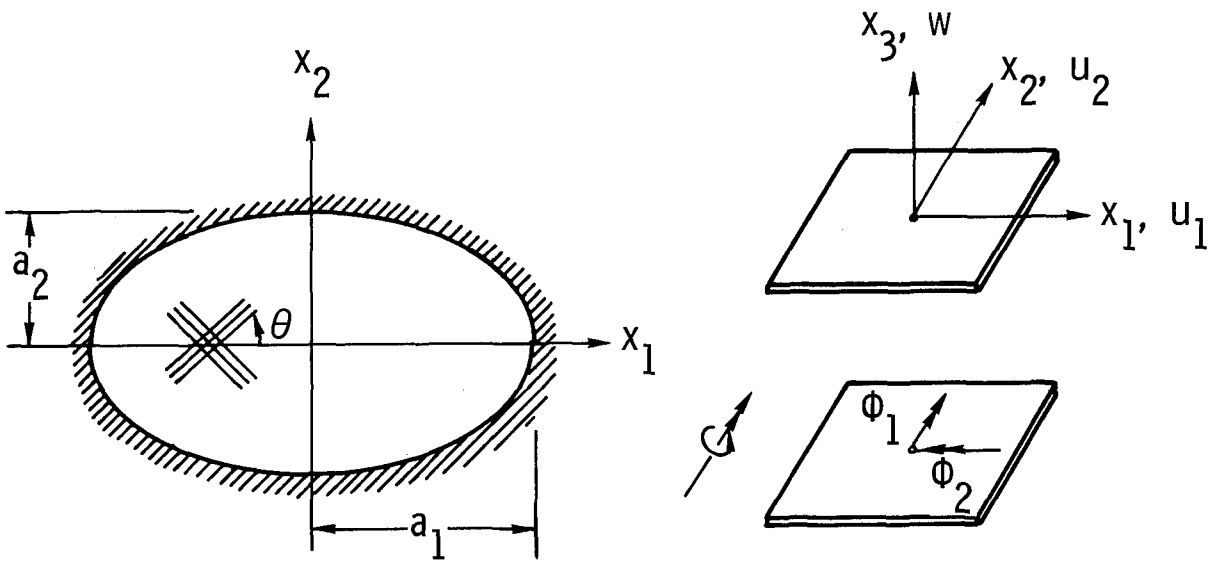

Figure 1.- Elliptic plate and sign convention.

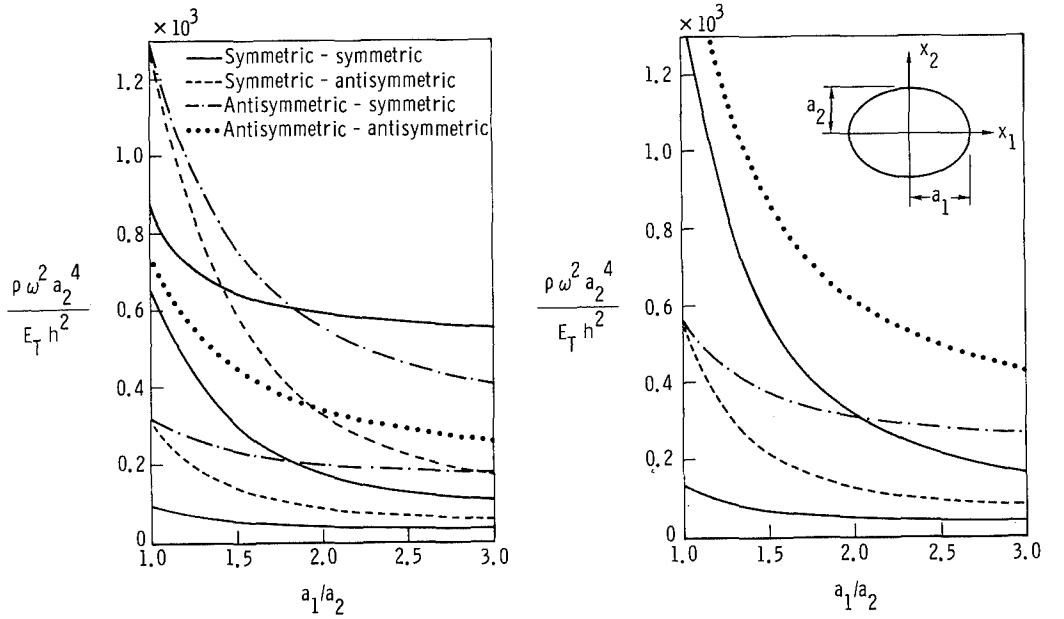

(a) $h/a_2 = 0.1$. (b) $h/a_2 = 0.01$.

Figure 2.- Effect of a_1/a_2 on the frequencies of clamped elliptic plates with antisymmetric lamination. Eight-layered plates with fiber orientation 45°/-45°/45°/-45°/45°/-45°/45°/-45°.

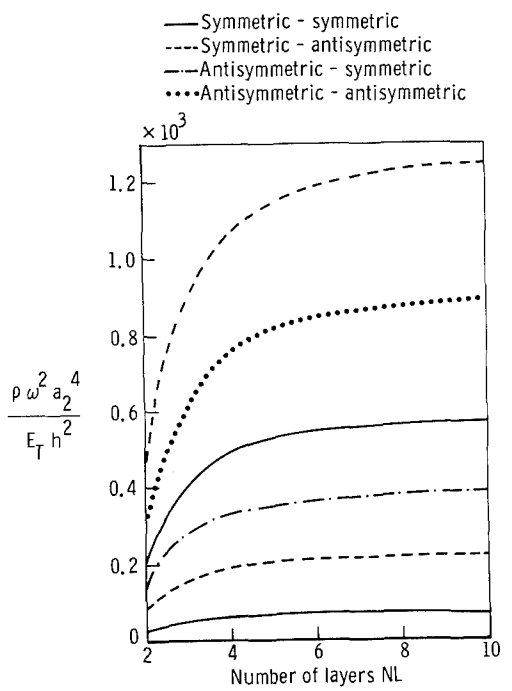

Figure 3.- Effect of number of layers on the frequencies of clamped elliptic plates with antisymmetric lamination. $h/a_2 = 0.01$; $a_1/a_2 = 1.5$; fiber orientation 45°/-45°/...

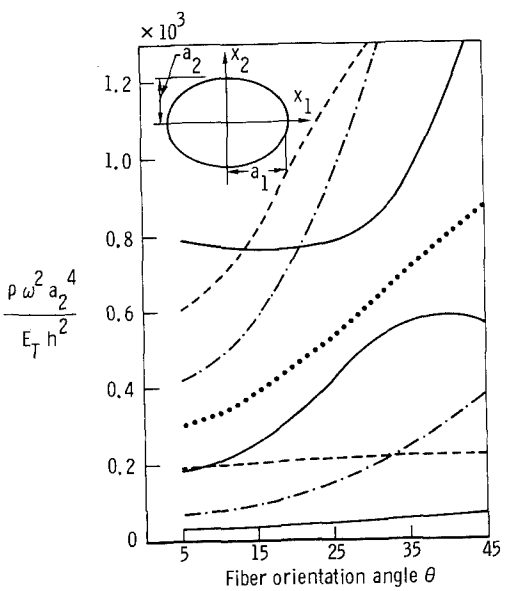

Figure 4.- Effect of fiber orientation θ on the frequencies of clamped elliptic plates with antisymmetric lamination. Eight-layered plates; $h/a_2 = 0.01$; $a_1/a_2 = 1.5$; fiber orientation θ/-θ/θ/-θ/θ/-θ/θ/-θ.

SOME DYNAMIC PROBLEMS OF ROTATING WINDMILL SYSTEMS*

John Dugundji
Massachusetts Institute of Technology

SUMMARY

The basic whirl stability of a rotating windmill on a flexible tower is reviewed. Effects of unbalance, gravity force, gyroscopic moments, and aerodynamics are discussed. Some experimental results on a small model windmill are given.

INTRODUCTION

There has been a renewed interest in the use of large windmills for generating power. Such large, rotating structures mounted on tall flexible towers may give rise to significant vibration and fatigue problems. A good deal of the experience and knowledge gained during the last few years in connection with helicopter rotors and tilt-wing proprotors can be applied to such large windmill systems. However, there are unique features of windmills and their operating environment that will have to be explored individually.

A basic description of general rotating machinery problems can be found in Den Hartog's book, (ref. 1). Loewy (ref. 2) presents a good review of rotary wing dynamic and aeroelastic problems. More recently, a NASA special publication (ref. 3) gives a good sampling of current problems dealing with rotor dynamics. References 4, 5, 6 are typical of recent investigations of problems of large windmill systems. The present article will first review some dynamic problems of a rotating windmill on a flexible tower, then present some preliminary experimental results on a small windmill model.

REVIEW OF THEORY

Figure 1 shows the model used for representing a windmill rotor mounted on a flexible tower. There is an absolute axis system x, y, z fixed in space, and also an axis system x_s, y_s, z_s along the windmill shaft and having x_s lie in the vertical plane (plane of xz). The i^{th} blade rotates about the axis z_s with a constant speed Ω, and can lag an angle ϕ_i in $x_s y_s$ plane and flap an angle β_i perpendicular to $x_s y_s$ plane. Any point, ξ, on the blade can be expressed relative to the shaft axes x_s, y_s, z_s as

*The author would like to acknowledge the support of National Science Foundation Grant AER75-00826.

$$x_s = e \cos \psi_i + \xi \cos (\psi_i + \phi_i) \cos \beta_i$$
$$y_s = e \sin \psi_i + \xi \sin (\psi_i + \phi_i) \cos \beta_i$$
$$z_s = \xi \sin \beta_i \qquad (1)$$

In the above, ψ_i represents the angular position of the i^{th} blade and e is the hinge off-set. The origin of the shaft axis is assumed to translate fore-and-aft a distance q_F and laterally a distance q_L. Associated with these deflections are an angular rotation $\theta_F q_F$ about the y_s axis, another possible rotation $\theta_L q_L$ about the x_s axis, and a vertical deflection $h_v q_F$ in the x direction. The coefficients θ_F, θ_L, h_v can be obtained from the vibration modes of the tower (often, $h_v \approx -h_F$). The shaft axes can be located relative to the fixed axes by performing a rigid body rotation about the y_s axis and about the x_s axis respectively. This gives the relation

$$\begin{Bmatrix} x \\ y \\ z \end{Bmatrix} = \begin{bmatrix} \cos \theta_F q_F & \sin \theta_F q_F \sin \theta_L q_L & -\sin \theta_F q_F \cos \theta_L q_L \\ & \cos \theta_L q_L & \sin \theta_L q_L \\ \sin \theta_F q_F & -\cos \theta_F q_F \sin \theta_L q_L & \cos \theta_F q_F \cos \theta_L q_L \end{bmatrix} \begin{Bmatrix} x_s \\ y_s \\ z_s \end{Bmatrix} \qquad (2)$$

Using the small angle approximation, $\sin \theta_F q_F \approx \theta_F q_F$, $\cos \theta_F q_F \approx 1 - \theta_F^2 q_F^2/2$ etc. in equation (2) and combining with equation (1) and the appropriate deflections gives,

$$x = h_v q_F + (1 - \theta_F^2 q_F^2/2) x_s + \theta_F q_F \, \theta_L q_L \, y_s - \theta_F q_F \, z_s$$
$$y = q_L + (1 - \theta_L^2 q_L^2/2) y_s + \theta_L q_L \, z_s \qquad (3)$$
$$z = q_F + \theta_F q_F \, x_s - \theta_L q_L \, y_s + (1 - \theta_F^2 q_F^2/2 - \theta_L^2 q_L^2/2) \, z_s$$

where x_s, y_s, z_s are given by equation (1). The velocity components $\dot{x}$, $\dot{y}$, $\dot{z}$ are obtained from equations (3) by differentiation with respect to time t. Then, by forming the kinetic energy of the blades and tower, and placing into Lagrange's equations, one can obtain the equations of motion of the windmill system. To simplify the lengthy algebra involved, it was assumed the hinge offset e = 0, and only those terms leading to linear terms in the final equations of motion were retained. The following standard mass integrals were defined for the i^{th} blade,

$$M_i = \int dm, \qquad S_i = \int \xi \, dm, \qquad I_i = \int \xi^2 \, dm \qquad (4)$$

In the development, a two-bladed rotor was assumed with slightly unequal masses, such that $M_1 = M_\beta + M_u/2$ and $M_2 = M_\beta - M_u/2$ where M_β was the average mass and M_u the unbalance in mass of the blades. Similar definitions were made for the average and unbalance in moment S_β and S_u, and in moment of inertia I_β and I_u. The vertical gravity loads were put in by writing the

incremental work as,

$$\delta W = \int [f_x \delta x + f_y \delta y + f_z \delta y] d\xi = \Sigma Q_n \delta q_n \tag{5}$$

where $f_x = -mg$, $f_y = f_z = 0$, δq_n represents δq_F, δq_L, $\delta \beta_i$, $\delta \phi_i$ respectively, and δx, δy, δz are found by differentiating equation (3). A similar procedure could be used for obtaining the aerodynamic forces acting on the blade. However there, it is convenient to relate the air forces perpendicular and parallel to the blade axis ξ.

The final, linear equations of motion in terms of the six coordinates q_F, q_L, β_1, β_2, ϕ_1, ϕ_2 are,

$$\begin{aligned}
&[M_{TF} + 2M_\beta(1 + h_v^2) + 2\theta_F S_u \cos\psi_1 + \theta_F^2 I_\beta(1 + \cos 2\psi_1)]\ddot{q}_F - \theta_F[S_u \sin\psi_1 \\
&+ \theta_F I_\beta \sin 2\psi_1]2\Omega\dot{q}_F - \theta_F S_u \cos\psi_1 \Omega^2 q_F + c_F\dot{q}_F + k_F q_F - \theta_L[S_u \sin\psi_1 \\
&+ \theta_F I_\beta \sin 2\psi_1]\ddot{q}_L - \theta_L[S_u \cos\psi_1 + \theta_F I_\beta(1 + \cos 2\psi_1)]2\Omega\dot{q}_L + \theta_L S_u \sin\psi_1 \Omega^2 q_L \\
&+ \dot{\Sigma}(S_i + \theta_F I_i \cos\psi_i)\ddot{\beta}_i + \dot{\Sigma}\theta_F I_i \cos\psi_i \Omega^2 \beta_i - \dot{\Sigma}(h_v S_i \sin\psi_i)\ddot{\phi}_i \\
&- \dot{\Sigma} h_v S_i \cos\psi_i \, 2\Omega\dot{\phi}_i + \dot{\Sigma} h_v S_i \sin\psi_i \Omega^2 \phi_i = h_v S_u \Omega^2 \cos\psi_1 + g[-h_v 2M_\beta \\
&+ \theta_F^2 S_u \cos\psi_1 q_F - \theta_F \theta_L S_u \sin\psi_1 q_L + \dot{\Sigma}\theta_F S_i \beta_i] + Q_{FA}
\end{aligned} \tag{6}$$

$$\begin{aligned}
&- \theta_L[S_u \sin\psi_1 + \theta_F I_\beta \sin 2\psi_1]\ddot{q}_F + \theta_L \theta_F I_\beta(1 - \cos 2\psi_1)2\Omega\dot{q}_F + [M_{TL} + 2M_\beta \\
&+ \theta_L^2 I_\beta(1 - \cos 2\psi_1)]\ddot{q}_L + \theta_L^2 I_\beta \sin 2\psi_1 \, 2\Omega\dot{q}_L + c_L\dot{q}_L + k_L q_L - \dot{\Sigma}\theta_L I_i \sin\psi_i \ddot{\beta}_i \\
&- \dot{\Sigma}\theta_L I_i \sin\psi_i \Omega^2 \beta_i + \dot{\Sigma} S_i \cos\psi_i \ddot{\phi}_i - \dot{\Sigma} S_i \sin\psi_i \, 2\Omega\dot{\phi}_i - \dot{\Sigma} S_i \cos\psi_i \Omega^2 \phi_i \\
&= S_u \Omega^2 \sin\psi_1 - g\theta_F \theta_L S_u \sin\psi_1 q_F + Q_{LA}
\end{aligned} \tag{7}$$

$$\begin{aligned}
&[S_i + \theta_F I_i \cos\psi_i]\ddot{q}_F - \theta_F I_i \sin\psi_i \, 2\Omega\dot{q}_F - \theta_L I_i \sin\psi_i \ddot{q}_L - \theta_L I_i \cos\psi_i \, 2\Omega\dot{q}_L \\
&+ I_i\ddot{\beta}_i + I_i \Omega^2 \beta_i + c_\beta\dot{\beta}_i + k_\beta \beta_i = g[\theta_F S_i q_F + S_i \cos\psi_i \beta_i] + Q_{\beta_i A} \qquad i = 1,2
\end{aligned} \tag{8}$$

$$\begin{aligned}
&- h_v S_i \sin\psi_i \ddot{q}_F + S_i \cos\psi_i \ddot{q}_L + I_i\ddot{\phi}_i + c_\phi\dot{\phi}_i + k_\phi \phi_i = g[S_i \sin\psi_i \\
&+ S_i \cos\psi_i \phi_i] + Q_{\phi_i A} \qquad i = 1,2
\end{aligned} \tag{9}$$

In the above equations, the $k_n q_n$ and $c_n \dot{q}_n$ terms represent structural stiffness and damping, the g terms represent the effect of gravity loads, and the Q_{nA} terms represent the aerodynamic forces. The M_{TF} and M_{TL} are the generalized tower masses corresponding to q_F and q_L respectively.

Some of the gravity loads act as stiffness terms in the equations. The blade coordinates $\psi_1 = \Omega t$ and $\psi_2 = \psi_1 + \pi$. For the two-bladed case, it is sometimes convenient to introduce the symmetric and antisymmetric blade variables,

$$\beta_s = (\beta_1 + \beta_2)/2, \qquad \beta_A = (\beta_1 - \beta_2)/2, \qquad \phi_s, \phi_A = \text{etc.} \tag{10}$$

to lessen the coupling between the degrees of freedom. Indeed, for a completely balanced rotor without gravity effects, the ϕ_s would be uncoupled from the other equations. In general though, all six coordinates are involved.

Equations (6) to (9) are a linear set of equations with periodic coefficients, subjected to gravity, rotor unbalance S_u, and aerodynamic wind forcing functions. The gravity loads act directly on the blades while the unbalance loads shake the tower which in turn couples into the blades. In addition to forced response, the homogeneous equations themselves may have strong instabilities present. These are generally investigated by the use of Floquet theory for these periodic coefficient equations. It should also be mentioned that for a three or more bladed rotor, the analysis is generally easier since one can eliminate the periodic coefficients by a suitable transformation of coordinates (at least for the balanced rotor, without gravity effects). See for example reference 7.

Various investigators have examined different subcases of equations (6) to (9). Coleman and Feingold (ref. 8) first looked at the case $q_F = 0$, $\beta_i = 0$, $\theta_L = 0$, with no gravity, unbalance, or aerodynamics present. Strong mechanical instabilities of a whirling nature were found to be possible at certain rotational speeds, involving coupling of lateral motion q_L with lag angle ϕ_A. This is the so-called "ground resonance" helicopter phenomenon. Reed (ref. 9) looked at the case $\beta_i = 0$, $\phi_i = 0$ with aerodynamics present. Again, strong instabilities were found involving q_L and the vertical $h_v q_F$ coupling through the mechanical and aerodynamic gyroscopic forces ($\Omega\dot{q}_F$, $\Omega\dot{q}_L$ terms). This is the so-called "propellor whirl" flutter. Young and Lytwyn (ref. 10) looked at the case $\phi_i = 0$ with aerodynamics present. This is essentially "propeller whirl" with flapping. Johnson (ref. 11) has looked in detail at the whole coupled system, but without gravity and unbalance effects in connection with his studies of proprotors. Equations very similar to the ones here are presented there. Finally, it should be mentioned there is a whole series of detailed investigations of rotors attached to fixed hubs ($q_F = 0$, $q_L = 0$) which emphasize the aerodynamic interaction between blade flapping, lagging, pitching and nonlinear dynamic effects brought on by large initial coning angles for the blades. See for example, references 4, 5, and 6.

EXPERIMENT

Some preliminary tests were run on a small .915 m (3.0 ft) diameter windmill placed in a wind tunnel. The general layout is shown in figure 2. The windmill had generally 2 blades, cantilevered in both the flap and lag directions. The approximately uniform, untwisted blades had a .0762 m(3 in) chord, and could be set at any incidence angle. For a few runs, 4 blades were

attached to the windmill.

The weight of a typical blade was .175 kg (.386 lbs). The cantilever natural frequencies of the non-rotating blades were measured as 33, 93, 172, and 310 Hz for the 1st flap bending, 1st lag bending, 2nd flap bending, and 1st torsion modes respectively. These were corrected for rotational effects in the standard manner, $\omega_R^2 = \omega_{NR}^2 + L\Omega^2$, to give the rotating natural frequencies shown in figure 3. The tower stand had natural frequencies of 8.8, 16, 25 and 75 Hz for the lateral yawing, vertical pitching, lateral translation and vertical translation modes respectively. The windmill was instrumented to measure flap and lag bending moments at the blade root, and also lateral and vertical accelerations of the tower near the front bearing.

The wind tunnel was run to about 18 m/sec (59.1 ft/sec), and after taking data on windmill performance, the wind was turned off and the windmill would coast down to zero rotational speed. This gave a continuous frequency record through all the resonances of the system. Figures 4, 5, and 6 show the measured bending moments and accelerations from such sweeps for a blade setting angle $\theta = 0°$. Many superharmonic resonances can be seen for the flap and lag bending moments. These occur near integer orders of the rotation frequency as can be seen from figure 3. Particularly strong vibrations occured at 2 per revolution for both flap and lag. Indeed, lag moments near 10 times the static gravity moments are present at 50 Hz. The corresponding accelerations show a strong lateral resonance near 24 Hz. In these tests there was a small static unbalance due to unequal blade weights. Subsequent tests with another set of blades having a greater unbalance showed the same vibration patterns, but with peak amplitudes increased more than double. Also, tests run with four blades on the rotor showed similar strong resonances at 2 per revolution. The strong resonances in figures 4 to 6 seem then to have been caused by the rotating unbalance of the blade exciting tower stand frequencies which in turn excite blade frequencies superharmonically. Further details of these tests can be found in reference 12.

CONCLUSIONS

A brief review of some of the dynamic problems associated with large rotating windmills has been given, together with some preliminary experimental results. The importance of flexible towers and their interaction with the rotating blade dynamics has been discussed. Although much work has already been done in this area, many interesting dynamic problems remain to be resolved, particularly those involving rotors with built-in coning angles where nonlinear dynamics must be considered.

REFERENCES

1. Den Hartog, J.P.: Mechanical Vibrations. McGraw-Hill, New York, 4th Ed., 1956.

2. Loewy, R.G.: Review of Rotary-Wing V/STOL Dynamic and Aeroelastic Problems. J. of Amer. Helicopter Soc., Vol. 14, July 1969, pp. 3-24.

3. Rotorcraft Dynamic, NASA Special Publication, NASA SP-352, 1974.

4. Ormiston, R.A.: Rotor Dynamic Considerations for Large Wind Power Generator Systmes. Wind Energy Conversion Systems Workshop Proceedings, National Science Foundation NSF/RA/W-73-006, Dec. 1973.

5. Friedman, P.P.: Aeroelastic Modeling of Large Wind Turbines. Preprint No. S-990, 31st Annual National Forum of Amer. Helicopter Soc., Washington, D.C., May 1975.

6. Kaza, K.R.V.; and Hammond, C.E.: An Investigation of Flap-Lag Stability of Wind Turbine Rotors in the Presence of Velocity Gradients and Helicopter Rotors in Forward Flight. Proceedings of AIAA/ASME/SAE 17th Structures, Structural Dynamics, and Materials Conf., King of Prussia, Pennsylvania, May 5-7, 1976, pp. 421-431.

7. Hohenemser, K.H.; and Yin, S.K.: Some Applications of the Method of Multiblade Coordinates. J. of Amer. Helicopter Soc., Vol. 17, July 1972, pp. 3-12.

8. Coleman, R.P.; and Feingold, A.M.: Theory of Self-Excited Mechanical Oscillations of Helicopter Rotors with Hinged Blades. NACA Report 1351, 1958.

9. Reed, Wilmer H., III: Review of Propeller-Rotor Whirl Flutter. NASA Technical Report, TR R-264, July 1967.

10. Young, M.I.; and Lytwyn, R.T.: The Influence of Blade Flapping Restraint on the Dynamic Stability of Low Disk Loading Propeller-Rotors. J. of Amer. Helicopter Soc., Vol. 12, Oct. 1967, pp. 38-54.

11. Johnson, W.: Dynamics of Tilting Proprotor Aircraft in Cruise Flight. NASA Technical Note, TN D-7677, May 1974.

12. Miller, R.H.; et al: Wind Energy Conversion. Progress Report for Period July 15, 1975 - February 15, 1976 on NSF Grant No. AER 75-00826, RANN Document No. ERDA/NSF-00826/75-2, UC-60, Appendix III.

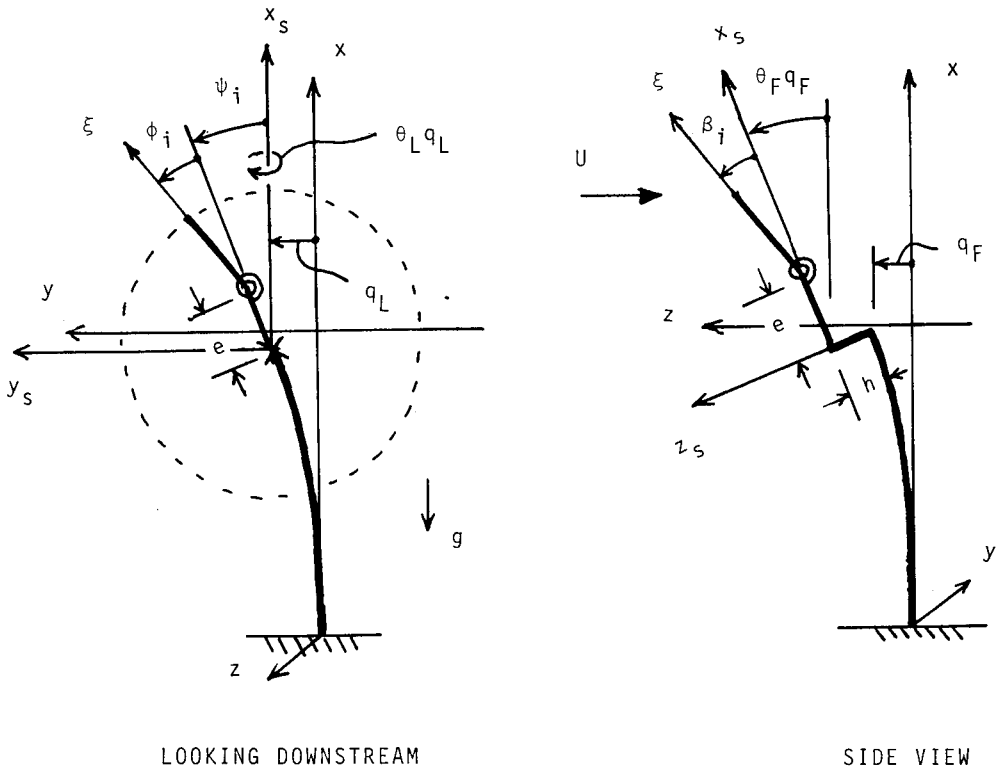

Figure 1.- Analytic model for windmill-tower systems.

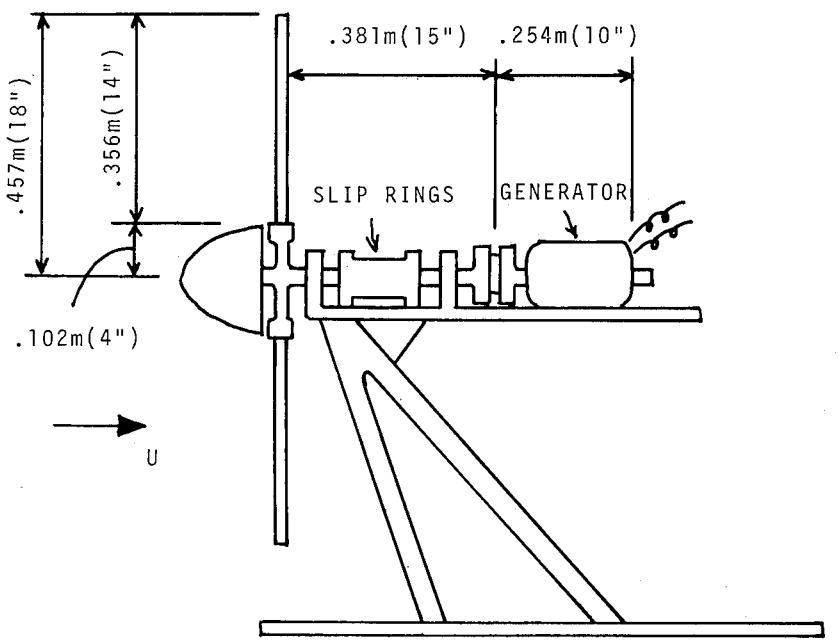

Figure 2.- Experimental layout of windmill assembly.

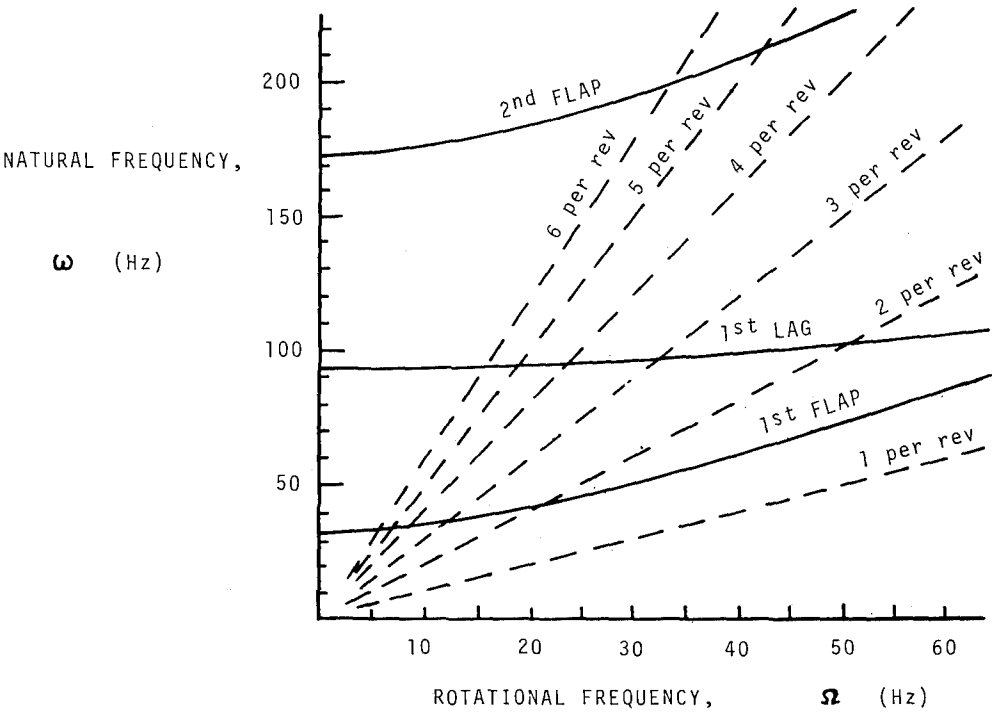

Figure 3.- Rotating natural frequencies of blades.

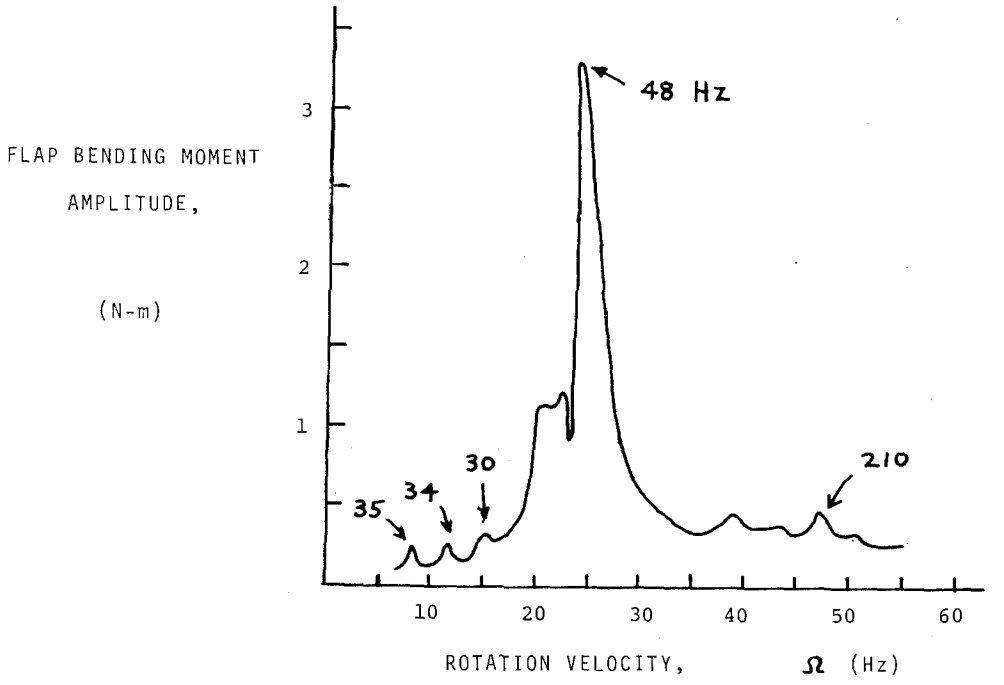

Figure 4.- Flap bending moment vibrations.

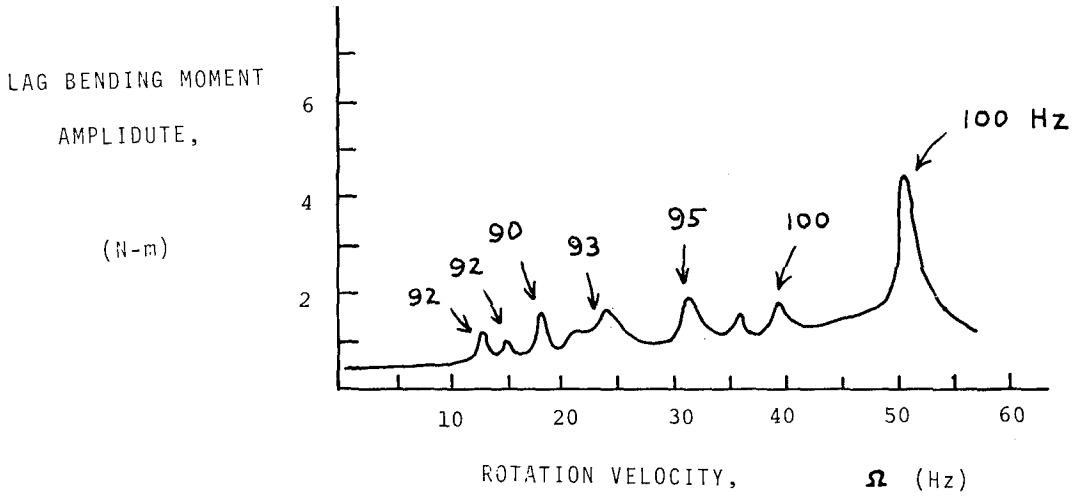

Figure 5.- Lag bending moment vibrations.

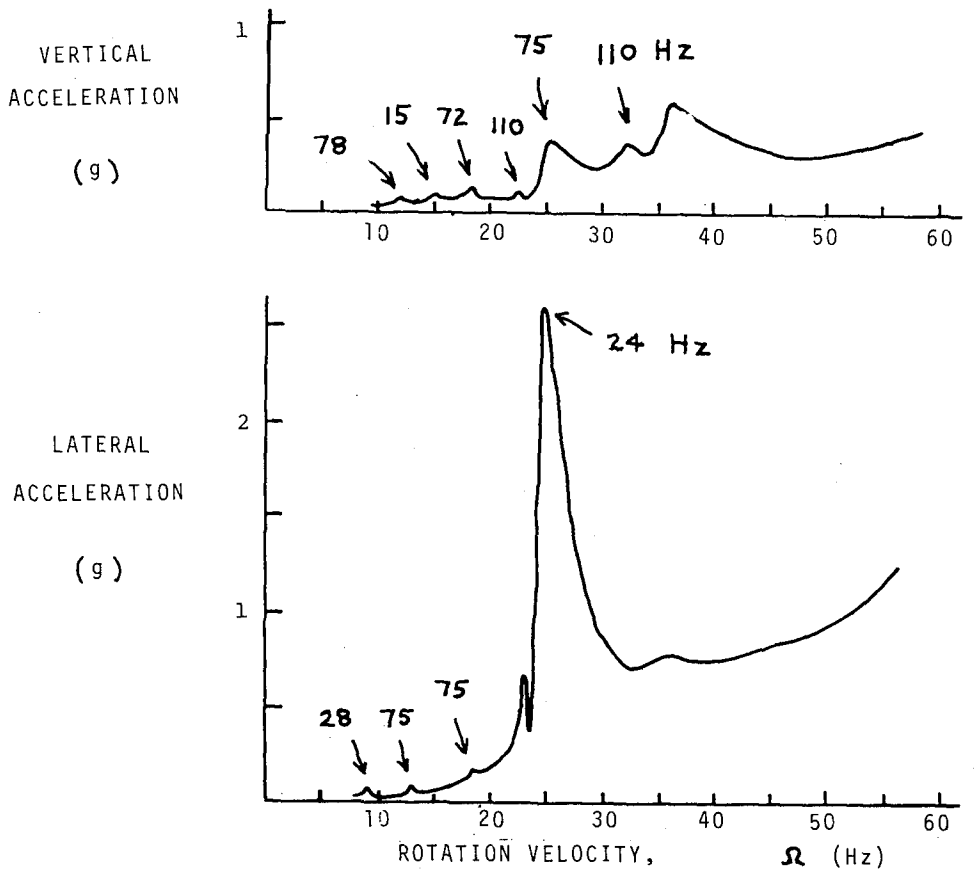

Figure 6.- Vertical and lateral tower accelerations.

DYNAMIC INELASTIC RESPONSE OF THICK SHELLS USING ENDOCHRONIC THEORY AND THE METHOD OF NEARCHARACTERISTICS*

Hsuan-Chi Lin
Argonne National Laboratory

SUMMARY

The endochronic theory of plasticity originated by Valanis has been applied to study the axially symmetric motion of circular cylindrical thick shells subjected to an arbitrary pressure transient applied at its inner surface. The constitutive equations for the thick shells have been obtained. The governing equations are then solved by means of the nearcharacteristics method.

INTRODUCTION

The problem of dynamic plastic response of shells has received considerable attention in recent years. Most of the published works are based on the flow theory of plasticity and usually limited to isotropic linear work-hardening materials. Theoretically, the flow theory is based on the existence of an initial yield surface coupled with an assumed hardening rule to obtain subsequent yield surfaces; an extensive bookkeeping is necessary to trace the evolution of the yield surface which changes as deformation progresses. The analysis of inelastic responses of the bodies is therefore complicated by path dependence and the yield condition, which introduces different governing equations in the distinct regions - elastic and inelastic. Valanis (ref. 1) presented a new theory of plasticity termed endochronic theory, which completely abandoned the concept of a yield surface and its subsequent hardening rule.

The endochronic theory of plasticity is based on thermodynamic theory of internal variables and conforms to experimentally observed material behavior. The basis of the endochronic theory is the assumption that the current state of stress is a functional of the entire history of deformation. The influence of past deformation on the current stress is measured in terms of a monotonically increasing time scale of strain-defined (ref. 1) or stress-defined (ref. 2) endochronic time. This theory has been applied to give analytic predictions for the quasi-static mechanical response of engineering materials (metallic (ref. 3) and non-metallic (ref. 4)), the dynamic response of a

*This work was performed under the auspices of the U. S. Energy Research and Development Administration. The author wishes to express his gratitude to Drs. C. A. Kot and R. A. Valentin for valuable comments.

thin-walled tube subjected to a combined longitudinal and torsional step loading (refs. 5,6), and the dynamic plastic response of circular cylindrical thin shells (refs. 7, 8). It has been shown that the theory does indeed have the capability of explaining the observed phenomena quantitatively with sufficient accuracy.

In this paper, the endochronic theory is applied to thick axially-symmetric cylindrical shell subjected to dynamic loading. The governing equations are then solved by the method of nearcharacteristics.

FORMULATION OF THE PROBLEM

Consider a circular cylindrical thick shell with mean radius R and thickness H. For the axisymmetric motion of shell, the stress and strain states are

$$\underset{\sim}{\sigma} = \begin{pmatrix} \sigma_x & \sigma_{xr} & 0 \\ \sigma_{xr} & \sigma_r & 0 \\ 0 & 0 & \sigma_\theta \end{pmatrix} \qquad \underset{\sim}{s} = \frac{1}{3}\begin{pmatrix} 2\sigma_x-\sigma_r-\sigma_\theta & 3\sigma_{xr} & 0 \\ 3\sigma_{xr} & 2\sigma_r-\sigma_x-\sigma_\theta & 0 \\ 0 & 0 & 2\sigma_\theta-\sigma_x-\sigma_r \end{pmatrix} \tag{1}$$

$$\underset{\sim}{\varepsilon} = \begin{pmatrix} \varepsilon_x & \varepsilon_{xr} & 0 \\ \varepsilon_{xr} & \varepsilon_r & 0 \\ 0 & 0 & \varepsilon_\theta \end{pmatrix} \qquad \underset{\sim}{e} = \frac{1}{3}\begin{pmatrix} 2\varepsilon_x-\varepsilon_r-\varepsilon_\theta & 3\varepsilon_{xr} & 0 \\ 3\varepsilon_{xr} & 2\varepsilon_r-\varepsilon_x-\varepsilon_\theta & 0 \\ 0 & 0 & 2\varepsilon_\theta-\varepsilon_x-\varepsilon_r \end{pmatrix} \tag{2}$$

where $\underset{\sim}{\sigma}$ is the Cauchy stress tensor, $\underset{\sim}{\varepsilon}$ is small strain tensor, $\underset{\sim}{s}$ and $\underset{\sim}{e}$ are the deviatoric stress and strain tensors, respectively, and subscripts x, r, θ refer to the components in longitudinal, radial, and circumferential directions, respectively, Let U and W denote the displacements in the axial and radial directions respectively at time t of the cross section a distance x from a reference section, and u and w are the corresponding velocity components. The equation of motion in the x and r directions have the following form:

$$\frac{\partial \sigma_x}{\partial x} + \frac{\partial \sigma_{xr}}{\partial r} - \rho \frac{\partial u}{\partial t} = -\frac{\sigma_{xr}}{R} \tag{3}$$

$$\frac{\partial \sigma_r}{\partial r} + \frac{\partial \sigma_{xr}}{\partial x} - \rho \frac{\partial w}{\partial t} = \frac{\sigma_\theta - \sigma_r}{R} \tag{4}$$

where ρ is the density.

The strain-displacement relations and the corresponding compatibility conditions are

$$\varepsilon_x = \frac{\partial U}{\partial x} \qquad \frac{\partial \varepsilon_x}{\partial t} = \frac{\partial u}{\partial x} \tag{5}$$

$$\varepsilon_\theta = \frac{W}{r} \qquad \frac{\partial \varepsilon_\theta}{\partial t} = \frac{w}{r} \tag{6}$$

$$\varepsilon_r = \frac{\partial W}{\partial r} \qquad \frac{\partial \varepsilon_r}{\partial t} = \frac{\partial w}{\partial r} \tag{7}$$

$$\varepsilon_{xr} = \frac{1}{2}\left(\frac{\partial U}{\partial r} + \frac{\partial W}{\partial x}\right) \qquad \frac{\partial \varepsilon_{xr}}{\partial t} = \frac{1}{2}\left(\frac{\partial u}{\partial r} + \frac{\partial w}{\partial x}\right) \tag{8}$$

For isotropic material under isothermal condition with the assumption of elastic hydrostatic response, the constitutive equations in the endochronic theory can be found from reference 1 as follows:

$$2\mu \frac{d\underset{\sim}{e}}{d\zeta} = \frac{\alpha \underset{\sim}{s}}{1+\beta\zeta} + \frac{d\underset{\sim}{s}}{d\zeta} \tag{9}$$

$$\sigma_{kk} = 3K\varepsilon_{kk} \tag{10}$$

$$d\zeta^2 = K_1 d\varepsilon_{kk} d\varepsilon_{\ell\ell} + K_2 d\varepsilon_{ij} d\varepsilon_{ij} \tag{11}$$

where α, β, K_1, K_2 are the material parameters, μ is shear modulus, K is bulk modulus, kk, $\ell\ell$, and ij are subscripts denoting coordinates, $d\zeta$ is the endochronic time measure with the restriction that $K_1 + K_2/3 \geq 0$, $K_2 \geq 0$, and K_1 and K_2 may not both be zero. From the definition of $\underset{\sim}{s}$ and $\underset{\sim}{e}$ considered in this problem, it is possible to express the time measure approximately as

$$\beta d\zeta = \pm \beta_1 \left[1 + \left(\frac{d\varepsilon_x}{d\varepsilon_\theta}\right)^2 + \left(\frac{d\varepsilon_r}{d\varepsilon_\theta}\right)^2\right]^{1/2} d\varepsilon_\theta \tag{12}$$

where $\beta_1 = E_t/\sigma_o$, E_t is the asymptotic slope of the uniaxial stress-strain curve for large strain, σ_o is the intercept of this slope with the stress axis, and the positive sign holds for straining while the negative sign is for unstraining of $d\varepsilon_\theta$. Using (12), and equations (9), (10) and the compatibility conditions (5) to (8) results in the following:

$$\frac{\partial \sigma_x}{\partial t} - \nu \frac{\partial \sigma_r}{\partial t} - \nu \frac{\partial \sigma_\theta}{\partial t} - E \frac{\partial u}{\partial x} = a_1 \tag{13}$$

$$-\nu \frac{\partial \sigma_x}{\partial t} - \nu \frac{\partial \sigma_r}{\partial t} + \frac{\partial \sigma_\theta}{\partial t} = a_2 \tag{14}$$

$$\frac{\partial \sigma_x}{\partial t} + \frac{\partial \sigma_r}{\partial t} + \frac{\partial \sigma_\theta}{\partial t} - 3K \frac{\partial u}{\partial x} - 3K \frac{\partial w}{\partial r} = a_3 \tag{15}$$

$$\frac{\partial \sigma_{xr}}{\partial t} - \mu \frac{\partial u}{\partial r} - \mu \frac{\partial w}{\partial x} = a^4 \tag{16}$$

where

$$a_1 = \mp \frac{1}{2} \frac{\alpha_1 (2\sigma_x - \sigma_r - \sigma_\theta)}{1 + \beta\zeta} \frac{w}{r}$$

$$a_2 = \left[E \mp \frac{1}{2} \frac{\alpha_1 (-\sigma_x - \sigma_r + 2\sigma_\theta)}{1 + \beta\zeta} \right] \frac{w}{r}$$

$$a_3 = 3K \frac{w}{r}$$

$$a_4 = \mp \frac{\alpha_2 \sigma_{xr}}{1 + \beta\zeta} \frac{w}{r}$$

$$\alpha_1 = \left[1 + \left(\frac{d\varepsilon_x}{d\varepsilon_\theta} \right)^2 + \left(\frac{d\varepsilon_r}{d\varepsilon_\theta} \right)^2 \right]^{1/2} \beta_1 \alpha$$

$$\alpha_2 = \beta_1 \alpha$$

and E is elastic modulus, ν is Poisson's ratio. Equations (3), (4), and (13) to (16) are the fundamental equations of the problem considered here.

NEARCHARACTERISTIC SOLUTION

The governing equations presented in the previous section together with the auxiliary equations can now be written in matrix form as follows:

$$[A]\{X\} = \{B\} \tag{17}$$

where

$$[A] = \left[\begin{array}{ccc|ccc|ccc}
 & -3K & & & & & -3K & 1 \quad 1 \quad 1 & \\
 & -E & & & & & & 1 \quad -\nu \quad -\nu & \\
 & & & & & & & -\nu \quad -\nu \quad 1 & \\
 & & -\mu & & -\mu & & & & 1 \\
1 & & & 1 & & & & & -\rho \\
 & 1 & & & 1 & & & & -\rho \\
\hline
dx & & & dr & & & dt & & \\
 & dx & & & dr & & & dt & \\
 & & dx & & & dr & & & dt \\
 & & & dx & & & dr & & \\
 & & & & dx & & & dr &
\end{array}\right]$$

$$\{X\} = \left\{ \frac{\partial \sigma_x}{\partial x} \frac{\partial \sigma_r}{\partial x} \frac{\partial \sigma_\theta}{\partial x} \frac{\partial \sigma_{xr}}{\partial x} \frac{\partial u}{\partial x} \frac{\partial w}{\partial x} \;\middle|\; \frac{\partial \sigma_x}{\partial r} \frac{\partial \sigma_r}{\partial r} \frac{\partial \sigma_\theta}{\partial r} \frac{\partial \sigma_{xr}}{\partial r} \frac{\partial u}{\partial r} \frac{\partial w}{\partial r} \right.$$
$$\left. \frac{\partial \sigma_x}{\partial t} \frac{\partial \sigma_r}{\partial t} \frac{\partial \sigma_\theta}{\partial t} \frac{\partial \sigma_{xr}}{\partial t} \frac{\partial u}{\partial t} \frac{\partial w}{\partial t} \right\}^T$$

and

$$\{B\} = \left\{ a_3 a_1 a_2 a_4 - \frac{\sigma_{xr}}{R} \frac{\sigma_\theta - \sigma_r}{R} \;\middle|\; d\sigma_x d\sigma_r d\sigma_\theta d\sigma_{xr} dudw \right\}^T$$

The above set of equations is of hyperbolic type; the conventional bicharacteristic method would be very tedious for six dependent variables. Using the method of nearcharacteristics first proposed by Sauer (ref. 9), we look for characteristic-like lines in the coordinate planes along which the solution can be extended. (Sauer called these lines nearcharacteristics.) The formulation and numerical technique in the nearcharacteristics resembles the one-dimensional approach except that those partial derivatives which do not lie in the plane of interest are considered of zeroth order in that particular calculation. For example, when the bicharacteristics in the x-t plane are of interest, then those terms in [A] containing partial derivative in r-direction are combined with terms in {B} in equation (17). Now following the same procedures as described in reference 8 for one-dimensional case, the nearcharacteristics in the x-t and r-t planes, respectively, are obtained as follows:

$$dx = dr = 0,0 \tag{18}$$

$$C_D = \frac{dx}{dt} = \frac{dr}{dt} = \pm \sqrt{\frac{(1-\nu)}{(1+\nu)(1-2\nu)} \frac{E}{\rho}} \tag{19}$$

$$C_S = \frac{dx}{dt} = \frac{dr}{dt} = \pm \sqrt{\frac{\mu}{\rho}} \tag{20}$$

The nearcharacteristics obtained here indicate that there are two characteristic cones existing in the present analysis; one of them (eq. (19)) corresponds to the longitudinal wave propagation while the other (eq. (20)) corresponds to shear wave. They are right circular cones with their center lines perpendicular to the x-r plane as shown in figure 1. This is an expected result, because the governing equations have constant coefficients for the highest order terms. There are no convected terms appearing in the present analysis. The compatibility equations along the nearcharacteristics can be found in the same way as in the one-dimensional case. In the x-t plane, we have:

$$d\sigma_x = \pm \rho C_D du + C_1 dx + C_2 dt \qquad \text{along } \frac{dx}{dt} = \pm C_D \tag{21}$$

$$d\sigma_{xr} = \pm \rho C_S dw + C_3 dx + C_4 dt \qquad \text{along } \frac{dx}{dt} = \pm C_S \tag{22}$$

$$d\sigma_r = \frac{\nu}{1-\nu} d\sigma_x + C_5 dt \qquad \text{along } dx = 0 \tag{23}$$

$$d\sigma_\theta = \frac{\nu}{1-\nu} d\sigma_x + C_6 dt \qquad \text{along } dx = 0 \tag{24}$$

where

$$C_1 = -\frac{\sigma_{xr}}{R} - \frac{\partial \sigma_{xr}}{\partial r}$$

$$C_2 = \frac{1}{1+\nu}\left[\frac{E\nu}{1-2\nu}\left(\frac{w}{r} + \frac{\partial w}{\partial r}\right) \mp \frac{\alpha_1}{2}\frac{(2\sigma_x - \sigma_r - \sigma_\theta)}{1+\beta\zeta}\frac{w}{r}\right]$$

$$C_3 = \frac{\sigma_\theta - \sigma_r}{R} - \frac{\partial \sigma_r}{\partial r}$$

$$C_4 = \mp \frac{\alpha_2 \sigma_{xr}}{1+\beta\zeta}\frac{w}{r} + \mu \frac{\partial u}{\partial r}$$

$$C_5 = \frac{1}{1-\nu^2}\left\{E\left(\nu \frac{w}{r} + \frac{\partial w}{\partial r}\right) \mp \frac{\alpha_1}{2}\frac{[(1+\nu)\sigma_x - (2-\nu)\sigma_r + (1-2\nu)\sigma_\theta]}{1+\beta\zeta}\frac{w}{r}\right\}$$

$$C_6 = \frac{1}{1-\nu^2}\left\{E\left(\frac{w}{r} + \nu \frac{\partial w}{\partial r}\right) \mp \frac{\alpha_1}{2}\frac{[(1+\nu)\sigma_x + (1-2\nu)\sigma_r - (2-\nu)\sigma_\theta]}{1+\beta\zeta}\frac{w}{r}\right\}$$

Similarly in the r-t plane, we have:

$$d\sigma_r = \mp \rho C_D dw + C_7 dr + C_8 dt \qquad \text{along } \frac{dr}{dt} = \mp C_D \tag{25}$$

$$d\sigma_{xr} = \mp \rho C_S du + C_9 dr + C_{10} dt \qquad \text{along } \frac{dr}{dt} = \mp C_S \tag{26}$$

$$d\sigma_x = \frac{\nu}{1-\nu} d\sigma_r + C_{11} dt \qquad \text{along } dr = 0 \tag{27}$$

$$d\sigma_\theta = \frac{\nu}{1-\nu} d\sigma_r + C_{12} dt \qquad \text{along } dr = 0 \tag{28}$$

where

$$C_7 = \frac{\sigma_\theta - \sigma_r}{R} - \frac{\partial \sigma_{xr}}{\partial x}$$

$$C_8 = \frac{1}{1+\nu}\left[\frac{E\nu}{1-2\nu}\left(\frac{w}{r} + \frac{\partial u}{\partial x}\right) \mp \frac{\alpha_1}{2}\frac{(\sigma_x - 2\sigma_r + \sigma_\theta)}{1+\beta\zeta}\frac{w}{r}\right]$$

$$C_9 = -\frac{\sigma_{xr}}{R} - \frac{\partial \sigma_{xr}}{\partial x}$$

$$C_{10} = \mp \frac{\alpha_2 \sigma_{xr}}{1+\beta\zeta}\frac{w}{r} + \mu \frac{\partial w}{\partial x}$$

$$C_{11} = \frac{1}{1-\nu^2}\left\{E\left(\nu \frac{w}{r} + \frac{\partial u}{\partial x}\right) \mp \frac{\alpha_1}{2}\frac{[(2-\nu)\sigma_x - (1+\nu)\sigma_r - (1-2\nu)\sigma_\theta]}{1+\beta\zeta}\frac{w}{r}\right\}$$

$$C_{12} = \frac{1}{1-\nu^2}\left\{E\left(\frac{w}{r} + \nu \frac{\partial u}{\partial x}\right) \mp \frac{\alpha_1}{2}\frac{[(2\nu-1)\sigma_x - (1+\nu)\sigma_r + (2-\nu)\sigma_\theta]}{1+\beta\zeta}\frac{w}{r}\right\}$$

Note that each set of the above characteristics lies entirely in planes parallel to one of coordinate planes. Equations (21) to (28) have the appearance of a one-dimensional method of characteristics formulation except that they contain the partial derivative terms in the other coordinate direction. The nearcharacteristics equation derived here can be solved numerically by the one-dimensional technique. Two independent solutions can be obtained, each corresponding to one of the coordinate planes.

NUMERICAL EXAMPLE

Consider a central segment of the Clinch River Breeder Reactor steam generator flow shroud with length 2ℓ = 1.0668 m, mean radius 0.47 m, and thickness 0.0127 m. The material is 2.25 Cr-1 Mo at 756 K. The pressure input function was generated by the hydrodynamics module (ref. 10). A constant volume, step pressure pulse of 13.79 MPa was taken as the source pressure p at the center. This is typical of the maxima observed in large sodium-water reaction experiments during the transient period. Since the pressure loading was supposed to be symmetric with respect to the mid-span, only half-length of the shell needed to be considered here. The boundary conditions for the example are shown in figure 2 as follows:

$$\left.\begin{aligned} u = 0 \quad &\text{and} \quad \sigma_{xr} = 0 \quad \text{at } x = 0 \\ u = 0 \quad &\text{and} \quad w = 0 \quad \text{at } x = \ell \\ \sigma_{xr} = 0 \quad &\text{and} \quad \sigma_r = -p(x,t) \quad \text{at } r = 0 \\ \sigma_{xr} = 0 \quad &\text{and} \quad \sigma_r = 0 \quad \text{at } r = H \end{aligned}\right\} \tag{29}$$

It has been shown in reference 11 that the two independent solutions, each based on one coordinate plane, are numerically unstable while a calculation method obtained by averaging the above mentioned independent solution yields a stable solution. In view of equations (21), (22) and the boundary conditions (29), it appears that the nearcharacteristics equations in x-t plane are not a proper choice at r = 0 and r = H because σ_r are being prescribed there. Therefore a combination technique is proposed here: on the boundaries r = 0 and r = H the solutions are obtained from r-t plane nearcharacteristics equations while at other points the solutions are obtained from the x-t plane. The numerical results here show that this leads to a stable solution. The advantage of this technique over the averaging method is a tremendous saving in computation time. The resulting pressure history at the midspan (x = 0) of the middle surface of the shell is shown in figure 3. The resultant dynamic response of radial displacement and velocity as a function of time for the same center point of the shell is also shown in the figure. In figure 4, shell displacement profiles are shown for several times.

CONCLUDING REMARKS

The endochronic theory of plasticity originated by Valanis has been applied to study the axially symmetric motion of circular cylindrical thick shells subjected to an arbitrary pressure transient applied at its inner

surface. The constitutive equations for the thick shells have been obtained. The governing equations are then solved by means of the nearcharacteristics method. It has been shown that a stable solution can be obtained by treating the radial boundaries in one coordinate plane while at other points the solutions obtain from the other coordinate plane.

REFERENCES

1. Valanis, K. C.: A Theory of Viscoplasticity without a Yield Surface, Part I, General Theory. Arch. Mech. Stosow., vol. 23, 1971, pp. 517-534.

2. Valanis, K. C.: On the Foundations of the Endochronic Theory of Viscoplasticity. Arch. Mech. Stosow., vol. 27, 1975, pp. 857-868.

3. Valanis, K. C.: A Theory of Viscoplasticity without a Yield Surface, Part II, Application to the Mechanical Behavior of Metals. Arch. Mech. Stosow., vol. 23, 1971, pp. 535-551.

4. Bazant, Z. P.: A New Approach to Inelasticity and Failure of Concrete, Sand and Rock-Endochronic Theory. Proceeding of 11th Annual Meeting, Soc. Eng. Sci., Duke Univ., 1974.

5. Wu, H. C.; and Lin, H. C.: Plastic Waves in a Thin-Walled Tube under Combined Longitudinal and Torsional Loads. 10th Anniversary Meeting, Soc. Eng. Sci., North Carolina State Univ., Nov. 1973.

6. Wu, H. C.; and Lin, H. C.: Combined Plastic Waves in a Thin-Walled Tube. Int. J. Solids Struct., vol. 10, 1974, pp. 903-917.

7. Lin, H. C.: Dynamic Plastic Deformation of Shell - An Endochronic Solution. Trans. Am. Nucl. Soc., vol. 22, 1975, pp. 567-568.

8. Lin, H. C.: Dynamic Plastic Deformation of Axi-Symmetric Circular Cylindrical Shells. Nucl. Eng. Design, vol. 35, 1975, pp. 283-293.

9. Sauer, R.: Differenzenverfahren für hyperbolishe Anfangswertprobleme bei mehr als zwei unabhängigen Veränderlichen mit Hilfe von Nebencharakteristiken. Numerische Mathematik, vol. 5, 1963, pp. 55-67.

10. Shin, Y. W.; and Valentin, R. A.: Dynamic Structural Loads Produced by Large Sodium-Water Reaction in LMFBR Steam Generators. 3rd SMiRT, London, UK, 1975, Paper E4/5*.

11. Shin, Y. W.; and Kot, C. A.: Two-Dimensional Fluid-Hammer Analysis by the Method of Nearcharacteristics. Argonne National Laboratory, ANL-75-21, 1975.

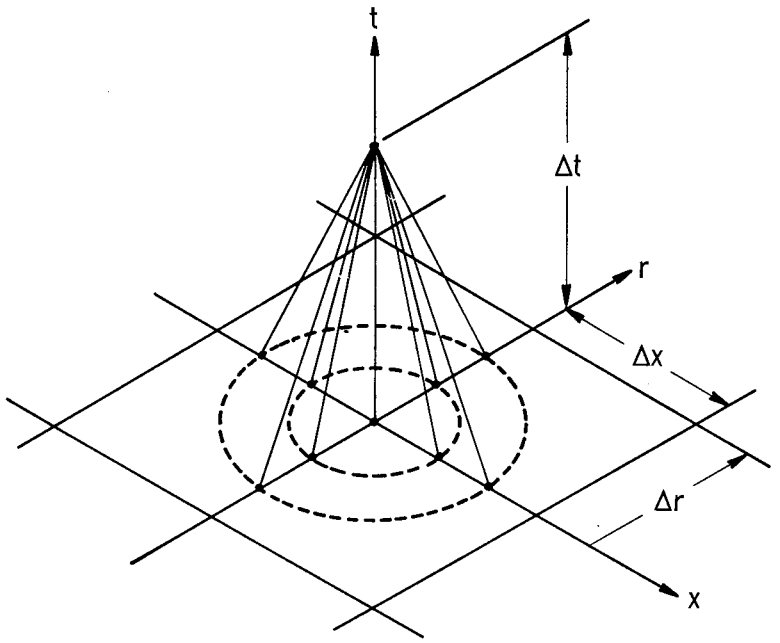

Figure 1.- Nearcharacteristics lines.

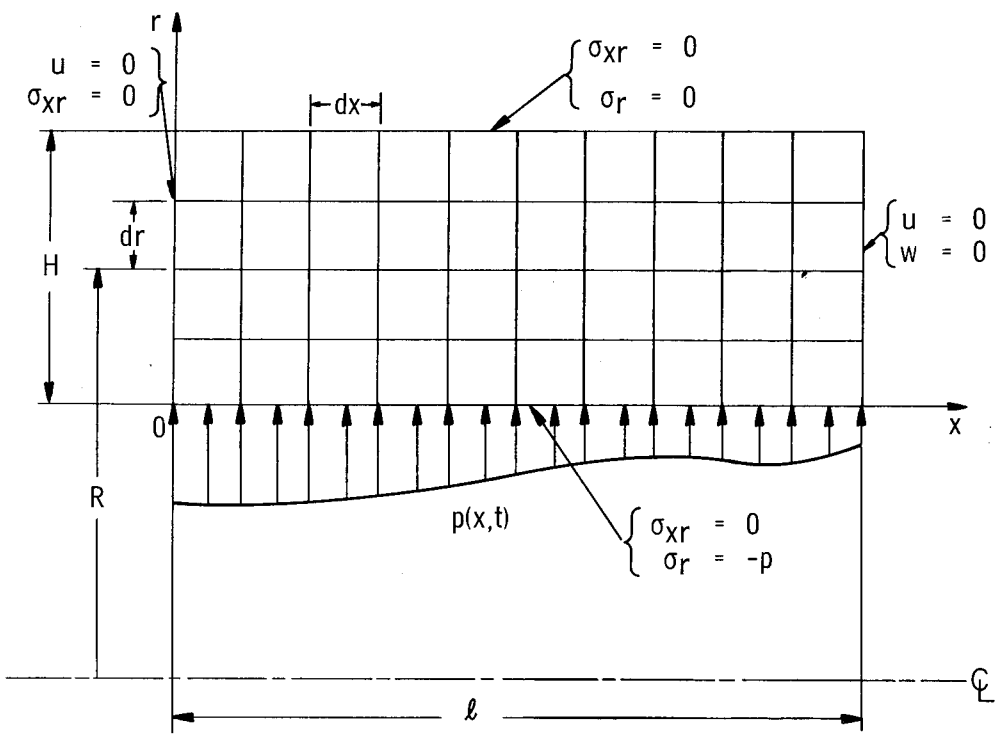

Figure 2.- Boundary conditions.

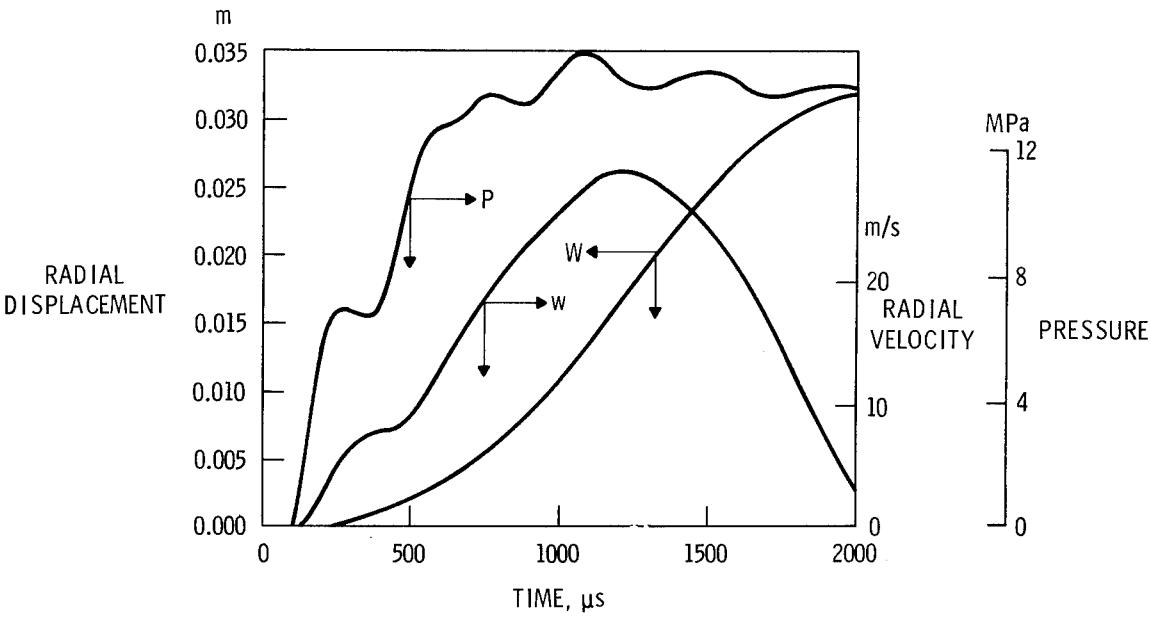

Figure 3.- Radial displacement velocity, pressure history at x = 0.

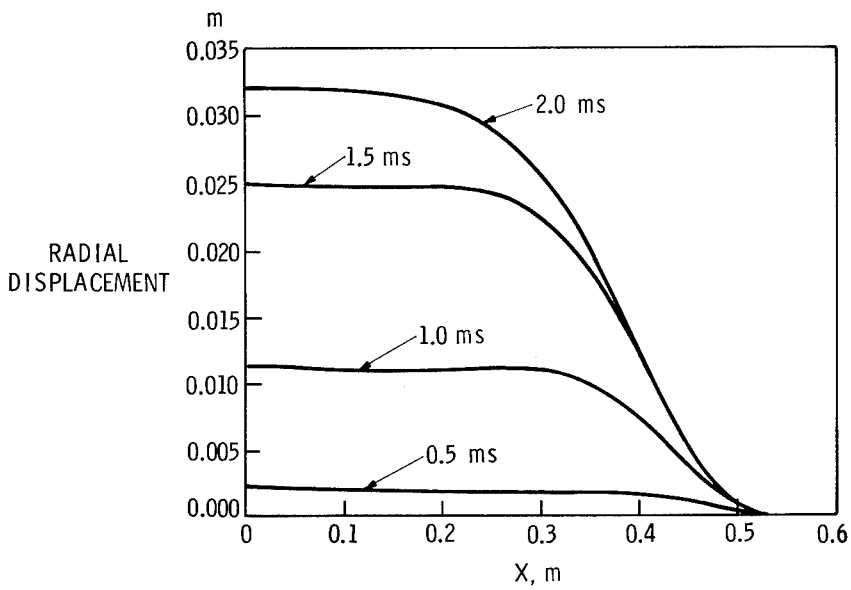

Figure 4.- Radial displacement profiles.

VIBRATIONS AND STRESSES IN LAYERED ANISOTROPIC CYLINDERS

G. P. Mulholland
New Mexico State University

B. P. Gupta
Fluor Engineers and Constructors, Inc.

SUMMARY

An equation describing the radial displacement in a k layered anisotropic cylinder has been obtained. The cylinders are initially unstressed but are subjected to either a time-dependent normal stress or a displacement at the external boundaries of the laminate. The solution is obtained by utilizing the Vodicka orthogonalization technique. Numerical examples are given to illustrate the procedure.

INTRODUCTION

The problems associated with the vibrations of plates and shells have been of concern to many investigators over the years. Most of these works for a single layered homogeneous material are summarized in two monographs by Leissa (ref. 1,2) and the reader is referred there for further references. Since composite materials have become popular due to their mechanical and thermal properties, it has become necessary to study their behavior to determine their unique characteristics before they can be used effectively. Recently Cobble (ref. 3) and Dong and Nelson (ref. 4) considered the vibration problem in laminated plates and the references contained in these papers summarize the work in this area quite well. For works concerned with anisotropic and layered cylinders, the book of Ambartsumyan (ref. 5) and Hearmon (ref. 6) and the papers of Gulati and Essenburg (ref. 7), Stavsky and Smolash (ref. 8), Cheung and Wu (ref. 9), and Nelson et al. (ref. 10) are representative.

In this paper, the radial vibrations of a layered anisotropic cylinder are considered. The cylinders are solidly joined at their interfaces, are initially unstressed, and can be subjected to either arbitrary time-dependent normal stresses or displacements at the external boundaries of the system. The solution is obtained by using a dependent variable transformation in the displacement equation thereby obtaining a new partial differential equation with homogeneous external boundary conditions; the Vodicka orthogonality conditions are then applied to this new system to obtain the final solution. The plane strain situation is considered for this analysis.

To illustrate the efficient and straight-forward manner in which solutions can be obtained with this method, numerical examples are given for a two-layered

composite. Results are presented for the displacement, normal stress, tangential stress, and axial stress components at two interior positions.

SYMBOLS

B_i, D_i	constants, (eq. (1))
C_{i11}, C_{i12}	constants, (eq. (2))
E_{i1}, E_{i2}, E_{i3}	Young's modulus for r, θ, and z directions, dyne/cm^2
$F_j(t)$	function of time, (eq. (5))
$H_{ij}(r,t)$	function of displacement and time, (eq. (10))
$J_{Di}(r)$	Bessel function of first kind of order D_i
$L_{ij}(r)$	function of r, (eq. (4))
p_m, q_m	constants, (eq. (23))
r	radial coordinate, cm
t	time, seconds
$u_i(r,t)$	radial displacement, cm
$u_m(t)$	function of time, (eq. (11))
W_i	weighting function, (eq. (17))
$X_{im}(r)$	eigenfunction
Y_{Di}	Bessel function of the second kind of order D_i
α_m	eigenvalues, 1/sec
Δ	constant
ν	Poisson's ratio
σ_{ir}, $\sigma_{i\theta}$, σ_{iz}	normal stress in r, θ, and z directions, dyne/cm^2
$\phi_1(t)$, $\phi_2(t)$	functions of time, (eq. (2))
$\psi_1(r)$, $\psi_2(r)$	functions of r, (eq. (9))

PROBLEM

The partial differential equation describing the displacement u_i for the i^{th} layer of a multilayered cylindrical composite whose material properties are constant for each layer is given by

$$\frac{\partial^2 u_i}{\partial r^2}(r,t) + \frac{1}{r}\frac{\partial u_i}{\partial r}(r,t) - \frac{D_i^2}{r^2}u_i(r,t) = \frac{1}{B_i^2}\frac{\partial^2 u_i}{\partial t^2}(r,t) \qquad (1)$$

where

$$D_i^2 = \frac{E_{2i}}{E_{1i}}\,\frac{1-\nu_{31i}\nu_{13i}}{1-\nu_{32i}\nu_{23i}}$$

$$B_i^2 = \frac{E_{1i}}{\rho_i}\,\frac{1-\nu_{32i}\nu_{23i}}{\Delta_i}$$

$$\Delta = (1-\nu_{31i}\nu_{13i})(1-\nu_{32i}\nu_{231}) - (\nu_{21i} + \nu_{31i}\nu_{23i})(\nu_{12i} + \nu_{32i}\nu_{13i})$$

The boundary and initial conditions associated with equation (1) are:

a) $$\sigma_r(r_1,t) = C_{111}\frac{\partial u_1}{\partial r}(r_1,t) + C_{112}\frac{u_1(r_1,t)}{r_1} = \phi_1(t)$$

b) $$\sigma_r(r_{k+1},t) = C_{k11}\frac{\partial u_k}{\partial r}(r_{k11},t) + C_{k12}\frac{u_k}{r_{k+1}}(r_{k+1},t) = \phi_2(t)$$

c) $$u_i(r_{k+1},t) = u_{i+1}(r_{i+1},t)$$

d) $$C_{i11}\frac{\partial u_i}{\partial r}(r_{i+1},t) + C_{i12}\frac{u_i}{r_{i+1}}(r_{i+1},t) = C_{i+1,11}\frac{\partial u_{i+1}}{\partial r}(r_{i+1},t) + C_{i+1,12}\frac{u_{i+1}(r_{i+1},t)}{r_{i+1}} \qquad (2)$$

e) $$u_i(r,o) = 0$$

f) $$\frac{\partial u_i}{\partial t}(r,o) = 0$$

where

$$C_{i11} = \frac{E_{1i}}{\Delta_i}(1-\nu_{32i}\nu_{23i})$$

$$C_{i12} = \frac{E_{1i}}{\Delta_i}(\nu_{21i} + \nu_{31i}\nu_{23i})$$

The boundary and initial conditions given by equation (2) assume that either the radial stresses or displacements are known at the external boundaries and that the radial stresses and displacements are continuous at the interfaces.

To obtain homogeneous external boundary conditions, let

$$u_i(r,t) = U_i(r,t) + \sum_{j=1}^{2} L_{ij}(r)F_j(t) \tag{3}$$

where

$$L_{ij}(r) = A_{ij}r^{Di} + B_{ij}/r^{Di}, \quad j=1,2 \tag{4}$$

$$F_j(t) = \phi_j(t), \quad j=1,2 \tag{5}$$

and

$$\nabla^2 L_{ij}(r) - \frac{D_i^2}{r^2} L_{ij}(r) = 0 \tag{6}$$

For a cylinder with $r_1 = 0$ (solid cylinder) and $D_1 \leq 1$, Eq. (4) and (6) take the following form for i = 1:

$$L_{1j}(r) = A_{1j}$$

and

$$\nabla^2 L_{1j} - \frac{D_1^2}{r^2} L_{1j}(r) = \frac{-A_{1j}D_1^2}{r^2}$$

The functions $L_{ij}(r)$ satisfy the following boundary conditions:

a) $$C_{111}\frac{dL_{ij}}{dr}(r_1) + C_{112}\frac{L_{ij}(r_1)}{r_1} = \begin{cases} 1, & j=1 \\ 0, & j=2 \end{cases}$$

b) $$C_{k11}\frac{dL_{kj}}{dr}(r_{k+1}) + C_{k12}\frac{L_{kj}}{r_{k+1}}(r_{k+1}) = \begin{cases} 0, & j=1 \\ 1, & j=2 \end{cases} \qquad (7)$$

c) $$L_{ij}(r_{i+1}) = L_{i+1,j}(r_{i+1})$$

d) $$C_{i11}\frac{dL_{ij}}{dr}(r_{i+1}) + C_{i12}\frac{L_{ij}(r_{i+1})}{r_{i+1}} = C_{i+1,11}\frac{dL_{ij}}{dr}(r_{i+1}) + C_{i+1,12}\frac{L_{i+1,j}(r_{i+1})}{r_{i+1}}$$

Substitution of equation (3) into equations (1) and (2) yields the following partial differential equation with homogeneous external boundary conditions:

$$\frac{\partial^2 U_i}{\partial r^2}(r,t) + \frac{1}{r}\frac{\partial U_i}{\partial r}(r,t) - \frac{D_i^2}{r^2}U_i(r,t) = \frac{1}{B_i^2}\frac{\partial^2 U_i}{\partial t^2}(r,t) + H_{ij}(r,t) \qquad (8)$$

with

a) $$C_{111}\frac{\partial U_1}{\partial r}(r_1,t) + C_{112}\frac{U_1(r_1,t)}{r_1} = 0$$

b) $$C_{k11}\frac{\partial U_k}{\partial r}(r_{k+1},t) + C_{k12}\frac{U_k(r_{k+1},t)}{r_{k+1}} = 0 \qquad (9)$$

c) $$U_i(r_{i+1},t) = U_{i+1}(r_{i+1},t)$$

d) $$C_{i11}\frac{\partial U_i}{\partial r}(r_{i+1},t) + C_{i12}\frac{U_i(r_{i+1},t)}{r_{i+1}} = C_{i+1,11}\frac{\partial U_{i+1}}{\partial r}(r_{i+1},t) + C_{i+1,12}\frac{U_{i+1}(r_{i+1},t)}{r_{i+1}}$$

e) $$U_i(r,o) = -\sum_{j=1}^{2} L_{ij}(r)\,F_j(0) = \psi_1(r)$$

f) $$\frac{\partial U_i}{\partial t}(r,o) = -\sum_{j=1}^{2} L_{ij}(r)\, F_j'(0) = \psi_2(r)$$

and where

$$H_{ij}(r,t) = \frac{1}{B_i^2} \sum_{j=1}^{2} L_{ij}(r) F_j''(t) \tag{10}$$

SOLUTION: $U_i(r,t)$

The problem has now been sufficiently simplified so that a series solution for $U_i(r,t)$ can be assumed where the orthogonality conditions developed by Vodicka (ref. 11) can be utilized. Let

$$U_i(r,t) = \sum_{m=1}^{\infty} u_m(t) X_{im}(r)$$

$$r_i \leq r \leq r_{i+1},\ i = 1,2,3,\ldots,k, t \geq 0 \tag{11}$$

where the function $u_m(t)$ is to be determined from the initial conditions and the functions $X_{im}(r)^m$ are eigenfunctions of the eigenvalue problem

$$\frac{B_i^2}{r}\frac{d}{dr}\left[r\frac{dX_{im}}{dr}(r)\right] - \frac{B_i^2 D_i^2}{r^2} X_{im}(r) + \alpha_m^2 X_{im}(r) = 0 \tag{12}$$

with

a) $$C_{111}\frac{dX_{1m}}{dr}(r_1) + C_{112}\frac{X_{1m}(r_1)}{r_1} = 0$$

b) $$C_{k11}\frac{dX_{km}}{dr}(r_{k+1}) + C_{k12}\frac{X_{km}(r_{k+1})}{r_{k+1}} = 0 \tag{13}$$

c) $$X_{im}(r_{k+1}) = X_{i+1,m}(r_{k+1})$$

d) $$C_{i11}\frac{dX_{im}}{dr}(r_{i+1}) + C_{i12}\frac{X_{im}(r_{i+1})}{r_{i+1}} = C_{i+1,11}\frac{dX_{i+1,m}}{dr}(r_{i+1})$$

$$+C_{i+1,12}\frac{X_{i+1,m}(r_{i+1})}{r_{i+1}}$$

The solution of equation (12) is

$$X_{im}(r) = A_{im} J_{Di}\left(\frac{\alpha_m}{B_i} r\right) + B_{im} J_{-Di}\left(\frac{\alpha_m}{B_i} r\right), \quad D_i = \text{non-integer} \tag{14}$$

$$X_{im}(r) = A_{im} J_{Di}\left(\frac{\alpha_m}{F_i} r\right) + B_{im} Y_{Di}\left(\frac{\alpha_m}{B_i} r\right), \quad D_i = \text{integer} \tag{15}$$

The eigenvalues, α_m, are found by substituting equations (14) or (15) into the boundary conditions, (eq. (13)). The 2k linear homogeneous equations that result from this substitution are then solved for the constants A_{im} and B_{im} (ref. 12).

The orthogonality condition for the eigenfunctions is

$$\sum_{i=1}^{k} \int_{r_1}^{r_{i+1}} W_1^2 \, r \, X_{im}(r) \, X_{in}(r) dr = \begin{cases} \text{(const. } m = n) \\ 0, \; m \neq n \end{cases} \tag{16}$$

where

$$W_i^2 = C_{i11}/B_i^2 = \rho_i \tag{17}$$

The functions $L_{ij}(r)$ and $H_{ij}(r,t)$ will satisfy Dirichlet's conditions so they can be expanded in an infinite series of the eigenfunctions

$$L_{ij}(r) = \sum_{m=1}^{\infty} \ell_{mj} X_{im}(r), \; j = 1,2 \tag{18}$$

and

$$B_i^2 \, H_{ij}(r,t) = \sum_{m=1}^{\infty} [\ell_{mj} F_j''(t)] \, X_{im}(r), \; j = 1,2 \tag{19}$$

where

$$\ell_{mj} = \frac{1}{N_m} \sum_{i=1}^{k} \rho_i \int_{r_1}^{r_{i+1}} r L_{ij}(r) \, X_{im}(r) \, dr, \; j = 1,2 \tag{20}$$

and

$$N_m = \sum_{i=1}^{k} \rho_i \int_{r_1}^{r_{i+1}} r\,[X_{im}^2(r)]\,dr \tag{21}$$

Substituting equations (11), (18), and (19) into equation (8), we obtain the following relationship:

$$\sum_{m=1}^{\infty} \left[\frac{d^2 u_m}{dt^2}(t) + \alpha_m^2\, u_m(t) + \sum_{j=1}^{2} \ell_{mj} F_j''(t) \right] X_{im}(r) = 0 \tag{22}$$

The initial conditions asssociated with equation (28) are obtained in the following manner:

$$U_i(r,o) = \sum_{m=1}^{\infty} u_m(o)\, X_{im}(r) = \psi_1(r) = -\sum_{m=1}^{\infty} \ell_{mj} F_j(o)\, X_{im}(r)$$

and

$$\frac{\partial U_i}{\partial t}(r,o) = \sum_{m=1}^{\infty} u_m'(o)\, X_{im}(r) = \psi_2(r) = -\sum_{m=1}^{\infty} \ell_{mj} F_j'(o)\, X_{im}(r)$$

Thus

$$\text{a)}\quad u_m(o) = -\sum_{j=1}^{2} \ell_{mj}\, F_j(o) = p_m$$

$$\text{b)}\quad u_m'(o) = -\sum_{j=1}^{2} \ell_{mj}\, F_j'(o) = q_m \tag{23}$$

The solution of equation (22) subject to the initial conditions (eq. (23)) is

$$u_m(t) = \frac{q_m}{\alpha_m} \sin \alpha_m t + p_m \cos \alpha_m t - \sum_{j=1}^{2} \frac{\ell_{mj}}{\alpha_m} F_j''(t) * \sin(\alpha_m t) \tag{24}$$

where the symbol * denotes convolution. Substitution of equation (24) into equation (11) and that result into equation (3) gives the desired relationship for the radial displacement of the composite cylinders:

$$u_i(r,t) = \sum_{j=1}^{2} L_{ij}(r)\, F_j(t) + \sum_{m=1}^{2} u_m(t)\, X_{im}(r) \tag{3}$$

where the functions $L_{ij}(r)$, $F_j(t)$, $X_{im}(r)$ and $u_m(t)$ are given by equations (4), (5), (14) or (15), and (24), respectively.

STRESS

The stress in the i^{th} section of the composite is given by

$$\sigma_{ir} = \frac{E_1}{\Delta_i} \left((1-\nu_{32}\nu_{23}) \frac{\partial u_i}{\partial r}(r,t) + (\nu_{21} + \nu_{31}\nu_{23}) \frac{u_i(r,t)}{r} \right) \tag{25}$$

$$\sigma_{i\theta} = \frac{E_2}{\Delta_i} \left((\nu_{12} + \nu_{32}\nu_{13}) \frac{\partial u_i}{\partial r}(r,t) + (1 - \nu_{31}\nu_{13}) \frac{u_i(r,t)}{r} \right) \tag{26}$$

$$\sigma_{iz} = \frac{\nu_{13}E_3}{E_1} \left(\sigma_{ir} + \frac{\nu_{23}E_3}{E_2} \nu_{i\theta} \right) \tag{27}$$

EXAMPLE

Consider a two-layered composite with the following properties:

Layer 1	Layer 2
$\rho_1 = 1.73$ gm/cm^3	$\rho_2 = 1.75$ gm/cm^3
$\nu_{121} = \nu_{131} = 0.11$	$\nu_{122} = \nu_{132} = 0.14$
$\nu_{211} = \nu_{311} = 0.16$	$\nu_{212} = \nu_{312} = 0.18$
$\nu_{231} = \nu_{321} = 0.1$	$\nu_{232} = \nu_{322} = 0.22$
$E_{11} = 7.93 \times 10^5$ newton/cm^2	$E_{12} = 6.6 \times 10^5$ newton/cm^2
$E_{21} = E_{31} = 1.14 \times 10^6$ newton/cm^2	$E_{22} = E_{32} = 8.76 \times 10^5$ newton/cm^2

The above properties are typical of some of the more common graphites (ATJ and CHQ) (ref. 13). Assume further that there is a normal stress applied at the outer boundary of the cylinder.

$$\phi_2(t) = 6895 \sin (10t) \text{ N/cm}^2$$

and the physical dimensions are

$$r_1 = 0;\ r_2 = 2.54 \text{ cm};\ r_3 = 5.08 \text{ cm}$$

Following the procedures outlined in the text, the radial displacement and the radial and tangential stresses within the composite are obtained; values at two positions are shown in Figures 1 through 3.

SUMMARY

A closed-form solution for the radial displacement in layered orthotropic cylinders has been obtained. The solution can be programmed on a modern computer which enables one to calculate natural frequencies, displacements and stresses quite easily. The functions ℓ_{mj} and N_m can either be integrated directly by hand or a numerical integration subroutine can be written to perform the calculations.

REFERENCES

1. Leissa, A. W., Vibration of Plates, Scientific and Technical Information Office, NASA, Washington, D. C., 1969, NASA SP-160.

2. Leissa, A. W., Vibration of Shells, Scientific and Technical Information Office, NASA, Washington, D. C., 1973, NASA SP-288.

3. Cobble, M. H., "Dynamic Vibrations and Stresses in Composite Elastic Plates," Journal of the Acoustical Society of America, Vol. 46, No. 5, pp. 1969, pp. 1175-1179.

4. Dong, S. B. and Nelson, R. B., "On Natural Vibrations and Waves in Laminated Orthotropic Plates," ASME Paper No. 72-APM-14.

5. Ambartsumyan, S. A., Theory of Anisotropic Plates, Technomic Publishing Co., Stamford, Conn.

6. Hearmon, R. F. S., Applied Anisotropic Elasticity, Oxford University Press, London, 1961.

7. Gulati, S. T. and Essenburg, F., "Effects of Anisotropy in Axisymmetric Cylindrical Shells," Journal of Applied Mechanics, Vol. 34, No. 3, Trans., ASME, Vol. 89, Series E., 1967, pp. 659-666.

8. Stavsky, Y. and Smolash, I., "Thermoelasticity of Heterogeneous Orthotropic Cylindrical Shells," International Journal of Solids and Structures, Vol. 6, 1970, pp. 1211-1231.

9. Cheung, Y. K., and Wu, C. I., "Free Vibrations of Thick, Layered Cylinders Having Finite Length With Various Boundary Conditions," Journal of Sound and Vibrations, Vol. 24, No. 2, 1972, pp. 189-200.

10. Nelson, R. B., Dong, S. B. and Kalro, R. D., "Vibrations and Waves in Laminated Orthotropic Circular Cylinders," Journal of Sound and Vibration, Vol. 18, No. 3, 1971, pp 429-444.

11. Vodicka, B., "Warmeleitung in geschichteten Kugel and Zylinderkorpern Schweiz. Arch. Vol. 10, 1950, pp. 297-304.

12. Mulholland, G. P. and Cobble, M. H., "Diffusion Through Composite Media," International Journal of Heat and Mass Transfer, Vol. 15, 1972, pp. 147-159

13. Industrial Graphite Engineering Handbook, Union Carbide Corporation, New York, 1970.

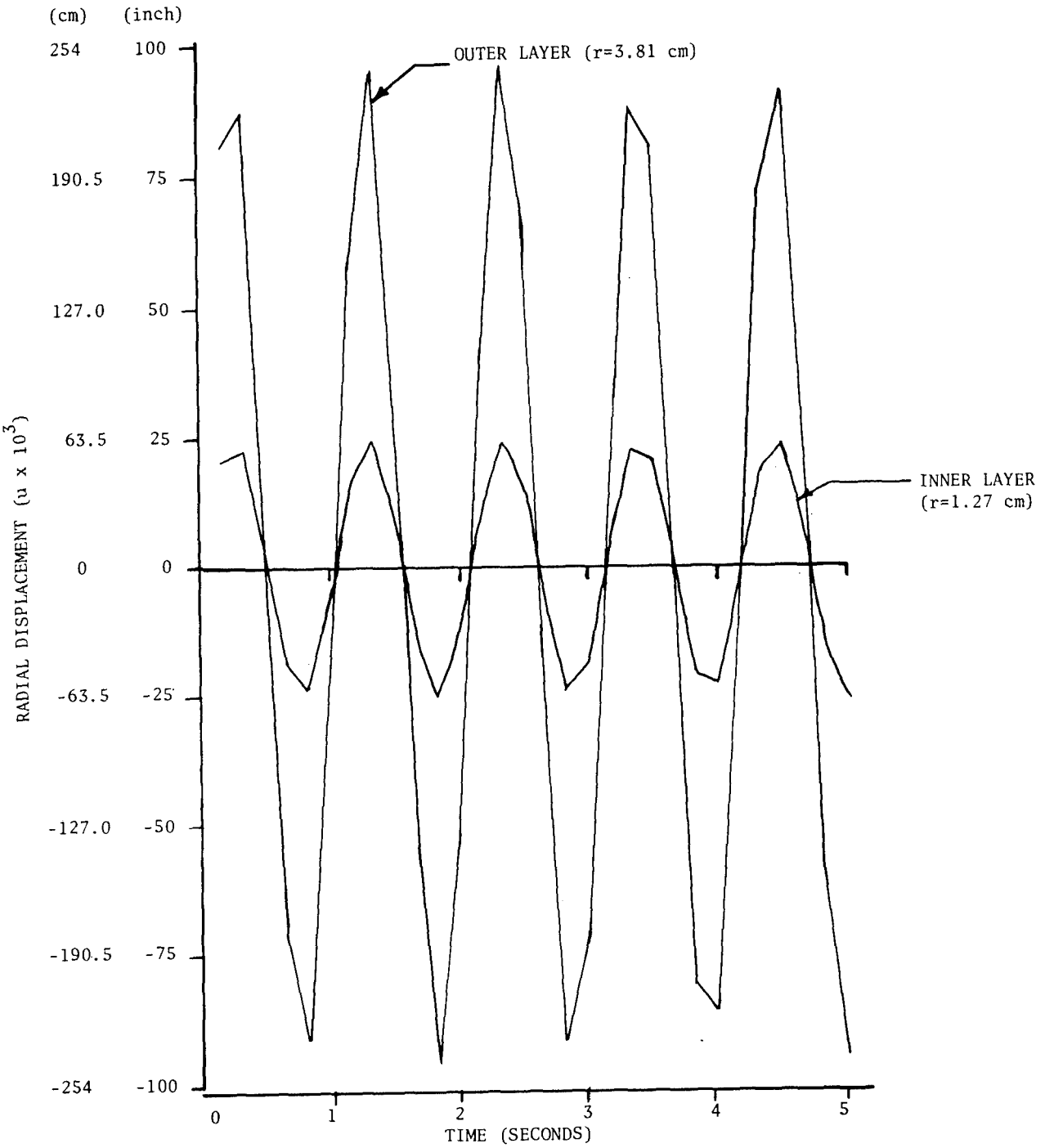

Figure 1.- Radial displacement of composite.

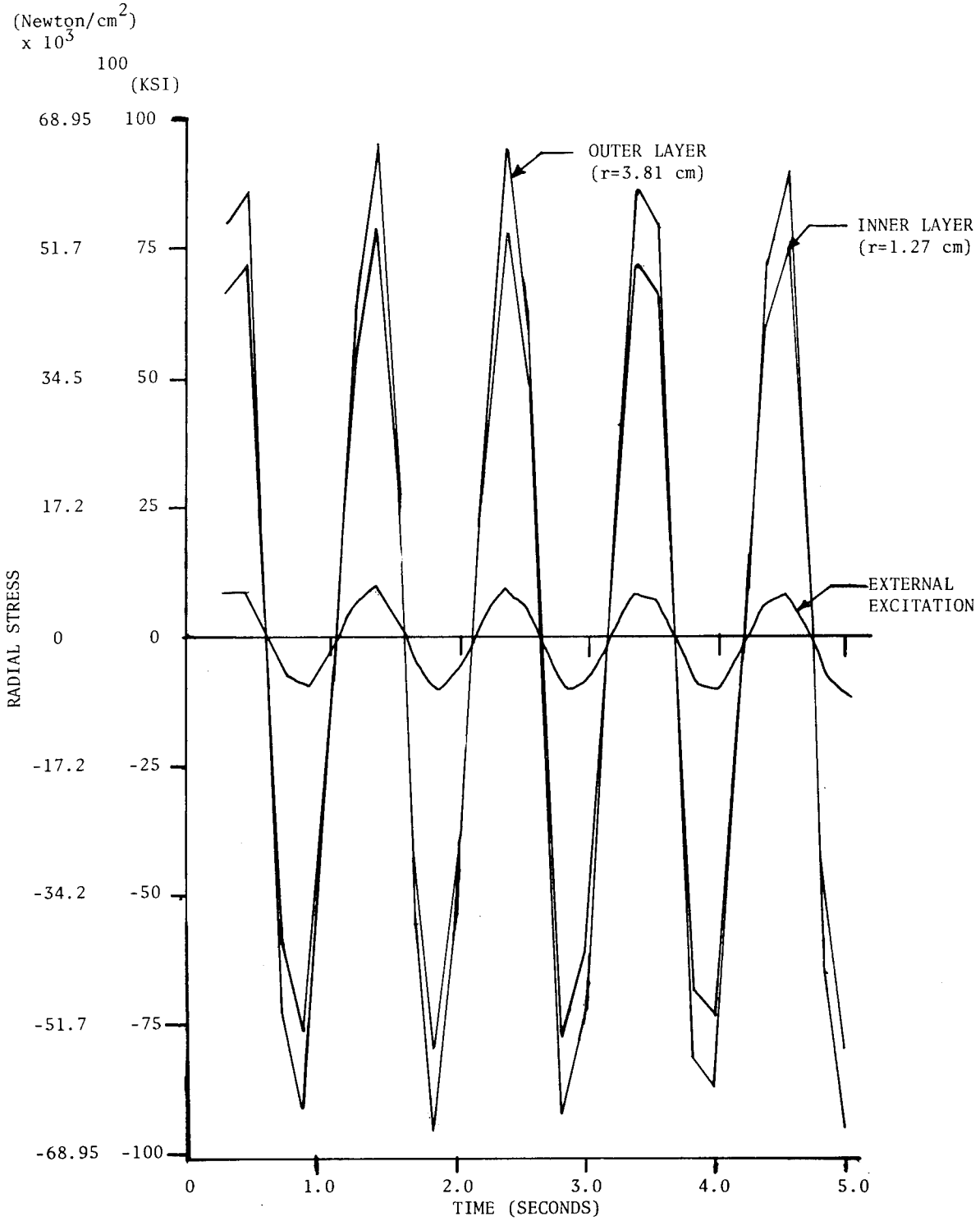

Figure 2.- Radial stress compared to external excitation.

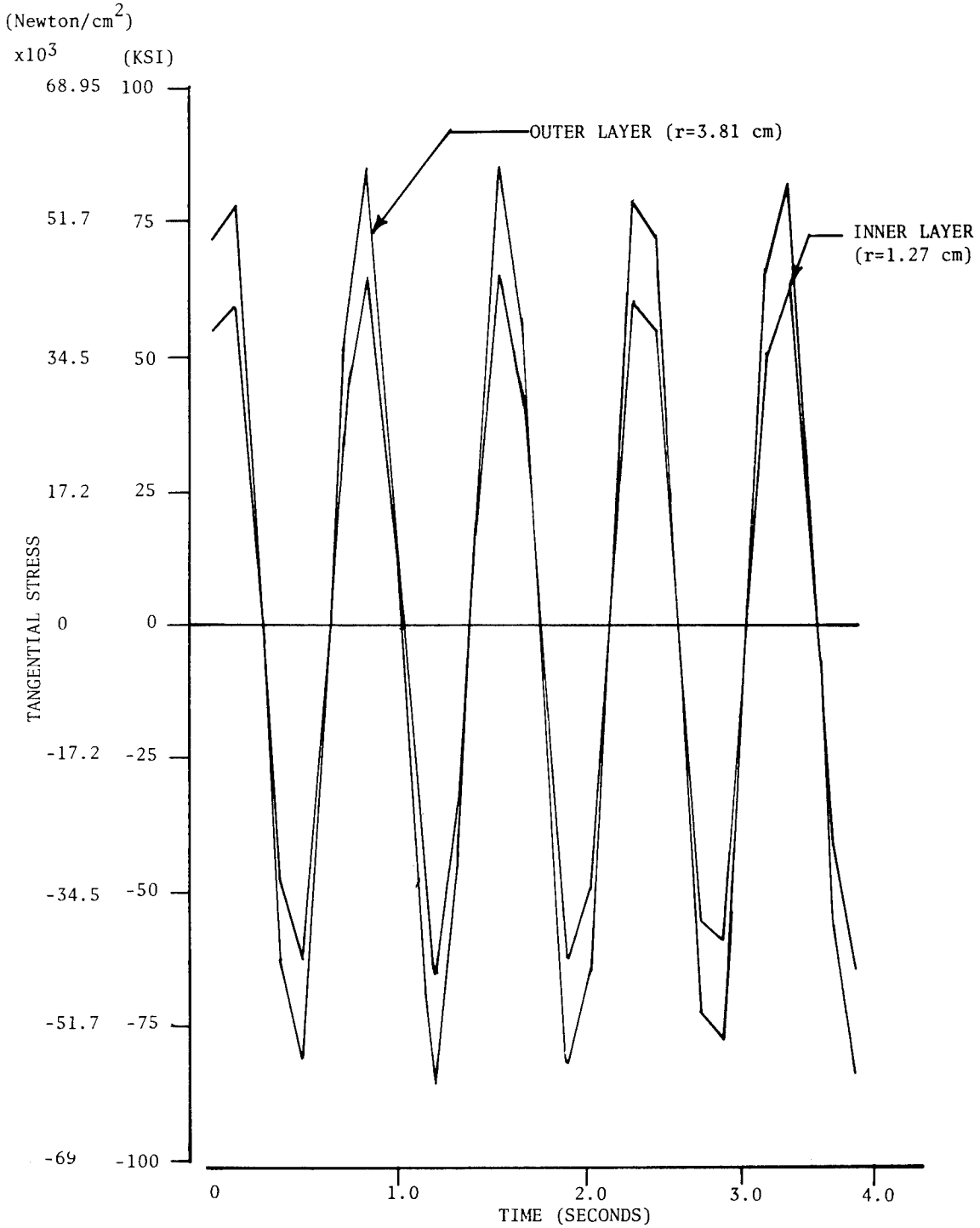

Figure 3.- Tangential stresses within composite.

INCREMENTAL ANALYSIS OF LARGE ELASTIC DEFORMATION OF A ROTATING CYLINDER

George R. Buchanan
Tennessee Technological University

INTRODUCTION

The effect of finite deformation upon a rotating, orthotropic cylinder was investigated by Sandman (ref. 1). He was able to predict the influence of finite deformations and relate his results to the degree of orthotropy. In this study an attempt has been made to study the same problem using a general incremental theory.

The incremental equations of motion are developed using the variational principle discussed by Washizu (ref. 2). A more than adequate development of the governing equations has been given by Atluri (ref. 3). Although his intention is to implement a finite element scheme to solve boundary value problems, the equations are given in general tensor notation. Hofmeister, Greenbaum, and Evensen (ref. 4) have presented an excellent discussion of the use of an incremental analysis; again, their goal is the application of a finite element analysis. The governing equations are also developed in the treatise by Biot (ref. 5), using both a geometrical viewpoint and a variational method. The governing equations are rederived here, in somewhat less detail, using the principle of virtual work for a body with initial stress (ref. 2).

The governing equations are reduced to those for the title problem and a numerical solution is obtained using finite difference approximations. Since the problem is defined in terms of one independent space coordinate, the finite difference grid can be modified as the incremental deformation occurs without serious numerical difficulties. The nonlinear problem is solved incrementally by totaling a series of linear solutions. This method was used to solve the same problem discussed in ref. 1 and gave identical results.

GOVERNING EQUATIONS

The derivation of the governing equations is based upon an incremental variational principle (ref. 2). The body is assumed to be in equilibrium at some arbitrary reference state along the load path. Let

$$\vec{x} = \vec{a} + \vec{u} \tag{1}$$

be the transformation of a particle at point $\vec{a}$ to point $\vec{x}$ in the same space, then $\vec{u}$ is the displacement of the particle. At the beginning of some increment of load, $\vec{a}$ is the initial coordinate and $\vec{x}$ is the current coordinate, and the

two are identical. Let initial stresses $\underline{\sigma}^o$, initial surface tractions $\vec{t}^o$, and initial body forces $\vec{f}^o$ act on the body before the addition of the load increment. These stresses and loads are with respect to the initial coordinate axis and are referred to a unit area before the loading increment is applied; hence, they are referred to an undeformed area and volume.

Assuming the initial stress system is in equilibrium, it follows that,

$$\text{div } \underline{\sigma}^o + \vec{f}^o = 0 \tag{2}$$

$$\underline{\sigma}^o \vec{n} = \vec{t}^o \tag{3}$$

where $\vec{n}$ is a unit normal vector. If the body is then loaded with some increment of surface traction or body force, the total stresses at the end of that increment of load are the sum of the initial stresses and incremental stresses.

In order to formulate the principle of virtual work, first define a nonlinear strain tensor, such as,

$$\underline{D} = \underline{E} + \underline{N} \tag{4}$$

where

$$\underline{E} = (\nabla \underline{u} + \nabla \underline{u}^T) \tag{5}$$

$$\underline{N} = (\nabla \underline{u}^T \nabla \underline{u}) \tag{6}$$

where $\vec{u}$ is the displacement field corresponding to $\underline{D}$ and $\underline{D}$ is referred to as Green's strain tensor (ref. 6). The notation is basically the direct notation used by Gurtin (ref. 7), although some symbols are different.

Introduce a virtual displacement $\delta\vec{u}$ and incremental stresses, body forces, and surface tractions, $\underline{\sigma}$, $\vec{f}$, and $\vec{t}$, respectively. The principle of virtual work for a body with initial stress may be written,

$$\int_V \{(\underline{\sigma}^o+\underline{\sigma})\cdot\delta\underline{D}-(\vec{f}^o+\vec{f})\cdot\delta u\}dv-\int_{S_1}(\vec{t}^o+\vec{t})\cdot\delta\vec{u}dS = 0 \tag{7}$$

where S_1 corresponds to the surface on which stresses are specified. Substituting equations (5) and (6) into (7) and noting that $\underline{\sigma}^o$ and $\underline{\sigma}$ are symmetric yields

$$\int_V \{\underline{\sigma}^o\cdot\delta\nabla\underline{u}+\underline{\sigma}^o\cdot\nabla\underline{u}^T\delta\nabla\underline{u}+\underline{\sigma}\cdot\delta\nabla\underline{u}+\underline{\sigma}\cdot\nabla\underline{u}^T\delta\nabla\underline{u}\}dv-\int_V(\vec{f}^o\cdot\delta\vec{u}+\vec{f}\cdot\delta\vec{u})dv-$$
$$\int_{S_1}(\vec{t}^o\cdot\delta\vec{u}+\vec{t}\cdot\delta\vec{u})dS = 0 \tag{8}$$

Making use of 18(1) (ref. 7), equation (8) can be rewritten as

$$\int_V \delta\vec{u}\cdot[\text{div } \underline{\sigma} + \text{div}(\underline{\sigma}^o \nabla\underline{u}^T) + \text{div}(\underline{\sigma}\nabla\underline{u}^T) + \vec{f}]dv$$
$$-\int_{S_1}\delta\vec{u}\cdot[\underline{\sigma}\vec{n} + (\underline{\sigma}^o\nabla\underline{u}^T)^T\vec{n} + (\underline{\sigma}\nabla\underline{u}^T)^T\vec{n} - \vec{t}]dS =$$
$$\int_{S_1}\delta\vec{u}\cdot[\underline{\sigma}^o\vec{n} - \vec{t}^o]dS - \int_V\delta\vec{u}\cdot[\text{div } \underline{\sigma}^o + \vec{f}^o]dv \tag{9}$$

According to equations (2) and (3) the righthand side of equation (9) should be zero; therefore, the equations of equilibrium become

$$\text{div } \underline{\sigma} + \text{div}[(\underline{\sigma}^{\circ} + \underline{\sigma})\nabla \underline{u}^{T}] + \vec{f} = 0 \tag{10}$$

and the boundary condition is

$$\underline{\sigma}\vec{n} + [(\underline{\sigma}^{\circ} + \underline{\sigma})\nabla \underline{u}^{T}]^{T}\vec{n} = \vec{t} \tag{11}$$

The assumption that the incremental strains are small implies that $\vec{u}$ is small incrementally and

$$\underline{D} = \underline{E}, \quad \text{i.e. } N = 0 \text{ in equation (4).} \tag{12}$$

The initial stress may not be small; hence, we retain $\underline{\sigma}^{\circ}$ terms in equations (10) and (11). It follows from equation (12) that for a linear incremental stress-strain relation the incremental stress will be small. Therefore products of $\underline{\sigma}\nabla \underline{u}^{T}$ can be neglected and the governing equations become

$$\text{div } \underline{\sigma} + \text{div}(\underline{\sigma}^{\circ}\nabla \underline{u}^{T}) + \vec{f} = 0 \tag{13}$$

$$\underline{\sigma}\vec{n} + (\underline{\sigma}^{\circ}\nabla \underline{u}^{T})^{T}\vec{n} = \vec{t} \tag{14}$$

Equations (2) and (3) serve as an error check and can be used at any increment to determine the equilibrium status of the initial stress system.

The total stress $\underline{\sigma}$ at the end of any load increment becomes the initial stress $\underline{\sigma}^{\circ}$ for the next load increment. Then, $\underline{\sigma}$ must be referred to the initial coordinates $\vec{a}$ and the deformed area in order to become $\underline{\sigma}^{\circ}$. The transformation has been given by Fung (ref. 6) and can be rewritten as

$$\underline{\sigma}^{\circ} = (\rho/\rho_{o})\nabla_{a}\underline{x}\,\underline{\sigma}\,\nabla_{a}\underline{x}^{T} \tag{15}$$

where ρ/ρ_{o} is the ratio of final mass to initial mass and ∇_{a} indicates that the operator is with respect to the initial coordinates $\vec{a}$. It follows from equation (1) that

$$\nabla_{a}\underline{x} = \nabla_{a}(\underline{a+u}) = \underline{\delta} + \nabla_{a}\underline{u} \tag{16}$$

where $\underline{\delta}$ is a unit tensor. For an incremental theory equation (16) may be written

$$\underline{\delta} + \nabla_{a}\underline{u} = \underline{\delta} + \nabla \underline{u} = \underline{J} \tag{17}$$

It follows that

$$\rho/\rho_{o} = \det|\nabla a| \simeq 1 - \text{tr}(\nabla \underline{u}) \tag{18}$$

where tr( ) represents the trace of a tensor. Combining equations (15) through (18) gives the transformation

$$\underline{\sigma}^{\circ} = [1 - \text{tr}(\nabla \underline{u})]\underline{J}\,\underline{\sigma}\,\underline{J}^{T} \tag{19}$$

where

$$\underline{J}^T = (\underline{\delta} + \nabla\underline{u})^T = \underline{\delta} + \nabla\underline{u}^T \tag{20}$$

GOVERNING EQUATIONS FOR A ROTATING CYLINDER

The general equations can be reduced to plane cylindrical coordinates in order to implement the analysis of a rotating cylinder. The problem is one of axisymmetric plane strain; hence, the displacement vector $\vec{u}$ reduces to u_r, the radial component, which will be referred to as u.

The numerical method will be applied to the equation of equilibrium (13), which in plane cylindrical coordinates may be written

$$\sigma_r' + (\sigma_r - \sigma_\theta)/r + \sigma_r^{\circ\prime}\, u' + \sigma_r^\circ(u'' + u'/r) - \sigma_\theta^\circ\, u/r^2 + \rho\omega^2(r + u) = 0 \tag{21}$$

where $f = \rho(r+u)\omega^2$ the inertia force, σ_r and σ_θ are the radial and tangential stresses, respectively, and the prime denotes differentiation with respect to r.

Equation (12) is represented by the linear strains

$$E_r = u' \quad \text{and} \quad E_\theta = u/r \tag{22}$$

Following Sandman (ref. 1) we assume a linear anisotropic stress-strain relation

$$\sigma_r = C_{11}\, u' + C_{12}\, u/r \tag{23}$$

$$\sigma_\theta = C_{22}\, u/r + C_{12}\, u/r \tag{24}$$

Substituting equations (23) and (24) into equation (21) yields the incremental governing equation

$$u'' + u'/r - \alpha u/r^2 + \sigma_r^\circ\, u''/C_{11} + u'(\sigma_r^{\circ\prime} + \sigma_r^\circ/r)/C_{11} - \sigma_\theta^\circ\, u/C_{11}r^2 + \rho\omega^2(r+u)/C_{11} = 0 \tag{25}$$

where

$$\alpha = C_{22}/C_{11} \quad \text{and} \quad \beta = C_{12}/C_{11} \tag{26}$$

The boundary condition, equation (14), becomes

$$u'(1 + \sigma_r^\circ/C_{11}) + \beta\, u/r = 0 \tag{27}$$

The linearized incremental stress transformation, equation (19), becomes

$$\sigma_r^\circ = \sigma_r(1 + u' - u/r) \tag{28}$$

$$\sigma_\theta^\circ = \sigma_\theta(1 - u' + u/r) \tag{29}$$

NUMERICAL ANALYSIS

The governing equation (25) was solved using a finite difference technique. The primary constraint to be dealt with is the magnitude of each increment of strain. It must be small enough to insure that equation (12) is not violated. After each increment of displacement is calculated, the finite difference grid must be updated; hence, the finite difference equations must be reformulated after each incremental solution. The difference operations may be derived as follows

$$(du/dr)_i \simeq (u_{i+1}-u_i)/\Delta r_2 \simeq (u_i-u_{i-1})/\Delta r_1 \simeq (u_{i+1}-u_{i-1})/(\Delta r_1+\Delta r_2) \tag{30}$$

$$(d^2u/dr^2)_i \simeq \frac{2u_{i-1}}{\Delta r_1(\Delta r_1+\Delta r_2)} - \frac{2u_i}{\Delta r_1 \Delta r_2} + \frac{2u_{i+1}}{\Delta r_2(\Delta r_1+\Delta r_2)} \tag{31}$$

The first incremental solution is merely the linear solution for the first increment of body force. Before the second incremental solution is determined, the initial stresses are assumed to be equal to the stresses obtained for the first increment. These stresses are transformed according to equations (28) and (29). The incremental displacement associated with each finite difference node is added to the coordinate of that node; hence, a new initial stress problem is formulated. The nonlinear analysis for the equation developed by Sandman (ref. 1) was obtained by transposing all nonlinear terms to the right. The displacements for the previous analysis were used to evaluate the nonlinear terms, and a solution for u is obtained. The calculated displacements are then used to calculate new nonlinear terms, and the solution is repeated. This process continues until the two sets of displacements agree to within some tolerance. This method was used to verify the results obtained by Sandman (ref. 1) and appears to be accurate and efficient.

Equations (2) and (3) can be used at any increment to determine if the initial stress system is still in equilibrium. If the initial stress system is not in equilibrium, the solution can be corrected by including equation (2) in the governing equation (25).

NUMERICAL RESULTS

Solutions were obtained for three different materials. These material parameters were assumed to approximate the behavior of steel, aluminum, and a composite epoxy-fiber orthotropic material. The maximum radial and tangential stresses are shown in figure 1 as a function of ω^2. The cylinder was assumed to have an outside radius of 0.127 m (5 inches) and inside radius of 0.254 m (10 inches). The maximum radial stress occurs approximately halfway between the inside and outside, while σ_θ is maximum at the inside radius.

The percent deviation of the nonlinear solutions above the linear is illustrated in figures 2 and 3. The increase in stress using the equations of reference 1 appear to be almost linear in every case. The radial stress increase, using the incremental theory, is similar for both steel and aluminum and reflects a nonlinear behavior. The increase for the composite appears to become constant. The nonlinear tangential stress deviation increases and then tends to decrease for both isotropic materials; however, this behavior is not demonstrated for the composite.

In all cases the increase in stress level does not appear to be significant for stresses in the elastic range. The analysis presented herein should be extended to include nonlinear material behavior.

REFERENCES

1. Sandman, B. E.: Finite Deformation of a Rotating Orthotropic Cylinder with Linear Elasticity. Computers and Structures, Vol. 4, 1974, pp. 581-591.

2. Washizu, K.: Variational Principles in Elasticity and Plasticity. Pergamon Press, Oxford, 1968.

3. Atluri, S.: On the Hybrid Stress Finite Element Model for Incremental Analysis of Large Deflection Problems. Int. J. Solids Structures, Vol. 9, 1973, pp. 1177-1191.

4. Hofmeister, L. D.; Greenbaum, G. A.; and Evensen, D. A.: Large Strain, Elastic-Plastic Finite Element Analysis. AIAA J., Vol. 9, 1971, pp. 1248-1255.

5. Biot, M. A.: Mechanics of Incremental Deformation. John Wiley, New York, 1965.

6. Fung, Y. C.: Foundations of Solid Mechanics. Prentice-Hall, New Jersey, 1965.

7. Gurtin, M. E.: The Linear Theory of Elasticity. Handbuck der Physik, VIa/2, Springer-Verlag, 1972.

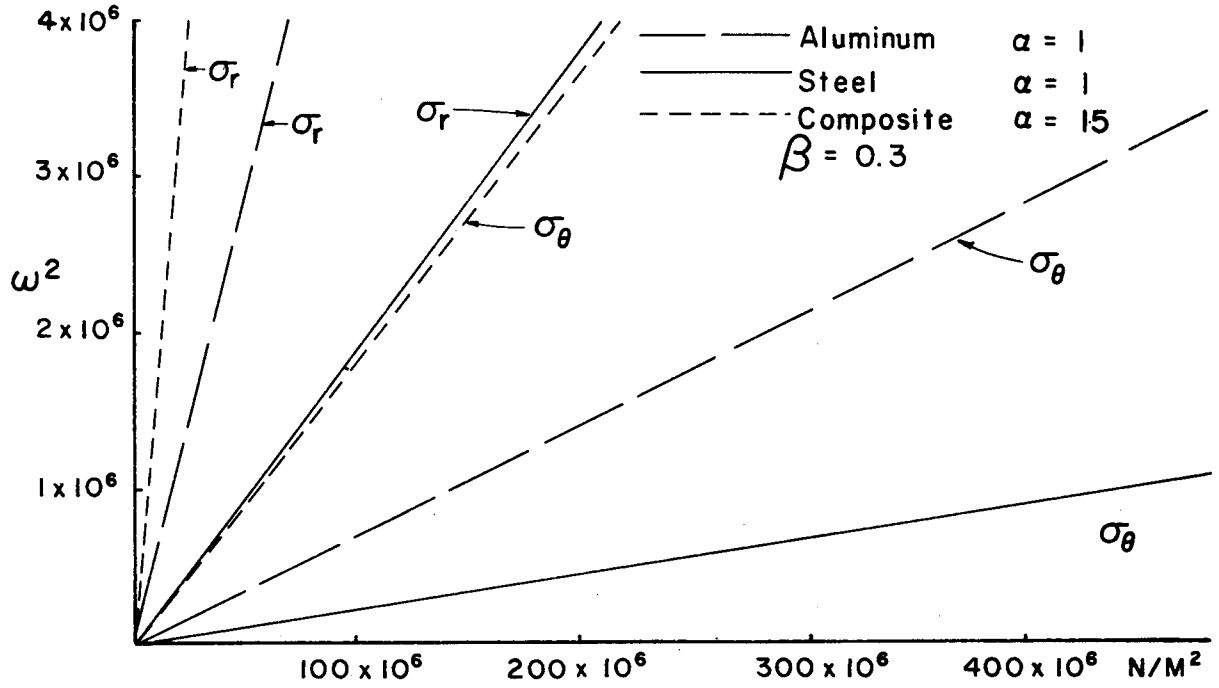

Figure 1.- Linear solution for maximum stress.

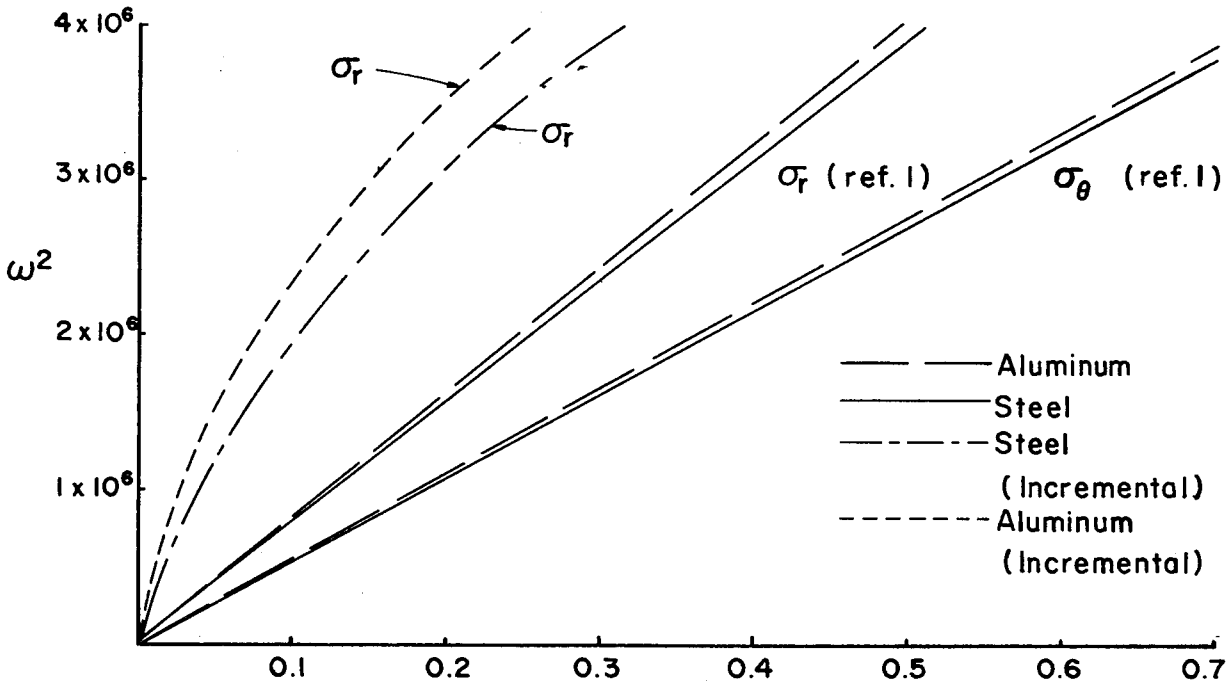

Figure 2.- Percent deviation from linear solution.

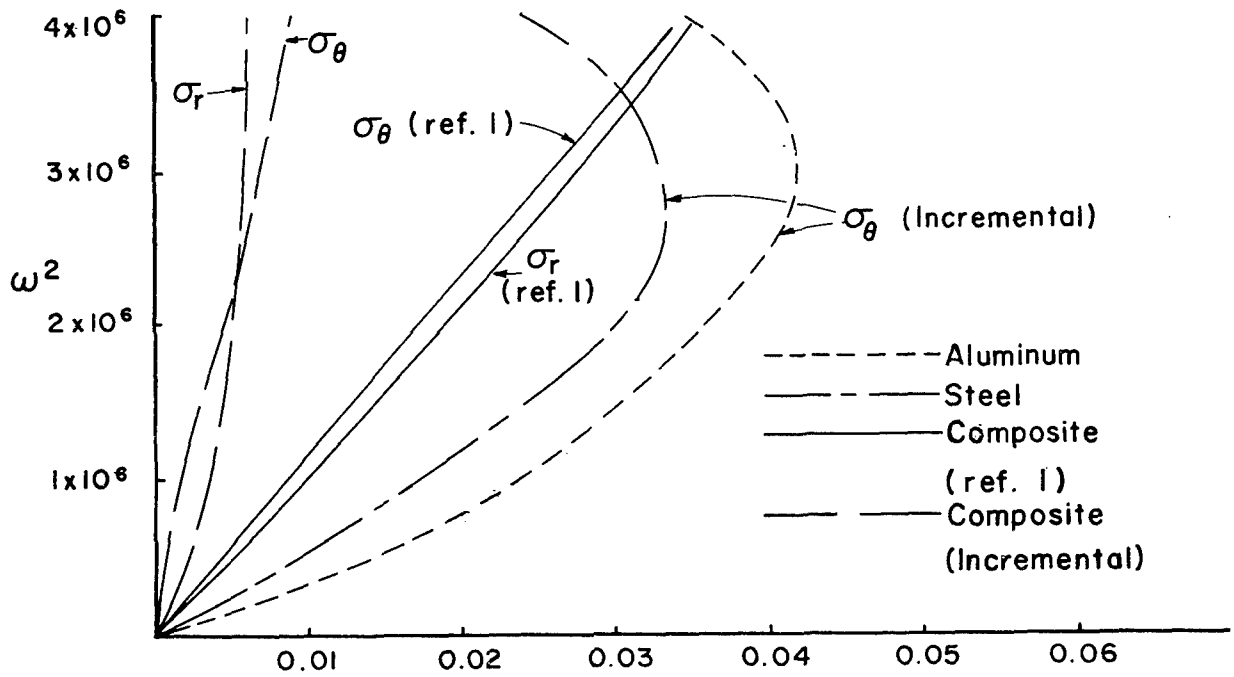

Figure 3.- Percent deviation from linear solution.

VARIATIONAL THEOREMS FOR SUPERIMPOSED MOTIONS IN ELASTICITY, WITH APPLICATION TO BEAMS

M. Cengiz Dökmeci
Technical University of Istanbul

SUMMARY

This study presents variational theorems for a theory of small motions superimposed on large static deformations and governing equations for prestressed beams on the basis of 3-D theory of elastodynamics. First, the principle of virtual work is modified through Friedrichs's transformation so as to describe the initial stress problem of elastodynamics. Next, the modified principle together with a chosen displacement field is used to derive a set of 1-D macroscopic governing equations of prestressed beams. The resulting equations describe all the types of superimposed motions in elastic beams, and they include all the effects of transverse shear and normal strains, and the rotatory inertia. The instability of the governing equations is discussed briefly.

INTRODUCTION

Small motions superimposed upon large static deformations have been tackled by a variety of investigators. And differential as well as variational formulations have been derived for both the so-called initial stress and initial strain problems (see, e.g., refs. 1-3, and references cited there). A classical variational formulation for the initial stress problem is deduced from a general principle of physics and has certain advantages over a differential formulation (see, e.g., ref. 3, where the principle of virtual work is taken as fundamental). This yields only the stress equations of motion and the natural boundary conditions. The remaining equations of the initial stress problem should be introduced as constraints. The constraints, however, can be removed through Friedrichs's transformation. This has been illustrated by de Veubeke (ref. 4) for classical elastodynamics.

All the past efforts reveal how the static and dynamic behavior of structures may significantly change by the presence of initial stress or initial strain. Among those, we mention here references 5-8 and references 9-12 on initially stressed shells and plates, respectively. On initially stressed beams, the works of Brunelle (ref. 13) and Sun (ref. 14) are cited. Brunelle

derived the governing equations for a prestressed, transversely isotropic beam via the direct integration of 3-D field equations. Sun studied the equations for a Timoshenko beam having an initial, in-plane compressive stress by the use of both Trefftz's and Biot's formulations.

The purpose of this investigation is twofold. The first aim is to modify the principle of virtual work, and then to obtain a generalized variational theorem which describes an arbitrary state of initial stress. The procedure used in achieving this is analogous to the one used in reference 4. The second aim is to construct the governing equations of anisotropic beams under initial stress by the use of the generalized variational theorem together with an incremental displacement field chosen a priori. The displacement field allows to include all the effects of transverse shear and normal strains, and the rotatory inertia for the prestressed thick beam in which they are significant. The resulting equations describe all the types of superimposed extensional, flexural, and torsional motions of thick anisotropic, elastic beam of uniform cross section. The dynamic instability of the prestressed beam is also discussed.

SYMBOLS

In a Euclidaen 3-space, Cartesian tensors are used, and Einstein's summation convention is implied for all repeated Latin (1,2,3) and Greek (1,2) indices, unless indices are put within parantheses.

L, A; C	length and cross-sectional area of beam; Jordan curve which bounds A
V, S	entire volume of beam and its total boundary surface
S', S''	complementary subsurfaces of S, where stresses and displacements are, respectively, prescribed
x_i; x_α, x_3	a system of right-handed Cartesian convected coordinates; lateral coordinates and beam axis
u_i, $u_i^{m,n}$	components of displacement vector, displacement functions of order (m,n)
ρ	mass density
n_i, ν_i	components of unit outward vector normal to S and C
ε_{ij}, s_{ij}	components of strain and symmetric stress tensors
Θ	prescribed steady temperature field

C_{ijkl}, α_{ij} isothermal elastic stiffnesses and strain-temperature constants

I_{mn} moment of inertia of order (m,n)

$a_i = \ddot{u}_i$, t_i components of acceleration and traction vectors

$T_{ij}^{m,n}$ stress resultants of order (m,n)

$F_i^{m,n}$, $A_i^{m,n}$ body force and acceleration resultants of order (m,n)

$Q_i^{m,n}$, $P_i^{m,n}$ effective load and external force of order (m,n)

$(\dot{})$, $(\ )_{,i}$ partial differentiation with respect to time, t, and x_i

$(^0)$, $(*)$ field quantities belong to the reference state and prescribed quantities

C_{mn} functions with derivatives of order up to and including m and n with respect to space coordinates x_i and time,t

FUNDAMENTAL EQUATIONS

Consider a simply connected elastic body V+S, with its boundary S, in a 3-D Euclidean space Ξ. The elastic body is referred to a x_i-fixed system of Cartesian convected coordinates in this space. When this body is prestressed, we distinguish two states of the body: its reference (or initial) and spatial (or final) state. The reference state is considered to be self-equilibrating following static loading in the natural (or undisturbed) state of the body at time, $t=t_0$. We may summarize, for ease of quick reference, the fundamental equations (see, e.g., ref. 2) in the form

$$s^0_{ij,i} + \rho^0 f^0_j = 0 \quad \text{in} \quad V \tag{1}$$

$$n_i s^0_{ij} - t^{0*}_j = 0 \quad \text{on} \quad S' \,, \quad u^0_i - u^{0*}_i = 0 \quad \text{on} \quad S'' \tag{2}$$

$$s^0_{ij} = C_{ijkl}\, \varepsilon^0_{kl} \qquad \varepsilon^0_{ij} = 1/2(u^0_{i,j} + u^0_{j,i}) \quad \text{in} \quad V \tag{3}$$

for this state. Here, ρ^0 is the known mass density of the body material, s^0_{ij} the symmetric stress tensor, f^0_i the body force vector per unit mass in V, u^0_i the displacement vector, n_i the unit outward vector normal to S, u^{0*}_i and t^{0*}_i the prescribed displacement and traction vectors on the complementary subsurfaces S" and S' of S, ε^0_{ij} the linear strain tensor, and C_{ijkl} ($C_{ijkl} = C_{jikl} = C_{klij}$) the isothermal elastic stiffnesses.

Now, suppose that an infinitesimal (or small) motion is

superimposed upon the reference state. For this motion, we have the following fundamental equations:

$$(s_{ij} + s^0_{ir}u_{j,r})_{,i} + \rho^0(f_j - a_j) = 0 \quad \text{in} \quad V \tag{4}$$

$$n_i(s_{ij} + s^0_{ir}u_{j,r}) - t^*_j = 0 \quad \text{on} \quad S' \tag{5}$$

$$u_i - u^*_i = 0 \quad \text{on} \quad S'' \tag{6}$$

$$\varepsilon_{ij} = 1/2(u_{i,j} + u_{j,i}) \quad \text{in} \quad V \tag{7}$$

$$s_{ij} = C_{ijkl}(\varepsilon_{kl} - \theta\alpha_{kl}) \quad \text{in} \quad V \tag{8}$$

$$u_i - v^*_i = 0 \quad \& \quad \dot{u}_i - w^*_i = 0 \quad \text{in} \quad V(t_0) \tag{9}$$

in the spatial state. In these equations, s_{ij}, u_i, t_i and so on indicate small incremental quantities superimposed upon those of the reference state (i.e., s^0_{ij}, u^0_i, t^0_i). And $a_i=\ddot{u}_i$ is the acceleration vector, v^*_i and w^*_i are the prescribed displacement vectors. θ is an incremental prescribed steady temperature field and $\alpha_{ij} = \alpha_{ji}$ the strain-temperature coefficients at constant stress. Also, $V(t_0)$ is used to designate V at $t=t_0$.

Equations (1)-(9) describe completely the initial stress problem of interest.

VARIATIONAL THEOREMS

To begin with, we express a principle of virtual work as the assertation

$$\int_V (s^0_{ij} + s_{ij})\delta\gamma_{ij}dV = \int_V \rho^0(f^0_i + f_i)\delta u_i dV - \int_V \rho^0 a_i \delta u_i dV + \int_S (t^0_i + t^*_i)\delta u_i dS \tag{10}$$

in the spatial state. Here, γ_{ij} denotes the Lagrangian strain tensor, and it is given by

$$\gamma_{ij} = \varepsilon_{ij} + 1/2(u_{i,r}u_{j,r}) \tag{11}$$

In equation (10), through the use of equation (11), we first carry out the indicated variations, apply Green - Gauss integral transformations and combine the resulting surface and volume integrals. Next, we recall the usual arguments on incremental field quantities (see, e.g., ref. 2), take into account equations (1) and (2), and finally arrive at the variational equation of the

form:

$$\delta J = \delta J_{\alpha\alpha} = 0 \tag{12 a}$$

with

$$\delta J_{11} = \int_V (s_{ij} + s^0_{ir} u_{j,r})_{,i} \delta u_i dV + \int_V \rho^0 (f_i - a_i)\delta u_i dV$$

$$\delta J_{22} = \int_S [(s_{ij} + s^0_{ir} u_{j,r})n_i - t^*_j]\delta u_j dS \tag{12 b}$$

The variations of displacements are arbitrary and independent in this equation. Hence, equation (12) leads evidently to the stress equations of motion (4) in V and the natural boundary conditions (5) on S, as the appropriate Euler equations.

Variational Theorem: Let V+S denote a regular, finite region of space (see, e.g., ref. 15) in Ξ, with its boundary S, and define the functional J whose the first variation is given by equation (12). Then, of all the admissible displacement states $u_i \varepsilon C_{12}$, if and only if, the one which satisfies the stress equations of motion (4) and the natural boundary conditions (5) as the appropriate Euler equations, renders $\delta J = 0$.

This is a one-field variational theorem in which equations (6) -(9) of the initial stress problem remain to be satisfied as constraints.

To include the rest of equations of the initial stress problem in the variational formulation, we introduce dislocation potentials and use Friedrichs's transformation, and we closely follow de Veubeke (ref. 4). Thus, we obtain the following theorem.

Generalized Variational Theorem: Let V+S denote a regular, finite region of space in Ξ, with its boundary S ($S' \eta S'' = 0$ and $S' \cup S'' = S$), and define the functional I whose first variation is given by

$$\delta I = \delta I_{ii} + \delta J_{11} \tag{13 a}$$

with

$$\delta I_{11} = \int_{S'} [(s_{ij} + s^0_{ir} u_{j,r})n_i - t^*_j]\delta u_j dS + \int_{S''} (u_i - u^*_i)\delta t_i dS \tag{13 b}$$

$$\delta I_{22} = \int_V [s_{ij} - C_{ijkl}(\varepsilon_{kl} - \Theta\alpha_{kl})]\delta\varepsilon_{ij} dV \tag{13 c}$$

$$\delta I_{33} = \int_V [\varepsilon_{ij} - 1/2(u_{i,j} + u_{j,i})]\delta s_{ij} dV \tag{13 d}$$

Then, of all the admissible states of $u_i \varepsilon C_{12}$, $\varepsilon_{ij} \varepsilon C_{00}$, $t_i \varepsilon C_{00}$, and

$s_{ij} \varepsilon C_{1\sigma}$, if and only if, those which satisfy the stress equations of motion (4) in V, the natural boundary conditions (5) and (6) for displacements and tractions on S" and S', the strain-displacement relations (7) in V, and the constitutive equations (8) in V, as the appropriate Euler equations, render $\delta I=0$.

In the generalized variational equation (13), the incremental field quantities (s_{ij}, u_i, t_{ij} and ε_{ij}) are varied independently. And this is a four-field variational theorem. The admissible states are not required to meet any of the fundamental equations of the initial stress problem but the initial conditions (9) only.

BEAMS UNDER INITIAL STRESS

Geometry and Kinematics

A straight elastic beam is embedded in the space Ξ. The beam is of uniform cross section, A, and it occupies a regular, finite region of space V with its boundary S in Ξ. The total surface S consists of two right and left faces, A_r and A_1, and a cylindrical lateral surface S_1. The beam is referred to the x_i-system of Cartesian convected coordinates located at the centroid of A_1. The x_3-axis is chosen to be the beam axis, and the x_α-axes indicate the principal axes of A which is bounded by a Jordan curve C. The beam is under an initial stress field in the reference state.

The incremental displacements of the prestressed elastic beam are taken of the form:

$$u_i(x_j,t) = \sum_{m,n=0}^{M=1} [x_1^m x_2^n \, u_i^{(m,n)}] \tag{14}$$

Here, the $u_i^{(m,n)}$ are functions of x_3 and time, t, only. These terms readily accommodate low-frequency extensional, flexural and torsional superimposed motions. However, it should be kept in mind that, in the case of torsion, equation (14) can represent only the displacements of beams of elliptic and circular cross-sections, and for all other sections, more terms should be retained in the expansion. The displacement field (14) is like the one Mindlin (ref. 16) used in his recent derivation of the governing equations for a non-initially stressed elastic bar.

Stress and Load Resultants

We define the stress resultants of order (m,n):

$$T_{ij}^{(m,n)} = \int_A x_1^m x_2^n \, s_{ij} dA \tag{15 a}$$

This represents the weighted, averaged values of stress tensor over a cross section of the prestressed beam in the reference state.

In addition, we introduce the body force, acceleration and load resultants, and the moment of inertia of order (m,n):

$$F_i^{(m,n)} = \int_A x_1^m x_2^n f_i dA, \quad T_i^{*(m,n)} = \int_A x_1^m x_2^n t_i^* dA$$

$$I_{mn} = \int_A x_1^m x_2^n dA, \quad A_i^{(m,n)} = \sum_{p,q=0}^{M=1} I_{m+p,n+q} \ddot{u}_i^{(p,q)}$$

$$[P_i^{(m,n)}, P_i^{0(m,n)}] = \oint_C x_1^m x_2^n \nu_\alpha [s_{\alpha i}, s_{\alpha i}^0] ds$$

$$R_i^{0(m,n)} = \sum_{p,q=0}^{M=1} [(pP_1^{0(m+p-1,n+q)} + qP_2^{0(m+p,n+q-1)}) u_i^{(p,q)} + P_3^{0(m+p,n+q)} u_{i,3}^{(p,q)}]$$

$$N_i^{0(m,n)} = \sum_{p,q=0}^{M=1} \{ [mpT_{11}^{0(m+p-2,n+q)} + (np+mq)T_{12}^{0(m+p-1,n+q-1)} + qnT_{22}^{0(m+p,n+q-1)} + pT_{31,3}^{0(m+p-1,n+q)} + qT_{32,3}^{0(m+p,n+q-1)}] u_i^{(p,q)} + T_{33}^{0(m+p,n+q)} u_{i,33}^{(p,q)} + [(p+m)T_{13}^{0(m+p-1,n+q)} + (q+n)T_{23}^{0(m+p,n+q-1)} + T_{33,3}^{0(m+p,n+q-1)}] u_{i,3}^{(p,q)} \}$$

$$N_{3i}^{0(m,n)} = \sum_{p,q=0}^{M=1} [(pT_{31}^{0(m+p-1,n+q)} + qT_{32}^{0(m+p,n+q-1)}) u_i^{(p,q)} + T_{33}^{0(m+p,n+q)} u_{i,3}^{(p,q)}] \qquad (15\ b)$$

Prestressed Beam Equations — Instability

Now, we shall derive the prestressed beam equations by the use of the generalized variational theorem (13) together with the incremental displacement field (14). First, upon substituting the expansion (14) into equation (13 a), we find the variational equation (16). In this equation, the variations $\delta u_i^{m,n}$ are arbitrary and independent for any choice of m(=0,1) and n(=0,1), and hence it evidently leads to the macroscopic equations of

motion (17) as follows:

$$\int_0^L \sum_{m,n=0}^{M=1} U_i^{(m,n)} \delta u_i^{(m,n)} \, dx_3 = 0, \quad m,n=0,1 \tag{16}$$

$$U_i^{(m,n)} = T_{3i,3}^{(m,n)} - mT_{1i}^{(m-1,n)} - nT_{2i}^{(m,n-1)} + P_i^{(m,n)} + Q_i^{0(m,n)} + \rho^0 (F_i^{(m,n)} - A_i^{(m,n)}) = 0, \quad m,n=0,1 \tag{17}$$

Here, $Q_i^{0(m,n)}$ is the effective initial load given by

$$Q_i^{0(m,n)} = N_i^{0(m,n)} + R_i^{0(m,n)} \tag{18}$$

Similarly, we evaluate the variational equation (13 b) and obtain the natural displacement and traction boundary conditions in the form

$$u_i^{(m,n)} - u_i^{*(m,n)} = 0, \quad m,n=0,1 \quad \text{on} \quad S_1 \tag{19}$$

$$T_i^{*(m,n)} + n_3 (T_{3i}^{(m,n)} + N_{3i}^{0(m,n)}) = 0, \quad m,n=0,1 \text{ on } A_r \text{ and } A_1$$

Here, $S'=A_r \cup A_1$ and $S''=S_1$, and $n_3=+1$ for A_r and $n_3=-1$ for A_1.

Upon using of equations (13 c) and (13 d) together with (14), we have the strain distribution:

$$\varepsilon_{ij} = \sum_{m,n=0,1}^{M=1} x_1^m x_2^n \, \varepsilon_{ij}^{(m,n)} (x_3,t) \tag{20 a}$$

with

$$\varepsilon_{ij}^{(m,n)} = 1/2 \, [u_{i,j}^{(m,n)} + u_{j,i}^{(m,n)} + (m+1)(\delta_{1i} u_j^{(m+1,n)} + \delta_{1j} u_i^{(m+1,n)}) + (n+1)(\delta_{2i} u_j^{(m,n+1)} + \delta_{2j} u_i^{(m,n+1)}) \,] \tag{20 b}$$

and the macroscopic constitutive equations:

$$T_{ij}^{(m,n)} = C_{ijkl} \sum_{p,q=1}^{M=1} I_{m+p,n+q} (\varepsilon_{kl}^{(p,q)} - \alpha_{kl} \theta^{(p,q)}) \tag{21}$$

where we take the temperature increment of the form:

$$\theta(x_i) = \sum_{m,n=0}^{M=1} x_1^m x_2^n \, \theta^{(m,n)}(x_3) \tag{22}$$

Lastly, the initial conditions, based on equations (9) and (14),

$$u_i^{(m,n)} - v_i^{*(m,n)} = 0 \quad \dot{u}_i^{(m,n)} - w_i^{*(m,n)} = 0 \quad \text{in } L(t_o) \tag{23}$$

complete the beam equations (cf., ref. 17, where non-initially stressed beams are treated) under an arbitrary state of initial stress field.

The beam equations of equilibrium may be derived similarly on the basis of equations (1)-(3); they are not written out here in order to conserve space.

To examine the stability of the prestressed beam equations, we first consider the beam with a set of initial forces χ. Next, we replace χ by a prescribed set χ^*. And, as usual, we arrive at a system of linear homogeneous differential equations which describes the instability problem under consideration. The sets are defined by

$$\chi = (T_{ij}^{0(m,n)} \text{ in } L,\ F_i^{0(m,n)} \text{ in } L,\ T_i^{0(m,n)} \text{ on } A)$$

$$\chi^* = \lambda(T_{ij}^{0*(m,n)} \text{ in } L,\ F_i^{0*(m,n)} \text{ in } L,\ T_i^{0*(m,n)} \text{ on } A)$$

where λ is a monotonically increasing factor, and whenever it reaches certain values the equilibrating reference configuration becomes unstable. The behavior of the eigenvalues of this factor is to be investigated in each particular case of interest. Some examples of instability will be reported elsewhere.

REFERENCES

1. Truesdell, C.; and Noll, W.: The Non-linear Field Theories of Mechanics. Handbuch der Physik, Bd. III/3. Springer-Verlag, 1965.

2. Bolotin, V. V.: Nonconservative Problems of the Theory of Elastic Stability. Pergamon Press, 1963.

3. Washizu, K.: Variational Methods in Elasticity and Plasticity Pergamon Press, 1974.

4. Fraeijs de Veubeke, B.: Diffusion des Inconnues

Hyperstatiques dans les Voilures a Longerons Couples. Bull. du Service Tech. de l'Aeronautique, N. 24, 1951.

5. Koiter, W. T.: General Equations of Elastic Stability for Thin Shells. Proc. Symp. Theory of Shells, Univ. Houston, 1967, pp. 185-227.

6. Budiansky, B.: Notes on Nonlinear Shell Theory. J. Appl. Mechs., vol. 35, 1968, pp. 393-401.

7. Danielson, D. A.; and Simmonds, J. G.: Accurate Buckling Equations for Arbitrary and Cylindrical Elastic Shells. Int. J. Engng. Sci., vol. 7, 1969, pp. 459-468.

8. Kalnins, A.; and Biricikoglu, V.: Theory of Vibration of Initially Stressed Shells. J. Acoust. Soc. Am., vol. 51, 1971, pp. 1697-1704.

9. Herrmann, G.; and Armenakas, A. E.: Vibrations and Stability of Plates under Initial Stress. ASCE, J. Eng. Mechs., vol. 86, 1960, pp. 65-94.

10. Dökmeci, M. C.; and AlpD, Mg.: On the Dynamic Stability of Composite Structures. Composite Materials in Engineering Design, Amer. Soc. Metals, 1972, pp. 147-162.

11. Brunelle, E. J.; and Robertson, S. R.: Initially Stressed Mindlin Plates. AIAA, vol. 12, 1974, pp. 1036-1045.

12. Brunelle, E. J.; and Robertson, S. R.: Vibration of an Initially Stressed Thick Plate. J. Sound Vibration, vol. 45 1976, pp. 405-416.

13. Brunelle, E. J.: Stability and Vibration of Transversely Isotropic Beams under Initial Stress. J. Appl. Mechs., vol. 39, 1972, pp. 819-821.

14. Sun, C. T.: On the Equations for a Timoshenko Beam under Initial Stress. J. Appl. Mechs., vol. 39, 1972, pp. 282-285.

15. Kellog , O. D.: Foundations of Potential Theory. Dover Pub., 1953.

16. Mindlin, R. D.: Low Frequency Vibrations of Elastic Bars, Int. J. Solids Structs., vol. 12, 1976, pp. 27-49.

17. Dökmeci, M. C.: A General Theory of Elastic Beams. Int. J. Solids Structs., vol. 8, 1972, pp. 1205-1222.

RESPONSE OF LONG, FLEXIBLE CANTILEVER BEAMS TO APPLIED ROOT MOTIONS

Robert W. Fralich
NASA Langley Research Center

SUMMARY

Results are presented for an analysis of the response of long, flexible cantilever beams to applied root rotational accelerations. Maximum values of deformation, slope, bending moment, and shear are found as a function of magnitude and duration of acceleration input. Effects of tip mass and its eccentricity and rotatory inertia on the response are also investigated. It is shown that flexible beams can withstand large root accelerations provided the period of applied acceleration can be kept small relative to the beam fundamental period.

INTRODUCTION

In the design of large space structures, it is necessary to understand the dynamic response of flexible, low-frequency structures. A typical design problem is shown in figure 1, where a 100-meter beam is deployed from the space shuttle orbiter for a proposed molecular vacuum facility. The design of a lightweight boom requires a knowledge of the motion caused by input accelerations produced by control forces applied at the shuttle orbiter. The duration of these control forces is a small fraction of the first natural period of the boom. The purpose of this paper is to present results of an analysis of lightweight flexible booms to short-duration acceleration impulses and to find the permissible values of these input accelerations. Effects of tip mass magnitude, eccentricity, and rotatory inertia are included in the analysis.

DESCRIPTION OF ANALYSIS

The configuration analyzed in this paper is the cantilever beam shown in figure 2. The beam of length L, depth D, stiffness EI, and mass per unit length ρ has a tip mass $\bar{M}$ with a rotatory inertia $I_{\bar{M}}$ and an eccentricity B. The analysis considers a constant rotational input acceleration A which is applied for a time T_0 and is then removed. The duration of input T_0 varies over the range from an impulsive input ($T_0 \to 0$) to a step input ($T_0 \to \infty$). A nondimensional measure of the duration of input acceleration is given by the ratio T_0/T where T is the period of the first natural frequency of the cantilever beam. In the present study, the region with low values of T_0/T is of main interest.

Simple beam theory is used to obtain the differential equation of motion

$$EI \frac{\partial^4 Y(X,t)}{\partial X^4} + \rho \left[\frac{\partial^2 Y(X,t)}{\partial t^2} + X \frac{d^2\theta(t)}{dt^2} \right] = 0 \tag{1}$$

where $\theta(t)$ is the rigid body rotation and $Y(X,t)$ is the elastic deformation of the rotating beam. The deflection $Y(X,t)$ satisfies the boundary conditions

$$\left.\begin{aligned} Y(0,t) &= 0 \\ \frac{\partial Y(0,t)}{\partial X} &= 0 \\ -EI \frac{\partial^3 Y(L,t)}{\partial X^3} + \bar{M} \left[(B + L) \frac{d^2\theta}{dt^2} + \frac{\partial^2 Y(L,t)}{\partial t^2} + B \frac{\partial^3 Y(L,t)}{\partial X\, \partial t^2} \right] &= 0 \\ EI \frac{\partial^2 Y(L,t)}{\partial X^2} + B\bar{M} \left[(B + L) \frac{d^2\theta}{dt^2} + \frac{\partial^2 Y(L,t)}{\partial t^2} + B \frac{\partial^3 Y(L,t)}{\partial X\, \partial t^2} \right] & \\ + I_M \left[\frac{d^2\theta}{\partial t^2} + \frac{\partial^3 Y(L,t)}{\partial X\, \partial t^2} \right] &= 0 \end{aligned}\right\} \tag{2}$$

and the initial conditions

$$\left.\begin{aligned} Y(X,0) &= 0 \\ \frac{\partial Y(X,0)}{\partial t} &= 0 \end{aligned}\right\} \tag{3}$$

The rigid body rotation is given by

$$\left.\begin{aligned} \theta &= \frac{1}{2} At^2 \qquad \text{for} \qquad 0 < t < T_0 \\ \text{and} & \\ \theta &= AT_0 \left(t - \frac{1}{2} T_0 \right) \qquad \text{for} \qquad t > T_0 \end{aligned}\right\} \tag{4}$$

In the analysis the elastic deformation $Y(X,t)$ is given by

$$Y(X,t) = \sum_{n=1}^{\infty} a_n(t)\, \phi_n(X) \tag{5}$$

where $\phi_n(X)$ are the beam vibration modes for the cantilever beam and $a_n(t)$ are generalized coordinates. Results are obtained for elastic beam deflection $Y(X,t)$, slope $\frac{\partial Y(X,t)}{\partial X}$, bending moment $M(X,t)$, and shear resultant $Q(X,t)$

Modal equations for these responses were programed on a digital computer and the maximum value of each was found at several stations along the beam.

RESULTS AND DISCUSSION

The number of modes required for convergence is indicated in figure 3 for a beam without a tip mass subjected to input rotational accelerations with a large enough variation of input durations to include all possible types of responses. Although not shown, similar curves have been established for other tip mass configurations. These curves give the maximum values of nondimensional response parameters for the deflection Y_T and slope $\partial Y_T/\partial X$ at the beam tip and for bending moment M_0 and shear resultant Q_0 at the beam root. Accurate calculations of these response parameters are obtained by using only one mode for tip deflection, two modes for tip slope, and five modes for root bending moment and shear resultant. A six-mode solution is used herein as a completely converged standard of comparison.

The curves of figure 3, showing the effects of duration of acceleration input, can be divided into two regions of response types. For short-duration inputs ($T_0/T < 0.5$) the maximum responses always occur after the input root acceleration has been removed. For long-duration inputs ($T_0/T > 0.5$) the maximum responses always occur while the input acceleration is being applied and approach the values for a step input ($T_0/T \to \infty$) which have the values of two times the values for the quasi-static solution for rigid body inertia loading. The nearly horizontal curves for $T_0/T > 0.5$ show that in this region the maximum values of beam responses can be calculated by use of the simple quasi-static solution.

When the nondimensional parameters of figure 3 are used, the results for nearly impulsive input acceleration ($T_0/T \to 0$) are all compressed near the origin. Inputs in this region are of particular interest since typical control inputs are for short intervals of time while space booms have long periods. To overcome this difficulty, the results of figure 3 are repeated in figure 4 by using a different set of nondimensional parameters. These parameters have finite nonzero values for the pure impulse and are in agreement with calculated values from reference 1, which considers the instantaneous arrest of a rotating cantilever beam. These response parameters that have input acceleration impulse (T_0A) in their nondimensionalizations, for short-duration inputs ($T_0/T < 0.5$), do not have the large variation with T_0/T that is obtained by using the response parameters of figure 3. For this reason, the nondimensional parameters of figure 4 are used throughout the remainder of the paper.

Effect of tip mass on maximum response is shown in figure 5 for a pure impulsive input ($T_0/T \to 0$) and for a short-duration input ($T_0/T = 0.1$). Curves are shown for the nondimensional parameters for elastic tip deflection and root bending moment. For short duration of input acceleration, the effect of duration has very little effect on the elastic tip deflection curve but has some effect on the root bending-moment curve. Note that effects of tip mass are included not only in the tip mass parameter ($\bar{M}/\rho L$) but also in the period T. Even though the nondimensional response is shown to decrease with tip mass,

the physical quantities increase as expected. For example, for a tip mass equal to the beam mass, the root bending moment increases 75 percent and the tip deflection 100 percent.

Effects of tip mass eccentricity and rotatory inertia are shown in figure 6 for a pure impulse ($T_0/T \to 0$) and for a short duration of input ($T_0/T = 0.1$). Here nondimensional tip deflection and root bending moment are shown as functions of rotatory inertia $I_M/\bar{M}L^2$ for two values of eccentricity B/L which are chosen as representative extreme values. Effects of rotatory inertia and eccentricity also appear in two parts of this figure; first, in the parameters $I_M/\bar{M}L^2$ and B/L and, second, in the period T which is used in nondimensionalizing the response parameters. Again, for short-duration inputs, the elastic tip deflection parameter is only slightly affected by duration of input but the root bending-moment parameter decreases appreciably with an increase in T_0/T.

When a limiting design or maximum value is assigned to any of the calculated values of response, curves can be obtained to give maximum permissible input acceleration as a function of structural parameters. For example, if limiting values are assigned to the maximum bending strain ε at the root of a cantilever with a symmetrical cross section, the curves of figure 7 are obtained which give permissible nondimensional input acceleration TT_0A as a function of span to depth L/D. The $\varepsilon = 0.003$ and 0.005 curves bound values of limiting bending strain that are appropriate for most isotropic and composite materials while the $\varepsilon = 0.001$ curve represents a practical value of limiting bending strain that has been reduced to take into account effects such as buckling. The curves, shown for no tip mass, show that for given values of L/D and ε, a slightly higher value of impulse T_0A is permitted if the impulse is applied over a longer duration of time T_0.

Sample curves with physical units are given in figure 8 for determining permissible input acceleration A. These curves are shown for a beam with no tip mass and for the reduced limiting strain condition ($\varepsilon = 0.001$). The curves show the variation of permissible input rotational acceleration with the lowest natural frequency ($1/T$) and the span-to-depth ratio L/D for two values of input duration T_0/T. The $T_0/T = 0.5$ value represents the most severe case where the response approaches that of the step input and the beam behavior can be estimated from a simple quasi-static solution. The $T_0/T = 0.001$ value represents a nearly impulsive input. As the duration of input decreases, the permissible magnitude of input rotational acceleration increases. As illustrated in figure 8, a hundred-fold increase in permissible acceleration can be achieved by applying very short-duration inputs.

CONCLUDING REMARKS

A modal solution has been obtained to study the response of long, flexible cantilever beams to applied values of root rotational acceleration. Effects of tip mass with various eccentricities and rotatory inertias have been included. Results were obtained for duration of input that cover the range from near-impulsive to the step function. A set of nondimensional parameters has been

identified that facilitates looking at the response for the near-impulsive type of input accelerations. When the duration of input is more than half the period of the first natural frequency of the beam, the maximum response is nearly equal to that of the step-function input and is found to be twice the response given by simple quasi-static analysis based on rigid body inertia loading. Examples are included of application of these results to the problem of determining maximum input acceleration so that design values of maximum strain are not exceeded. These results show that large flexible booms can experience high root rotational accelerations without inducing large strains provided the duration of controlling forces are kept to a small fraction of the period of the first natural frequency.

REFERENCE

1. Stowell, Elbridge Z.; Schwartz, Edward B.; and Houbolt, John C.: Bending and Shear Stresses Developed by the Instantaneous Arrest of the Root of a Cantilever Beam Rotating With Constant Angular Velocity About a Transverse Axis Through the Root. NACA Wartime Report L-27 (ARR No. L5E25) 1945.

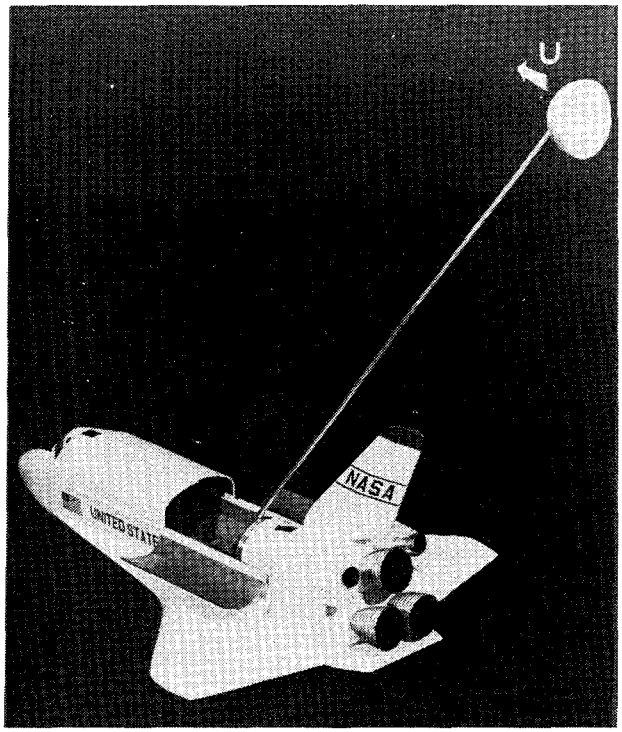

Figure 1. Long, flexible boom for molecular vacuum facility.

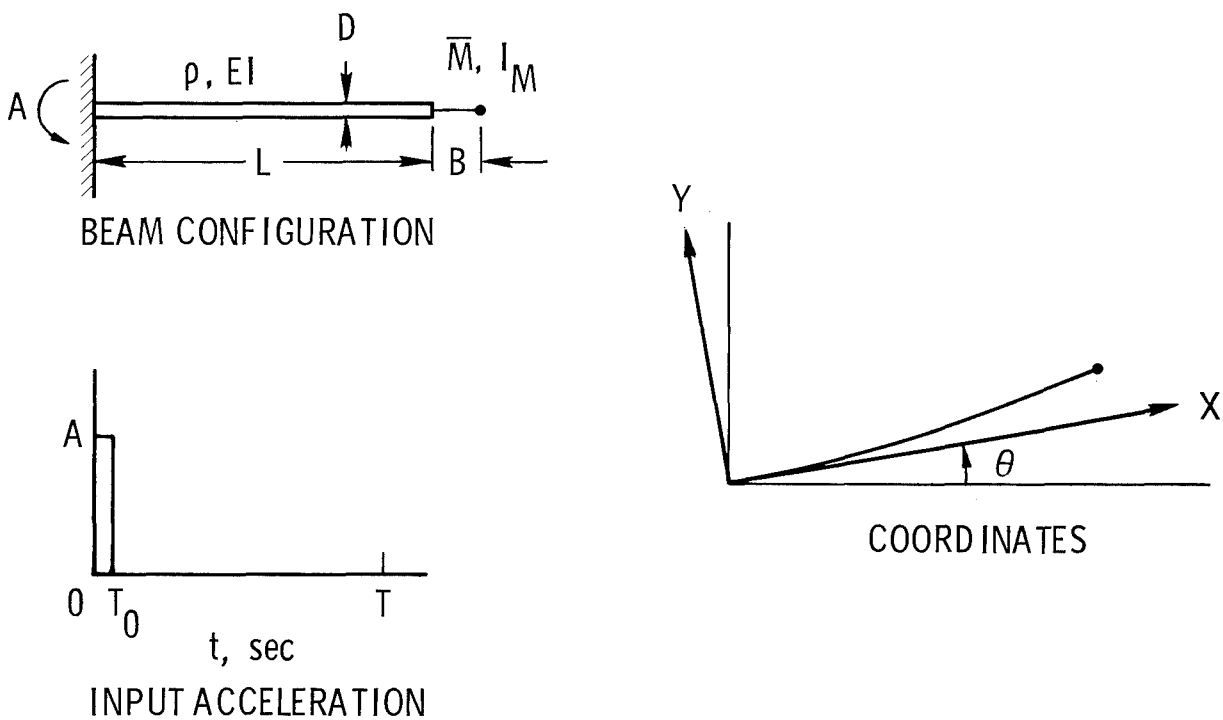

Figure 2. Flexible cantilever beam subjected to input rotational acceleration.

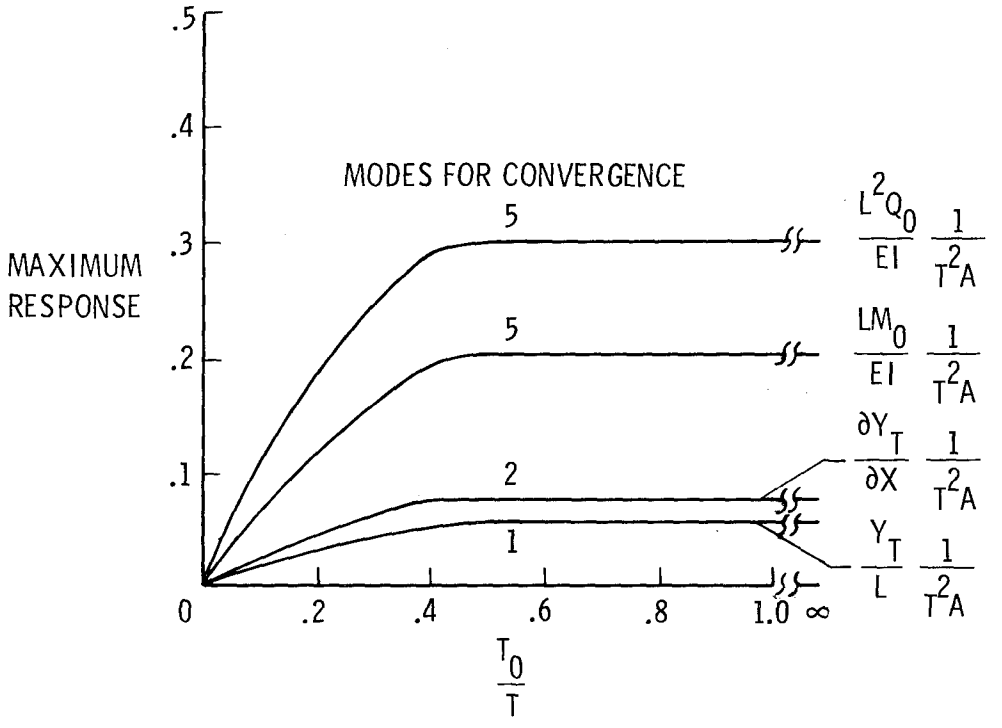

Figure 3. Effect of duration (T_0/T) of input rotational acceleration on maximum response. No tip mass ($\bar{M}/\rho L = 0$).

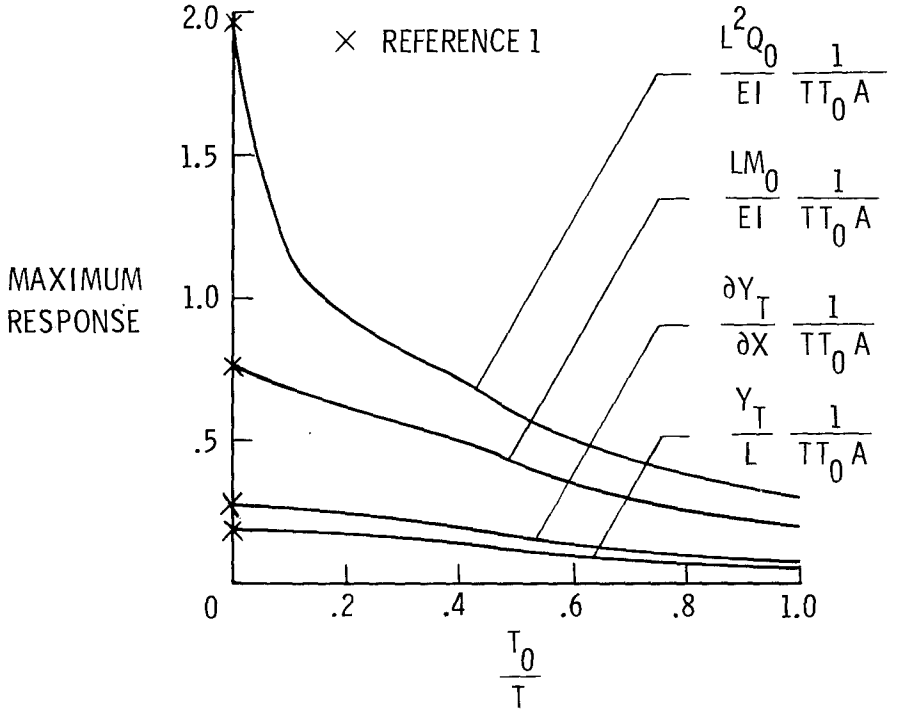

Figure 4. Response parameters appropriate for nearly impulsive input acceleration ($T_0/T \to 0$). No tip mass ($\bar{M}/\rho L = 0$).

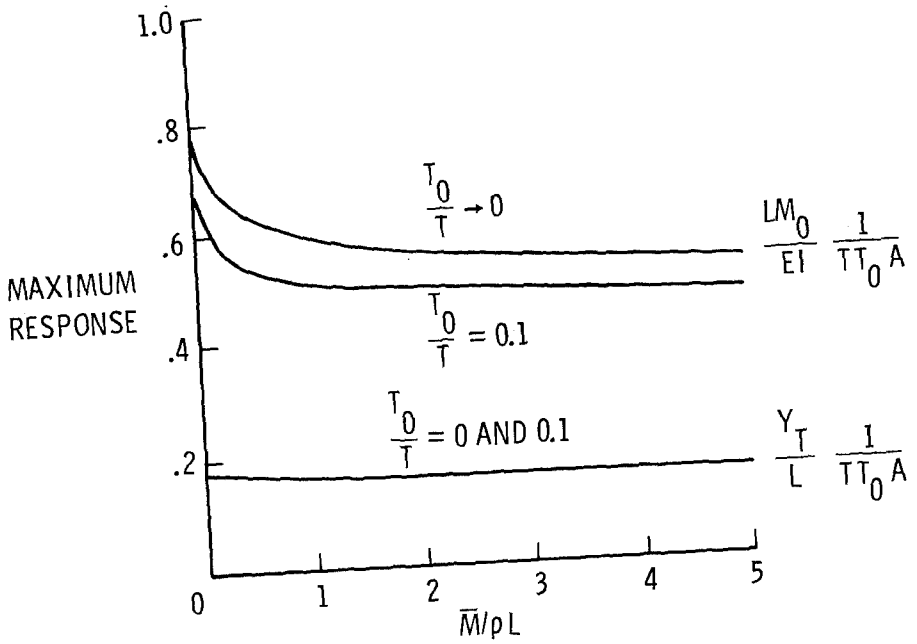

Figure 5. Effect of tip mass ($\bar{M}/\rho L$) on maximum response of beam.

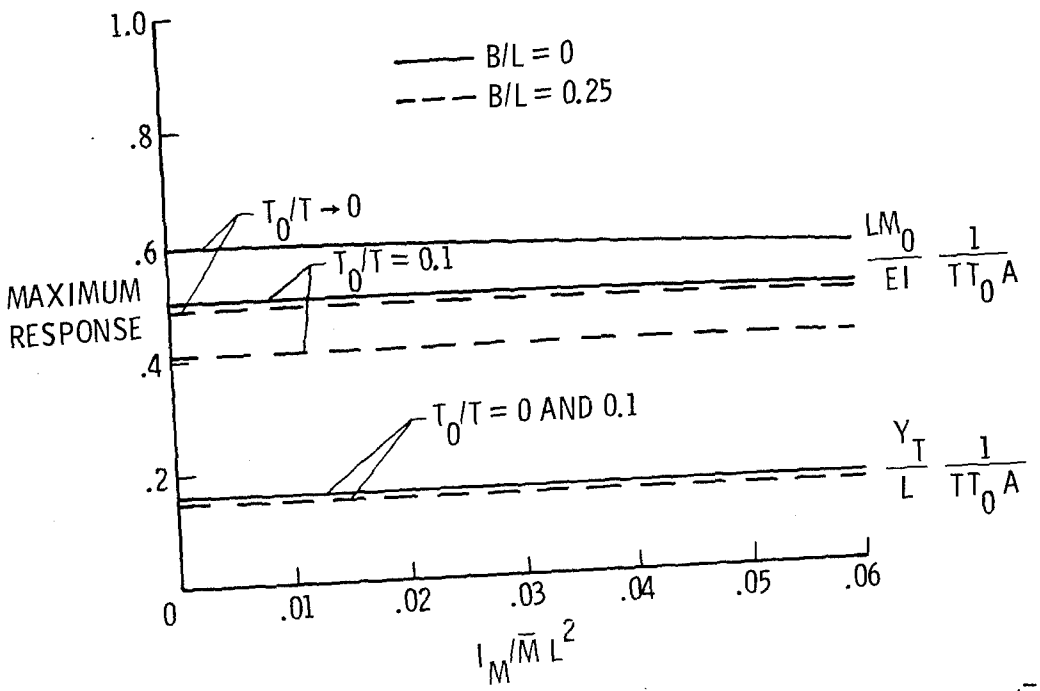

Figure 6. Effects of eccentricity (B/L) and rotatory inertia ($I_M/\bar{M}L^2$) of tip mass on maximum response of beam. $\bar{M}/\rho L = 1$.

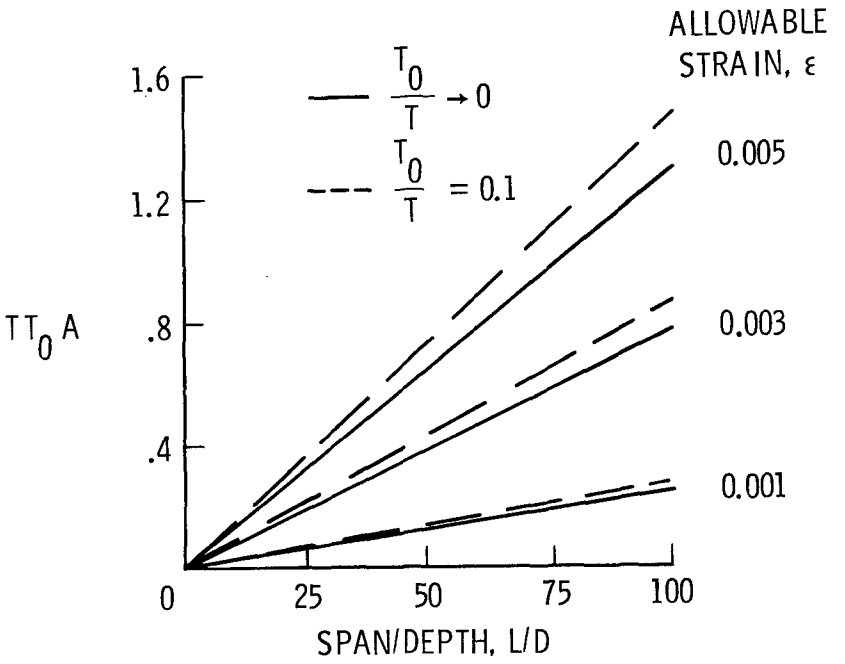

Figure 7. Nondimensional parameter (TT_0A) for permissible root rotational acceleration. $\bar{M}/\rho L = 0$.

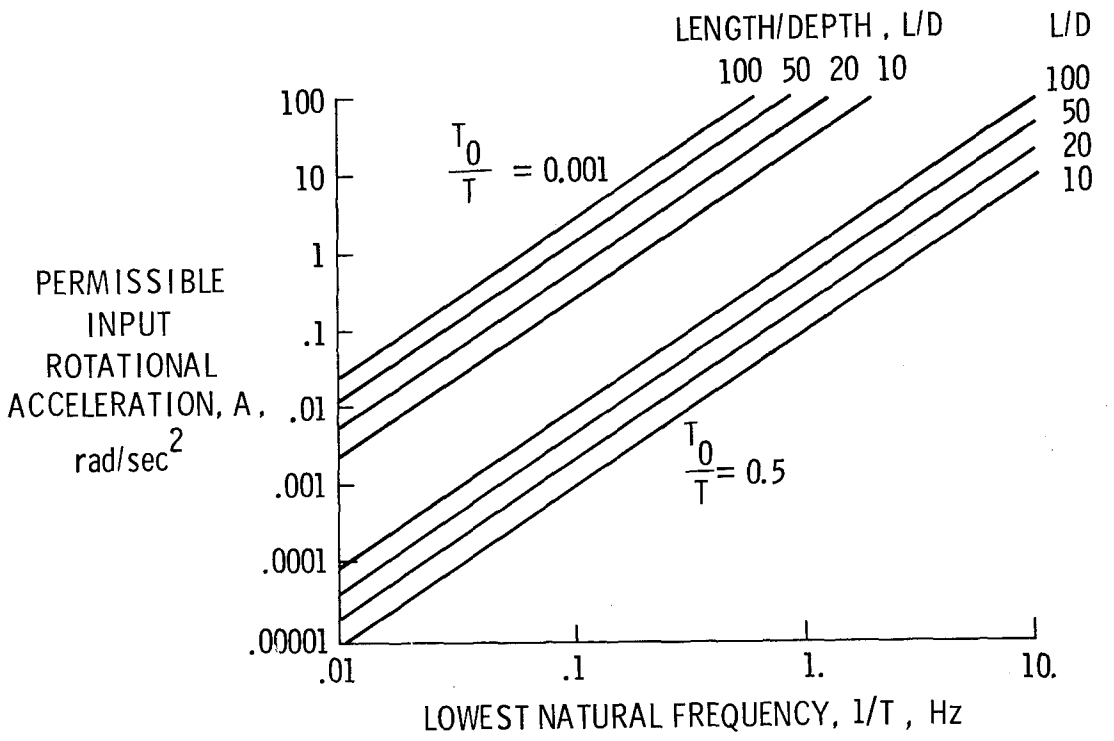

Figure 8. Permissible root rotational acceleration. $\bar{M}/\rho L = 0$, $\varepsilon = 0.001$.

OPTIMAL DESIGN AGAINST COLLAPSE AFTER BUCKLING

E. F. Masur
University of Illinois at Chicago Circle

SUMMARY

After buckling, statically indeterminate trusses, beams, and other "strictly symmetric" structures may collapse under loads which reach limiting magnitudes. The current paper discusses optimal design for prescribed values of these collapse loads.

INTRODUCTION

The principles and techniques of optimally designing structural elements against buckling have been widely investigated. For example, there exists an extensive literature on the problem of finding the least weight design for a column of prescribed Euler buckling strength (see, for example, ref. 1,2,3), and two recent publications (ref. 4,5) deal with the analogous problem of finding the lightest beam to resist lateral buckling under prescribed loads. The common feature of these problems is the fact that the structures considered are statically determinate in the sense that the prebuckling stresses themselves are independent of the design.

If the structure is indeterminate, and if the prebuckling stresses themselves are therefore affected by design changes, the problem becomes vastly more complicated and no general optimality principles appear to have been developed. On the other hand, it is likely that in cases of this type the buckling load itself does not represent an important design criterion. Some structures buckle under decreasing loads and are therefore imperfection-sensitive. Others may buckle under increasing loads, and their actual strength is again governed by factors other than the critical buckling load.

It has been shown that certain "strictly symmetric" types of structures necessarily buckle under increasing loads, and that these loads often approach limiting values as buckling deformations increase indefinitely. Examples of structures of this kind are statically indeterminate trusses (ref. 6) or beams buckling laterally (ref. 7), and recent numerical (ref. 8,9) and experimental (ref. 10) results have confirmed the general theory (ref. 11). It may therefore be realistic to study the optimal design of such structures as their collapse strength, rather than their buckling strength, is prescribed. The object of this paper is to introduce a general discussion of this problem and to indicate a method of solution.

POSTBUCKLING MODEL

The postbuckling behavior of strictly symmetric structures has been described in total generality in reference 11. It can easily be visualized by means of a simple model consisting of a pin-jointed truss of n (say, $n = 2$) degrees of indeterminacy. If the external loads are increased by increasing a common load parameter λ, then the "critical" load value is reached when the compressive force in one of the bars (say, bar 1) reaches the Euler value for that bar. Nevertheless, the load-carrying capacity of the truss is obviously not yet exhausted. While member 1 buckles under sensibly constant compressive force, λ continues to increase until member 2 similarly starts to buckle. Collapse occurs when member 3 also buckles, and $\lambda = \lambda_c$ then remains constant.

This simple process can be visualized within a format that is applicable to all strictly symmetric structures. Let $\underset{\sim}{S}$, the vector of all bar forces, be of the form

$$\underset{\sim}{S} = \lambda \underset{\sim}{S}_o + \alpha_r \underset{\sim}{S}_r \ , \tag{1}$$

in which, for simplicity, the self-equilibrated bar force systems $\underset{\sim}{S}_r$ are selected so as to satisfy the orthonormality condition

$$\sum_i \frac{S_r^i S_s^i \ell_i}{A_i E_i} \equiv \underset{\sim}{S}_r \cdot \underset{\sim}{S}_s = \delta_{rs} \qquad (r,s = 1,2) \tag{2}$$

where the summation extends over all the bars and ℓ_i, A_i, E_i represent, respectively, the length, cross-sectional area, and Young's modulus of the i^{th} bar. Moreover, if $\underset{\sim}{S}_o$ is the actual force system in the unbuckled structure, $(\alpha_r = 0)$, then

$$\underset{\sim}{S}_o \cdot \underset{\sim}{S}_r = 0 \qquad (r = 1,2) \ . \tag{3}$$

In the absence of any limitations on the tensile strength of any member, the condition of "statical admissibility" is given by

$$S^i \geqq -N^i \qquad (N^i > 0 = \text{Euler force}) \ , \tag{4}$$

which, in view of equation (1), becomes

$$\alpha_r S_r^i \geqq -N^i - \lambda S_o^i \qquad (i = 1,2,\ldots,n) \tag{5}$$

For given value of λ equations (5) define a statically admissible region in the α_r space, whose convex boundary consists of hyperplanes whose normal vectors are proportional to S_r^i (fig. 1). The region so defined need not be closed. For definiteness we assume $\lambda > 0$ and $S_o^i < 0$ $(i = 1,2,3,\ldots,p \leqq n)$; in that case the region "shrinks" for increasing values of λ.

For the sake of brevity we rule out the possibility of multiple buckling modes; then the critical value $\lambda = \lambda_1$ is reached when

$$\lambda_1 S_o^1 = -N^1 \; ; \qquad \lambda_1 S_o^i > -N^i \qquad (i = 2,3,\ldots,n) \; . \tag{6}$$

As bar 1 buckles under constant compressive Euler force the first $(i = 1)$ of equations (5), in view of equation (6), becomes

$$\alpha_r S_r^1 = -(\lambda - \lambda_1) S_o^1 \; . \tag{7}$$

At the same time the changes in the bar chord lengths are given by

$$\begin{aligned} \delta_1 &= \frac{S^1 \ell_1}{A_1 E_1} - \delta_1' \\ \delta_i &= \frac{S^i \ell_i}{A_i E_i} \qquad\qquad (i = 2,3,\ldots,n) \end{aligned} \tag{8}$$

in which $\delta_1' > 0$ represents the nonlinear effect of the curvature. Hence

$$\sum_i S_r^i \delta_i = \underset{\sim}{S}_r \cdot \underset{\sim}{S} - S_r^1 \delta_1' = 0 \qquad (r = 1,2) \; , \tag{9}$$

or, with equations (1), (2), and (3),

$$\alpha_r = S_r^1 \delta_1' \qquad\qquad (r = 1,2) \; . \tag{10}$$

Finally, when equation (10) is substituted into equation (7),

$$\lambda - \lambda_1 = -\frac{\sum_r \left(S_r^i\right)^2}{S_o^1} \delta_1' > 0 \; , \tag{11}$$

confirming, once again, that strictly symmetric structures have stable points of bifurcation.

For $\lambda < \lambda_1$ the origin 0 of the coordinate system in figure 1 is in the statically admissible region and therefore represents the actual stress point. At bifurcation $(\lambda = \lambda_1)$ the hyperplane B_1 passes through the origin and, for increasing values of λ, the origin moves outside of the statically admissible region, while the stress point P moves with B_1. According to equation (10) the vector $\overline{OP}$ is parallel to the normal to B_1 and, because of the convexity of the stable region, P is therefore closer to 0 than any other statically admissible point.

After bar 2 also buckles, point P lies on the intersection of two hyperplanes, and

$$\alpha_r = S_r^1 \delta_1' + S_r^2 \delta_2' \ . \tag{12}$$

Finally, collapse is reached, for $\lambda = \lambda_c$, when the statically admissible region has shrunk to the point P_c representing the intersection of three hyperplanes. In that case the constant values of α_r are given by

$$\alpha_r^c = S_r^1 \delta_1' + S_r^2 \delta_2' + S_r^3 \delta_3' \qquad (r = 1,2) \ , \tag{13}$$

and as collapse proceeds according to

$$\delta_i' = \omega \delta_i^c \qquad (\omega \to \infty) \ , \tag{14}$$

the collapse mechanism satisfies

$$S_r^1 \delta_1^c + S_r^2 \delta_2^c + S_r^3 \delta_3^c = 0 \qquad (r = 1,2) \ . \tag{15}$$

We also note that, in general, this mode as well as the value of λ_c is independent of initial imperfections.

OPTIMALITY

For the more general case we may identify the major state of stress by means of

$$\underset{\sim}{\sigma} = \lambda \underset{\sim}{\sigma}_o + \alpha_r \underset{\sim}{\sigma}_r \ . \tag{16}$$

The equations of compatibility are given by

$$\underset{\sim}{\sigma}_r^T \left[\underset{\sim}{C}\, \underset{\sim}{\sigma} - \frac{1}{2} \underset{\sim}{\ell}_2(\underline{v}) \right] = 0 \qquad (r = 1,2,\ldots,n) \tag{17}$$

in which $\underset{\sim}{C}$ is the compliance density with respect to σ, $\underset{\sim}{\ell}_2$ is the quadratic contribution to the major strain associated with the buckling mode $\underline{v}$, and the notation implies an integral or a summation over the entire structure.

The condition of equilibrium is given in variational form by

$$\underset{\sim}{k}^T(\underline{v})\, \underset{\sim}{K}\, \underset{\sim}{k}(\delta \underline{v}) - \underset{\sim}{\sigma}^T \underset{\sim}{\ell}_{11}(\underline{v}\, \delta \underline{v}) = 0 \ , \tag{18}$$

where $\underset{\sim}{k}$ is the linear buckling strain tensor and $\underset{\sim}{K}$ the stiffness density with respect to $\underset{\sim}{k}$. We note that both $\underset{\sim}{K}$ and $\underset{\sim}{C}$ are, in general, functions of the design variable h.

For optimality we vary the design by replacing h by $h + \dot{h}$, subject to the condition of constant volume

$$\dot{V} = \frac{dA}{dh}\dot{h} = 0 \ . \tag{19}$$

Since the load is prescribed it follows that $\dot{\lambda} = 0$; nevertheless, the major stress system (identified by α_r) and the buckling mode $\underline{v}$ may change. Variation of equations (17) and (18) then leads to

$$\underset{\sim}{\sigma}_r^T \left[\frac{d\underset{\sim}{C}}{dh}\underset{\sim}{\sigma}\dot{h} + \underset{\sim}{C}\underset{\sim}{\sigma}_s\dot{\alpha}_s - \underset{\sim}{\ell}_{11}(\underline{v}\,\dot{\underline{v}})\right] = 0 \qquad (r = 1,2,\ldots,n) \tag{20}$$

$$\underset{\sim}{k}^T(\dot{\underline{v}})\,\underset{\sim}{K}\,\underset{\sim}{k}(\delta\underline{v}) - \underset{\sim}{\sigma}^T\underset{\sim}{\ell}_{11}(\dot{\underline{v}}\,\delta\underline{v}) = \dot{\alpha}_s\underset{\sim}{\sigma}_s^T\underset{\sim}{\ell}_{11}(\underline{v}\,\delta\underline{v}) - \left[\underset{\sim}{k}^T(\underline{v})\frac{d\underset{\sim}{K}}{dh}\underset{\sim}{k}(\delta\underline{v}) - \Lambda^2\frac{dA}{dh}\right]\dot{h} \tag{21}$$

in which Λ^2 has been introduced as Lagrangian multiplier to account for equation (19). Equation (18) represents a homogeneous eigenvalue problem, and equation (21) has therefore no solution unless the condition of integrability

$$\dot{\alpha}_s\,\underset{\sim}{\sigma}_s^T\underset{\sim}{\ell}_2(\underline{v}) - \left[\underset{\sim}{k}^T(\underline{v})\frac{d\underset{\sim}{K}}{dh}\underset{\sim}{k}(\underline{v}) - \Lambda^2\frac{dA}{dh}\right]\dot{h} = 0 \tag{22}$$

is satisfied. We note that equations (20) and (22) are similar to the equations derived for the initial buckling case in reference 4, except for the last term in equation (20) representing the contribution of the postbuckling condition.

Letting once again

$$\underline{v} = \omega\underline{v}_c \qquad \Lambda = \omega\Lambda_c \qquad (\omega \to \infty) \tag{23}$$

and assuming collapse under finite load and stress conditions we obtain

$$\underset{\sim}{\sigma}_r^T\underset{\sim}{\ell}_2(\underline{v}_c) = 0 \qquad (r = 1,2,\ldots,n) \tag{24}$$

$$\underset{\sim}{k}^T(\underline{v}_c)\,\underset{\sim}{K}\,\underset{\sim}{k}(\delta\underline{v}) - \underset{\sim}{\sigma}_c^T\underset{\sim}{\ell}_{11}(\underline{v}_c\,\delta\underline{v}) = 0 \tag{25}$$

$$\underset{\sim}{k}^T(\underline{v}_c)\frac{d\underset{\sim}{K}}{dh}\underset{\sim}{k}(\underline{v}_c) = \Lambda^2\frac{dA}{dh} \tag{26}$$

of which the first two equations represent the collapse condition, and the last constitutes the condition of optimality. It is noted that once again this optimality condition requires constant strain energy density in the design fibers. It is also noted that for collapse (in contrast to initial buckling) the direct effect of a design change on the collapse mode via the compatibility conditions has disappeared. In other words, we see once again a parallel behavior pattern between collapse through buckling and collapse through perfect plasticity.

EXAMPLE

As an example to illustrate the theory, we consider a beam of length ℓ which is fixed in its own major plane at the right end and subjected to a bending moment λ at the simply supported left end. Collapse occurs when

$$\sigma_c = \lambda_c\left(1 - \frac{3}{2}\frac{x}{\ell}\right) + \alpha_c \frac{x}{\ell} , \tag{27}$$

while the equations of equilibrium (25) assume the form

$$K_1 u_c'' - \sigma_c \beta_c = 0 \qquad (K_2 \beta_c')' + \sigma_c u_c'' = 0 \qquad (0 \leqq x \leqq \ell) \tag{28}$$

where u and β represent the lateral displacement and rotation, respectively, with associated bending and torsional stiffnesses K_1 and K_2. In the development of equations (28), it is assumed that $u = u'' = \beta = 0$ at both ends and that the effect of warping can be neglected. In terms of β alone equations (28) reduce to

$$(K_2 \beta_c')' + \frac{\sigma_c^2}{K_1} \beta_c = 0 \qquad (0 \leqq x \leqq \ell) \tag{29}$$

The collapse condition equation (24) becomes

$$\int_0^\ell x\, u_c'' \beta_c \, dx = \int_0^\ell \frac{x}{K_1} \sigma_c \beta_c^2 \, dx = 0 , \tag{30}$$

while the optimality criterion equation (26) assumes the form

$$\frac{dK_1}{dh}\left(\frac{\sigma_c}{K_1}\right)^2 \beta_c^2 + \frac{dK_2}{dh} \beta_c'^2 = \Lambda_c^2 \frac{dA}{dh} \qquad (0 \leqq x \leqq \ell) . \tag{31}$$

For the specific case of a thin rectangular beam, in which $K_1 = b^3h/12$, $K_2 = b^3h/3$, and $A = bh$, and in view of equation (29), equation (31) can be written in the form

$$h = -\frac{b^2}{3\Lambda_c^2}\beta_c^2\left(\frac{h\beta_c'}{\beta_c}\right)' \qquad (32)$$

which lends itself well to an iterative solution scheme. It is also interesting to note that equation (32) is satisfied for constant value of h provided $\beta = \sin \pi x/\ell$; this confirms the curious conclusion arrived at recently by Popelar (ref. 4) that the prismatic design represents an optimum for simply supported beams under constant bending moment.

Numerical results covering equations (29), (30) and (32) for the case under consideration are currently being developed. Because of the variation in the major bending moment, it is expected that in this case the prismatic beam is not optimum, and that optimal design for collapse may lead to a noticeable reduction in weight.

REFERENCES

1. Keller, J. B.: The Shape of the Strongest Column. Arch. Rat. Mech. Anal., Vol. 5, 1960, pp. 275-285.

2. Prager, W. and Taylor, J. E.: Problems of Optimal Structural Design. J. Appl. Mech., Vol. 35, 1968, pp. 102-106.

3. Masur, E. F.: Optimal Placement of Available Sections in Structural Eigenvalue Problems. J. Optim. Theory Appl., Vol. 15, 1975, pp. 69-84.

4. Popelar, C. H.: Optimal Design of Beams against Buckling: A Potential Energy Approach. J. Struc. Mech., Vol. 4, 1976, pp. 181-196.

5. Popelar, C. H.: Optimal Design of Structures against Buckling: A Complementary Energy Approach. J. Struc. Mech., Vol. 5, 1977.

6. Masur, E. F.: Post-Buckling Strength of Redundant Trusses. Trans. ASCE, Vol. 119, 1954, pp. 699-716.

7. Masur, E. F. and Milbradt, K. P.: Collapse Strength of Redundant Beams after Lateral Buckling. J. Appl. Mech., Vol. 24, 1957, pp. 283-288.

8. Bazant, Z. P. and Nimeiri, M. E.: Large Deflection Spatial Buckling of Thin-Walled Beams and Frames. J. Engr. Mech. Div., ASCE, Vol. 99, 1973, pp. 1259-1282.

9. Woolcock, S. T. and Trahair, N. S.: Post-Buckling of Redundant Rectangular Beams. J. Engr. Mech. Div., ASCE, Vol. 101, 1975, pp. 301-316.

10. Trahair, N. S.: Elastic Stability of Continuous Beams. J. Struc. Div., ASCE, Vol. 95, 1969, pp. 1295-1312.

11. Masur, E. F.: Buckling, Post-Buckling and Limit Analysis of Completely Symmetric Structures. Int. J. Sol. Struc., Vol. 6, 1970, pp. 587-604.

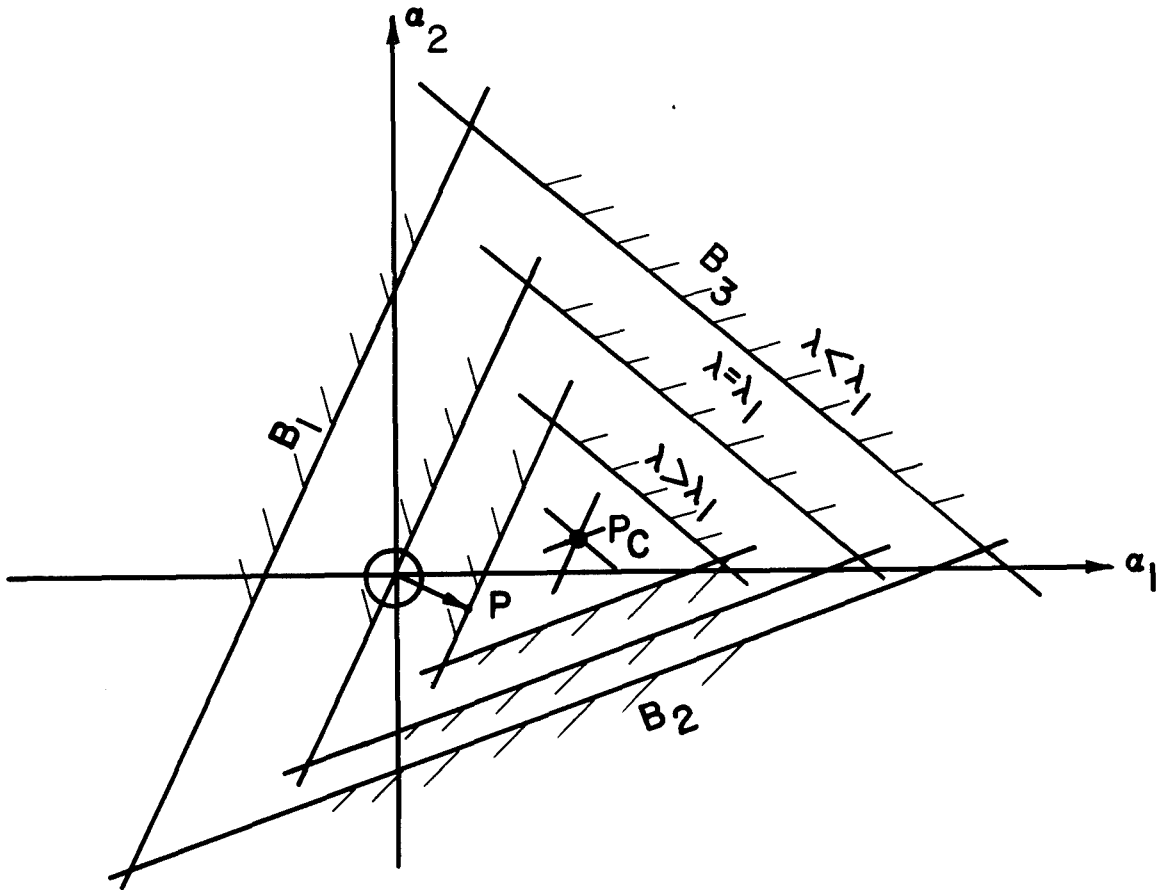

Figure 1.- Redundant stress space.

OPTIMUM VIBRATING BEAMS WITH STRESS AND DEFLECTION CONSTRAINTS

Manohar P. Kamat
Virginia Polytechnic Institute and State University

SUMMARY

The fundamental frequency of vibration of an Euler-Bernoulli or a Timoshenko beam of a specified constant volume is maximized subject to the constraint that under a prescribed loading the maximum stress or maximum deflection at any point along the beam axis will not exceed a specified value. In contrast with the inequality constraint which controls the minimum cross-section, the present inequality constraints lead to more meaningful designs. The inequality constraint on stresses is as easily implemented as the minimum cross-section constraint but the inequality constraint on deflection uses a treatment which is an extension of the matrix partitioning technique of prescribing displacements in finite-element analysis.

INTRODUCTION

The problem of maximizing the fundamental frequency of vibration of beams of a fixed, prescribed volume and likewise its dual problem have been investigated by a great many investigators (see reference 1). It appears that no consensus has been reached however, on the existence of non-trivial solutions for beams with certain types of boundary conditions. While the numerical experiments do strongly emphasize the existence of such solutions (see refs. 2 and 3), mathematical proofs have been constructed (see ref. 4) to prove otherwise. This situation is rather unique since more often than not it is the dismal failure of the numerical techniques in obtaining a solution, which is only presumed to exist, that calls upon mathematics to establish its existence or non-existence.

The difficulty stems from singularities which result from vanishing stiffness at some points along the beam axis. Although at such points the curvature $w,_{xx}$ assumes an infinite value, the products $I(x)w,_{xx}$ and $I(x)w,^{2}_{xx}$ are nonetheless finite at such points. Furthermore, the function $I(x)w,^{2}_{xx}$ is required to be integrable over the length of the beam. Fallacies of the mathematical proofs, if any, could well result from a failure to take proper account of these properties for the functions $I(x)$ and $w(x)$.

Finite-element solutions of reference 3, which incidently emphasize existence even in the absence of any inequality constraints appear to have very limited practical value because the resulting designs are far from being useful as load-carrying members. Controlling the minimum cross section of the beam does not appear to be the answer. The optimized beam must sustain a given loading, presumably the worst loading, without exceeding a prescribed level of

stress or a prescribed value for the maximum deflection. In general, the cross section with the least area is not necessarily the critical section in terms of stress nor are the constraints on deflections met in a rational and an expeditious manner simply by controlling the minimum cross-sectional area of the beam.

To generate more practical designs, it is deemed appropriate to require that the optimum beam shall not (i) be stressed to more than a specified multiple of the maximum stress or (ii) deflect more than a specified multiple of the maximum deflection of the corresponding uniform beam of the same volume. The present formulation allows the specification of an arbitrary vector of stresses or of deflections, with those corresponding to the uniform beam case being specializations of the arbitrarily specified vectors.

PROBLEM FORMULATION

The formulation is restricted to discretized finite-element models of beams. Since the case of an Euler-Bernoulli beam can be obtained as a special case of a Timoshenko beam, the latter will be implied in the formulation.

The approach is exactly similar to the one used in ref. 3. It consists of maximizing the minimum value of the Rayleigh quotient, ω^2, for a Timoshenko beam subject to the equality and the inequality constraints. For a discretized finite-element model

$$\omega^2 = \frac{[q][K]\{q\}}{[q][M]\{q\}} \tag{1}$$

where [K] and [M] are, respectively, the assembled stiffness and mass matrices derived on the basis of a uniform cross-section beam element and {q} is the mode shape of free vibration. In the case of a Timoshenko beam the stiffness matrix accounts for the effects of shear deformations and the mass matrix accounts for the effects of rotary inertia. Furthermore, for a general case, the stiffness matrix may include the effect of a specified distribution of axial loading and elastic foundation and likewise the mass matrix may include the effects of a specified distribution of non-structural mass.

The optimization is to be carried out subject to the equality constraint of a fixed, given total volume V which for a beam with elements each of length ℓ_i and cross-sectional area A_i, i=1,2...m, reduces to

$$\sum_{i=1}^{m} A_i \ell_i = V \tag{2}$$

The required relation between the cross-sectional area and the moment of inertia is provided by a consideration of cross-sectional shapes for which

$$I_i = \rho A_i^n \tag{3}$$

$\rho>0$ and n being appropriate constants depending upon the type of cross section.

Stress Constraint

It is required that for a beam satisfying eqs. (1) through (3), the Rayleigh quotient of eq. (1) be maximized subject to the constraint that

$$\{\sigma\} \leq k_\sigma^2 \{\tilde{\sigma}\} \tag{4}$$

where $\{\sigma\}$ is the vector of nodal stresses for the optimum beam under a prescribed loading and $\{\tilde{\sigma}\}$ is the vector of prescribed stresses. Since stress at an internal node is discontinuous, the vectors $\{\sigma\}$ and $\{\tilde{\sigma}\}$ are assumed to be of size 2m by one.

A beam element with a cubic transverse displacement field has a linear variation of bending moment within an element. Thus, the maximum bending moment within an element can occur only at the two nodes and hence, as in eq. (4), only the nodal stresses need be monitored for the purposes of implementing the stress constraints.

The stress σ_{1i} due to a bending moment M_{1i} at node 1 of element i is

$$|\sigma_{1i}| = \left|\frac{M_{1i} c_i}{I_i}\right| \tag{5}$$

For cross-sections specified by eq. (3), it can be easily verified that

$$\frac{c_i}{\overset{0}{c_i}} = \left(\frac{I_i}{\overset{0}{I_i}}\right)^{\frac{n-1}{2n}} \tag{6}$$

where quantities with superscript 0 pertain to the uniform beam of total volume V. Equations (5) and (6) together imply that

$$\{\sigma\} = \left\{\frac{M}{(I)^{\frac{n+1}{2n}}}\right\} \tag{7}$$

Accordingly, eq. (4) can be written as

$$\left\{\frac{M}{(I)^{\frac{n+1}{2n}}}\right\} \leq k_\sigma^2 \{\tilde{\sigma}\} \tag{8}$$

The inequality constraint, eq. (8), can be transformed into an equivalent equality constraint by Valentine's principle. An auxiliary functional which is the original functional of eq. (1) modified by the two equality constraints with the aid of undetermined Lagrange multipliers is constructed. In terms of

non-dimensional quantities this functional can be shown to be

$$(\omega^2)^* = \frac{[q^*][K^*]\{q^*\}}{[q^*][M^*]\{q^*\}} - \lambda_0^*\left(\sum_{i=1}^{m} A_i^* \ell_i^* - 1\right)$$

$$- \sum_{i=1}^{m} \left\langle \lambda_{1i}^* \left[\left(\frac{M_{1i}^*}{(I^*)_i^{\frac{n+1}{2n}}}\right) - k_\sigma^2 (\tilde{\sigma}_{1i}^*) + \phi_{1i}^{*2}\right] \right. \tag{9}$$

$$\left. + \lambda_{2i}^* \left[\left(\frac{M_{2i}^*}{(I^*)_i^{\frac{n+1}{2n}}}\right) - k_\sigma^2 (\tilde{\sigma}_{2i}^*) + \phi_{2i}^{*2}\right] \right\rangle$$

where

$(\omega^2)^*$ = square of the non-dimensional fundamental frequency

$$= \frac{\gamma}{g} \frac{A^0 \ell^4 \omega^2}{EI^0}$$

A^* = non-dimensional cross-sectional area

$$= \frac{A}{A^0} = \frac{A\ell}{V} \tag{10}$$

I^* = non-dimensional cross-sectional moment of inertia

$$= \frac{I}{I^0}$$

M^* = non-dimensional bending moment

$$= \frac{M\ell}{EI^0}$$

$\tilde{\sigma}_i^*$ = non-dimensional stress

$$= \frac{\tilde{\sigma}_i \ell}{Ec^0}$$

where ℓ, A^0, I^0, and c^0 are, respectively, the length, the cross-sectional area, moment of inertia and distance of the extreme fiber from the centroidal axis of the cross-section of the equivalent uniform beam of volume V. ϕ_1^* and ϕ_2^* are the non-dimensional auxiliary functions of $\xi=x/\ell$, which transform the inequality constraints into equivalent equality constraints.

The requirement of the vanishing of the variation of $(\omega^2)^*$ with respect to $\{q^*\}$, λ_j^* and ϕ^* yields the necessary optimality conditions. Based on the work of ref. 3, these conditions can be shown to be the following:

In those portions of the beam where the inequality constraint is not effective, the conditions

$$(nU^*_{bi} + U^*_{si} - T^*_{ti} - nT^*_{ri})/V_i = \text{constant}, \quad i=1,2...m \qquad (11)$$

hold true; while in other portions the stress constraint is effective. In eq. (11) U^*_{bi} and U^*_{si} denote non-dimensional strain energies due to pure bending and shear deformations, respectively; T^*_{ti} and T^*_{ri} denote non-dimensional kinetic energy densities due to translational and rotary inertia, respectively, and V_i denotes the volume of the i-th element.

Implementation of the stress inequality constraint in the optimization procedure proceeds in a manner very similar to the one used for the minimum cross-section inequality constraint of ref. 3. The moments of inertia of elements leading to improved designs are determined by recurrence relations designed to force the specific energy density of eq. (11) to be a constant for all elements assuming initially that none of the elements are governed by any inequality constraint. (See reference 3 for details of these recurrence relations.) In each iteration, however, determining if the stress constraint is effective or not requires a complete static stress analysis of the beam to obtain the vector of nodal stresses. The cross-sectional inertias of those elements which violate the constraint are then set equal to

$$I_i^* = \max\left[\left(\frac{M^*_{1i}}{\sigma^*_{1i}}\right)^{\frac{2n}{n+1}}, \left(\frac{M^*_{2i}}{\sigma^*_{2i}}\right)^{\frac{2n}{n+1}}\right] \qquad (12)$$

The cross-sectional inertias of the other elements which do not violate the inequality constraint are adjusted to meet the volume equality constraint, eq. (2).

Although for statically determinate beams eq. (12) guarantees the satisfaction of the stress constraint in any given iteration of the frequency optimization the same is not true of statically indeterminate beams. For the latter, one could conceivably iterate within the static stress analysis to determine the appropriate element stiffnesses so as to satisfy the stress constraints to within a desired tolerance. However, in view of the iterative nature of the frequency optimization procedure, such additional effort is not warranted especially if stiffness changes in successive iterations are kept small enough.

In view of the equality constraint, eq. (2), it is obvious that the maximum number of elements which may be governed by this constraint is at most m-1 for a consistent constrained optimization.

Deflection Constraint

In this case it is required that for a beam satisfying eqs. (1) through (3), the Rayleigh quotient of eq. (1) be maximized subject to the constraint that

$$\{r\} \leq k_\delta^2 \{\tilde{r}\} \tag{13}$$

where $\{r\}$ is the vector of nodal displacements for the optimum beam under a prescribed loading and $\{\tilde{r}\}$ is the vector of prescribed displacements. Both vectors are of size (2m+2) by one. As with the stress constraint the maximum number of elements whose cross-sectional moment of inertia can be arbitrarily specified is at most m-1. Hence, under the limiting case of a strict equality in eq. (13), the number of equations which imply prescribed displacements cannot exceed m-1 for a consistent constrained optimization.

In this case, the auxiliary functional in terms of non-dimensional quantities is

$$(\omega^2)^* = \frac{[q^*][K^*]\{q^*\}}{[q^*][M^*]\{q^*\}} - \lambda_0^* \left(\sum_{i=1}^{m} A_i^* \ell_i^* - 1\right) - \sum_{i+1}^{m+1} \lambda_i^* [(r_i^*)^2 - k_\delta^2 (\tilde{r}_i^*)^2 + (\psi_i^*)^2] \tag{14}$$

where

$$\begin{aligned} r_i^* &= r_i/\ell \quad \text{for translational degree of freedom} \\ &= r_i \quad \text{for rotational degree of freedom} \end{aligned} \tag{15}$$

Proceeding as before the optimality conditions can be shown to be eq. (11) in those portions of the beam for which the deflection constraint is not effective; while in other portions the deflection constraint is effective. Since the transverse displacement field varies cubically over the length of the element, satisfaction of the constraint at the two nodes of the element does not guarantee that the constraint is not violated in the interior, especially if large changes in curvatures take place within the element. This is circumvented by refining the discretization sufficiently.

Strictly speaking, the implementation of the stress constraint is, in general, an implicit, nonlinear phenomenon which is rendered explicit by the use of a very simple and approximate relation, eq. (12). No such approximations are necessary for the implementation of deflection constraints. The problem

in this case reduces to determing element stiffnesses which guarantee prescribed displacements under prescribed loads. Let $[K^*_s]$ denote the assembled matrix of the supported beam and let $\{r^*_\beta\}$ denote those nodal displacements which violate the constraints, eq.(13). The matrix $[K^*_s]$ and the corresponding displacement and load vectors are accordingly partitioned as

$$\begin{bmatrix} K^*_{\alpha\alpha} & K^*_{\alpha\beta} \\ K^*_{\beta\alpha} & K^*_{\beta\beta} \end{bmatrix} \begin{Bmatrix} r^*_\alpha \\ \tilde{r}^*_\beta \end{Bmatrix} = \begin{Bmatrix} \tilde{Q}^*_\alpha \\ \tilde{Q}^*_\beta \end{Bmatrix} \tag{16}$$

where $\{\tilde{Q}^*_\alpha\}$ and $\{\tilde{Q}^*_\beta\}$ are the vectors of externally prescribed loads with the latter being associated with those degrees of freedom which violate the displacement constraints and are accordingly prescribed as being equal to $\{\tilde{r}^*_\beta\}$. Equations (16) yield

$$[K^*_{\alpha\alpha}]\{r^*_\alpha\}+[K^*_{\alpha\beta}]\{\tilde{r}^*_\beta\}= \{\tilde{Q}^*_\alpha\} \tag{17 a}$$

$$[K^*_{\beta\alpha}]\{r^*_\alpha\}+[K^*_{\beta\beta}]\{\tilde{r}^*_\beta\}= \{\tilde{Q}^*_\beta\} \tag{17 b}$$

Simultaneous solution of equations (17 a) and (17 b) yields

$$[K^*_{\beta\beta}]\{\tilde{r}^*_\beta\}=\{\tilde{Q}^*_\beta\}-[K^*_{\beta\alpha}][K^*_{\alpha\alpha}]^{-1}(\{\tilde{Q}^*_\alpha\}-[K^*_{\alpha\beta}]\{\tilde{r}^*_\beta\}) = \{F^*_\beta\} \tag{18}$$

If the elements of the matrix $[K^*_{\beta\beta}]$ are assumed to be functions of moments of inertia of as many beam elements as the number of prescribed displacements $\{\tilde{r}^*_\beta\}$, then the system of equations (18) can be uniquely solved for the unknown moments of inertia which guarantee the satisfaction of the deflection constraint, eq. (13).

Those displacements which violate the constraints are prescribed as being equal to the specified values. Invariably, more than one alternative will exist for the specification of stiffnesses with prescribed displacements. If both the degrees of freedom of a joint are prescribed, then the moments of inertia of both elements common to the joint must be prescribed. However, if a single degree of freedom is prescribed at a joint, then it is not obvious which of the two elements should have a prescribed stiffness. Herein may lie the nonuniqueness of the resulting solution for beams with certain boundary conditions with certain loadings. A rational criterion for making such a decision should be based on the magnitudes of displacements of one joint relative to the other, since such relative displacements are functions of the properties of the element alone. Accordingly, relative displacements of joints, on either side of the joint whose displacement is prescribed, are determined. The element with the joint which has a higher relative displacement is selected for the purposes of prescribing the moment of inertia.

The procedure is straightforward from this point onwards. The moments of

inertia of the constrained elements which guarantee the satisfaction of the deflection constraints are obtained by the solution of eq. (18). The inertias of the remaining elements initially obtained through the use of energy based recurrence relation of reference 3 are finally adjusted to satisfy the equality volume constraint, eq. (2).

RESULTS AND DISCUSSION

In general, because of the necessity of satisfying the equality constraint, eqs. (12) and (18) do not guarantee the satisfaction of the stress and deflection constraints exactly. This causes the optimization procedure to fail to converge or converge extremely slowly to the optimum solution. This is avoided by modifying the inequality constraints with a multiplicative constraint factor, R^{β}, which tends to unity with convergence to the optimum solution. The parameter R is chosen to be the least of the ratios of the prescribed displacements to the actual displacements in the case of displacement constraints or to be the maximum of the ratios of the actual stress to the prescribed stress in the case of stress constraints. β is chosen to be greater than unity. Increasingly higher values of β imply increasingly stiffer designs.

Figures 1 and 2 portray the effects of the implementation of the stress constraints on the optimum design of vibrating beams with two different support conditions. Figure 3 illustrates the effect of implementing the deflection constraint on the optimum design of a vibrating cantilever beam.

Figure 1 considers the case of a cantilever beam subjected to two different types of loading for the implementation of stress constraints in the optimization of its fundamental frequency of free vibration. In one case the loading consists of a concentrated load at the tip with $k_{\sigma}^2=5$ and $\{\tilde{\sigma}\}=(\sigma_{max})^0_{load}\{1\}$. In the other case the loading consists of a concentrated bending moment at the tip with $k_{\sigma}^2=5$ and $\{\tilde{\sigma}\}=(\sigma_{max})^0_{load}\{1\}$. As expected, the constraint corresponding to the moment loading is much more severe and accordingly leads to a drastic reduction of the optimized fundamental frequency. A comparison of these designs with the optimized beam without these constraints emphasizes the importance of such constraints in optimal design.

Figure 2 considers the case of a clamped-clamped beam subjected to a concentrated load at the center with $\{\tilde{\sigma}\}=(\sigma_{max})^0\{1\}$ for two distinct values of k_{σ}^2. If it were not for the stress constraints, the moment of inertia would approach zero at the center of the beam as in reference 3. Severity of the stress constraints brings about increased quantities of material to be disposed around the center of the beam.

Figure 3 illustrates the material distribution of an optimum cantilever beam subject to the deflection inequality constraint with $k_{\delta}^2=5$ and $\{\tilde{r}\}=\{r\}^0_{load}$ under a concentrated load at the free end of the beam. Since no singularity exists with inequality constraints of either the displacement or stress type and since the deflected shape of the beam under a concentrated end load or a moment involves no change of curvature, it can be expected that the solution

obtained using only ten elements for the cantilever beam model is a good approximation to the optimum continuous model.

In conclusion, it may be remarked that with only a minor change of the computer logic the formulation extends quite easily to cases wherein both deflection and stress constraints are specified simultaneously.

REFERENCES

1. Olszowski, B.,: Some Problems of Optimum Design Problems of Vibrating Systems. Archives of Mechanics, Vol. 27, No. 4, 1975, pp. 605-616.

2. Karihaloo, B. L. and Niordson, F. I.: Optimum Design of Vibrating Cantilevers. J. Optimization Theory Appl., Vol. 11, 1973, pp. 638-654.

3. Kamat, M. P.: Effect of Shear Deformations and Rotary Inertia on Optimum Beam Frequencies. Int. J. Num. Meth. Engrg., Vol. 9, 1975, pp. 51-62.

4. Vepa, K.: On the Existence of Solutions to Optimization Problems with Eigenvalue Constraints. Quart. Appl. Math., Vol. 31, No. 3, 1973, pp. 329-341.

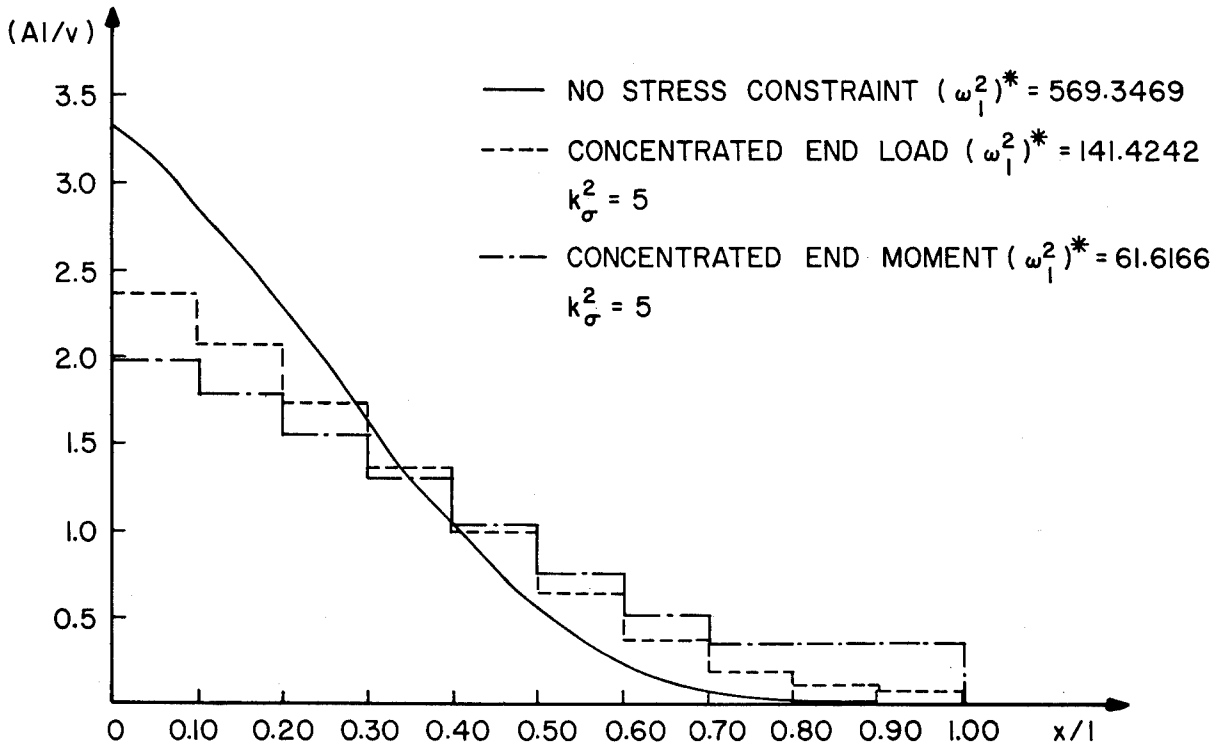

Figure 1.- Optimum area distribution for a beam clamped at x=0 and free at x=ℓ under stress constraints; n=2.

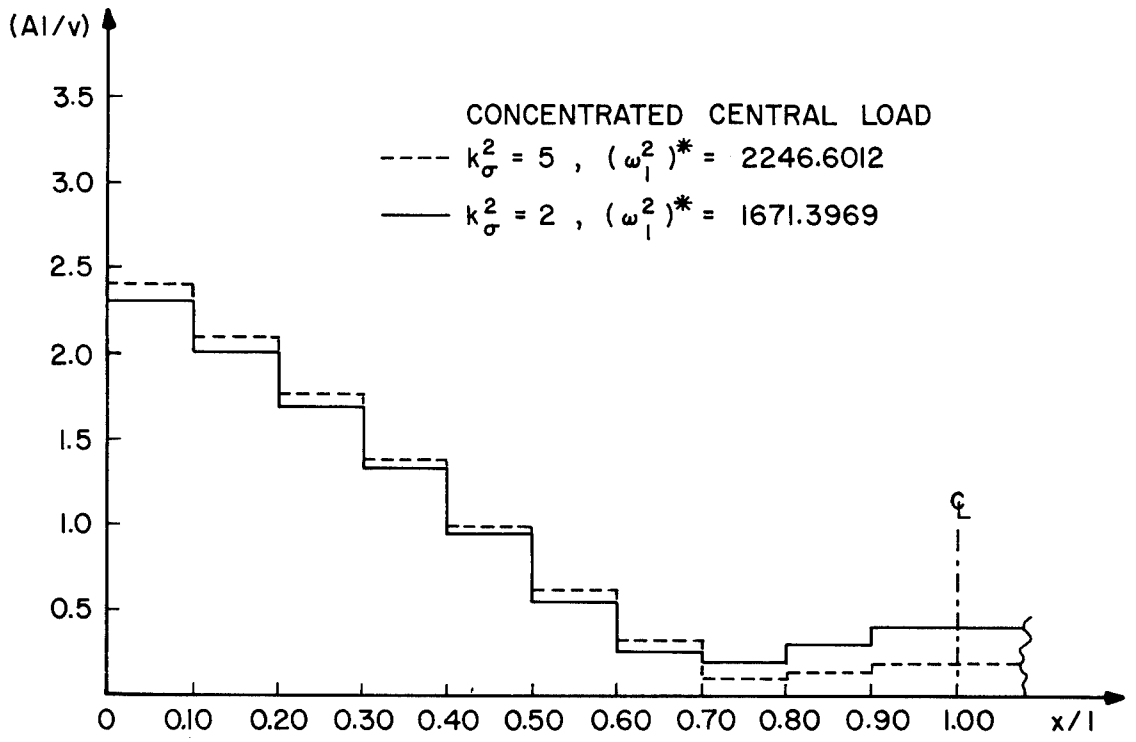

Figure 2.- Optimum area distribution for a beam clamped at both ends under stress constraints; n=2.

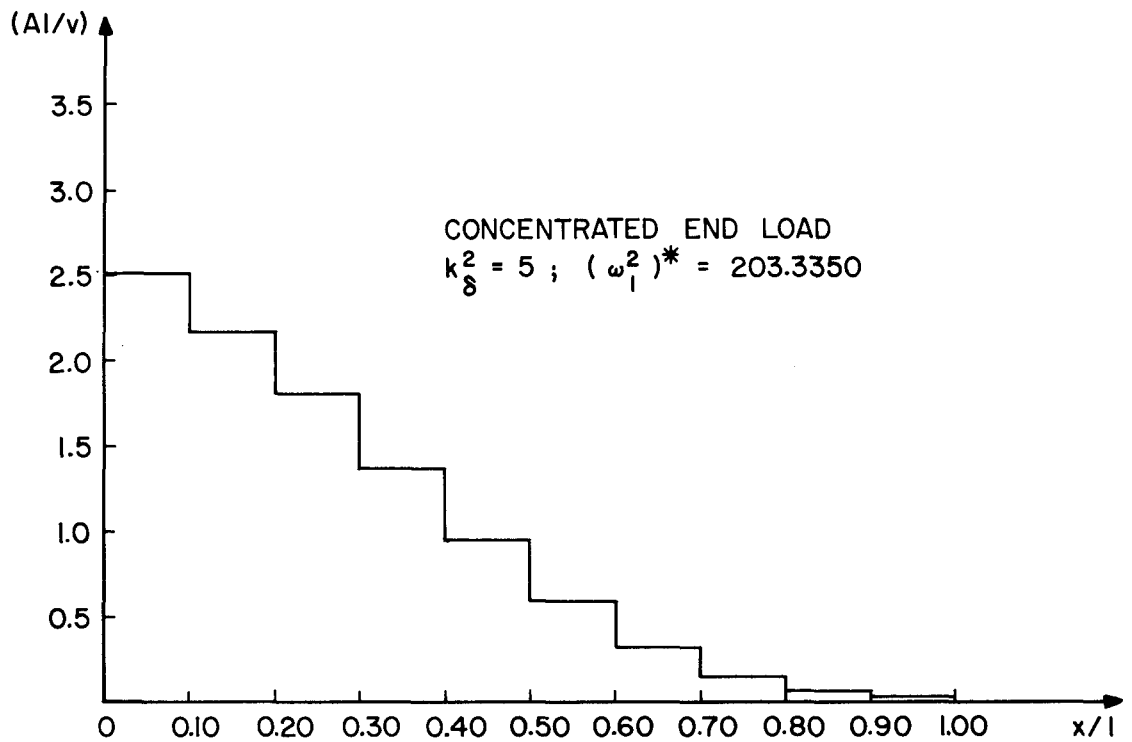

Figure 3.- Optimum area distribution for a beam clamped at x=0 and free at x=ℓ under a deflection constraint; n=2.

AN OPTIMAL STRUCTURAL DESIGN ALGORITHM USING OPTIMALITY CRITERIA

John E. Taylor
University of Michigan

Mark P. Rossow
Washington University, St. Louis, Missouri

SUMMARY

An algorithm for optimal design is given which incorporates several of the desirable features of both mathematical programming and optimality criteria, while avoiding some of the undesirable features. The algorithm proceeds by approaching the optimal solution through the solutions of an associated set of constrained optimal design problems. The solutions of the constrained problems are recognized at each stage through the application of optimality criteria based on energy concepts. Two examples are described in which the optimal member size and layout of a truss is predicted, given the joint locations and loads.

INTRODUCTION

In the field of optimal structural design, two general techniques for finding the optimum design may be distinguished: mathematical programming methods and the use of optimality criteria. In the present paper, an algorithm is given which resembles a technique of mathematical programming in that it proceeds by stages, with an improved design generated at each stage. However, in contrast to most mathematical programming methods, the improved design is identified at each stage by the application of optimality criteria, rather than by a search technique. In this way, the computationally expensive search procedure is avoided, yet the principle of approaching the optimum through a succession of small changes is preserved. The algorithm is explained and illustrated by application to the optimal design of a truss, where member cross-sectional areas are taken as the design variables.

SYMBOLS

A_i cross-sectional area of truss member i

a_r slack function

$D(p,S^*)$ trial design corresponding to p and S^*

E	elastic modulus
F_j	x and y components of external loads applied at nodes and numbered consecutively
L	augmented function
ℓ_i	length of member i
m	total number of nodes
n	total number of truss members, assuming each node connected to every other node by a member
P	potential energy
S	value of lower bound constraint
V	specified volume of material
δ_j	nodal displacements, numbered corresponding to F_j
ε_i	strain of member i
Λ_i	Lagrange multipliers for area constraints
λ	Lagrange multiplier for volume constraint (also equal to specific strain energy of fully-stressed members)
$\eta_k, \eta_k(p,S)$	specific strain energy of member k, corresponding to fully-stressed set p and constraint value S

ENERGY FORMULATION

Consider the problem of finding the maximum stiffness design of a planar truss, given a specified total volume of material to be allocated to the various members of the truss, and specifying inequality constraints on the truss members' cross-sectional areas. The connectivity of the truss is unrestricted; however, locations of nodes are specified beforehand, and the possibility of member buckling is ignored. Taylor (ref. 1) and Hiley (ref. 2) have shown how a problem of the type just described may be formulated by the use of the potential energy function of the structure. In the present paper a similar energy formulation will be used. The potential energy of the truss may be written

$$P = \sum_{i=1}^{n} \ell_i A_i \eta_i - \sum_{j=1}^{2m} F_j \delta_j \tag{1}$$

(See the list of symbols for definitions of the parameters.)

The specific strain energy η_i is related to the strain ε_i by

$$\eta_i = E\varepsilon_i^2/2 \tag{2}$$

where E is the elastic modulus.

The volume constraint is

$$\sum_{i=1}^{n} A_i \ell_i = V \tag{3}$$

where V is the specified volume of material. The inequality constraints are

$$A_i \geq S \tag{4}$$

where S is the specified lower bound constraint.

It can be shown that the problem of maximum stiffness design is equivalent to that of maximizing the potential energy P (refs. 1,3).

The constraints may be introduced directly into the problem formulation by defining the slack functions a_r by

$$A_r - a_r^2 = S, \qquad r = 1,2,\ldots,n \tag{5}$$

and introducing Lagrange multipliers λ and Λ_i to form the augmented function

$$L = P + \lambda(V - \sum_{i=1}^{n} A_i \ell_i) + \sum_{i=1}^{n} \Lambda_i (S - A_i + a_i^2) \tag{6}$$

Requiring the first derivatives of L with respect to δ_k, A_r, and a_r to vanish gives

$$\sum_{i=1}^{n} \ell_i A_i \frac{\partial \eta_i}{\partial \delta_k} - F_k = 0 \tag{7}$$

$$\eta_r \ell_r - \lambda \ell_r - \Lambda_r = 0 \tag{8}$$

$$\Lambda_r a_r = 0 \tag{9}$$

while application of the Kuhn-Tucker theorem of non-linear programming gives

$$\Lambda_r \leq 0 \tag{10}$$

These equations can be shown to be both necessary and sufficient for optimality (refs. 1,4,5).

A basic assumption about the optimal design problem formulated above will now be made. It is assumed that for every value of S in the interval $0<S\leq V/(\sum_{i=1}^{n} \ell_i)$ an optimal design exists. That is, the optimal design is assumed to be a function of S. Furthermore, this function is assumed continuous.

It is of interest to note that at least one optimal design can always be found easily for the value of the lower bound constraint given by

$$S = V/(\sum_{i=1}^{n} \ell_i) \tag{11}$$

For by equation (4) all admissible designs must satisfy

$$A_j \geq S^* \equiv V/(\sum_{i=1}^{n} \ell_i), \qquad j = 1,2,\ldots,n \tag{12}$$

However the strict inequality in equation (12) cannot apply for any j since this would violate the volume constraint in equation (3). Thus the optimal design for the value of S in equation (11) must be the "equally-sized" design

$$A_j = V/(\sum_{i=1}^{n} \ell_i), \qquad j = 1,2,\ldots,n$$

OBSERVATIONS ON GOVERNING EQUATIONS

Inspection of the preceding set of governing equations (3)-(10) leads to several observations of later use in this paper. First note that when a member area A_r in the optimal design is strictly greater than the lower bound constraint value S, then the corresponding slack function $a_r \neq 0$ by equation (5) and $\Lambda_r = 0$ by equation (9), but then equation (8) yields

$$\eta_r = \lambda \tag{13}$$

Thus all members with areas greater than S are stressed to the same level.

Note that by equation (2), equation (13) may be written as a linear equation in the strain ε_r and hence linear in the nodal displacements:

$$\varepsilon_r = \pm\sqrt{2\lambda/E} \tag{14}$$

Next consider a member t in the optimal design which is stressed below the level λ (eqs. (8) and (10) exclude the possibility that an element in the optimal design is stressed <u>above</u> the level λ.):

$$\eta_t < \lambda \tag{15}$$

Then by equation (8) $\Lambda_t \neq 0$ and so equations (9) and (5) imply

$$A_t = S \tag{16}$$

The implication of equations (14) and (16) may be summarized by saying that the members of the optimal design may be divided into two groups: fully-stressed members ($\eta_r = \lambda$ and $A_r > S$) and members at the constraint ($\eta_t < \lambda$ and $A_t = S$). As shall be discussed later in this paper, under certain conditions borderline cases exist where a member is both fully-stressed and at the constraint.

A second observation about the governing equations for the optimal design problem can be made with the help of the fully-stressed condition, equation (14). Introducing equations (14) and (2) into the equilibrium relations (equation 7) yields

$$\sqrt{2\lambda E}\sum_r e_r \ell_r A_r \frac{\partial \varepsilon_r}{\partial \delta_k} + S\sum_t \ell_t \frac{\partial \eta_t}{\partial \delta_k} - F_k = 0 \tag{17}$$

where the first summation is over the set of fully-stressed members, and the second summation is over the set of members at the constraint (hence areas equal S). e_r is the sign associated with member r (compression or tension).

Equations (14) and (17) have been formulated for the problem of maximum stiffness design for a fixed volume of material V. The maximum specific strain energy λ is found as part of the solution. However, this problem may be shown

(ref. 6) to be equivalent to the problem of minimum volume design for specified λ. From now on in this paper it will be assumed that a value of λ is specified. The solution corresponding to this value of λ may later be made to correspond to some specified volume of material by multiplying all results by a common factor.

With λ specified, equations (14) and (17) become linear equations in the remaining unknowns δ_k and A_r. Thus once it has been determined which members are to be fully-stressed in the optimal design, the areas and nodal displacements may be calculated by solving a linear system of equations.

FULLY-STRESSED SET AND TRIAL DESIGN

Suppose that a subset of the n members of the truss have specific strain energy λ, as well as specified signs, and do not violate nodal displacement compatibility. These members will be called a "fully-stressed set".

Suppose that a fully-stressed set p has been designated and a value of the lower bound constraint specified, $S = S^*$. In general, it is not known beforehand if p corresponds to an optimal design for $S = S^*$. However, knowing p and S^*, we can nevertheless determine a corresponding set of areas and displacements by writing equations (17) and (14) for the fully-stressed set p and then solving these equations.

The set of areas and displacements found in this way will be written $D(p,S^*)$ and will be called the "trial design corresponding to p and S^*." Note that by assumption the trial design is a continuous function of the lower bound constraint, for fixed p.

Once a trial design $D(p,S^*)$ has been calculated, equations (10) and (4) may be used to determine if the trial design is also an optimal design. If $D(p,S^*)$ is optimal, then p will be called the "optimal fully-stressed set corresponding to S^*."

BASIS FOR ALGORITHM

Using the definitions just introduced, we can now discuss the basis for an algorithm for finding the optimal design.

Starting with a fully-stressed set r and a value of $S = S^*$ such that $D(r,S^*)$ is optimal (finding such a starting design presents no difficulties, as was observed earlier), S is repeatedly reduced and D(r,S) recalculated until a value of S is found for which D(r,S) is non-optimal. Since the cause of the non-optimality must lie in the incorrect choice of fully-stressed members, a method is needed for identifying those members which must be added to or deleted from the optimal fully-stressed set as S decreases. Such a method may be derived from a close examination of the optimal designs in the neighborhood of a point where the optimal fully-stressed set changes.

Consider the particular case where a single member, for example, j, is to be added to the optimal fully-stressed set. In figure 1, $S = S_c$ is the value of the lower bound constraint for which η_j first equals the constraint value λ as S is decreased from a value S_2 slightly above S_c to a value S_1 slightly below S_c. Note that, for $S = S_c$, member j is an example of a "borderline" case referred to earlier ($A_j = S_c$ and $\eta_j = \lambda$).

If p denotes the fully-stressed set for which D(p,S) is optimal for $S_2 \geq S \geq S_c$, then D(p,S) is non-optimal for $S_c > S \geq S_1$, since by hypothesis p lacks the fully-stressed member j.

Denote by q the fully-stressed set obtained from p by adding member j and consider a member, for example, k, which belongs to neither p nor q. By hypothesis,

$$\eta_k(p,S_c) = \eta_k(q,S_c) < \lambda$$

Furthermore since $\eta_k(p,S)$ and $\eta_k(q,S)$ are continuous functions of S, it follows that

$$\eta_k(p,S) < \lambda \text{ and } \eta_k(q,S) < \lambda$$

for $S_1 \leq S < S_c$. For the same range of S, it must also be true that

$$\eta_j(p,S) > \lambda$$

since D(p,S) has been assumed to be non-optimal. Thus the member to be added to the fully-stressed set p to form the optimal fully-stressed set q (for $S_1 \leq S < S_c$) may be determined by examining the non-optimal design $D(p,S_1)$ - the member to be added is that member with specific strain energy exceeding λ. The sign associated with the member j to be added is identical to the sign of member j in $D(q,S_1)$, as may be established by a continuity argument similar to that given above.

The preceding discussion dealt with the procedure for identifying the member to be added to the optimal fully-stressed set as S decreases. An analogous procedure can be developed for identifying the member to be deleted from the optimal fully-stressed set. Proceeding as in the previous paragraphs, it can be shown that the members of the optimal fully-stressed set can be identified by inspection of a non-optimal design $D(p,S_1)$ - the criterion being that the member in p whose area is less than S_1, is to be deleted from p to form the optimal fully-stressed set.

A final remark on the algorithm should be added here. In developing the method for adding or deleting fully-stressed members, the assumption was made that only one element at a time could be both fully-stressed and have area equal

to the constraint value. In certain problems, especially where a high degree of symmetry is present, this assumption may be violated. The argument presented above for identifying additions or deletions to the optimal fully-stressed set is no longer generally valid. In the examples considered in the course of this study, several instances were observed where more than one member was fully-stressed and also at the constraint for the same value of S. However, the algorithm had no difficulty in these instances and found the optimal fully-stressed set. The information gained by examining the non-optimal design in the vicinity of a change in the fully-stressed set was a reliable guide in determining the elements to be added or deleted. Thus the lack of theoretical justification for the algorithm in this situation does not appear to be serious.

EXAMPLE PROBLEMS

In figure 2 an example is presented, involving sixteen interior nodes loaded as shown and also two support nodes located far from the interior nodes and not shown in the figure. The optimal design (shown in the figure) is self-equilibrated. In this example, the algorithm was able to select the appropriate sixteen members comprising the optimal design from among all possible members. In achieving this result, no advantage was taken of the symmetry of the problem.

In figure 3, seven internal and four support nodes are specified, and a single applied load is to be carried by the truss. The optimum design is found to contain ten members and is reminiscent of a Michell truss.

REFERENCES

1. Taylor, J.E.: "Maximum Strength Elastic Structural Design," Proc. ASCE vol. 95, no. EM3, June 1969, pp. 653-663.

2. Hiley, D.J.: "On the Optimal Design of Trusses," M.S. thesis (University of California at Los Angeles), 1968.

3. Rossow, M.P. and Taylor, J.E.: "A Finite Element Method for the Optimal Design of Variable Thickness Sheets," AIAA J., vol. 11, 1973, pp. 1566-1567.

4. Rossow, M.P.: "A Finite Element Approach to Optimal Structural Design," Ph.D. thesis (University of Michigan) 1973.

5. Mroz, Z.: "Multi-parameter Optimal Design of Plates and Shells," J. Structural Mechanics, vol. 1, 1973, pp. 371-392.

6. Salinas, D.: On Variational Formulations for Optimal Structural Design, Ph.D. thesis (University of California at Los Angeles) 1968.

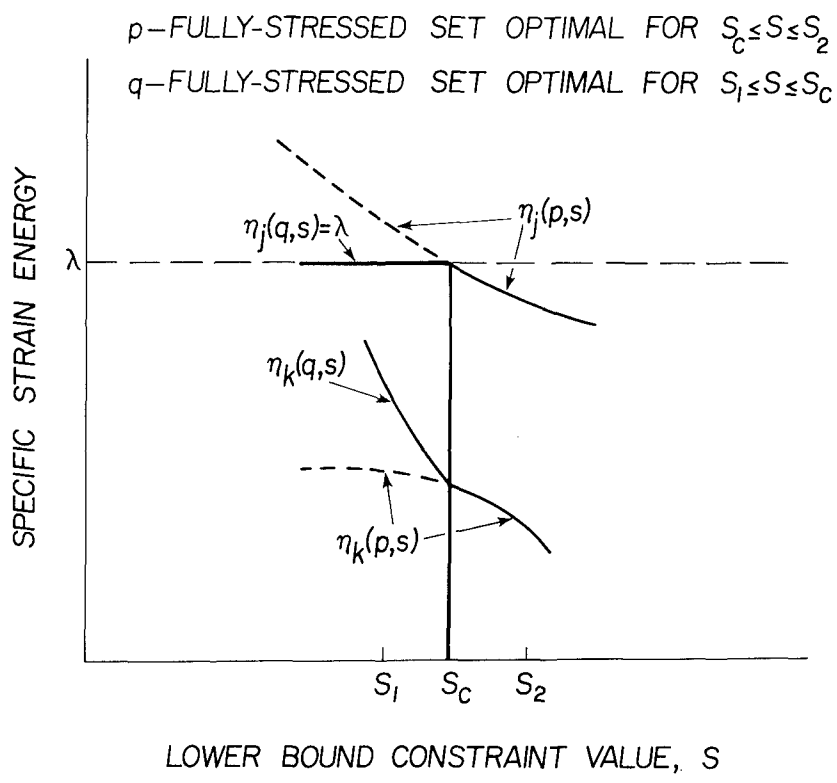

Figure 1.- Specific energies near point where member j is to be added to optimal fully-stressed set.

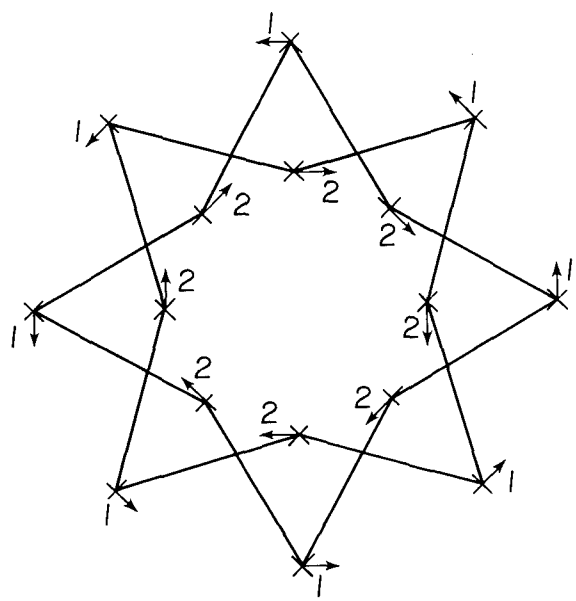

Figure 2.- Optimal truss, with sixteen interior nodes.

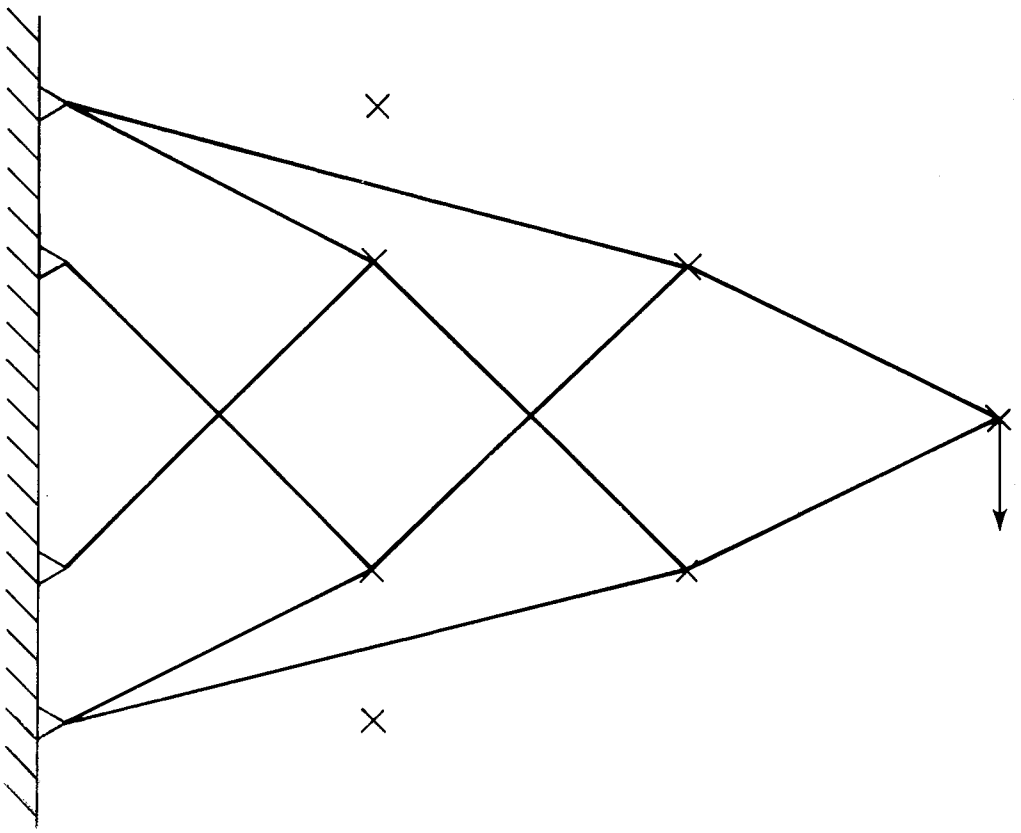

Figure 3.- Optimal truss, with seven interior nodes and four support nodes.

A RAYLEIGH-RITZ APPROACH TO THE SYNTHESIS OF LARGE STRUCTURES WITH ROTATING FLEXIBLE COMPONENTS*

L. Meirovitch** and A. L. Hale***
Department of Engineering Science and Mechanics
Virginia Polytechnic Institute and State University

SUMMARY

The equations of motion for large structures with rotating flexible components are derived by regarding the structure as an assemblage of substructures. Based on a stationarity principle for rotating structures, it is shown that each continuous or discrete substructure can be simulated by a suitable set of admissible functions or admissible vectors. This substructure synthesis approach provides a rational basis for truncating the number of degrees of freedom both of each substructure and of the assembled structure.

INTRODUCTION

The methodology for analyzing large complex structures has developed along different lines. One approach represents a natural extension of methods developed originally for civil and aircraft structures, culminating in the finite-element method (ref. 1) and the component-mode synthesis (refs. 2,3). Although rotation of the structure could be accounted for through rigid-body modes, work using the approach of references 1-3 has been concerned mainly with nonspinning structures. On the other hand, an entirely different approach was developed in conjunction with spinning and nonspinning spacecraft structures. This approach was dominated by the fact that early spacecraft could be treated as entirely rigid. Hence, in the early stages of development, structures were assumed to consist of point-connected rigid bodies arranged in "topological trees" (refs. 4,5). With time, the rigidity assumption was relaxed gradually by first allowing for flexible "terminal bodies" (refs. 6,7) and then finally for all flexible bodies (ref. 8). A third approach to the problem of spinning flexible spacecraft was concerned with spacecraft consisting of a rigid body with flexible appendages (ref. 9,10). This latter approach can be regarded as an early application of the component-mode synthesis to spinning structures.

Most papers concerned with structures simulated by point-connected rigid bodies, such as references 4, 5, proposed to derive the equations of motion by

---

*Supported in part by the NASA Research Grant NSG 1114 sponsored by the Structures and Dynamics Division, Langley Research Center.

**Professor. ***Graduate Research Assistant.

the Newtonian approach, on the assumption that such a derivation was more suitable for digital computation. Of course, an early difficulty became immediately apparent in the form of the handling of interbody constraints, a major criticism of the Newtonian approach in most circumstances. Another difficulty was the relatively large number of degrees of freedom involved, a difficulty only compounded by permitting various bodies to be flexible. As a result, there are no meaningful ways of truncating the problem.

This paper is concerned with the mathematical simulation of large structures, where the structure is regarded as an assemblage of substructures. Indeed, the mathematical model is assumed to consist of a central substructure with a number of appended substructures, where some of the latter can rotate relative to the central substructure. To ensure that the various substructures act as parts of a whole structure, an orderly kinematical procedure is used which takes into account automatically the superposition of motion of the central substructure on the motion of the interconnected substructures. The system equations of motion are derived by means of the Lagrangian approach, which, when used in conjunction with the kinematical procedure just described, does away with the question of constraints. The equations of motion are derived from scalar functions, namely, the kinetic and potential energy, where the first requires the calculation of velocities only. In addition, discretization of the kinetic and potential energy in conjunction with linearization ensures proper symmetry and skew symmetry of the coefficient matrices in the final equations of motion. Using a Rayleigh-Ritz approach, the motion of each continuous (discrete) substructure can be represented by a linear combination of admissible functions (vectors) rather than substructure natural modes. This approach is based on a stationarity principle for rotating structures developed recently by the first author (ref. 11). Finally, the truncation problem can be handled much more efficiently by the substructure synthesis approach, as the possibility of truncating the number of degrees of freedom both of the individual substructures and of the assembled structure provides a much more rational basis for an overall truncation decision.

KINEMATICAL CONSIDERATIONS

Let us consider a general structure consisting of a central substructure C and a given number of appended substructures (see fig. 1), where the latter are of three types: rigid and rotating relative to the central substructure (type R), elastic and nonrotating relative to the central substructure (type E), and elastic and rotating relative to the central substructure (type A). Clearly, there can be more than one appendage of a given type, but we shall confine our discussion to a representative one of each type, with summation implied over the entire number of substructures. Although we consider here only peripheral substructures, the formulation can be easily extended to chains of substructures, as discussed later.

Let us introduce the inertial system of axes XYZ with the origin at O and identify a system of axes $x_C y_C z_C$ with the origin at an arbitrary point C of the central substructure. Then, denoting by $\underset{\sim}{w}_{OC}$ the radius vector from O to C, by $\underset{\sim}{r}_C$ the position vector of any mass point in the substructure, and by $\underset{\sim}{u}_C$ the

elastic displacement of that point measured relative to $x_C y_C z_C$, and recognizing that w_{OC} is in terms of components along XYZ and r_C and u_C are in terms of components along $x_C y_C z_C$, the absolute position of the mass point in question in terms of components along $x_C y_C z_C$ is $w_C = T_{OC} w_{OC} + r_C + u_C$, where T_{OC} is the matrix of direction cosines between XYZ and $x_C y_C z_C$. Moreover, if Ω_C is the angular velocity of the frame $x_C y_C z_C$ relative to XYZ, the absolute velocity of the mass point is

$$\dot{w}_C = T_{OC}\dot{w}_{OC} - (\tilde{r}_C + \tilde{u}_C)\Omega_C + \dot{u}_C \tag{1}$$

where $\tilde{r}_C + \tilde{u}_C$ is a skew symmetric matrix associated with $r_C + u_C$ and $\dot{u}_C$ is the elastic velocity of the point relative to axes $x_C y_C z_C$.

To calculate the absolute velocity of a point in the substructure R, we must first obtain the velocity of point R as well as the angular velocity of a reference frame $x_{CR} y_{CR} z_{CR}$ attached to the central substructure at R and with axes parallel to the rotor axes $x_R y_R z_R$ when at rest and when the central substructure is undeformed. Due to geometry alone the orientation of axes $x_{CR} y_{CR} z_{CR}$ relative to $x_C y_C z_C$ is given by the constant matrix of direction cosines L_{GR}. Denoting by u_{CR} the elastic deformation vector at point R of the central substructure and assuming that the components u_{CRx}, u_{CRy}, u_{CRz}, of u_{CR} are small, the rotation vector of axes $x_{CR} y_{CR} z_{CR}$ due to elastic deformation can be written in the form

$$\tilde{\nabla}_{CR}(L_{GR} u_{CR}) = \left[\frac{\partial u_{CRz}}{\partial y_{CR}} - \frac{\partial u_{CRy}}{\partial z_{CR}} \quad \frac{\partial u_{CRx}}{\partial z_{CR}} - \frac{\partial u_{CRz}}{\partial x_{CR}} \quad \frac{\partial u_{CRy}}{\partial x_{CR}} - \frac{\partial u_{CRx}}{\partial y_{CR}}\right]^T \tag{2}$$

where $\tilde{\nabla}_{CR}$ is a skew symmetric differential operator matrix corresponding to the curl operator. Hence, the matrix of direction cosines between axes $x_{CR} y_{CR} z_{CR}$ before and after deformation is

$$L_{CR} = \begin{bmatrix} 1 & \frac{\partial u_{CRy}}{\partial x_{CR}} - \frac{\partial u_{CRx}}{\partial y_{CR}} & -\left(\frac{\partial u_{CRx}}{\partial z_{CR}} - \frac{\partial u_{CRz}}{\partial x_{CR}}\right) \\ -\left(\frac{\partial u_{CRy}}{\partial x_{CR}} - \frac{\partial u_{CRx}}{\partial y_{CR}}\right) & 1 & \frac{\partial u_{CRz}}{\partial y_{CR}} - \frac{\partial u_{CRy}}{\partial z_{CR}} \\ \frac{\partial u_{CRx}}{\partial z_{CR}} - \frac{\partial u_{CRz}}{\partial x_{CR}} & -\left(\frac{\partial u_{CRz}}{\partial y_{CR}} - \frac{\partial u_{CRy}}{\partial z_{CR}}\right) & 1 \end{bmatrix} \tag{3}$$

Moreover, letting L_R be the matrix of direction cosines between axes $x_R y_R z_R$ and $x_{CR} y_{CR} z_{CR}$, the transformation matrix between axes $x_R y_R z_R$ and $x_C y_C z_C$ is simply $T_{CR} = L_R L_{CR} L_{GR}$.

Denoting by ω_R the angular velocity of the rotor relative to axes $x_{CR} y_{CR} z_{CR}$, the absolute angular velocity of $x_R y_R z_R$ in terms of components along $x_R y_R z_R$ is

$$\Omega_R = T_{CR}\,\Omega_C + L_R\,\tilde{\nabla}_{CR}(L_{GR}\,\dot{u}_{CR}) + \omega_R \tag{4}$$

where the second term in equation (4) is the angular velocity of axes $x_{CR}y_{CR}z_{CR}$ due to the elastic motion of the central substructure. Because the rotor is rigid, the position of a mass point relative to R is simply $\underset{\sim}{r}_R$. Hence, the absolute velocity of the point in question is simply

$$\dot{\underset{\sim}{w}}_R = T_{CR}\,\dot{\underset{\sim}{w}}_{CR} - \tilde{\underset{\sim}{r}}_R\,\underset{\sim}{\Omega}_R \tag{5}$$

where $\dot{\underset{\sim}{w}}_{CR}$ is the velocity of point R obtained from $\dot{\underset{\sim}{w}}_C$ by substituting the coordinates of the point R for those of an arbitrary point.

Next, let us turn our attention to the substructure E and denote by $x_{E}y_{E}z_{E}$ any convenient set of axes with the origin at E and attached to the substructure. Using the analogy with equation (4), the angular velocity of $x_{E}y_{E}z_{E}$ is

$$\underset{\sim}{\Omega}_E = T_{CE}\,\underset{\sim}{\Omega}_C + \tilde{\nabla}_{CE}(L_{GE}\,\dot{\underset{\sim}{u}}_{CE}) \tag{6}$$

where $T_{CE} = L_{CE}L_{GE}$. Moreover, by analogy with equation (5), the absolute velocity of a mass point in the substructure is

$$\dot{\underset{\sim}{w}}_E = T_{CE}\,\dot{\underset{\sim}{w}}_{CE} - (\tilde{\underset{\sim}{r}}_E + \tilde{\underset{\sim}{u}}_E)\underset{\sim}{\Omega}_E + \dot{\underset{\sim}{u}}_E \tag{7}$$

where $\dot{\underset{\sim}{u}}_E$ is the elastic displacement relative to axes $x_{E}y_{E}z_{E}$.

The extension to elastic substructures rotating relative to the central substructure is quite obvious. Letting $\underset{\sim}{\omega}_A$ be the angular velocity of the substructure A relative to a set of axes $x_{CA}y_{CA}z_{CA}$ attached to the central body at point A, the absolute angular velocity of $x_{A}y_{A}z_{A}$ is simply

$$\underset{\sim}{\Omega}_A = T_{CA}\,\underset{\sim}{\Omega}_C + L_A\,\tilde{\nabla}_{CA}(L_{GA}\,\dot{\underset{\sim}{u}}_{CA}) + \underset{\sim}{\omega}_A \tag{8}$$

where $T_{CA} = L_AL_{CA}L_{GA}$, and the absolute velocity of an arbitrary point in A is

$$\dot{\underset{\sim}{w}}_A = T_{CA}\,\dot{\underset{\sim}{w}}_{CA} - (\tilde{\underset{\sim}{r}}_A + \tilde{\underset{\sim}{u}}_A)\underset{\sim}{\Omega}_A + \dot{\underset{\sim}{u}}_A \tag{9}$$

Finally, let us consider chains of substructures. First, we note that the angular velocity of a peripheral substructure and the absolute velocity of an arbitrary point in a peripheral substructure are written in terms of the angular velocity of a set of axes attached to the central substructure and with origin at the interconnecting point and the translational velocity of the interconnecting point. As an example, see equations (4) and (5). To write the angular velocity and absolute velocity of an arbitrary point of a substructure in a chain, we simply replace quantities pertaining to the central substructures, such as T_{CR}, $\underset{\sim}{\Omega}_C$, $\nabla_{CR}(L_{GR}\,\dot{\underset{\sim}{u}}_{CR})$, and $\dot{\underset{\sim}{w}}_{CR}$ in equations (4) and (5), by analogous quantities pertaining to the immediately preceding substructure in the chain.

SYSTEM DISCRETIZATION AND/OR TRUNCATION

In general, each elastic substructure possesses a large number of degrees of freedom. In fact, if the substructure is continuous, then its number of degrees of freedom is infinite. For practical reasons, we must limit the formulation not only to a finite number of degrees of freedom but also to as small a number as possible consistent with a good simulation of the system dynamic characteristics. In this regard, we wish to use a Rayleigh-Ritz approach and represent the elastic displacements of a continuous substructure by a linear combination of space-dependent admissible functions multiplied by time-dependent generalized coordinates of the substructure. If the substructure is discrete, then instead of admissible functions we must use admissible vectors. Note that it is common practice to use as admissible functions and admissible vectors the eigenfunctions and eigenvectors of the substructure. In view of the stationarity principle for gyroscopic systems developed in reference 11, however, this is not really necessary, and a reasonable set of admissible functions or admissible vectors should suffice. Hence, we shall use the discretization and/or truncation scheme

$$\underset{\sim}{u}_C = {}^{\Phi}_{C}\,\underset{\sim}{\eta}_C \quad , \quad \underset{\sim}{u}_E = {}^{\Phi}_{E}\,\underset{\sim}{\eta}_E \quad , \quad \underset{\sim}{u}_A = {}^{\Phi}_{A}\,\underset{\sim}{\eta}_A \tag{10}$$

where $\underset{\sim}{\eta}_C$, $\underset{\sim}{\eta}_E$, and $\underset{\sim}{\eta}_A$ are time-dependent vectors of generalized displacements with dimensions n_C, n_E, and n_A, respectively, and Φ_C, Φ_E, and Φ_A are $3 \times n_C$, $3 \times n_E$, and $3 \times n_A$ space-dependent matrices of admissible functions or admissible vectors, as the case may be. Note that for a continuous substructure $\underset{\sim}{u}$ depends on continuous space variables and for a discrete substructure it depends on discrete space variables. In the latter case, the partial derivatives involved in the quantity $\nabla \underset{\sim}{u}$ are to be replaced by corresponding slopes.

Although we have mentioned both continuous and discrete substructures in the above, we have made no attempt to make clear distinction between the two types of mathematical models. Neither have we elaborated on the various types of discrete models, such as lumped models, finite-element models, etc. Of course, the mathematical model used depends on the substructure mass and stiffness distributions, but this is of no particular concern here. The reason for this is that, independently of the mathematical model postulated for the substructure, the general idea is the same, namely, to eliminate the spatial dependence by the use of admissible functions or admissible vectors and to truncate the problem by limiting the number of these functions or vectors.

LAGRANGE'S EQUATIONS OF MOTION

To derive Lagrange's equations of motion it is necessary to produce first expressions for the kinetic energy, potential energy, and nonconservative virtual work. Assuming that in equilibrium the central substructure C, substructure R, and substructure A rotate with the uniform angular velocities $\underset{\sim}{\Omega}_C$ about z_C, $\underset{\sim}{\Omega}_R$ about z_R, and $\underset{\sim}{\Omega}_A$ about z_A, respectively, while any other motion is zero, we can write $\underset{\sim}{\omega}_C = \Omega_C \underset{\sim}{\ell}_C + \Theta_C \dot{\underset{\sim}{\theta}}_C$, $\underset{\sim}{\omega}_R = \Omega_R \underset{\sim}{\ell}_R + \Theta_R \dot{\underset{\sim}{\theta}}_R$, $\underset{\sim}{\omega}_A = \Omega_A \underset{\sim}{\ell}_A + \Theta_A \dot{\underset{\sim}{\theta}}_A$, where $\underset{\sim}{\ell}_A$ is the vector of direction cosines between z_C and $\tilde{X}\tilde{Y}\tilde{Z}$, $\underset{\sim}{\ell}_R$ is the vector of

direction cosines between z_R and $x_{CR}y_{CR}z_{CR}$, and $\underset{\sim}{\ell}_A$ is the vector of direction cosines between z_A and $x_{CA}y_{CA}z_{CA}$. Moreover, Θ_C, Θ_R, and Θ_A are 3 x 3 matrices depending on oscillation of the axes $x_Cy_Cz_C$ relative to XYZ, etc. Using equations (10) and retaining only linear terms, the absolute velocities of typical points in the various substructures become

$$\dot{\underset{\sim}{w}}_C = C_1\,\dot{\underset{\sim}{q}}_C + C_2\,\underset{\sim}{q}_C \quad , \quad \dot{\underset{\sim}{w}}_R = R_1\,\dot{\underset{\sim}{q}}_R + R_2\,\underset{\sim}{q}_R$$

$$\dot{\underset{\sim}{w}}_E = E_1\,\dot{\underset{\sim}{q}}_E + E_2\,\underset{\sim}{q}_E \quad , \quad \dot{\underset{\sim}{w}}_A = A_1\,\dot{\underset{\sim}{q}}_A + A_2\,\underset{\sim}{q}_A \tag{11}$$

where $\underset{\sim}{q}_C = [\underset{\sim}{w}_{OC}^T \vdots \underset{\sim}{\theta}_C^T \vdots \underset{\sim}{\eta}_C^T]^T$, $\underset{\sim}{q}_R = [\underset{\sim}{w}_{OC}^T \vdots \underset{\sim}{\theta}_C^T \vdots \underset{\sim}{\eta}_C^T \vdots \underset{\sim}{\theta}_R^T]^T$, $\underset{\sim}{q}_E = [\underset{\sim}{w}_{OC}^T \vdots \underset{\sim}{\theta}_C^T \vdots \underset{\sim}{\eta}_C^T \vdots \underset{\sim}{\eta}_E^T]^T$, and $\underset{\sim}{q}_A = [\underset{\sim}{w}_{OC}^T \vdots \underset{\sim}{\theta}_C^T \vdots \underset{\sim}{\eta}_C^T \vdots \underset{\sim}{\theta}_A^T \vdots \underset{\sim}{\eta}_A^T]^T$ are configuration vectors for the substructures.

The system kinetic energy can be written in the form

$$T = T_C + T_R + T_E + T_A \tag{12}$$

where

$$T_C = \frac{1}{2}\int_{m_C} \dot{\underset{\sim}{w}}_C^T\,\dot{\underset{\sim}{w}}_C\,dm_C = \frac{1}{2}\,\dot{\underset{\sim}{q}}_C^T\,\overline{C}_{11}\,\dot{\underset{\sim}{q}}_C + \underset{\sim}{q}_C^T\,\overline{C}_{12}\,\dot{\underset{\sim}{q}}_C + \frac{1}{2}\,\underset{\sim}{q}_C^T\,\overline{C}_{22}\,\underset{\sim}{q}_C$$

$$T_R = \frac{1}{2}\int_{m_R} \dot{\underset{\sim}{w}}_R^T\,\dot{\underset{\sim}{w}}_R\,dm_R = \frac{1}{2}\,\dot{\underset{\sim}{q}}_R^T\,\overline{R}_{11}\,\dot{\underset{\sim}{q}}_R + \underset{\sim}{q}_R^T\,\overline{R}_{12}\,\dot{\underset{\sim}{q}}_R + \frac{1}{2}\,\underset{\sim}{q}_R^T\,\overline{R}_{22}\,\underset{\sim}{q}_R$$

$$T_E = \frac{1}{2}\int_{m_E} \dot{\underset{\sim}{w}}_E^T\,\dot{\underset{\sim}{w}}_E\,dm_E = \frac{1}{2}\,\dot{\underset{\sim}{q}}_E^T\,\overline{E}_{11}\,\dot{\underset{\sim}{q}}_E + \underset{\sim}{q}_E^T\,\overline{E}_{12}\,\dot{\underset{\sim}{q}}_E + \frac{1}{2}\,\underset{\sim}{q}_E^T\,\overline{E}_{22}\,\underset{\sim}{q}_E \tag{13}$$

$$T_A = \frac{1}{2}\int_{m_A} \dot{\underset{\sim}{w}}_A^T\,\dot{\underset{\sim}{w}}_A\,dm_A = \frac{1}{2}\,\dot{\underset{\sim}{q}}_A^T\,\overline{A}_{11}\,\dot{\underset{\sim}{q}}_A + \underset{\sim}{q}_A^T\,\overline{A}_{12}\,\dot{\underset{\sim}{q}}_A + \frac{1}{2}\,\underset{\sim}{q}_A\,\overline{A}_{22}\,\underset{\sim}{q}_A$$

in which

$$\overline{C}_{ij} = \int_{m_C} C_j^T\,C_i\,dm_C \quad , \quad \overline{R}_{ij} = \int_{m_R} R_j^T\,R_i\,dm_R$$

$$\overline{E}_{ij} = \int_{m_E} E_j^T\,E_i\,dm_E \quad , \quad \overline{A}_{ij} = \int_{m_A} A_j^T\,A_i\,dm_A \tag{14}$$

Note that the square matrices $\overline{C}_{ij}$, $\overline{R}_{ij}$, $\overline{E}_{ij}$, and $\overline{A}_{ij}$ have partitioned forms, with many of the off-diagonal submatrices equal to zero. Introducing the n-dimensional configuration vector for the entire system in the form $\underset{\sim}{q} = [\underset{\sim}{w}_{OC}^T \vdots \underset{\sim}{\theta}_C^T \vdots \underset{\sim}{\theta}_R^T \vdots \underset{\sim}{\theta}_A^T \vdots \underset{\sim}{\eta}_C^T \vdots \underset{\sim}{\eta}_E^T \vdots \underset{\sim}{\eta}_A^T]^T$, where n is the number of degrees of freedom of the system, the kinetic energy can be written in the general form

$$T = \frac{1}{2}\dot{\underset{\sim}{q}}^T M \dot{\underset{\sim}{q}} + \underset{\sim}{q}^T F \dot{\underset{\sim}{q}} + \frac{1}{2}\underset{\sim}{q}^T K_T \underset{\sim}{q} \tag{15}$$

where M and K_T are symmetric matrices. Similarly, the potential energy for the entire system is

$$V = \frac{1}{2}\underset{\sim}{q}^T K_V \underset{\sim}{q} \tag{16}$$

where K_V is a symmetric matrix, and the nonconservative virtual work has the form

$$\delta W = \underset{\sim}{Q}^T \delta\underset{\sim}{q} \tag{17}$$

where $\underset{\sim}{Q}$ is the nonconservative generalized force vector.

In general, the matrices M and F depend explicitly on time. However, under certain circumstances, such as when the substructures R and A are symmetric, the time dependence disappears. A helicopter with a symmetric rotor rotating relative to an airframe while in hover is an example, where the entire rotor is considered as a substructure. Another possibility is to consider each rotor blade as a separate substructure. In this case, a combination of substructures forms a symmetric rotor and M and F will once again be constant matrices.

Lagrange's equations can be written in the symbolic form

$$\frac{d}{dt}\frac{\partial L}{\partial \dot{\underset{\sim}{q}}} - \frac{\partial L}{\partial \underset{\sim}{q}} = \underset{\sim}{Q} \tag{18}$$

where L = T - V is the system Lagrangian. Assuming that M and F are constant, introducing equations (15) and (16) into the Lagrangian L, and using equation (18), we obtain the Lagrange's equations of motion

$$M\ddot{\underset{\sim}{q}} + (F^T - F)\dot{\underset{\sim}{q}} + (K_V - K_T)\underset{\sim}{q} = \underset{\sim}{Q} \tag{19}$$

where $F^T - F$ is a skew symmetric matrix. Hence, equation (19) represents a typical gyroscopic system. The natural frequencies and natural modes of the complete structure and the closed-form solution of equation (19) can be obtained by the methods developed in references 12 and 13. The interest here is not so much in the response as in the dynamic characteristics of the system, and in particular, the truncation effect on these characteristics.

THE EIGENVALUE PROBLEM AND TRUNCATION IMPLICATIONS

Introducing the 2n-dimensional state vector $\underset{\sim}{x}(t)$ and the associated 2n-dimensional force vector $\underset{\sim}{X}(t)$ in the form

$$\underset{\sim}{x}(t) = [\underset{\sim}{q}^T(t) \vdots \dot{\underset{\sim}{q}}^T(t)]^T \quad , \quad \underset{\sim}{X}(t) = [\underset{\sim}{Q}^T(t) \vdots \underset{\sim}{0}^T]^T \tag{20}$$

where $\underset{\sim}{0}$ is the n-dimensional null vector, as well as the 2n x 2n matrices

$$I = \begin{bmatrix} M & 0 \\ 0 & K_V - K_T \end{bmatrix} \qquad G = \begin{bmatrix} F^T - F & K_V - K_T \\ K_T - K_V & 0 \end{bmatrix} \tag{21}$$

where 0 is the null matrix of order n, the n second-order differential equations of motion, equation (19), can be replaced by the 2n first-order differential equations in the state space $\underset{\sim}{x}(t)$, where the equations have the eigenvalue problem

$$\lambda I \underset{\sim}{x} + G \underset{\sim}{x} = \underset{\sim}{0} \tag{22}$$

It is shown in reference 12 that the eigenvalue problem (22) can be reduced to the real symmetric form

$$\omega^2 I \underset{\sim}{y} = K \underset{\sim}{y} \quad , \quad \omega^2 I \underset{\sim}{z} = K \underset{\sim}{z} \tag{23}$$

where $K = G^T I^{-1} G$ is a real symmetric matrix. The eigenvalue problem (23) is in terms of two real symmetric matrices and is known to possess real eigenvalues. Assuming that I is positive definite, it follows that K is positive definite, so that the eigenvalues are not only real but also positive. Moreover, the eigenvalues ω_r^2 (r = 1,2,...,n) have multiplicity two, so that to each ω_r^2 belong the eigenvectors $\underset{\sim}{y}_r$ and $\underset{\sim}{z}_r$. Because I and K are positive definite all the eigenvectors are independent. In fact, they are orthogonal with respect to the matrix I.

Next, let us use the Cholesky decomposition and write I in the form $I = LL^T$, where L is a lower triangular matrix. Introducing the notation $\underset{\sim}{y}'_r = L^T \underset{\sim}{y}_r$, $\underset{\sim}{z}'_r = L^T \underset{\sim}{z}_r$, (r = 1,2,...,n), the eigenvalue problem (23) becomes

$$\omega_r^2 \underset{\sim}{y}'_r = K' \underset{\sim}{y}'_r \quad , \quad \omega_r^2 \underset{\sim}{z}'_r = K' \underset{\sim}{z}'_r \tag{24}$$

where $K' = L^{-1} K L^{-T}$ is a real symmetric positive definite matrix, in which $L^{-T} = (L^{-1})^T$.

Denoting by $\underset{\sim}{v}$ an arbitrary 2n-vector, Rayleigh's quotient associated with the eigenvalue problem (24) can be written in the form (ref. 11)

$$R(v) = \frac{\underset{\sim}{v}^T K' \underset{\sim}{v}}{\underset{\sim}{v}^T \underset{\sim}{v}} \tag{25}$$

Because K' is real and symmetric, it is well known that Rayleigh's quotient has a stationary value in the neighborhood of an eigenvalue. Note that the symmetric formulation (24) permits us to conclude that a stationarity principle exists also for gyroscopic systems.

Next, we wish to examine the truncation effect on the system characteristics. To this end, let us examine the eigenvalue problem $A\underset{\sim}{v} = \lambda\underset{\sim}{v}$, where A is a real symmetric matrix of order N, and assume that the eigenvalues of A are ordered so that $\lambda_1 \leq \lambda_2 \leq \ldots \leq \lambda_N$. Now, let us form the matrix B by deleting the last row and column of A and write the eigenvalue problem $B\underset{\sim}{u} = \gamma\underset{\sim}{u}$, where the eigenvalues γ_j (j = 1,2,...,N-1) are ordered so that $\gamma_1 \leq \gamma_2 \leq \ldots \leq \gamma_{N-1}$. The question arises as to how the eigenvalues γ_j relate to the eigenvalues λ_i. To this end, one can use the Courant's maximum-minimum theorem (ref. 14) and prove that

$$\lambda_1 \leq \gamma_1 \leq \lambda_2 \leq \gamma_2 \leq \cdots \leq \lambda_{N-1} \leq \gamma_{N-1} \leq \lambda_N \tag{26}$$

We shall refer to inequalities (26) as the inclusion principle.

Now, let us return to the truncation problem. The 2n x 2n matrix K' was obtained as the result of representing the spinning structure by an n-degree-of-freedom system. Note that the rotational coordinates are also included in these degrees of freedom. This representation is tantamount to the imposition of a given number of constraints on the original structure. For example, the first of equations (10) can be written in the form

$$\underset{\sim}{u}_C = \sum_{i=1}^{n_C} \underset{\sim}{\Phi}_{Ci}\, \eta_{Ci} \tag{27}$$

so that the constraints imposed on the system are $\eta_{C,n_{C+1}} = \eta_{C,n_{C+2}} = \ldots = 0$. Truncating the series (27) by assuming that $\eta_{C,n_C} = 0$, we obtain a matrix K" obtained from K' by deleting two rows and the corresponding two columns. If the eigenvalues ω_r^2 of K' are such that $\omega_1^2 \leq \omega_2^2 \leq \ldots \leq \omega_n^2$ and the eigenvalues β_r^2 of K" are such that $\beta_1^2 \leq \beta_2^2 \leq \ldots \leq \beta_{n-1}^2$, then we have

$$\omega_1^2 \leq \beta_1^2 \leq \omega_2^2 \leq \beta_2^2 \leq \cdots \leq \omega_{n-1}^2 \leq \beta_{n-1}^2 \leq \omega_n^2 \tag{28}$$

Note that the fact that the eigenvalues of K' and K" have multiplicity two is automatically taken into account in inequalities (28). On the other hand, by relaxing one constraint, i.e., by adding one term to the series (27), we obtain a (2n + 2) x (2n + 2) matrix K"' which is obtained by adding two rows and columns to K'. The eigenvalues α^2 of K"' are such that

$$\alpha_1^2 \leq \omega_1^2 \leq \alpha_2^2 \leq \omega_2^2 \leq \cdots \leq \alpha_n^2 \leq \omega_n^2 \leq \alpha_{n+1}^2 \tag{29}$$

The above developments permit us to conclude that the system estimated natural frequencies tend to decrease monotonically with each additional degree of freedom. At the same time there is a new frequency added which is higher than any of the previous ones.

The question remains as to how to select the admissible functions or admissible vectors. The first thing that comes to mind is to take them as the

eigenfunctions and eigenvectors of the various substructures. In many cases, the solution of the eigenvalue problem for a substructure can be quite a task in itself, so that in such cases one may wish to use deformation patterns only approximating the actual modes. This can be regarded as imposing additional constraints on the system, which tends to raise the natural frequencies of the system, but this may be considered as a viable alternative, particularly when the validity of the solution of the eigenvalue problem is questionable. Experience with the Rayleigh-Ritz approach shows that the system natural frequencies are not very sensitive to the admissible functions used, which can be traced to the stationarity principle. But a stationarity principle exists also for discrete systems, so that the same conclusion can be extended to admissible vectors.

The truncation by substructures has a clear advantage over truncation of the structure as a whole. The reason is that it permits a more rational judgement based on the substructure properties, such as the mass and stiffness distributions. Generally one is interested in only a limited number of lower modes of the complete structure. Hence, a very stiff and light substructure is likely to have less effect on the modes of the complete structure than a flexible heavy substructure. Hence, one can truncate the first more severely than the second. Some ideas for truncation can be obtained by estimating the natural frequencies of the substructures. This by no means implies that one need solve the eigenvalue problem for the substructures exactly. Indeed, using a Rayleigh-Ritz procedure for continuous or discrete systems, in conjunction with a preselected set of admissible functions or admissible vectors, it is possible to obtain a reasonable estimate of the lower frequencies of each substructure. Note that the Rayleigh-Ritz method can be used to produce and solve an eigenvalue problem of considerably lower dimension than that of the full eigenvalue problem for the substructure. The estimated lower natural frequencies of the substructure, when compared to those of other substructures, can be used merely as a guide for truncation purposes. In fact, the eigenvectors serve no useful purpose and need not be calculated, as the same admissible functions or vectors can be used to represent the substructure in the generation of the eigenvalue problem for the complete assembled structure. This conclusion is based on results shown in reference 11.

If the dimension of the eigenvalue problem for the complete assembled structure is still too large, and the higher modes are not really necessary, then one can solve only for a given number of lower modes by using such techniques as subspace iteration.

CONCLUDING REMARKS

A procedure has been shown whereby the equations of motion for large structures with rotating flexible components can be derived by the Lagrangian approach. A fundamental consideration in the derivation of Lagrange's equations is the superposition of substructure motions by means of an orderly kinematical procedure, which automatically eliminates the problem of constraints. Using a Rayleigh-Ritz approach, it is shown that each continuous or discrete flexible substructure can be simulated by a finite number of ad-

missible functions or admissible vectors and exact substructure modes are not really necessary. This conclusion is based on a stationarity principle for rotating structures developed recently by the first author (ref. 11). Finally, the substructure synthesis approach provides a rational basis for truncating the number of degrees of freedom both of each individual substructure and of the assembled substructure.

REFERENCES

1. Turner, M. J., Clough, R. W., Martin, H. C., and Topp, L. J., "Stiffness and Deflection Analysis of Complex Structures", Journal of Aeronautical Sciences, Vol. 23, 1956, pp. 805-824.

2. Hurty, W. C., "Dynamic Analysis of Structural Systems Using Component Modes", AIAA Journal, Vol. 3, No. 4, 1965, pp. 678-685.

3. Benfield, W. A. and Hruda, R. F., "Vibration Analysis of Structures by Component Mode Substitution", AIAA Journal, Vol. 9, No. 7, 1971, pp. 1255-1261.

4. Hooker, William W. and Margulies, G., "The Dynamical Equations for an n-Body Satellite", Journal of Astronautical Sciences, Vol. 12, No. 4, 1965, pp. 123-128.

5. Roberson, R. E. and Wittenburg, J., "A Dynamical Formalism for an Arbitrary Number of Interconnected Rigid Bodies, with Reference to the Problem of Satellite Attitude Control", Proceedings of the Third Congress of the International Federation of Automatic Control, London, 1966.

6. Hooker, William W., "Equations of Motion for Interconnected Rigid and Elastic Bodies: A Derivation Independent of Angular Momentum", Celestial Mechanics Journal, Vol. 11, 1975, pp. 337-359.

7. Ho, J. Y. L., "The Direct Path Method for Deriving the Dynamic Equations of Motion of a Multibody Flexible Spacecraft with Topological Tree Configuration", Presented as AIAA Paper No. 74-786 at the AIAA Mechanics and Control of Flight Conference, August 5-9, 1974.

8. Frisch, Harold P., "A Vector-Dyadic Development of the Equations of Motion for N-Coupled Flexible Bodies and Point Masses", NASA TN D-8047, August 1975.

9. Meirovitch, L. and Nelson, H. A., "On the High-Spin Motion of a Satellite Containing Elastic Parts", Journal of Spacecraft and Rockets, Vol. 3, No. 11, 1966, pp. 1597-1602.

10. Meirovitch, L., "Liapunov Stability Analysis of Hybrid Dynamical Systems with Multi-Elastic Domains", International Journal of Non-Linear Mechanics, Vol. 7, 1972, pp. 425-443.

11. Meirovitch, L., "A Stationarity Principle for the Eigenvalue Problem for Rotating Structures", Presented as AIAA Paper No. 76-184 at the AIAA 14th Aerospace Sciences Meeting, Washington, D. C., January 26-28, 1976. To appear in the AIAA Journal.

12. Meirovitch, L, "A New Method of Solution of the Eigenvalue Problem for Gyroscopic Systems", AIAA Journal, Vol. 12, No. 10, 1974, pp. 1337-1342.

13. Meirovitch, L., "A Modal Analysis for the Response of Linear Gyroscopic Systems", Journal of Applied Mechanics, Vol. 42, No. 2, 1975, pp. 446-450.

14. Franklin, J. N., Matrix Theory, Prentice-Hall, Inc., Englewood Cliffs, N. J., 1968.

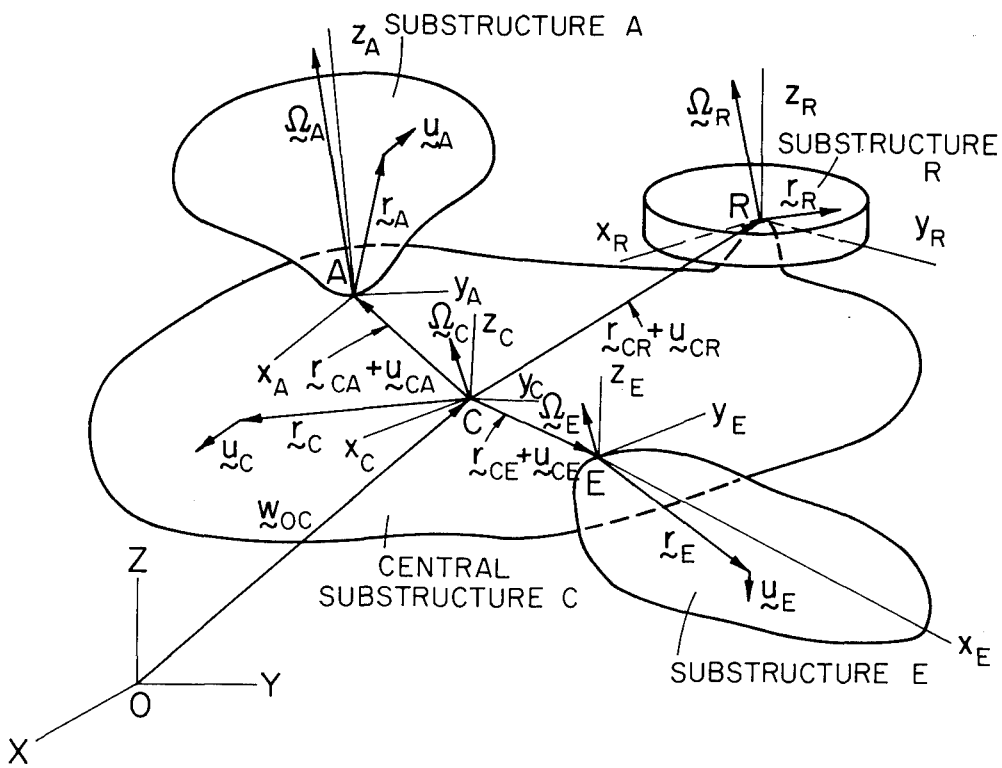

Figure 1.- The mathematical model.

THE STAGING SYSTEM:

DISPLAY AND EDIT MODULE

Ed Edwards
Battelle Columbus Laboratories

Leo Bernier
Air Force Flight Dynamics Laboratory

SUMMARY

The Display and Edit (D&E) Module, described in this paper, is one of six major modules being developed for the STAGING (STructural Analysis through Generalized INteractive Graphics) System. Several remarks are included concerning the computer environment and the architecture of the data base. But the thrust of the paper is, clearly, to provide an understanding of the utility of this module. This is accomplished by defining, to a reasonable level of detail, the more prominent features of D&E.

INTRODUCTION

To assure an adequate appreciation for the D&E capabilities, it is important to have a good conceptual understanding of STAGING and of the need for STAGING. Over recent years, the finite element technology has literally "burst" onto the scene, becoming one of the most powerful and popular analytical methods available today. One result of this popularity has been a proliferation of computer programs, all claiming to be unique or better than other similar programs. In some cases, the claim is simply untrue. In more cases, capabilities do overlap, but the programs are still unique enough to justify their existence. In all cases, the programs cannot communicate easily with one another and are cumbersome to use. The net result is that we have less capability than we need, but more than we can use effectively. To cope with this problem, efforts are underway to develop STAGING.

STAGING is a highly interactive capability intended to: (a) synthesize the finite element methodology into a cohesive, user-oriented capability, and (b) radically reduce the time required to conduct a finite element analysis. The system will allow potential users to rapidly generate finite element models and interpret analysis results independent of the analysis program chosen to conduct the analysis. Although STAGING is specifically being aimed at the finite element methodology, early consideration is being given for its eventual extension to other technical disciplines.

STAGING (fig. 1) consists of six major modules; (a) Executive Monitor, (b) Preprocessor, (c) Display and Edit, (d) Postprocessor, (e) Analysis

Programs, and (f) Generalized Data Base. The Executive Monitor will serve as a "traffic cop" to help a user find and use a particular capability, and to ensure the proper flow of information between modules. The Preprocessor will be used to generate bulk information for the analysis codes. D&E will provide a host of interactive graphic utilities to assist in "fine tuning" previously generated data, and effectively display the analysis results. The Postprocessor will allow easy generation of additional engineering information from the basic output files of the analysis codes. The Analysis Module will simply be a file of available design and analysis computer programs. And, finally, the Generalized Data Base will provide efficient storage for all geometric and non-geometric information associated with a particular analysis.

A number of general purpose subroutines are provided to facilitate the transfer of information to and from the data base. Conversion programs are written, using these subroutines, to allow each of the major system modules to communicate with the data base through the Executive Monitor.

COMPUTER ENVIRONMENT

Hardware

The major hardware components include: a CDC 6000 series computer, the CDC CYBER Graphics terminal (ref. 1), and the CDC System 17 mini-computer. The System 17 mini-computer is being used to perform a limited amount of local processing (e.g. continuous 3-D rotation), while the CYBER Graphics terminal is being used as the primary interface between the host computer and the user. Within the year, D&E will also be accessible from a Tektronix 4014 scope.

In the more distant future, networking techniques will be used to make D&E available to the user community. A part, or all, of D&E will be downloaded from a central host computer to a mini-computer and used in a local mode. The current feeling is that networking can provide an effective answer to maintaining large software systems, reduce the time required to streamline these same systems, and consequently, provide more time for implementing new features.

Software

The code for most routines is FORTRAN, with the exception of a few specialized routines for character manipulation and permanent file management which are written in 6000 assembly language. These routines are isolated in the code and clearly identified. The program uses the CDC segmentation loader (ref. 2) and operates in less than 60K octal words of core memory on the CDC 6600. Also, a strong emphasis is placed on isolating the graphics code to reduce the amount of frustration for future implementations of D&E on other graphics devices. And finally, the DTNSRDC data handler routines (ref. 3) are being used to manage the data base.

DATA BASE

The data base provides a convenient mechanism for storing the geometric model and all related information, including the analysis results. Functionally, the data base is composed of the following four levels: structures, substructures, elements and nodes (fig. 2). This hierarchical concept is important and is used extensively by D&E. Associated with the individual items within a level is an attribute list that contains specific information about each particular entity. The data base handler routines are used to allow a user to interrogate and modify the data base efficiently and effectively. An understanding of these basic concepts is all that is required to use D&E effectively.

DISPLAY AND EDIT FEATURES

The power and flexibility of D&E can best be characterized by simply defining the discrete capabilities of the module. To put some order into the litany of features that is about to follow, they will be grouped into these broader categories: (a) Substructure Definition, (b) Displaying the Input Model, (c) Picture Manipulation, (d) Displaying the Results, (e) Editing, and (f) Global Commands. The actual mechanics of the interactive process are contained in a command tree (ref. 4). The command tree structures the user's options, and allows the user to systematically progress through the D&E capabilities. Examples of these capabilities are illustrated in figure 3.

Substructure Definition

A substructure is defined as any arbitrary collection of nodes and elements that are present in the data base. The actual definition of a particular substructure is left completely to the user, and is used by him to improve his visual interpretation, and interaction, with that portion of the model in which he is most interested. A substructure can be defined using one, or more, of the following features:

a. Specifying a range of element/node numbers.

b. Specifying individual elements/nodes.

c. Specifying a range of values for any attribute.

d. Merging two or more substructures to form a new substructure.

e. Identifying geometric bounds.

Geometric specified bounds are defined using keyboard entries to specify an area or volume in either rectangular, cylindrical, or spherical coordinates. In a more limited sense, the lightpen can also be used to define the desired area or volume.

Displaying the Input Model

The input model can be viewed in one of three ways: in two-space (2D), in three-space rotatable (3DR), or in three-space non-rotatable (3DNR). The distinction between 2D and 3D is obvious. However, a 3D model can be displayed as a 2D model and vice versa. If the third coordinate is present in 2D, it will be ignored, and if absent in 3D, it will be given a default value of zero. 3DR and 3DNR present a more subtle distinction. The basic difference lies in where the 3D to 2D projection is carried out. The CYBER Graphics terminal features software (ref. 5) that will project a model using its mini-computer controller to describe the picture. The small core memory of the controller severely limits the size of the display. In the 3DNR mode the same projection is carried out on the host computer. Consequently, it is possible to display approximately twice the information in 3DNR as it is in 3DR. The tradeoff is that it takes longer to generate the picture in the 3DNR mode. Therefore, the 3DNR mode is used only when the 3DR mode would generate too much information.

In addition to displaying the actual geometry, all of the attributes associated with each entity can be displayed as alphameric or vector quantities superimposed on the geometric model. Examples of alphameric quantities include geometric and material properties. Examples of vector quantities include forces, moments and constraints.

Picture Manipulation

Picture manipulation varies from 2D to 3D. The base capabilities of 2D do, however, apply in exactly the same way for both 3D and 3DNR modes. These capabilities include:

a. picture zooming and recentering. These functions are performed through software in the controller and are considered LOCAL to the CYBER Graphics terminal.

b. generating a split screen view (fig. 3a). Up to four views can be generated simultaneously using the split screen option. Either a "free" (in which rotation can still occur) or "freeze" left side can be generated. In either case, only the main picture can be zoomed or used for lightpen selection.

c. shrinking elements (fig. 3b). Each element on the screen can be reduced about its center to 80% of its original size.

d. rescaling the picture. A new scale can be applied to the picture, or the picture can be scaled to fill the entire screen.

e. restoring the original picture. This option removes the effects of split screening and shrunk members, and restores the original picture re-centered.

It should be noted that 3DNR and 3DR have provisions for two more capabilities:

f. displaying of an X-Y-Z axis system. The axis system is centered in the middle of the picture and points along the X, Y, Z axes of the model.

g. generating a perspective view.

Finally, 3DR adds a feature its name implies: a capability to rotate around any of the three screen coordinate axes in a continuous or discrete mode. Continuous mode provides for automatic updating of the rotation. The discrete mode allows the user to rotate the model quickly, but in fixed steps.

Displaying the Results

After conducting the analysis, the answers are stored in the data base in the correct attribute arrays. Four basic capabilities are available to help the user review his results. They include X-Y plots, contour plots, deformed plots, and dynamic plots. Of course, the entire complement of picture manipulation capabilities is still available to help the user improve his visual interpretation of the results. As with the input model display section, the user need not pre-select the results displays he may wish to use.

The X-Y plotting capability (fig. 3c) is very flexible. The user may interactively activate the following options:

a. line style
   1. points
   2. connected points
   3. solid lines
   4. short dashed lines
   5. long dashed lines

b. grid
   1. full grid
   2. tic marks

c. graph style
   1. linear X/linear Y
   2. log X/linear Y
   3. linear X/log Y
   4. log X/log Y

d. titling
   1. X-axis
   2. Y-axis
   3. graph title

As many as ten curves can be generated on each plot. The user may also plot any attribute in the data base against any other attribute. And, finally, provisions have been made for automatic rescaling to ensure a reasonable picture every time.

Contour plots are available for 2-D displays only. As with the X-Y plotting capability, the user has control over the data to be plotted and the labelling of the graph. Scaling is performed automatically. The user can select the distance between contours, or use a value supplied by the system, to generate the contour intervals.

Deformed plots (fig. 3d) can be displayed alone, or superimposed on an undeformed plot. Dashed lines are used to easily distinguish the deformed plot from the undeformed plot. A magnification factor can be applied to the displacements to improve their visual appearance.

The dynamic plot capability is provided to facilitate film strip generation. In operation, the user need only specify the number of analysis time steps he wishes to process and the time-length of the film strip. The remaining process is automatic. The user has the option of previewing the information on the graphics scope or disposing it directly to an off-line plotting device.

Editing

Provisions are available to allow a user to easily alter the contents of the data base. Specifically, it is possible to add, delete, or modify any value of any attribute list in the data using keyboard entries and lightpen interaction. In a similar fashion, it is also possible to add or delete substructures, elements and nodes from the same data base.

Certain convenience features have been added to accelerate the editing process. For example, a user wishing to make the same changes to several different elements can activate the attribute lists of these elements by "picking" them from the graphics scope using the lightpen. Then, using the keyboard, the user can enter the new value for the particular attribute he wishes to change. The system will process this information and ensure that the change is reflected in each of the activated attribute lists.

Another useful feature is that the user can search a part, or all, of the data base for a particular value, or range of values, and replace them with a new one. A final example is that node points can be easily moved about in 2-D space. This feature is particularly helpful for moving the interior points of a model. An application of this feature could be to improve the aspect ratio of certain elements in a 2-D model.

GLOBAL Commands

GLOBAL commands initialize features that are accessible to the user any time during his session. Because these features will be made available to the user in other STAGING modules, they will eventually be included as features of the Executive Monitor. GLOBAL features that are currently available include:

a. STOP - the stop option ends execution of the user session. The option must be "picked" twice to actually stop. The first "pick" reminds the user that the new data base has not been automatically catalogued.

b. SAVE DATA BASE - the current data base can be saved in one of two ways. First, it is possible to overwrite the original copy of the data base. In this case, the contents of the old file will be purged automatically and the new data base will be catalogued with the same file name. The second option is

to enter a new copy of the file name by entering a new permanent file name, or cycle number. This new name will then become the current permanent file name.

c. CLOCK - this feature allows the user to check on how much time he has left in his current session.

d. STATISTICS - this feature provides information to the user to help him track the size of his model. The information includes such things as the number of nodes, elements, and substructures, and the limit values of the display.

e. HELP - this feature can be used to provide further definition of the "pickable" options available to the user. It can also be used to display the options at the next level up and the next level down in the command tree. And finally, the HELP feature can be used to display the history of "picks" a user has made to get from the top of the command tree down to his current level.

f. HARDCOPY - the CYBER Graphics terminal has no inherent hardcopy capability because it is a refresh terminal. Consequently, software is provided to process the current display to a suitable hardcopy device.

g. SKIP - this command is intended for experienced users who know their way around the command tree. It allows the user to skip up as many levels as the user has traveled through. The user is cautioned that subroutines normally called, as he progresses through the normal RETURN mechanism, are not called in the SKIP mode. Consequently, this feature can cause problems for the inexperienced user later in the session.

h. COMMENT - the comment log is provided to improve communication between the program developers and the program users. Users are encouraged to use the log to ask questions, criticize, or make general comments. The comment log is periodically reviewed by the program developer and has proved to be an effective mechanism for debugging, and streamlining, the D&E capability.

i. RETURN - this option re-activates the menu for the module the user was working in before activating the GLOBAL command feature. The only exception is when input is required for type-ins. In this case, RETURN must be "picked" and the segment re-entered.

j. Error Recovery - occasionally an error will occur that causes the program to abort on the host computer. The host will recover the error and ask the user if he wishes to continue. If the user says yes, the screen will erase and control will be transferred to that menu from which the abort was initiated.

CONCLUDING REMARKS

The D&E module represents an important first step toward a much more ambitious goal, that goal being to integrate the entire spectrum of design and analysis computer programs, while maximizing the utility and efficiency of these same programs. Efforts will continue to be made to streamline the D&E

module and to add new features to it. But even in this unpolished state, user reaction has been surprisingly good. This reaction tends to lend further credence to the old adage that a picture, in the right place and at the right time, is still worth a thousand words.

The remaining five major STAGING modules are being developed concurrent with D&E. It is estimated that, within this calendar year, the six major system modules will be integrated to form the first tangible version of STAGING.

REFERENCES

1. 777 Interactive Graphics System, Version 2.0, User's Guide/Training Manual. Control Data Corporation Publication No. 17322500, 1976.

2. Loader Reference Manual. Control Data Corporation Publication No. 60344200, 1976.

3. Haas, M.; and Control Data Corporation: Data Handler Reference Manual. Control Data Corporation Publication No. 17322100, 1976.

4. Kasik, D. J.: Controlling User Interaction. Proceedings of the Third Annual SIGGRAPH Conference, July 1976.

5. 3D 777/IGS Reference Manual, Version 1.0. Control Data Corporation Publication No. 17326500, 1976.

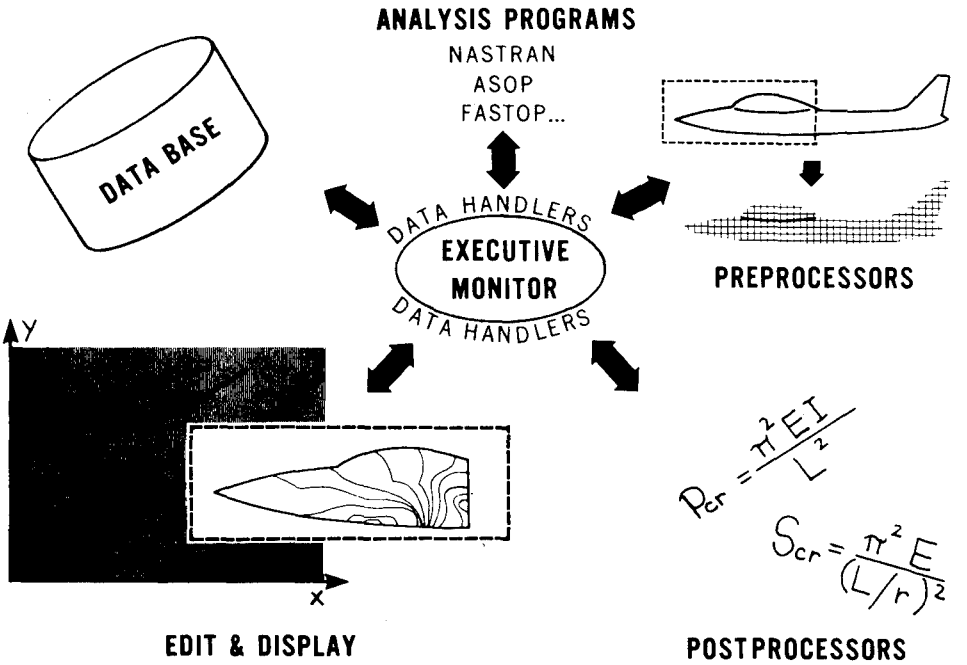

Figure 1.- STAGING modules.

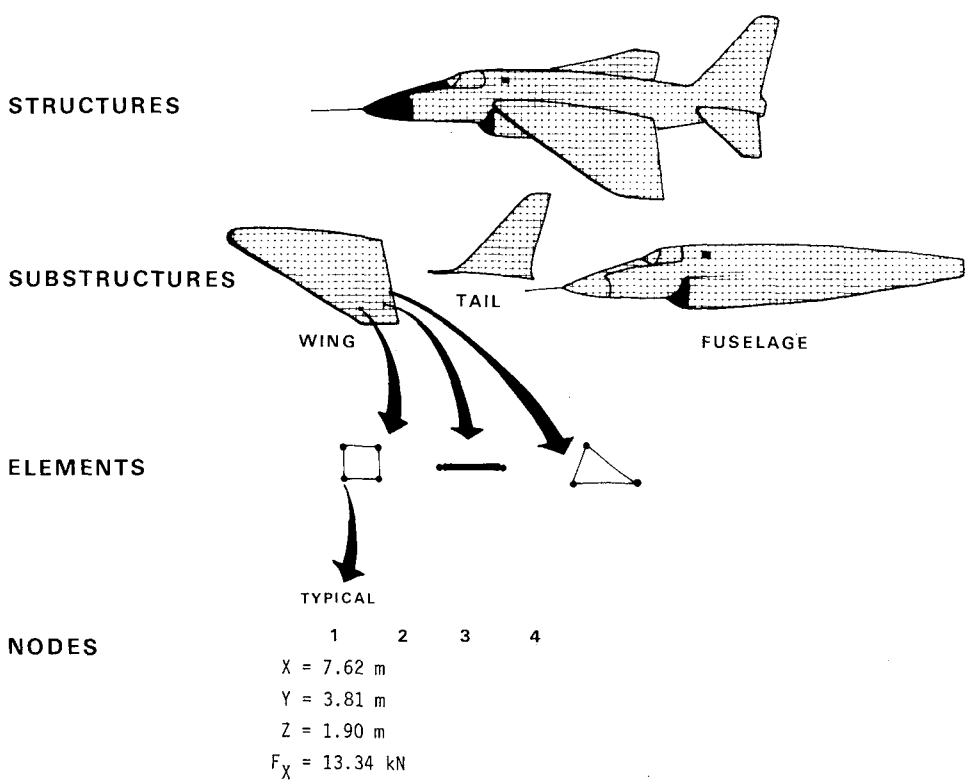

Figure 2.- Conceptual view of the data base.

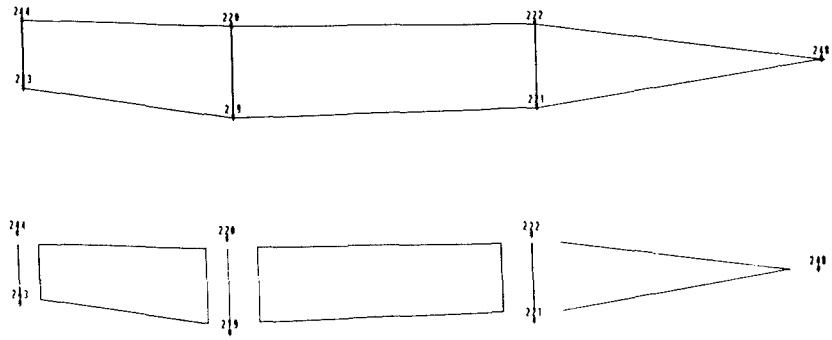

(a) An 80-percent shrink shows rod elements.

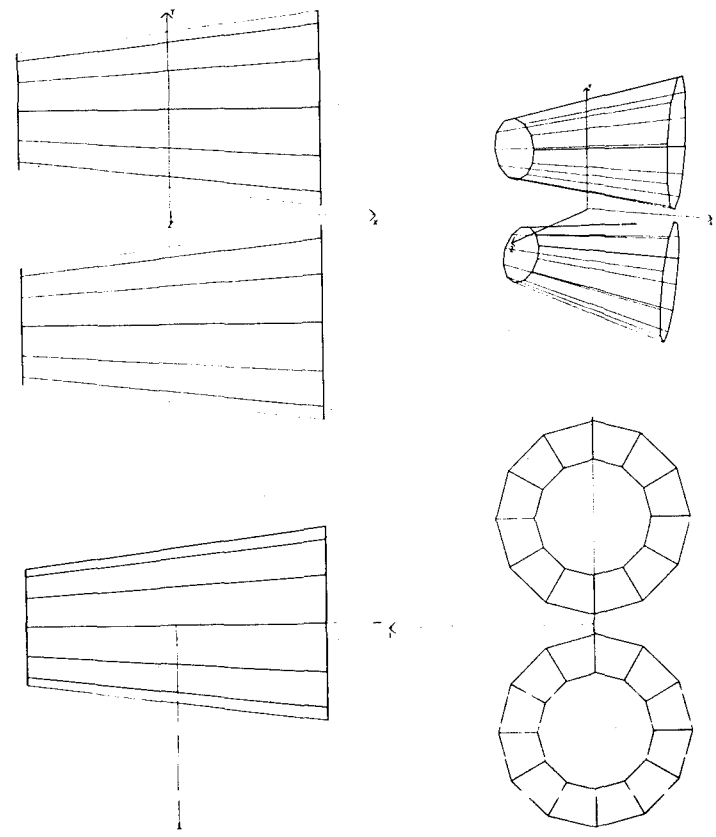

(b) 4-way split screen with top, side, front, and perspective views.

Figure 3.- Four examples of D&E display capabilities.

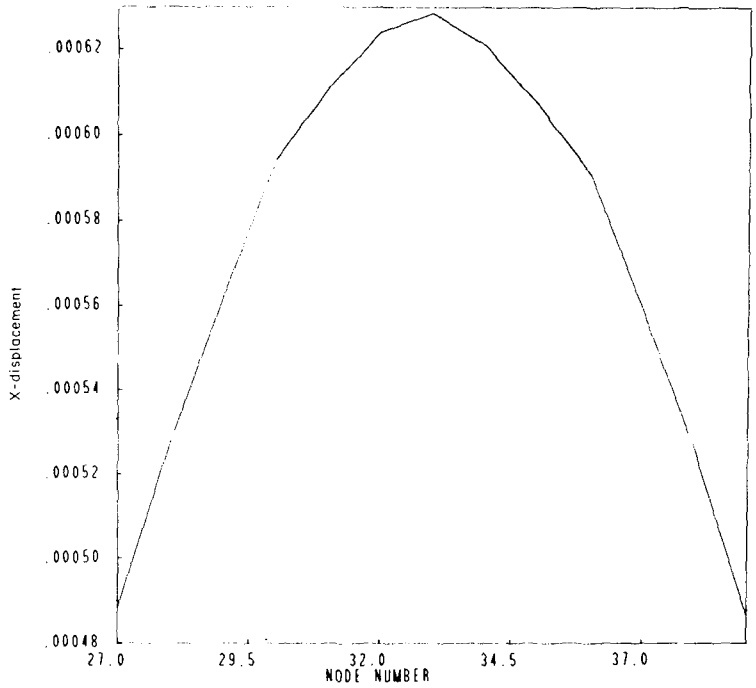

(c) X-Y plot of node number versus X-displacement.

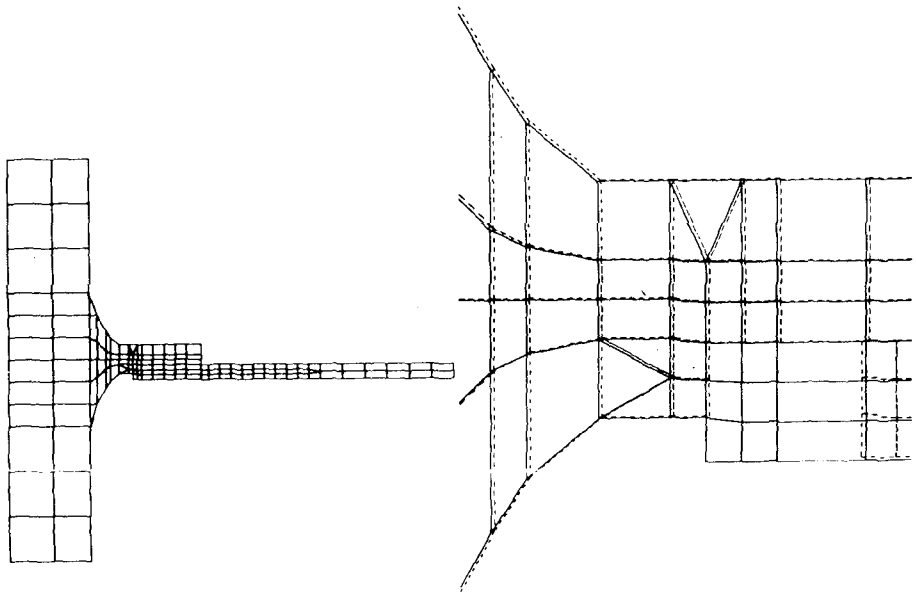

(d) 2-way split screen with zoomed deformed plot.

Figure 3.- Concluded.

SOME CONVERGENCE PROPERTIES OF FINITE ELEMENT APPROXIMATIONS OF PROBLEMS IN NONLINEAR ELASTICITY WITH MULTI-VALUED SOLUTIONS*

J. T. Oden
Texas Institute for Computational Mechanics
The University of Texas

SUMMARY

Some results of studies of convergence and accuracy of finite element approximations of certain nonlinear problems encountered in finite elasticity are presented. A general technique for obtaining error bounds is also described together with an existence theorem. Numerical results obtained by solving a representative problem are also included.

INTRODUCTION

In this note I summarize some recent results obtained on finite element approximations of certain nonlinear elliptic-boundary-value problems in finite elasticity. The results I quote here are given in a more elaborate form elsewhere. In reference 1, Ricardo Nicolau and I reported some results on a class of problems in which bifurcations occur. There we consider cases in which, for a given set of external forces, not only can multiple solutions occur, but a loss of regularity can apparently result on certain solution paths. A complete account of these results is to be published in a lengthier article.

The principal features of this work are (1) a priori error estimates and proofs of convergence of finite element approximations of highly nonlinear elasticity problems (these estimates are optimal), (2) error estimates for multiple solutions of a nonlinear elliptic problem (these estimates are also optimal, but the predicated bounds are different for different solution paths), (3) a discussion of specific numerical results and certain special problems connected with the numerical analysis of this class of problems.

NOTATION AND PRELIMINARIES

We shall employ the following notations and conventions:

$\underset{\sim}{w} = (u,v,w)$ = displacement vector in a material body $\mathcal{B}$, u, v, and w being the cartesian components of displacement in the material directions X, Y, Z.

---

* This work was supported by the National Science Foundation under Grant ENG-75-07846.

$\nabla \underset{\sim}{w}$ = gradient of $\underset{\sim}{w}$

W = strain energy per unit volume of the body in a reference configuration, W being an appropriately invariant twice-continuously differentiable function of $\nabla \underset{\sim}{w}$.

$V = V(\underset{\sim}{w},p)$ = potential of the external forces per unit reference volume, p being a real loading parameter.

$\underset{\sim}{\Sigma} = \partial W/\partial \nabla \underset{\sim}{w}$ = stress tensor $\equiv \underset{\sim}{\Sigma}(\underset{\sim}{w})$

$\mathcal{U}$ = space of admissible displacements $= \{ \underset{\sim}{w}: \int_{\Omega} (W + V) dXdYdZ < \infty; \ \underset{\sim}{w} = \underset{\sim}{0} \text{ on } \partial\Omega \}$

(Here Ω is a bounded open set of particles composing the interior of the body $\mathcal{B}$ and $\partial\Omega$ is its boundary)

To indicate various dependences, we also use such notations as $\underset{\sim}{\Sigma}(\underset{\sim}{w})$, $\nabla V(\underset{\sim}{w},p)$, etc.

The potential $V(\underset{\sim}{w},p)$ is assumed to be of the form

$$V(\underset{\sim}{w},p) = - (p\underset{\sim}{f},\underset{\sim}{w}) + V_o(\underset{\sim}{w},p)$$

where $p\underset{\sim}{f}$ is a body force term and $V_o(\underset{\sim}{w},p)$ is nonlinear in $\underset{\sim}{w}$. To simplify notations, we also introduce the operator

$$\langle A(\underset{\sim}{w},p),\underset{\sim}{\eta} \rangle = \int_{\Omega} (\underset{\sim}{\Sigma} \cdot \nabla \underset{\sim}{\eta} - \frac{\partial V_o}{\partial \underset{\sim}{w}} \cdot \underset{\sim}{\eta}) dXdYdZ \tag{1}$$

Then, formally, A is given by

$$A(\underset{\sim}{w},p) = - \operatorname{Div} \underset{\sim}{\Sigma}(w) - \frac{\partial V_o(\underset{\sim}{w},p)}{\partial \underset{\sim}{w}} \tag{2}$$

We are concerned with nonlinear boundary-value problems of the following type: find $\underset{\sim}{w} \in \mathcal{U}$ such that

$$\langle A(\underset{\sim}{w},p),\underset{\sim}{\eta} \rangle = (p\underset{\sim}{f},\underset{\sim}{\eta}) \qquad \forall \ \underset{\sim}{\eta} \in \mathcal{U} \tag{3}$$

We are particularly concerned with Galerkin approximations of (3). We introduce a real parameter h, $0 < h \leq 1$, which, of course, corresponds to the mesh parameter in finite element approximations, and denote $\{ \mathcal{U}_h \}_{0<h\leq 1}$ = a family of finite-dimensional subspaces of $\mathcal{U}$ such that $\bigcup_{0<h\leq 1} \mathcal{U}_h$ is dense in $\mathcal{U}$.

The Galerkin approximation of (3) then amounts to resolving the following problem: find $\underset{\sim}{w}_h \in U_h$ such that

$$\langle A(\underset{\sim}{w}_h, p), \underset{\sim}{\eta}_h \rangle = (p\underset{\sim}{f}, \underset{\sim}{\eta}_h) \qquad \forall\, \underset{\sim}{\eta}_h \in U_h \tag{4}$$

Upon subtracting (4) from (3) evaluated on $\underset{\sim}{\eta} = \underset{\sim}{\eta}_h$, we obtain the orthogonality condition:

$$\langle A(\underset{\sim}{w}, p) - A(\underset{\sim}{w}_h, p), \underset{\sim}{\eta}_h \rangle = 0 \qquad \forall\, \underset{\sim}{\eta}_h \in U_h \tag{5}$$

SOME HYPOTEHSES ON THE STRESS AND POTENTIAL OPERATORS

In many problems in finite elasticity, it appears to be justified to make hypotheses of the following type concerning the operator A and the space U:

I. The operator A of (1) maps U into its topological dual U'; U is a reflexive Banach space with norm $||\underset{\sim}{w}||_U$.

II. The displacement field in the body corresponding to a given load p is contained in a space $\hat{U}$ with stronger topology than U, $\hat{U}$ being densely and continuously imbedded in U.

III. The operator A is weakly continuous; i.e. if $\{\underset{\sim}{w}_n\}$ is any sequence converging weakly to $\underset{\sim}{w}_o$, then $A(\underset{\sim}{w}_n, p)$ converges weakly to $A(\underset{\sim}{w}_o, p)$.

IV. The operator A is coercive; i.e.

$$\lim_{||\underset{\sim}{w}||_U \to +\infty} \frac{\langle A(\underset{\sim}{w}, p), \underset{\sim}{w} \rangle}{||\underset{\sim}{w}||_U} = +\infty \tag{6}$$

V. A sufficient condition that II holds is that A be a potential operator with a Gateaux differential DA such that $\langle DA(\underset{\sim}{w}_o + \theta(\underset{\sim}{w}_n - \underset{\sim}{w}_o)) \cdot \underset{\sim}{\eta}, \underset{\sim}{w}_n - \underset{\sim}{w}_o \rangle = 0$ as $n \to \infty$ for any sequence $\{\underset{\sim}{w}_n\}$ converging weakly to $\underset{\sim}{w}_o$, $\forall\, \underset{\sim}{\eta} \in U$.

VI. A sufficient condition for coerciveness is that there exists a constant $\mu > 0$ such that

$$\langle A(\underset{\sim}{w}_1, p) - A(\underset{\sim}{w}_2, p), \underset{\sim}{w}_1 - \underset{\sim}{w}_2 \rangle \geq \gamma_o ||\underset{\sim}{w}_1 - \underset{\sim}{w}_2||_U^p - \mu \tag{7}$$

where γ_o is a positive constant and $p > 1$.

VII. There exist functions B: $U \times U \to \mathbb{R}$ and C: $U \times U \to \mathbb{R}$, B weakly continuous, such that $\forall\ \underset{\sim}{w}_1, \underset{\sim}{w}_2, \underset{\sim}{w}_3 \in U$,

$$|\langle A(\underset{\sim}{w}_1, p) - A(\underset{\sim}{w}_2, p), \underset{\sim}{w}_3\rangle| \leq ||\underset{\sim}{w}_3||_U ||\underset{\sim}{w}_1 - \underset{\sim}{w}_2||_U B(\underset{\sim}{w}_1, \underset{\sim}{w}_2) \tag{8}$$

$$|\langle A(\underset{\sim}{w}_1, p) - A(\underset{\sim}{w}_2, p),\ \underset{\sim}{w}_1 - \underset{\sim}{w}_2\rangle| \geq \gamma ||\underset{\sim}{w}_1 - \underset{\sim}{w}_2||_U^p \tag{9}$$

where γ is a positive constant and $p > 0$.

Theorem 1 (Existence). Let either of the following hold:

(i) Conditions I, III, and IV above, or

(ii) Conditions I, IV, and V, or

(iii) Conditions I, III, and VI, or

(iv) Conditions I, IV, and VI.

Then there exists at least one vector $\underset{\sim}{w} \in U$ that satisfies (3) for each $\underset{\sim}{pf} \in U'$. ■

We emphasize that the operator A is not necessarily monotone.

FINITE ELEMENT APPROXIMATIONS AND ERROR BOUNDS

The subspaces U_h in (4) are assumed to be constructed using finite element methods. Thus, the solution domain Ω is partitioned into E subdomains Ω_e over which $\underset{\sim}{w}$ is approximated by piecewise polynomials of degree $\leq k$. If $\underset{\sim}{w} \in \hat{U} \cap U$ and $\underset{\sim}{\tilde{w}}_h$ is its projection into U_h, it is well known that the subspace U_h can be designed so that the following hold:

(i)

$$||\underset{\sim}{w} - \underset{\sim}{\tilde{w}}_h||_U \leq C_o h^{\sigma} ||\underset{\sim}{w}||_{\hat{U}} \tag{10}$$

h being the mesh parameter and σ a positive number.

(ii)

$$\frac{||\underset{\sim}{w}_h||_U^2}{||\underset{\sim}{w}_h||_U^p} \leq C_1 h^{\nu}, \qquad \nu \geq 0 \tag{11}$$

In (10) and (11), C_o and C_1 are constants independent of h.

We proceed to determine error bounds as follows:

1. The approximation error is $\underset{\sim}{e} = \underset{\sim}{w} - \underset{\sim}{w}_h$:

$$||\underset{\sim}{e}||_u \leq ||\underset{\sim}{w} - \tilde{\underset{\sim}{w}}_h||_u + ||\underset{\sim}{w}_h - \tilde{\underset{\sim}{w}}_h||_u \qquad \text{(by the triangle inequality)}$$

$$\leq C_o h^{\sigma} ||\underset{\sim}{w}||_u + ||\underset{\sim}{w}_h - \underset{\sim}{w}_h||_u \qquad \text{(by (10))}$$

2.

$$||\underset{\sim}{w}_h - \tilde{\underset{\sim}{w}}_h||_u^2 \leq C_1 n^{\nu} ||\underset{\sim}{w}_h - \tilde{\underset{\sim}{w}}_h||_u^p \qquad \text{(by (11))}$$

$$\leq C_1 h^{\nu} 1/\gamma |\langle A(\underset{\sim}{w}_h,p) - A(\tilde{\underset{\sim}{w}}_h,p), \underset{\sim}{w}_h - \tilde{\underset{\sim}{w}}_h\rangle| \qquad \text{(by (9))}$$

$$= C_1 1/\gamma\ h^{\nu} |\langle A(\underset{\sim}{w},p) - A(\tilde{\underset{\sim}{w}}_h;p), \underset{\sim}{w}_h - \tilde{\underset{\sim}{w}}_h\rangle| \qquad \text{(by (5))}$$

$$\leq \frac{C_1}{\gamma} B(\underset{\sim}{w}, \tilde{\underset{\sim}{w}}_h) ||\underset{\sim}{w}_h - \tilde{\underset{\sim}{w}}_h||_u ||\underset{\sim}{w} - \underset{\sim}{w}_h||_u\ h^{\nu} \qquad \text{(by (8))}$$

3. For sufficiently small h, we assume that

$$B(\underset{\sim}{w}, \tilde{\underset{\sim}{w}}_h) = B(\underset{\sim}{w}, \underset{\sim}{w}_h - \underset{\sim}{w} + \underset{\sim}{w})$$

$$= B(\underset{\sim}{w}, \underset{\sim}{w}) + O(h^{\mu}) \qquad \mu > 0 \qquad (12)$$

owing to the continuity of $B(\cdot,\cdot)$. Thus

$$||\underset{\sim}{w}_h - \tilde{\underset{\sim}{w}}_h||_u \leq (\frac{C_1 C_o}{\gamma})\ h^{\sigma+\nu} ||\underset{\sim}{w}||_{\hat{u}} B(\underset{\sim}{w}) \qquad (13)$$

by virtue of (10), wherein $B(\underset{\sim}{w}) = B(\underset{\sim}{w}, \underset{\sim}{w})$.

4. Combining the result 1 with (13), we see that as $h \to 0$, a positive constant C_2 exists such that

$$||\underset{\sim}{e}|| \leq C_2||\underset{\sim}{w}||_{\hat{U}}(h^{\sigma} + h^{\sigma+\nu}B(\underset{\sim}{w})) \tag{14}$$

Thus, for sufficiently smooth w, we obtain the optimal rate of convergence for the nonlinear problem so long as $\nu \geq 0$.

Theorem 2. Let (8), (9), and (13) hold and let there exist solutions to the nonlinear boundary-value problem (3). Let $w_h \in U_h$ be a finite element approximation of w in a subspace U_h in possessing properties (10) and (11). Then the approximation error $\underset{\sim}{e} = \underset{\sim}{w} - \underset{\sim h}{w}$ satisfies the bound (14) as $h \to 0$. Moreover, if $\nu \geq 0$ and w is sufficiently smooth, the optimal rate of convergence is obtained for the nonlinear problem.

AN EXAMPLE AND NUMERICAL EXPERIMENTS

The following example is described in [1]:

$$W = -E_o \ell n\lambda + E_1(\lambda^2 + v'^2 - 1) + E_2(\lambda^2 + v'^2 - 1)^2 + E_3(\lambda^2 + v'^2 - 2) + E_4(\lambda - 1) \tag{15}$$

$$V = -pu + \frac{1}{4} K_o p v^3 \tag{16}$$

where $\lambda = 1 + u'$ ($u = u(x)$, $v = v(x)$), $E_o, \cdots, E_4$, K_o are constants, and $p \geq 0$, In this case,

1. $U = \{(u,v): \int_0^L (W + V)dX < \infty\} \cap \underset{\sim 4}{\overset{\circ}{W}}{}^1_1(I)$

$\underset{\sim 4}{\overset{\circ}{W}}{}^1_1(I)$ = Reflexive Sobolev space $= \{(u,v): \int_0^L (|u'|^4 + |v'|^4)dx < \infty,$

$$u(0) = u(L) = v(0) = v(L) = 0\}.$$

$$|||\underset{\sim}{w}||| = ||u||_{\overset{\circ}{W}{}^1_4(I)} + ||v||_{\overset{\circ}{N}{}^1_4(I)} = \{\int_0^1 |u'|^4\, dx\}^{\frac{1}{4}} + \{\int_0^L |v'|^4\, dx\}^{\frac{1}{4}}$$

$$||\underset{\sim}{w}||_U = [||u||^4_{\overset{\circ}{W}{}^1_4(I)} + ||v||^4_{\overset{\circ}{W}{}^1_4(I)}]^{\frac{1}{4}}$$

3. $\hat{U} = W^{\ell}_4(I) \cap \overset{\circ}{W}{}^1_4(I) \qquad I = (0,L)$

4. $p = 4$, $\sigma = \min(k, \ell-1)$, $\nu = 3/2$

The functions $B(\underset{\sim}{w},\underset{\sim}{w})$ and $C(\underset{\sim}{w},\underset{\sim}{w})$ are complicated functions of the components u and v and are given in [1]. In this case, the operator A is not monotone.

Test problems were solved using piecewise linear finite element (k = 1). The problem does not have unique solutions for $p > p_{cr}$. Figure 1 shows the computed solutions for various values of p for the case L = 10, $E_1 = 1$, $E_2 = 0.8$, $E_3 = 0.5$, $E_3 = -0.1$, $E_4 = -0.2$, $K_o = 1.0$. Observe that a bifurcation is reached at p = 0.5.

Figure 2 shows the rate of convergence actually obtained in the analysis computed by comparing the solution for coarse meshes with that obtained for 100 elements. As predicted, the rate of convergence is

$$O(h^{\sigma} + h^{\sigma+\nu}) = O(h + h^{5/2}) = O(h)$$

REFERENCES

1. Oden, J. T. and Nicolau, R., "Analysis of Finite Element Approximations of a Boundary-Value Problem in Finite Elasticity," Formulations and Computational Algorithms in Finite Element Analysis, Edited by J. Bathe, J. T. Oden, and W. Wunderlich, M.I.T. Press, Cambridge, Mass., 1976.

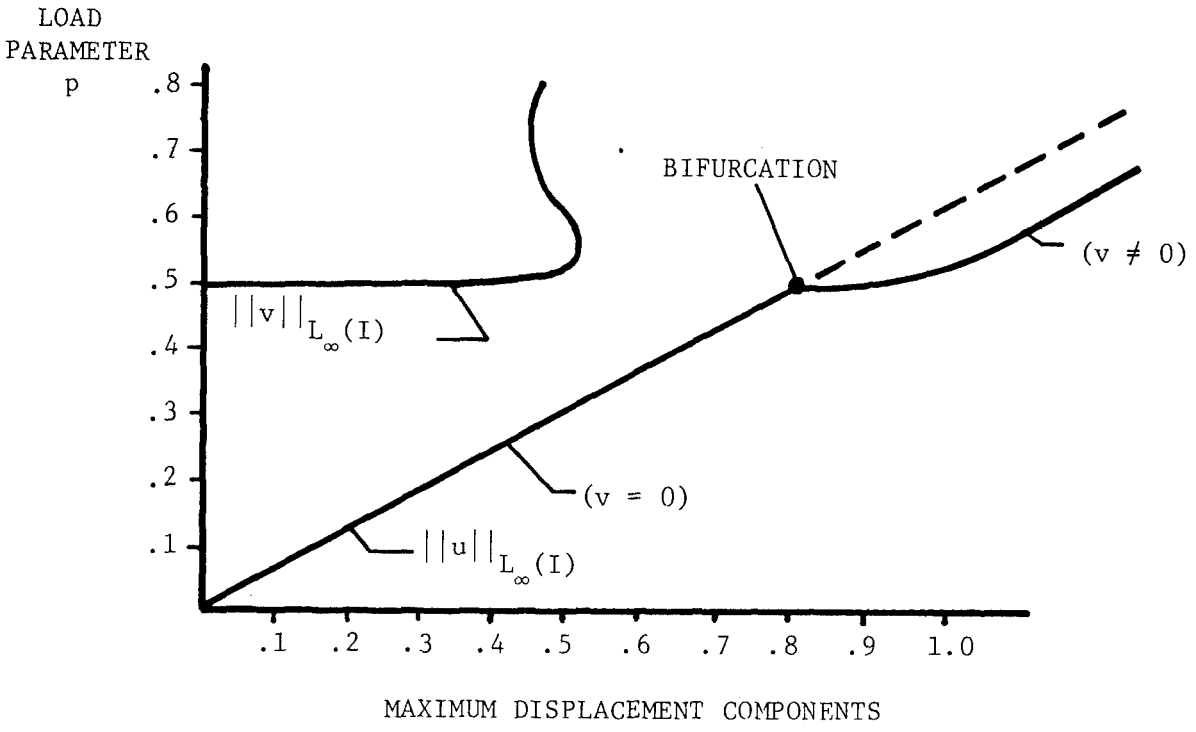

Figure 1.- Computed equilibrium paths.

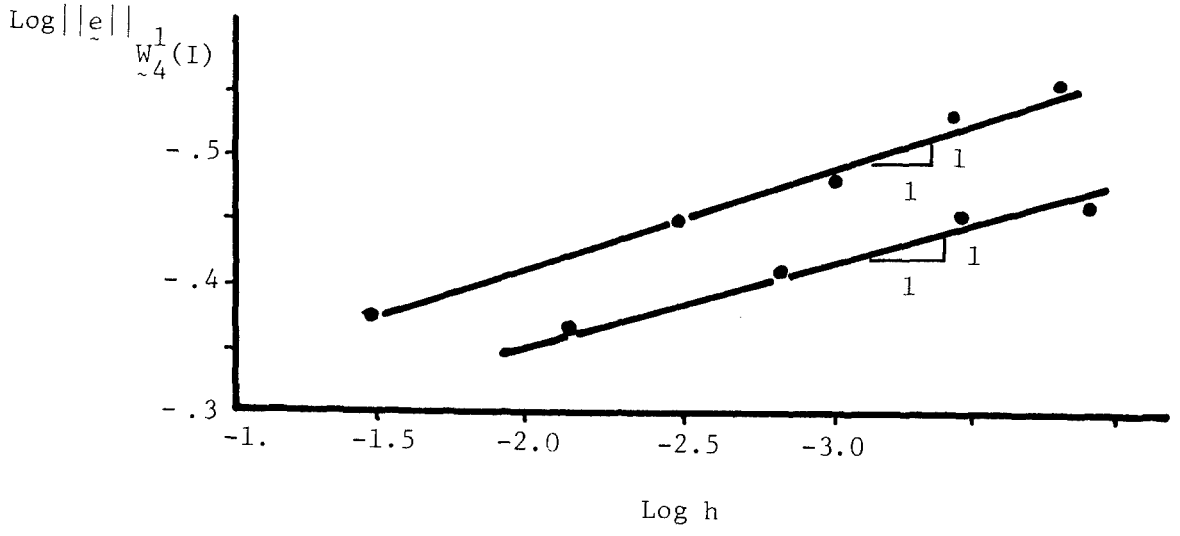

Figure 2.- Computed rates of convergence.

ELASTO-PLASTIC IMPACT OF HEMISPHERICAL SHELL IMPACTING ON HARD RIGID SPHERE

D. D. Raftopoulos
Professor of Mechanical Engineering
The University of Toledo

A. L. Spicer
Research Engineer, New Departure-Hyatt
Division of General Motors Corp.

ABSTRACT

This paper extends an analysis of plastic stress waves, originated by G. I. Taylor in reference 1, for cylindrical metallic projectile in impact to an analysis of a hemispherical shell suffering plastic deformation during the process of impact. In that, it is assumed that the hemispherical shell with a prescribed launch velocity impinges a fixed rigid sphere of diameter equal to the internal diameter of the shell. Particularly this study is directed in order to investigate the dynamic biaxial state of stress present in the shell during deformation.

The results of this analysis are compared with Taylor's reference 1 and it has been found that this analysis is an extension of the one-dimensional analyses of references 1, 2, 3, and 4, to spherical coordinates. It is valuable for studying the state of stress during large plastic deformation of a hemispherical shell.

INTRODUCTION

The object of this paper is to develop an analysis of plastic hemispherical stress-wave propagation and to use this analysis for determining the dynamic biaxial yield stress. The Tresca yield criteria is used as the yield condition. Higher order terms are included in the derivations; thus, this analysis is valid for large deformations.

G. I. Taylor in reference 1 used the governing physical laws and the geometry during plastic deformation of the cylindrical projectile to formulate differential equations which are solved in order to determine the dynamic yield stress in impact. This analysis of a hemispherical shell impacting a fixed rigid sphere, of diameter equal to the internal diameter of the shell, is similar to the analysis of a cylindrical projectile impacting a rigid target of references 1, 2, 3, and 4. In fact, in all these cases during impact it is assumed that when the stress rise exceeds the elastic limit of the material,

two waves are generated. The first of these is the elastic wave, which travels with a velocity c. It is followed by the plastic stress wave which travels with a slower velocity v. Through an analysis of the propagation of these two stress waves, a method is formed which can be used to determine the dynamic yield stress of the material of a hemispherical shell. The proper choice of the time increment, dt, simplifies the analysis greatly. The choice is to make the time increment equal to the length of time required for the elastic wave to complete a double passage of the elastic zone. If the difference equations are derived by utilizing this time increment, which is eliminated by combining the derived difference equations, the governing equations which are derived are free of this time increment. This mathematical approach, for the biaxial state of stress of the hemispherical shell, closely parallels Taylor's analysis of the cylindrical projectile.

NOMENCLATURE

A_o	Projection at the elastic-plastic boundary undeformed area at time t
A	Projection at the elastic-plastic boundary deformed area at time t + dt
a	Initial inside radius
b	Initial outside radius
c	Elastic wave velocity
dh	Incremental plastic radius
dr	Incremental elastic radius
dt	Time for a double passage of elastic region by elastic wave
E	Young's modulus
h	Thickness of plastic region at time t
r_o	Initial elastic length of shell in the radial direction = b - a
r_1	Final total length of shell in the radial direction
r	Thickness of shell in the elastic zone at time t
R	Final thickness of the elastic region
S_1	Dynamic yield stress - calculated by the approximate method
S	Dynamic yield stress - calculated by the exact method
t	Time

U Initial radial velocity due to launch velocity

u Particle velocity in the elastic region

v Absolute velocity of the plastic wave front

Y Yield stress in uniaxial tension

ε_1 Initial radial strain

ε Radial strain at time t

ρ Density

ν Poisson's ratio

ANALYSIS

Problem Description

A hemispherical metallic shell strikes with a prescribed velocity a rigid sphere (of diameter equal to the internal diameter of the shell) which is permanently fixed at a base retaining zero velocity during the process of impact. During this impact, a radial motion is directed from the internal surface of the shell toward the external surface of the same. The radial particle velocity of the internal surface of the shell is initially the same as the impact velocity and is denoted by U. If the biaxial stress exceeds the elastic limit, two waves are generated at the internal surface of the shell. The first wave is the elastic wave which travels with velocity c. The second is the plastic wave which travels with velocity v. The elastic compressive stress wave, which propagates radially outward in the elastic region with velocity c, will reduce the impact velocity U to $U-(S/\rho c)$. During this time, the stress reaches the elastic limit. This elastic wave will reflect at the external surface of the sphere, resulting in an elastic tensile wave being superposed on the compressive elastic wave. The material which has been passed by this reflected elastic wave is stress free and has a velocity equal to $U-(2S/\rho c)$. At the particular time when this wave reaches the elastic-plastic boundary, the shell is in a condition similar to the initial impact, except that its speed is equal to $U-(2S/\rho c)$ and its elastic thickness is less than the original value. At this time, it is assumed that the plastically deformed material will be attached to the sphere and acts on the elastic part of the shell as a rigid material. This continues until the speed of the shell becomes equal to zero.

Assumptions

In order to work out the mathematical analysis of this problem, several basic assumptions are needed.

First, for axially symmetrical analysis, the shell must be symmetric with respect to its axis of symmetry and maintain this symmetry during the process of impact. The second assumption is that the elastic strain is negligible. This assumption is valid if the plastic strain is large, thus making the elastic strain very small in comparison with the plastic strain. Along the same lines as the previous assumption, the third assumption is that the material is taken to be perfectly plastic. Although no material behaves exactly in a perfectly plastic manner, some materials approach this type of behavior at high strain rates. This dynamic-plastic stress-wave analysis is for extremely high strain rates. Thus it is possible to assume that the material is perfectly plastic without the loss of much generality in the solution. The fourth assumption, which is usually made in plasticity problems, is that the density of the shell material remains constant. The fifth and final assumption is that the material in the plastic region, after being deformed, does not possess elastic properties; thus it behaves as a rigid material with zero velocity.

Physical Laws

By considering the problem description, and assumptions, the governing physical laws can be formulated.

Choose the time increment, dt, to be equal to the time required for a complete double passage of the elastic wave through the elastic region. Since the length of material in the elastic zone is defined as r and the elastic wave velocity is c, it follows that

$$dt = 2r/c \tag{1}$$

where

$$c = \{E\,(1 - \nu)/\,\{\rho(1 + \nu)(1 - 2\nu)\}\}^{1/2}$$

$$dh = v\,(2r/c) \tag{2}$$

$$dr = -(u + v)\,(2r/c) \tag{3}$$

$$du = -\,2S/(\rho c) \tag{4}$$

Using equation (1) to eliminate c from equations (2), (3), and (4) results in

$$\frac{dh}{dt} = v \tag{5}$$

$$\frac{dr}{dt} = -(u + v) \tag{6}$$

$$\frac{du}{dt} = - S/(\rho r) \tag{7}$$

for conservation of mass

$$A\ v = (u + v)\ A_o \tag{8}$$

The momentum equation reduces to

$$S\ (A - A_o) = 1/2(A + A_o)\ (u + v)\ u\ \rho \tag{9}$$

The radial strain is defined, at the plastic boundary, by

$$\varepsilon = 1 - A_o/A \tag{10}$$

Combining equations (8), (9), and (10)

$$\rho u^2/S = 2\ \varepsilon^2/(2 - \varepsilon) \tag{11}$$

Combining equations (6), (7), (8), and (10)

$$\frac{dr}{du} = \rho u r/(S\varepsilon) \tag{12}$$

Integrating equation (12)

$$\text{Log}_e(r^2) = \int 1/\varepsilon\ d\{\varepsilon^2/(1 - \varepsilon/2)\}$$

$$= 4/(2 - \varepsilon) - 2\ \text{Log}_e\ (1 - \varepsilon/2) + \text{Constant} \tag{13}$$

At time $t = 0$, $u = U$, $r = r_o$, and $\varepsilon = \varepsilon_1$; thus equation (11) and equation (13) become, respectively

$$\rho U^2/S = 2\ \varepsilon_1^2\ /(2 - \varepsilon_1) \tag{14}$$

$$\text{Log}_e(r/r_o)^2 = 4/(2 - \varepsilon) - 2\ \text{Log}_e\ (1 - \varepsilon/2) - 4/(2 - \varepsilon_1)$$

$$+ 2\ \text{Log}_e\ (1 - \varepsilon_1/2) \tag{15}$$

When all motion has ceased, $r = R$, and $\varepsilon = 0$, and R can be measured.

$$\text{Log}_e(R/r_o)^2 = 2 - 4/(2 - \varepsilon_1) + 2\ \text{Log}_e(1 - \varepsilon_1/2) \tag{16}$$

Combining equations (5), (6), (8) and (10)

$$h = \int dh = - \int_{r_o}^{r} (1 - \varepsilon).\ dr \tag{17}$$

Combining equations (7), (11), and (14)

$$Ut/r_o = \varepsilon_1(1 - \varepsilon_1/2)^{-1/2}\int_{\varepsilon}^{\varepsilon_1} r/r_o\,(1 - \varepsilon/4)/(1 - \varepsilon/2)^{3/2}d\varepsilon \quad (18)$$

If uniformly spaced values of ε_1 are placed in equations (14) and (16), $\rho U^2/S$ vs R/r_o can be plotted. Evaluation of equation (17) for h is accomplished by Simpson's rule integration. Results of these calculations are plotted in Figure 1.

Two different methods of integration were employed to evaluate the integral equations (17) and (18). The first method used was a Simpson's rule integration. Results for various ε_1 are plotted in Figure 2.

The second method of integration was using the asymptotic expansion of the integrals. References 5, 6, and 7 provide information on asymptotic power-series expansions. Values obtained by asymptotic expansion agreed well with those obtained by Simpson's rule integration.

To develop a simple formula for calculating the dynamic yield stress from measurements made before and after the impact, it will be additionally assumed that the plastic boundary propagates at a constant velocity from the inside radius a to its final position. The velocity of the plastic boundary equals C.

Combining equations (6) and (7)

$$\frac{du}{dr} = S/\{\rho r(u + C)\} \quad (19)$$

Integrating equation (19) results in

$$S/\rho\ \mathrm{Log}_e\,(r/r_o) = 1/2u^2 + C\,u - 1/2U^2 - C\,U \quad (20)$$

When $u = 0$, $r = R$ and equation (20) becomes

$$S/\rho\ \mathrm{Log}_e\,(R/r_o) = -\,1/2U^2 - C\,U \quad (21)$$

At time $t = 0$, $u = U$. Assuming u decreases to zero uniformly with time, in a time equal to T

$$T = (r_1 - R)/C = 2(r_o - r_1)/U$$

Rearranging $\quad C/U = 1/2\,(r_1 - R)/(r_o - r_1)$

Therefore, equation (21) becomes

$$S_1/\rho U^2 = (r_o - R)/[2(r_o - r_1)\ \mathrm{Log}_e\,(r_o/R)] \quad (22)$$

The fact that the decrease in u is not uniform results in an error which can be calculated. Combining equations (3) and (20)

$$\left[\frac{dr}{dt}\right]^2 = 2S/\rho \ \mathrm{Log}_e \ (r/r_o) + (U + C)^2 \qquad (23)$$

When all motion has ceased, $u = 0$, $r = R$, and $\varepsilon = 0$. Therefore, equation (21) becomes

$$2S/\rho \ \mathrm{Log}_e \ (R/r_o) = C^2 - (U + C)^2 \qquad (24)$$

Letting

$$2S/\rho = \alpha^2$$
$$K = (U + C)/\alpha$$
$$R_1 = r/r_o$$
$$t_1 = \alpha t/r_o$$
$$T_1 = \alpha T/r_o$$

where T is the time from the initial impact until the plastic zone velocity equals zero

$$\frac{dR_1}{dt_1} = (K^2 + \mathrm{Log}_e \ R_1)^{1/2}$$

so that

$$T_1 = \int_{\exp[\,(\frac{C}{\alpha})^2 - K^2\,]}^{1} (K^2 + \mathrm{Log}_e \ R_1)^{-1/2} dR_1 \qquad (25)$$

Letting

$$Z^2 = K^2 + \mathrm{Log}_e \ R_1$$

results in

$$T_1 = 2 \ e^{-K^2} \int_{C/\alpha}^{K} e^{Z^2} \ dZ \qquad (26)$$

Values of $F(K) = e^{-K^2} \int_o^K e^{Z^2} \ dZ$ have been tabulated in references 5 and 6. Equation (26) can be expanded using this function, F(K), to give

$$T_1 = 2 \ \{F(K) - \mathrm{Exp} \ (-K^2 + (C/\alpha)^2) \ F(C/\alpha)\} \qquad (27)$$

Previously it was assumed that the plastic boundary moves with a constant velocity C, or

$$C \ T = r_1 - R$$

or in dimensionless form

$$C/\alpha\ T_1 = r_1/r_o - R/r_o \tag{28}$$

Rearranging, equation (24) becomes

$$\mathrm{Log}_e\ (r_o/R) = K^2 - (C/\alpha)^2 \tag{29}$$

Since R/r_o and r_1/r_o can be measured, C/α, U/α, K and T can be evaluated from equations (27), (28), (29), and

$$K = U/\alpha + C/\alpha \tag{30}$$

Combining equations (27), (28), and (29)

$$r_1/r_o = 2\ C/\alpha\ F(K) - \{2\ C/\alpha\ F(C/\alpha) - 1\}\ R/r_o \tag{31}$$

Since

$$2S/\rho U^2 = \alpha^2/U^2 = 1/(K - C/\alpha)^2$$

dividing this equation by equation (22) therefore results in

$$S/S_1 = (r_o - r_1)/(r_o - R)\ [\mathrm{Log}_e\ (r_o/R)/(K - C/\alpha)^2] \tag{32}$$

Due to the complexity of these equations, the correction factor, S/S_1, cannot be determined directly. To determine S/S_1 given R/r_o and r_1/r_o it is easiest to first form the curves of S/S_1 vs r_1/r_o with contours of equal h/r_o. Values for this curve can be obtained by taking a value of R/r_o and values of C/α which cover the desired range. Therefore, using equation (29), equations (31) and (32) can be evaluated.

The asymptotic expansion of F(K) is

$$F(K) = 1/(2K) + 1/(4K^3) + 3/(8K^5) + 15/(16K^7) + \ldots \tag{33}$$

Through some complex manipulations, it can be shown, although it will not be presented here, that as $C/\alpha \to \infty$

$$r_1/r_o \to 1.0 \tag{34}$$

and

$$S/S_1 = 2\ \{1/(1 - R/r_o) - 1/(\mathrm{Log}_e(r_o/R))\} \tag{35}$$

From this equation, the limiting values of S/S_1 can be determined as $r_1/r_o \to 1.0$.

This completes the analysis of the problem. Thus, if values of r_o, r_1, and h are given, the dynamic yield stress can be calculated for the hemispherical shell.

DISCUSSION AND CONCLUDING REMARKS

In this paper, a method is developed to investigate the propagation of plastic stress waves in a hemispherical shell. In particular, this study investigates the dynamic yield stress due to the impulsive loading initiated at the interface of the shell. This mathematical approach, for determining the biaxial state of stress of the hemispherical shell, closely parallels Taylor's analysis of the cylindrical projectile. It is interesting to note that if all higher order terms were dropped from this analysis, the results would be the same as those of reference 1 except that the components are defined differently. Graphs which are drawn from this analysis in Figures 1 and 2 are similar to Figures 2 and 3 of reference 1. In addition, comparison between the results of this analysis and the analysis of reference 1 is possible. In fact, when these two analyses are compared, one can observe that the results of the present work parallel the experimental data more closely than the results of reference 1. This is due to the fact that one-dimensional analysis may not possibly explain the spreading out of the projectile near the target. This phenomenon requires taking into account the inertia in the radial direction.

The derivation of the yield stress correction factor is almost identical with the results of reference 1 on page 297. Singularities were observed which were not discussed in reference 1. The discontinuities occurred just before $r_1/r_o \to 1.0$. If the discontinuity is ignored, the results are similar to those of reference 1.

A method has been presented by which the dynamic yield stress can be calculated, using the Tresca yield criteria, from the radial expansion of a hemispherical shell. The approximate yield stress can be calculated from equation (22), if the initial conditions, final conditions, U, and ρ are specified. The dynamic yield stress could also be calculated from Figure 1. Thus, the dynamic yield stress can be determined if certain initial and final experimental conditions are specified, including the launch velocity, density, and geometrical considerations of the shell. The motion of the plastic boundary, as shown in Figure 2, is similar to the results obtained in Figure 4 of reference 8. Their choice of coordinates is different, which accounts for many of the differences between the shape of their curve and of Figure 2.

REFERENCES

1. Taylor, G. I., "The Use of Flat-ended Projectiles for Determining Dynamic Yield Stress", I: Theoretical Considerations, Proceedings of the Royal Society, London, England, Series A., Vol. 194.

2. Raftopoulos, D. and Davids N., "Elasto-Plastic Impact on Rigid Targets" AIAA Journal, July 5, 1967, pp. 2254-2260.

3. Raftopoulos, D. "Longitudinal Impact of Two Mutually Plastically-Deformable Missiles", Int. Journal of Solids and Structures - Vol. 5, No. 4, pp. 399-412, 1969.

4. Raftopoulos, D. and Al-Salihi, M. "Direct Analysis of Elasto-Plastic Wave Interaction in Impact", Proceeding of the 11th Midwstern Mechanics Conference, Vol. 5, 1969.

5. Jeffreys, Harold and Jeffreys, Bertha Swirles, Methods of Mathematical Physics, University Press, Cambridge, 1950, pp. 498-528.

6. Handbook of Mathematical Functions with Formulas, Graphs, and Mathematical Tables, edited by Milton Abramowitz and Irene A. Stegun, United States Department of Commerce, 1964, pp. 319-320.

7. Wosow, Wolfgang, Asymptotic Expansions for Ordinary Differential Equations, New York - John Wiley & Sons, Inc., 1965, p. 31.

8. Davids, N., Mehta, P. K., and Johnson, O. T., "Spherical Elasto-Plastic Waves in Materials". Colloquium on "Behavior of Materials Under Dynamic Loading", ASME Winter Annual Meeting, Chicago, November 9, 1965, pp. 125-137.

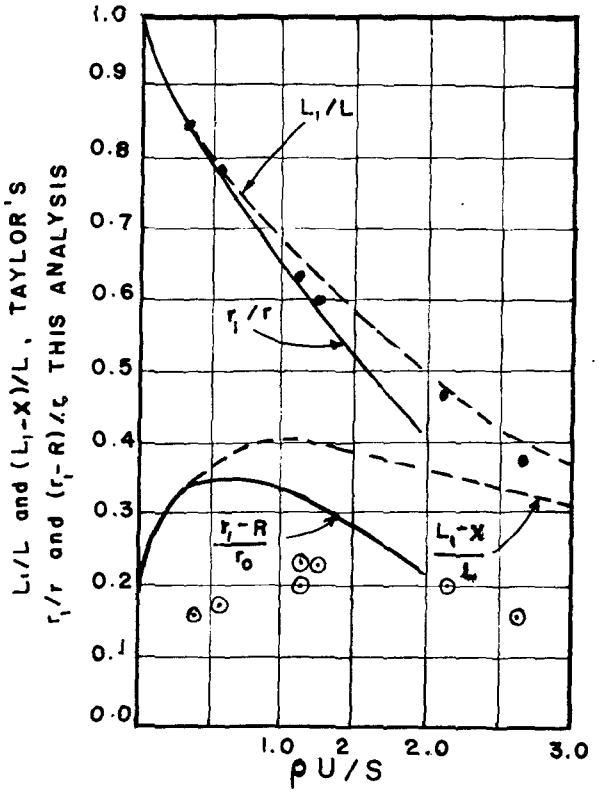

--- TAYLOR'S SIMPLE THEORETICAL MODEL

—— SIMPLE THEORETICAL MODEL, THIS ANALYSIS

• TAYLOR'S MEASURED VALUES L_1/L

⊙ TAYLOR'S MEASURED VALUES $(L_1-X)/L$

Figure 1.- Calculated results compared with Taylor's theoretical and experimental data.

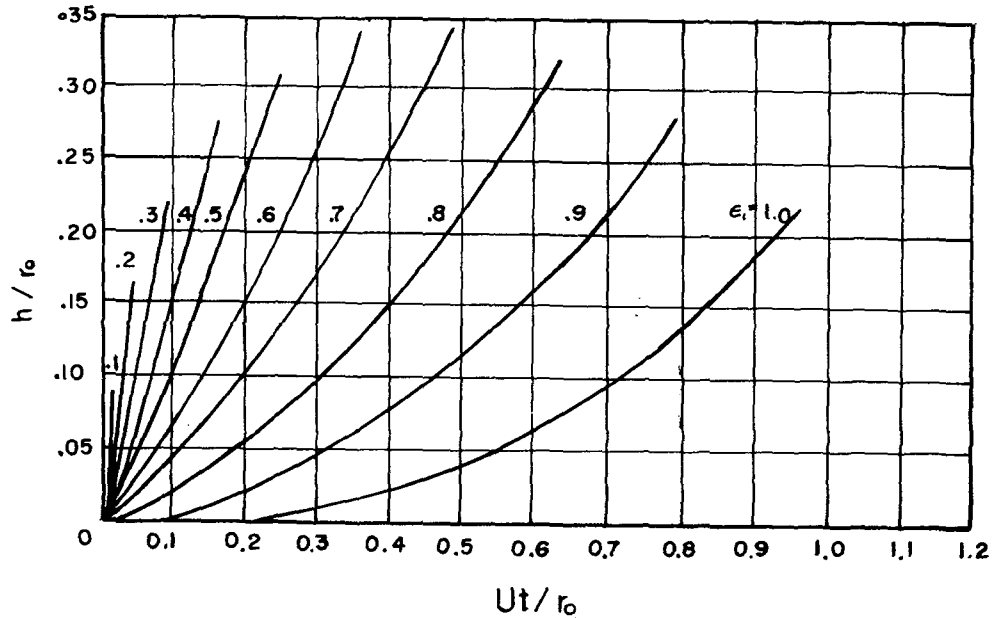

Figure 2.- Propagation of plastic boundary.

LARGE DEFLECTIONS OF A SHALLOW CONICAL MEMBRANE

Wen-Hu Chang and John Peddieson, Jr.
Tennessee Technological University

SUMMARY

This work is concerned with large deflections of a shallow elastic conical membrane fixed at the outer edge and loaded by either uniform or hydrostatic pressure. The governing equations were solved by the method of matched asymptotic expansions and by a finite-difference method. Agreement between the two methods was excellent for the small values of the perturbation parameter.

INTRODUCTION

This paper is concerned with the moderately large axisymmetric deformation of a shallow elastic conical membrane. The purpose of this work is to further investigate the application of the method of matched asymptotic expansions (see Van Dyke, reference 1) to the solution of membrane-shell problems involving large deflections. The success of this method is based on the fact that for small loads the linear membrane solution is a good approximation to the actual solution everywhere except in the immediate vicinity of boundaries. In these regions thin boundary layers exist where the variables undergo rapid changes to accommodate themselves to the boundary conditions that cannot be satisfied by the linear membrane solution. In the method of matched asymptotic expansions separate perturbation expansions are found in the interior and boundary-layer regions and matched in an appropriate way to insure that they join smoothly.

Bromberg and Stoker (ref. 2) initiated this type of analysis of membrane shells when they found one term of both the interior and boundary-layer expansions for a uniformly pressurized shallow spherical shell. The next two terms in the interior and boundary-layer expansions were found by Smith, Peddieson, and Chung (ref. 3) and used by them to investigate the accuracy of finite-difference solutions of the same problem. One term of the interior and boundary-layer expansions for deep membranes of arbitrary shape has been given by Rossettos (ref. 4). This work generalizes the results given in the references listed in reference 4.

In the present paper three terms of the interior and boundary-layer expansions are found for the case of a shallow conical membrane loaded by either uniform or hydrostatic pressure. It is found that complications arise which do not appear in the solution of the corresponding sphere problem. The solution method is modified somewhat to account for this. Numerical results are presented to illustrate some of the interesting features of the solution.

GOVERNING EQUATIONS

Consider a shallow conical membrane (opening upward) with base radius a, thickness h, and initial angle ϕ_o with the horizontal made of a linearly elastic material with modulus of elasticity E and Poisson's ratio ν. The equations governing moderately large axisymmetric deflections of such a structure can be obtained from the work of Reissner (ref. 5). The resulting equations are (in dimensionless form)

$$\psi'' + \psi'/r - \psi/r^2 + (1+\varepsilon^2\beta/2)(\beta/r) = 0$$

$$(1+\varepsilon^2\beta)\psi = rV$$

$$N_r = \psi/r, \quad N_\theta = \psi'$$

$$u = r\psi' - \nu\psi, \quad w' = \beta \tag{1}$$

where ar is the radial coordinate, $V_o a\psi/\phi_o$ is a stress function (V_o being a characteristic vertical force resultant), $V_o V$ is the vertical force resultant, $V_o N_r/\phi_o$ is the radial stress resultant, $V_o N_\theta/\phi_o$ is the transverse stress resultant, ε is a load parameter, $a\phi_o^2\varepsilon^2 u$ is the horizontal displacement, $a\phi_o\varepsilon^2 w$ is the vertical displacement, $\phi_o\varepsilon^2\beta$ is the rotation, and a prime denotes differentiation with respect to r.

In the present paper a uniform pressure p_o and a hydrostatic loading $\gamma_o\phi_o a(1-r)$ are considered. It can be shown by considering the vertical equilibrium of the membrane centered on the vertex and having radius r that

$$V = r/2 - jr^2/3 \tag{2}$$

where j = 0 for the uniform pressure and j = 1 for the hydrostatic pressure. The characteristic vertical force resultant is given by

$$V_o = \begin{cases} p_o a, & j = 0 \\ \gamma_o a^2 \phi_o, & j = 1 \end{cases} \tag{3}$$

The load parameter ε is defined to be

$$\varepsilon = (V_o/Eh\phi_o^3)^{\frac{1}{2}} \tag{4}$$

In the present work it is desired to solve equations (1) subject to the boundary conditions

$$u(1) = w(1) = 0 \tag{5}$$

Special attention will be given to situations where $\varepsilon << 1$.

STRAIGHTFORWARD SOLUTION

To begin the solution process a straightforward perturbation solution to equations (1) is sought for $\varepsilon << 1$. To do this it is convenient to rearrange equations (1a) and (1b) to yield

$$\varepsilon^2(\psi'' + \psi'/r - \psi/r^2) - (1 - (rV/\psi)^2)/(2r) = 0$$

$$\beta = (rV/\psi - 1)/\varepsilon^2 \tag{6}$$

A straightforward perturbation solution for $\varepsilon << 1$ has the form

$$\psi_s \sim \psi_{s0} + \varepsilon\psi_{s1} + \varepsilon^2\psi_{s2} + \ldots \tag{7}$$

where the subscript s indicates the straightforward solution. Substituting equation (7) into equation (6a), expanding for $\varepsilon << 1$, setting the coefficient of each power of ε equal to zero in the usual way, and solving the resulting algebraic equations yields

$$\begin{aligned}\psi_s \sim\ & (r^2/2 - jr^3/3) + \varepsilon^2(r^2/2 - jr^3/3)(3r/2 \\ & - 8jr^2/3) + \varepsilon^4(r^2/2 - jr^3/3)(75r^2/8 \\ & - j(79r^3/2 - 32r^4)) + \ldots\end{aligned} \tag{8}$$

From equations (1) and (6b) it can then be shown that

$$\begin{aligned}N_{rs} \sim\ & (r/2 - jr^2/3) + \varepsilon^2(r/2 - jr^2/3)(3r/2 \\ & - 8jr^2/3) + \varepsilon^4(r/2 - jr^2/3)(75r^2/8 \\ & - j(79r^3/2 - 32r^4)) + \ldots \\ N_{\theta s} \sim\ & (r - jr^2) + \varepsilon^2(9r^2/4 - j(22r^3/3 - 40r^4/9)) \\ & + \varepsilon^4(75r^3/4 - j(915r^4/8 - 175r^5 \\ & + 224r^6/3)) + \ldots \\ \beta_s \sim\ & -(3r/2 - 8jr^2/3) - \varepsilon^2(57r^2/8 \\ & - j(63r^3/2 - 224r^4/9)) + \ldots \\ u_s \sim\ & (1 - \nu/2)r^2 - j(1 - \nu/3)r^3 + \varepsilon^2(3(3 - \nu)r^3/4 \\ & - j(11(4 - \nu)r^4/6 - 8(5 - \nu)r^5/9)) \\ & + \varepsilon^4(75(4 - \nu)r^4/16 - j(183(5 - \nu)r^5/8 \\ & - 175(6 - \nu)r^6/6 + 32(7 - \nu)r^7/3)) + \ldots\end{aligned}$$

$$w_s \sim -3(r^2 - 1)/4 + j8(r^3 - 1)/9 - \varepsilon^2(19(r^3 - 1)/8$$

$$- j(63(r^4 - 1)/8 - 224(r^4 - 1)/45)) + \ldots \qquad (9)$$

where equation (5b) has been used to determine the constants of integration in equation (9c). By comparison with the results given in Kraus (ref. 6) it can be seen that the first term in each series expansion is the linear membrane solution. It should also be noted that the first terms in equations (9d) and (9e) are due to the second term in equation (8). Thus to obtain β_s and w_s to $0(\varepsilon^2)$ it is necessary to find ψ_s to $0(\varepsilon^4)$. The boundary condition represented by equation (5a) cannot be satisfied by equation (9d). Thus a boundary-layer expansion is needed in the vicinity of $r = 1$.

BOUNDARY-LAYER SOLUTION

There are several ways to carry out the boundary-layer analysis in this problem. One is to work in terms of the original stress function ψ. If this is done the differential equation for the first boundary-layer approximation turns out to be nonlinear. Bromberg and Stoker (ref. 2) discovered that a linear equation could be obtained in the first approximation for a spherical membrane by a method which is equivalent to working with a dependent variable which is the difference between the actual and the linear stress functions. This was tried in the present problem but matching difficulties were encountered. These were due to the fact that equations (8) and (9) do not terminate with one term for the cone as the corresponding straightforward expansions do for a sphere. It was, therefore, decided to use the difference between the actual stress function and the straightforward stress function as the dependent variable. This guarantees that the outer expansion for this dependent variable will be zero. Thus it is necessary to find only the inner expansion.

Substituting

$$\psi = \psi_s + \psi_b \qquad (10)$$

(where the subscript b denotes the boundary-layer solution) into equation (6), defining the boundary-layer variables F and ξ by the equations

$$\psi_b = \varepsilon F, \quad r = 1 - \varepsilon\xi, \qquad (11)$$

expanding F as

$$F \sim F_0 + \varepsilon F_1 + \varepsilon^2 F_2 + \ldots, \qquad (12)$$

and carrying out the usual perturbation analysis yields

$$\ddot{F}_0 - S^2 F_0 = 0 \qquad (13)$$

and two other equations governing F_1 and F_2 where

$$S = (6/(3 - 2j))^{\frac{1}{2}} \qquad (14)$$

In equation (13) $(\dot{})$ = d( )/dξ. Define N_{rb}, $N_{\theta b}$, β_b, u_b, and w_b by the following equations

$$N_r = N_{rs} + \varepsilon N_{rb}, \quad N_\theta = N_{\theta s} + N_{\theta b}$$

$$\beta = \beta_s + \beta_b/\varepsilon, \quad u = u_s + u_b, \quad w = w_s + w_b \tag{15}$$

Now expand as follows

$$A_b \sim A_{b0} + \varepsilon A_{b1} + \varepsilon^2 A_{b2} + \ldots \tag{16}$$

where A_b is any one of the boundary-layer variables. Substituting equations (10), (11), (12), (15), and (16) into equations (1), expanding for $\varepsilon \ll 1$, and equating the coefficients of like powers of ε to zero one obtains

$$N_{rb0} = F_0, \quad N_{\theta b0} = -\dot{F}_0, \quad \beta_{b0} = -S^2 F_0$$

$$u_{b0} = -\dot{F}_0, \quad w_{b0} = S^2 \int_0^\infty F_0 d\xi \tag{17}$$

and two similar sets of equations relating A_{b1} and A_{b2} to F_0, F_1, and F_2. A similar procedure applied to equation (5a) leads to boundary condition

$$\dot{F}_0(0) = 1 - j - (1/2 - j/3)\nu \tag{18}$$

and boundary conditions for $\dot{F}_1(0)$ and $\dot{F}_2(0)$.

To illustrate the solution procedure the first approximation will now be carried out in detail. The solution of equation (13) is easily seen to be

$$F_0 = c_1 \exp(S\xi) + c_2 \exp(-S\xi) \tag{19}$$

Since the outer expansion has been forced to vanish because of equation (10) the matching process (see Van Dyke, reference 1) is equivalent in this case to a statement that positive exponential terms must vanish. Thus

$$c_1 = 0 \tag{20}$$

Substituting equations (19) and (20) into equation (18) yields

$$c_2 = -(1 - j - (1/2 - j/3)\nu)/S \tag{21}$$

Thus

$$F_0 = -(1 - j - (1/2 - j/3)\nu)\exp(-S\xi)/S \tag{22}$$

Substituting equation (22) into equations (17) one obtains

$$N_{rb0} = -(1 - j - (1/2 - j/3)\nu)\exp(-S\xi)/S$$

$$N_{\theta b0} = (1 - j - (1/2 - j/3)\nu)\exp(-S\xi)$$

$$\beta_{b0} = (1 - j - (1/2 - j/3)\nu)S \exp(-S\xi)$$

$$u_{b0} = -(1 - j - (1/2 - j/3)\nu)\exp(-S\xi)$$

$$w_{b0} = -(1 - j - (1/2 - j/3)\nu)(1 - \exp(-S\xi)) \tag{23}$$

The results for higher approximations are found in a similar way but the calculations are quite lengthy. For the sake of brevity this work is omitted.

To find the complete solution the boundary-layer expansions must be added to the corresponding straightforward expansions. The first approximations to these expressions are

$$\psi_0 = r^2/2 - jr^3/3 - \varepsilon(1 - j - (1/2 - j/3)\nu)\exp(-S(1 - r)/\varepsilon)/S$$

$$N_{r0} = r/2 - jr^2/3 - \varepsilon(1 - j - (1/2 - j/3)\nu)\exp(-S(1 - r)/\varepsilon)/S$$

$$N_{\theta 0} = r - jr^2 + (1 - j - (1/2 - j/3)\nu)\exp(-S(1 - r)/\varepsilon)$$

$$\beta_0 = (1 - j - (1/2 - j/3)\nu)S \exp(-S(1 - r)/\varepsilon)/\varepsilon$$

$$u_0 = (1 - \nu/2)r^2 - j(1 - \nu/3)r^3 - (1 - j$$
$$- (1/2 - j/3)\nu)\exp(-S(1 - r)/\varepsilon)$$

$$w_0 = 3(1 - r^2)/4 - 8j(1 - r^3)/9 - (1 - j$$
$$- (1/2 - j/3)\nu)(1 - \exp(-S(1 - r)/\varepsilon)) \tag{24}$$

In writing equations (24) the boundary-layer solution was treated as the fundamental expansion. All terms in the straightforward expansion with magnitude equal to or greater than the first term in the boundary-layer expansion were added to this term to form the first approximation. The same method was used to obtain the second and third approximations.

RESULTS AND DISCUSSION

Numerical results were computed for the first, second, and third approximations to the variables ψ, N_r, N_θ, β, u, and w. These calculations were made for a variety of values of the load parameter ε and Poisson's ratio ν. To evaluate the accuracy of the perturbation method, selected cases were compared with numerical solutions to equation (6a) obtained by the finite-difference method discussed by Smith, Peddieson, and Chung (ref. 3). It was found that the third approximation to the perturbation solution agreed with the finite-difference results up to $\varepsilon = 0.1$. It should be pointed out that for small values of ε, the numerical method is difficult to apply because a variable step size must be used near the edge and the optimum arrangement of step sizes can only be approached by trial and error. The explicit formulas obtained in the present work are much easier to use for $\varepsilon << 1$.

To illustrate the behavior of the solution some of the computed results are shown in figures 1 - 4. For the sake of brevity, data are presented for only the radial stress resultant N_r, the transverse stress resultant N_θ, and the vertical deflection w. The solid lines represent the three-term perturbation solution while the dashed lines represent the linear membrane solution. The linear membrane solution is shown only when it differs significantly from the perturbation solution.

Figures 1 and 2 present results for uniform pressurization (j = 0). Figure 1 shows that thin boundary layers exist for N_θ and w for $\varepsilon = 0.01$ while N_r does not exhibit boundary-layer behavior. As ε increases the boundary layers become wider for all variables. This is illustrated by figure 2. Figures 3 and 4 contain results for hydrostatic loading (j = 1). The parametric trends illustrated by these results are identical to those discussed above but the behavior of the solution variables is more complicated. These results illustrate the utility of the perturbation method. Complicated functions of this type can be represented numerically only if extreme care is used.

Results were also computed for several other values of ν. It was found that the qualitative behavior of the solution is not significantly influenced by this parameter.

CONCLUSION

In this paper, the rotationally symmetric moderately large deformation of a linearly elastic shallow conical membrane subjected to either uniform or hydrostatic pressure was investigated. A single differential equation having a stress function as dependent variable was solved by the method of matched asymptotic expansions. The accuracy of the solution was verified by comparison with a finite-difference numerical solution of the governing equation for the stress function. Selected results were presented graphically to illustrate interesting features of the solutions.

REFERENCES

1. Van Dyke, M.: Perturbation Methods in Fluid Mechanics. Academic Press, 1964, Chapter 5.

2. Bromberg, E.; and Stoker, J. J.: Nonlinear Theory of Curved Elastic Sheet. Quarterly of Applied Mathematics, Vol. 3, 1950, pp. 27-52.

3. Smith, Dallas G.; Peddieson, John, Jr.; and Chung, Chin-Jer: Finite Deflection of a Shallow Spherical Membrane. AIAA Journal, Vol. 11, 1973, pp. 736-738.

4. Rossettos, John N.: Nonlinear Membrane Solutions for Symmetrically Loaded Deep Membranes of Revolution. NASA TN D-3297, 1966.

5. Reissner, E.: Rotationally Symmetric Problems in the Theory of Thin Elastic Shells. Proceedings of the Third U. S. National Congress of Applied Mechanics, 1958, pp. 51-69.

6. Kraus, H.: Thin Elastic Shells. John Wiley & Sons, Inc., 1967, Chapter 4.

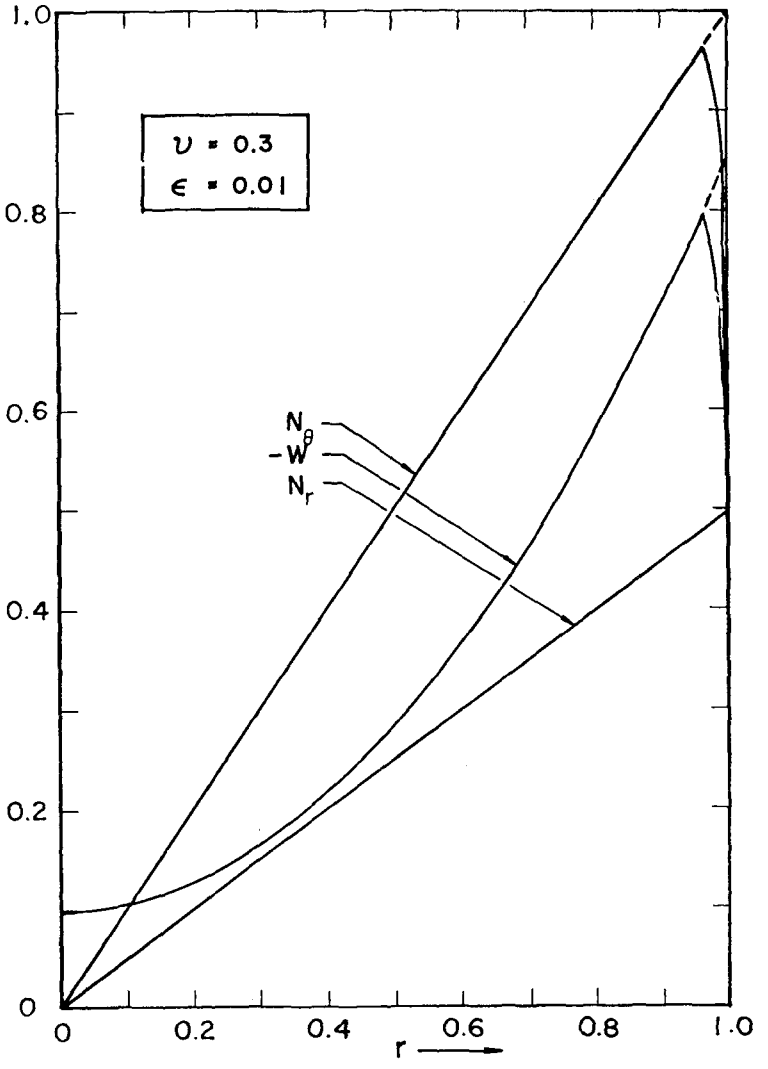

Figure 1.- Stress resultants and axial displacement for uniform pressurization. $\varepsilon = 0.01$.

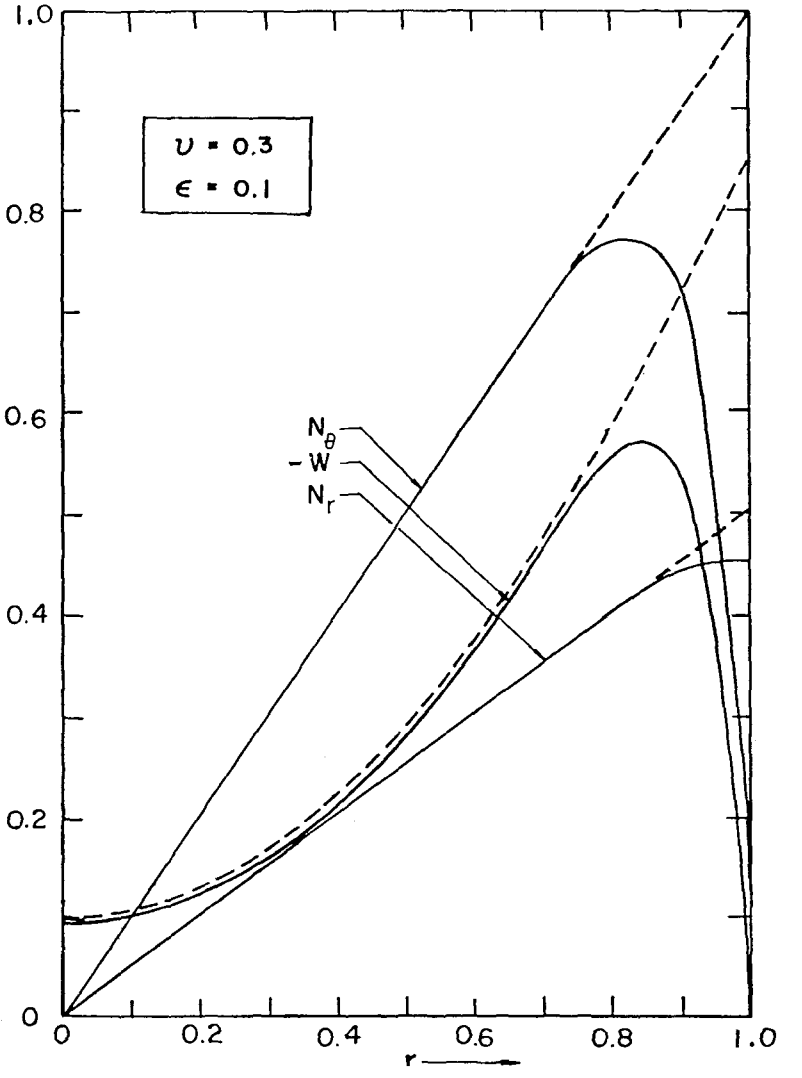

Figure 2.- Stress resultants and axial displacement for uniform pressurization. $\varepsilon = 0.1$.

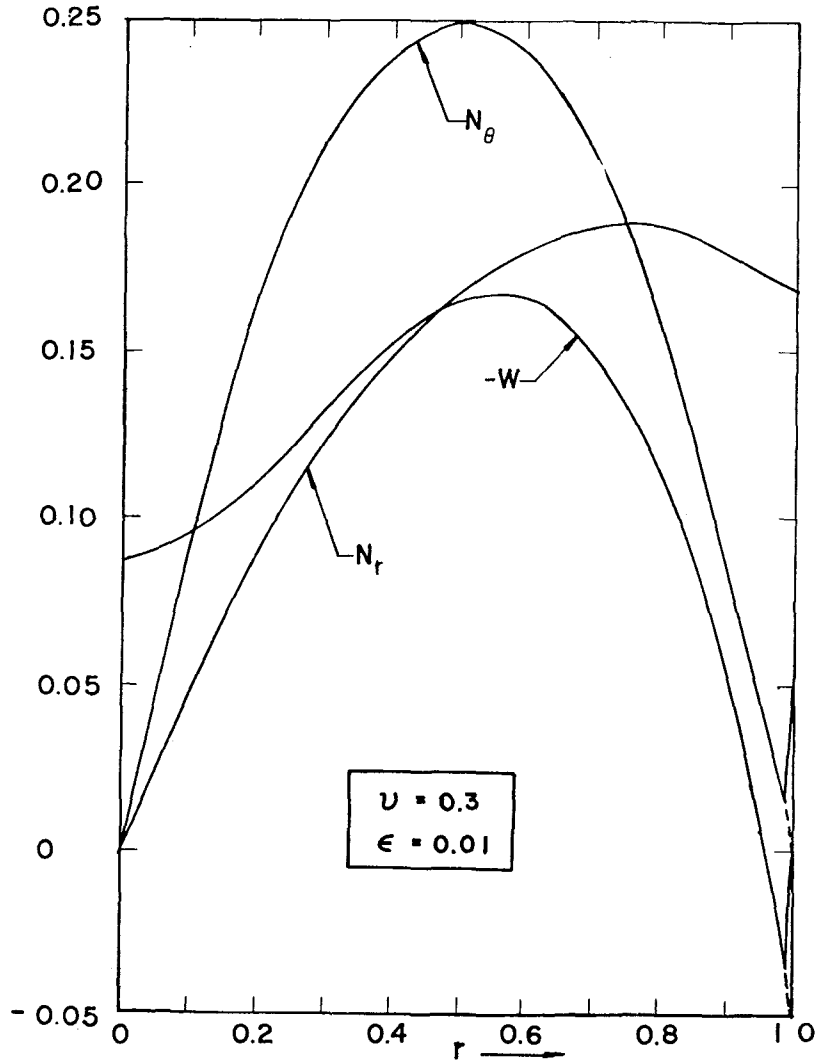

Figure 3.- Stress resultants and axial displacement for hydrostatic loading. $\varepsilon = 0.01$.

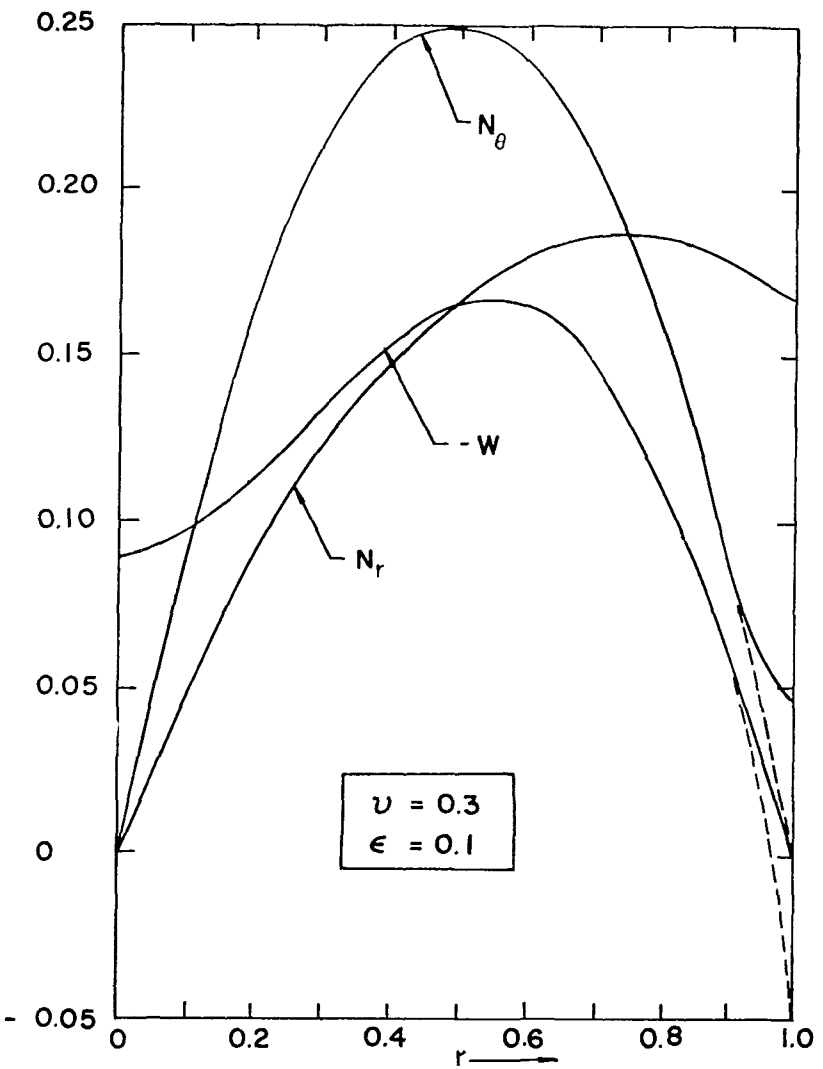

Figure 4.- Stress resultants and axial displacement for hydrostatic loading. $\varepsilon = 0.1$.

A PLANE STRAIN ANALYSIS OF THE BLUNTED CRACK TIP USING SMALL STRAIN DEFORMATION PLASTICITY THEORY*

J. J. McGowan and C. W. Smith
Virginia Polytechnic Institute and State University

SUMMARY

This paper presents a deformation plasticity analysis of the tip region of a blunted crack in plane strain. The power hardening material is incompressible both elastically and plastically, in order to simulate behavior of a stress freezing material above critical temperature. The study represents a full field, finite difference solution to the Mode I problem. Stress and displacement fields surrounding the crack tip are presented. The results of this study indicate that the maximum stress seen at the crack tip is indeed limited and is determined by the tensile properties; however, the scale over which the stresses act is dependent on the loading. Comparisons are good between the forward crack tip displacement and micro-fractographic measurements of "stretch" zones observed in plane strain fracture toughness tests.

INTRODUCTION

In recent years Cherepanov (ref. 1), Rice (ref. 2,3), Hutchinson (ref. 4, 5), and Rice and Rosengren (ref. 6) have shown the asymptotic behavior of stress and strain fields surrounding sharp crack tips in plane strain. Using these studies as a guide, full field solutions with finite elements have been obtained by Levy, Marcal, Ostergren and Rice (ref. 7) and Hilton and Hutchinson (ref. 8). These two studies give accurate near and far field behavior due to the inclusion of singular elements reflecting plasticity at the crack tip. Other numerical solutions by Marcal and King (ref. 9), Mendelson (ref. 10), Swedlow and coworkers (ref. 11,12) and Tuba (ref. 13) show qualitative features of the near field, but may not yield accurate stress field definition due to the large gradients there.

In order to have an accurate description of the near field surrounding crack tips, and hence a good understanding of the mechanisms of failure, Rice and Johnson (ref. 14) have pointed out that crack tip blunting must also be included. Their analysis accounted in an approximate manner for the blunting at the crack tip and for strain hardening in the plastic zone. As a result they showed that the stresses near the crack tip are indeed finite and that the maximum σ_{yy} stress occurred at some small distance from the deformed crack tip. A finite deformation analysis by McGowan and Smith (ref. 15) of blunted cracks in a linear (stress-strain) incompressible material shows the same general behavior. The maximum σ_{yy} stress occurs in front of the blunted crack tip and the magnitude is independent of the remote loading.

---

*This work was supported by the National Science Foundation Engineering Mechanics Program under Grant No. GK-39922

The purpose of the present study is to gain a full field solution around a blunted crack tip in a strain hardening incompressible material under Mode I loading. This work will provide an accurate description of the stress and deformation fields immediately surrounding the blunted tip, and thereby gain insight to fracture behavior. Deformation theory of plasticity with a Mises yield condition is used. The resulting set of equations is solved for the blunted crack tip in the deformed state under load by finite differences. The linear theory of Inglis (ref. 16) gives the necessary asymptotic boundary conditions.

An initial goal of the present study was to gain a more complete understanding of the near field behavior of stress freezing photoelastic materials above critical temperature; however, this study should also give considerable insight to the general behavior of engineering materials under Mode I loading.

SYMBOLS

c	One-half crack length	ε_o	Initial yield strain
E	Young's Modulus	ε_p	Effective plastic strain
K	Stress intensity factor	ε_T	Effective total strain = $\varepsilon_p + \sigma_e/E$
n	Strain hardening exponent	ρ	Deformed crack root radius
r,θ	Cylindrical coordinates measured from crack tip	ν	Poisson's ratio
T	Secant modulus = σ_e/ε_T	σ_{ij}	Stress tensor
u_i	Displacement vector	σ_{yy}	Hoop stress
U	Strain energy density	σ_e	Effective stress
X	Distance in front of deformed crack tip	σ_o	Tensile yield stress
Y	Distance perpendicular to deformed crack tip	Φ	Airy stress function
ε_{ij}	Strain tensor	α	Constant in eq. (2)

FORMULATION OF THE PROBLEM

Using small strain deformation theory of plasticity for an incompressible ($\nu = 1/2$) material the governing equation for the field can be shown to be:

$$\frac{1}{T}\left(\Phi_{,2222} + \Phi_{,1111} + 2\Phi_{,1122}\right) + 2\left(\frac{1}{T}\right)_{,1}\left(\Phi_{,111} + \Phi_{,122}\right)$$

$$+ 2\left(\frac{1}{T}\right)_{,2}\left(\Phi_{,222} + \Phi_{,112}\right) + \left(\Phi_{,22} - \Phi_{,11}\right)\left[\left(\frac{1}{T}\right)_{,22} - \left(\frac{1}{T}\right)_{,11}\right] \qquad (1)$$

$$+ 4\left(\frac{1}{T}\right)_{,12}\Phi_{,12} = 0 \quad .$$

(The details of this analysis are given in ref. 17)
For this study a Ramberg-Osgood material will be used

$$\frac{E}{\sigma_o}\varepsilon_T = \sigma_e/\sigma_o + b\alpha[(\sigma_e/\sigma_o)^{1/n} - 1]$$

$$\text{or } \frac{E}{T} = 1 + b\alpha[(\sigma_e/\sigma_o)^{(1-n)/n} - \sigma_o/\sigma_e] \qquad (2)$$

where $b = 0$ if $\sigma_e < \sigma_o$

$b = 1$ if $\sigma_e \geq \sigma_o$.

Thus the governing equation (1) will be solved subject to the constitutive laws (eq. (2)).

The geometry of the blunted cracks in the deformed state under Mode I loading will resemble small elliptical perforations as shown in figure 1. The size of the deformed crack tip root radius will be determined through integration of the strain displacement relationships

$$u_{i,j} + u_{j,i} = 2\varepsilon_{ij}$$

The affected strain hardening region will be divided into a small grid utilizing elliptical coordinates and the governing set of equations will be solved through the method of finite differences. At some distance from the deformed crack tip the linear solution of Inglis (ref. 16) will apply. The stress at the outer boundary of the inner strain hardening region will be then matched to the Inglis solution. The outer boundary will be enlarged until there is no change in the inner stress field. (A detailed description of the solution procedure is given in ref. 18.)

PRESENTATION OF RESULTS

The stress and displacement fields in the field surrounding a deformed crack tip in a strain hardening material which is incompressible in both the elastic and plastic regions are examined. Strain hardening exponents of 0.2 through 0.01 are presented. The range of initial yield strain values is from 0.01 through 0.0001. The value of α in the effective stress-effective strain relationship, equation (2), is taken to be 1.0 in this study. (The authors have found that small changes in α and ν do not influence the solution significantly.) The "linear" results reported here are those of Inglis (ref. 16) for a deformed crack tip in a linear material. The "singular" results are those corresponding to a crack which has no root radius in a linear material.

The plastic zone shape for the smallest ellipse investigated ($\rho = 0.0018\ (K/\sigma_o)^2$) is shown in figure 2. Note that with decreasing hardening ($n \to 0$)

the plastic zone grows in maximum extent and leans progressively in the direction of crack propagation. For comparison, the singular plastic zone from McClintock and Irwin (ref. 19) and that of Levy et al (ref. 7) for a non-hardening (n = 0) material are also shown. As shown by figure 2, the plastic zone shape predicted by McClintock and Irwin (ref. 19) is approached by the present study as $n \to \infty$. The difference between the plastic zone shape predicted by Levy et al (ref. 7) and the present study for n = 0.01 is primarily due to the inclusion of blunting effects and use of ν of 0.5 in the latter; the difference should be negligible as $\varepsilon_o \to 0$.

The effective stress σ_e is shown versus the distance ahead of the deformed crack tip in figure 3. This figure shows that the effective stress varies as $(r^{n/n+1})^{-1}$ in the plastic zone ahead of the tip. (The behavior for other values of θ is similar). It can be shown that the strain energy has the form:

$$\frac{2EU}{\sigma_o^2} = \left[\frac{\sigma_e}{\sigma_o}\right]^2 + \frac{2}{1+n}\,\alpha\, b\left[\left[\frac{\sigma_e}{\sigma_o}\right]^{(1+n)/n} - 1\right] \quad \text{for a power hardening material}$$

Therefore, the strain energy varies approximately as 1/r in the plastic zone. This was a key assumption in the analysis of Rice and Rosengren (ref. 6) and Hutchinson (ref. 4).

The σ_{yy} stress in front of the crack tip is shown for various values of yield strain for n = 0.01 in figure 4. As shown in this figure, this stress is substantially reduced near the crack tip because of blunting and strain hardening, with the maximum value developed at some distance forward of the crack tip. (The σ_{yy} stress distributions for other values of n is quite analogous.) The analysis of Rice and Johnson (ref. 14) gives the same qualitative behavior; the correlation is believed to be quite reasonable in view of the several approximations involved. For a non-hardening material Rice (ref. 2) has shown that the maximum σ_{yy} stress is 2.97 σ_o. This stress, as predicted by Levy et al (ref. 7), approaches this limit at the crack tip as shown in figure 4. The σ_{yy} stress distribution of the present study in this figure reflects the presence of blunting and should coincide with the work of Levy et al (ref. 7) as $\varepsilon_o \to 0$.

Figure 5 shows the variation of maximum σ_{yy} stress with initial yield strain for varying hardening. As shown in the figure, blunting alone (the "linear" curve) forces the peak σ_{yy} stress to be finite and the inclusion of finite deformations (ref. 15) reduces the magnitude somewhat. However, the effects of blunting and plasticity taken together are significant: the peak σ_{yy} stress is reduced by a factor of 10 from that with blunting alone. From figure 5, one observes the peak σ_{yy} stress to be $3\sigma_o$ to $7\sigma_o$ depending upon n and σ_o/E. The peak σ_{yy} stress increases with n and decreases with σ_o/E. (The large value of peak σ_{yy} stress compared to the uniaxial yield stress, σ_o, is believed due to the presence of triaxiality in the crack tip region.)

The crack tip displacement in the direction of propagation (which is also the deformed crack root radius, ρ) is shown in figure 6 for varying initial yield strain and hardening exponent. The present study predicts that the forward crack tip displacement increases with σ_o/E and decreases with n. For

comparison one-half the crack tip opening displacement calculated by Levy (ref. 7) is shown. The forward crack tip displacement as predicted by the present study and the work of Levy et al (ref. 7) show parallel behavior, although they are separated by some distance. This disagreement is believed due to the shape of the crack tip being elliptical in the present study instead of cylindrical.

Included also on figure 6 is the width of the "transition" or "stretch" zone which exists on the fracture surface between the cracked and the overload regions in fatigue. As Broek (ref. 20) has discussed, the depth of this transition zone is the crack tip opening displacement, and, therefore the width is the tip forward displacement.

Examination of the figure shows the correlation between the forward tip displacement and failure. The measurements of the stretch zone fall close to $n = 0.2$. For the steels and aluminums shown values of n around 0.05 have been reported in references 20, 21 and 22. However, it is known that for this class of materials the value of n varies with plastic strain (ref. 23). For large plastic strain ($\varepsilon_p > 10\%$), the strain hardening exponent is close to 0.2 as shown by Jones and Brown (ref. 24) for 4340 steel. The strains in the tip region are clearly greater than 10% so that the agreement between the measurements and the analysis appears quite reasonable. The scatter band shown on the figure is an indication of the span of actual measurements (authors typically report a 40% variation).

DISCUSSION

Previously McGowan and Smith (ref. 15) performed a finite deformation analysis of the region surrounding deformed crack tips for a linear (stress-strain) material. The results of the finite deformation work showed that the maximum σ_{yy} stress occurred in front of the deformed crack tip. It was determined that the stress distribution around the crack tip was "similar", in the sense that one stress distribution could be used to describe the response of the material under load. The size of the affected zone would depend upon the load and crack length through K. The self-similarity of the stress field was a direct result of the blunting process, and would be expected to remain as long as the affected zone stayed small with respect to the crack length, thickness, or any other in-plane dimension.

The behavior is quite similar for a power hardening material. The stress field is self-similar with the size of the affected zone varying with K. The maximum σ_{yy} stress will only then be a function of the material properties E, n, and σ_o. The stretching of the similar stress distribution will depend upon K as well as the other material properties. One may conjecture that failure would depend upon the growth in size of a critical dimension, such as plastic zone size, which increases with K.

Wells (ref. 25) and others have used the crack opening displacement as a fracture criterion. Broek (ref. 20) has used this concept to correlate the depth of transition zones in aluminum with fracture toughness. The present study shows good correlation of fracture toughness and transition zone width. Krafft (ref. 26), Hahn and Rosenfield (ref. 27) and Rice and Johnson (ref. 14)

have all shown good correlation of plane strain fracture toughness with some minute particle size or process zone size for specific cases.

SUMMARY AND RECOMMENDATIONS

Following the pioneering studies of Hutchinson (ref. 4), Rice and Rosengren (ref. 6), Levy et al (ref. 7) and Hilton and Hutchinson (ref. 8), the authors have obtained a full field deformation plasticity finite difference solution to the Mode I plane strain problem including the effects of blunting. The material was incompressible in both the elastic and plastic regions, and followed a power hardening rule. Stress and displacement fields surrounding the deformed crack tip are presented, and are found to compare favorably both with the analysis of other investigators as well as experimental results. Because of the improved accuracy expected from a full field solution, it would be appropriate to incorporate such a solution into theories concerning void coalescence and final instability. Efforts are currently being devoted to such an approach.

REFERENCES

1. Cherepanov, G. P., "Crack Propagation in Continuous Media," Appl. Math. Mech. (PMM), Vol. 31, p. 476, 1967.
2. Rice, J. R., "A Path Independent Integral and the Approximate Analysis of Strain Concentrations by Notches and Cracks", J. Appl. Mech., Vol. 35, p. 379, 1968.
3. Rice, J. R., "Mathematical Analysis in the Mechanics of Fracture", Ch. 3 of Fracture, An Advanced Treatise, Vol. II (H. Liebowitz, ed.), Academic Press, New York, 1968.
4. Hutchinson, J. W., "Singular Behavior at the End of a Tensile Crack in a Hardening Material", J. Mech. Phys. Solids, Vol. 16, p. 13, 1968.
5. Hutchinson, J. W., "Plastic Stress and Strain Fields at a Crack Tip", J. Mech. Phys. Solids, Vol. 16, p. 337, 1968.
6. Rice, J. R. and Rosengren, G. F., "Plane Strain Deformation Near a Crack Tip in a Power Law Hardening Material", J. Mech. Phys. Solids, Vol. 16, p. 1, 1968.
7. Levy, N., Marcal, P. V., Ostergren, W. J., and Rice, J. R., "Small Scale Yielding Near a Crack in Plane Strain: A Finite Element Analysis", Int. J. Frac. Mech., Vol. 7, No. 2, p. 143, 1971.
8. Hilton, P. D. and Hutchinson, J. W., "Plasticity Intensity Factors for Cracked Plates", Eng. Frac. Mech., Vol. 3, p. 435, 1971.
9. Marcal, P.V. and King, I.P., "Elastic-Plastic Analysis of Two-Dimensional Stress Systems By the Finite Element Method", Int. J. Mech Sci., Vol. 9, p. 143, 1967.
10. Mendelson, A., Plasticity: Theory and Application, The Macmillan Company, New York, 1968.

11. Swedlow, J. L., Yang, A. H., and Williams, M. L., "Elasto-Plastic Stresses and Strains in a Cracked Plate", in Proc. of the First Int. Conf. on Fracture, 1965, Vol. 1, p. 259, 1966.

12. Swedlow, J. L., "Elasto-Plastic Cracked Plates in Plane Strain", Int. J. Frac. Mech., Vol. 5, p. 33, 1969.

13. Tuba, I. S., "A Method of Elastic Plastic Plane Stress and Strain Analysis", J. of Strain Analysis, Vol. 1, p. 115, 1966.

14. Rice, J. R. and Johnson, M. A., "The Role of Large Crack Tip Geometry Changes in Plane Strain Fracture", Inelastic Behavior of Solids (M. F. Kanninen, et al, eds.), McGraw-Hill, New York, p. 641, 1970.

15. McGowan, J. J. and Smith, C. W., "A Finite Deformation Analysis of the Near Field Surrounding the Tip of Crack-Like Elliptical Perforations", Int. J. Frac., Vol. 11, No. 6, p. 977, 1975.

16. Inglis, C. E., "Stresses in a Plate Due to the Presence of Cracks and Corners", Trans. Instn. Naval Archit., 55, p. 219, 1913.

17. McGowan, J. J. and Smith, C. W., "A Deformation Plasticity Analysis of the Blunted Crack Tip in Plane Strain," VPI-E-76-4, March 1976.

18. McGowan, J. J. and Smith, C. W., "A Finite Deformation Analysis of the Near Field Surrounding the Tip of Crack-Like Ellipses", VPI-E-74-10, May 1974.

19. McClintock, F. A. and Irwin, G. R., "Plasticity Aspects of Fracture Mechanics", Fracture Toughness Testing and Its Applications, STP-381, ASTM p. 84, 1965.

20. Broek, D., "Correlation Between Stretched Zone Size and Fracture Toughness", Eng. Frac. Mech., Vol. 6, No. 1, p. 173, 1974.

21. Bates, R. C., Clark, Jr., W. G., and Moon, D. M., "Correlation of Fractographic Features with Fracture Mechanics", Electron Microfractography, STP-453, ASTM, p. 192, 1969.

22. Pandey, R. K. and Banerjee, S., "Studies on Fracture Toughness and Fractographic Features in Fe-Mn Base Alloys", Eng. Frac. Mech., Vol. 5, No. 4, p. 965, 1973.

23. Lauta, F. J. and Steigerwald, E. A., "Influence of Work Hardening Coefficient on Crack Propagation in High Strength Steels", AFML TR 65-31, Air Force Materials Laboratory, May 1965.

24. Jones, M. H. and Brown, Jr., W. B., "The Influence of Crack Length and Thickness in Plane Strain Fracture Toughness Tests", Review of Developments in Plane Strain Fracture Toughness Testing, STP-463, ASTM, p. 63, 1970.

25. Wells, A. A., "Crack Opening Displacements from Elastic-Plastic Analyses of Externally Notched Tension Bars", Eng. Frac. Mech., Vol. 1, No. 3, p. 399, 1969.

26. Krafft, J., "Correlation of Plane Strain Crack Toughness with Strain Hardening Characteristics of a Low, a Medium, and a High Strength Steel", Applied Material Research, Vol. 3, p. 1964, 1964.

27. Hahn, G. and Rosenfield, A., "Source of Fracture Toughness: The Relation Between K_{Ic} and the Ordinary Tensile Properties of Metals", Applications Related Phenomena in Titanium Alloys, STP-432, ASTM, p. 5, 1968.

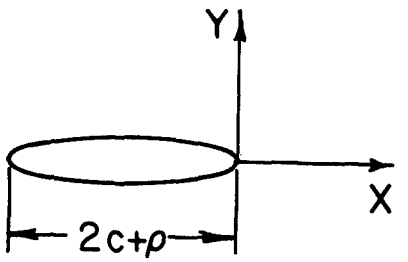

Deformed crack geometry

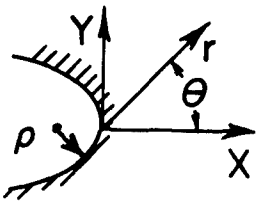

Enlarged view of deformed crack tip region

Figure 1.- Problem geometry.

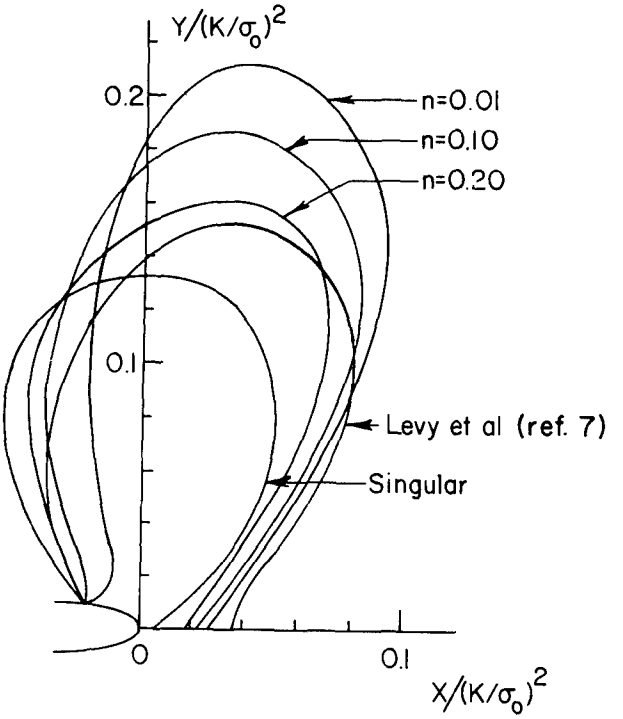

Figure 2.- Plastic zone shape.

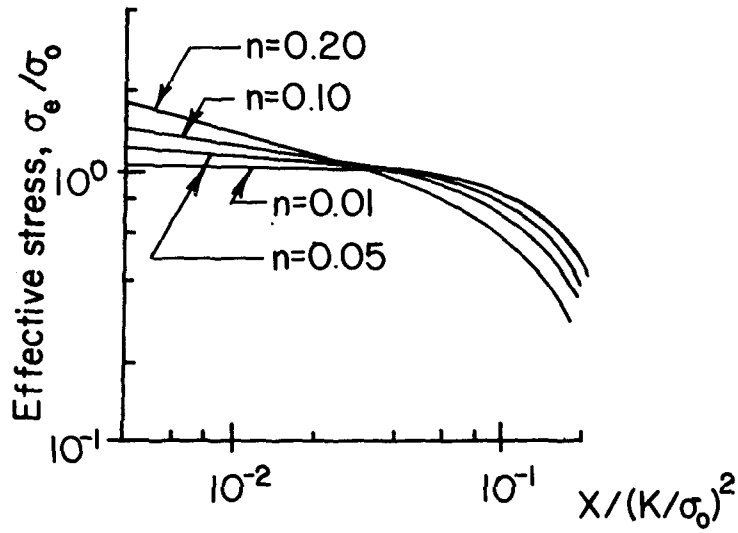

Figure 3.- Effective stress distribution forward of the blunted crack tip.

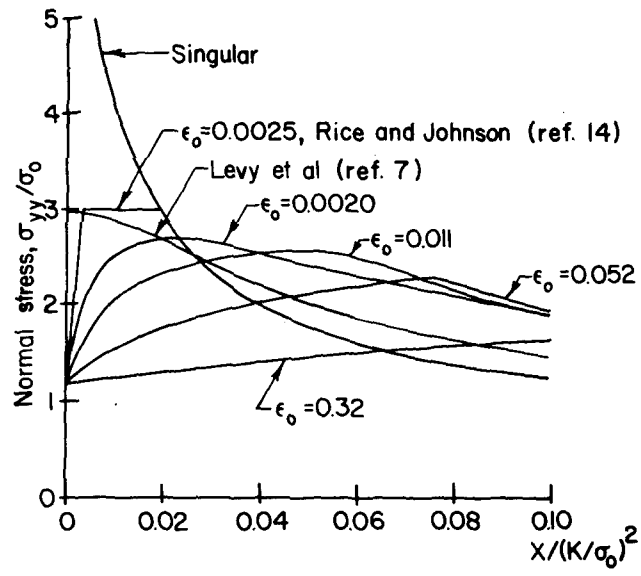

Figure 4.- Distribution of σ_{yy} stress forward of the blunted crack tip for n = 0.01.

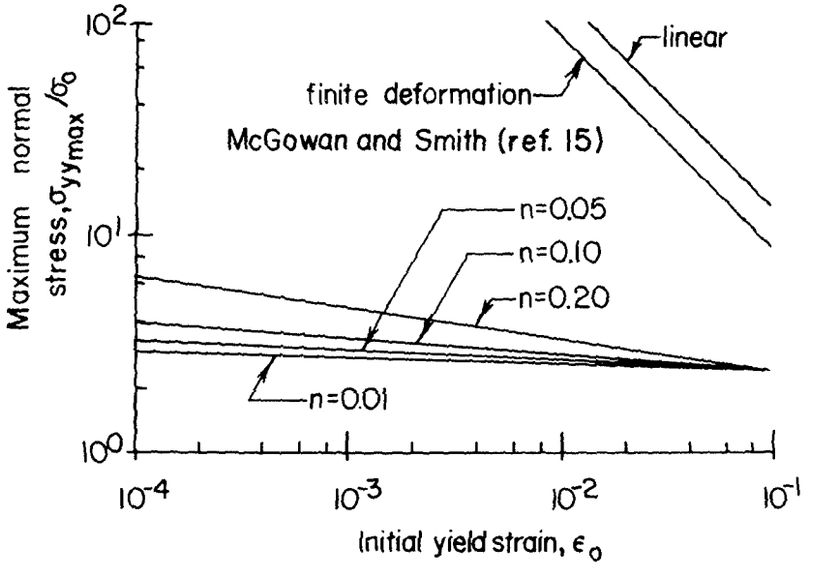

Figure 5.- Variation of σ_{yy} stress maximum with ε_o and n.

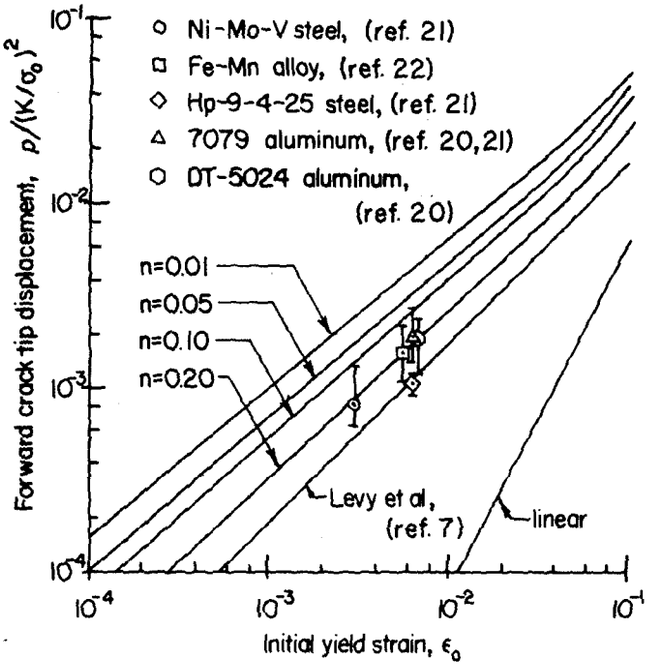

Figure 6.- Forward crack tip displacement and stretch zone variation with n and ε_o.

GAUSSIAN IDEAL IMPULSIVE LOADING OF RIGID VISCOPLASTIC PLATES

Robert J. Hayduk
NASA Langley Research Center

ABSTRACT

The response of a thin, rigid viscoplastic plate subjected to a spatially axisymmetric Gaussian ideal impulse loading was studied analytically. The Gaussian ideal impulse distribution instantaneously imparts a Gaussian initial velocity distribution to the plate, except at the fixed boundary. The plate deforms with monotonically increasing deflections until the initial dynamic energy is completely dissipated in plastic work. The simply supported plate of uniform thickness obeys the von Mises yield criterion and a generalized constitutive equation for rigid, viscoplastic materials. For the small deflection bending response of the plate, neglecting the transverse shear stress in the yield condition and rotary inertia in the equations of dynamic equilibrium, the governing system of equations is essentially nonlinear. A proportional loading technique, known to give excellent approximations of the exact solution for the uniform load case, was used to linearize the problem and obtain analytical solutions in the form of eigenvalue expansions. The linearized governing equation required the knowledge of the collapse load of the corresponding static problem.

The effects of load concentration and an order of magnitude change in the viscosity of the plate material were examined while holding the total impulse constant. In general, as the load became more concentrated, the peak central velocity increased and the time for plate motion to cease increased. For the less viscous plate, these increases of velocity and time were more pronounced. The final plate profile became more conical as the load concentration increased, but did not approach the purely conical shape predicted for the point impulse by the rigid, perfectly plastic analysis with the Tresca yield criteria. Profiles of the less viscous plate were influenced more by the load concentration.

SYMBOLS

A_n^I	series coefficient, equation (A6)
a	Gaussian distribution parameter
$B = \frac{\sqrt{3}\,\gamma}{2h}$	plate geometry and material constant
$\bar{C}_1$, $\bar{C}_2$	constants defined by equation (A5)
$F' = \frac{\sqrt{3}\,p_o'\,R^2}{4\,M_o}$	nondimensional collapse load amplitude

F	yield function
h	plate half-thickness
I	impulse per unit area amplitude at the plate center
$I' = \frac{IR^2}{M_o}$	impulse parameter, sec
$J_p(x)$, $I_p(x)$	Bessel function of the first kind of real and imaginary arguments, respectively
J_2'	second invariant of the deviatoric stress tensor
$\dot{K}_r$, $\dot{K}_\phi$	radial and circumferential curvature rates
k	yield stress in simple shear
M_r, M_ϕ	radial and circumferential bending-moment resultants
$\bar{M}_r$, $\bar{M}_\phi$	radial and circumferential bending-moment resultants at initial yield
$M_o = \sigma_o h^2$	yield moment of the plate
$m = \frac{M_r}{M_o}$	nondimensional radial bending-moment resultant
$n = \frac{M_\phi}{M_o}$	nondimensional circumferential bending-moment resultant
p_o'	pressure amplitude at the plate center at collapse
$\bar{p}_o' = \frac{p_o' R^2}{M_o}$	nondimensional pressure amplitude at the plate center at collapse
Q	shear stress resultant
$q = \frac{RQ}{M_o}$	nondimensional shear stress resultant
R	plate radius
r	radial coordinate
S_{ij}	deviator stress tensor

$\bar{S}_{ij}$	deviator stress tensor at initial yield
t	time
t_f	time for motion to cease
$u(\rho,t)$	dynamic component of velocity
$U(\rho)$	steady component of velocity
V	initial velocity
v	nondimensional plate velocity
w	transverse deflection of the plate
z	transverse coordinate
$\alpha = \frac{\mu\ BR^4}{M_o}$	plate geometry and material constant, sec
$\beta = a^2R^2$	nondimensional Gaussian shape parameter
γ, γ^o	material constants
∇^2, ∇^4	harmonic and biharmonic operators in cylindrical coordinates
δ	final center deflection
$\dot{\varepsilon}_{ij}$	strain rate tensor
λ_n	eigenvalues determined from equation (A7)
μ	mass density per unit area of the plate
ρ	nondimensional radial coordinate
σ_{ij}	stress tensor
σ_o	yield stress in simple tension
$\Phi(F)$	function defined by equation (3)
ϕ	circumferential coordinate
$\phi(\lambda_n,\beta)$	function defined by equation (A13)
$\psi(\lambda_n,\rho,\beta)$	function defined by equation (A12)

INTRODUCTION

This paper presents the results of an analysis of the small-deflection bending response of a simply supported circular plate of rigid, viscoplastic material subjected to a spatially axisymmetric Gaussian ideal impulse. The effects of load concentration and an order of magnitude change in the viscosity of the plate material are examined while holding the total impulse constant. Approximate expressions are developed for the time at which plate motion ceases, the final shape of the plate, and the final central displacement.

Although there have been a number of papers (refs. 1, 2, 3) which permit a time variation of the load, there have been few papers which consider a radial variation other than linear (refs. 3, 4). The only general spatial distribution of load which has received significant analytical attention is the Gaussian distribution. By varying a single parameter, this general distribution can span the extremes from the point load to the uniformly distributed load. This versatility was recognized by Sneddon (ref. 5) who approximated the dynamic loading of a projectile on a thin, infinite elastic plate by a Gaussian distribution of pressure. Madden (ref. 6), in his study of shielding of space vehicle structures against meteoroid penetration, related the meteoroid-shield debris loading of the main vehicle wall to a Gaussian initial velocity distribution. The first study of this loading on a plastic plate was by Thomson (ref. 7). He obtained the solution of a rigid, perfectly plastic plate of material obeying the Tresca yield condition subjected to an initial impulse of Gaussian distribution. Weidman (ref. 2), in considering the response of simply supported circular plastic plates to distributed time-varying loadings, presented an example case of a radial Gaussian distribution of pressure with an exponential decay. The plate material was also rigid, perfectly plastic obeying the Tresca yield conditions.

A generalized constitutive equation for rigid, viscoplastic materials is presented in the next section. Material elasticity is neglected in order to simplify the analysis, as is frequently done in theoretical investigations of dynamic plastic response of structures. Rigid-plastic analyses are generally believed to be valid when the dynamic energy is considerably larger than the maximum energy which could be absorbed in a wholly elastic manner and the duration of loading is short compared with the fundamental period of vibration.

LINEARIZATION OF THE GENERALIZED CONSTITUTIVE EQUATIONS FOR RIGID, VISCOPLASTIC MATERIALS

Perzyna (ref. 8) developed a generalized constitutive equation for rate sensitive plastic materials by incorporating a general function in the relationship to take the place of the yield function as used by previous researchers (Hohenemser and Prager, ref. 9; and Prager, ref. 10). Utilizing the definition of the second invariant of the stress deviator, $J_2' = \frac{1}{2} S_{ij} S_{ij}$, the yield function is expressed as

$$F = \frac{J_2'^{1/2}}{k} - 1 \tag{1}$$

where S_{ij} is the stress deviator tensor and k is the yield stress. The generalized constitutive equation proposed by Perzyna is

$$\dot{\varepsilon}_{ij} = \gamma^{o}\Phi(F)\frac{\partial F}{\partial \sigma_{ij}} \tag{2}$$

where $\dot{\varepsilon}_{ij}$ is the strain rate tensor,

$$\begin{aligned} \Phi(F) &= 0 \quad \text{if} \quad F \leq 0 \\ \Phi(F) &\neq 0 \quad \text{if} \quad F > 0 \end{aligned} \tag{3}$$

and γ^{o} denotes a physical constant of the material.

Perzyna (ref. 11) has shown that the generalized constitutive equation for viscoplastic materials reduces to the constitutive equations of an incompressible, perfectly plastic material first considered by von Mises and to the flow law of perfect plasticity theory. As in the theory of perfectly plastic solids, convexity of the subsequent dynamic loading surfaces and orthogonality of the inelastic strain-rate vector to the yield surface follow from Drucker's postulates defining a stable, inelastic material with inclusion of time-dependent terms (Perzyna, ref. 8).

A method of linearizing boundary-value problems in the theory of viscoplastic solids is described by Wierzbicki in reference 12. In this method, as shown graphically in figure 1, the concept of proportional loading is used to relate the state of stress $\bar{S}_{ij}$ on the initial yield surface $F = 0$ to subsequent states of stress, namely, proportional loading requires the direction cosine tensor of the state of stress in deviatoric space to be independent of time:

$$\frac{S_{ij}}{J_2'^{1/2}} = \frac{\bar{S}_{ij}}{k} \tag{4}$$

This is a reasonable approximation for axisymmetrically loaded simply supported circular plates because the plate center and boundary are automatically proportionally loaded, that is, the bending moments must always be equal at the plate center and the circumferential bending moment must always be zero at the plate boundary.

Utilizing equation (4), the generalized constitutive equation (2) becomes

$$\dot{\varepsilon}_{ij} = \frac{\gamma}{k} \Phi \left(\frac{S_{ij}}{\bar{S}_{ij}} - 1 \right) \bar{S}_{ij} \tag{5}$$

where the viscosity constant $\gamma = \gamma^{\circ}/2k$. For this analysis, the linear form

$$\Phi(F) = F \tag{6}$$

is chosen. This simplified constitutive equation still is nonlinear in stresses However, in the solution of dynamical plate and rotationally symmetric shell problems, the constitutive equation (5) with the linear function $\Phi(F) = F$ produces full linearization of the governing equations.

For the problem of a uniformly loaded, simply supported circular plate with $\Phi(F) = F$, Wierzbicki (ref. 12) has shown that the approximate solution obtained using the proportional loading hypothesis agrees very well with a numerical finite-difference solution of the exact equations. The solution of the linearized problem also agrees well with experimental data on impulsively loaded plates by Florence (ref. 13).

For the linear function equation (5) becomes

$$\dot{\varepsilon}_{ij} = \frac{\gamma}{k} (S_{ij} - \bar{S}_{ij}) \tag{7}$$

where equation (7) is really a flow relation for a given structure rather than a constitutive equation describing a given material (ref. 14).

GOVERNING EQUATIONS, BOUNDARY AND INITIAL CONDITIONS

A Gaussian ideal impulse is suddenly applied to the entire surface of a rigid, viscoplastic plate of radius R and thickness $2h$ resulting in an initial velocity distribution described by

$$V(r, 0) = \frac{I}{\mu} e^{-a^2 r^2} \tag{8}$$

where I is the impulse per unit area at the center of the plate and μ is the mass density per unit area of the plate middle surface. The boundary of the plate at $r = R$ is simply supported. The geometry of the plate and initial velocity are shown in figure 2.

The parameter a in the distribution function is a shape parameter which controls the distribution of the impulse. For $a = 0$ equation (8) describes a uniform impulse; and as $a \to \infty$, $I \to \infty$ equation (8) describes a point impulse at the plate center.

The internal forces and moments acting on a typical plate element are shown in figure 3. If rotary inertia is neglected, but transverse inertia taken into account, the equations of motion are

$$\frac{\partial}{\partial r}(rQ) = \mu r \frac{\partial^2 w}{\partial t^2}$$

$$\frac{\partial}{\partial r}(rM_r) - M_\phi = rQ \tag{9}$$

Utilizing the Love-Kirchoff hypotheses, the curvature-rate-moment relations, derived from the linearized constitutive equation, equation (7), are

$$\dot{K}_r = \frac{B}{M_o}\left[(2M_r - M_\phi) - (2\bar{M}_r - \bar{M}_\phi)\right]$$

$$\dot{K}_\phi = \frac{B}{M_o}\left[(2M_\phi - M_r) - (2\bar{M}_\phi - \bar{M}_r)\right] \tag{10}$$

where $B = \sqrt{3}\,\gamma/2h$. $\bar{M}_r$ and $\bar{M}_\phi$ are moments satisfying for any r the equation of the initial yield surface

$$M_r^2 - M_r M_\phi + M_\phi^2 = M_o^2 \tag{11}$$

$M_o = \sigma_o h^2$ is the yield moment of the plate material and σ_o is the yield stress in simple tension.

For small deflections of the plate the curvature rates $\dot{K}_r$ and $\dot{K}_\phi$ are related to the deflection rate $\dot{w}$ by

$$\dot{K}_r = -\frac{\partial^2 \dot{w}}{\partial r^2}\,; \qquad \dot{K}_\phi = -\frac{1}{r}\frac{\partial \dot{w}}{\partial r} \tag{12}$$

Equations (9), (10), and (12) form a linear parabolic system of partial differential equations with six unknown functions — M_r, M_ϕ, Q, w, $\dot{K}_r$, and $\dot{K}_\phi$ — plus the unknown static moment distribution $\bar{M}_r$ and $\bar{M}_\phi$.

By eliminating all unknowns except $\dot{w}$, the system of governing equations can be reduced to the single, fourth-order equation

$$\frac{2M_o}{3B}\nabla^4 \dot{w} + \mu \frac{\partial \dot{w}}{\partial t} = \frac{1}{r}\frac{\partial}{\partial r}\left[\frac{\partial}{\partial r}(r\bar{M}_r) - \bar{M}_\phi\right] \tag{13}$$

where

$$\nabla^4 = \left[\frac{\partial^2}{\partial r^2} + \frac{1}{r}\frac{\partial}{\partial r}\right]\left[\frac{\partial^2}{\partial r^2} + \frac{1}{r}\frac{\partial}{\partial r}\right]$$

The right-hand side of equation (13) represents the internal force distribution at the initiation of collapse in the static case.

Let p_o' denote the static load-carrying capacity of the plate, then the right-hand side of equation (13) can be replaced by $-p_o' e^{-a^2r^2}$ and the governing equation becomes

$$\frac{2M_o}{3B} \nabla^4 \dot{w} + \mu \frac{\partial \dot{w}}{\partial t} = - p_o' e^{-a^2r^2} \tag{14}$$

This method of solution, proposed by Wierzbicki (ref. 12), has the important property of replacing the unknown static moment distribution $\bar{M}_r$ and $\bar{M}_\phi$, whose explicit formulas are not known for the von Mises yield condition, by the static load-carrying capacity p_o'. Thus, the need for explicit formulas has been reduced to finding the value of a constant, p_o', corresponding to a particular value of the shape parameter, a. The determination of the load-carrying capacity, p_o', of a circular plate under a Gaussian distribution of pressure is presented in reference 15.

Define the dimensionless quantities

$$m = \frac{M_r}{M_o} , \quad n = \frac{M_\phi}{M_o} , \quad q = \frac{RQ}{M_o}$$

$$\rho = \frac{r}{R} , \quad \beta = a^2R^2 \tag{15}$$

$$v = \frac{1}{BR^2} \frac{\partial w}{\partial t} , \quad F' = \frac{\sqrt{3}\, p_o' R^2}{4\, M_o}$$

and let $\nabla^2 = \frac{\partial^2}{\partial \rho^2} + \frac{1}{\rho} \frac{\partial}{\partial \rho}$. Then the final form of the governing equation, equation (14), is

$$\nabla^4 v + \frac{3}{2} \alpha \frac{\partial v}{\partial t} = - 2\sqrt{3}\, F' e^{-\beta\rho^2} \tag{16}$$

where $\alpha = \mu BR^4/M_o$.

The boundary conditions of the simply supported plate are

$$m = n, \quad q = 0 \quad \text{at} \quad \rho = 0 \tag{17}$$

$$v = m = 0 \quad \text{at} \quad \rho = 1$$

Using equations (10), (12), and (9), equations (17), in terms of rate of deflection become

$$\lim_{\rho \to 0} \left(\frac{\partial^2 v}{\partial \rho^2} - \frac{1}{\rho} \frac{\partial v}{\partial \rho} \right) = 0; \quad \lim_{\rho \to 0} \left(\frac{\partial^3 v}{\partial \rho^3} + \frac{1}{\rho} \frac{\partial^2 v}{\partial \rho^2} - \frac{1}{\rho^2} \frac{\partial v}{\partial \rho} \right) = 0;$$

$$2 \frac{\partial^2 v}{\partial \rho^2} + \frac{\partial v}{\partial \rho} \Bigg|_{\rho = 1} = 0; \quad v(1,t) = 0 \tag{18}$$

For the Gaussian ideal impulsive loading the plate is initially flat and the initial velocity has a Gaussian distribution

$$w(\rho, 0) = 0; \quad v(\rho, 0) = \frac{I'}{\alpha} e^{-\beta \rho^2} \tag{19}$$

where $I' = \frac{IR^2}{M_o}$.

RESULTS AND DISCUSSION

The solution to the governing equation, equation (16), with associated boundary and initial conditions, equations (18) and (19) are presented in the Appendix. The effects of load distribution and plate viscosity on plate response are examined in this section while holding the total impulse constant.

The impulse amplitude, $I' = IR^2/M_o$, sec, at the plate center is related to the total impulse, I^T, and distribution parameter, β, by the relation

$$I' = \frac{I^T}{\pi M_o} \left(\frac{\beta}{1 - e^{-\beta}} \right) \tag{20}$$

For comparison purposes the total impulse is held constant at $\frac{I^T}{\pi M_o} = 1 \times 10^{-3}$ sec. The impulse becomes more concentrated at the center of the plate as β is increased and the amplitude grows almost linearly as β becomes large. For $\beta = 0$, the impulse has a uniform distribution.

The graphical results were obtained by programing the solution (equations (A14) and (A15)) and summing the series term-by-term. The rapidly convergent series with $1/\lambda_n^5$ and $1/\lambda_n^9$ factors did not present any computational difficulties; however, the last series in the velocity expression equation (A14)

has a $1/\lambda_n$ factor and prohibited the calculation of velocity-time histories for small β and t. For $t = 0$ the series is slowly convergent.

A representative plot of the plate central velocity is shown in figure 4 for $\beta = 10$ and viscosity parameter $\alpha = 1 \times 10^{-2}$ sec. The initial central velocity is seen to rapidly decline during the first 0.025 msec after which the velocity more slowly tends to zero.

The plate is seen to deform monotonically with increasing deflection until the initial dynamic energy is completely dissipated in plastic work and the plate comes to rest. The deformed profiles of the plate at rest are shown in figure 5 for two values of α (1×10^{-2}, 1×10^{-3}) and various values of β. The profile becomes more conical as the impulse becomes more concentrated and the profiles of the less viscous plate ($\alpha = 1 \times 10^{-2}$ sec) exhibit a wider variation, thus are influenced more by the shape parameter β than are those for the $\alpha = 1 \times 10^{-3}$ sec case.

Approximations

An approximation to the deflection of the plate is obtained from equation (A15) by retaining only the first terms of series and using the approximation

$$\bar{C}_1 + \bar{C}_2\rho^2 + \frac{1}{2\beta} e^{-\beta\rho 2} + \left(\frac{1}{\beta} + \rho^2\right) \sum_{n=1}^{\infty} \frac{(-1)^n(\beta\rho^2)^n}{(2n)\ n!}$$

$$\cong - \frac{16\beta}{3} \frac{1}{\lambda_1^5} \psi(\lambda_1, \rho, \beta)$$

The result is

$$\frac{1}{BR^2} w(\rho,t) = - \frac{\sqrt{3}\ F'}{4\beta} \left[\bar{C}_1 + \bar{C}_2\rho^2 + \frac{1}{2\beta} e^{-\beta\rho^2} + \left(\frac{1}{\beta} + \rho^2\right) \sum_{n=1}^{\infty} \frac{(-1)^n(\beta\rho^2)^n}{(2n)\ n!}\right]$$

$$\left\{\left(1 - e^{-\frac{2\lambda_1^4}{3\alpha} t}\right) \left(\frac{3\alpha}{2\lambda_1^4} + \frac{\sqrt{3}\ I'}{4F'}\right) - t\right\} \tag{21}$$

An approximate expression for the time for motion to cease can be obtained by setting the derivative of the approximate displacement expression to zero, that is, $\left.\frac{\partial w}{\partial t}\right|_{t_f} = 0$, is

$$t_f = \frac{3\alpha}{2\lambda_1^4} \ln\left(1 + \frac{\lambda_1^4\ I'}{2\sqrt{3}\ F'\alpha}\right) \tag{22}$$

Equation (22) is plotted in rigure 6 for $0 \leq \beta \leq 100$ and several values of α. Equation (22) is an implicit function of β since I' and F' vary with β. The effect of β diminishes after an initial rapid rise of t_f with increasing β. The symboled points represent computed times using the complete equation for the velocity, equation (A14). Equation (22) is a very good approximation for the case $\alpha = 1 \times 10^{-3}$ sec. However, except for small values of β, the approximation is poor for the $\alpha = 1 \times 10^{-2}$ sec case.

For $\alpha \to \infty$ equation (22) limits to

$$t_f = \frac{\sqrt{3}\, I'}{4F'} = \frac{I}{\bar{p}_o'} \tag{23}$$

and represents the rigid, perfectly plastic case ($\gamma \to \infty$) with the von Mises yield condition. Equation (23) has the same form as Wang's (ref. 16) result for the uniform ideal impulse problem using the Tresca yield condition for a rigid perfectly plastic material. However, equation (23) gives slightly smaller values of t_f since $\bar{p}_o' = 6.51$ for the von Mises yield condition rather than 6 in the case of the Tresca yield condition.

The curve labeled Tresca, r.p.p. was obtained from the results of reference 7 where a simply supported circular plate of rigid, perfectly plastic material obeying the Tresca yield condition and associated flow rule was analyzed for a general Gaussian ideal impulse loading. For small β the two curves differ only slightly, but as β grows larger and the impulse becomes more concentrated, the two analyses predict drastically different times for the plate motion to cease. The Tresca yield condition predcits very large times for plate motion to cease, whereas the von Mises yield condition predicts more realistic times for concentrated loads.

The substitution of equation (22) for t_f into equation (21) provides an approximate expression for the final plate displacements:

$$\frac{1}{BR^2} w(\rho,t) = -\frac{\sqrt{3}\, F'}{4\beta}\left[\bar{C}_1 + \bar{C}_2\rho^2 + \frac{1}{2\beta} e^{-\beta\rho^2} + \left(\frac{1}{\beta} + \rho^2\right)\sum_{n=1}^{\infty} \frac{(-1)^n(\beta\rho^2)^n}{(2n)\, n!}\right]$$

$$\left\{\frac{\sqrt{3}\, I'}{4F'} - \frac{3\alpha}{2\lambda_1^4} \ln\left(1 + \frac{\lambda_1^4 I'}{2\sqrt{3}\, F'\alpha}\right)\right\} \tag{24}$$

and for the final center displacement $\delta(0,t_f) = w(0,t_f)$:

$$\frac{\mu R^2}{\alpha M_o}\,\delta(0,t_f) = -\frac{\sqrt{3}\,F'}{4\beta}\left(\bar{C}_1 + \frac{1}{2\beta}\right)\left\{\frac{\sqrt{3}\,I'}{4F'} - \frac{3\alpha}{2\lambda_1^4}\,\ell n\left(1 + \frac{\lambda_1^4 I'}{2\sqrt{3}\,F'\alpha}\right)\right\} \tag{25}$$

Equation (25) is plotted as a function of β for the two values of α in figure 7. The approximations are in excellent agreement with the points computed from the exact equations for both $\alpha = 1 \times 10^{-3}$ sec and 1×10^{-2} sec, even though the t_f-approximations for the larger α were poor for large β as shown in figure 6. The nondimensional central displacements are shown smaller for the $\alpha = 1 \times 10^{-2}$ sec case when, in reality the real displacements are larger than for the $\alpha = 1 \times 10^{-3}$ sec case. This is caused by α being in the denominator of the expression for the nondimensional central displacement.

Profiles obtained from the approximation, equation (24), were compared with profiles obtained from the exact equation. For $\alpha = 1 \times 10^{-3}$ sec, the differences between the approximate and exact profiles were negligibly small for the entire range of β considered, 10^{-3} to 10,000. However, for the less viscous plates, $\alpha = 1 \times 10^{-2}$ sec, the differences were not negligible and the approximation, equation (23), should therefore be restricted accordingly.

CONCLUDING REMARKS

A thin, simply supported rigid, viscoplastic plate subjected to a Gaussian ideal impulse has been analyzed within the realm of small deflection bending theory. The plate material obeys the von Mises yield criteria and constitutive equations due to Perzyna (ref. 11). These considerations lead, essentially, to nonlinear equations governing the dynamic response of the thin plate. A proportional loading hypothesis, proposed by Wierzbicki (ref. 12) and shown to be an excellent approximation of the exact solution for the uniform load case, was used to linearize the problem and obtain analytical solutions in the form of eigenvalue expansions. The linearized governing equation on the velocity of the plate required the knowledge of the collapse load of the corresponding static problem, that is, the collapse load for the specific load distribution parameter, β.

The effects of impulse concentration and an order of magnitude change in the viscosity of the plate material were examined while holding the total impulse constant. In general, as the impulse became more concentrated, the peak central velocity increased and the time for plate motion to cease increased. For the less viscous plate material, these increases of velocity and time, t_f, for plate motion to cease are more pronounced. The final plate profile became more conical as the load concentration increased, but did not approach the purely conical shape predicted by the rigid, perfectly plastic analysis with the Tresca yield condition for a point impulse. As the viscosity of the plate decreases, the shape parameter has more effect on the final deformed plate profiles.

Approximate expressions were developed for the time at which plate motion ceases, t_f, the final shape of the plate, and the final central displacement. Comparisons with the series solution indicated that the approximations were excellent for the $\alpha = 1 \times 10^{-3}$ sec case. The approximation for the final central deflection was good for the entire range of shape parameter β, the other approximations were limited in usefulness.

APPENDIX

SOLUTION OF EQUATION (16) BY EIGENVALUE EXPANSION*

Since the right-hand side of equation (16) is not a function of time, it can be solved by means of an eigenvalue expansion method. Substitution of

$$v(\rho,t) = u(\rho,t) + U(\rho) \tag{A1}$$

into equation (16) results in

$$\nabla^4 u(\rho,t) + \frac{3}{2}\,\alpha\,\frac{\partial u(\rho,t)}{\partial t} + \nabla^4 U(\rho) = -\,2\sqrt{3}\;F'\;e^{-\beta\rho^2}$$

which separates into

$$\nabla^4 u + \frac{3}{2}\,\alpha\,\frac{\partial u}{\partial t} = 0 \tag{A2}$$

and

$$\nabla^4 U = -\,2\sqrt{3}\;F'\;e^{-\beta\rho^2} \tag{A3}$$

Equation (A3) is the same as equation (16) except for the absence of the inertia term. Thus, $U(\rho)$ is an equilibrium solution of equation (16) with the same boundary conditions, equations (17).

The solution to equation (A3) satisfying the boundary conditions, equations (18), is

$$U(\rho) = \frac{\sqrt{3}}{4\beta}\,F'\left\{\bar{C}_1 + \bar{C}_2\rho^2 + \frac{1}{2\beta}\,e^{-\beta\rho^2} + \left(\frac{1}{\beta} + \rho^2\right)\sum_{m=1}^{\infty}\frac{(-1)^m(\beta\rho^2)^m}{(2m)\;m!}\right\} \tag{A4}$$

where

$$\bar{C}_1 = \frac{1}{6\beta} - \frac{7}{6} - \frac{2}{3\beta}\,e^{-\beta} - \frac{1}{\beta}\sum_{m=1}^{\infty}\frac{(-1)^m\beta^m}{(2m)\;m!} \tag{A5}$$

---

*For more details, the reader can consult "Gaussian Impulsive Loading of Rigid Viscoplastic Plates," by R. J. Hayduk, Ph. D. Thesis, Virginia Polytechnic Institute and State University, Blacksburg, Virginia, 1972.

and

$$\bar{C}_2 = -\frac{1}{6\beta} + \frac{7}{6} - \frac{1}{6\beta} e^{-\beta} - \sum_{m=1}^{\infty} \frac{(-1)^m \beta^m}{(2m)\ m!}$$

A general solution due to Wierzbicki (ref. 12) satisfying equation (A2) and all prescribed boundary conditions can be written in the form

$$u(\rho,t) = \sum_{n=1}^{\infty} A_n^I \left[I_o(\lambda_n)J_o(\lambda_n\rho) - J_o(\lambda_n)I_o(\lambda_n\rho)\right] e^{-(2\lambda_n^4/3\alpha)t} \tag{A6}$$

where $J_o(x)$ and $I_o(x)$ denote the Bessel functions of the first kind of real and imaginary arguments. The solution (A6) identically satisfies boundary conditions (18 a, b, and d). The eigenvalues, λ_n, are roots of the following transcendental equation stemming from the boundary condition (18c) of zero bending moment at the plate edge

$$I_o(\lambda_n)J_1(\lambda_n) + I_1(\lambda_n)J_o(\lambda_n) - 4\lambda_n I_o(\lambda_n)J_o(\lambda_n) = 0 \tag{A7}$$

The only remaining unknowns in the solution are the series coefficients A_n^I. These coefficients are evaluated from the initial condition (19), that is,

$$v(\rho,0) = u(\rho,0) + U(\rho) = \frac{I'}{\alpha} e^{-\beta\rho^2}$$

Thus,

$$u(\rho,0) = -U(\rho) + \frac{I'}{\alpha} e^{-\beta\rho^2} \tag{A8}$$

and after substituting equation (A6) for $u(\rho,0)$ there results

$$\sum_{n=1}^{\infty} A_n^I \left[I_o(\lambda_n)J_o(\lambda_n\rho) - J_o(\lambda_n)I_o(\lambda_n\rho)\right] = -U(\rho) + \frac{I'}{\alpha} e^{-\beta\rho^2} \tag{A9}$$

The coefficients A_n^I can be determined from (A9) by virtue of the orthogonality of the system $[I_o(\lambda_n)J_o(\lambda_n\rho) - J_o(\lambda_n)I_o(\lambda_n\rho)]$ on the interval $[0,1]$ where ρ is used as a weighting function. Therefore, coefficients A_n^I can be determined as

$$A_n^I = -\frac{\int_0^1 \left(\rho U(\rho) - \rho \frac{I'}{\alpha} e^{-\beta\rho^2}\right)\left[I_o(\lambda_n)J_o(\lambda_n\rho) - J_o(\lambda_n)I_o(\lambda_n\rho)\right] d\rho}{\int_0^1 \rho\left[I_o(\lambda_n)J_o(\lambda_n\rho) - J_o(\lambda_n)I_o(\lambda_n\rho)\right]^2 d\rho} \tag{A10}$$

where $U(\rho)$ is defined by equation (A4). The resulting coefficients are

$$A_n^I [I_o(\lambda_n)J_o(\lambda_n\rho) - J_o(\lambda_n)I_o(\lambda_n\rho)] = [\frac{4}{\sqrt{3}} F' \frac{1}{\lambda_n^5} + \frac{2}{3}\frac{I'}{\alpha}\frac{1}{\lambda_n}]\psi(\lambda_n,\rho,\beta) \tag{A11}$$

where the functions $\psi(\lambda_n,\rho,b)$ are defined by the relation

$$\frac{16\beta}{3\lambda_n^5}\psi(\lambda_n,\rho,\beta) = \phi(\lambda_n,\beta)[I_o(\lambda_n)J_o(\lambda_n\rho) - J_o(\lambda_n)I_o(\lambda_n\rho)] \tag{A12}$$

with

$$\phi(\lambda_n,\beta) = \frac{\begin{aligned}&\frac{1}{\lambda_n}\bar{C}_1 I_o(\lambda_n)J_1(\lambda_n) - \frac{1}{\lambda_n}\bar{C}_1 J_o(\lambda_n)I_1(\lambda_n) + \bar{C}_2 I_o(\lambda_n)\left[\frac{1}{\lambda_n}J_1(\lambda_n) - \frac{4}{\lambda_n^3}J_1(\lambda_n) + \frac{2}{\lambda_n^2}J_o(\lambda_n)\right]\\ &- \bar{C}_2 J_o(\lambda_n)\left[\frac{1}{\lambda_n}I_1(\lambda_n) - \frac{2}{\lambda_n^2}I_o(\lambda_n) + \frac{4}{\lambda_n^3}I_1(\lambda_n)\right] + \frac{1}{2\beta}I_o(\lambda_n)\int_0^1 xe^{-\beta x^2}J_o(\lambda_n x)dx\\ &- \frac{1}{2\beta}J_o(\lambda_n)\int_0^1 xe^{-\beta x^2}I_o(\lambda_n x)dx + I_o(\lambda_n)\int_0^1 x(\frac{1}{\beta}+x^2)\sum_{m=1}^{\infty}\left[\frac{(-1)^m(\beta x^2)^m}{(2m)m!}\right]J_o(\lambda_n x)dx\\ &- J_o(\lambda_n)\int_0^1 x(\frac{1}{\beta}+x^2)\sum_{m=1}^{\infty}\left[\frac{(-1)^m(\beta x^2)^m}{(2m)m!}\right]I_o(\lambda_n x)dx\end{aligned}}{I_o(\lambda_n)J_o(\lambda_n)\{2\lambda_n[I_o(\lambda_n)J_1(\lambda_n) - I_1(\lambda_n)J_o(\lambda_n)] - 3I_o(\lambda_n)J_o(\lambda_n)\}} \tag{A13}$$

When equations (A4) and (A6) are summed and equation (A11) is used, the complete solution becomes

$$v(\rho,t) = \frac{\sqrt{3}}{4\beta}F'\left\{\bar{C}_1 + \bar{C}_2\rho^2 + \frac{1}{2\beta}e^{-\beta\rho^2} + (\frac{1}{\beta}+\rho^2)\sum_{n=1}^{\infty}\frac{(-1)^n(\beta\rho^2)^n}{(2n)\,n!}\right\}$$

$$+ \frac{4}{\sqrt{3}}F'\sum_{n=1}^{\infty}\frac{1}{\lambda_n^5}\psi(\lambda_n,\rho,\beta)e^{-(2\lambda_n^4/3\alpha)t} + \frac{2}{3}\frac{I'}{\alpha}\sum_{n=1}^{\infty}\frac{1}{\lambda_n}\psi(\lambda_n,\rho,\beta)e^{-(2\lambda_n^4/3\alpha)t} \tag{A14}$$

The displacement of the plate is determined by integrating (A14) with respect to time. Taking the initial condition of zero displacement into account, the displacement becomes

$$\frac{1}{BR^2} w(\rho,t) = \frac{\sqrt{3}}{4\beta} F' t \left[\bar{C}_1 + \bar{C}_2 \rho^2 + \frac{1}{2\beta} e^{-\beta\rho^2} + \left(\frac{1}{\beta} + \rho^2\right) \sum_{n=1}^{\infty} \frac{(-1)^n (\beta\rho^2)^n}{(2n)\ n!} \right]$$

$$+ \frac{4}{\sqrt{3}} F' \frac{3\alpha}{2} \sum_{n=1}^{\infty} \frac{1}{\lambda_n^9} \psi(\lambda_n,\rho,\beta)\left(1 - e^{-(2\lambda_n^4/3\alpha)t}\right)$$

$$+ I' \sum_{n=1}^{\infty} \frac{1}{\lambda_n^5} \psi(\lambda_n,\rho,\beta)\left(1 - e^{-(2\lambda_n^4/3\alpha)t}\right) \qquad \text{(A15)}$$

Equations (A14) and (A15) represent the complete solution for the velocity and displacement of the plate. In the limit as $\beta \to 0$, the Gaussian ideal impulse becomes the uniform ideal impulse and this solution reduces to the solution presented by Wierzbicki (ref. 12).

REFERENCES

1. Perzyna, P.: Dynamic Load Carrying Capacity of a Circular Plate. Arch. Mech. Stos., Vol. 10, No. 5, 1958, pp. 635-647.

2. Weidman, D. J.: Response of a Plastic Circular Plate to a Distributed Time-Varying Loading. Ph. D. Thesis, Virginia Polytechnic Institute and State University, 1968.

3. Youngdahl, C. K.: Influence of Pulse Shape on the Final Plastic Deformation of a Circular Plate. Int. J. Solids Structures, Vol. 7, 1971, pp. 1127-1142.

4. Florence, A. L.: Annular Plate Under a Transverse Line Impulse. AIAA Journal, Vol. 3, No. 9, 1965, pp. 1726-1732.

5. Sneddon, I. E.: Fourier Transforms. McGraw-Hill Book Co., Inc., 1951, pp. 145-147.

6. Madden, R.: Ballistic Limit of Double-Walled Meteoroid Bumper Systems. NASA TN D-3916, 1967.

7. Thomson, R. G.: Plastic Behavior of Circular Plates Under Transverse Impulse Loadings of Gaussian Distribution. NASA TR R-279, 1968.

8. Perzyna, P.: The Constitutive Equations for Work-Hardening and Rate Sensitive Plastic Materials. Proc. Vib. Problems, Vol. 4, 1963, pp. 281-290; Bull. Acad. Polon. Sci., Ser. Sci. Tech., Vol. 12, 1964, pp. 199-206.

9. Hohenemser, K.; and Prager, W.: Über die Ansätze der Mechanik isotroper Konitinua. ZAMM, Vol. 12, 1932, pp. 216-226.

10. Prager, W.: Mechanique des solides isotropes an dela du domaine elastique. Memorial Sci. Math. 87, Paris, 1937, Eq. (47) on p. 27.

11. Perzyna, P.: Fundamental Problems in Viscoplasticity. Advances in Applied Mechanics. Vol. 9, 1966, pp. 202-243.

12. Wierzbicki, T.: Impulsive Loading of Rigid Viscoplastic Plates. Int. J. Solids Structures, Vol. 3, 1967, pp. 635-647.

13. Florence, A. L.: Circular Plate Under a Uniformly Distributed Impulse. Int. J. Solids Structures, Vol. 2, 1966, pp. 37-47.

14. Wierzbicki, T.: A Method of Approximate Solution of Boundary Value Problems for Rigid, Viscoplastic Structures. Acta Mechanica, Vol. 3, No. 1, 1967, pp. 56-66.

15. Hayduk, R. J.; and Thomson, R. G.: Static Load-Carrying Capacity of Circular Rigid-Plastic Plates Under Gaussian Distribution of Pressure. Int. J. of Solids and Structures, Vol. 12, 1976, pp. 555-558.

16. Wang, A. J.: The Permanent Deflection of a Plastic Plate Under Blast Loading. J. Appl. Mech., Vol. 22, No. 3, 1955, pp. 375-376.

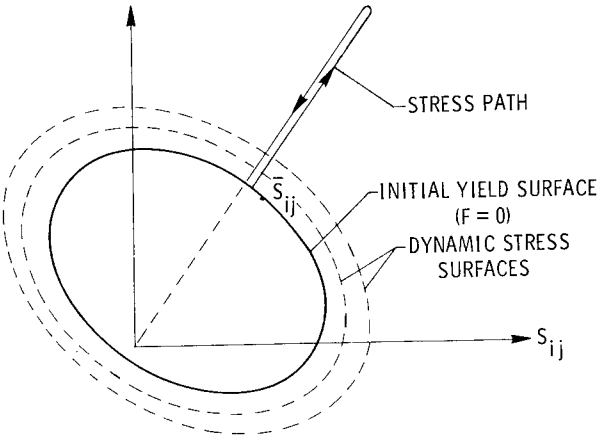

Figure 1.- Representation of proportional loading in deviatoric space.

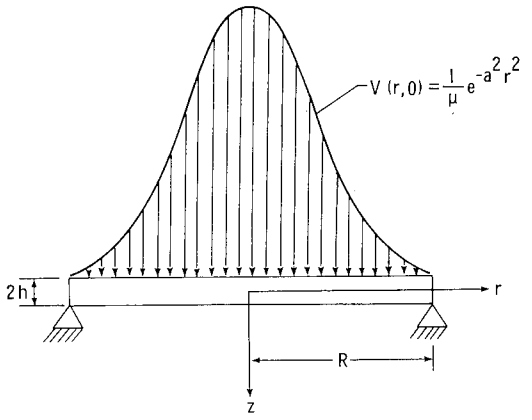

Figure 2.- Simply supported circular plate with Gaussian distribution of initial velocity.

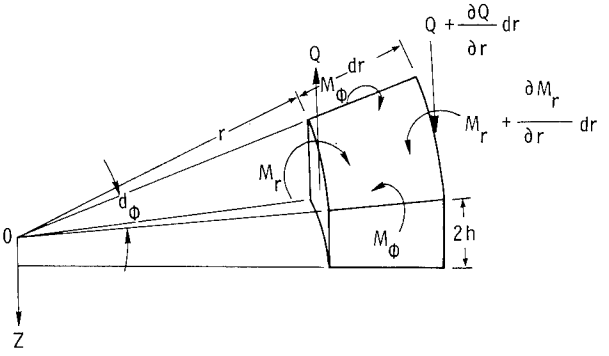

Figure 3.- Element of the circular plate with internal forces and moments.

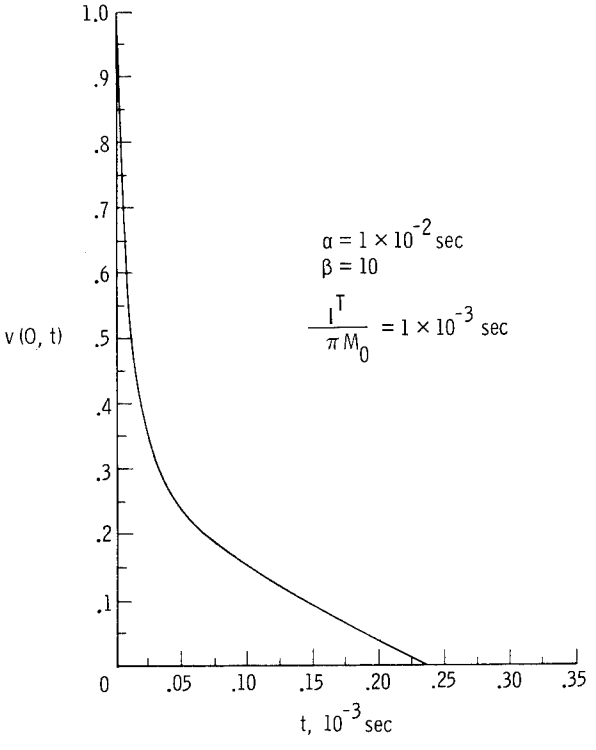

Figure 4.- Representative time history of plate central velocity for the Gaussian ideal impulse loading.

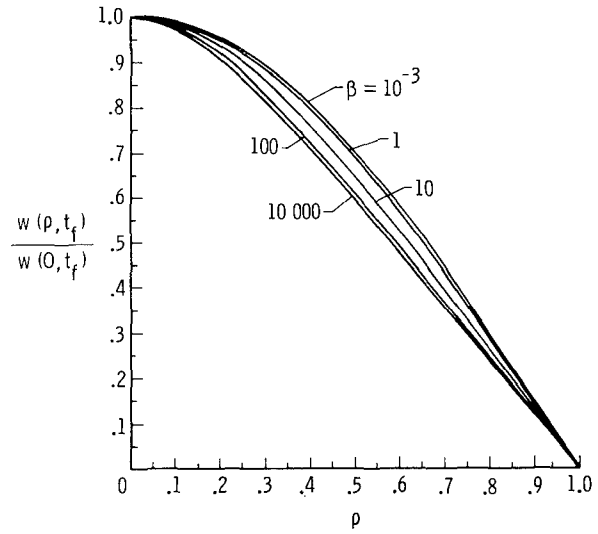

(a) $\alpha = 1 \times 10^{-3}$ sec.

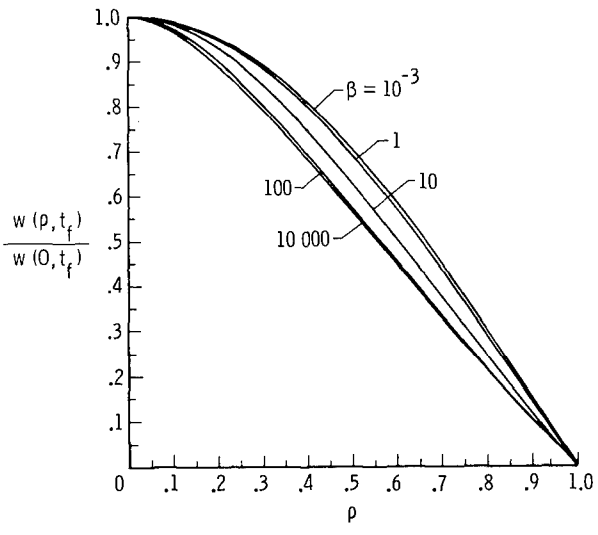

(b) $\alpha = 1 \times 10^{-2}$ sec.

Figure 5.- Final plate profiles for various values of the ideal impulse shape parameter, β.

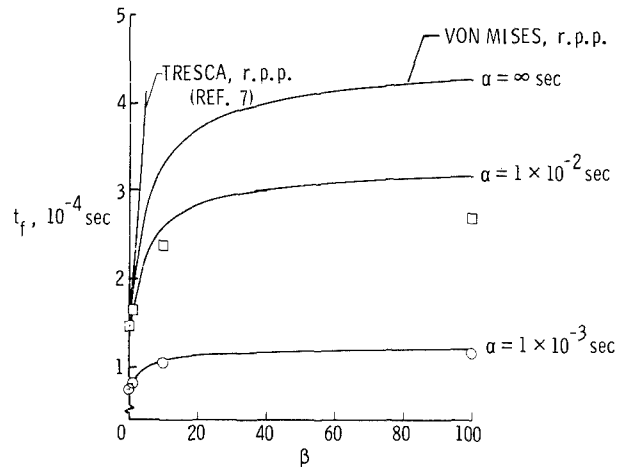

Figure 6.- Comparison of approximate expression (eq. (22)) for motion to cease, t_f, and points determined from the complete equations for the ideal impulse loading.

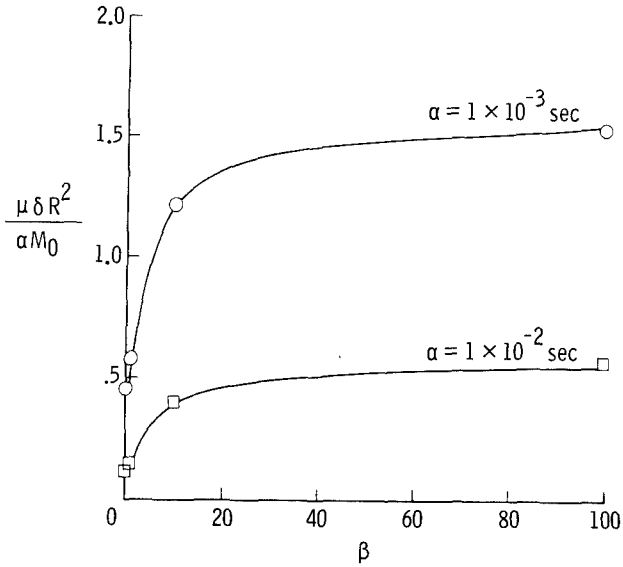

Figure 7.- Comparison of approximate expression (eq. (25)) for the final central deflection and points determined from the complete equations for the ideal impulse loading.

RECENT ADVANCES IN SHELL THEORY

James G. Simmonds

Department of Applied Mathematics & Computer Science

University of Virginia

INTRODUCTION

The results to be reviewed are divided into two categories: those that relate two-dimensional shell theory to three-dimensional elasticity theory and those concerned with shell theory per se. In the second category I further distinquish between results for general elastic systems that carry over, by specialization or analogy, to shells and results that are unique to shell theory itself. Because of the limitations of space and my interests, I do not mention multilayered or sandwich shells. A good discussion of these with an ample list of references may be found in Librescu's book [1]. Also, in view of the excellent review articles by Stein [2] and Hutchinson and Koiter [3], I have not attempted to review the enormous literature on shell buckling.

TWO APPROACHES TO SHELL THEORY

Most texts derive shell theory by a mixture of two-and three-dimensional considerations. However, a number of recent papers have adopted one of the following two extreme approaches:

A. A shell is idealized as a material surface in three-dimensional Euclidean space capable of transmitting forces and moments. The physical laws for this two-dimensional continuum are postulated in analogy with those for a three-dimensional one. Stress-strain laws and even failure criteria are formulated in terms of two-dimensional variables and may be deduced directly from experiments on the shell material. The papers by Sanders [4], Ericksen and Truesdell [5], Serbin [6], Budiansky [7], Simmonds and Danielson [8], and Reissner [9], to mention but a few, as well as much of the monumental treatise by Naghdi [10] are written in this spirit.

B. No matter how thin, a shell must be regarded as a three-dimensional continuum. However, the governing equations can be enormously simplified by considering various formal asymptotic expansions of the unknowns in terms of appropiate "thinness" parameters. In the interior of the shell (i.e. away from edges, concentrated loads or geometric discontinuities of one sort or another) the leading terms of the expansions satisfy various sets of two-dimensional equations that we call, collectively, the shell equations. Among those who have contributed recently to this second approach are Green [11], Johnson and Reissner [12], Cicala [13], Van der Heijden [14], and especially Goldenveiser (see the references cited in [15].)

The virtue of the first approach is also its shortcoming: there is no way to estimate intrinsically the errors made by neglecting three-dimensional effects. Or, from another viewpoint, there is no systematic way to construct a refined shell theory.

A drawback of the second approach, aside from its tediousness, is that it requires a knowledge at the edges of the shell of the distribution in the thickness direction of the applied stresses or displacements. As Koiter has emphasized [16], we never know these distributions precisely, except at a free edge. Another drawback of the second approach is that, because the thickness of the shell is always incorporated in the expansion parameters, one set of uniformly valid interior (i.e. shell) equations does not emerge. Rather there is one set of equations for a "membrane" state, another for an "inextensional bending" state, another for a "simple edge effect", another for a "degenerate edge effect", and, if one is dealing, for example, with an infinite cylindrical shell subject to self-equilibrating edge loads, still another set of equations is needed to recover the "semi-membrane" theory of Vlasov [17, p. 254].

THE ASYMPTOTIC APPROACH

The goal here is to provide a systematic method of refining the analysis of thin-walled bodies. One important consequence of the asymptotic approach is the verification and refinement of the classical Kirchhoff boundary conditions. Another useful result is that it gives a method for computing the dominant stresses in the immediate vicinity of an edge without the need of solving a full three-dimensional problem. We shall first illustrate the essence of the asymptotic method by means of a simple example drawn from the work of Goldenveiser and Van der Heijden. Then we shall indicate the implication of the results for nonlinear shell theory.

Let (r,θ,z) denote a set of cylindrical coordinates and consider a homogeneous, elastically isotropic plate that occupies the region $0\leqslant r\leqslant R$, $-H\leqslant z\leqslant H$. Let the plate be free of body forces and edge tractions but subject to self-equilibrating normal tractions on its upper and lower faces. The linear equations of elasticity may be expressed as three equilibrium equations for the six independent components $(\sigma_r, \tau, \sigma_\theta, \tau_r, \tau_\theta, \sigma)$ of the symmetric stress tensor plus six stress-strain relations with the strains expressed in terms of the components (u,v,w) of the displacement vector. Let $\rho=r/R$ and $\zeta=z/H$. Then the boundary conditions read

$$\sigma(\rho,\theta,\pm 1)=\pm \tfrac{1}{2}H^2\sigma_o p(\rho,\theta),\quad \tau_r(\rho,\theta,\pm 1)=\tau_\theta(\rho,\theta,\pm 1)=0 \tag{3.1}$$

$$\sigma_r(1,\theta,\zeta)=\tau(1,\theta,\zeta)=\tau_r(1,\theta,\zeta)=0, \tag{3.2}$$

where σ_o is a reference stress chosen so that $|p|\leqslant 1$. The boundary conditions induce a state of pure bending in which $(\sigma_r,\tau,\sigma_\theta,\sigma,u,v)$ are odd in ζ and (τ_r,τ_θ,w) are even.

Goldenveiser's approach, following earlier work by Friedrichs and Dressler [18] and Green [11], is to express each unknown as the sum of a "basic" or interior contribution plus two distinct "auxiliary" or edge zone contributions.

The edge zone contributions are expressed in terms of the scaled variable $\zeta=(R-r)/H\equiv\varepsilon^{-1}(1-\rho)$ so that, for example,

$$\sigma_r(\rho,\theta,\zeta;\varepsilon)=\sigma_o[\Sigma_r(\rho,\theta,\zeta;\varepsilon)+\tilde{\sigma}_r(\xi,\theta,\zeta;\varepsilon)+\hat{\sigma}_r(\xi,\theta,\zeta;\varepsilon)]$$

$$\text{and } u(\rho,\theta,\zeta;\varepsilon)+(R/E)[U(\rho,\theta,\zeta;\varepsilon)+\tilde{u}(\xi,\theta,\zeta;\varepsilon)+\hat{u}(\xi,\theta,\zeta;\varepsilon)].$$

For a traction free edge, Goldenveiser [19] assumes the following formal asymptotic expansions

$$(\Sigma_r,T,\Sigma_\theta,T_r,T_\theta,\Sigma,U,V,W)$$

$$\sim\sum_0^\infty\varepsilon^n(\Sigma_r^n,T^n,\Sigma_\theta^n,\varepsilon T_r^n,\varepsilon T_\theta^n,\varepsilon^2\Sigma^n,U^n,V^n,\varepsilon^{-1}W^n) \tag{3.3}$$

$$(\tilde{\sigma}_r,\ldots,\tilde{W})\sim\sum_0^\infty\varepsilon^n(\varepsilon\tilde{\sigma}_r^n,\tilde{\tau}^n,\varepsilon\tilde{\sigma}_\theta^n,\varepsilon\tilde{\tau}_r^n,\tilde{\tau}_\theta^n,\varepsilon\tilde{\sigma}^n,\varepsilon^2\tilde{u},\varepsilon\tilde{v},\varepsilon^2\tilde{w}) \tag{3.4}$$

$$(\hat{\sigma}_r,\ldots,\hat{W})\sim\varepsilon\sum_0^\infty\varepsilon^n(\hat{\sigma}_r^n,\varepsilon\hat{\tau}^n,\hat{\sigma}_\theta^n\ \hat{\tau}_r^n,\varepsilon\hat{\tau}_\theta^n,\hat{\sigma}^n,\varepsilon\hat{u}^n,\varepsilon^2\hat{v}^n,\varepsilon\hat{w}^n). \tag{3.5}$$

The edge zone contributions are assumed to vanish exponentially as $\zeta\to\infty$.

When these representations are substituted into the elasticity equations and their assumed asymptotic character accounted for, there results an infinite sequence of differential equations for each infinite sequence of coefficients $\{\Sigma_r^n,\ldots,W^n\},\{\tilde{\sigma}_r^n,\ldots,\tilde{w}^n\},\{\hat{\sigma}_r^n,\ldots,\hat{w}^n\}$. Furthermore, the boundary conditions (3.1) and (3.2) imply that for $\zeta=\pm1$,

$$\Sigma^o=\pm\tfrac{1}{2}p,\quad(\Sigma^{n+1},T_r^n,T_\theta^n)=0 \tag{3.6}$$

$$(\tilde{\tau}_\theta,\tilde{\tau}_\theta^1,\tilde{\tau}_\theta^{n+2}+\hat{\tau}_\theta^n,\tilde{\tau}_r^n+\hat{\tau}_r^n,\tilde{\sigma}^n+\hat{\sigma}^n)=0 \tag{3.7}$$

and that for $\rho=1$ and $\xi=0$:

$$(\Sigma_r^o,T^o+\tilde{\tau}^o,T^1+\tilde{\tau}^1,\Sigma_r^{n+1}+\tilde{\sigma}_r^n+\hat{\sigma}_r^n,T^{n+2}+\tilde{\tau}^{n+2}+\hat{\tau}^n,T_r^n+\tilde{\tau}_r^n+\hat{\tau}_r^n)=0 \tag{3.8}$$

where $n=0,1,2,\ldots$.

The equations for the interior coefficients may be integrated systematically with respect to ζ. Application of the face boundary conditions (3.6) leads, in the first instance, to the classical equation of plate bending

$$(2/3)\Delta\Delta W^o=(1-\nu^2)p,\quad\Delta W^o=W^o_{,\xi\xi}+W^o_{,\zeta\zeta}. \tag{3.9}$$

All of the remaining lowest order interior coefficients are expressible in terms of W^o; in particular

$$\Sigma_r^o=-(1-\nu^2)^{-1}\zeta[W^o_{,\rho\rho}+\nu(\rho^{-1}W^o_{,\rho}+\rho^{-2}W^o_{,\theta\theta}]\equiv2/3\zeta M_r^o(\rho,\theta) \tag{3.10}$$

$$T^{o}=(1+\nu)^{-1}\zeta[\rho^{-2}W^{o}_{,\theta}-\rho^{-1}W^{o}_{,\rho\theta}]\equiv 2/3\zeta H^{o}(\rho,\theta) \tag{3.11}$$

$$T^{o}_{r}=-\frac{1}{2}(1-\nu^{2})^{-1}(1-\zeta^{2})(\Delta W^{o})_{,\rho}\equiv 3/4\ (1-\zeta^{2})Q^{o}_{r}(\rho,\theta). \tag{3.12}$$

The first of the edge boundary conditions in (3.8), namely $\Sigma^{o}_{r}=0$, yields only one of the two boundary conditions needed for W^{o}. To obtain the second, the edge zone solutions must be considered.

The infinite sequence of differential equations for the set of edge zone coefficients $(\tilde{\sigma}_{r},\ldots,\tilde{w})$ can be grouped into sets which resemble the nonhomogeneous St.-Venant equations for the torsion of a prism whose cross-section is the semi-infinite strip $\xi\geq 0, |\zeta|\leq 1$. Likewise the differential equations for the coefficients $(\hat{\sigma}_{r},\ldots,\hat{w})$ can be grouped into sets which resemble the nonhomogeneous equations of plane strain for the same semi-infinite strip. The solutions of the torsion and plane strain problems are coupled through the nonhomogeneous terms in the differential equations as well as through the boundary conditions (3.7) and (3.8) which also link these solutions with the interior solutions. It should be noted that in the edge zone differential equations, θ appears only as a parameter.

In order that the edge zone solutions decay as $\xi\to\infty$, it is necessary that the forces and moments applied to the boundary of the semi-infinite strip be equilibrated by the non-homogeneous terms in the torsion and plane strain equilibrium equations. These integral conditions yield, ultimately, the additional boundary conditions needed for the various interior solutions. For example, the Kirchhoff boundary condition that relates the shear stress resultant Q^{o}_{r} and the derivative along the edge of the twisting stress couple H^{o} is obtained as follows.

The solution of the lowest order torsion problem may be expressed in terms of a stress function ψ^{o}, where

$$\Delta\psi^{o}=0, \quad \psi^{o}_{,\zeta}(\xi,\pm 1)=0, \quad \psi^{o}_{,\xi}(0,\zeta)=-\zeta \tag{3.13}$$

and

$$\tilde{\tau}^{o}= -2/3\zeta H^{o}(1,\theta)\psi^{o}_{,\xi}, \quad \tilde{\tau}^{o}_{\theta}= -2/3\zeta H^{o}(1,\theta)\psi^{o}_{,\zeta} \tag{3.14}$$

The lowest order equation for equilibrium in the ζ-direction for the plane strain problem is

$$(\hat{\tau}^{o}_{r}+\tilde{\tau}^{o}_{r})_{,\xi} + (\hat{\sigma}^{o}+\tilde{\sigma}^{o})_{,\zeta}= -\tilde{\tau}^{o}_{\theta,\theta}\equiv R^{o}_{\zeta}. \tag{3.15}$$

From the last of the boundary conditions (3.7) and (3.8), the condition that the net forces in the ζ-direction add to zero, to lowest order, is

$$-\int_{-1}^{1}[T^{o}_{r}(1,\theta,\zeta) + \int_{0}^{\infty} R^{o}_{\zeta}(\xi,\theta,\zeta)d\xi]d\zeta=0. \tag{3.16}$$

With the aid of (3.12) and (3.13) to (3.15), (3.16) reduces to

$$Q^{o}_{r} + H^{o}_{,\theta}= 0 \text{ at } \rho=1, \tag{3.17}$$

which is the second boundary condition for W^o. It is important to note that one never needs to actually solve for ψ^o to obtain this result.

GOLDENVEISER'S EXTENSION AND KOITER'S SIMPLIFICATION OF THE PRECEDING RESULTS

The solution for $(\Sigma_r^1, \ldots, W^1)$ reduces to the solution of a biharmonic equation for W^1. To obtain boundary conditions for W^1 one again considers the integral conditions of overall equilibrium necessary to guarantee decaying edge zone solutions. To evaluate these, one must solve explicitly for ψ^o (which is easily done) but needs only to consider the form of the solution of the lowest order plane strain problem. After a straightforward but tedious analysis, there results the refined boundary conditions of Goldenveiser [19]:

$$M_r^1 = AH,_\theta^o, \quad Q_r^1 + H,_\theta^1 + AH,_\theta^o = 0, \tag{4.1}$$

where A=1.260...is computed from the solution for ψ^o. The details of the calculations leading to (4.1) may be found in a report by Van der Heijden [20].

Goldenveiser's results may be restated in the following useful way. Consider a plate of radius R and thickness 2H subject to a self-equilibrated normal pressure p but otherwise free of surface and edge tractions. Solve the classical equation of plate bending subject to the refined boundary conditions.

$$M_r - A(H/R)H,_\theta = 0, \quad Q_r + H,_\theta + A(H/R)H,_\theta = 0 \text{ at } \rho=1. \tag{4.2}$$

Then the stresses in the interior of the plate, to within a relative error of $O(H^2/R^2)$, are given by the formulas for Σ_r^o, T^o, etc. but with W^o replaced by W. Moreover, in the edge zone of the plate, the dominant stresses, to within a relative error of $O(H/R)$, are given by these same formulas except that T^o is replaced by $T^o+\tilde{T}^o$, and T_θ^o is replaced by $\tilde{\tau}_\theta^o$, where $\tilde{\tau}^o$ and $\tilde{\tau}_\theta^o$ are given by (3.14)

These results are simple and satisfying. Though derived for, perhaps, the simplest, non-trivial problem imaginable, their qualitative implications for shells with free edges undergoing large deformations is clear, namely 1), the most importnat refinement of the classical shell equations are in the boundary conditions and 2), the dominant stresses near a free edge can be inferred from the solution of the shell equations and the solution of a torsion problem for a semi-infinite strip. To give these statements a quantitative form via an asymptotic analysis would seem to be a formidable task.

The problem of refining the Kirchhoff boundary conditions at a free edge has, fortunately, been solved by Koiter [15] in an alternate way, using an ingenious energy argument. As Danielson [21], and Koiter [22] have shown, the three-dimensional tangential shear stress predicted by shell theory at a free edge does not vanish, even though the Kirchhoff boundary conditions are satisfied exactly. Thus the conventional strain energy expression of shell theory overestimates the torsional energy in the neighborhood of a free edge. To assess this error, Koiter considers the torsional rigidity of a flat strip whose thickness is equal to that of the shell. By comparing this expression with that given by classical plate theory he is able to identify an edge zone correction factor which is proportional to the twist per unit length of the edge of the strip. The torsional energy associated with this term is therefore

expressible as a line integral. For an arbitrary shell with a smooth edge curve Koiter argues that one merely needs to insert an appropiate expression for the edge twisting per unit length for the shell into this line integral and then subtract this expression from the conventional surface integral for the shell energy.

Koiter's result may be of limited practical value. If the shell has other edges that are not free of stress, it is most likely that the associated shell boundary conditions cannot be refined because the corresponding boundary conditions of elasticity theory cannot be determined precisely. The shell equations are elliptic, hence the influence of boundary conditions extend everywhere, and it would be inconsistent to use refined boundary conditions at a free edge but unrefined ones at another edge.

The results of this section also imply that so-called thick shell theories are meaningless if applied to homogeneous shells with edges. We should note, however, that Van der Heijden has shown that Reissner's latest thick plate theory [23] does give fairly good numerical results for stress concentration factors for circular holes in infinite plates.

THE DIRECT APPROACH TO SHELL THEORY

Here and in the following section we mention briefly — space limitations permit no more — some recent work concerning different formulations, implications, simplifications and the reduction of certain problems of the now generally accepted equations of first-approximation shell theory.

Formulations of the Nonlinear Theory

A strictly mechanical theory of shells may be expressed entirely in terms of the midsurface displacement components [5]. If dynamic effects are excluded, alternate formulations are possible in terms of the components of a stress function and rotation vector [8], or in terms of stress resultants and bending strains [15]. In the last case, any displacement boundary conditions need to be reformulated in terms of strains [24,25]. This in itself has advantages, for it automatically leads to the boundary conditions for inextensional deformation and, in the linear theory, it gives boundary conditions that are the geometric analogues of the Kirchhoff conditions.

Thermodynamic Considerations

These are important for at least three reasons. 1) heating a shell may cause it to fail, buckle, or vibrate; 2) the best justification of the static approach to stability for a continuous body is a thermodynamic one; and 3) the coupling of mechanical and thermal effects produces damping.

There is a plethora of papers on 1) that we shall not attempt to review; a few texts give a discussion of the underlying ideas. The thermodynamic aspects of stability in general elastic systems are discussed in [26,27,28]. These results are directly transferable to shell theory. The specific form and role of the laws of thermodynamics in shell theory are discussed in [10]. The effect of thermal damping on the free vibrations of shells is considered in [29] where it is also shown that, because the damping is light, perturbation

methods may be used to advantage.

Variational Principles

A problem of long standing in nonlinear elasticity has been to formulate a principle of complementary energy. Recent work [30,31,32] has established conditions under which this is possible. In particular, in [33] and [34], these results have been applied to the nonlinear von Karman plate equations and Marguerre shallow shell equations to obtain upper and lower bounds on an associated energy functional.

SOME NEW RESULTS IN LINEAR SHELL THEORY

Shells As Beams

For general cylindrical shells and shells of revolution, one may consider special classes of solutions that, in a St. Venant sense, correspond to the stretching, bending, twisting, and flexure of a beam. In many cases the resulting equations can be solved explicitly. See [35,36].

Reduction of the Governing Equations

The shell equations constitute a system of eighth order. For analytical purposes, especially for the application of perturbation methods, it is often convenient to attempt to express these equations as two coupled fourth order equations. (A single eighth order equation destroys the very useful static-geometric duality). Such reductions have been found for spherical, general cylindrical, and minimal shells as well as for shells of revolution. A reduction for arbitrary, non-developable shells is also possible, but does involve some loss of accuracy. See [37] where other references are cited.

Membrane Theory

It is well known that shells with the proper shape and boundary support can be analyzed with good accuracy by membrane theory. The details of such an approach are spelled out in a very general but useful way in [38].

Cracks and Cutouts

Shells may contain cutouts by design and cracks by accident. In practice the dimensions of these cracks and cutouts is apt to be small compared to some characteristic geometric dimension of the shell, permitting shallow shell theory to be applied. The calculation of the stresses has been reduced to the solution of coupled singular integral equations [39] that have been solved numerically for several important problems. See [40] and the references cited there.

Pointwise Estimates For Approximate Solutions

The Prager-Synge hypercircle method is useful for constructing approximate solutions to linear shell problems, and provides mean square error estimates for the approximate stress field. More desirable are pointwise estimates for both the approximate stress field and the approximate displacement field. For recent work on this problem see [41] and the references cited

therein.

Wave Propagation, Asymptotics, and St-Venant's Principle

These are three additional areas in which there has been significant recent progress but which cannot be reviewed for lack of space.

Acknowledgement

This work was supported by the National Science Foundation under grant MPS-73-08650A02.

REFERENCES

1. Librescu, L., Elastostatics and Kineties of Anisotropic and Heterogeneous Shell-Type Structures, Noordhoff, 1975.

2. Stein, M., "Some Recent Advances in the Investigation of Shell Buckling," AIAA J., 6:2339-2345 (1968).

3. Hutchinson, J.W. and Koiter, W.T., "Postbuckling Theory," Appl. Mech. Revs., 23: 1353-1366 (1970).

4. Sanders, J.L., Jr., "An Improved First Approximation Theory of Thin Shells", NASA Rept. No. 24, 1959.

5. Ericksen, J.L., and Truesdell, C.A. "Exact Theory of Stress and Strain in Rods and Shells," Arch. Rat. Mechs. & Anal., 1:295-323 (1958).

6. Serbin, H., "Quadratic Invariants of Surface Deformation and the Strain Energy of Thin Elastic Shells," J. Math. & Phys., 4:838-851 (1963).

7. Budiansky, B., "Notes on Nonlinear Shell Theory," J. Appl. Mechs., 35: 393-401 (1968).

8. Simmonds, J.G. and Danielson, D.A., "Nonlinear Shell Theory with Finite Rotation and Stress-Function Vectors," J. Appl. Mechs., 39:1085-1090 (1972).

9. Reissner, E., "Linear and Nonlinear Theory of Shells," Thin Shell Structures, Ed. Y.C. Fung and E.E. Sechler, Prentice-Hall, 1974, pp. 29-44.

10. Naghdi, P.M., "The Theory of Shells and Plates," Handbuch der Physik, 2nd Ed., Vol VIa/2, Springer-Verlag, 1972.

11. Green, A.E., "Boundary-Layer Equations in the Theory of Thin Elastic Shells," Proc. Roy. Soc. London, A269:481-491 (1962).

12. Johnson, M.W., and Reissner, E., "On the Foundations of the Theory of Thin Elastic Shells," J. Math & Phys.,37:375-392 (1958).

13. Cicala, P., Systematic Approximation Approach to Linear Shell Theory, Levrotto & Bella, 1966.

14. Van der Heijden, A., "On the Calculation of the Stress and Displacement Field in a Plate with a Circular Hole Loaded by Bending Couples at Infinity," Rept. 518, Lab. for Engr. Mechs., Univ. of Delft, 1973.

15. Koiter, W.T., and Simmonds, J.G., "Foundations of Shell Theory," Proc. 13th Int. Cong. Theor. & Appl. Mechs., Springer-Verlag, 1973, pp. 150-176.

16. Koiter, W.T., "On the Foundations of the Linear Theory of Thin Elastic Shells," Proc. Kon. Ned. Ak. Wet., B73:169-195 (1970).

17. Novozhilov, V.V., The Theory of Thin Shells, Noordhoff, 1959.

18. Friedrichs, K.O., and Dressler, R.F., "A Boundary-Layer Theory of Elastic Plates, "Comm. Pure & Appl. Math, 14:1-33 (1961).

19. Goldenveiser, A.L., "The Principles of Reducing Three-Dimensional Problems of Elasticity to Two-Dimensional Problems of the Theory of Plates and Shells," Proc. 11th Int. Cong. Appl. Mechs., Springer-Verlag, 1966, pp. 306-311.

20. Van der Heijden, A., "On the Derivation of the Modified Boundary Conditions for a Free Edge of an Infinite Plate with a Circular Hole,...," Rept. 502, Lab. for Engr. Mechs., Univ. of Delft, 1973.

21. Danielson, D.A., "Improved Error Estimates in the Linear Theory of Thin Elastic Shells," Proc. Kon. Ned. Ak. Wet., B74:294-300 (1971).

22. Koiter, W.T., "On the Mathematical Foundation of Shell Theory," Actes Cong. Int. Math., 3:123-130 (1970).

23. Reissner, E., "On Transverse Bending of Plates Including the Effect of Transverse Shear Deformation," Int. J. Solids & Structures, 11:569:573 (1975).

24. Wan, F.Y.M., "Two Variational Theorems in Thin Shells," J. Math & Phys., 47:429-431 (1968).

25. Chernykh, K.F. and Mikhailovskii, E.I., "Separation of Boundary Conditions in Linear Shell Theory," Probs. of Kydrodynamics and Cont. Mechs., SIAM, 1969, pp. 170-177.

26. Gurtin, M.E., "Thermodynamics and Stability," Arch. Rat. Mechs, and Anal., 59:63-96 (1975).

27. Koiter, W.T., "On the Thermodynamic Backround of Elastic Stability Theory," Probs. of Hydrodynamics and Cont. Mechs., SIAM, 1969, pp. 423-433.

28. Ericksen, J.L. "A Thermo-Kinetic View of Elastic Stability Theory," Int. J. Solids & Structures, 2:573:580 (1966).

29. Adelman, H.A., "Coupled Thermoelastic Vibrations of Thin Shells of Revolution," Ph.D. thesis, Univ. of Va., 1974.

30. Zubov, L.M., "The Stationary Principle of Complementary Work in Nonlinear Theory of Elasticity," J. Appl. Math & Mechs., 34:228-232 (1970).

31. Fraeijs de Veubeke, B., "A New Variational Principle for Finite Elastic Displacements," Int. J. Engr. Sci, 10:745-763 (1972).

32. Koiter, W.T., "On the Principle of Stationary Complementary Energy in the Nonlinear Theory of Elasticity," SIAM J. Appl. Math., 25:424-434 (1973).

33. Stumpf, H., "Dual Extremum Principles and Error Bounds in the Theory of Plates with Large Deflections," Arch. Mech., 27:485-496 (1975).

34. Stumpf, H., "Generating Functionals and Extremum Principles in Nonlinear Elasticity with Applications to Nonlinear Plate and Shallow Shell Theory," Joint IUTAM/IMU Sympos. on Appl. of Methods of Fcl. Anal. to Probs. of Mechs., 1975.

35. E. Reissner, "On Stretching, Bending, Twisting, and Flexure of Cylindrical Shells," to appear in Int. J. Solids & Structures.

36. Wan, F.Y.M., "Laterally loaded Elastic Shells of Revolution," Ing. Arch., 42: 245-258 (1973).

37. Simmonds, J.G., "Reduction of the Linear Sanders-Koiter Shell Equations for Nondevelopable Midsurfaces to Two Coupled Equations," J. Appl. Mechs., 42:511-513 (1975).

38. Steele, C.R., "Membrane Solutions for Shells with Edge Constraints," J. Engr. Mech. Div., Proc. A.S.C.E., 100:497-510 (1974).

39. Sanders, J.L., Jr., "Cutouts in Shallow Shells," J. Appl. Mechs,37:374-383 (1970).

40. Tsai, C.J., and Sanders, J.L.,Jr., "Elliptical Cutouts in Cylindrical Shells," J. Appl. Mechs., 42:326-334 (1975).

41. Antes, H., "Punktweise Eingrenzung bei Flachen Schalen," Acta Mechanica, 23:235-245 (1975).

FLUID-PLASTICITY OF THIN CYLINDRICAL SHELLS*

Dusan Krajcinovic
University of Illinois at Chicago Circle

M. G. Srinivasan and Richard A. Valentin
Argonne National Laboratory

SUMMARY

The paper considers dynamic plastic response of a thin cylindrical shell, immersed in a potential fluid initially at rest, subjected to internal pressure pulse of arbitrary shape and duration. The shell is assumed to respond as a rigid-perfectly plastic material while the fluid is taken as inviscid and incompressible. The fluid back pressure is incorporated into the equation of motion of the shell as an added mass term. Since arbitrary pulses can be reduced to equivalent rectangular pulses, the equation of motion is solved only for a rectangular pulse. The influence of the fluid in reducing the final plastic deformation is demonstrated by a numerical example.

FORMULATION OF THE PROBLEM

Consider a rigid-ideally plastic, thin-walled, circular, cylindrical shell of infinite length. The shell is surrounded by a pool of potential (inviscid and incompressible) fluid infinitely extended in all directions. The shell is subjected to an internal pressure pulse $P(z,t)$, varying both along the axis and with time. $P(z,t)$ is further assumed to be axisymmetric and symmetric in z with respect to $z = 0$ (fig. 1).

This paper examines the influence of the fluid in reducing the plastic (residual) deformation of the shell. It is known that the pressure with which potential fluid resists the motion of a deforming solid can be considered as an increase in the inertia of the solid. Therefore in order to solve the problem it is necessary to establish the so-called effective mass consisting of the actual mass of the shell and the added (virtual) mass reflecting the fluid resistance. Then the problem is reduced to the analysis of a shell deforming in vacuum. For the sake of continuity, we will adopt the notation introduced in reference 1.

GOVERNING EQUATIONS

The equation of motion of the shell is:

*Research performed under the auspices of the U. S. Energy Research and Development Administration

$$\frac{\partial^2 M}{\partial z^2} = P - P_f - \frac{N}{R} - \rho H \frac{\partial V}{\partial t} \tag{1}$$

where M is the axial bending moment, N the circumferential (hoop) normal force, R, H and ρ the radius, the wall thickness and the mass density of the shell respectively, V the radial velocity of the points on the middle surface of the shell, and $P(z,t)$ and $P_f(z,t)$ are the externally applied pressure pulse and the back pressure of the fluid resisting the motion of the shell respectively.

We assume that the yield condition in the M,N space is defined by the limited interaction curve of fig. 2. The implications of this assumption are discussed in detail by Drucker (ref. 2) and Hodge (ref. 3). The yield values M_y and N_y are given by

$$M_y = \frac{1}{4} HRP_o \qquad N_y = RP_o \tag{2}$$

where

$$P_o = \sigma_y \frac{H}{R} \tag{3}$$

with σ_y being the yield stress.

It is known (see, for example, ref. 1) that four different phases (modes) of plastic deformation may occur during the motion. We will consider herein only one of these phases which occurs for all possible types of loading, though this restricts the magnitude of the loading to a certain limit. In the considered phase the deformation is characterized by a stationary plastic hinge circle at $z = 0$ and two moving hinge circles at $z = \pm \zeta(t)$.

It can be shown (see, for example, Eason and Shield (ref. 4)) that the plastic regimes (see fig. 2) are as follows:

$$\begin{aligned}
z = 0: &\quad M = -M_y, &\quad N = N_y &\qquad \text{Regime A} \\
z = \zeta: &\quad M = M_y, &\quad N = N_y &\qquad \text{Regime B} \\
0 < z < \zeta: &\quad -M_y < M < M_y, &\quad N = N_y &\qquad \text{Regime AB}
\end{aligned} \tag{4}$$

Thus, from the normality of the strain-rate vector to the yield surface,

$$\frac{\partial^2 V}{\partial z^2} = 0 \quad , \qquad V > 0 \quad \text{for} \quad 0 < z < \zeta \tag{5}$$

For this deformation mode the velocity, $V(z,t)$, is therefore a linear function of z, i.e.,

$$V(z,t) = \begin{cases} V_o(t) \left\{ 1 - \dfrac{z}{\zeta(t)} \right\} & 0 < z \leq \zeta \\ 0 & z > \zeta \end{cases} \tag{6}$$

In the above equations and in the sequel because of symmetry it is enough to consider only half of the shell $z \geq 0$.

DETERMINATION OF THE ADDED MASS

Before attempting to solve equation (1), the backpressure $P_f(z,t)$ should be determined as a function of $V(z,t)$ and its derivatives. The equation governing the flow of the potential fluid is in polar coordinates

$$\frac{\partial^2 F}{\partial r^2} + \frac{1}{r}\frac{\partial F}{\partial r} + \frac{\partial^2 F}{\partial z^2} = 0 \quad \text{in} \quad r \geq R \tag{7}$$

where $F(r,z,t)$ is the fluid velocity potential.

As the shell is impermeable, the velocities of the fluid and the shell at the points of contact must be identical, i.e.,

$$\frac{\partial F}{\partial r} = V \quad \text{at} \quad r = R \tag{8}$$

Furthermore, from the radiation principle,

$$V \to 0 \ , \quad \frac{\partial F}{\partial r} \to 0 \ , \quad \frac{\partial F}{\partial z} \to 0 \quad \text{as} \quad \max(r,z) \to \infty \tag{9}$$

Once the fluid velocity potential is determined from the Laplace equation (7), subject to the boundary conditions (eqs. (8) and (9)) the pressure exerted by the fluid on the shell can be computed from the Cauchy integral,

$$P_f(z,t) = -\rho_f \frac{\partial F}{\partial t} \quad \text{at} \quad r = R \tag{10}$$

where ρ_f is the mass density of the fluid.

The equations (7) and (10) imply the assumption that the perturbations about average values can be neglected.

As a further approximation, we will assume that the functional relation between $P_f(z,t)$ and ζ is not sensitive to the time dependence of ζ, and hence ζ may be treated as a constant for the determination of this relation. Then in view of equations (6), (7) and (8), we may write

$$F(r,z,t) = V_o(t)\, f(r,z) \tag{11}$$

and from equation (10),

$$P_f(z,t) = -\rho_f f(R,z) \frac{dV_o}{dt} \tag{12}$$

where $-\rho_f f(R,z)$ is the added (virtual) mass arising due to the resistance of the fluid being displaced by the shell.

Substituting equations (11) and (6), (with ζ being constant) into equations (7) to (9), it follows

$$\frac{\partial^2 f}{\partial r^2} + \frac{1}{r}\frac{\partial f}{\partial r} + \frac{\partial^2 f}{\partial z^2} = 0 \tag{13}$$

subject to

$$\frac{\partial f}{\partial r} = \begin{cases} \left(1 - \frac{z}{\zeta}\right) & \text{at } r = R, \quad z \leq \zeta \\ 0 & \text{at } r = R, \quad z > \zeta \end{cases} \tag{14}$$

and

$$f \to 0 \quad , \quad \frac{\partial f}{\partial r} \to 0 \quad , \quad \frac{\partial f}{\partial z} \to 0 \quad \text{as} \quad \max(r,z) \to \infty \tag{15}$$

The details of the solution of equation (13) are omitted herein for the sake of brevity. A closed form integral solution is obtained after introducing the Fourier cosine transform. The argument of this integral is rather complicated and the integration is performed in three stages using asymptotic formulae and Filon's method, subject to the restriction, $\zeta \leq R$ which is subsequently seen to be not severe. In order to make this numerical solution amenable for substitution into equation (1), the result is subjected to a series of polynomial regression analyses. Finally we obtain

$$f(R,z) = -R\left\{g_0\left(\frac{\zeta}{R}\right) + g_1\left(\frac{\zeta}{R}\right)\frac{z}{\zeta}\right\} \tag{16}$$

where

$$g_0(x) = \beta_0 + \beta_1 x + \beta_2 x^2 + \beta_3 x^3 \tag{17}$$

and

$$g_1(x) = \alpha_0 + \alpha_1 x + \alpha_2 x^2 + \alpha_3 x^3 \tag{18}$$

with

$$\begin{aligned} \alpha_0 &= .004994512 & \beta_0 &= .02050149 \\ \alpha_1 &= -.5420473 & \beta_1 &= 1.664447 \\ \alpha_2 &= -.1058701 & \beta_2 &= -1.105309 \\ \alpha_3 &= .1627719 & \beta_3 &= .4096600 \end{aligned} \tag{19}$$

Note α_i and β_i are dimensionless constants that do not depend on the shell/fluid parameters.

PLASTIC DEFORMATION OF THE SHELL

Equation (1) now becomes, in view of equations (2), (6), (12) and (16),

$$\frac{\partial^2 M}{\partial z^2} = P(z,t) - P_o - \left[\left\{\rho H + \rho_f R g_0\left(\frac{\zeta}{R}\right)\right\} - \left\{\rho H - \rho_f R g_1\left(\frac{\zeta}{R}\right)\right\}\frac{z}{\zeta}\right]\frac{dV_o}{dt} \quad \text{in } 0 < z < \zeta \tag{20}$$

In equation (20), $\zeta = \zeta(t)$. For arbitrary $P(z,t)$ the above equation may only be solved by numerical methods. As a first step in simplifying the work, the approach introduced by Youngdahl (ref. 1) will be used to approximate a complex loading function by (i.e., correlate it to) a simple rectangular pulse. Since the standard limit analysis of the shell is independent of any surrounding medium, the method given by Youngdahl (ref. 1) to determine the equivalent rectangular pulse does not need any modification in this case. Thus correlated, $P(z,t)$ can be expressed as

$$\begin{aligned} P(z,t) &= P_e \qquad |z| \le L_e \quad \text{and} \quad 0 \le t \le t_e \\ P(z,t) &= 0 \qquad |z| > L_e \quad \text{or} \quad t > t_e \end{aligned} \tag{21}$$

where P_e is the magnitude, t_e the duration and $2L_e$ the length of the loaded area of the equivalent rectangular pulse (see ref. 1 for their derivation).

For plastic deformation to occur, P_e must be greater than the limit load. This condition is expressed by (see ref. 1)

$$P_e > \frac{P_o}{2}\left(1 + \sqrt{1 + \frac{4RH}{L_e^2}}\right) \tag{22}$$

For the deformation to take place in the assumed phase, the following boundary conditions must be satisfied

$$\begin{aligned} M = -M_y \;, \quad \frac{\partial M}{\partial z} = 0 \quad \text{at} \quad z = 0 \\ M = M_y \;, \quad \frac{\partial M}{\partial z} = 0 \quad \text{at} \quad z = \zeta \end{aligned} \tag{23}$$

Further, the condition that the bending moment does not exceed M_y at the hinge circle at $z = \zeta$ implies

$$\frac{\partial^2 M}{\partial z^2} < 0 \quad \text{at} \quad z = \zeta \tag{24}$$

In addition the condition that the bending moment cannot be less than $-M_y$ at the hinge circle at $z = 0$ implies

$$\frac{\partial^2 M}{\partial z^2} > 0 \quad \text{at} \quad z = 0 \tag{25}$$

For the interval $0 \le t \le t_e$, a trial solution as in the case of a shell deforming in vacuum is assumed. This is taken in the form

$$\left.\begin{aligned} \zeta(t) &= z_1 \\ \text{and} \qquad V_o(t) &= \frac{K_1}{\rho H}\, t \end{aligned}\right\} \quad 0 \le t \le t_e \tag{26}$$

where z_1 and K_1 are constants. Substituting equation (26) into equation (20) and integrating twice subject to the boundary conditions (23) yields in the

end two equations for z_1 and K_1. These two can be reduced to:

$$\alpha(z_1)P_o z_1^2 + \{6 - 4\alpha(z_1)\}P_e L_e z_1 - \{6 - 3\alpha(z_1)\}(P_e L_e^2 + P_o RH) = 0 \tag{27}$$

and

$$K_1 = \frac{6\rho H(P_e L_e z_1 - P_e L_e^2 - P_o RH)}{z_1^2 \left\{\rho H - \rho_f R g_1\left(\frac{z_1}{R}\right)\right\}} \tag{28}$$

where

$$\alpha(z_1) = \frac{\rho H - \rho_f R g_1\left(\frac{z_1}{R}\right)}{\rho H + \rho_f R g_0\left(\frac{z_1}{R}\right)} \tag{29}$$

The inequalities (24) and (25) can be written in the form

$$P_o z_1^2 + K_1 \frac{\rho_f}{\rho}\frac{R}{H}\left\{g_0\left(\frac{z_1}{R}\right) + g_1\left(\frac{z_1}{R}\right)\right\} z_1^2 > 0 \tag{30}$$

and

$$4P_e L_e z_1 - P_e z_1^2 - 3P_e L_e^2 - 3P_o RH < 0 \tag{31}$$

From equations (17), (18) and (19) it is easily verified that inequality (30) is always satisfied. If inequality (31) is not satisfied motion cannot start in the phase assumed. When the inequality becomes an equality, P_e takes the bounding value. To determine the bounding value of P_e, the non-linear equations (27) and (31) should be solved simultaneously. This is done numerically. Figure 3 shows the range of values of P_e that satisfies inequalities (22) and (31) and hence gives rise to deformation in the assumed mode. For a P_e belonging to this range, the non-linear equation (27) may be solved numerically. Also it may be verified that the restriction $z_1 < R$ is always satisfied if $L_e < R$. Thus, the solution discussed in this paper is valid for $L_e < R$ and P_e satisfying inequalities (22) and (31).

For $t > t_e$, there is no internal pressure. Letting $P(z,t) = 0$ in equation (20), integrating it twice with respect to z and substituting the result into the boundary conditions (23), we arrive at the following equations

$$\frac{dV_o}{dt} = \frac{-P_o(\zeta^2 + 3RH)}{\zeta^2\left\{\rho H + \rho_f R g_0\left(\frac{\zeta}{R}\right)\right\}} \equiv \phi(\zeta) \tag{32}$$

$$\frac{d}{dt}\left(\frac{V_o}{\zeta}\right) = \frac{-6P_o RH}{\zeta^3\left\{\rho H - \rho_f R g_1\left(\frac{\zeta}{R}\right)\right\}} \equiv \psi(\zeta) \tag{33}$$

Equations (32) and (33) constitute a system of non-linear first order differential equations for V_o and ζ, the initial conditions being given by

$$\zeta(t_e) = z_1 \tag{34}$$

$$V_o(t_e) = \frac{K_1 t_e}{\rho H} \tag{35}$$

The above differential equations are valid only for $t_e \le t \le t_f$, where t_f is defined by

$$V_o(t_f) = 0 \tag{36}$$

We will denote

$$\zeta_f \equiv \zeta(t_f) \tag{37}$$

From equations (32) and (33), we can express V_o as,

$$V_o(t) = \frac{P_o}{\zeta\left(\frac{d\zeta}{dt}\right)}\left\{\frac{6RH}{\rho H - \rho_f R g_1\left(\frac{\zeta}{R}\right)} - \frac{3RH+\zeta^2}{\rho H+\rho_f R g_0\left(\frac{\zeta}{R}\right)}\right\} \tag{38}$$

From (36) and (37), we see that ζ_f can be obtained from the equation,

$$\frac{6RH}{\rho H - \rho_f R g_1\left(\frac{\zeta_f}{R}\right)} - \frac{3RH+\zeta_f^2}{\rho H+\rho_f R g_0\left(\frac{\zeta_f}{R}\right)} = 0 \tag{39}$$

Equation (39) can be solved numerically to obtain ζ_f. It is noted that ζ_f depends only on the shell parameters H and R and the density ratio ρ_f/ρ. Since ζ_f is the quantity that is known and not t_f, the equations (32) and (33) are now reformulated with ζ being the independent variable and $t(\zeta)$ and $V_o(\zeta)$ being the dependent variables. Thus,

$$\left.\begin{aligned} \frac{dV_o}{d\zeta} &= \frac{dt}{d\zeta}\,\phi(\zeta) \qquad (40)\\ \text{and}\quad \frac{d}{d\zeta}\left(\frac{V_o}{\zeta}\right) &= \frac{dt}{d\zeta}\,\psi(\zeta) \qquad (41)\end{aligned}\right\} \quad z_1 \le \zeta \le \zeta_f$$

The new initial conditions are

$$t(z_1) = t_e \tag{42}$$

and

$$V_o(z_1) = \frac{K_1 t_e}{\rho H} \tag{43}$$

Equations (40) and (41) are solved numerically. Finally, the maximum plastic deformation $U_o(t)$ can be obtained as,

$$U_o(t) = \frac{K_1 t^2}{2\rho H} \qquad 0 \le t \le t_e \tag{44}$$

and $$U_o(t) = U_o(t_e) + \int_{t_e}^{t} V_o(\bar{t})d\bar{t} \qquad 0 < t \le t_f$$

or $$U_o(t) = \frac{K_1 t_e^2}{2\rho H} + \int_{z_1}^{\zeta} V_o(\bar{\zeta}) \frac{dt}{d\bar{\zeta}} d\bar{\zeta} \qquad z_1 \le \zeta \le \zeta_f \tag{45}$$

The integral in equation (45) can be numerically evaluated after the numerical solutions $V_o(\zeta)$ and $t(\zeta)$ have been obtained.

For the special case in which z_1 coincides with ζ_f, the solution for $t > t_e$ discussed above is not valid. For this case, equations (32) and (33) with (35) yield,

$$\zeta = z_1 = \zeta_f \tag{46}$$

$$V_o(t) = (t - t_e)\phi(z_1) + \frac{K_1 t_e}{\rho H} \tag{47}$$

where $\phi(\zeta)$ is defined in equation (32). Note $\phi(z_1) < 0$. From equation (47) we see

$$t_f = t_e \left\{1 - \frac{K_1}{\rho H \phi(z_1)}\right\} \tag{48}$$

From equations (47) and (44) we can show that

$$U_o(t) = \frac{\phi(z_1)}{2} (t - t_e)^2 + \frac{K_1 t_e}{2\rho H} (2t - t_e) \tag{49}$$

Finally we have, for the maximum plastic deformation in this special case

$$U_o(t_f) = \frac{K_1 t_e^2}{2\rho H} \left(1 - \frac{K_1}{\rho H \phi(z_1)}\right) \tag{50}$$

NUMERICAL EXAMPLE

For a shell with $H/R = 1/36$, $L_e/R = 1/4$ surrounded by a fluid of $\rho_f/\rho = 1/10$, the complete numerical solution is determined for the admissible range of loads P_e. As is seen from figure 3, the range of P_e/P_o that will give rise to motion in the assumed phase is between: 1.33 and 2.97. The same range for a shell in vacuum is 1.33 to 2.19. Figure 4 shows the final maximum plastic deformation, $U_o(t_f)$, (non-dimensionalized as $\rho H U_o/P_o t_e^2$) as a function of P_e/P_o. For the sake of comparison the corresponding curve for a shell deforming in vacuum is also shown in the same figure.

In the numerical methods used, non-linear algebraic equations such as (27) and (39) were solved by Newton's iteration method and the system of

differential equations (40), (41) by a method using automatic step change (ref. 5).

REFERENCES

1. Youngdahl, C. K.: Correlating the Dynamic Plastic Deformation of a Circular Cylindrical Shell Loaded by an Axially Varying Pressure. Report ANL-7738, Argonne National Laboratory, 1970.

2. Drucker, D. C.: Limit Analysis of Cylindrical Shells Under Axially-Symmetric Loading. Proc. of the First Midwest Conf. on Solid Mech., 1953, pp. 158-163.

3. Hodge, P. G.: Limit Analysis of Rotationally Symmetric Plates and Shells. Prentice-Hall Inc., Englewood Cliffs, N.J., ch. 3, 1963.

4. Eason, G.; and Shield, R. T.: Dynamic Loading of Rigid-Plastic Cylindrical Shells. J. Mech. Phys. Solids, vol. 4, 1956, pp. 53-71.

5. Christianson, J.: Numerical Solution of Ordinary Simultaneous Differential Equations of 1st Order using a Method of Automatic Step Change. Numerische Mathematik, vol. 14, no. 4, 1970, pp. 317-324.

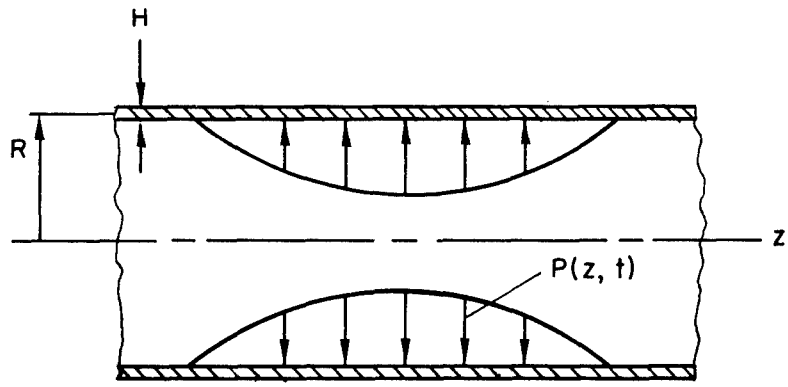

Figure 1.- Circular cylindrical shell immersed in fluid and loaded by internal pressure pulse.

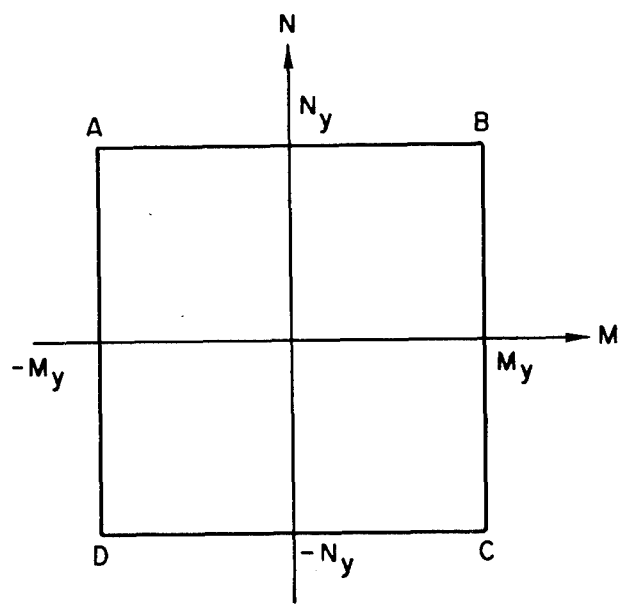

Figure 2.- Yield condition.

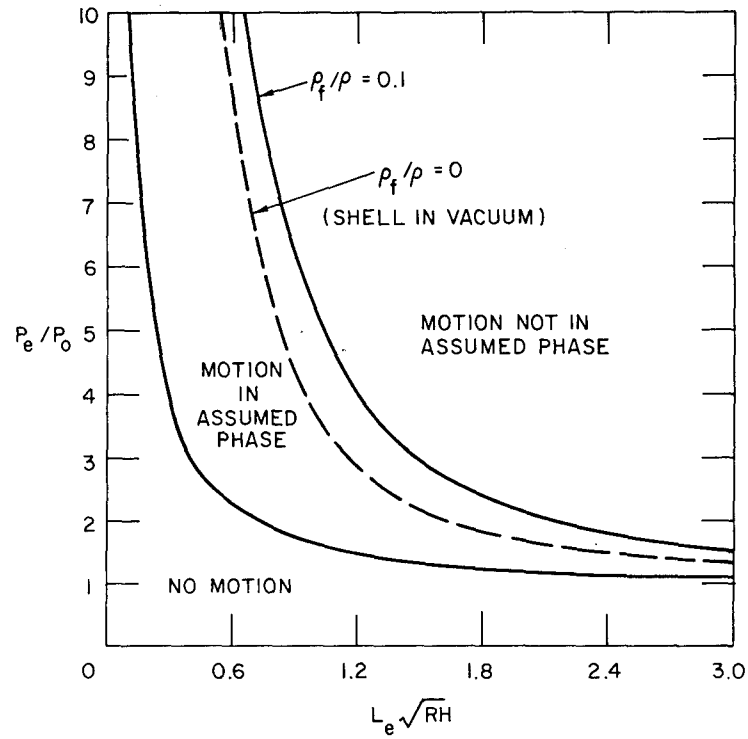

Figure 3.- Range of pulse intensity initiating motion in assumed phase.

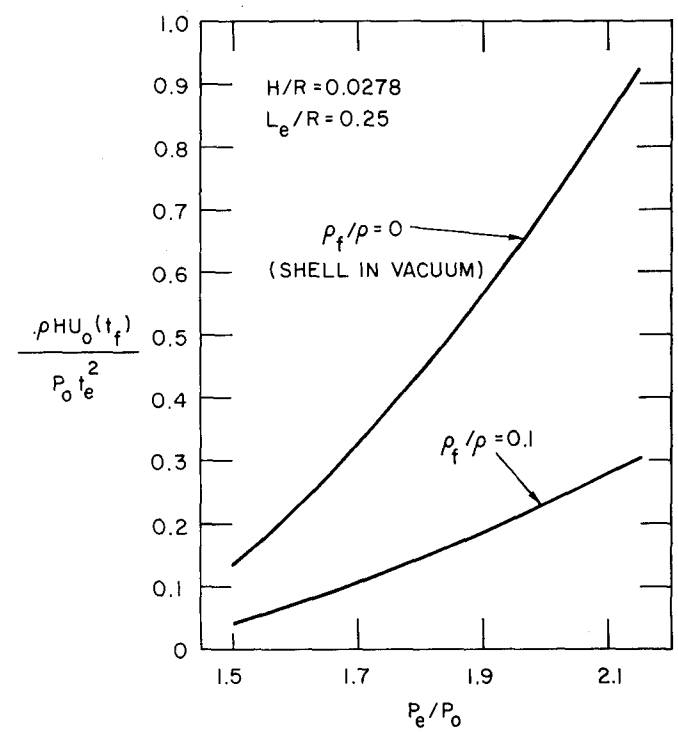

Figure 4.- Maximum plastic deformation as a function of pulse intensity.

THERMAL STRESSES IN A SPHERICAL PRESSURE VESSEL HAVING TEMPERATURE-DEPENDENT, TRANSVERSELY ISOTROPIC, ELASTIC PROPERTIES

T. R. Tauchert
University of Kentucky

SUMMARY

Rayleigh-Ritz and modified Rayleigh-Ritz procedures are used to construct approximate solutions for the response of a thick-walled sphere to uniform pressure loads and an arbitrary radial temperature distribution. The thermoelastic properties of the sphere are assumed to be transversely isotropic and nonhomogeneous; variations in the elastic stiffness and thermal expansion coefficients are taken to be an arbitrary function of the radial coordinate and temperature. Numerical examples are presented which illustrate the effect of the temperature-dependence upon the thermal stress field. A comparison of the approximate solutions with a finite element analysis indicates that Ritz methods offer a simple, efficient, and relatively accurate approach to the problem.

INTRODUCTION

Modern engineering structures are often subject to thermal environments in which the temperature causes significant variations in the thermal and mechanical properties of the material. Over certain temperature ranges the material may behave elastically, but have variable stiffness and thermal expansion characteristics. In addition, modern materials of construction (e.g. composites) often possess anisotropy and nonhomogeneity. While most classical thermoelastic solutions are not applicable to situations involving temperature-dependent anisotropic behavior, some progress has been made in this direction. For example, the problem of a hollow sphere with temperature-sensitive isotropic elastic properties has been studied by Nowinski (ref. 1) and Stanisic and McKinley (ref. 2). More recently Hata and Atsumi (ref. 3) investigated the response of a transversely isotropic sphere exposed to a sudden temperature rise on its internal surface.

In the present paper a transversely isotropic hollow sphere having temperature sensitivity and/or initial nonhomogeneity is considered. The variability of the thermoelastic properties may result from manufacturing processes, in which case the properties depend upon position but not temperature, or the nonhomogeneity may be a consequence of the materials' temperature sensitivity.

FORMULATION OF THE PROBLEM

Consider a hollow elastic sphere of inner radius r_1 and outer radius r_2, exposed to a temperature distribution $T(r)$ in addition to internal and external pressures, p_I and p_{II}, respectively. Owing to the spherical symmetry of the problem, the nonvanishing strain components depend upon the radial displacement u according to the relations

$$e_{rr} = \frac{du}{dr} \qquad e_{\phi\phi} = e_{\theta\theta} = \frac{u}{r} \tag{1}$$

Assuming transverse isotropy, the thermal stresses are related to the strains and temperature rise by

$$\begin{Bmatrix} \sigma_{rr} \\ \sigma_{\phi\phi} \\ \sigma_{\theta\theta} \end{Bmatrix} = \begin{Bmatrix} A_{11} \\ A_{12} \\ A_{12} \end{Bmatrix} e_{rr} + \begin{Bmatrix} A_{12} \\ A_{22} \\ A_{23} \end{Bmatrix} e_{\phi\phi} + \begin{Bmatrix} A_{12} \\ A_{23} \\ A_{22} \end{Bmatrix} e_{\theta\theta} - \int_0^T \begin{Bmatrix} \beta_1(T,r) \\ \beta_2(T,r) \\ \beta_2(T,r) \end{Bmatrix} dT \tag{2}$$

in which $A_{ij}(T,r)$ denote the elastic stiffnesses and $\beta_i(T,r)$ are the stress-temperature coefficients. Alternatively, the strains may be expressed in terms of the stresses and temperature as

$$\begin{Bmatrix} e_{rr} \\ e_{\phi\phi} \\ e_{\theta\theta} \end{Bmatrix} = \begin{Bmatrix} a_{11} \\ a_{12} \\ a_{12} \end{Bmatrix} \sigma_{rr} + \begin{Bmatrix} a_{12} \\ a_{22} \\ a_{23} \end{Bmatrix} \sigma_{\phi\phi} + \begin{Bmatrix} a_{12} \\ a_{23} \\ a_{22} \end{Bmatrix} \sigma_{\theta\theta} + \int_0^T \begin{Bmatrix} \alpha_1(T,r) \\ \alpha_2(T,r) \\ \alpha_2(T,r) \end{Bmatrix} dT \tag{3}$$

where $a_{ij}(T,r)$ and $\alpha_i(T,r)$ are the compliances and the coefficients of thermal expansion, respectively.

For convenience in later operations the following dimensionless quantities are introduced:

$$\left.\begin{array}{lll} \rho = r/r_2 & \rho_1 = r_1/r_2 & v = u/r_2 \\ \Theta = T/T_o & q_I = p_I/\beta_o T_o & q_{II} = p_{II}/\beta_o T_o \\ t_{\rho\rho} = \sigma_{rr}/\beta_o T_o & t_{\phi\phi} = \sigma_{\phi\phi}/\beta_o T_o & t_{\theta\theta} = \sigma_{\theta\theta}/\beta_o T_o \\ B_{ij}(\Theta,\rho) = A_{ij}(T,r)/\beta_o T_o & & b_{ij}(\Theta,\rho) = a_{ij}(T,r)\beta_o T_o \end{array}\right\} \tag{4}$$

$$\gamma_i(\Theta,\rho) = \beta_i(T,r)/\beta_o \qquad \varepsilon_i(\Theta,\rho) = \alpha_i(T,r)T_o \quad \Big)$$

in which β_o denotes an arbitrary reference stress-temperature coefficient and T_o represents some reference temperature.

In formulating the problem through the use of energy principles, we require specification of the total potential energy of the sphere. For the case of quasi-static loading, the *total potential energy* Π consists of the strain energy U plus the potential V_E of the external forces. General expressions for the strain energy in anisotropic, temperature-sensitive, elastic bodies are given in reference 4. Based upon these expressions the total potential energy for a transversely isotropic sphere with strains given by equation (1) is

$$\Pi = 4\pi\beta_o T_o r_2^3 \left\{ \int_{\rho_1}^{1} \left[\tfrac{1}{2}B_{11}\left(\frac{dv}{d\rho}\right)^2 + 2B_{12}\left(\frac{dv}{d\rho}\right)\left(\frac{v}{\rho}\right) + \left(B_{22}+B_{23}\right)\left(\frac{v}{\rho}\right)^2 \right.\right.$$

$$- \frac{dv}{d\rho}\int_0^{\Theta}\gamma_1(\Theta,\rho)d\Theta - 2\frac{v}{\rho}\int_0^{\Theta}\gamma_2(\Theta,\rho)d\Theta + \tfrac{1}{2}\int_0^{\Theta}\varepsilon_1(\Theta,\rho)d\Theta\int_0^{\Theta}\gamma_1(\Theta,\rho)d\Theta \qquad (5)$$

$$\left.\left. + \int_0^{\Theta}\varepsilon_2(\Theta,\rho)d\Theta\int_0^{\Theta}\gamma_2(\Theta,\rho)d\Theta \right] \rho^2 d\rho - \rho_1^2\, q_I v(\rho_1) + q_{II}v(1) \right\}$$

in which the integral expressions constitute the strain energy, and the terms involving q_I and q_{II} represent the potential of the pressure loads.

A complementary variational approach to the problem, in which stresses rather than displacements represent the varied quantities, involves the *total complementary energy*. When tractions are specified over the entire boundary of the body, the total complementary energy Π^* is equal to the complementary strain energy U^*. From the general results given in reference 4 it can be shown that for the sphere

$$\Pi^* = 4\pi\beta_o T_o r_2^3 \int_{\rho_1}^{1} \left[\tfrac{1}{2}b_{11}t_{\rho\rho}^2 + b_{12}t_{\rho\rho}(t_{\phi\phi}+t_{\theta\theta}) + \tfrac{1}{2}b_{22}(t_{\phi\phi}^2+t_{\theta\theta}^2) \right.$$

$$\left. + b_{23}t_{\phi\phi}t_{\theta\theta} + t_{\rho\rho}\int_0^{\Theta}\varepsilon_1(\Theta,\rho)d\Theta + (t_{\phi\phi}+t_{\theta\theta})\int_0^{\Theta}\varepsilon_2(\Theta,\rho)d\Theta \right] \rho^2 d\rho \qquad (6)$$

Before developing approximate solutions to the problem, it is noted that the governing differential equation and natural boundary conditions can be derived through direct application of the *principle of minimum potential energy*. Requiring that the first variation of the total potential energy be equal to zero ($\delta\Pi = 0$), and performing integration by parts, one obtains the displacement

equation of equilibrium

$$B_{11}\left(\frac{d^2v}{d\rho^2}+\frac{2}{\rho}\frac{dv}{d\rho}\right)-2(B_{22}+B_{23}-B_{12})\frac{v}{\rho^2}+\frac{dB_{11}}{d\rho}\frac{dv}{d\rho}+2\frac{dB_{12}}{d\rho}\frac{v}{\rho}$$
$$=\frac{d}{d\rho}\int_0^{\Theta}\gamma_1(\Theta,\rho)\,d\Theta+\frac{2}{\rho}\int_0^{\Theta}[\gamma_1(\Theta,\rho)-\gamma_2(\Theta,\rho)]\,d\Theta \tag{7}$$

and the natural boundary conditions

$$\left.\begin{aligned} &B_{11}(\rho_1)\frac{dv(\rho_1)}{d\rho}+2B_{12}(\rho_1)\frac{v(\rho_1)}{\rho_1}-\int_0^{\Theta(\rho_1)}\gamma_1(\Theta,\rho_1)\,d\Theta=-q_I\\ &B_{11}(1)\frac{dv(1)}{d\rho}+2B_{12}(1)\,v(1)-\int_0^{\Theta(1)}\gamma_1(\Theta,1)\,d\Theta=-q_{II}\end{aligned}\right\} \tag{8}$$

Finding an exact solution to these equations does not appear possible for a sphere of general nonhomogeneity.

RAYLEIGH-RITZ METHOD

In the Rayleigh-Ritz method a kinematically admissible displacement field is assumed, and the principle of minimum potential energy is used to determine unknown coefficients in the assumed solution. Here we shall represent the radial displacement $v(\rho)$ by the power series

$$v=\sum_{i=-m}^{n}a_i\rho^i=a_{-m}\rho^{-m}+\ldots+a_o+\ldots+a_n\rho^n \tag{9}$$

in which the number of nonzero coefficients a_i is arbitrary. Although it is only necessary to satisfy displacement boundary conditions when applying the Rayleigh-Ritz method, generally it is desirable to satisfy traction conditions as well. Relations (8) will be satisfied identically by the displacement field (9) if the coefficients a_i satisfy

$$\left.\begin{aligned} &f_1(a_i)=B_{11}(\rho_1)\sum_i i\,a_i\,\rho_1^{i-1}+2B_{12}(\rho_1)\sum_i a_i\rho^{i-1}-\int_0^{\Theta(\rho_1)}\gamma_1(\Theta,\rho_1)\,d\Theta+q_I=0\\ &f_2(a_i)=B_{11}(1)\sum_i i\,a_i+2B_{12}(1)\sum_i a_i-\int_0^{\Theta(1)}\gamma_1(\Theta,1)\,d\Theta+q_{II}=0\end{aligned}\right\} \tag{10}$$

These equations can be used in order to eliminate two of the coefficients a_i from the assumed solution. Alternatively, equation (9) can be retained in its original form and conditions (10) satisfied by the method of Lagrange multipliers, as described in reference 4. In this case the restrictions (10) are written in terms of Lagrange multipliers λ_1 and λ_2 as

$$\lambda_1 f_1(a_i) = 0, \quad \lambda_2 f_2(a_i) = 0 \tag{11}$$

Necessary conditions for a minimum value of the total potential energy Π, subject to the subsidiary conditions (11), then are given by

$$\frac{\partial \tilde{\Pi}}{\partial a_j} = 0 \ (j = -m, \ldots, n), \quad \frac{\partial \tilde{\Pi}}{\partial \lambda_s} = 0 \ (s = 1,2) \tag{12}$$

where

$$\tilde{\Pi} = \Pi + \lambda_1 f_1 + \lambda_2 f_2 \tag{13}$$

Substituting the assumed solution (9) into the potential energy expression (5), and differentiating $\tilde{\Pi}$ with respect to a_j as indicated in equation (12), gives

$$\sum_{i=-m}^{n} G_{ji}\, a_i + \sum_{s=1}^{2} g_{js}\, \lambda_s = H_j \ (j = -m, \ldots, n) \tag{14}$$

in which

$$\left.\begin{aligned} G_{ji} &= \int_{\rho_1}^{1} \left[ijB_{11} + 2(i+j)B_{12} + 2(B_{22} + B_{23}) \right] \rho^{i+j} d\rho \\ H_j &= \int_{\rho_1}^{1} \left[\int_0^{\Theta} [j\gamma_1(\Theta,\rho) + 2\gamma_2(\Theta,\rho)]\, d\Theta \right] \rho^{j+1} d\rho + \rho_1^{j+2} q_I - q_{II} \end{aligned}\right\} \tag{15}$$

$$g_{j1} = B_{11}(\rho_1)\ j\ \rho_1^{j-1} + 2B_{12}(\rho_1)\rho_1^{j-1}, \quad g_{j2} = B_{11}(1)\ j + 2B_{12}(1)$$

The Ritz coefficients a_i are then found by solving the algebraic equations (14) together with the constraint equations (10).

MODIFIED RAYLEIGH-RITZ METHOD

The modified Rayleigh-Ritz method consists of assuming a state of stress which satisfies equilibrium and traction boundary conditions, and then determining unknown coefficients in the assumed solution by applying the *principle of minimum complementary energy*.

It is easily verified that equilibrium is satisfied if the dimensionless stress components are expressed in terms of a stress function ψ as

$$t_{\rho\rho} = \frac{\psi}{\rho}, \quad t_{\phi\phi} = t_{\theta\theta} = \tfrac{1}{2}\left(\frac{\psi}{\rho} + \frac{d\psi}{d\rho}\right) \tag{16}$$

In this case the total complementary energy becomes

$$\Pi^* = 4\pi\beta_o T_o r_2^3 \int_{\rho_1}^{1} \left[\tfrac{1}{2} b_{11}\left(\frac{\psi}{\rho}\right)^2 + b_{12}\left(\frac{\psi}{\rho}\right)\left(\frac{\psi}{\rho}+\frac{d\psi}{d\rho}\right) + \tfrac{1}{4}(b_{22}+b_{23})\left(\frac{\psi}{\rho}+\frac{d\psi}{d\rho}\right)^2 + \frac{\psi}{\rho}\int_0^{\Theta} \varepsilon_1(\Theta,\rho)\,d\Theta + \left(\frac{\psi}{\rho}+\frac{d\psi}{d\rho}\right)\int_0^{\Theta} \varepsilon_2(\Theta,\rho)\,d\Theta \right] \rho^2 d\rho \tag{17}$$

We choose to represent the stress function ψ by the power series

$$\psi = \sum_{i=-m}^{n} a_i^* \rho^i = a_{-m}^* \rho^{-m} + \ldots + a_o^* + \ldots + a_n^* \rho^n \tag{18}$$

in which the number of nonzero coefficients a_i^* is arbitrary. In order that expression (18) yields stresses which satisfy the traction boundary conditions (8), the coefficients a_i^* must satisfy the relations

$$\begin{aligned} f_1^*(a_i^*) &= \sum_i a_i^* \rho_1^{i-1} + q_I = 0 \\ f_2^*(a_i^*) &= \sum_i a_i^* + q_{II} = 0 \end{aligned} \tag{19}$$

Proceeding as in the standard Rayleigh-Ritz technique outlined earlier, conditions (19) are next written in terms of the Lagrange multipliers λ_1^* and λ_2^*. Application of the principle of minimum complementary energy then leads to the set of equations

$$\sum_{i=-m}^{n} G_{ji}^* a_i^* + \sum_{s=1}^{2} g_{js}^* \lambda_s^* = H_j^* \tag{20}$$

where

$$\left.\begin{aligned} G_{ji}^* &= \int_{\rho_1}^{1} \left[b_{11} + (2+i+j) b_{12} + \tfrac{1}{2}(1+i)(1+j)(b_{22}+b_{23}) \right] \rho^{i+j} d\rho \\ H_j^* &= -\int_{\rho_1}^{1} \left[\int_0^{\Theta} [\varepsilon_1(\Theta,\rho) + (1+j)\varepsilon_2(\Theta,\rho)]\,d\Theta \right] \rho^{j+1} d\rho \end{aligned}\right\} \tag{21}$$

$$g^*_{j1} = \rho_1^{j-1} \quad , \quad g^*_{j2} = 1$$

The coefficients a_i^* and the Lagrange multipliers λ_s^* then are found by solving equations (19) and (20).

FINITE ELEMENT TECHNIQUE

The energy formulation developed earlier also provides a convenient basis for constructing a finite element solution to the problem. In this case the sphere is idealized as a series of N hollow spherical subregions. A typical element j has an inner radius ρ_i and an outer radius ρ_j; the corresponding radial displacement components are denoted by v_i and v_j, and the radial stresses are taken to be $(t_{\rho\rho})_i$ and $(t_{\rho\rho})_j$, respectively.

It is assumed that the displacement varies linearly with ρ within each element, so that

$$v(\rho) = \left(\frac{\rho_j - \rho}{\rho_j - \rho_i}\right) v_i + \left(\frac{-\rho_i + \rho}{\rho_j - \rho_i}\right) v_j \tag{22}$$

The thermoelastic properties are taken to be constant over each element, in which case the following average values will be used

$$\left.\begin{aligned} \overline{B}_{kl} &= \tfrac{1}{2}\left[B_{kl}(\rho_j) + B_{kl}(\rho_i)\right] \quad , \quad \overline{\Gamma}_k = \tfrac{1}{2}\left[\int_0^{\Theta(\rho_j)} \gamma_k(\Theta,\rho_j)\,d\Theta + \int_0^{\Theta(\rho_i)} \gamma_k(\Theta,\rho_i)\,d\Theta\right] \\ \overline{E}_k &= \tfrac{1}{2}\left[\int_0^{\Theta(\rho_j)} \varepsilon_k(\Theta,\rho_j)\,d\Theta + \int_0^{\Theta(\rho_i)} \varepsilon_k(\Theta,\rho_i)\,d\Theta\right] \end{aligned}\right\} \tag{23}$$

By analogy with equation (5), the total potential energy for element j is

$$\begin{aligned} \Pi^{(j)} = 4\pi\beta_o T_o r_2^3 \Bigg\{ \int_{\rho_i}^{\rho_j} \Bigg[&\tfrac{1}{2}\overline{B}_{11}\left(\frac{dv}{d\rho}\right)^2 + 2\overline{B}_{12}\left(\frac{dv}{d\rho}\right)\left(\frac{v}{\rho}\right) + \left(\overline{B}_{22} + \overline{B}_{23}\right)\left(\frac{v}{\rho}\right)^2 \\ &- \overline{\Gamma}_1 \frac{dv}{d\rho} - 2\overline{\Gamma}_2 \frac{v}{\rho} + \tfrac{1}{2}\left(\overline{E}_1\overline{\Gamma}_1 + \overline{E}_2\overline{\Gamma}_2\right)\Bigg] \rho^2 d\rho + \rho_i^2 (t_{\rho\rho})_i v_i - \rho_j^2 (t_{\rho\rho})_j v_j \Bigg\} \end{aligned} \tag{24}$$

Substituting equation (22) into (24), and minimizing $\Pi^{(j)}$ with respect to v_i and v_j gives

$$-\rho_i^2 (t_{\rho\rho})_i - \frac{(\rho_j^3 - \rho_i^3)}{3(\rho_j - \rho_i)}\overline{\Gamma}_1 + \frac{(\rho_j^3 - 3\rho_j\rho_i^2 + 2\rho_i^3)}{3(\rho_j - \rho_i)}\overline{\Gamma}_2 = k_{11}v_i + k_{12}v_j \tag{25a}$$

$$\rho_j^2 (t_{\rho\rho})_j + \frac{(\rho_j^3 - \rho_i^3)}{3(\rho_j - \rho_i)} \bar{\Gamma}_1 + \frac{(\rho_i^3 - 3\rho_i\rho_j^2 + 2\rho_j^3)}{3(\rho_j - \rho_i)} \bar{\Gamma}_2 = k_{12} v_i + k_{22} v_j \tag{25b}$$

where the element stiffness coefficients k_{ij} are

$$\left.\begin{aligned} k_{11} &= \frac{(\rho_j^3 - \rho_i^3)}{3(\rho_j - \rho_i)^2} \bar{B}_{11} - \frac{2(\rho_j^3 - 3\rho_j\rho_i^2 + 2\rho_i^3)}{3(\rho_j - \rho_i)^2} \bar{B}_{12} + \frac{2(\rho_j - \rho_i)}{3} (\bar{B}_{22} + \bar{B}_{23}) \\ k_{22} &= \frac{(\rho_j^3 - \rho_i^3)}{3(\rho_j - \rho_i)^2} \bar{B}_{11} + \frac{2(\rho_i^3 - 3\rho_i\rho_j^2 + 2\rho_j^3)}{3(\rho_j - \rho_i)^2} \bar{B}_{12} + \frac{2(\rho_j - \rho_i)}{3} (\bar{B}_{22} + \bar{B}_{23}) \\ k_{12} &= -\frac{(\rho_j^3 - \rho_i^3)}{3(\rho_j - \rho_i)^2} \bar{B}_{11} + \frac{(\rho_j - \rho_i)}{3} (\bar{B}_{22} + \bar{B}_{23} - \bar{B}_{12}) \end{aligned}\right\} \tag{26}$$

Application of equations (25) to each of the N elements provides a system of 2N linear equations for the N+1 displacement components and the N-1 interface stresses. The interface stresses can be eleminated, resulting in a set of N+1 equations for the unknown displacement components.

NUMERICAL EXAMPLES

To illustrate the influence of temperature-dependent material properties upon the thermoelastic response, and at the same time to demonstrate the applicability of Ritz methods in thermal stress problems, numerical results are presented for a sphere subject to various temperature and pressure conditions. The ratio of the sphere's inner and outer radii is taken to be $\rho_1 = 0.8$. It is assumed that the body is initially homogeneous, and that the thermal expansion coefficients vary linearly with temperature, while the elastic stiffnesses exhibit a quadratic variation. In particular we let

$$\varepsilon_i = \varepsilon_i^{\circ} (1 + b\Theta), \quad B_{ij} = B_{ij}^{\circ} (1 - c\Theta^2) \tag{27}$$

in which b and c are constants. The initial (zero-temperature) thermoelastic coefficients are taken to be

$$\left.\begin{aligned} B_{11}^{\circ} = 3.0 \times 10^4 \quad B_{12}^{\circ} = 1.0 \times 10^4 \quad B_{22}^{\circ} + B_{23}^{\circ} = 31.0 \times 10^4 \\ \gamma_1^{\circ} = 1.0 \quad \gamma_2^{\circ} = 1.5 \end{aligned}\right\} \tag{28}$$

These values are representative of certain fiber reinforced composite materials, reinforced in the circumferential (ϕ and θ) directions.

As a first example let us consider a sphere subject to a uniform temperature rise $\Theta = 1$ and zero internal and external pressure. Values of the thermal displacements and stresses found using the Rayleigh-Ritz and the modified Rayleigh-Ritz methods are compared with the exact solution (ref. 5) for the limiting case of temperature-independent properties (b=c=0) in Table I. It is evident that the accuracy of the approximate solutions generally improves as additional terms are included in the assumed solution. When the Rayleigh-Ritz approximation contains 3 independent coefficients (i.e., a total of the 5 coefficients $a_{-2}, a_{-1}, a_0, a_1, a_2$ of which 2 may be eliminated using the boundary conditions), the value of the maximum stress amplitude $|t_{\phi\phi}(0.8)|$ exceeds the exact value by 0.9%. For 5 independent coefficients the error is reduced to 0.3%. On the other hand the maximum stresses predicted by the modified Rayleigh-Ritz procedure using 3 and 5 independent coefficients are 2.3% and 1.6% smaller than the exact value. When the powers of ρ in either the standard or modified Rayleigh-Ritz approximation are taken to be -5, 4, and 1, the computed values of the displacements and stresses are exact, since the assumed solution then has precisely the form of the exact solution.

Results of finite element analyses are compared with the exact solution to this same problem in Table II. Naturally the accuracy of the finite element solutions improves as the number of independent displacement components is increased. When the finite element solution is based upon 3 independent displacement components (2 elements), the maximum stress $|t_{\phi\phi}(0.8)|$ exceeds the exact value by 2.6%. The error is reduced to 0.7% when 13 displacement components (12 elements) are used. However for this problem it was found that the computations required to achieve a given level of accuracy were less time consuming when one of the Ritz methods was used than when the finite element technique was applied.

To demonstrate the influence of temperature-dependent behavior upon the circumferential stress in the sphere, Ritz solutions based upon 5 independent coefficients are plotted in figures 1-3. Each of the figures shows the stress distributions associated with various values of the temperature-dependent parameters b and c for temperature alone and for combined temperature plus internal pressure. Figure 1 shows the stresses induced by a uniform temperature rise $\Theta=1$. Results for the linearly varying temperature distributions $\Theta=5-5\rho$ and $\Theta=-4+5\rho$ are given in figure 2 and 3, respectively. Each of the Ritz solutions plotted in the figures was compared with a finite element solution based upon a 12-element model. Agreement between the values of the maximum absolute stress predicted by the two methods varied between 0.1% and 1.6%, with one exception. In the case of $\Theta=-4+5\rho$ and zero internal pressure $q_I=0$ (fig. 3) the maximum stress was relatively small, and the discrepancy was nearly 5.0%.

As would be expected for the purely temperature loadings ($q_I=q_{II}=0$), the maximum stresses diminish with increasing values of c(i.e., with decreasing stiffness), whereas they become larger with increasing values of b (increasing thermal expansion). The influence of temperature sensitivity is less predictable in the case of combined temperature and pressure, since both the pressure-induced and temperature-induced stresses are affected by the nonhomogeneity.

REFERENCES

1. Nowinski, J.: Thermoelastic Problem for an Isotropic Sphere with Temperature Dependent Properties. Zeitschrift für Angewandte Mathematik und Physik, vol. 10, 1959, pp. 565-575.

2. Stanisic, M.M.; and McKinley, R.M.: The Steady-State Thermal Stress Field in an Isotropic Sphere with Temperature Dependent Properties. Ingenieur-Archiv vol. 31, 1962, pp. 241-249.

3. Hata, T.; and Atsumi, A.: Transient Thermoelastic Problem for a Transversely Anisotropic Hollow Sphere with Temperature-Dependent Properties. Bulletin of Japan Society of Mechanical Engineers, vol. 12, 1969, pp. 445-452.

4. Tauchert, T.R.: Thermal Stresses in an Orthotropic Cylinder with Temperature-Dependent Elastic Properties. Developments in Theoretical and Applied Mechanics, vol. 8, Virginia Polytech. Inst. and State Univ., 1976, pp.201-212.

5. Birger, B.I.: Temperature Stresses in Anisotropic Bodies. Soviet Applied Mechanics, vol. 7, 1971, pp. 292-296.

Table I. Ritz approximations for the thermal displacements and stresses caused by a uniform temperature rise $\Theta = 1$ when $b = c = 0$.

		Rayleigh-Ritz		Modified Rayleigh-Ritz		Exact
Powers of ρ		-2,-1,0,1,2	-3,-2,-1, 0,1,2,3	-2,-1,0,1,2	-3,-2,-1, 0,1,2,3	-5,4,1
No. of indep. coefs.		3	5	3	5	3
Radial displ. $\times 10^7$	$v(0.8)$	.058	.059	.066	.064	.060
	$v(0.9)$	.355	.355	.354	.354	.354
	$v(1.0)$	.636	.634	.633	.632	.634
Radial stress	$t_{\rho\rho}(0.8)$	0	0	0	0	0
	$t_{\rho\rho}(0.9)$	-.084	-.091	-.092	-.092	-.091
	$t_{\rho\rho}(1.0)$	0	0	0	0	0
Circumf. stress	$t_{\phi\phi}(0.8)$	-.948	-.943	-.918	-.925	-.940
	$t_{\phi\phi}(0.9)$	.001	-.001	-.006	-.003	-.003
	$t_{\phi\phi}(1.0)$	.762	.757	.755	.750	.758

Table II. Finite element solutions for the thermal displacements and stresses caused by a uniform temperature rise $\Theta = 1$ when $b = c = 0$.

		Finite Element				Exact
No. elements		2	4	6	12	-
No. indep. displ. comps.		3	5	7	13	-
Radial displ. $\times 10^7$	$v(0.8)$	.062	.060	.060	.060	.060
	$v(0.9)$	.356	.355	.355	.355	.354
	$v(1.0)$	.636	.635	.635	.635	.634
Radial stress	$t_{\rho\rho}(0.8)$	-.105	-.064	-.046	-.025	0
	$t_{\rho\rho}(0.9)$	-.073	-.092	-.092	-.091	-.091
	$t_{\rho\rho}(1.0)$	-.033	-.022	-.016	-.008	0
Circumf. stress	$t_{\phi\phi}(0.8)$	-.965	-.959	-.954	-.947	-.940
	$t_{\phi\phi}(0.9)$	.012	.001	-.001	-.001	-.003
	$t_{\phi\phi}(1.0)$	.750	.752	.753	.756	.758

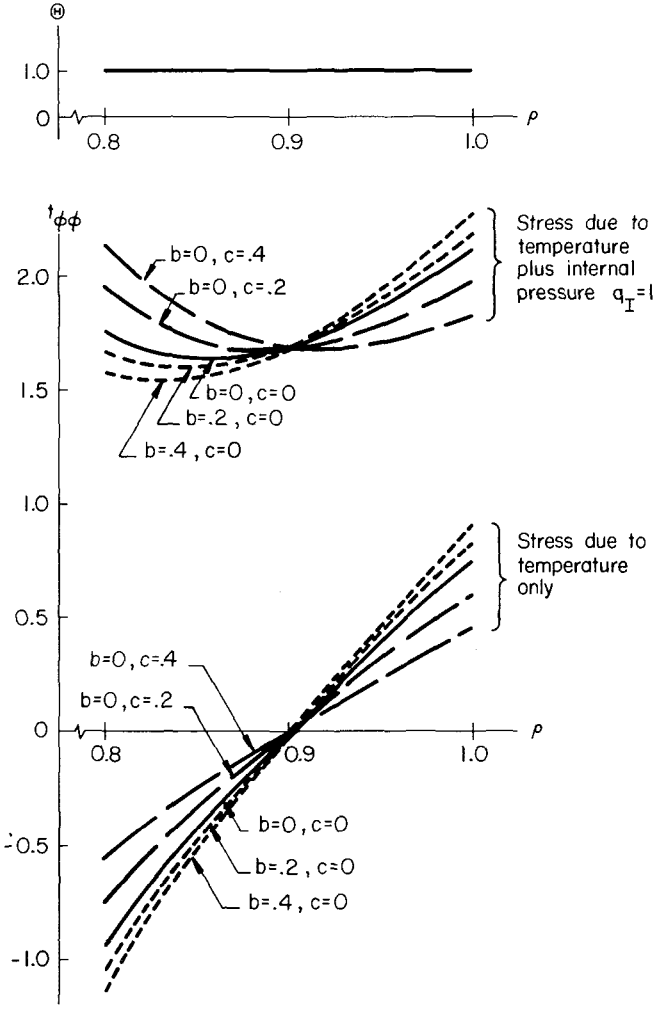

Figure 1.- Influence of temperature sensitivity coefficients b and c upon the circumferential stress distribution for the uniform temperature rise $\Theta = 1$.

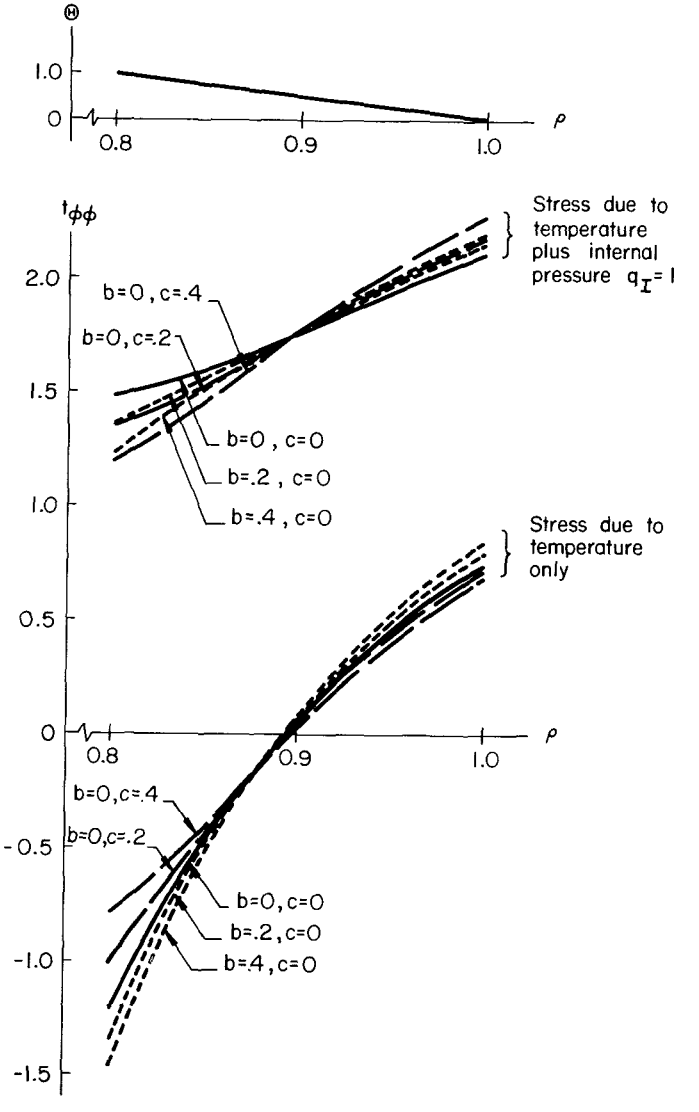

Figure 2.- Influence of temperature sensitivity coefficients b and c upon the circumferential stress distribution for the temperature field $\Theta = 5 - 5\rho$.

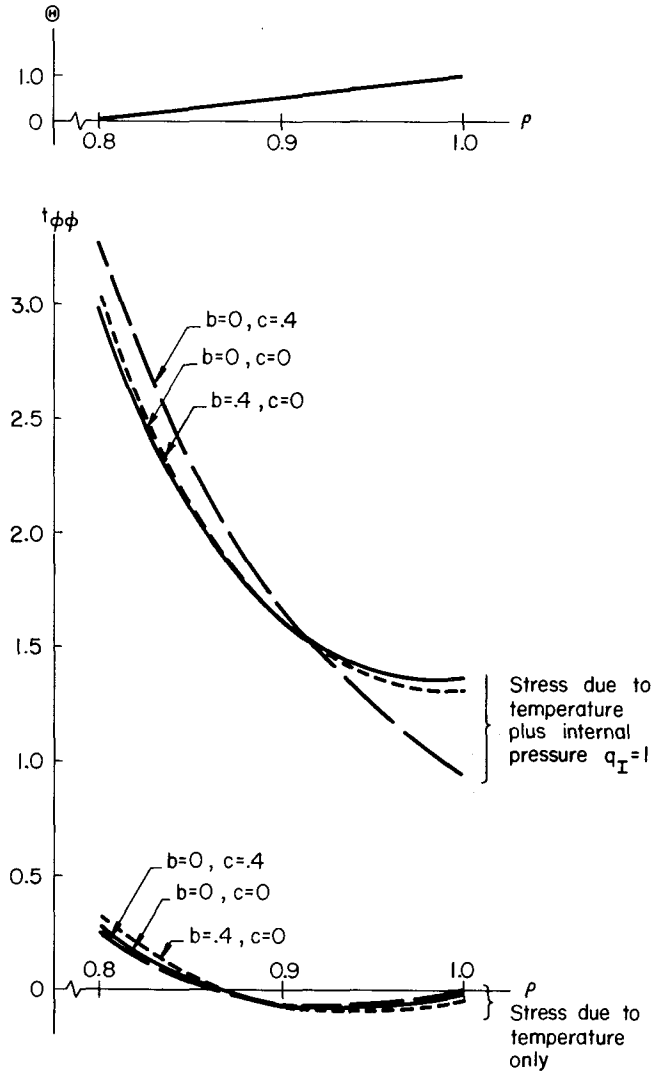

Figure 3.- Influence of temperature sensitivity coefficients b and c upon the circumferential stress distribution for the temperature field $\Theta = -4 + 5\rho$.

ANALYSIS OF PANEL DENT RESISTANCE

Chi-Mou Ni
General Motors Research Laboratories

SUMMARY

An analytical technique for elastic-plastic deformation of panels has been developed, which may be employed to analyze the denting mechanisms of panels resulting from point projectile impacts and impulsive loadings. The correlations of analytical results with the experimental measurements are considered quite satisfactory.

The effect of elastic springback on the dent-resistance analysis is found to be very significant for the panel (122 cm x 60.9 cm x 0.076 cm) subjected to a point projectile impact at 16.45 m/sec. While the amount of springback decreases as the loading speed increases, the effect due to the strain-rate hardening of material, such as low-carbon steel, becomes more dominant and has been demonstrated in the analysis of dent resistance of a rectangular steel plate impulsively loaded.

INTRODUCTION

One of the primary concerns in exposed panels of automotive vehicles and aircraft is their ability to resist damage by denting during fabrication and in service. Generally speaking, the mechanical properties of the material, panel geometry, and loading conditions are the primary factors in determining panel dent resistance. These factors are related in a complicated way, however; therefore, it is not easy to use an intuitive approach to develop their mathematical relationship, and we must resort to an analytical approach instead.

Generally speaking, the loadings which dent the panel are somewhat random in nature. Dents may be produced in automotive panels during fabrication, for example, by the impact of one panel on another and by dropping a panel onto a holder or conveyor projection. In service, dents are commonly produced by flying stones, door impact in a parking lot, and even hail. For aerospace structures, quite often the exposed aircraft components are subjected to impact loadings, including hail and runway stones, etc. Nevertheless, in this study it is assumed that the loading conditions may be characterized with (a) projectile impact over a period of time; and (b) an impulse having a very short duration.

In this study, an analytical approach is developed to analyze the denting mechanism of panels under impact and impulsive loadings. Panel denting is usually the consequence of ductile plastic flow. The dent resistance is

referred to as the panel-dent strength, measured in terms of permanent plastic deformation (not the deformation resulting from any elastic buckling). Over the past few years, the analysis and prediction of large dynamic and permanent deformations of structures caused by impact and impulsive loadings have received increasing interest (refs. 1 to 6).

Three analytical approaches to these problems are commonly used. The rigid-plastic idealization (refs. 1 to 2) has been frequently applied to analyze impulsively loaded beams, rings, flat plates, and axisymmetric cylindrical shells. There are limitations to this idealization, however. For instance, once the large deflection or geometry change is taken into account, a rigid-plastic analysis may be too complicated to use (ref. 2). Furthermore, the rigid-plastic analysis is applicable only to problems for which the initial kinetic energy is much larger than the maximum elastic strain energy. Another approach often employed for structural problems is the energy method (ref. 6) in which the energy input to the structure is equated to the plastic work done. The success of this method depends on how reasonable an estimate is made of the primary mode of deformation. For a complex structure under arbitrary transient loading, it can be difficult to make such an estimate.

The deficiencies in the two analytical methods can be skirted by various numerical methods, such as the finite difference method (refs. 3 to 5) and the finite element method (ref. 5). In this paper, a numerical scheme extended from Reference 4 is employed to analyze the panel denting as a result of being subjected to impact and impulsive loadings.

THEORETICAL FORMULATIONS

Minimum Principle

Consider a body of a continuum occupying in its natural state a region V_O and bounded by a piecewise smooth surface, A. The body is subjected to time-dependent body force, F_m (per unit mass) and Lagranian surface traction (per unit area) T_m over that part of the initial surface area A_T. At time t, let $\{U_k\}$ be the displacement vector of a particle of the body which has an initial position of $\{X_k\}$ in a curvilinear coordinate system. The displacements are prescribed over that part of the boundary surface, A_u. The deformation of the body may be described in terms of the covariant components of the Lagrangian strain tensor, E_{kL}, defined by

$$E_{kL} = \frac{1}{2}\left(U_{k;L} + U_{L;k} + U^{M}_{;k}U_{M;L}\right) \tag{1}$$

Herein, a covariant derivative of a variable with respect to X_k is designated by the semicolon in the subscript position, as $(\,)_{;k}$, and the repetition of an index in a term indicates summation. The Lagrangian strain may be expressed as the sum of two parts: elastic strain, E^{e}_{kL} and plastic strain E^{p}_{kL}. It is postulated that the constitutive relationships, in

terms of the symmetric Kirchhoff stress tensor S_{kL}, may be plastic-strain velocity dependent but are not influenced by strain accelerations. In other words, it is assumed that

$$S_{kL} = S_{kL}\left(E^{e}_{MN}, E^{p}_{MN}, \dot{E}^{p}_{MN}, \theta\right) \tag{2}$$

in which θ is the temperature and $\dot{E}^{p}_{MN}$ is the velocity rate of plastic straining. The contravariant components of the Kirchhoff stress tensor, S^{kL}, satisfy the boundary conditions

$$S^{kL}\left(g_{ML} + U_{M;L}\right) N_k = T_M \text{ on } A_T \tag{3}$$

in which N_k is the covariant outward unit normal to A, and g_{ML} is the metric tensor.

It has been shown (ref. 7) that the time acceleration field, $\ddot{U}_M = D^2U_M/Dt^2$, of the body, which has known or predetermined displacement and velocity fields at time t, is distinguished from all kinematically admissible ones by having the minimum value of the following functional:

$$I = \int_{V_o} S^{kL}\ddot{E}_{kL}\,dV_o + \frac{1}{2}\int_{V_o} \rho_o \ddot{U}^{M}\ddot{U}_M\,dV_o - \int_{A_T} T^{M}\ddot{U}_M\,dA - \int_{V_o} \rho_o F^{M}\ddot{U}_M\,dV_o \tag{4}$$

in which ρ_o is the initial mass density. The minimum principle is valid for continuous as well as sectionally discontinuous acceleration fields. Ordinarily, it is sufficient to use the first variation with respect to the acceleration, $\delta_{acc}I = 0$, to establish governing equations or to solve a problem by a direct method of variational calculus.

Kinematics

Consider a cylindrical-shell panel of mean radius R, thickness h, axial length L, and arc width $R\beta$. Let (x,y,z) be the axial, circumferential and (outward) normal coordinates, and (U_x,U_y,U_z) be the corresponding physical components of the displacement vector of a point in the shell, respectively. Then, by utilizing the Love-Kirchhoff assumption for thin shells and by neglecting wave propagation through the thickness, the displacement components of a particle can be expressed in terms of the corresponding displacement (and its derivatives) of the middle surface as

$$\left.\begin{aligned} U_r &= u - zw_{,x} \\ U_y &= v - \frac{z}{R}(w,y + v) \\ U_z &= w \end{aligned}\right\} \tag{5}$$

where u, v, and w denote the axial, tangential, and (outward) normal displacement components of a point on the mid-surface. Having the displacement components, the strain accelerations can then be defined as

$$\ddot{E}_{xx} = (1 + u_{,x})\ddot{u}_{,x} + v_{,x}\ddot{v}_{,x} + w_{,x}\ddot{w}_{,x} - z\ddot{w}_{,xx} + \dot{u}^2_{,x} + \dot{v}^2_{,x} + \dot{w}^2_{,x}$$

$$\ddot{E}_{xy} = \frac{1}{2}\Big[u_{,y}\ddot{u}_{,x} + (1 + v_{,y} - \ddot{w})v_{,x} + (v + w_{,y})\ddot{w}_{,x} + (1 + u_{,x})\ddot{u}_{,y}$$
$$+ v_{,x}(\ddot{v}_{,y} - \ddot{w}) + w_{,x}(\ddot{v} + \ddot{w}_{,y}) - z(2\ddot{w}_{,xy} + \ddot{v}_{,x}) + \dot{u}_{,x}\dot{u}_{,y}$$
$$+ \dot{v}_{,x}(\dot{v}_{,y} - w)\Big] \qquad (6)$$

$$\ddot{E}_{yy} = u_{,y}\ddot{u}_{,y} + (1 + v_{,y} - w)(\ddot{v}_{,y} - \ddot{w}) + (v + w_{,y})(\ddot{w}_{,y} + \ddot{v})$$
$$- z(\ddot{w}_{,yy} + \ddot{v}_{,y}) + \dot{u}^2_{,y} + (\dot{v}_{,y} - \dot{w})^2 + (\dot{v} + \dot{w}_{,y})^2$$

Constitutive Relationship

For an isotropic and homogeneous material, the elastic stress-strain relationship may be reasonably expressed by

$$\dot{E}^e_{kL} = \frac{1}{E}\left[(1 + \nu)\,\dot{S}_{kL} - \nu\delta_{kL}\dot{S}_{MM}\right] \qquad (7)$$

where ν is Poisson's ratio and δ_{kL} is the Kronecker symbol. The plastic stress-strain relationship based on the isothermal, incremental theories of plasticity may be derived from Drucker's postulate of positive work in plastic deformation. Drucker's postulate establishes two requirements:

(a) The loading surface is convex and (b) at a smooth point of the yield surface, the plastic strain rate vector is always directed along the normal to the loading surface or

$$\dot{E}^p_{kL} = \begin{cases} G\,\dfrac{\partial f}{\partial S_{kL}}\dfrac{\partial f}{\partial S_{MN}}\dot{S}_{MN} & \text{for } f = 0 \text{ and } \dfrac{\partial f}{\partial S_{MN}}\dot{S}_{MN} > 0 \\ 0 & \text{for } f < 0 \text{ or } \dfrac{\partial f}{\partial S_{MN}}\dot{S}_{MN} \le 0 \end{cases} \qquad (8)$$

where G is a scalar proportionality function depending on the state of the material and may be determined, based on the concept of isotropic hardening, as (ref. 4)

$$\left.\begin{aligned} G &= \frac{3}{4J_2}\left(\frac{1}{E_t} - \frac{1}{E}\right) \quad \text{for } f = 0 \text{ and } \frac{\partial f}{\partial S_{MN}}\dot{S}_{MN} > 0 \\ &= 0 \qquad\qquad\qquad \text{for } f < 0 \text{ or } \frac{\partial f}{\partial S_{MN}}\dot{S}_{MN} \le 0 \end{aligned}\right\} \qquad (9)$$

in which E_t , a function of J_2 , is the tangent modulus which may be obtained from the uniaxial Kirchhoff stress vs Lagrangian strain curve of the material. Herein, a generalized J_2 criterion based on the Mises yield function is employed for the shell problem as

$$f = J_2 - \kappa^2 = \frac{1}{3}\left(S_{xx}^2 - S_{yy} + S_{yy}^2\right) + S_{xy}^2 - \kappa^2 = 0 \tag{10}$$

where κ is the strain-hardening parameter.

It has been long recognized that the strain-rate sensitivity of material may be one of the important factors affecting the dynamic responses of elastic-plastic structures. A generalized formula which accounts approximately for the multiaxial behavior of a strain-rate sensitive material is employed and expressed as

$$\frac{\sigma_e}{\sigma_o} = 1 + \left(\frac{\dot{\varepsilon}_e}{D}\right)^{\frac{1}{p}} \tag{11}$$

where σ_e (effective stress) $= \left(\frac{3}{2}\bar{S}'_{ij}\bar{S}'_{ij}\right)^{\frac{1}{2}}$, $\bar{S}'_{ij} = \sigma_{ij} - \frac{1}{3}\delta_{ij}\sigma_{kk}$

$\dot{\varepsilon}_e$ (effective strain rate) $= \left(\frac{2}{3}\dot{\varepsilon}_{ij}\dot{\varepsilon}_{ij}\right)^{\frac{1}{2}}$

D and p = material constants

Finite-Difference Energy Method

A numerical approach based on the finite-difference direct method in conjunction with the minimum principle (as shown in Eq. (4)) is developed to analyze the large dynamic responses of cylindrical shell panel under impact and impulsive loadings. To make the amount of computation tenable, an idealized sandwich shell having a number of discrete, thin load-carrying sheets made of a work-hardening material is employed. The indices i, j, and k are introduced to indicate the spatial position of a point in the shell as follows: $x = i\Delta x$, $i = 1,\ldots m$; $y = j\Delta y$, $j = 1,\ldots n$; $z = k\Delta z$, $k = 0, \pm 1,\ldots \pm \ell$; where Δx, Δy, and Δz are chosen spacings of coordinates x, y, and z, respectively. The spatial derivatives of accelerations and displacements are replaced by discrete values of accelerations and displacements through a central finite-difference scheme. The functional I , by Equation (4), may be replaced by a finite summation through using the trapezoidal rule for the integration. The explicit expressions for accelerations at any time step $t = q\Delta t$ may be obtained by minimizing the functional I^q with respect to the discrete accelerations as follows:

$$\frac{\partial I^q}{\partial \ddot{u}^q_{i,j}} = 0; \quad \frac{\partial I^q}{\partial \ddot{v}^q_{i,j}} = 0; \quad \frac{\partial I^q}{\partial \ddot{w}^q_{i,j}} = 0 \tag{12}$$

The discrete accelerations must also satisfy the boundary conditions for the clamped cylindrical shell panels which require that three displacement components and their slopes all have a value of zero.

It is assumed that at time $t = q\Delta t$, the displacements, velocities, strains and stresses, have been previously determined at all nodal points of the domain. Then Equation (12) may be used to determine the accelerations $\ddot{u}^q_{i,j}$, $\ddot{v}^q_{i,j}$, $\ddot{w}^q_{i,j}$ at time t. Subsequently, the displacements at time $t + \Delta t$ may be obtained by the central difference approximation. Knowing the displacements at $t + \Delta t$, the strain increments that occurred in the time interval $(t + \Delta t - t)$ may also be determined by using the central difference scheme. Furthermore, the corresponding stress increments may be obtained by the constitutive relationships provided that the condition of loading or unloading is known. This may be accomplished by first calculating a set of stress increments corresponding to $G = 0$. Then the loading criterion, $df \gtrless 0$, may be checked and the appropriate value of G in Equation (9) is used in the calculation of the correct stress increments. By repeating the foregoing steps for each subsequent time increment, the entire history of deformation of the shell panel may be obtained.

Impact and Impulsive Loadings

In the case of projectile impact, the actual situation could be very complex and not amenable to analysis due to the irregular shapes of the panels and the indentors and their interactions during deformations. However, for simplicity the projectile is considered here to be rigid and small in size compared with the dimensions of the panel. In engineering analysis, there are, in general, two approximate methods to incorporate the impact loadings by the projectile into the mathematical system: one is termed "Collision-Imparted Velocity Method" (ref. 8) and the other, the "Collision-Force Method" (ref. 8). For the "Collision-Force Method," the contact force is included in the analysis; the contact force is neglected in the "Collision-Imparted Velocity Method," which makes it much simpler to implement. In Reference 9 it has been shown that in cases of small ratio of beam mass to impactor mass, these two methods may offer the same degree of accuracy in solutions of a simply supported beam under central impact. In this study of panel dent resistance, a point-projectile-impact loading is assumed in the analysis. Furthermore, the impactor mass is considered as rigid and attached to the panel at the impact point and then an initial velocity equal to the original impactor velocity is assumed at the panel impact point. Subsequently, the motion of the panel is then analyzed.

In the low-speed impact situation, the stress due to the impactor is dispersed continuously throughout the panel. As impact speed increases, the regions not in the immediate vicinity of the impact point will not immediately feel a stress, and it will cause more localized deformation at the impact point. In order to simplify the analysis for the very localized dents as a result of very high speed impact, a small portion of the panel around the impact point under high-intensity impulse is analyzed. In general, a solid under an impulsive loading of very short duration may be considered to be equivalent to a solid moving with a prescribed initial velocity.

RESULTS AND DISCUSSION

Since the primary concern in the analysis of panel dent resistance is the dent size, which is, in general, inversely proportional to panel resistance to loading, the dent size (or permanent set) of the impacted panel is here used as an index to calibrate its resistance to denting. As mentioned previously, the actual loading conditions are usually not deterministic and vary widely with the manufacturing and service environments of the panel. In any event, the analytical technique presented herein may be employed to analyze the panel dent sizes resulting from point projectile impacts and impulses, which should provide some fundamental understandings of panel dent resistance.

In order to validate the present analytical technique, numerical results have been obtained for the dynamic responses of a cylindrical shell panel subjected to a point projectile impact and of a rectangular plate subjected to impulsive loading:

The cylindrical shell panel clamped on its boundaries is made of aluminum alloy 6061-T6 and has the geometric properties as shown in Figure 1. The material has a mass density of 2750 kg/m^3 and a Poisson's ratio of 1/3. The uniaxial stress-strain relationship may be approximated as a bilinear relationship with E(Young's modulus) = $8 \times 10^{10} N/m^2$, E_t(tangent modulus) = $10.7 \times 10^7 N/m^2$ and σ_o(initial yield stress) = $27 \times 10^7 N/m^2$. The panel is impacted by a 0.45 kg steel ball (0.79 mm in diameter) at 16.5 m/sec. Figure 1 illustrates the analytical results of the central deflection-time relationships of the impacted panel, and the measured maximum deflection and permanent deflection in experiment. It should be noted that the maximum deflection and the permanent deflection predicted are larger than those determined experimentally. The reason for this overestimation of deflections at the impacted point may be that in this analysis, the projectile is assumed to be a point so that the predicted deformed profiles around the impact point are deeper than those observed in experiment. It is believed that the correlations can be improved by matching the contact surface instead of the point in the analysis. As one can see in Figure 1, however, the analytical results obtained can still be reasonable enough to provide understanding of the panel dent resistance. Indicated in Figure 1, the impacted point of panel with the projectile reaches its peak deflection by elastic-plastic deformation, and then springs back to its saddle point, at which time the projectile and the impacted point of panel separate, and finally it oscillates about its permanent deformation; the permanent deformation is defined as the dent. When the panel reaches peak deflection, the kinetic energy of the projectile before impact is transformed within the panel in two parts, elastic strain energy and the work of plastic strain. Since the elastic deformation is assumed to be reversible, the panel springs back, causing rebound of the projectile. The elastic strain energy released is related to the elastic stiffness of the panel, which depends on the Young's modulus, panel geometry, and on the impact speed. Evidently, for this case, the elastic springback plays an important role in determining the degree of dent resistance.

Furthermore, under certain circumstances, the impact speed can be so high that only a very localized dent occurs, with insignificant springback (Ref. 10). This phenomenon may be analyzed and reproduced by only treating the immediate impacted area being subjected to high intensity of impulse, which would simplify the analysis and still provide enough insight of the panel dent-resistance. Also, in some other circumstances, the loading conditions may be explicitly characterized as impulsive loadings with relatively short durations. To understand the denting mechanisms of panel resulting from impulsive loadings, the present analytical technique has been applied to analyze the dynamic responses of a rectangular plate subjected to a uniform impulse with equivalent initial velocity of 91.4 m/sec. The geometric dimensions of this plate are shown in Figure 2 and the material is aluminum alloy 6061-T6, whose mechanical properties are described previously. Presented in Figure 2 are the analytical results of the central deflection-time history and the experimentally measured permanent set (Ref. 11) for comparison. It is evident that the predicted dent depth of the center agrees very well with the test data. Note that the springback is insignificant compared with the previous case. The amount of spring-back back generally depends on the Young's modulus, panel geometry, and the impact speed. As the springback effect decreases as the impact speed increases, the strain-rate hardening of material may become dominant when deformation rate increases. The degree of strain-rate hardening can vary with material and temper condition. For example, low-carbon mild steel generally has greater strain-rate hardening than aluminum alloy and high-strength steel.

Finally, to quantify the effect of strain-rate hardening of steel on the panel dent-resistance, the central deflection-time relationships of a rectangular steel plate (as shown in Fig. 3) subjected to a uniform impulse of 61.32 m/sec have been obtained by using the present analysis with three sets of strain-rate coefficients of Equation 11, and the test data (Ref. 11) for comparison. The steel has a mass density of 7830 kg/m^3, and a Poisson's ratio of 0.28. The uniaxial stress-strain relation may be approximated as a bilinear relationship with $E = 21 \times 10^{10} N/m^2$, $E_t = 10^3 N/m^2$ and $\sigma_o = 21.7 \times 10^7 N/m^2$. As one can see in Figure 3, the dent depths (or permanent sets) vary significantly with the degree of strain-rate hardening.

From the aforementioned two loading conditions under which dents of panels occur, it is quite evident that how two important factors--panel elastic springback and strain-rate hardening of material--influence the panel dent-resistance. In addition to these two factors, other factors such as strain-hardening, material density, and yield stress could be important.

CONCLUDING REMARKS

An analytical technique for elastic-plastic deformation of panels has been developed, which may be employed to analyze the denting mechanisms of panels resulting from point projectile impacts and impulsive loadings. The correlations of analytical results with the experimental measurements are considered quite satisfactory.

The effect of elastic springback on the dent-resistance analysis is found to be very significant for the panel (122 cm x 60.9 cm x 0.076 cm) subjected to a point projectile impact at 16.45 m/sec. While the springback decreases as the loading speed increases, the amount due to the strain-rate hardening of material, such as low-carbon steel, becomes more dominant, which has been demonstrated in the analysis of dent resistance of a rectangular steel plate impulsively loaded.

REFERENCES

1. Symonds, P. S.: Survey of Methods of Analysis for Plastic Deformation of Structures Under Dynamic Loading. Brown University, Report BU/NSRDC/ 1-67 (1967).

2. Jones, N.: The Influence of Large Deflections on the Behavior of Rigid-Plastic Cylindrical Shells Loaded Impulsively. J. Appl. Mech. 37, 416 (1970).

3. Morino, L.; Leech, J. W.; Witmer, E. A.: An Improved Numerical Calculation Technique for Large Elastic-Plastic Transient Deformations of Thin Shells, Part 1 and Part 2. J. Appl. Mech. 38, 423 (1971).

4. Ni, C. M.; Lee, L.H.N.: Dynamic Behavior of Inelastic Cylindrical Shells at Finite Deformation. Int. J. Non-Linear Mech., Vol. 9 (1974).

5. Wu, R. W.; Witmer, E. A.: The Dynamic Responses of Cylindrical Shells Including Geometric and Material Nonlinearities. Int. J. Solids Structures 10 (1974).

6. Greenspon, J. E.: Elastic and Plastic Behavior of Cylindrical Shells Under Dynamic Loads Based On Energy Criteria. Tech. Report 3. J. G. Engr. Research Associates, Baltimore, MD (1963).

7. Lee, L.H.N.; Ni, C. M.: A Minimum Principle in Dynamics of Elastic-Plastic Continua at Finite Deformation. Arch. Mech. 25 (1973).

8. Wu, R. W.; Witmer, E. A.: Finite-Element Analysis of Large Transient Elastic-Plastic Deformations of Simple Structures, With Application to the Engine Rotor Fragment Containment/Deflection Problem. NASA CR-120886 ASRL TR 154-4, 1972.

9. Chon, P. C.; Flis, W. J.: Design Curves for Structural Response Due to Impact Loading. Proceedings of AIAA/ASME/SAE 17th SDM (1976).

10. Calder, C. A.; Goldsmith, W.: Plastic Deformation and Perforation of Thin Plates Resulting from Projectile Impact. Int. J. Solids Structures, Vol. 7, 1971.

11. Jones, N.; Uran, T. O.; Tekin, S.A.: The Dynamic Plastic Behavior of Fully Clamped Rectangular Plages. Int. J. Solids Structures, Vol. 6, 1970.

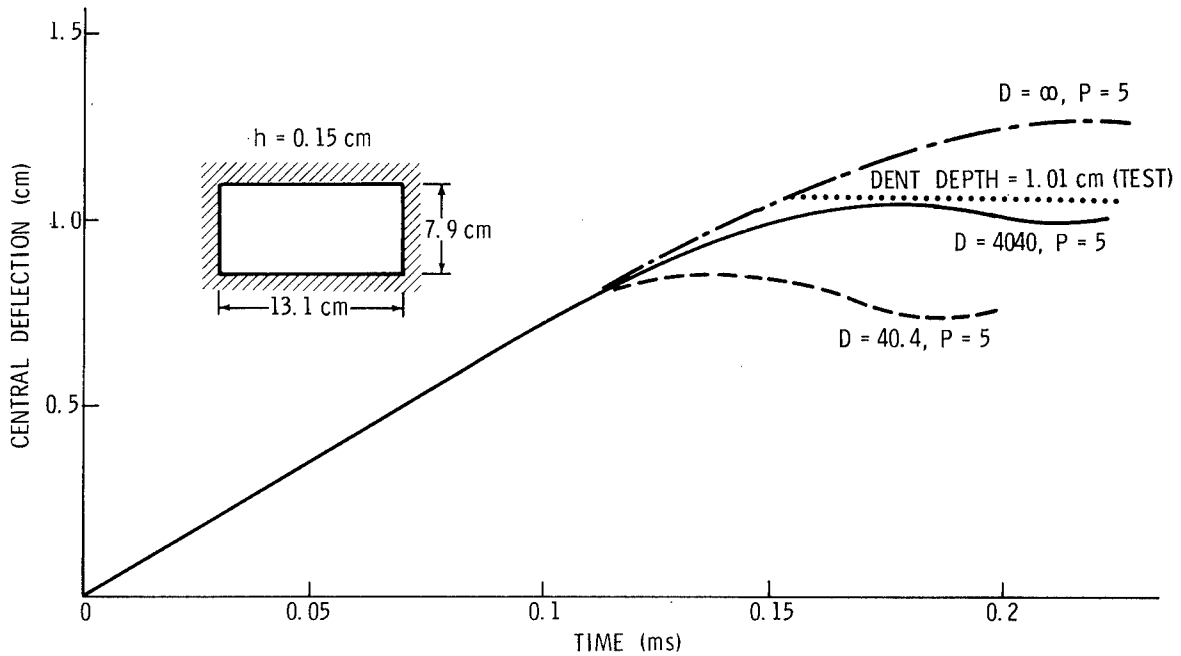

Figure 3.- Predicted deflection histories of a steel plate subjected to a uniform initial velocity of 61.32 m/sec, showing the strain-rate effect via parameter D.

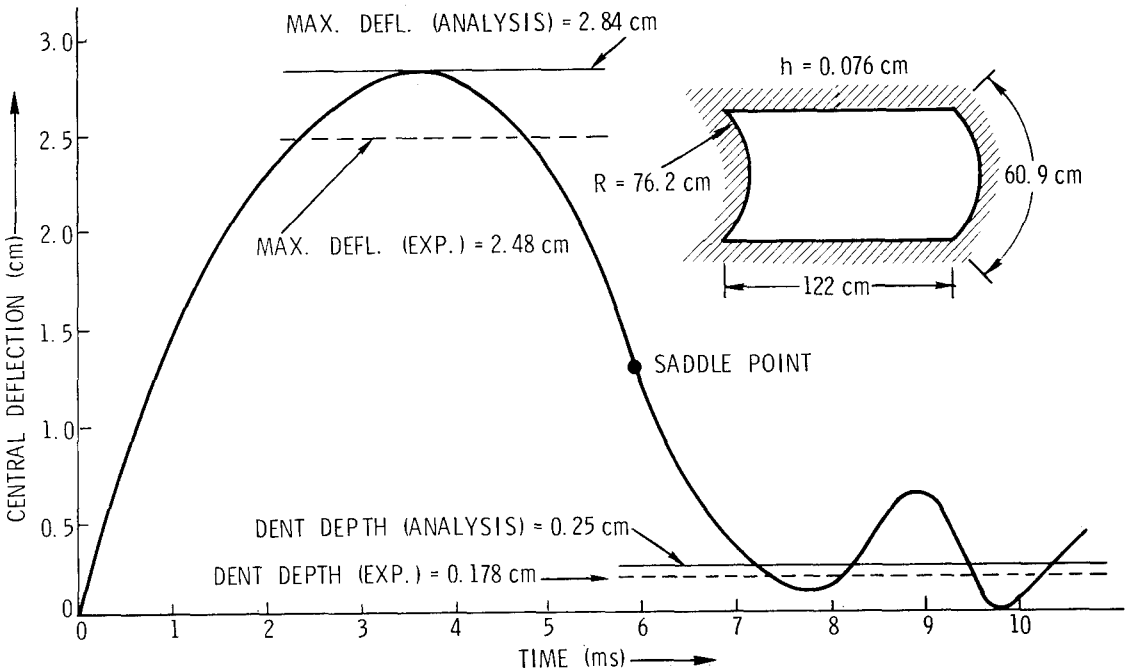

Figure 1.- Predicted deflection history of the center of a panel impacted by a 0.45-kg steel ball at 16.45 m/sec.

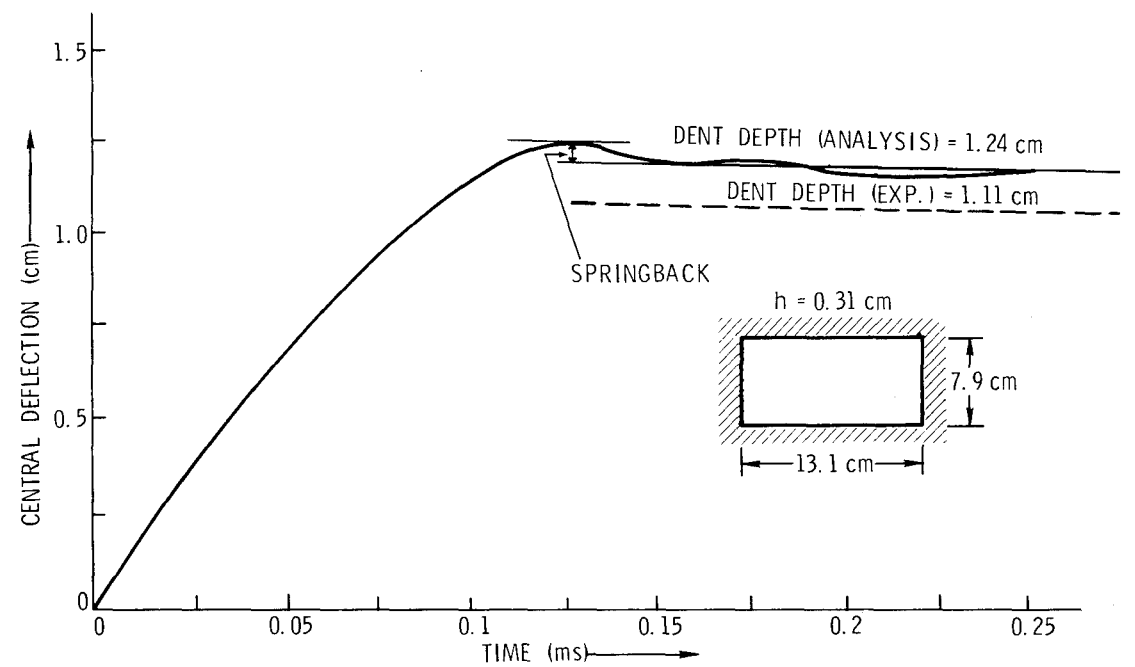

Figure 2.- Predicted deflection history of the center of a rectangular plate subjected to a uniform initial velocity of 121.9 m/sec.

NEUTRAL ELASTIC DEFORMATIONS

Metin M. Durum
Roy C. Ingersoll Research Center, Borg-Warner Corp.

ABSTRACT

Elastic bodies or systems may not require external energy for certain finite and continuous deformations. Conditions providing these kinds of effortless, or neutral, deformations are the subject of this paper.

INTRODUCTION

If the total strain energy in a solid body or system remains constant during its elastic deformation, a neutral equilibrium state is obtained. No external effort then is needed for this deformation assuming the supports or guides are frictionless. If friction is considered during such a deformation, then the losses due to friction would introduce the only demand for external effort. Although an elasticity approach to determine the strain energy level would be extremely difficult for large deformations, simplified approaches such as beam or shell theories offer practical solutions.

Time independent stress or strain fields in Eulerian coordinates may be the simplest form of neutral deformation. In this special case, a stress or strain dependent boundary also remains fixed, and the deformation takes place in a rigid envelope similar to a steady fluid flow. These non-apparent deformations can be identified by inspection as illustrated in the following examples. It is generally not difficult to determine whether or not the macroscopic condition of a system, and consequently its stress field, are time independent.

PRACTICAL EXAMPLES FOR NEUTRAL DEFORMATIONS

Flexible Shaft and a Spinor Problem

An initially straight, flexible shaft or rod having cross sections of equal principal moments of inertia and being guided or supported along a fixed curve can be rotated freely about its deformed axis (fig. 1). During this deformation, the stress distribution in the rod (not necessarily prismatic) is generally time dependent. However, since the bending stiffness around any cross section is constant, the deformed

rod axis (elastica) and, consequently, the total strain energy remain time independent within the approximations of beam theory. The stress distribution also becomes time independent if the rod is axisymmetrical. A steady torque transmission through a guided flexible shaft does not change the foregoing discussion, and the deformation still remains neutral.

As an aside, it can be noted that if the angular velocity vectors at A and B ends are collinear and in opposite direction ($\boldsymbol{\omega}_B=-\boldsymbol{\omega}_A$) and if the supports' frame is rotated by $\boldsymbol{\Omega}_F=-\boldsymbol{\omega}_A$ then the absolute velocities become $\boldsymbol{\Omega}_A=0$ and $\boldsymbol{\Omega}_B=-2\boldsymbol{\omega}_A=2\boldsymbol{\Omega}_F$. This spinor problem (ref. 1) was employed to provide a direct connection between a rotating and a fixed platform which was patented in 1971 (ref. 2).

Free Invertible Rings

If the free ends A and B of a flexible rod are bonded together, a free invertible ring is obtained. Without the guides, the ring becomes circular (fig. 2).

A free invertible ring can also be obtained by bonding two molded rings of certain cross sections (such as semi circular sections) after inverting one through 180° (fig. 3). The split ring idea was applied to rollable belts and patented in 1928 (ref. 3).

In general, the uniform inversion of a non-strained slender ring about a given circular axis requires a uniformly distributed torque and a uniformly distributed radial load. The torque is a sum of the first and second harmonic functions of toroidal displacement (θ) while the radial load is a first harmonic function of toroidal displacement (ref. 4 and author's disclosure, Oct. 1973). When two bonded rings are being inverted about their common circular axis, the second harmonic torques can be eliminated by a suitable choice of cross sections. Also, the sum of the first harmonic torques on the radial loads can be eliminated by introducing a difference of 180° between the inversion phases of the two rings.

Belt and Pulleys

During a steady load transmission, the stress distribution in a uniform belt (fig. 4) remains the same, ignoring non-elastic properties of conventional belt materials. The deformation of this belt can, therefore, be called neutral. In this system, load transmission requires friction between the belt and pulleys, but then the microslips at their contacts produce an unavoidable small resistance.

If a belt of non-uniform stiffness is considered, its deformation will no longer be neutral.

Rolamite (ref. 5)

Two rollers wrapped by a flat band move almost freely between parallel guides (fig. 5). The pretensioned elastic band presents constant stress and strain energy level in the straight portions (AB + CD) and time independent stress distribution in the wrapped portion (BC).

Rolling Elements

Stress distribution in load-carrying rolling elements such as locomotive wheels remains constant in a transported frame. A small rolling resistance accompanies their neutral deformation, but this is mainly due to microslips at wheel-track contacts (ref. 6).

Some common load-carrying elements, e.g. radial ball bearings, undergo a non-neutral deformation because of a cyclic load and stress variation at ball-race contacts.

CONCLUSION

A neutral deformation concept is defined, and two basic rules are employed to identify a large deformation of this kind with or without help of additional assumptions. Some practical applications have been presented. It is hoped that further investigations in this field may lead to new developments.

REFERENCES

1. Adams, D. A., 'Direct Energy Communication Between Continuously Rotating and Stationary Platforms', U.S. Patent 3,586,413, June 22, 1971.

2. Bolker, E. D., 'The Spinor Spanner', American Mathematical Monthly, Nov. 1973.

3. Keiser, A. J., 'Feeding or Displacing Belt', U.S. Patent 1,667,120, April 24, 1928.

4. Biezeno & Grammel, 'Engineering Dynamics', Vol. II, Blackie & Son, Ltd., 1956.

5. Wilkes, D. F., 'Rolamite - A New Mechanical Design Concept', Research Report, Sandia Lab., Oct. 1967.

6. Poritsky, H., 'Microslip and Creep in Contacts', Interdisciplinary Approach to the Lubrication of Concentrated Contacts, NASA SP-237, 1970.

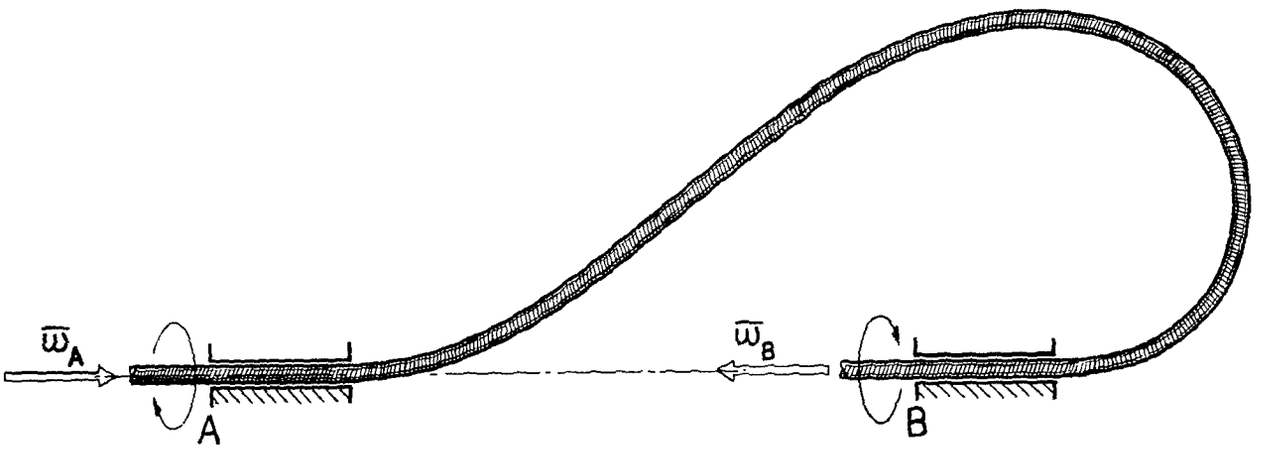

Figure 1.- Flexible shaft.

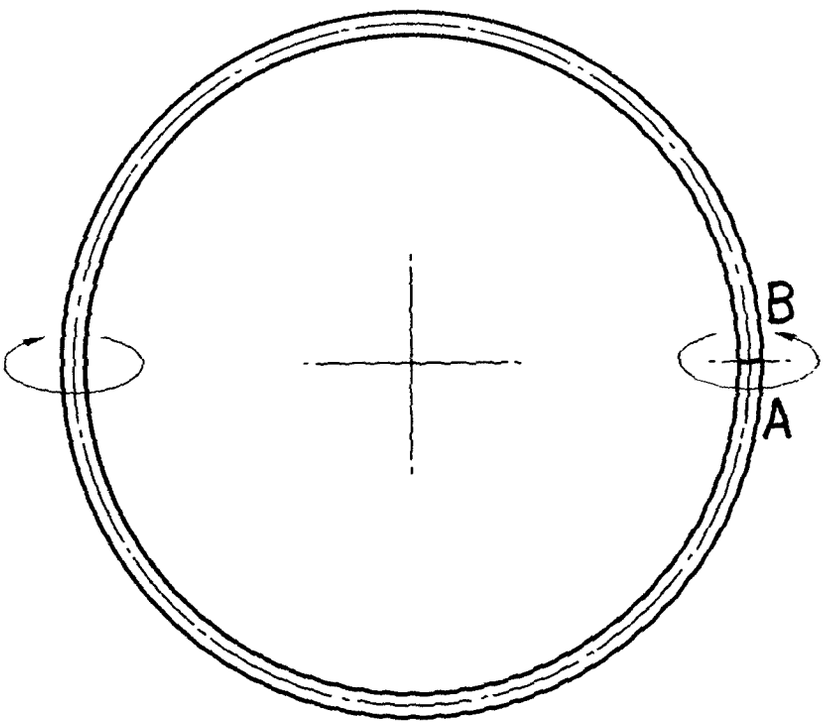

Figure 2.- Ring made of rod.

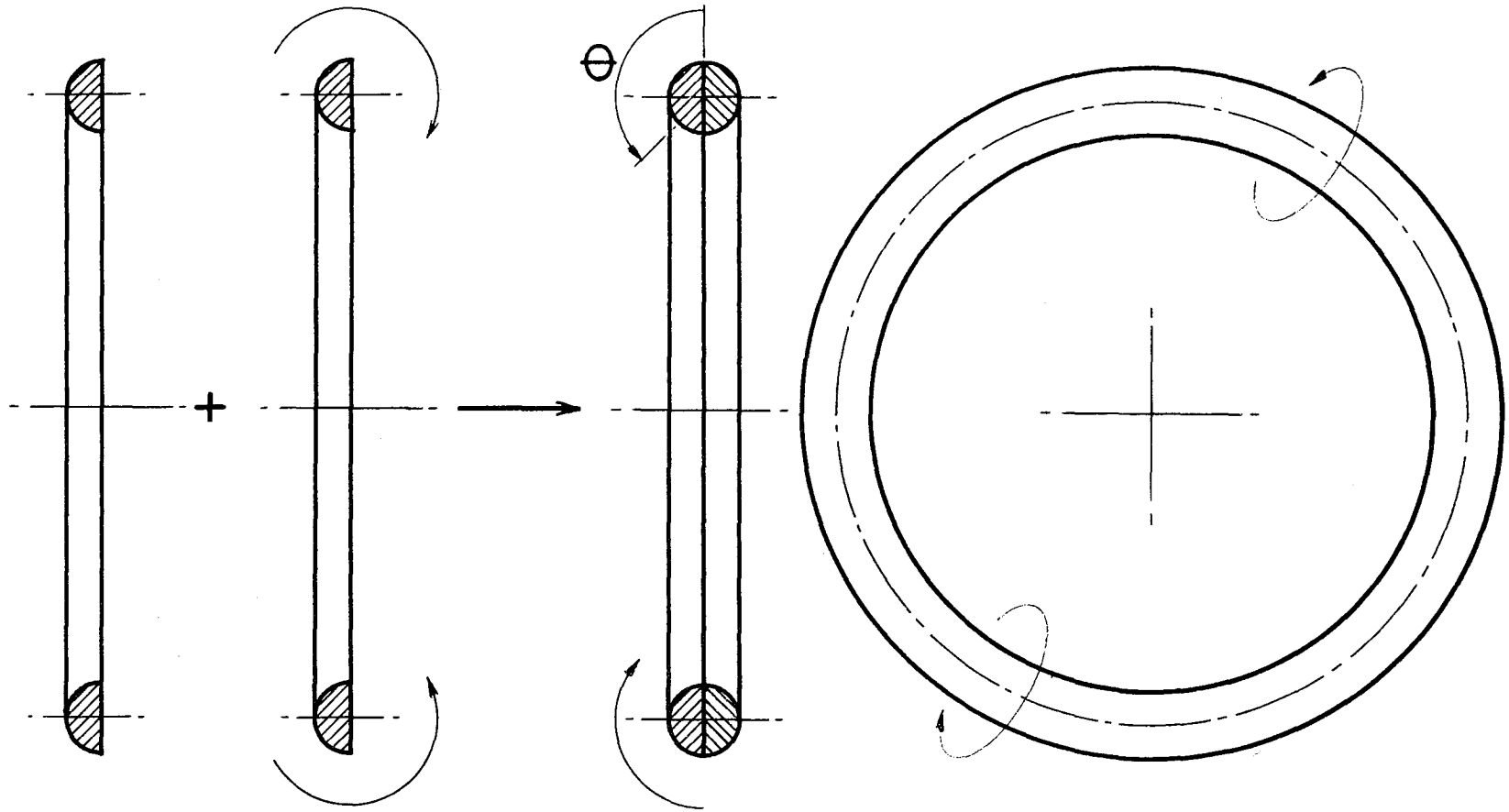

Figure 3.- Free invertible split ring.

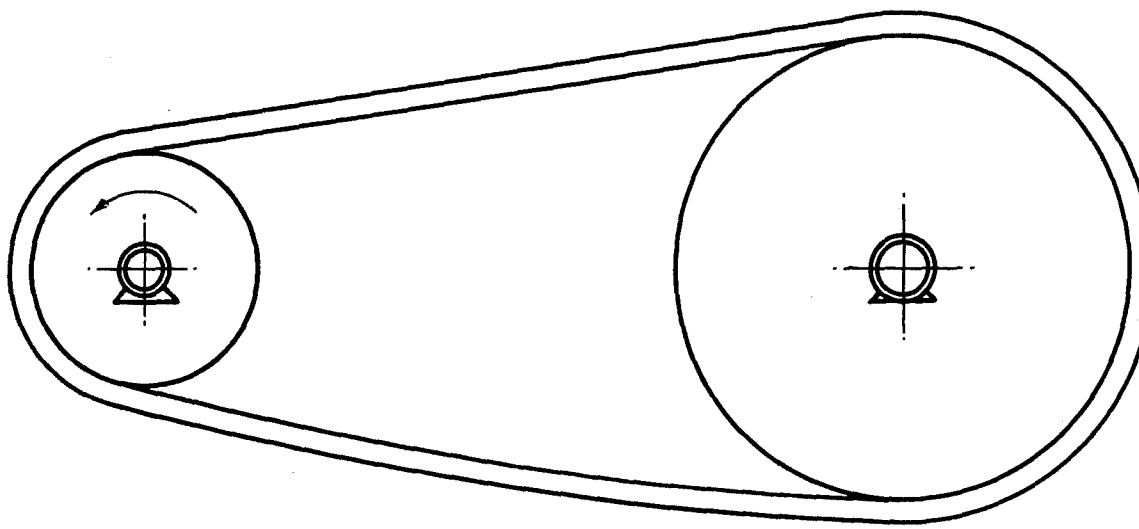

Figure 4.- Belt and pulleys.

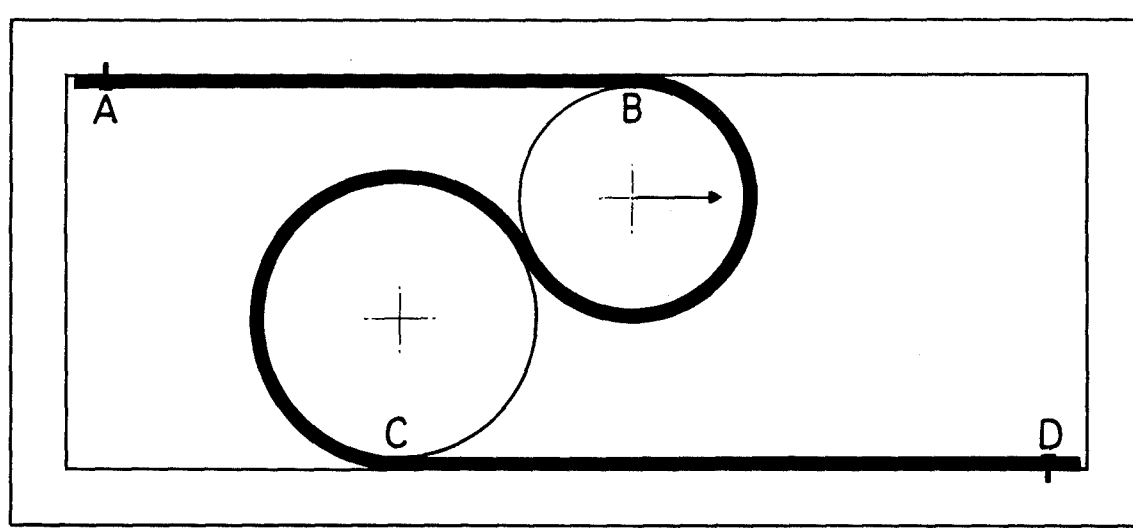

Figure 5.- Rolamite.

A STUDY ON THE FORCED VIBRATION OF A TIMOSHENKO BEAM

Bucur Zainea

SUMMARY

By using Galerkin's variational method we build up an approximate solution for a system of two differential equations with linear partial derivatives of the second order. This system of differential equations corresponds to the physical model, known in the literature as the Timoshenko Beam. The results obtained can be finally applied to two particular cases representing respectively:
the case of a beam with a rectangular section, with a constant height and a basis with a linear variation:
the case of a beam with a constant basis and a height with cubic variation.

INTRODUCTION

We are taking into consideration a heterogenous elastic straight beam possessing variable geometrical and mechanical characteristics all along the beam.

We are considering the small, cross-cut non-damping forced oscillations. The mathematical model chosen to be subjected to analysis consists in a system of two linear equations with partial derivatives of second order, corresponding to the physical model known in the literature under the name of Timoshenko Beam. This model is more exact than the classical one usually employed in the engineering calculations, that is the Euler-Bernoulli model. The difference between them consists in the fact that while for the Euler-Bernoulli model only the deformations given by the bending moment or by the translation inertia are taken into

account, in the Timoshenko model the transverse shear and the rotational inertia are also taken into consideration. As a result the Timoshenko model reflects more exactly the physical reality. It is well-known that (ref. 1) the differences between the two theories become significant in the case of (relatively) short beams and this cannot be neglected any longer.

Although the literature referring to the dynamics of the Timoshenko Beam is abundant enough, the matter of the non-damping beam has been insufficiently treated.

In the present paper we try to determine the approximate solutions of the phenomenon by means of the Galerkin variational method. We are of the opinion that the above mentioned method is most suitable in solving the subject considered. The choosing of the system of coordinates required by the Galerkin method assures the convergence of the obtained solutions.

SYMBOLS

$\delta(x-\zeta)$	Dirac function
$\beta(p,g)$	Euler's Beta function: $\beta(p,g) = \int_0^1 x^{p-1}(1-x)^{g-1}dx$
K	coefficient of the form of the section
G	cross-cut modulus of elasticity
ρ	density of material
E	longitudinal modulus of elasticity (Young)
A(x)	area of cross-cut section

$I(x)$	moment of inertia of cross-cut section
$W(x,t)$	cross-cut displacement
$\psi(x,t)$	rotation angle
$(f(x),g(x))$	scalar product: $(f,g) = \int_0^1 f(x)g(x)dx$
ℓ	length of beam
$V(x)$	time-independent cross-cut displacement
$U(x)$	time-independent rotation angle
α,λ	cross-sectional area parameters
β	moment of inertia parameter
$C_o^\infty[0,1]$	class of functions defined on 0 to 1

THE DIFFERENTIAL EQUATIONS OF THE PHENOMENON

The differential equations for the phenomenon are as follows: (ref. 2)

$$KGA(x)\frac{\partial^2 W}{\partial x^2} - KGA(x)\frac{\partial \psi}{\partial x} = \rho A(x)\frac{\partial^2 W}{\partial t^2} - f(x,t)$$
$$EI(x)\frac{\partial^2 \psi}{\partial x^2} + KGA(x)\left[\frac{\partial W}{\partial x} - \psi\right] = \rho I(x)\frac{\partial^2 \psi}{\partial t^2} \qquad (1)$$

Solutions for the differential equations are determined as follows:

$$W(x,t) = V(x)e^{i\omega t}; \quad \psi(x,t) = U(x)e^{i\omega t} \qquad (2)$$

for boundary conditions

$$W(0,t) = W(b,t) = 0 \; ; \; \psi(0,t) = \psi(b,t) = \infty \tag{3}$$

and f(x,t) is a perturbance force, a mobile, but concentrated force for a unit magnitude:

$$f(x,t) = \delta(x-\zeta)e^{i\omega t}$$

By considering equation (2) the system of equation (1) becomes two differential equations of the fourth order for V(x) and U(x) as follows:

$$a_0(x)U^{IV} + a_1(x)U''' + a_2(x)U'' + a_3(x)U' + a_4(x)U = a_5(x) \tag{4}$$

$$b_0(x)V^{IV} + b_1(x)V''' + b_2(x)V'' + b_3(x)V' + b_4(x)V = b_5(x) \tag{5}$$

The differential equations (4) and (5) for the following two cases are as follows:

Case 1: $A(x) = \alpha(1+\lambda x) \; ; \; I(x) = \beta(1+\lambda x)$

$$\begin{aligned}&(a_{30}x^3 + a_{31}x^2 + a_{32}x + a_{33})U^{IV} + (a_{10}x + a_{11})U''' + \\ &(b_{30}x^3 + b_{31}x^2 + b_{32}x + b_{33})U'' + (b_{10}x + b_{11})U' + \\ &(c_{30}x^3 + c_{31}x^2 + c_{32}x + c_{33})U = \\ &= (a_{20}x^2 + a_{21}x + a_{22})\delta'(x-\zeta) - (c_{10}x + c_{11})\delta(x-\zeta)\end{aligned} \tag{6}$$

$$(a_{50}x^5+a_{51}x^4+a_{52}x^3+a_{53}x^2+a_{54}x+a_{55})V^{IV}+$$
$$+(a_{30}x^3+a_{31}x^2+a_{32}x+a_{33})V'''+$$
$$+(b_{50}x^5+b_{51}x^4+b_{52}x^3+b_{53}x^2+b_{54}x+b_{55})V''+$$
$$+(b_{30}x^3+b_{31}x^2+b_{32}x+b_{33})V'+ \qquad (7)$$
$$+(c_{50}x^5+c_{51}x^4+c_{52}x^3+c_{53}x^2+c_{54}x+c_{55})V=$$
$$=(a_{40}x^4+a_{41}x^3+a_{42}x^2+a_{43}x+a_{44})\delta(x-\zeta)+$$
$$+(c_{30}x^3+c_{31}x^2+c_{32}x+c_{33})\delta'(x-\zeta)-(b_{40}x^4+b_{41}x^3+b_{42}x^2+b_{43}x+b_{44})\delta''(x-\zeta)$$

Case 2: $A(x)=\alpha(1+\lambda x)\,;\quad I(x)=\beta(1+\lambda x)^3$

$$(a_{50}x^5+a_{51}x^4+a_{52}x^3+a_{53}x^2+a_{54}x+a_{55})U^{IV}+(a_{40}x^4+a_{41}x^3+a_{42}x^2+a_{43}x+a_{44})U'''+$$
$$(b_{50}x^5+b_{51}x^4+b_{52}x^3+b_{53}x^2+b_{54}x+b_{55})U''+(b_{40}x^4+b_{41}x^3+b_{42}x^2+b_{43}x+b_{44})U'+$$
$$(c_{50}x^5+c_{51}x^4+c_{52}x^3+c_{53}x^2+c_{54}x+c_{55})U= \qquad (8)$$
$$=(a_{20}x^2+a_{21}x+a_{22})\delta'(x-\zeta)-(a_{10}x+a_{11})\delta(x-\zeta)$$

$$(a_{90}x^9+a_{91}x^8+a_{92}x^7+a_{93}x^6+a_{94}x^5+a_{95}x^4+a_{96}x^3+a_{97}x^2+a_{98}x+a_{99})V^{IV}+$$
$$+(a_{60}x^6+a_{61}x^5+a_{62}x^4+a_{63}x^3+a_{64}x^2+a_{65}x+a_{66})V'''+$$
$$+(b_{90}x^9+b_{91}x^8+b_{92}x^7+b_{93}x^6+b_{94}x^5+b_{95}x^4+b_{96}x^3+b_{97}x^2+b_{98}x+b_{99})V''+$$
$$+(b_{60}x^6+b_{61}x^5+b_{62}x^4+b_{63}x^3+b_{64}x^2+b_{65}x+b_{66})V'+$$

$$+(c_{90}x^9+c_{91}x^8+c_{92}x^7+c_{93}x^6+c_{94}x^5+c_{95}x^4+c_{96}x^3+c_{97}x^2+c_{98}x+c_{99})V =$$
$$=(a_{80}x^8+a_{81}x^7+a_{82}x^6+a_{83}x^5+a_{84}x^4+a_{85}x^3+a_{86}x^2+a_{87}x+a_{88})\delta(x-\zeta)+ \quad (9)$$
$$+(a_{70}x^7+a_{71}x^6+a_{72}x^5+a_{73}x^4+a_{74}x^3+a_{75}x^2+a_{76}x+a_{77})\delta'(x-\zeta)-$$
$$-(b_{80}x^8+b_{81}x^7+b_{82}x^6+b_{83}x^5+b_{84}x^4+b_{85}x^3+b_{86}x^2+b_{87}x+b_{88})\delta''(x-\zeta)$$

THE APPROXIMATE SOLUTION

We shall integrate the differential equations (6), (7), (8), and (9) by means of the Galerkin method.

In the case of boundary conditions of equation (3) we shall consider l=unit which is always possible by

$$\frac{x}{l}=X : \quad 0\le x\le l \Rightarrow \quad 0\le X\le 1$$

Using the Galerkin method, we shall determine an approximate solution for equation (6) as follows:

$$U_n(x)=\sum_{K=1}^{n}\alpha_K\varphi_K(x) \qquad (10)$$

We choose $\phi_k(x)$ of the form (ref. 3)

$$\varphi_K(x)=x^K(1-x)^{m-K}; \quad m=n+1$$

The system of coordinate functions $\phi_k(x)$ has to satisfy the boundary conditions of equation (3) which become equivalent with the following conditions:

$$U(0) = U(1) = 0$$

The approximate solution (10) becomes:

$$U_n(x) = \sum_{k=1}^{n} \alpha_k x^k (1-x)^{m-k} \tag{11}$$

The α_k constants are determined out of the following algebraic system:

$$\sum_{k=1}^{n} \alpha_k (L\varphi_k, \varphi_j) = (g, \varphi_j) \; ; \; j = 1, 2, \ldots, n. \tag{12}$$

where L is the left part of equation (6), and g is the right part of the same equation, that is:

$$L = (a_{30}x^3 + a_{31}x^2 + a_{32}x + a_{33})\frac{d^4}{dx^4} + (a_{10}x + a_{11})\frac{d^3}{dx^3} +$$
$$+ (b_{30}x^3 + b_{31}x^2 + b_{32}x + b_{33})\frac{d^2}{dx^2} + (b_{10}x + b_{11})\frac{d}{dx} +$$
$$+ (c_{30}x^3 + c_{31}x^2 + c_{32}x + c_{33}) \; ;$$

$$L\varphi_k = (a_{30}x^3 + a_{31}x^2 + a_{32}x + a_{33})\frac{d^4\varphi_k}{dx^4} + (a_{10}x + a_{11})\frac{d^3\varphi_k}{dx^3} +$$
$$+ (b_{30}x^3 + b_{31}x^2 + b_{32}x + b_{33})\frac{d^2\varphi_k}{dx^2} + (b_{10}x + b_{11})\frac{d\varphi_k}{dx} +$$
$$+ (c_{30}x^3 + c_{31}x^2 + c_{32}x + c_{33})\varphi_k \; ;$$

$$g = (a_{20}x^2 + a_{21}x + a_{22})\delta'(x-\zeta) - (c_{10}x + c_{11})\delta(x-\zeta)$$

$$(L\varphi_k, \varphi_j) = \int_0^1 \varphi_j L\varphi_k \, dx \; ; \; (g, \varphi_j) = \int_0^1 g\varphi_j \, dx$$

The system of equation (11) is a non-damped algebraic system of n equations with n indeterminates. This system is compatible because the determinant formed with the coefficients of the undeterminants is a Gramm determinant of a linear independent system of functions. For the calculation of the scalar product $(L\phi_k, \phi_j)$ and (g, ϕ_j), we have kept in view the following points:

We have used the Euler's Beta function

$$B(p,q) = \int_0^1 x^{p-1}(1-x)^{q-1} dx$$

We have used the following formula (ref. 4) in calculating the scalar product:

if $\varphi \in C_0^\infty [0,1]$ then

$$\int_0^1 \varphi(x)\delta^{(n)}(x-\zeta)dx = \left(\delta^{(n)}(x-\zeta), \varphi(x)\right) = (-1)^n \varphi^{(n)}(\zeta)$$

For equation (7) with the boundary conditions of equation (3) which mean V(o)=V(1)=o we are going to give an approximate solution of the following form:

$$V_n(x) = \sum_{k=1}^{n} \beta_k x^k (1-x)^{m-k} \; ; \; m = n+1 \qquad (13)$$

where the constant β_k is drawn from the following algebraic system:

$$\sum_{k=1}^{n} \beta_k (L\varphi_k, \varphi_j) = (g, \varphi_j) \; ; \; j = 1, 2, \ldots, n.$$

where L is the left side of equation (7) and g is the right side of the same equation.

Analogous to equation (8) we build up an approximate solution of the following form:

$$U_n(x) = \sum_{k=1}^{n} \gamma_k x^k (1-x)^{m-k} \; ; \; m = n+1$$

where the γ_k constants are determined from the following algebraic system:

$$\sum_{k=1}^{n} \gamma_k (L\varphi_k, \varphi_j) = (g, \varphi_j) \; ; \; j = 1, 2, \ldots, n.$$

where L is the left side of equation (8) and g the right side of the same equation.

Finally, for equation (9) we build up a solution of the following form:

$$V_n(x) = \sum_{k=1}^{n} \delta_k x^k (1-x)^{m-k} \; ; \; m = n+1$$

where the δ_k constants are determined from the following algebraic system:

$$\sum_{k=1}^{n} \delta_k (L\varphi_k, \varphi_j) = (g, \varphi_j) \; ; \; j = 1, 2, \ldots, n.$$

where L and g are the left side and right side of equation (9).

As a conclusion to case 1 the approximate solutions built up by the Galerkin method are the following:

$$\psi_n(x,t) = e^{i\omega t}\sum_{k=1}^{n}\alpha_k x^k(1-x)^{m-k}\ ;\ W_n(x,t) = e^{i\omega t}\sum_{k=1}^{n}\beta_k x^k(1-x)^{m-k}$$

and, for case 2 the approximate solutions are the following

$$\psi_n(x,t) = e^{i\omega t}\sum_{k=1}^{n}\gamma_k x^k(1-x)^{m-k}\ ;\ W_n(x,t) = e^{i\omega t}\sum_{k=1}^{n}\delta_k x^k(1-x)^{m-k}$$

PECULIAR CASES

In the following lines we shall use the obtained solution for two particular cases, which will be also an indirect checking of the accuracy of the obtained results.

We build up the first two approximations ψ_1; ψ_2 and respectively W_1; W_2 for the following situations:

$$A(x) = A_0(1+\lambda x)\ ;\ J(x) = J_0(1+\lambda x) \tag{14}$$

$$A(x) = A_0(1+\lambda x)\ ;\ J(x) = J_0(1+\lambda x)^3 \tag{15}$$

They represent respectively the case of a beam with a rectangular section, having a constant height and a base with a linear variation, and the case of a beam with a constant base and a height with a cubic variation and this because, from an applicative point of view the beam sections are in many cases considered

rectangular. Case (a) The equation (6), if we consider (14) is reduced to the following equation

$$(1+\lambda x)^2\left[EI_0U^{IV}+\rho\omega^2\left(1+\frac{E}{kG}\right)I_0U''+\rho\omega^2\left(\frac{\rho\omega^2}{kG}I_0-A_0\right)U\right]=$$
$$=(1+\lambda x)\delta'(x-\zeta)-\lambda\delta(x-\zeta)$$

The first and second approximations are respectively:

$$\psi_1=\alpha x(1-x)e^{i\omega t}\ ;\ \psi_2=\left[\alpha_1 x(1-x)^2+\alpha_2 x^2(1-x)\right]e^{i\omega t}$$

If we compare ψ_1 with ψ_2 for a rectangular beam made of steel we come to the conclusion that the two approximations are comparable: $\psi_1 = \psi_2$ for certain λ values and for certain x values

λ	0,1	0,2	0,3	0,4	0,5
x	0,252	0,541	0,528	0,573	0,525

This conclusion results from the following calculation:

$$\alpha=\frac{(g,\varphi)}{(L\varphi,\varphi)}=\frac{4\lambda\zeta^2-3\lambda\zeta+2\zeta-1}{\rho\omega^2\left(\frac{\rho\omega^2}{kG}I_0-A_0\right)\left(\frac{1}{105}\lambda^2+\frac{1}{30}\lambda+\frac{1}{30}\right)-\rho\omega^2\left(1+\frac{E}{kG}\right)I_0\left(\frac{1}{10}\lambda^2+\frac{1}{3}\lambda+\frac{1}{3}\right)}$$

The α_1,α_2 constants are determined from the following algebraic system:.

$$\alpha_1(L\varphi_1,\varphi_1)+\alpha_2(L\varphi_2,\varphi_1)=(g,\varphi_1)$$
$$\alpha_1(L\varphi_1,\varphi_2)+\alpha_2(L\varphi_2,\varphi_2)=(g,\varphi_2)$$

where

$$(g,\varphi_1) = -5\lambda\zeta^3 + (8\lambda-3)\zeta^2 + (4-3\lambda)\zeta - 1 \; ; \; (g,\varphi_2) = 5\lambda\zeta^3 + (3-4\lambda)\zeta^2 - 2\zeta$$

$$(L\varphi_1,\varphi_1) = \rho\omega^2\left(\frac{\rho\omega^2}{KG}I_0 - A_0\right)\left(\frac{1}{630}\lambda^2 + \frac{1}{140}\lambda + \frac{1}{105}\right) - \rho\omega^2\left(1+\frac{E}{KG}\right)I_0\left(\frac{1}{105}\lambda^2 + \frac{1}{15}\lambda + \frac{2}{15}\right)$$

$$(L\varphi_1,\varphi_2) = \rho\omega^2\left(\frac{\rho\omega^2}{KG}I_0 - A_0\right)\left(\frac{1}{504}\lambda^2 + \frac{1}{140}\lambda + \frac{1}{140}\right) + \rho\omega^2\left(1+\frac{E}{KG}\right)I_0\left(\frac{1}{105}\lambda^2 - \frac{1}{30}\right)$$

$$(L\varphi_2,\varphi_1) = \rho\omega^2\left(\frac{\rho\omega^2}{KG}I_0 - A_0\right)\left(\frac{1}{504}\lambda^2 + \frac{1}{140}\lambda + \frac{1}{140}\right) - \rho\omega^2\left(1+\frac{E}{KG}\right)I_0\left(\frac{1}{42}\lambda^2 + \frac{1}{15}\lambda + \frac{1}{30}\right)$$

$$(L\varphi_2,\varphi_2) = \rho\omega^2\left(\frac{\rho\omega^2}{KG}I_0 - A_0\right)\left(\frac{1}{252}\lambda^2 + \frac{1}{84}\lambda + \frac{1}{105}\right) - \rho\omega^2\left(1+\frac{E}{KG}\right)I_0\left(\frac{8}{105}\lambda^2 + \frac{1}{5}\lambda + \frac{2}{15}\right)$$

and for the steel in S.I. units

$$k = \frac{5}{6}\,h \; ; \; G = 8\cdot 9{,}8\times 10^9 \frac{N}{m^2} \; ; \; E = 2{,}1\times 9{,}8\times 10^{10}\frac{N}{m^2} \; ; \; l = 1\,m.$$
$$h = 10^{-1}\,m. \; ; \; \rho = 8\times 10^3 \frac{Kg}{m^3} \; ; \; A_0 = a_0 h \; ; \; I_0 = a_0\frac{h^3}{12}$$

Equation (7) then becomes:

$$(1+\lambda x)^4\left(aV^{IV} + bV'' + cV\right) = \left[d_1(1+\lambda x)^3 - 2\lambda^2 d(1+\lambda x)\right]\delta(x-\zeta) +$$
$$+ 2\lambda d(1+\lambda x)\delta'(x-\zeta) - d(1+\lambda x)^3\delta''(x-\zeta)$$

where $a = EGKA_0^4 \; ; \; b = \rho\omega^2(E+kG)I_0A_0^3 \; ; \; d = EI_0A_0^2$

$$c = \rho\omega^2(\rho\omega^2 I_0 - kGA_0)A_0^3 \; ; \; d_1 = (KGA_0 - \rho\omega^2 I_0)A_0^2$$

The first and second approximations are

$$W_1 = \beta x(1-x)e^{i\omega t} \quad ; \text{ and } \quad W_2 = \left[\beta_1 x(1-x)^2 + \beta_2 x^2(1-x)\right]e^{i\omega t}$$

where

$$\beta = \frac{A_1 d_1 + B_1 d}{Ac + Bb}$$

$$A = \frac{1}{252}\lambda^4 + \frac{1}{42}\lambda^3 + \frac{2}{35}\lambda^2 + \frac{1}{15}\lambda + \frac{1}{30}$$

$$B = -\left(\frac{1}{21}\lambda^4 + \frac{4}{15}\lambda^3 + \frac{3}{5}\lambda^2 + \frac{2}{3}\lambda + \frac{1}{3}\right)$$

$$A_1 = \frac{1}{4}\left(1+\frac{\lambda}{2}\right)^3$$

$$B_1 = -\frac{3}{4}\lambda^3 - \lambda^2 + 3\lambda + 2$$

$$\beta_1 = \frac{1}{\Delta}\left[(A_2 d_1 + B_2 d)(P_6 c + P_7 b) - (A_3 d_1 + B_3 d)(P_3 c + P_5 b)\right]$$

$$\beta_2 = \frac{1}{\Delta}\left[(A_3 d_1 + B_3 d)(P_1 c + P_2 b) - (A_2 d_1 + B_2 d)(P_3 c + P_4 b)\right]$$

$$\Delta = (P_1 c + P_2 b)(P_6 c + P_7 b) - (P_3 c + P_4 b)(P_3 c + P_5 b)$$

$$A_2 = \frac{1}{8}\left(1+\frac{\lambda}{2}\right)^3$$

$$B_2 = 1 + \frac{7}{2}\lambda + \frac{5}{4}\lambda^2$$

$$A_3 = \frac{1}{8}\left(1+\frac{\lambda}{2}\right)^3$$

$$B_3 = 1 - \frac{1}{2}\lambda - \frac{9}{4}\lambda^2 - \frac{3}{4}\lambda^3$$

$$P_1 = \frac{1}{2310}\lambda^4 + \frac{1}{315}\lambda^3 + \frac{1}{105}\lambda^2 + \frac{1}{70}\lambda + \frac{1}{105}$$

$$P_2 = -\left(\frac{1}{105}\lambda^3 + \frac{2}{35}\lambda^2 + \frac{2}{15}\lambda + \frac{2}{15}\right)$$

$$P_3 = \frac{1}{1320}\lambda^4 + \frac{1}{210}\lambda^3 + \frac{1}{84}\lambda^2 + \frac{1}{70}\lambda + \frac{1}{140}$$

$$P_4 = \frac{1}{84}\lambda^4 + \frac{1}{21}\lambda^3 + \frac{2}{35}\lambda^2 - \frac{1}{30}$$

$$P_5 = -\left(\frac{1}{84}\lambda^4 + \frac{1}{15}\lambda^3 + \frac{1}{7}\lambda^2 + \frac{2}{15}\lambda + \frac{1}{30}\right)$$

$$P_6 = \frac{1}{495}\lambda^4 + \frac{1}{90}\lambda^3 + \frac{1}{42}\lambda^2 + \frac{1}{42}\lambda + \frac{1}{105}$$

$$P_7 = -\left(\frac{1}{21}\lambda^4 + \frac{5}{21}\lambda^3 + \frac{16}{35}\lambda^2 + \frac{2}{5}\lambda + \frac{2}{15}\right)$$

Because $W_2 = W_1\left[1 + \frac{(\beta_1-\beta) + (\beta_2-\beta_1)x}{\beta}\right]$ the conclusion is made that the two approximations are comparable for certain λ values and for certain x values such as

λ	0,1	0,2	0,3	0,4	0,5
x	0,675	0,515	0,585	0,525	0,567

CONCLUSIONS TO THESE PECULIAR CASES

For equations (8) and (9) we come to the same result, that is: the first two approximate solutions are equal for the given values of λ for the same value of x :0,5: $0 \leq x \leq 1$ that is, the approximate solutions are comparable among themselves in the vicinity of where the concentrated perturbance force is applied: when $x = \zeta = \frac{1}{2}$.

REFERENCES

1. Newmann, K.: Viscous Damping in Flexural Vibrations of Bars. Journal of Applied Mechanics. September 1959.

2. Sun, C. T.: On the Equations for a Timoshenko Beam Under Initial Stress. Journal of Applied Mechanics. March 1972.

3. Zainea, Bucur: Concernant à la Convergence de la Méthode de Galerkin. Buletinul Stiintific al Institutului de Constructii Bucuresti. Anul XVI Nr. 3/ 1973.

4. Schwarts, Laurent: Methodesmathématiques poursciences physiques (Chapitre II. Dérivation des distributions).

ENVIRONMENTAL EFFECTS ON POLYMERIC MATRIX COMPOSITES

J. M. Whitney and G. E. Husman
Air Force Materials Laboratory

SUMMARY

Current epoxy resins utilized in high performance structural composites absorb moisture from high humidity environments. Such moisture absorption causes plasticization of the resin to occur with concurrent swelling and lowering of the glass transition temperature. Similar effects are observed in composites. Data are presented showing the effects of absorbed moisture on Hercules AS/3501-5 graphite/epoxy composites. Prediction of moisture content and distribution in composites, along with reduction in mechanical properties, are discussed.

INTRODUCTION

The glass transition temperature, T_g, of a polymer is defined as the temperature above which the polymer is soft and below which it is hard. For epoxy resins the T_g is the temperature at which the polymer goes from a glassy solid to a rubbery solid. From a practical standpoint it is more appropriate to discuss a glass transition temperature region rather than a single glass transition temperature, as the change from a hard polymeric material to a soft material takes place over a temperature range. The concept of a T_g is for convenience and refers to the temperature at which there is a very rapid change in physical properties. As a result, there is no precise T_g.

It is well recognized (ref. 1) that the T_g of a polymer can be lowered by mixing with it a miscible liquid (diluent) that has a lower glass transition temperature than the polymer. This process is referred to as plasticization. Thus, moisture acts as a diluent in current resins being utilized in high performance structural composites, resulting in a lowering of the T_g. There are indications (ref. 2) that similar effects occur in epoxy matrix composites. Data (ref. 2) also indicates that the lowering of the T_g in both neat resins and

derived composites can be estimated from the Kelley-Bueche plasticization theory (ref. 3). Thus, absorbed moisture reduces the temperature range over which matrix dominated composite properties remain stable. From a practical standpoint, change of failure mode due to plasticization is of primary concern.

In the present paper, the prediction of moisture content in conjunction with laboratory characterization is discussed in detail. In addition, data is presented which shows the effect of absorbed moisture on the flexure strength of unidirectional Hercules AS/3501-5 graphite/epoxy composites. The flexure test is an excellent example of absorbed moisture inducing a change in failure mode.

PREDICTION OF MOISTURE DIFFUSION

Fick's Law

It has been shown (ref. 4) that moisture diffusion in laminated composites can be predicted by Fick's second law. For diffusion through the thickness of an infinite plate, the diffusion equation is given by

$$\frac{\partial m}{\partial t} = D_z \frac{\partial^2 m}{\partial z^2} \tag{1}$$

where m is the percent moisture gain per unit thickness, D_z is the diffusivity through the thickness, t denotes time, and z is the thickness coordinate. Consider the following boundary and initial conditions for a plate of thickness h

$$m(z, 0) = m_i = \text{constant} \tag{2}$$

$$m(0, t) = m(h, t) = m_1 = \text{constant} \tag{3}$$

where m_i is the initial moisture distribution in the material, and m_1 is the surface moisture concentration, which is a function of the relative humidity. A solution to equation (1) which satisfies the conditions of equations (2) and (3) can be obtained by classical separation of variables with the result

$$m(z,t) = m_1 - \frac{4}{\pi}(m_1 - m_i) \sum_{n=1}^{\infty} \frac{1}{(2n-1)} \times \left[\sin \frac{(2n-1)\pi z}{h} \exp\left[-(2n-1)^2 \pi^2 t^*\right] \right] \quad (4)$$

where

$$t^* = \frac{D_z t}{h^2} \quad (5)$$

The total weight gain of moisture in the plate is given by

$$M = \int_0^h m \, dz \quad (6)$$

Integration of equation (4) yields

$$M(t) = M_1 - \frac{8}{\pi^2}(M_1 - M_i) \sum_{n=1}^{\infty} \frac{\exp\left[-(2n-1)^2 \pi^2 t^*\right]}{(2n-1)^2} \quad (7)$$

Application to Characterization

Consider an experiment where an initially dry specimen is exposed to a constant environment (temperature and humidity) for a given period of time t_1. It is then put in a dry environment and the temperature ramped at a constant rate to a given level at time t_2. A test is then performed on the specimen over some period of time. Such a procedure is used during laboratory characterization of moisture effects on the mechanical behavior of laminates. It is often desirable to control both the moisture content and distribution during such a characterization. Equations (4) and (7) can be modified for such a purpose.

For the interval $0 \leq t \leq t_1$, equations (4) and (7) can be used directly with $m_i = M_i = 0$ and $D_z = D_z(T_1)$, where T_1 denotes the temperature during this time interval. It should be noted that the diffusivity is a function of temperature. In the interval $t_1 \leq t \leq t_2$ the temperature will be varying with time and as a result, D_z will vary with time. This can be accounted for by defining t^* in the following manner (ref. 5)

$$t^* = \frac{1}{h^2} \int_{t_1}^{t} D_z(s)\, ds \tag{8}$$

Note that in the derivation of equation (8) it is assumed that the temperature gradient has negligible effect on diffusivity, as the heat diffusivity is several orders of magnitude greater than moisture diffusivity. For this interval the initial distribution can be obtained from equation (4), with the result

$$m_i(z) = m_1 \left[1 - \frac{4}{\pi} \sum_{n=1}^{\infty} \frac{1}{(2n-1)} \sin\frac{(2n-1)\pi z}{h} \right. \tag{9}$$

$$\left. \times \exp\left[-(2n-1)^2 \pi^2 t_1^*\right] \right]$$

where

$$t_1^* = \frac{D_z(T_1)t_1}{h^2} \tag{10}$$

In addition,

$$m(0,t) = m(h,t) = 0 \tag{11}$$

$$D_z = D_z(T) = D_z(t) \tag{12}$$

If equation (9) is expressed as a Fourier series, then the moisture profile for this time interval becomes

$$m(z,t) = \frac{4}{\pi} m_1 \sum_{n=1}^{\infty} \frac{1}{(2n-1)} \left\{ 1 \right. \tag{13}$$

$$\left. - \exp\left[-(2n-1)^2 \pi^2 t_1^*\right] \right\} \sin\frac{(2n-1)\pi z}{h}$$

$$\times \exp\left[\frac{-(2n-1)^2 \pi^2}{h^2} \int_{t_1}^{t} D_z(s)\, ds \right]$$

$$M(t) = \frac{8M_1}{\pi^2} \sum_{n=1}^{\infty} \frac{1 - \exp\left[-(2n-1)^2 \pi^2 t_1^*\right]}{(2n-1)^2}$$

$$x \quad \exp\left[\frac{-(2n-1)^2 \pi^2}{h^2} \int_{t_1}^{t} D_z(s)\, ds\right] \tag{14}$$

For the interval $t_2 \leq t$

$$m_i(z) = \frac{4m_1}{\pi} \sum_{n=1}^{\infty} \frac{1}{(2n-1)} \left\{1 - \exp\left[-(2n-1)^2 \pi^2 t_1^*\right]\right\}$$

$$x \quad \exp\left[-(2n-1)^2 \pi^2 t_2^*\right] \quad \sin\frac{(2n-1)\pi z}{h} \tag{15}$$

where

$$t_2^* = \frac{1}{h^2} \int_{t_1}^{t_2} D_z(s)\, ds \tag{16}$$

The boundary conditions are those of equation (11). Since equation (14) is in the form of a Fourier series, the moisture profile for this time interval becomes

$$m(z,t) = \frac{4m_1}{\pi} \sum_{n=1}^{\infty} \frac{1}{(2n-1)} \left\{1 - \exp\left[-(2n-1)^2 \pi^2 t_1^*\right]\right\} \quad \sin\frac{(2n-1)\pi z}{h}$$

$$x \quad \exp\left[-(2n-1)^2 \pi^2 (t_2^* + \bar{t})\right] \tag{17}$$

and the total moisture gain is given

$$M(t) = \frac{8M_1}{\pi^2} \sum_{n=1}^{\infty} \frac{1}{(2n-1)^2} \left\{1\right.$$

$$- \exp\left[-(2n-1)^2\ {}^2t_1^*\right]\Bigg\} \quad \exp\left[-(2n-1)^2\ {}^2(t_2^* + \bar{t})\right] \tag{18}$$

where

$$\bar{t} = \frac{D_z(T_2)}{h^2}\ (t - t_2) \tag{19}$$

CHANGE IN FAILURE MODES

Filament Dominated Laminates

In most engineering usage of fiber reinforced composites, laminate stacking geometry is chosen such that stiffness and strength are controlled by fiber modulus and strength, respectively. Thus, some matrix softening can be accommodated in such applications without serious consequences. If considerable matrix softening occurs, however, the ability of the resin to support the fiber is severely reduced, along with the ability to transfer load through the matrix to the fibers. The result is a change in failure mode from filament dominated to matrix dominated. The classical example is that of unidirectional compression, where a significant loss in matrix stiffness leads to local instabilities and a reduction in compression strength. Thus, any loss in resin T_g due to moisture absorption can lead to a reduction in the useful temperature range of the composite laminate.

Flexure Strength

Unidirectional flexure tests are commonly used for quality control, and 0 degree flex strength is considered to be a filament dominated property. For state-of-the-art high-performance epoxy resins, 0 degree dry flex strength is relatively insensitive to temperatures below 300°F. With increasing moisture content, however, measurable strength degradation can occur at temperatures considerably below 300°F. This is illustrated in Table I, where 0 degree flex strengths are shown for Hercules AS/3501-5 graphite/epoxy composites. These results were obtained on eight-ply composites subjected to a standard four-point bend test with a 32:1 span-to-depth ratio. A cursory examination of these results reveals that a severe loss in 0 degree flex strength occurs at a temperature as low as 200°F after exposure to equilibrium moisture content in a 95% relative humidity environment. The T_g of this material under these conditions has been shown to be approximately 210°F (ref. 2).

Under dry conditions the shear strength of the matrix, for temperatures less than 300°F, is high enough to prevent interlaminar shear failure and assure that the flex strength is governed by fiber breakage. As moisture induces matrix softening below 300°F, the high temperature flex strength becomes dominated by interlaminar shear yielding. This conclusion can be supported by examining failed specimens and noting that the 300°F wet composites did not display fiber breakage as the mode of failure, but were permanently deformed near the load noses where the shear stress was largest. Furthermore, the load deflection curves for these cases produced a classic example of an elastic-plastic material. For conditions under which brittle failure was induced, fiber breakage occured between the loading pins where the interlaminar shear stress vanishes. Thus, the 0 degree flex strength is another classic example of a change in failure mode induced by matrix softening.

Interlaminar shear stress-strain behavior relative to the 0 degree flex test is illustrated in figure 1. These 0 degree shear results were obtained from a ± 45 degree tensile test as described by Rosen (ref. 6). The entire stress-strain curve is not shown, but is terminated at the stress level where the maximum interlaminar shear stress occurs in the 0 degree flex test. This value can be calculated from classical beam theory with the following result for quarter-point loading.

$$\tau_{max} = \frac{\sigma_f}{S} \tag{20}$$

where τ_{max} is the maximum value of the interlaminar stress obtained during the flex test, σ_f is the flex strength, and S is the span-to-depth ratio of the test specimen. For the high temperature tests considerable non-linear shear stress-strain behavior is observed. For the wet tests, the non-linear behavior occurs at very low stress levels.

To further illustrate the change in failure mode, 0 degree flex strength is plotted on a log scale in figure 2 as a function of temperature for wet and dry conditions. This plot resembles typical log modulus versus temperature curves found in classical viscoelastic polymeric materials. Thus, the flex test may be useful in assessing T_g for composites or for assessing the useful temperature range of the material for various moisture contents.

CONCLUDING REMARKS

It has been shown that a solution to Fick's law can be obtained which is relavent to laboratory characterization of composite materials containing moisture. This solution provides a detailed moisture profile in addition to determining total weight gain due to moisture absorption. Data presented also indicates that the widely utilized unidirectional flexure test can be a valuable tool in assessing the useful temperature range of composite laminates for various moisture contents.

REFERENCES

1. Bueche, F.: Physical Properties of Polymers. Interscience Publishers, New York, 1962.

2. Browning, C.E.; Husman, G.E.; and Whitney, J.M.: Moisture Effects in Epoxy Matrix Composites. Composite Materials: Testing and Design (Fourth Conference), American Society for Testing and Materials, 1976.

3. Bueche, F.; and Kelley, F.N.: Viscosity and Glass Temperature Relations for Polymer-Diluent Systems. Journal of Polymer Science, vol. 45, 1961, pp. 549-556.

4. Shen, Chi-Hung; and Springer, G.S.: Moisture Absorption and Desorption of Composite Materials. Journal of Composite Materials, vol. 10, January, 1976, pp. 2-20.

5. Weitzman, Y.: Diffusion With Time-Varying Diffusivity, With Application to Moisture-Sorption in Composites. Journal of Composite Materials, vol. 10, July, 1976.

6. Rosen, B.W.: A Simple Procedure for Experimental Determination of the Longitudinal Shear Modulus of Unidirectional Composites. Journal of Composite Materials, vol. 6, October, 1972, pp. 552-554.

TABLE I.- UNIDIRECTIONAL FLEX STRENGTH, AS/3501-5 GRAPHITE/EPOXY

TEMPERATURE	σ_f(DRY)	σ_f(WET-1.1%)*	σ_f(WET-1.7%)**
RT	259 KSI	265 KSI	252 KSI
200° F	259 KSI	210 KSI	180 KSI
250° F	242 KSI	166 KSI	135 KSI
300° F	233 KSI	125 KSI	90 KSI

* EXPOSED TO EQUILIBRIUM AT 75% RELATIVE HUMIDITY AND 160°F, % WT. GAIN = 1.1%.

** EXPOSED TO EQUILIBRIUM AT 95% RELATIVE HUMIDITY AND 160°F, % WT. GAIN = 1.7%.

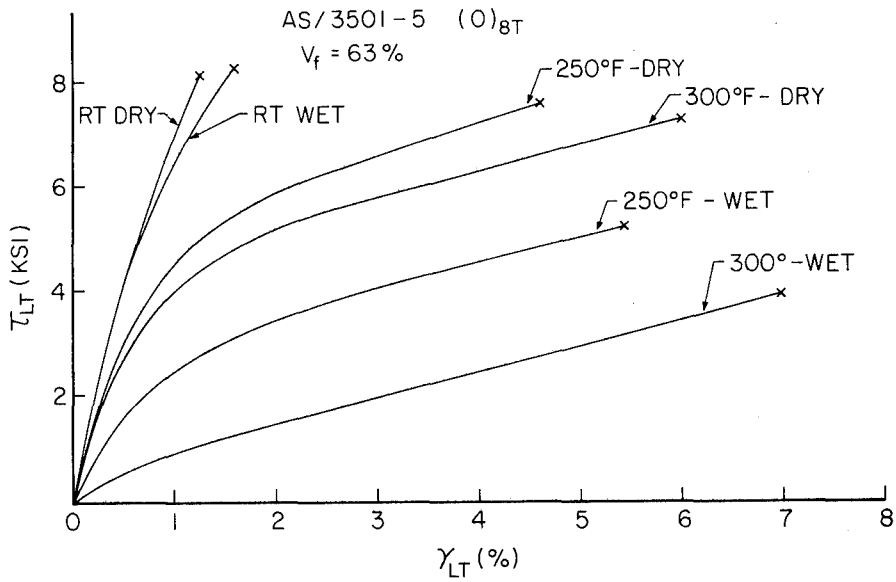

Figure 1.- Shear stress-strain curves for unidirectional composites. Wet = 1.1% equilibrium weight gain at 75% relative humidity and 160°F.

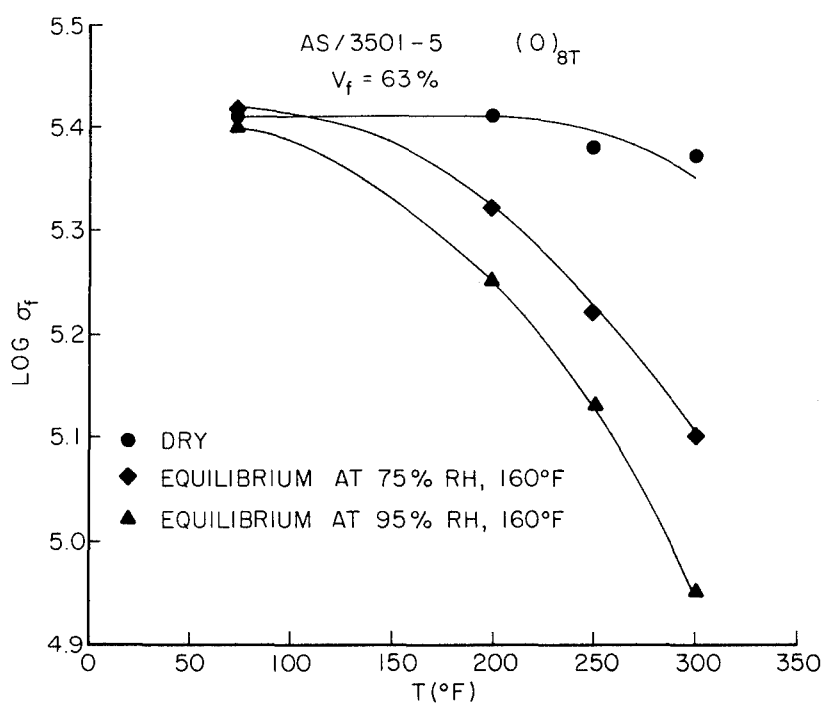

Figure 2.- Unidirectional flex strength as a function of temperature.

INTERLAYER DELAMINATION IN FIBER REINFORCED COMPOSITES WITH AND WITHOUT SURFACE DAMAGE

S. S. Wang
Department of Materials Science and Engineering
Massachusetts Institute of Technology
Cambridge, Massachusetts

ABSTRACT

Fracture problems of interlayer delamination in fiber reinforced composites with and without surface damage are studied in this paper. The singular hybrid-stress finite element method employing a crack tip super-element based on a complex variable formulation is used. The applied loads are either uniform stretching or pure bending as in standard experimental tensile and interlaminar tests. Combined fracture modes and the corresponding stress intensity factors are obtained for different ply orientations and stacking sequences for a graphite/epoxy system. The results also serve to elucidate the interlaminar stress transfer mechanism for this type of fracture problem. Using Erdogan-Sih's brittle fracture criterion, the initiation and direction of growth from the delamination crack are calculated.

STRESS INTENSITY AT A CRACK BETWEEN BONDED DISSIMILAR MATERIALS[1]

Morris Stern and Chen-Chin Hong
The University of Texas at Austin

INTRODUCTION

The nature of the stress field in front of a crack lying in the surface between bonded dissimilar materials was first investigated by Williams (ref. 1). He observed that not only do the stresses grow at a rate inversely proportional to the square root of distance from the crack tip, they also exhibit an oscillatory singularity with wave length inversely proportional to the absolute value of the logrithm of distance from the crack tip. The problem of calculating stress intensity factors for various special loadings and geometries has been treated by other authors, among them Erdogan (ref. 2 and 3), England (ref. 4), Rice and Sih (ref. 5), and Erdogan and Gupta (ref. 6). In all cases for which results are given the region is unbounded and the loads are uniform.

For more general boundary value problems involving imperfect bonding of dissimilar materials numerical methods must be resorted to, and both the growth and oscillatory nature of the singularity can be expected to cause numerical difficulties. In addition, because the elastic moduli of the materials are generally different, discontinuities in components of stress and strain develop naturally on the bond. Recently we extended the contour integral method to problems of this type. It turns out that the nature of the loading and restraints, even on remote edges, can have a significant effect on the stress intensity. In this paper we treat some example problems to illustrate this.

[1]This work was supported in part by a grant from the National Science Foundation.

CONTOUR INTEGRAL METHOD

The basic boundary value problem is illustrated in Fig. 1. Two dissimilar materials are joined along a straight edge with one or more cracks present. The composite is loaded or restrained on the remote boundary, and the crack faces are free of load. Local cartesian and polar coordinates are introduced with origin at a crack tip and the negative x-axis ($\theta = \pm \pi$) along the crack edges. The subscript 1 is arbitrarily assigned to material below the axis ($-\pi \leq \theta \leq 0$), and the subscript 2 is used for the other material ($0 \leq \theta \leq \pi$). Also introduced is the so-called bimaterial constant

$$\gamma = \frac{\mu_1 + \mu_2 \kappa_1}{\mu_2 + \mu_1 \kappa_2} \tag{1}$$

where μ_1, μ_2 are the respective shear moduli and $\kappa = 3-4\nu$ for plane strain, or $\kappa = (3-4\nu)(1+\nu)$ for plane stress, ν being Poisson's Ratio.

Notation for complex displacement and stress fields in terms of components referred to the local polar coordinate system are introduced as follows:

$$u = u_r + iu_\theta$$

$$\sigma_r = \sigma_{rr} + i\tau_{r\theta} \tag{2}$$

$$\sigma_\theta = \sigma_{\theta\theta} - i\tau_{r\theta}$$

Then the displacement and stress fields in the neighborhood of the crack tip in each material are of the form[2]

$$u_1 = \frac{\bar{K}}{2\mu_1(1+\gamma)\lambda} r^{\lambda}[\kappa_1 e^{i(\lambda-1)\theta} - \gamma e^{i(-\lambda-1)\theta}]$$

$$+ \frac{K}{2\mu_1(1+\gamma)} r^{\bar{\lambda}}[e^{i(-\bar{\lambda}-1)\theta} - e^{i(-\bar{\lambda}+1)\theta}] + \text{remainder}$$

$$u_2 = \frac{\bar{K}}{2\mu_2(1+\gamma)\lambda} r^{\lambda}[\kappa_2\gamma e^{i(\lambda-1)\theta} + e^{i(-\lambda-1)\theta}]$$

$$+ \frac{K}{2\mu_2(1+\gamma)} r^{\bar{\lambda}}[e^{i(-\bar{\lambda}+1)\theta} - e^{i(-\lambda+1)\theta}] + \text{remainder}$$

$$\sigma_{1r} = \frac{\bar{K}}{(1+\gamma)} r^{\lambda-1}[e^{i(\lambda-1)\theta} - \gamma e^{i(-\lambda-1)\theta}]$$

$$+ \frac{K}{(1+\gamma)} r^{\bar{\lambda}-1}[\bar{\lambda}e^{i(\bar{\lambda}-1)\theta} - (\bar{\lambda}-2)e^{i(-\bar{\lambda}+1)\theta}] + \text{remainder}$$

$$\sigma_{2r} = \frac{\bar{K}}{(1+\gamma)} r^{\lambda-1}[\gamma e^{i(\lambda-1)\theta} - e^{i(-\lambda-1)\theta}] \qquad (3)$$

$$+ \frac{K\gamma}{(1+\gamma)} r^{\bar{\lambda}-1}[\bar{\lambda}e^{i(-\bar{\lambda}-1)\theta} - (\bar{\lambda}-2)e^{i(-\bar{\lambda}+1)\theta}] + \text{remainder}$$

$$\sigma_{1\theta} = \frac{\bar{K}}{(1+\gamma)} r^{\lambda-1}[e^{i(\lambda-1)\theta} + \gamma e^{i(-\lambda-1)\theta}]$$

$$+ \frac{K\bar{\lambda}}{(1+\gamma)} r^{\bar{\lambda}-1}[e^{i(-\bar{\lambda}+1)\theta} - e^{i(-\bar{\lambda}-1)\theta}] + \text{remainder}$$

$$\sigma_{2\theta} = \frac{\bar{K}}{(1+\gamma)} r^{\lambda-1}[\gamma e^{i(\lambda-1)\theta} + e^{i(-\lambda-1)\theta}]$$

$$+ \frac{K\gamma\bar{\lambda}}{(1+\gamma)} r^{\bar{\lambda}-1}[e^{i(-\bar{\lambda}+1)\theta} - e^{i(-\bar{\lambda}-1)\theta}] + \text{remainder}$$

[2]Except for notational differences these results were also obtained in references 3, 4 and 5.

where

$$\lambda = \frac{1}{2} + \frac{i}{2\pi} \ln \gamma = \frac{1}{2} + i\varepsilon \quad (\varepsilon = \frac{1}{2\pi} \ln \gamma) \tag{4}$$

and $K = K_o e^{i\beta}$ is a complex stress intensity factor with the following "physical" interpretation:

$$\lim_{r\to 0} \sigma_\theta \Big|_{\theta=0} = \lim_{x\to 0^+} (\sigma_{yy} - i\tau_{xy}) \Big|_{y=0}$$

$$= Kr^{\lambda-1} = K_o r^{-\frac{1}{2}} e^{i(\varepsilon \ln r + \beta)}$$

hence on the bond immediately in front of the crack tip we have

$$\sigma_{yy} = \frac{K_o}{\sqrt{r}} \cos(\varepsilon \ln r + \beta) + \text{remainder}$$

$$\tau_{xy} = \frac{K_o}{\sqrt{r}} \sin(\varepsilon \ln r + \beta) + \text{remainder} \tag{5}$$

Thus K_o governs the amplitude growth rate of both the normal stress and shear stress while β determines a nonsignificant phase shift. The complex crack opening displacement is also governed by the stress intensity factor:

$$\Delta u = u_2 \Big|_{\theta=\pi} - u_1 \Big|_{\theta=-\pi} = \left\{ \frac{\mu_1 + \mu_2 \kappa_1}{\mu_1 \mu_2} \right\} \frac{\cosh \varepsilon\pi}{(1+\gamma)\lambda} \bar{K} r^\lambda$$

The amplitude of the complex crack opening displacement can be put in the form

$$|\Delta u| = \frac{(\mu_1 + \mu_2 \kappa_1)(\mu_2 + \mu_1 \kappa_2)}{\mu_1 \mu_2 (\mu_1 + \mu_2 + \mu_1 \kappa_2 + \mu_2 \kappa_1)} \frac{\cosh \varepsilon\pi}{\sqrt{\frac{1}{4} + \varepsilon^2}} K_o \sqrt{r} \tag{6}$$

A contour integral representation for the stress intensity factor is obtained from the reciprocal work identity by introducing a suitable artificial singular elastic state. Briefly, we observe that for arbitrary values of the complex constant C,

a singular elastic state corresponding to zero body force and with no traction on the lines $\theta = \pm \pi$ is defined in the bimaterial region by

$$
\begin{aligned}
2\mu_1 u_1^* &= \bar{C}\lambda r^{-\lambda}[e^{i(\lambda+1)\theta} - e^{i(\lambda-1)\theta}] \\
&\quad + Cr^{-\bar{\lambda}}[\kappa_1 e^{i(-\bar{\lambda}-1)\theta} - \gamma e^{i(\bar{\lambda}-1)\theta}] \\
2\mu_2 u_2^* &= \bar{C}\lambda\gamma r^{-\lambda}[e^{i(\lambda+1)\theta} - e^{i(\lambda-1)\theta}] \\
&\quad + Cr^{-\bar{\lambda}}[\kappa_2\gamma e^{i(-\bar{\lambda}-1)\theta} - e^{i(\bar{\lambda}-1)\theta}] \\
\sigma_{r1}^* &= \bar{C}\lambda r^{-\lambda-1}[\lambda e^{i(\lambda-1)\theta} - (\lambda+2)e^{i(\lambda+1)\theta}] \\
&\quad + C\bar{\lambda} r^{-\bar{\lambda}-1}[\gamma e^{i(\bar{\lambda}-1)\theta} - e^{i(-\bar{\lambda}-1)\theta}] \\
\sigma_{r2}^* &= \bar{C}\gamma\lambda r^{-\lambda-1}[\lambda e^{i(\lambda-1)\theta} - (\lambda+2)e^{i(\lambda+1)\theta}] \\
&\quad + C\bar{\lambda} r^{-\bar{\lambda}-1}[e^{i(\bar{\lambda}-1)\theta} - \gamma e^{i(-\bar{\lambda}-1)\theta}] \\
\sigma_{\theta 1}^* &= \bar{C}\lambda^2 r^{-\lambda-1}[e^{i(\lambda+1)\theta} - e^{i(\lambda-1)\theta}] \\
&\quad - C\bar{\lambda} r^{-\bar{\lambda}-1}[e^{i(-\bar{\lambda}-1)\theta} + \gamma e^{i(\bar{\lambda}-1)\theta}] \\
\sigma_{\theta 2}^* &= \bar{C}\gamma\lambda^2 r^{-\lambda-1}[e^{i(\lambda+1)\theta} - e^{i(\lambda-1)\theta}] \\
&\quad - C\bar{\lambda} r^{-\bar{\lambda}-1}[\gamma e^{i(-\bar{\lambda}-1)\theta} + e^{i(\bar{\lambda}-1)\theta}]
\end{aligned}
\tag{7}
$$

This elastic state has the further property that on the contour C_ε (a circle of radius ε centered on the origin) we calculate a finite contribution from the reciprocal work as the contour shrinks to a point:

$$I_{tip} = \lim_{\varepsilon \to 0} \int_{C_\varepsilon} (\underset{\sim}{u}^* \cdot \underset{\sim}{t} - \underset{\sim}{u} \cdot \underset{\sim}{t}^*) ds$$

$$= \lim_{\varepsilon \to 0} \int_{C_\varepsilon} Re[\bar{u}^* \sigma_r - \bar{u} \sigma_r^*] ds \qquad (8)$$

$$= \frac{-\pi(\mu_1 + \mu_2 \kappa_1)}{\mu_1 \mu_2} Re\ \bar{C}K$$

Upon noting that the reciprocal work vanishes on the complete contour $C_o \cup C^+ \cup C_\varepsilon \cup C^-$ indicated in Fig. 1 as a consequence of Betti's theorem, and on the crack edges $C^+ \cup C^-$ since the tractions in any case vanish there, we obtain the representation

$$\begin{Bmatrix} Re\ K \\ Im\ K \end{Bmatrix} = \int_{C_o} (\underset{\sim}{u} \cdot \underset{\sim}{t}^* - \underset{\sim}{u}^* \cdot \underset{\sim}{t}) ds \qquad (9)$$

where for *Re* K we choose $C = -\frac{\mu_1 \mu_2}{\pi(\mu_1 + \mu_2 \kappa_1)}$ in Eq. (7) in calculating $\underset{\sim}{t}^*$ and $\underset{\sim}{u}^*$, whereas for *Im* K we take $C = -i \frac{\mu_1 \mu_2}{\pi(\mu_1 + \mu_2 \kappa_1)}$. The values of $\underset{\sim}{u}$ and $\underset{\sim}{t}$ on the contour C_o are obtained numerically. For the results given in this paper we used code TEXGAP (ref. 7) which performs isotropic linearly elastic plane analyses using conventional quadratic displacement triangles and isoparametric quadrilaterals.

NUMERICAL RESULTS

The four cases treated involve a finite bimaterial strip loaded in tension and are sketched in Fig. 2. From symmetry considerations we need to consider only the shaded region, and in Fig. 3 we show a typical grid (symmetrically defined in each half region) for the finite element analyses. Half the contour used for evaluation of the stress intensity factors is shown in dashed line in Fig. 3. We note that the four distinct problems considered are obtained from the same grid and boundary conditions on the edges parallel to the crack, but with the following boundary conditions on the vertical edges:

i) Central crack - free edges: AB restrained, CD unrestrained
ii) Central crack - fixed edges: AB and CD restrained
iii) Single edge crack: AB and CD unrestrained
iv) Double edge crack: AB unrestrained, CD restrained.

Two sets of results are plotted in Fig. 4 and 5. The first shows the effect of different crack sizes in a given strip for each case; the second shows the effect of changing the relative dimensions of the strip for a fixed crack length to width ratio. In each case the results are normalized using the stress intensity factor for an infinite region loaded uniformly in tension normal to the crack and restrained from motion parallel to the crack on the remote boundary. This case is equivalent to an infinite bimaterial plate with vanishing stresses at infinity and a uniformly pressurized crack on the bond, for which analytical results are given in references (4) and (5):

$$K_\infty = \sqrt{1 + 4\varepsilon^2}\ \sigma_o\sqrt{a/2} \tag{10}$$

It is interesting to note that for real materials the bimaterial constant γ is restricted to values between 1 and 3; consequently, the maximum variation in K_∞ that can be achieved by varying the properties of the two materials (this enters only through the parameter ε) is less than six percent, thus the isotropic case furnishes an excellent (lower bound) estimate for K_∞. The data plotted in Fig. 4 and 5 are based on material properties

$$\kappa_1 = 1.6, \quad \kappa_2 = 1.8, \quad \mu_2/\mu_1 = 17$$

which yields the value $\gamma = 1.5$.

REFERENCES

1. Williams, M.L.: The Stresses Around a Fault or Crack in Dissimilar Media. Bulletin of the Seismological Society of America, vol. 49, 1959, pp. 199-204.

2. Erdogan, F.: Stress Distribution in a Nonhomogeneous Elastic Plane With Cracks. Journal of Applied Mechanics, vol. 30, 1963, pp. 232-236.

3. Erdogan, F.: Stress Distribution in Bonded Dissimilar Materials With Cracks. Journal of Applied Mechanics, vol. 32, 1965, pp. 403-410.

4. England, A.H.: A Crack Between Dissimilar Media. Journal of Applied Mechanics, vol. 32, 1965, pp. 400-402.

5. Rice, J.R.; Sih, G.C.: Plane Problems of Cracks in Dissimilar Media. Journal of Applied Mechanics, vol. 32, 1965, pp. 418-423.

6. Erdogan, F.; Gupta, G.D.: Layered Composites with an Interface Flaw. International Journal of Solids and Structures, vol. 7, 1971, pp. 1089-1107.

7. Dunham, R.S.; Becker, E.B.: TEXGAP, The Texas Grain Analysis Program. TICOM Report 73-1, The University of Texas at Austin, August, 1973.

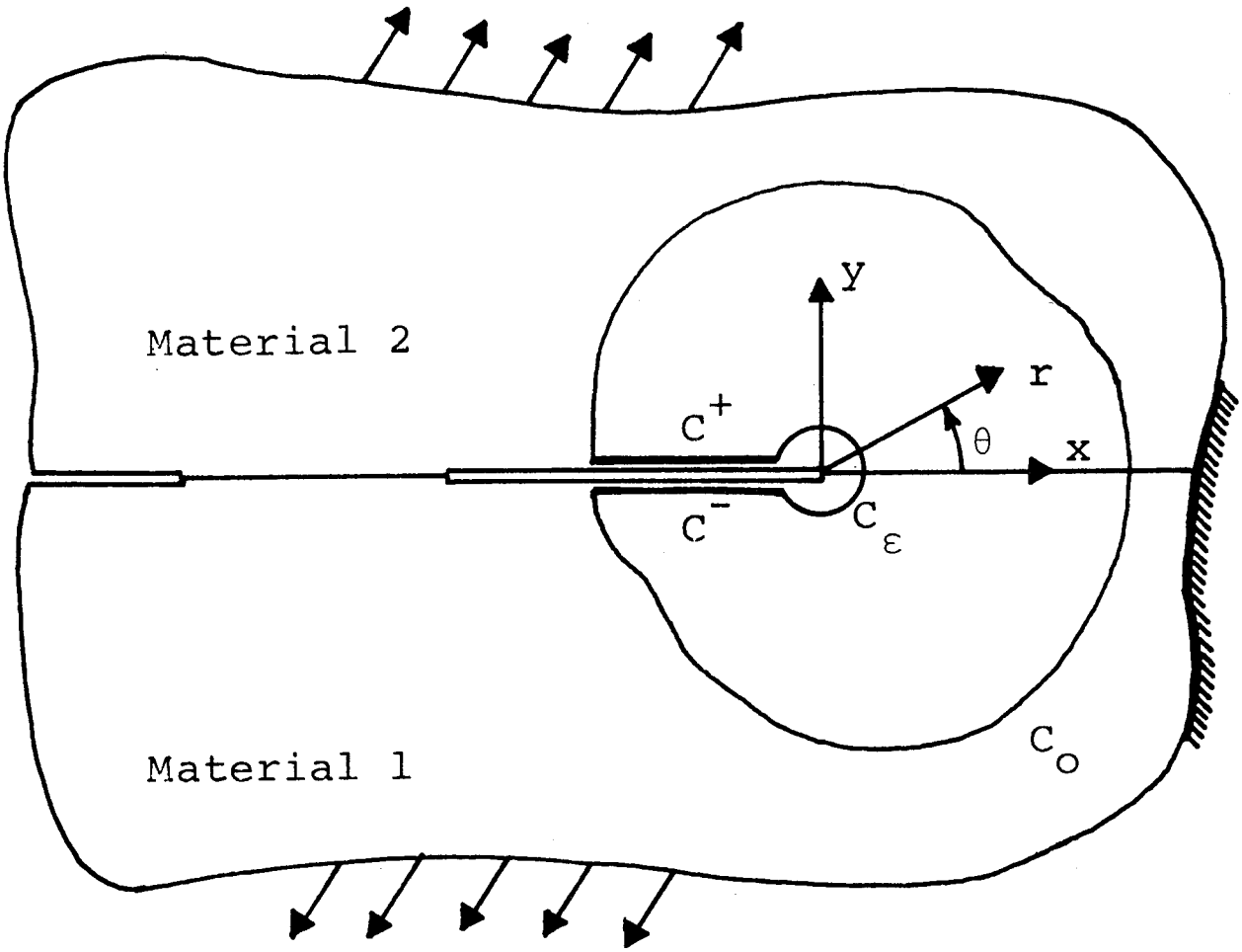

Figure 1.- Basic boundary value problem.

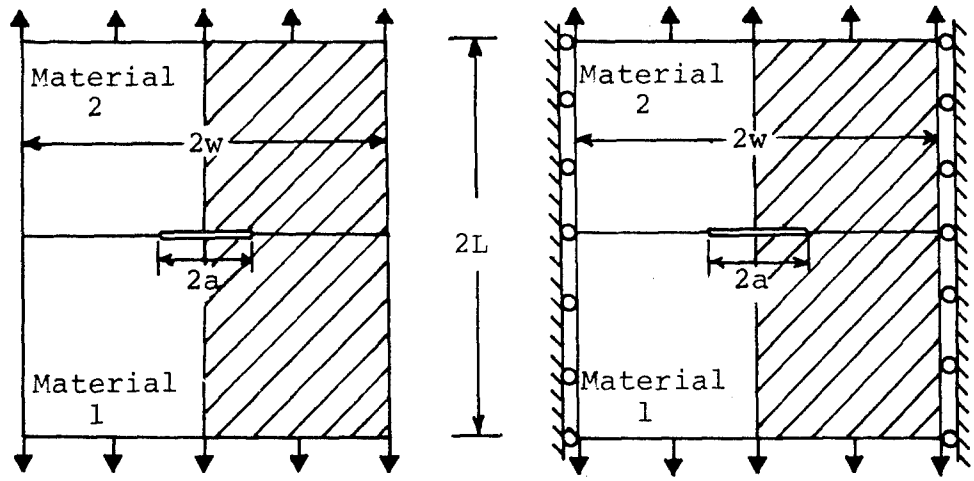

i) Central crack - free edges. ii) Central crack - restrained edges.

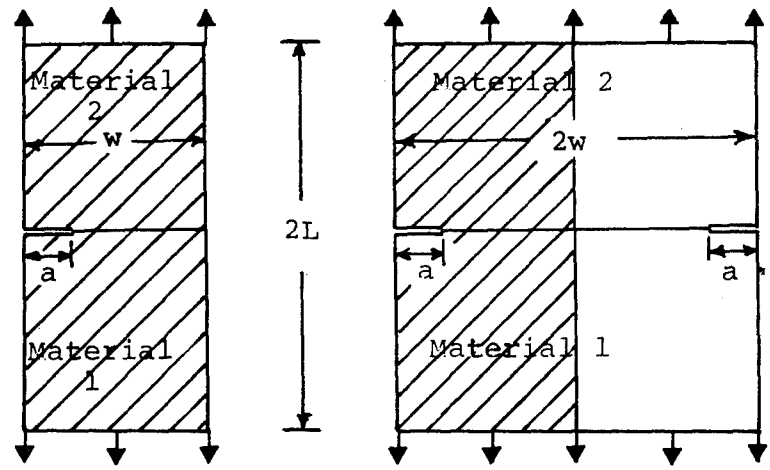

iii) Single edge crack. iv) Double edge crack.

Figure 2.- The four cases considered.

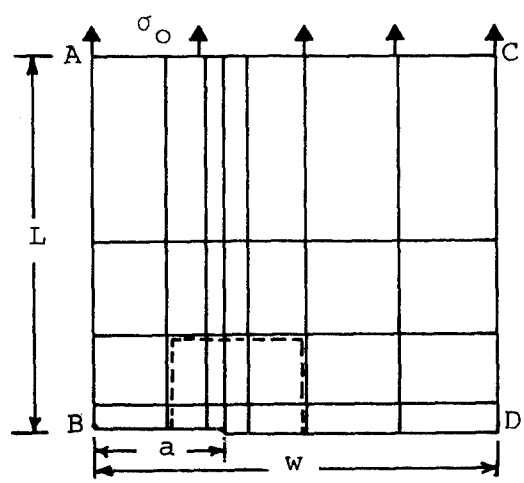

Figure 3.- Finite element grid.

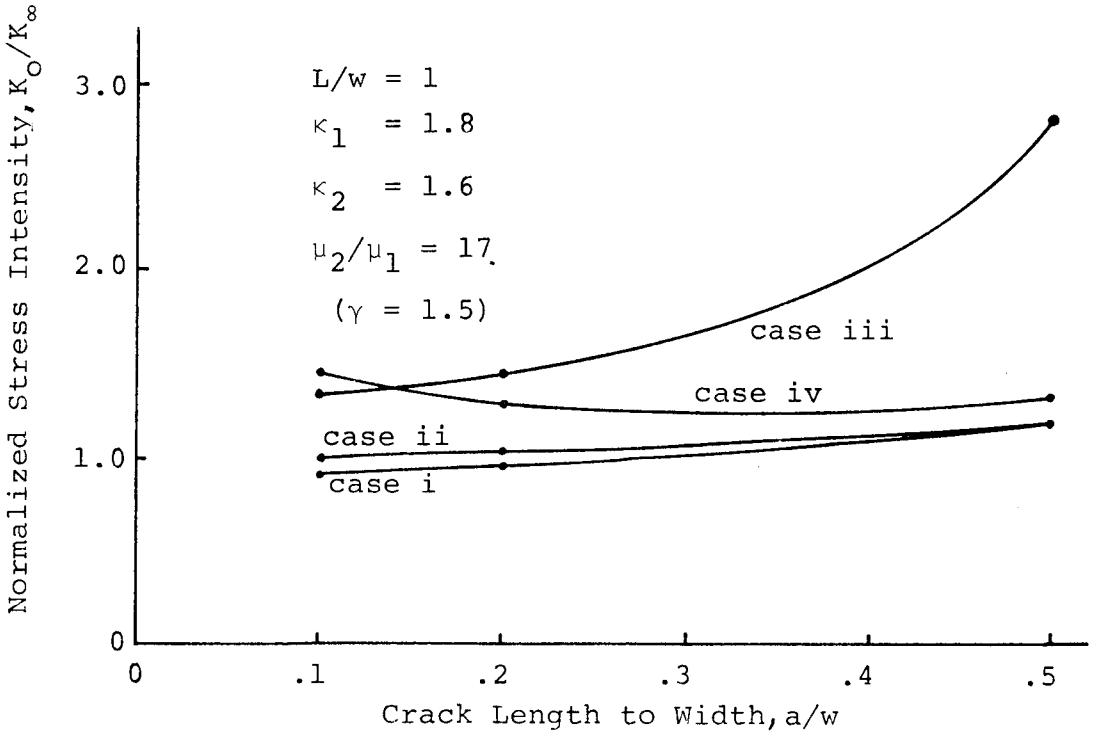

Figure 4.- Effect of crack length.

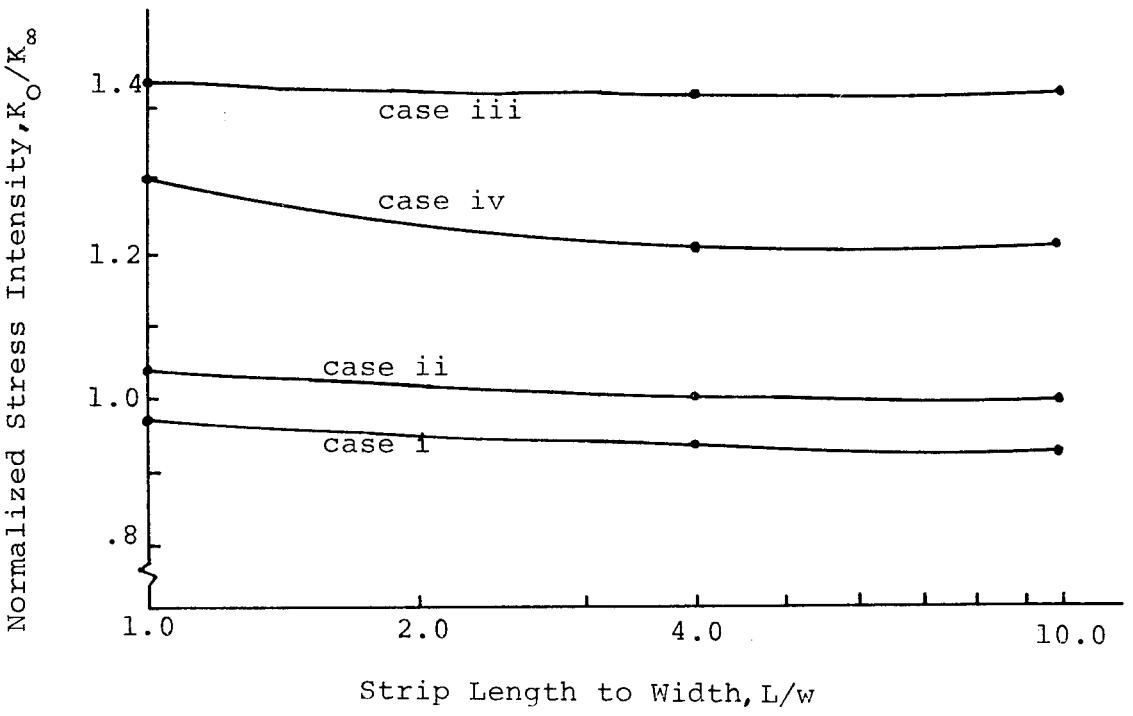

Figure 5.- Effect of strip length.

STRESS CONCENTRATION FACTORS AROUND A CIRCULAR HOLE IN LAMINATED COMPOSITES

C. E. S. Ueng
Georgia Institute of Technology

SUMMARY

This paper deals with the determination of stress concentration factors around a circular hole in a composite laminate. The specific case investigated is a four layer ($-45^o/45^o/45^o/-45^o$) graphite epoxy laminate. The factors are determined experimentally by means of electrical resistance strain gages, and analytically by using a hybrid finite-element analysis.

INTRODUCTION

In this study, the laminar stress concentrations around a circular hole in an angle-ply composite laminate are determined for the axial tension loading case. Of particular interest is the largest value of σ_θ present at the perimeter of the hole. This study proposes to determine these stresses experimentally and analytically. For the experimental analysis, electrical resistance strain gages are used. The analytic procedure uses the finite-element method of a two-dimensional hybrid model with an assumed stress field within the element and assumed displacements at the element interfaces.

The stress concentration factors around a circular hole in an infinite, isotropic sheet have been determined analytically through various approaches and confirmed experimentally. For an infinite plate, the stress components around the hole are (ref. 1)

$$\sigma_r = \frac{\sigma_o}{2}\left(1 - \frac{b^2}{r^2}\right) + \frac{\sigma_o}{2}\left(1 - \frac{b^2}{r^2}\right)\left(1 - \frac{3b^2}{r^2}\right)\cos 2\theta \tag{1a}$$

$$\sigma_\theta = \frac{\sigma_o}{2}\left(1 + \frac{b^2}{r^2}\right) - \frac{\sigma_o}{2}\left(1 + \frac{3b^4}{r^4}\right)\cos 2\theta \tag{1b}$$

$$\tau_{r\theta} = -\frac{\sigma_o}{2}\left(1 - \frac{b^2}{r^2}\right)\left(1 + \frac{3b^2}{r^2}\right)\sin 2\theta \tag{1c}$$

where b is the radius of the hole and σ_o is the applied load. The ratio of σ_θ/σ_o along the hole is plotted as shown in figure 1. Obviously, the maximum

of σ_θ is three times σ_o, and occurs at $\theta = \pm 90^o$, i.e., at the ends of the diameter perpendicular to the direction of tension.

Due to the increasing use of advanced laminated composites in flight structures and other potential applications, the stress concentration around a cutout in a fiber-reinforced laminate has been the subject of research by several investigators in recent years. Daniel and Rowland (ref. 2) used an experimental approach - the Moire technique, and determined the strain (stress) concentration around a circular hole in a tension loaded anisotropic plate. Hyman et al. (ref. 3) carried some exploratory tests on the same problem. Franklin (ref. 4) also investigated the hole stress concentrations in filamentary structures. By using linear elastic plane stress conditions with the help of finite-element method, Rybicki and Hooper (ref. 5) studied and obtained results for boron-epoxy lamina. In a reviewing article (ref. 6), Grimes and Greimann gave an up-to-date overall picture about the stress concentration around a circular hole in a fiber-reinforced composite. Several additional references are cited in this article.

In an experimental study of orthotropic composite materials, Kulkarni, Rosen, and Zweben (ref. 7) have found that the stress concentration factors are a function of the hole diameter, up to a diameter of 2.54 cm (1 in.). They observed that the actual number of filaments severed by the hole determined the strength of the specimen.

The present problem of a general angle-ply composite laminate with a circular hole is further complicated by the interaction of the individual layers.

EXPERIMENTAL WORK

Equipment

The orientation of the strain gages around the holes is shown for each of the four specimens in figure 2. The gages were mounted adjacent to the hole and were 4.8 mm (3/16 in.) wide, 120 ohm standard foil gages. The specimens were mounted in clamp grips and attached to a 90,000 N (20,000 lb.) capacity load cell through the use of swivel bearings. The gages were wired into the digital strain indicator with the indicator providing three arms of the Wheatstone bridge required in the electrical circuit. The load cell was wired into an electrical transducer and calibrated to measure the axial tension applied to the specimens.

The strain gages were applied to the specimens using Eastman 910 adhesive, following standard preparation of the surfaces.

Test Specimen Data

The four testing specimens were provided by Lockheed-Georgia Aircraft Company. Their assistance is greatly appreciated.

Material: graphite epoxy (Narmco 5209/T300)

65% graphite fiber, 35% epoxy matrix

Four layer angle-ply ($-45^{o}/45^{o}/45^{o}-45^{o}$)

Grip tabs of fiberglass epoxy molded integrally with specimens.

For a unidirectional single layer the macroscopic properties are

$$E_{0^o} = 137900 \sim 144795 \text{ MN/m}^2 \ (20 \sim 21(10)^6 \text{ psi})$$

$$E_{90^o} = 8274 \sim 9653 \text{ MN/m}^2 \ (1.2 \sim 1.4(10)^6 \text{ psi})$$

$$G = 4.55 \text{ MN/m}^2 \ (0.66(10)^6 \text{ psi})$$

Specimen No.	1	2	3	4
Width	10.16 cm (4 in)	10.16 cm (4 in)	10.16 cm (4 in)	10.16 cm (4 in)
Hole diameter	2.5522 cm (1.0048 in)	2.5527 cm (1.0050 in)	2.5527 cm (1.0050 in)	2.5530 cm (1.0051in)

The thickness of the four specimens around the hole was also carefully measured. Data were taken at eight stations, the end points of a horizontal diameter, a vertical diameter, and two more diameters which bisect the horizontal and vertical directions. The results are shown in table 1.

It can therefore be concluded that the assumed thickness 0.6350 mm (0.0250 in) is quite reasonable.

Testing Procedure

First, the testing specimen was mounted in the upper grips of the loading device. The loading indicator and the strain indicator were zeroed and calibrated. Then the other end of the specimen was mounted in the lower grips of the loading device. After the specimen was loaded up to the 100% load (2224 N or 500 lb), the load was then released. This was repeated six times in order to eliminate the strain gage error due to strain hardening. An increment of 20% of the maximum load was used each time, and the corresponding strain reading was then taken. The same steps were followed for the other three specimens.

Testing Results

The data obtained from the strain gage testing was the values for ε_θ at

four different locations around the hole. These values are given in table 2, and displayed graphically in figure 3.

The strain gage results can be easily repeated and showed very good stability with repeated loadings. The values obtained at 444.8 N (100 lb) of load are not as reliable as the incremental changes in strain for each incremental change in load. Normally, the tightening of the end clamps on the specimens resulted in an initial strain of some significance.

The assistance of Mr. W. H. Taylor in carrying out the testing program is acknowledged here.

Stresses

Based upon the available mechanical properties as previously mentioned, the stresses were calculated from the stress-strain relation and the transformation relations. The tangential stress component σ_θ obtained from the recorded strains are plotted in figure 4.

FINITE ELEMENT ANALYSIS

The finite-element method used here is a two-dimensional hybrid approach. The variational principle used is that of minimum complementary energy with the interelement stress continuity enforced by means of the Lagrange multipliers. The elements used are shown in figure 5.

The formulation of the problem at this stage follows a rather standard fashion as this method is typically applied to many stress analysis problems.

The stress function polynomial used in the computer program is

$$\psi = ax^3 + bx^2y + cxy^2 + dy^3 \tag{2}$$

which results in the following stresses:

$$\begin{aligned} \sigma_{xx} &= 2\,cx + 6\,dy \\ \sigma_{yy} &= 6\,ax + 2\,by \\ \tau_{xy} &= -2\,bx - 2\,cy \end{aligned} \tag{3}$$

It can be easily verified that these stress components automatically satisfy the equilibrium equations in the absence of body forces.

Arranged in matrix form, equations (3) become

$$[\sigma] = [Q]\,[a] \tag{4}$$

where

$$[Q] = \begin{bmatrix} 0 & 0 & 2x & 6y \\ 6x & 2y & 0 & 0 \\ 0 & -2x & -2y & 0 \end{bmatrix} \quad \text{and} \quad [a] = \begin{bmatrix} a \\ b \\ c \\ d \end{bmatrix}$$

By Cauchy's relation $T_i = \sigma_{ij} n_j$, one has

$$\begin{matrix} T_x \\ T_y \end{matrix} = \begin{bmatrix} n_x & 0 & n_y \\ 0 & n_y & n_x \end{bmatrix} \begin{bmatrix} \sigma_{xx} \\ \sigma_{yy} \\ \tau_{xy} \end{bmatrix} \tag{5}$$

or

$$[T] = [M]\,[a] \tag{6}$$

where

$$[M] = \begin{bmatrix} n_x & 0 & n_y \\ 0 & n_y & n_x \end{bmatrix} [Q] \tag{7}$$

Following a somewhat standard fashion, the circumferential stress around the hole is obtained and plotted also in figure 4 for the comparison purpose.

DISCUSSION OF RESULTS

The results presented in this paper represent an attempt to understand and predict the stress concentration around a circular hole in an angle-ply laminate. As shown in figure 4, the circumferential stresses, based upon the finite-element method and the one computed from the recorded strain data, are plotted together for comparison purpose. These two curves cross each other at a few places, but the discrepancy at some places is up to 35%. This degree of deviation is not hoped for, but it is tolerable. Similar experience indicates that such a difference is by all means possible.

The stress concentration factor at $b/r = 1$ and $\theta = \pm 90^{\circ}$ is about 5.8

which is considerably higher than the classical factor 3 for an infinite, isotropic plate. Therefore, special attention must be paid for the local stress concentration around such a circular hole. One possible reason for having such a high stress concentration factor is that a number of fibers were cut at the location of the hole. This weakens the ability of the fiber elements for transmitting the stresses. From an intuitive point of view, if the location of the hole is known in advance, then rerouting the fibers around the hole may cut down the high stress concentration factor.

REFERENCES

1. Timoshenko, S. P. and Goodier, J. N.: Theory of Elasticity, Third Edition, McGraw-Hill, 1970, p. 91.

2. Daniel, I. M. and Rowland, R. E.: Determination of Strain Concentration in Composites by Moiré Techniques, Journal of Composite Materials, vol. 5, April 1971, pp. 250-254.

3. Hyman, B. I., DeTurk, A., Diaz, R., and DiGiovanni, G.: Exploratory Tests on Fiber-Reinforced Plates with Circular Holes Under Tension, AIAA Journal, vol. 7, no. 9, September 1969, pp. 1820-1821.

4. Franklin, H. G.: Hole Stress Concentrations in Filamentary Structures, Fibre Science and Technology, vol. 2, 1970.

5. Rybicki, E. F., and Hooper, A. T.: Analytical Investigation of Stress Concentrations Due to Holes in Fiber Reinforced Plastic Laminated Plates, Two-Dimensional Models, AFML-TR-72-15, U.S. Air Force, 1972.

6. Grimes, G. C. and Greimann, L. F.: Analysis of Discontinuities, Edge Effects, and Joints, Chapter 10, vol. 8, Structural Design and Analysis, Part II, edited by C. C. Chamis, in Composite Materials, Academic Press, 1974.

7. Kulkarni, S. V., Rosen, B. W., and Zweben, C.: Load Concentration Factors for Circular Holes in Composite Laminates, Journal of Composite Materials, vol. 7, July 1973, pp. 387-393.

TABLE 1.- TEST SPECIMEN DATA

Station	Thickness, mm (in.) for specimen —			
	1	2	3	4
0°	0.5842 (0.0230)	0.6477 (0.0255)	0.6223 (0.0245)	0.5969 (0.0235)
45°	0.5969 (0.0235)	0.6477 (0.0255)	0.6350 (0.0250)	0.5842 (0.0230)
90°	0.6477 (0.0255)	0.6350 (0.0250)	0.6350 (0.0250)	0.5842 (0.0230)
135°	0.6731 (0.0265)	0.6604 (0.0260)	0.6096 (0.0240)	0.5842 (0.0230)
180°	0.6477 (0.0255)	0.6731 (0.0265)	0.6350 (0.0250)	0.5969 (0.0235)
-135°	0.6223 (0.0245)	0.6731 (0.0265)	0.6350 (0.0250)	0.5969 (0.0235)
-90°	0.5969 (0.0235)	0.6350 (0.0250)	0.6477 (0.0255)	0.5969 (0.0235)
-45°	0.5842 (0.0230)	0.6477 (0.0255)	0.6223 (0.0245)	0.6223 (0.0245)

TABLE 2.- TEST RESULTS

Applied load, N (lb)	Remote stress, kN/m^2 (ksi)	Strain recorded, mm/mm or in./in., for specimen —			
		1	2	3	4
448.8 (100)	6895 (1)	1520×10^6	-990×10^6	390×10^6	108×10^6
889.6 (200)	13790 (2)	2610×10^6	-1710×10^6	600×10^6	250×10^6
1334.4 (300)	20685 (3)	3730×10^6	-2690×10^6	830×10^6	398×10^6
1779.2 (400)	27580 (4)	4920×10^6	-3540×10^6	1020×10^6	551×10^6
2224 (500)	34475 (4)	6170×10^6	-4600×10^6	1230×10^6	710×10^6

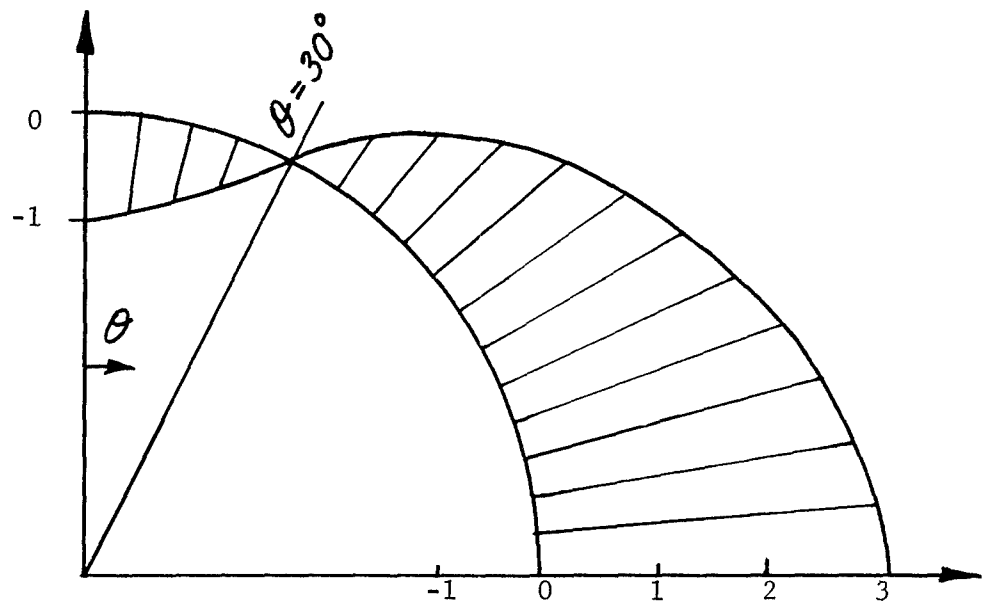

Figure 1.- Isotropic case, σ_θ/σ_o.

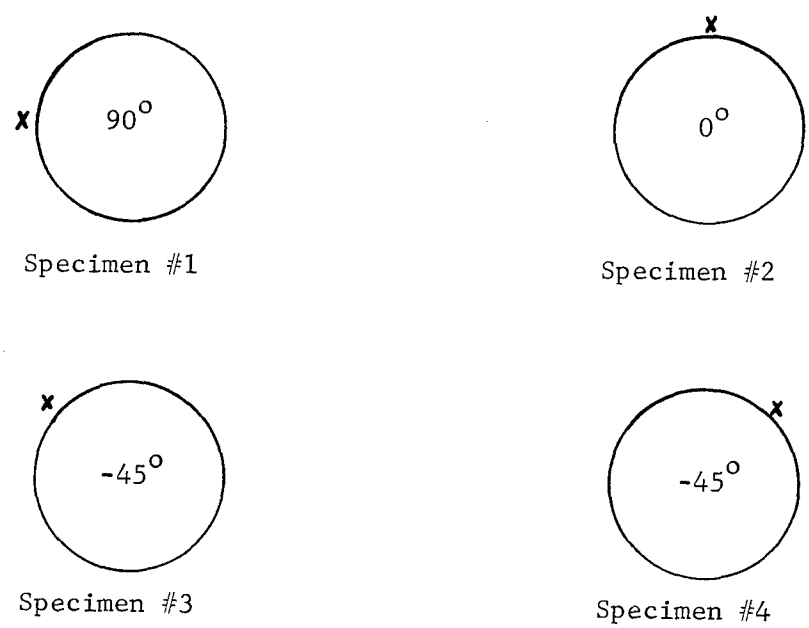

Figure 2.- Location of strain gages.

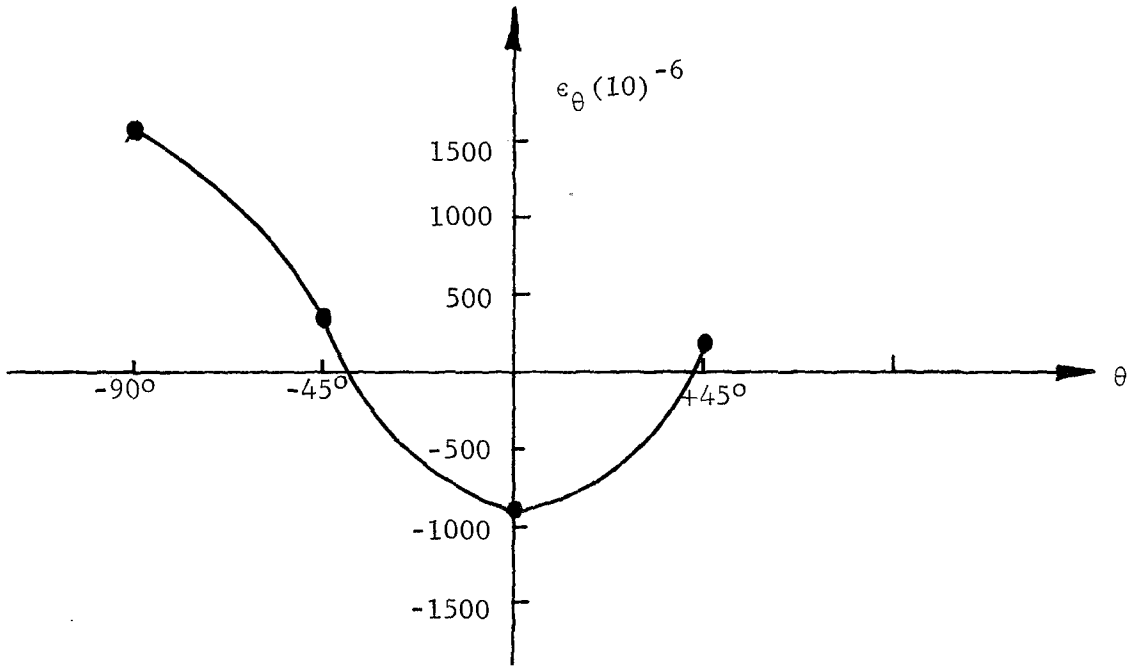

Figure 3.- Strain curve, σ_o = 6895 kN/m^2 (1 ksi).

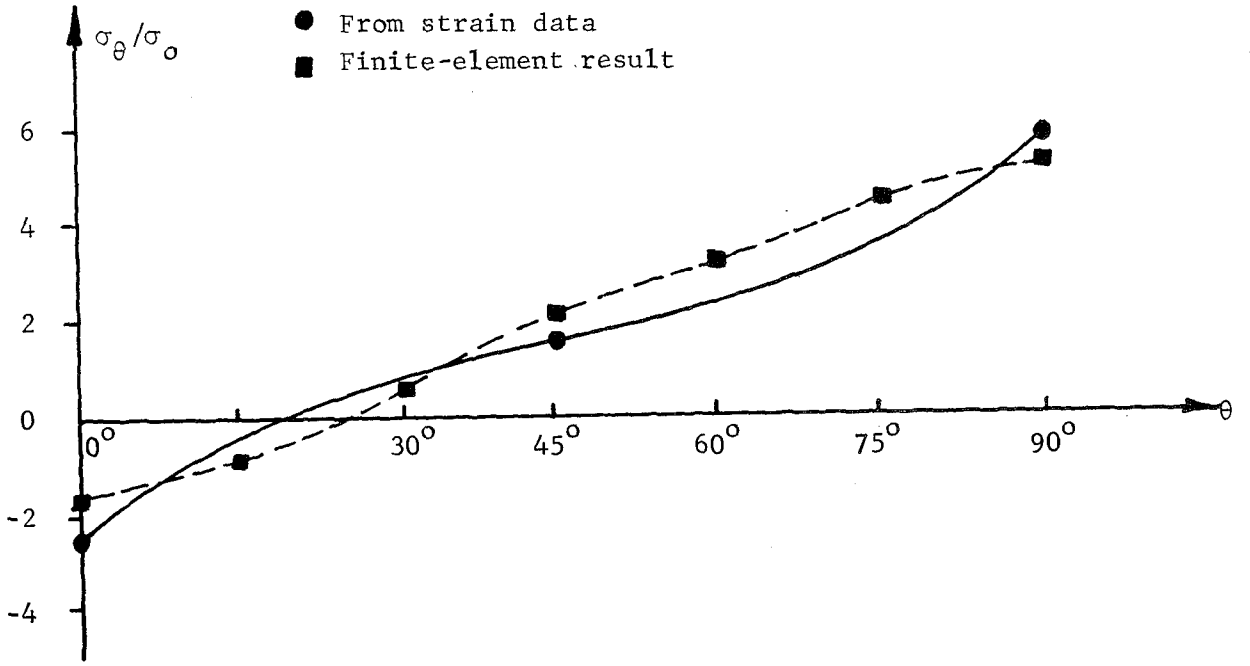

Figure 4.- Stress concentration factors.

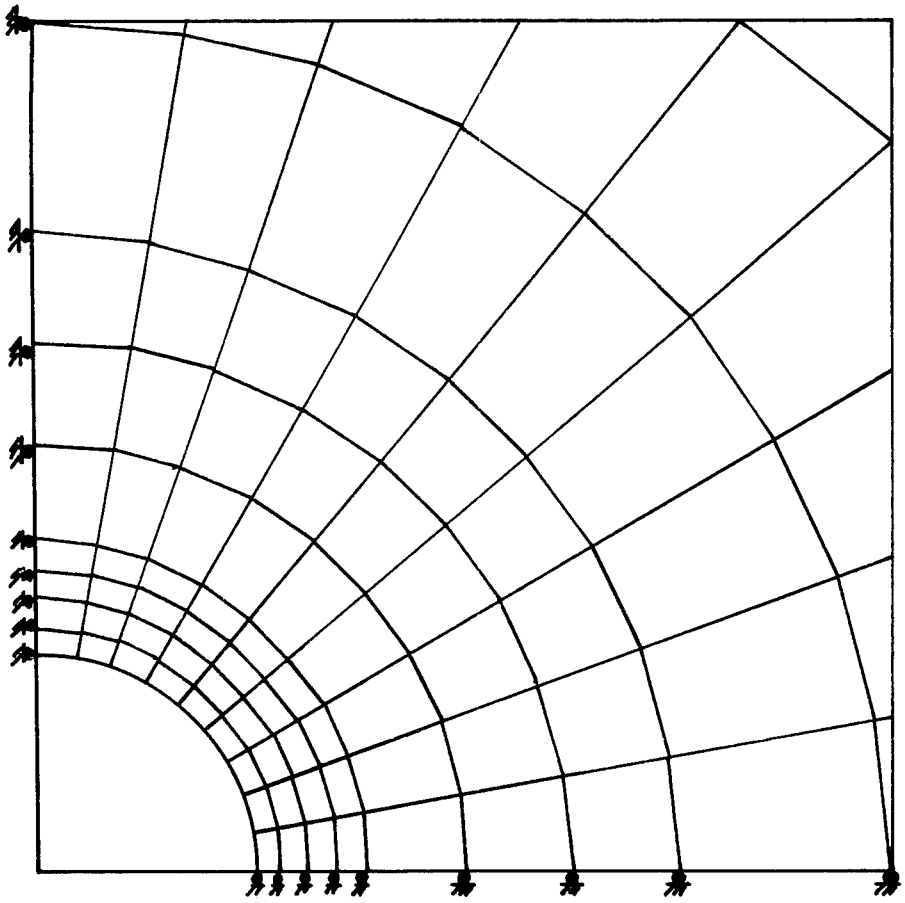

Figure 5.- Element assignment.

TRANSFER MATRIX APPROACH TO LAYERED SYSTEMS WITH AXIAL SYMMETRY

Leon Y. Bahar

Department of Mechanical Engineering and Mechanics
Drexel University

Philadelphia, Pennsylvania 19104

SUMMARY

The stress and displacement distribution in a layered medium is found by means of transfer matrices. The surface loading exhibits axial symmetry, and each layer is of infinite extent in the horizontal direction, of constant depth, and is considered to be linearly elastic, homogeneous, and isotropic. The method developed has the built-in advantage of enforcing interface continuity conditions automatically. Its application to layered composites shows the flexibility with which it predicts the local as well as the global response of the medium.

INTRODUCTION

Recently, this writer developed a transfer matrix approach to various problems in mechanics by combining the method of initial functions due to Vlasov (ref. 1), with the integral transform method developed by Sneddon (ref. 2).

The method employed by this writer consists in applying the state space approach, which has been used extensively to analyze linear systems in various areas of systems engineering, such as modern control theory (ref. 3), to the field of elastomechanics.

The topics so far analyzed through this approach cover two-dimensional elastostatics (ref. 4), one-dimensional elastodynamics (ref. 5), application to a typical elasticity problem (ref. 6), examination of the basic foundation of the theory (ref. 7), application to numerical integration of equations of motion to predict dynamic response (ref. 8), heat conduction (ref. 9), boundary value problems (ref. 10) and earthquake engineering with emphasis on soil-structure interaction (ref. 11). Additional references pertaining to each topic considered will be found in the references cited above and will not be repeated here.

This paper extends the work described in (ref. 4) which was restricted to a plane stress (or plane strain) problem, to a three-dimensional one with axially symmetric loading. The motivation for considering the present approach is to develop a flexible method for the analysis of layered media subjected for instance to concentrated loads, ranging from classical problems in soil mechanics, to the prediction of impulsive response of laminated composites. In the latter case inertial effects must be included.

The main advantage of the method is due to the fact that continuity of stresses and displacements at interfaces is automatically satisfied. Therefore, upon determination of the missing initial displacements from boundary conditions, the field quantities can be determined upon multiplication of the initial state vector by the chain of layer transfer matrices by the field matrix of the layer of interest. A Hankel inversion gives the actual field quantities.

In contrast, the classical formulation requires the construction of a transformed Airy stress function that contains four arbitrary parameters per layer, thus producing a total of 4n equations in 4n unknowns for a medium of n layers. These are determined by enforcing the continuity of stresses and displacements across each interface, which yields 4(n-1) conditions to which the four boundary conditions are added.

DERIVATION OF THE TRANSFER MATRIX

The equations governing the state of stress of an axially symmetric, homogeneous, isotropic, linearly elastic solid, are given by the equilibrium equations

$$\frac{\partial \sigma_r}{\partial r} + \frac{\partial \tau_{rz}}{\partial z} + \frac{\sigma_r - \sigma_\theta}{r} = 0 \tag{1a}$$

$$\frac{\partial \tau_{rz}}{\partial r} + \frac{\partial \sigma_z}{\partial z} + \frac{\tau_{rz}}{r} = 0 \tag{1b}$$

in the absence of body forces and inertial effects. These equations must be adjoined by the constitutive relations

$$\sigma_r = (\lambda + 2\mu)\frac{\partial u}{\partial r} + \lambda\left(\frac{u}{r} + \frac{\partial w}{\partial z}\right) \tag{2a}$$

$$\sigma_\theta = \lambda\left(\frac{\partial u}{\partial r} + \frac{\partial w}{\partial z}\right) + (\lambda + 2\mu)\frac{u}{r} \tag{2b}$$

$$\sigma_z = \lambda\left(\frac{\partial u}{\partial r} + \frac{u}{r}\right) + (\lambda + 2\mu)\frac{\partial w}{\partial z} \tag{2c}$$

$$\tau_{rz} = \mu\left(\frac{\partial u}{\partial z} + \frac{\partial w}{\partial r}\right) \tag{2d}$$

The four stresses given by equations (2) are functions of the partial derivatives of two displacements only; it follows that two of these stresses can be eliminated.

For reasons of convenience, σ_θ and σ_r are chosen for this purpose. Upon substitution of equations (2a) and (2b) into equation (1a), the latter can be rewritten as

$$(\lambda + 2\mu)\left[\frac{\partial^2 u}{\partial r^2} + \frac{1}{r}\frac{\partial u}{\partial r} - \frac{u}{r^2}\right] + \frac{\partial \tau_{rz}}{\partial z} + \lambda \frac{\partial^2 w}{\partial z \partial r} = 0 \qquad (3)$$

Differentiation of equation (2c) with respect to r yields

$$\frac{\partial \sigma_z}{\partial r} = \lambda\left[\frac{\partial^2 u}{\partial r^2} + \frac{1}{r}\frac{\partial u}{\partial r} - \frac{u}{r^2}\right] + (\lambda + 2\mu)\frac{\partial^2 w}{\partial z \partial r} \qquad (4)$$

Elimination of the mixed derivative between equations (3) and (4) results in the relation

$$\lambda \frac{\partial \sigma_z}{\partial r} + 4\mu(\lambda + \mu)\left[\frac{\partial^2 u}{\partial r^2} + \frac{1}{r}\frac{\partial u}{\partial r} - \frac{u}{r^2}\right] + (\lambda + 2\mu)\frac{\partial \tau_{rz}}{\partial z} = 0 \qquad (5)$$

Consider a semi-infinite elastic medium which extends to infinity in the r-direction as shown in figure 1. The medium is loaded by an axially symmetric load as shown. Under the circumstances, taking Hankel Transforms of order one of equations (5) and (2d), and of order zero of equations (2c) and (1b), results in the system of equations cast in matrix form as follows:

$$\frac{d}{dz}\begin{Bmatrix} \mu\bar{u}_1 \\ \mu\bar{w}_0 \\ \bar{\sigma}_0 \\ \bar{\tau}_1 \end{Bmatrix} = \begin{bmatrix} 0 & \xi & 0 & 1 \\ -\lambda\xi/(\lambda+2\mu) & 0 & \mu/(\lambda+2\mu) & 0 \\ 0 & 0 & 0 & -\xi \\ 4(\lambda+\mu)\xi^2/(\lambda+2\mu) & 0 & \lambda\xi/(\lambda+2\mu) & 0 \end{bmatrix} \begin{Bmatrix} \mu\bar{u}_1 \\ \mu\bar{w}_0 \\ \bar{\sigma}_0 \\ \bar{\tau}_1 \end{Bmatrix} \qquad (6)$$

where the subscripts indicate the order of the Hankel transform. Equation (6) can be integrated by considering the column vector of transformed stresses and displacements as the state vector $\bar{X}(\xi,z)$, and rewriting it as

$$\frac{d}{dz}\{\bar{X}(\xi,z)\} = [A(\xi)]\{\bar{X}(\xi,z)\} \qquad (7)$$

As shown in (ref. 4), equation (7) can be integrated to yield

$$\{\bar{X}(\xi,z)\} = \exp[zA(\xi)]\{\bar{X}(0)\} \qquad (8)$$

where the matrix exponential has to be evaluated explicitly. The characteristic roots of the determinant associated with the matrix $A(\xi)$ are the

double roots $\pm \xi$, identical to the result obtained in ref. 4 . Therefore, the results are analogous to those obtained in that paper, in which it is shown that

$$\exp(zA) = a_0 I + a_1 A + a_2 A^2 + a_3 A^3 \tag{9}$$

where

$$\begin{aligned} a_0 &= \cosh \xi z - (\xi z/2) \sinh \xi z \\ a_1 &= [3 \sinh \xi z - \xi z \cosh \xi z]/2\xi \\ a_2 &= [z \sinh \xi z]/2\xi \\ a_3 &= [\xi z \cosh \xi z - \sinh \xi z]/2\xi^3 \end{aligned} \tag{10}$$

Upon substitution of these values into equation (9), the transfer matrix is obtained, and equation (8) gives, in turn, the state vector which consists of the transformed stresses and displacements at an arbitrary depth in the field. The details pertaining to the evaluation of the transfer matrix are given in the Appendix. The results can be summarized in matrix form as

$$\begin{Bmatrix} \mu\bar{u}_1(\xi,z) \\ \mu\bar{w}_0(\xi,z) \\ \bar{\sigma}_0(\xi,z) \\ \bar{\tau}_1(\xi,z) \end{Bmatrix} = \begin{bmatrix} L_{11} & L_{12} & L_{13} & L_{14} \\ L_{21} & L_{22} & L_{23} & L_{24} \\ L_{31} & L_{32} & L_{33} & L_{34} \\ L_{41} & L_{42} & L_{43} & L_{44} \end{bmatrix} \begin{Bmatrix} \mu\bar{u}_1(\xi,0) \\ \mu\bar{w}_0(\xi,0) \\ \bar{\sigma}_0(\xi,0) \\ \bar{\tau}_1(\xi,0) \end{Bmatrix} \tag{11}$$

where the influence functions mapping the initial field quantities into those at an arbitrary depth in the field are given by

$$\left.\begin{aligned} L_{11} &= L_{44} = \cosh z\xi + [(\lambda+\mu)/(\lambda+2\mu)]z\xi \sinh z\xi \\ L_{12} &= -L_{34} = [\mu \sinh z\xi + (\lambda+\mu)z\xi \cosh z\xi]/(\lambda+2\mu) \\ L_{13} &= -L_{24} = [(\lambda+\mu)/(\lambda+2\mu)]z \sinh z\xi \\ L_{14} &= [1/2(\lambda+2\mu)\xi][(\lambda+3\mu) \sinh z\xi + (\lambda+\mu)z\xi \cosh z\xi] \\ L_{21} &= -L_{43} = [1/(\lambda+2\mu)][\mu \sinh z\xi - (\lambda+\mu)z\xi \cosh z\xi] \\ L_{22} &= L_{33} = \cosh z\xi - [(\lambda+\mu)/(\lambda+2\mu)]z\xi \sinh z\xi \\ L_{23} &= [1/2(\lambda+2\mu)\xi][(\lambda+3\mu) \sinh z\xi - (\lambda+\mu)z\xi \cosh z\xi] \\ L_{31} &= -L_{42} = -2z\xi^2 \sinh z\xi \\ L_{32} &= [2(\lambda+\mu)\xi/(\lambda+2\mu)][\sinh z\xi - z\xi \cosh z\xi] \\ L_{41} &= [2(\lambda+\mu)\xi/(\lambda+2\mu)][\sinh z\xi + z\xi \cosh z\xi] \end{aligned}\right\} \tag{12}$$

The actual physical quantities are then recovered through the inverse Hankel transform.

APPLICATION TO LAYERED SYSTEM

Consider a layered medium with perfect bonding along all interfaces as shown in figure 2. This implies the continuity of transformed stresses and displacements across each interface. In order to enforce this condition, the first two entries of the state vector which appear in equation (11) are divided by the shear modulus, to produce a new state vector consisting of transformed stresses and displacements. The elements of the new matrix G become $G_{13} = L_{13}/\mu$; $G_{14} = L_{14}/\mu$; $G_{23} = L_{23}/\mu$; $G_{24} = L_{24}/\mu$; $G_{31} = \mu L_{31}$; $G_{32} = \mu L_{32}$; $G_{41} = \mu L_{41}$; and $G_{42} = \mu L_{42}$. The remaining elements of the G matrix are identical to the corresponding elements of the L matrix.

The modified equation (11) can now be written in contracted form as

$$\{\bar{Y}(\xi,z)\} = [G(\lambda,\mu,z,\xi)]\ \{\bar{Y}(\xi,0)\} \tag{13}$$

Applying equation (13) to each interface in turn, in the sequence shown in figure 2, leads to

$$\{\bar{Y}(\xi,h_n)\} = [G(\lambda_n,\mu_n,h_n,\xi)\cdots G(\lambda_1,\mu_1,h_1,\xi)]\ \{\bar{Y}(\xi,0)\} \tag{14}$$

in which the missing initial conditions are determined from boundary conditions. Equation (14) then describes the overall response of the layered system.

Local information consisting of state vectors at interfaces can now be obtained by terminating the matrix multiplication indicated by equation (14) at the appropriate interface. These relations are shown by the block diagrams shown in figures 3 and 4.

The state vector in any arbitrary layer m can now be found by the relation

$$\{\bar{Y}(\xi,z)\} = [G(\lambda_m,\mu_m,z,\xi) \prod_{i=1}^{m-1} G(\lambda_i,\mu_i,h_i,\xi)]\{\bar{Y}(\xi,0)\} \tag{15}$$

in which the z coordinate is the local depth within the layer m, ranging from zero to h_m. The actual stresses and displacements are given by the inverse Hankel transformation of the state vector.

CONCLUDING REMARKS

In this paper, a transfer matrix method to determine the response of a layered medium subjected to an axially symmetric loading has been presented.

The matrix formulation shows that the need for matching interface conditions explicitly is avoided by imposing the continuity of the state vector across each interface. This is accomplished through the continued

multiplication of layer transfer matrices. Therefore, the size of the transfer matrix remains four by four, and is independent of the number of layers contained in the medium. This is the main conceptual as well as computational advantage of the proposed method.

APPENDIX

The transfer matrix is given by the expression $\exp(zA) = a_0 I + a_1 A + a_2 A^2 + a_3 A^3$, in which the matrices A, A^2, and A^3 are given by

$$A = \begin{bmatrix} 0 & \xi & 0 & 1 \\ -\lambda\xi/(\lambda+2\mu) & 0 & \mu/(\lambda+2\mu) & 0 \\ 0 & 0 & 0 & -\xi \\ 4(\lambda+\mu)\xi^2/(\lambda+2\mu) & 0 & \lambda\xi/(\lambda+2\mu) & 0 \end{bmatrix}$$

$$(\lambda+2\mu)A^2 = \begin{bmatrix} (3\lambda+4\mu)\xi^2 & 0 & (\lambda+\mu)\xi & 0 \\ 0 & -\lambda\xi^2 & 0 & -(\lambda+\mu)\xi \\ -4(\lambda+\mu)\xi^3 & 0 & -\lambda\xi^2 & 0 \\ 0 & 4(\lambda+\mu)\xi^3 & 0 & (3\lambda+4\mu)\xi^2 \end{bmatrix}$$

$$(\lambda+2\mu)A^3 = \begin{bmatrix} 0 & (3\lambda+4\mu)\xi^3 & 0 & (2\lambda+3\mu)\xi^2 \\ -(3\lambda+2\mu)\xi^3 & 0 & -\lambda\xi^2 & 0 \\ 0 & -4(\lambda+\mu)\xi^4 & 0 & -(3\lambda+4\mu)\xi^3 \\ 8(\lambda+\mu)\xi^4 & 0 & (3\lambda+2\mu)\xi^3 & 0 \end{bmatrix}$$

and the coefficients $a_0, a_1 a_2$, and a_3 are given by the set of relations (10). The elements of the matrix exponential are given explicitly by the expressions (12).

REFERENCES

1. Vlasov, V.Z., and Leontev, N.N.: Beams, Plates and Shells on Elastic Foundations. NASA TTF-357, TT65-50135, 1966.

2. Sneddon, I.N.: Fourier Transforms. McGraw-Hill Book Co., Inc., N.Y., N.Y., 1951.

3. Ogata, K.: State Space Analysis of Control Systems. Prentice-Hall Englewood Cliffs, N.J., 1967.

4. Bahar, L.Y.: Transfer Matrix Approach to Layered Systems. J. Eng. Mech. Div. (ASCE), Vol. 98, No. EM5, Oct. 1972, pp. 1159-1172.

5. Bahar, L.Y.: Transfer Matrix Approach to Elastodynamics of Layered Media. J. Acoust. Soc. Am., Vol. 57, No. 3, Mar. 1975, pp. 606-609.

6. Bahar, L.Y.: State Space Solution of the Infinite Elastic Strip. Proc. 4th Can. Cong. Appl. Mech., 1973, pp. 53-54.

7. Bahar, L.Y.: A State Space Approach to Elasticity. J. Franklin Inst., Vol. 299, No. 1, Jan. 1975, pp. 33-41.

8. Bahar, L.Y., and Sinha, A.K.: Matrix Exponential Approach to Dynamic Response. Int. J. Comp. and Struc. Vol. 5, No. 2/3, June 1975, pp. 159-165.

9. Bahar, L.Y.: A Transfer Matrix Approach to Heat Conduction in Layered Composites. Proc. 11th Meet. Soc. Eng. Sci., 1974, pp. 168-169.

10. Bahar, L.Y.: A State Space Approach to Boundary Value Problems. Proc. 11th Meet. Soc. Eng. Sci., 1974, pp. 170-171.

11. Bahar, L.Y., and Ebner, A.M.: Transfer Matrix Approach to Earthquake Amplification through Layered Soils. Nucl. Eng. and Des., Vol. 35, No. 1, Dec. 1975, pp. 59-67.

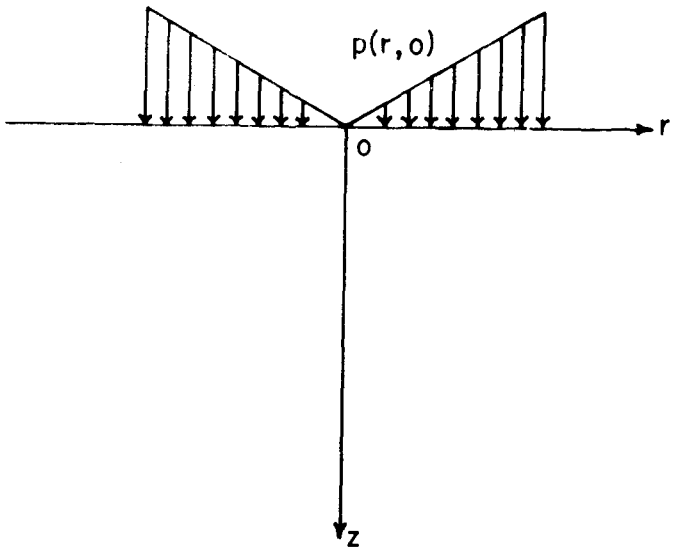

Figure 1.- Semi-infinite elastic medium.

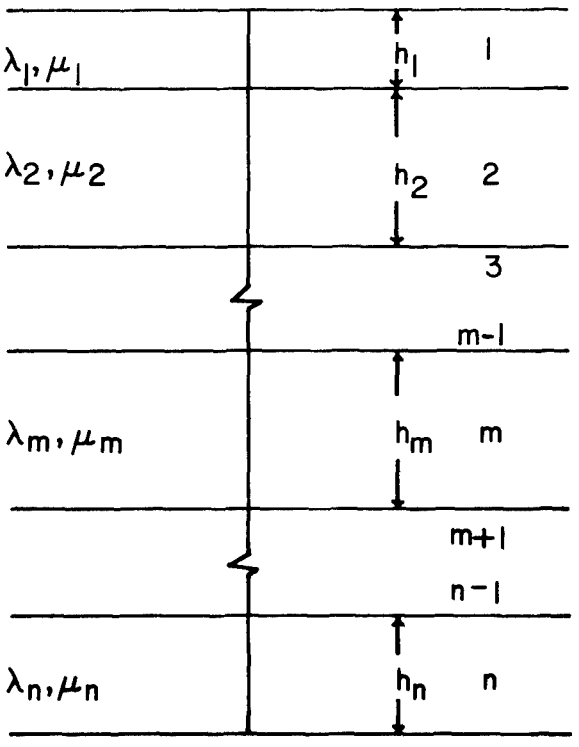

Figure 2.- Axially symmetric layered medium.

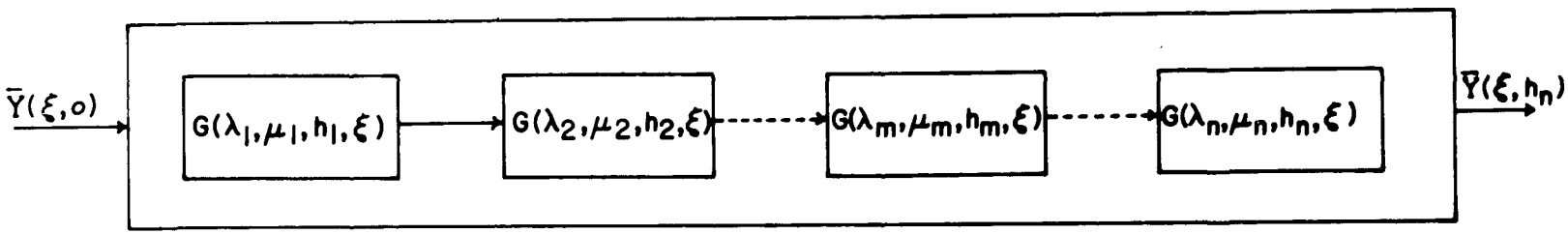

Figure 3.- Overall response of layered medium.

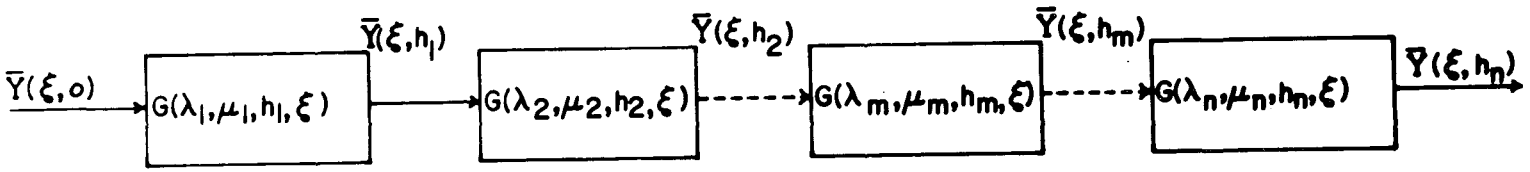

Figure 4.- Local response of layered medium.

APPLIED GROUP THEORY

APPLICATIONS IN THE ENGINEERING (PHYSICAL, CHEMICAL, AND MEDICAL), BIOLOGICAL, SOCIAL, AND BEHAVIORAL SCIENCES AND IN THE FINE ARTS

S.F. Borg
Stevens Institute of Technology

SUMMARY

A generalized "applied group theory" is developed and it is shown that phenomena from a number of diverse disciplines may be included under the umbrella of a single theoretical formulation based upon the concept of a "group" consistent with the usual definition of this term.

INTRODUCTION

The essence of the "group" concept as used herein is contained in the three terms, element, transformation and invariance, and it may be shown that they are included in the various analyses discussed in this paper. More formally, the mathematical definition of a group generally includes the "inverse" operation (however defined) and also an "identity" operation (also variously though consistently defined). These may be brought into the discussion of this report without difficulty, as will be shown, although the main emphasis will be placed upon the element, transformation and invariance properties of the groups being considered.

It must be noted at the outset that the various terms, quantities and operations will have different forms for the different disciplines considered. In some cases they take a mathematical form; in others they appear as curves, or as sounds or as visual entities. However, despite these differences, it will be shown that the requirements of the "group" representation will be satisfied in each case and in this sense all of the disciplines discussed fall within the overall province of the group concept.

The following manner of presentation will be utilized. In the next section a Table will be presented in which the entire theory will be summarized. All of the group requirements will be listed for the different disciplines considered in this paper. Others may be included, without difficulty, if desired.

After this an example from each discipline will be discussed in greater

detail.

THE GROUPS

A concise, detailed general classification scheme for the underlying theory is contained in Table 1.

Note especially how all of the formal requirements of group representation are satisfied - although these vary from group to group.

In particular two distinct typical types of group elements are shown: (1) tensor or (2) events. There appears to be a connection between these seemingly separate group types in that many "event" groups may, in fact, be "tensors". A discussion of this point in connection with "Behavior" is presented later in the paper and current continuing analyses indicate that this duality may be a general property of many event phenomena.

The transformation corresponding to the tensors is a rotation of axes. The transformation corresponding to an event is an alteration or change of the phenomenon caused by a change in the particular activity variable involved in the phenomenon. The invariants (which imply conservation of the structure of the element during the transformation) are the tensor invariants for tensor and the single equation or curve or other phenomenon representing events. All of the above will be explained in greater detail in the next section.

DISCUSSION OF TYPICAL GROUPS IN THE VARIOUS DISCIPLINES

In this section, one typical group from each of the disciplines will be described in more detail than given in Table 1. The references cover the subject in even greater detail.

Engineering-Physics Groups

A typical group element of many engineering-physical problems is the tensor - zero, first and second order (ref. 1). Zero order tensors are scalars, first order tensors are vectors and second order tensors are usually called "tensors".

Some typical familiar examples of tensors are the stress tensor and the inertia tensor. In three dimensional x-y-z space these may be shown in a 3x3 matric form, with each term of the matrix representing either a stress component or a moment of inertia with respect to x-y-z axes.

These tensors may be transformed by rotating the x-y-z axes arbitrarily about the origin of the axial system. If this is done, then it can be shown there are three invariants, that is, quantities whose values are not changed

by this rotation. In addition, the tensor itself is an invariant since it can be expressed without regard to axial orientation. Furthermore, the inverse operation and the identity (unit) tensor may be defined and we have, therefore, all second order tensors as elements of the group.

In an analogous manner, we may discuss a particular physical event (ref. 2) - an infinite straight-sided wedge impacting with constant velocity on an infinite ocean, with time t=0 the instant the point of the wedge touches the surface. At any time t>0, the wedge and water surface will be at particular locations, and each of these will be different for different times. The representation of the wedge and ocean, at any time t=t, corresponds to the element of the group. If, into this phenomenon, we introduce a change of coordinates, $\xi = \frac{x}{t}$, $\eta = \frac{y}{t}$, then the entire phenomenon, for all t>0, may be shown on a single map (the invariant) in the ξ,η plane. The time, t, is the transformation coordinate, since for each different value of t the event transforms to new wedge and water positions.

The fundamental behavior in the above group is the collapsing of multi-curve data (the elements) by a suitable change in coordinates to a single curve (the invariant) valid for all the separate elements for all values of the transformation coordinate, t. This concept is the basis for many of the group representations considered in the present paper.

We may define as a group, a set of objects, quantities, happenings or other items which, by means of a mathematical relation is transformed into a single event, this being the invariant representation of the separate items or phenomena. The separate items are called the elements of the group. The variable which transforms or alters the event is called the activity variable and the single equation or visual representation of the event is called the invariant of the group.

The identity relation for these phenomena is either

1) unity, a multiplier of the mathematical equation,

or

2) a transparent sheet placed over the curve such that the curve shows through unchanged.

The inverse relation for these phenomena is either

1) the negative equation, which when added to the original equation gives zero,

or

2) an obliterating cover sheet which annihilates the given curve, resulting in a blank sheet.

Chemical Groups

In reference 3 an experimental study is reported of the sensitivity of the DNA-RNA hybrid obtained from the CSCI density gradient to ribonuclease A and to fraction A (the transformation variables). Six different curves (elements) were drawn corresponding to six different sets of transformation variables.

As shown in reference 4 all six curves can be collapsed to a single curve (and mathematical equation), the invariant, in terms of a suitable change of variables. The details are presented in the reference.

The unity and inverse statements are as in the engineering-physical groups, case b.

Biological-Medical Groups

Orentreich and Selmanowitz, (ref. 5) discuss results of experiments dealing with healing of wounds in dogs and men. Their report shows curves of healing of originally 40 sq cm wounds on men of 20, 30 and 40 years indicating wound healing in relation to age (the activity variable).

In reference 3 it is shown that all three curves (the elements) can be collapsed into a single equation or curve (the invariant) by means of a suitable change of coordinates. The details are given in reference 3. The inverse and identity statements are equivalent to those of case b, engineering-physical groups.

Social Groups

A social application occurs in connection with a study reported by Sherman (ref. 6), dealing with total food intake of children from birth to age 13-15. His results are presented in a chart showing the food allowances (in calories) for children of about average weight for their age. The data is given separately for girls and for boys (the activity variables), these being the group elements. By means of a suitable change of variables (as shown in ref. 3) it is possible to collapse both sets of data to a single mathematical equation and curve - the invariant. The identity and inverse statements are again as in case b, engineering-physical groups.

Behavior Groups

Just as in the case of engineering-physical applications, in the area of behavior there appear to be two different types of group representation - the "tensoral" and the "event" forms.

As an example of the "tensoral" behavior group, the author (in an as yet

unpublished report) developed a theory in which it was hypothesized that certain variables related to behavior may be interpreted as tensors, satisfying the same transformation and other relations that engineering-physical tensors satisfy.

As a check against the hypothesis experimental data presented in a report (ref. 7) was used, dealing with a number of subjects who imagined happy, sad and angry situations. Different patterns of facial muscle activity were produced (the elements) and these were measured by electromyography. The facial expressions were recorded for depressed and for non-depressed subjects and, suitably calibrated, were presented in bar graph form. The subjects were tested on the Zung Self Rating Depression Scale and scored accordingly. These scores corresponded to the transformation variable. Complete details are given in the unpublished report.

It was shown that quantities satisfying the tensor transformations could be established for this one test, at least. A fair check on the hypothesis was obtained and, subject to further verification, it seems possible that many of the phenomena in the field of behavior may be treated utilizing tensor theory. If this is in fact true, it will permit one to predict by extrapolation various new relations in behavior theory which themselves may be capable of experimental verification. Also by modelling suitable mathematical tensoral equations one may be able to correlate measured behavior quantities with fundamental measurable central nervous system responses.

A typical "event" type of behavior group occurred (ref. 8) in an experimental study of the swimming ability of new-born rats treated with hormones, the activity variable. Three different groups of rats were studied and three separate curves were obtained. As shown, (ref. 3) it is possible, by means of a suitable change of coordinates, to collapse all three curves, the elements, to a single curve, the invariant. The identity and inverse statements are similar to the ones shown for case b, engineering-physical groups.

Music Groups

Several different types of music groups may occur. A particular arrangement of notes (as for example Ravel's "Bolero" or the Schönberg "twelve tone music") is a typical element. A discussion of the entire range of music composition, as it relates to "groups" including such factors as pitch, repetition, sequential treatment, counterpoint, loudness, etc., is clearly beyond the limits of this paper. One may, however, consider Ravel's Bolero as an example. In this composition we have the repetition of a single theme (the element), representable by means of a musical equation (the notes), being transformed while being performed by means of a continuing gradual crescendo into a composition (the invariant) all shown as a symbolic mathematical equation. It is also possible to represent musical forms in matrix equations. The identity and inverse statements may be taken as shown in Table 1. Reference 9 lists a number of additional studies in this area.

Art-Architectural Groups

In the art-architectural field one may think of piastre band treatments as being typical of group phenomena. In these cases one may have a series of "figures" (gargoyles or Saints or Kings or windows for example) in a "band" going along one side of the building, or completely around the building. These may be identical (as in the case of windows and possibly the human or other figures) or they may vary from one to the other as in the case of human and gargoyle figures.

It is possible to reduce these band figures, the elements, to a single mathematical equation or to collapse the different figures to a single visual quantity, as follows:

For, say, the identical windows, we have

(window)x(function of spacing) = n (identical windows)

For, say, the figures, we have (with a suitable definition of the summation process)

$$\Sigma(\text{figure})_n^{x\ \frac{(\text{face})n}{(\text{face})_o}\ldots.x\ \frac{(\text{clothes})n}{(\text{clothes})_o}\ldots.} = n(\text{identical figures})_o$$

in which all figures are transformed to an identical figure by means of the alterations noted. From these equations the invariant - identical window or identical figure - may be determined.

A somewhat different approach is presented in reference 9.

Poetry Groups

In the case of poetry (reference 10 for example) one deals with terms such as metre, rhyme, image, texture, triolet, stanza, etc. It is possible to indicate rhyming schemes by means of letters. As a typical example, the rondeau which may consist of ten lines has a rhyming scheme as follows:

abbaabRabbaR

In this, R, the refrain, is frequently simply a tail and may be the first word of the opening stanza.

The above scheme may be put in a rather more symmetrical matrix form (symmetry is desirable in some theories of composition),

$$\begin{pmatrix} (aba) & (ab) \end{pmatrix} \begin{pmatrix} \begin{pmatrix} b \\ a \\ bR \end{pmatrix} \\ \begin{pmatrix} b \\ aR \end{pmatrix} \end{pmatrix} = \text{rondeau}$$

in which the usual rules of matrix multiplication are used and "rondeau" is the invariant. One may, conceivably, invent new poetic forms by performing various matrix operations - an "inverse rondeau", for example. A much more elaborate treatment of this topic is presented in reference 9 with particular emphasis on its application to Russian literature.

CONCLUDING REMARKS

It was shown that the general mathematical definition of "group" may be applied to phenomena occurring in many different disciplines. The basic terms of the theory - element, invariant, identity, transformation and inverse - all have counterparts in the different fields considered, subject to suitable alterations as required, for example, with visual or tonal or other characteristic phenomena.

In some of the disciplines discussed, by using the group concept and developing the group invariant, new relations are obtained which permit one to predict new engineering, biological, etc. phenomena that are capable of experimental verification.

Finally, it is conceivable that some of the general theorems and properties of "mathematical group theory" may - by suitable modification - be applicable to the different disciplines considered, thereby permitting one to obtain new fundamental insights and knowledge in these fields.

REFERENCES

1. Borg, S.F.: Matrix - Tensor Methods in Continuum Mechanics, D. Van Nostrand Co., Inc. Princeton, N.J. 1963.

2. Borg, S.F.: Some Contributions to the Wedge-Water Entry Problem. Journal of the Engineering Mechanics Division, Proc. ASCE, April 1957, 1214-1 through 1214-28.

3. Stein, H. and P. Hansen, 1969 Science 166; 393-395

4. Borg, S.F.: Similarity Solutions in the Engineering, Physical-Chemical, Biological-Medical and Social Sciences, Proceedings of the Symposium on Symmetry, Similarity and Group Theoretic Methods in Mechanics, Eds. P.G. Glockner and M.C. Singh, The University of Calgary, Aug. 19-21, 1974, pp. 263-282.

5. Orentreich, N. and V.J. Selmanowitz, Levels of Biological Functions with Aging, Trans. N.Y. Acad. Sci. 31, 1966, p. 992.

6. Sherman, H.C. Chemistry of Food and Nutrition, 8th Ed. The Macmillan Co., New York, N.Y. 1952, p. 563.

7. Schwartz, Gary E. et al., 30 April 1976, Science 192, p. 489.

8. Schapiro, S., Salas, M., Vucovich, K., 1970, Science 168, pp. 147-151.

9. Shubnikov, A.V. and Koptsik, V.A., Symmetry in Science and Art, translated from the Russian Edition (Moscow 1972) by G.D. Archard. David Harker, Ed., Plenum Press, New York, London, 1974.

10. Deutch, B.: Poetry Handbook, 2nd. Ed. Funk and Wagnalls Co., New York, 1957, p. 136.

TABLE I - THE GROUPS

	THE DISCIPLINE	TYPICAL ELEMENTS	TYPICAL INVARIANT	TYPICAL TRANSFORMATION	TYPICAL IDENTITY STATEMENT	TYPICAL INVERSE	REFERENCE NUMBER
1	ENGINEERING-PHYSICAL	a)tensor components b) events	a)tensor invariants. The tensor b)a single mathematical equation or collapse of multi-curve data to a single curve	a)a rotation of axes b)alteration caused by a particular "activity variable" for the given phenomenon	a)the unit tensor b)unity or a transparent sheet	a)the inverse tensor b)the negative equation or the obliterating sheet	a)1 b)2
2	CHEMICAL	←		The same as 1b	→		3,4
3	BIOLOGICAL-MEDICAL	←		The same as 1b	→		5,3
4	SOCIAL	←		The same as 1b	→		6,3
5	BEHAVIOR	a)tensor components b) ←	a)tensor invariants The tensor	a)a rotation of axes The same as 1b	a)the unit tensor →	a)the inverse tensor	7 8,3
6	MUSIC	tones, melodies, time,etc. the events	a musical composition reduced to a single mathematical equation	tonal,melodic, loudness,etc. changes	unity	the negative equation or silence	9
7	ART-ARCHITECTURE	visual figures,parts of a strip or band, the events	a visual sequence reduced to a single mathematical equation representing the entire band	spatial or visual-spatial rearrangement of the elements	the transparent sheet	the obliterating sheet-blank band	9

TABLE I - THE GROUPS (CONCLUDED)

	THE DISCIPLINE	TYPICAL ELEMENTS	TYPICAL INVARIANT	TYPICAL TRANSFORMATION	TYPICAL IDENTITY STATEMENT	TYPICAL INVERSE	REFERENCE NUMBER
8	POETRY	syllables, lines, words stanzas, rhymes, etc. The events	a matrix equation representing the poetic scheme	rearrangement of the elements new words, etc.	unit matrix	the negative matrix-blank page	9,10

RESPONSE OF LINEAR DYNAMIC SYSTEMS

WITH RANDOM COEFFICIENTS

John Dickerson
University of South Carolina

INTRODUCTION

Numerous models of physical systems contain parameters whose values are not known exactly. This paper attempts to address some of the physical and mathematical complexities arrising in the prediction of the statistical behavior of such systems. Although the discussions in the paper are far from providing a satisfactory solution to such problems, they perhaps, by utilization of simple examples, will create a greater awareness of the statistical effect of random parameters.

PROBLEM FORMULATION

Consider the problem of determining the statistical properties of the response of a finite dimensional linear dynamical system with random coefficients (constant with respect to time) and subjected to stochastic forces. Mathematically the problem is represented by the following equation:

$$\frac{dx(t)}{dt} = Ax(t) + f(t) \qquad 0 \leq t$$
$$x(o) = x_o \tag{1}$$

where $x(t)$, $f(t)$, and x_o are n-dimensional random vectors, A is an nxn random matrix. The problem is to determine statistical properties (mean value, variance, correlation function, spectral density, distribution, etc.) of $x(t)$ knowing the statistical properties of x_o, $f(t)$, and A.

EXISTENCE OF SOLUTION

If the derivative in equation (1) is interpreted in the almost sure sense then existence and uniqueness of a solution follows from appropriate results in R^n and if $f(t)$ is almost surely continuous then a solution in this sense would exist and be given by:

$$x(t) = e^{At}x_o + \int_o^t e^{A(t-\tau)} f(\tau)d\tau \qquad (2)$$

However, since the discussions in this paper will be concerned with second moments of the solution, it would seem appropriate to require the derivative in (1) to be a mean square derivative and to consider the differential equation (1) over the Hilbert space Z^n where Z denotes the space of second order random variables. If A is a bounded operator over Z^n (probably equivalent to requiring A to be almost surely bounded) then the theory of ordinary differential equations would yield a unique solution given by (2), where the integral was a mean square integral, provided f(t) is mean square continuous. In general, however, A may not be bounded, i.e. the product of two second order random variables will not be a second order random variable and then the appropriate theory discussing existence of a solution to (1) would likely be a requirement that the solution be the action of a semigroup on the initial condition. For example, if there exists a real number λ_o such that:

$$||\lambda[\lambda+\lambda_o - A]^{-1}|| \leq C, \quad \text{for all complex } \lambda \text{ with Re } \lambda \geq 0,\ C_1 \text{ a real}$$

number and $||\ ||$ denoting the norm over R^n, then there will be a solution in the mean square sense to (1) and further:

$$E[(e^{At}x_o)^T(e^{At}x_o)] \leq C_2 e^{2\lambda_o t} E[x_o^T x_o]$$

In particular if λ_o can be chosen to be negative then the solution will be asymptotically stable. This approach to the problem exhibits a solution with the only stipulations that $x_o \varepsilon Z^n$ and f(t) be mean square continuous. Another approach to finding a mean square solution to (1) would be to require conditions on x_o, A, f(t) such that (2) is a solution to (1). If x_o, A, and f(t) are mutually independent, then requiring e^{At} and Ae^{At} to have second moments would insure that (2) satisfies (1). The following elementary examples attempt to illustrate the above discussion.

EXAMPLES

Example 1

Consider the first order homogeneous equation (n = 1).

$$\frac{dx}{dt} = ax \qquad x(o) = x_o$$

with a uniformly distributed between α and β. Clearly a is a bounded operator over Z thus, for example, if x_o is independent of a it follows that:

$$E[x(t)] = \frac{1}{(\beta-\alpha)t} \left(e^{\beta t} - e^{\alpha t}\right) E[x_o]$$

If $\beta>0$ then E[x(t)] becomes arbitrarily large even if the mean of a is negative.

Example 2

Consider the above problem with the density of a given by:

$$P_a(a) = \alpha e^{\alpha(a-\beta)}$$ shown:

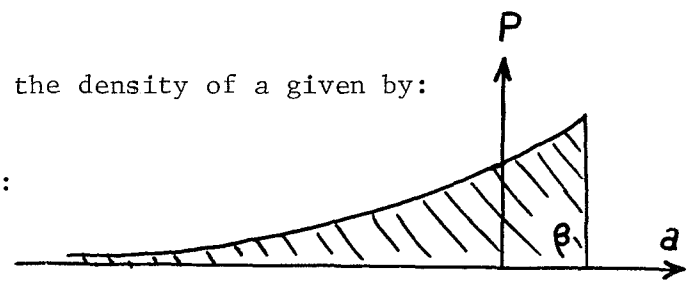

Although a is not a bounded operator over Z clearly $\left| \frac{\lambda}{\lambda+\lambda_o-a} \right| \leq C$ if $\lambda_o>\beta$

for all Re $\lambda>0$. Thus a solution exists. If x_o is independent of a then it can be shown that

$$E[x(t)] = \frac{\alpha e^{\beta t}}{t+\alpha} E[x_o].$$

Note again that if $\beta>0$ E[x(t)] becomes arbitrarily large.

Example 3

Consider the above example with a Gaussian with mean μ and variance σ. Clearly a is not bounded and further no λ_o can be chosen to make $\left|\frac{\lambda}{\lambda+\lambda_o-a}\right| \leq C$.

However if a is independent of x_o then ae^{at} and e^{at} do have second moments and it follows that:

$$E[x(t)] = \exp\left\{\frac{t^2\sigma^4 + 2\mu t\sigma^2}{\sigma^2}\right\} E[x_o].$$

However, regardless of σ and μ, E[x(t)] becomes arbitrarily large.

Example 4

Consider the above example with the density of a given by:

$$P_a(a) = \alpha e^{-\alpha(a-\beta)}$$ shown:

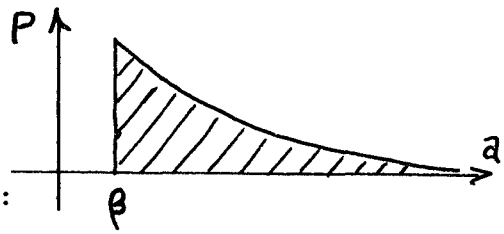

Again it is not possible to pick a λ_o such that:

$$\left|\frac{\lambda}{\lambda+\lambda_o-a}\right| \leq C$$ and even if x_o is independent of a it can be demonstrated that x(t) does not have a first moment for $t>\alpha$. Thus it makes no sense in this problem to attempt to calculate E[x(t)].

STATIONARY RESPONSE AND SPECTRAL DENSITY

Assume that the existence of the solution in the mean square sense to (1) is known and is expressible as:

$$x(t) = e^{At}x_o t \int_o^t e^{A(t-\tau)} f(\tau)d\tau$$

If A, x_o, and f(t) are mutually independent and further if f(t) is stationary with correlation matrix R_f then it follows that:

$$E[(x(t+\Delta) - E[x(t+\Delta)])\ (x(t) - E[x(t)])^T] = \int_o^{t+\Delta} \int_o^t E[e^{A(t+\Delta-\eta_1)}$$

$$R_f(\eta_1-\eta_2)e^{A^T(t-\eta_2)}\ ]\ d\eta_1\ d\eta_2$$

If it can further be shown that $||e^{At}|| \leq Ce^{\beta t}$ with $\beta<0$, then it follows in the usual way that as t goes to ∞ x(t) becomes stationary with:

$$R_x(\Delta) = \int_0^\infty \int_0^\infty E[e^{A\eta_1} R_f(\Delta-\eta_1+\eta_2)e^{A^T\eta_2}\ ]\ d\eta_1 d\eta_2$$

By taking the Fourier transform of $R_x(\Delta)$ it is easily shown that the spectral density of x(t) is given by:

$$S_x(\omega) = E[\ [A+i\omega]^{-1}\ S_f(\omega)\ [A-i\omega]^{-1}\ ]$$

Example 5

Of the previous examples only Example 1 with $\beta<0$ and Example 2 with $\beta<0$ eventually have stationary solutions. In example 1 (with $\beta<0$) it is easily seen that:

$$S_x(\omega) = \frac{1}{\omega} \left[\tan^{-1}\frac{\beta}{\omega} - \tan^{-1}\frac{\alpha}{\omega}\right] S_f(\omega)$$

If $S_f(\omega) = 1$ (white noise) then a plot of $S_x(\omega)$ follows:

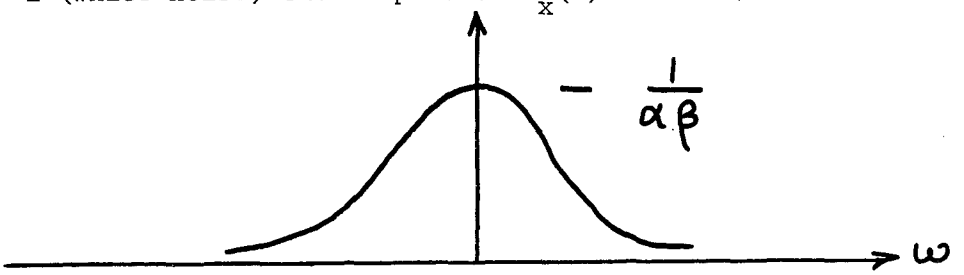

If a was not a random variable then $S_x(\omega) = \frac{1}{a^2+\omega^2}$ and a plot of this follows:

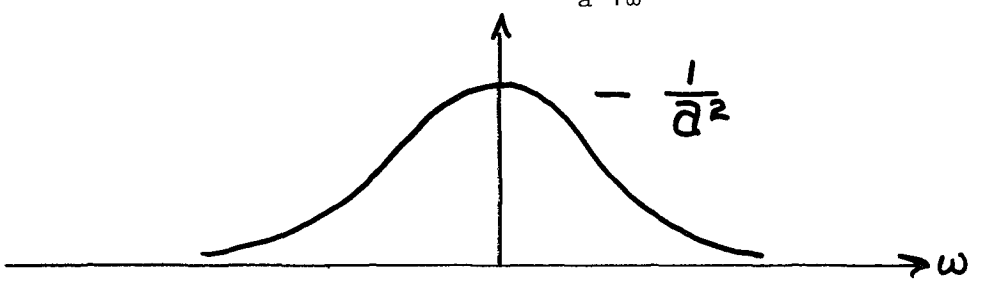

SUMMARY

Those readers who have gotten to this point in the paper recognize it as a fraud. The paper (1) presents a physical problem, i.e.: how do you calculate the statistical properties of the response of dynamical systems which have random parameters, (2) presents possible mathematical models that pertain to the physical problem and (3) presents, via simple examples, where the problems are in trying to solve the problem. The result in example 3, where a is Gaussian, shows that regardless of how negative the mean value and how small the variance of a, the mean value of the solution goes to ∞ as time goes to ∞. In particular, it makes no sense to talk about the spectral density of the solution.

In the opinion of the author closed form solutions to problems beyond n=1 are not feasible and current work centers around the study of the accuracy of approximate methods that have been proposed in the literature.

APPLICATIONS OF CATASTROPHE THEORY IN MECHANICS

Martin Buoncristiani and George R. Webb
Christopher Newport College

INTRODUCTION

Consider a system under the influence of control parameters c. It may happen that for some values of c the system has more than one stable equilibrium state and consequently a continuous change in control may cause a discontinuous change from one equilibrium state to another. This occurs, for example, in the "snap-through" of a compressed beam under transverse loading. This kind of abrupt transition between stable equilibrium states - a branching or bifurcation - has been the subject of much study (ref. 1 to 4) and recently the French topologist René Thom developed a theory which presents seven standard types of discontinuous behavior (ref. 5 to 6), called elementary catastrophes, and proved that any discontinuous behavior in systems controlled by not more than four variables is one of these seven elementary catastrophes. Thom's theorem is remarkable for providing a classification of discontinuous behavior but it is also useful as an aid to visualizing phenomena of this sort. The proof of the theorem is difficult but its results are easy to understand and to use in problems involving bifurcation.

Applications of Thom's theory to problems in mechanics are just beginning to appear. The first problem solved appears to have been an example by Zeeman (ref. 7) and his co-workers. This example has recently been generalized by Woodcock and Poston so that it can describe higher order catastrophes.

The most extensive studies come from the group of researchers that work with J. M. T. Thompson of University College, London. Thompson and Hunt (ref. 8) correlate their own theories of elastic stability for discrete systems with the work of Thom and suggest possible fields in which the theory will give significant insights. Troger (ref. 9) suggests the nature of such insights in his study of von Mises truss and a shallow arch from the point of view of catastrophe theory, and Fowler (ref. 10) in his paper on the Riemann-Hugoniot shock does the same.

Chillingworth and Guckenheimer apply the theory to continuous systems. Chillingworth (ref. 11) uses a generalization of Morse's Lemma to Hilbert spaces to reduce the study of the buckling of a beam to a problem in finite dimensions; Guckenheimer (ref. 12) discusses catastrophes and Hamiltonian systems.

The papers by Schulman (ref. 13) on phase transitions, Kozak and Benham (ref. 14) on denaturation, and Mehra and Blum (ref. 15) on the ignition of paper provide examples in the realm of thermodynamics. Detailed bibliographies of catastrophe theory and its applications to problems in other areas can be found in reference 16 .

STRUCTURAL STABILITY OF POTENTIAL FUNCTIONS

In this paper we will describe a method, using Thom's classification of catastrophes, for the analysis of stability of systems whose static behavior is derived from a potential function. Examination of the stability of singular points of potential functions will serve to illustrate the nature of the elementary catastrophes, which can also arise in non-conservative dynamical systems as well as in the static case of potential theory.

The first step in examining the stability of systems admitting discontinuous transitions is to clarify the notion of stable state. Early work of Poincaré (ref. 17), and Pontryagin and Andronov (ref. 18) developed the notion of structural stability which expresses two key ideas. First, equilibrium states of a system are characterized by their topological type; it is the general shape of a state which is important and not numerical values which it might take on. In the case of potential functions the topological type is given by the number of singular points. Second, discontinuous behavior of a system occurs for those (critical) values of control parameters at which the equilibrium state changes its topological type. Let $C(=R^p)$ be the space of control variables c, and $X(=R)$ the state space. The potential function is a smooth map, $V(x,c)$, $V:X \times R^p \to R$. A point x_0 is a singular point of V if $D_x V(x_0,c) = 0$. The collection of control points and their associated singular (state) points form a manifold, called the catastrophe manifold,

$$M = \{(x,c) \in X \times R^p \mid D_x V(x,c) = 0\} \tag{1}$$

The dimension of M is p. Figure 1 illustrates M for a quartic potential. For a fixed value of c, there is a fixed potential function $V_c(x)$ with a fixed number of singular points. As this number changes with c it stratifies (or subdivides) the control space into open and dense regions in which this number is constant, separated by boundaries across which it changes. Such a change will occur whenever the manifold M has a tangent parallel to X, i.e. when $D_x^2 V(x) = 0$. A singular point x_0 is said to be structurally stable when $D_x^2 V(x_0) \neq 0$. The set of points which are not structurally stable appears as a fold F in the manifold M.

$$F = \{(x,c) \in X \times R^p \mid D_x^2 V(x,c) = 0\} \tag{2}$$

These are points at which the map projecting M onto C is singular. The set of critical control variables at which the number of singular points changes (or equivalently which have structurally unstable singular points) is called the bifurcation set B. This set is given by eliminating x from (1) and (2):

$$B = M \cap F$$

In Figure 1, B appears as the cusp in the c-plane.

In the neighborhood of a structurally stable point $x_0 (D_x^2 V(x_0) \neq 0)$ the potential is quadratic, that is there is a curvilinear coordinate system $\bar{x}$ in which $V(x) - V(x_0) = \bar{x}^2$. To investigate the behavior of the potential in a

neighborhood of a structurally unstable point Thom developed the notion of a universal unfolding of a singularity. Consider a perturbation of the potential $V \to V + \delta V$ where δV and all of its derivatives are small. Two possibilities arise - either the perturbation gives rise to an infinite number of different topological types of the potential or only a finite number. In the latter case the variation of V can be parameterized by a finite number of variables which can be identified with the control variables, as

$$\delta V = c_1 h_1(x) + c_2 h_2(x) + \ldots \quad c_p h_p(x) \tag{3}$$

This variation is universal in the sense that any variation of V depending on p-parameters can be obtained by a transformation of (3). For example suppose we begin with a cubic potential $V(x) = x^3$, so that 0 is a structurally unstable point. If this potential is perturbed by $\delta V = ax$ the topological character of $V + \delta V$ is described by the value of the parameter a as follows: for $a \geq 0$, V has one root, an inflection point, and for $a < 0$, V has 3 roots, thus one maximum and one minimum, c.f. Figure 2. The importance of this result of Thom's work is that for all potentials with the same singularity type, perturbations need depend on only one parameter, and their behavior is of the fold type illustrated in the following examples. The number of parameters involved in the variation of V is called the codimension of the singularity. All singularities of codimension ≤ 4 have been analyzed by Thom. There are four potentials depending on one state variable and these have the following form:

$$x^{\ell} + a_{\ell-2}x^{\ell-2} + a_{\ell-1}x^{\ell-1} + \ldots \quad a_1 x$$

We now summarize these results by stating a version of Thom's Theorem that we will use in the examples of the next section. This version is given by Chow, Hale and Mallet-Paret in reference 4 .

Thom's Transversality Theorem and Catastrophes

Let $V(x,c) : X \times R^p \to R$ and $f(x,c) \equiv dV/dx$, so that the singular points of V are given by $f(x,c) = 0$. If $x = 0$ is a singular point of V, f can be expanded in the form

$$f(x,0) = Ax^k + 0\ (|x|^{k+1})$$

where $A \neq 0$ and k gives the order of the singular point. Expand the derivatives of f with respect to the parameters:

$$\frac{\partial f}{\partial c_i}(x,0) = \sum_{j=0}^{k-2} A_{ij} \frac{x^j}{j!} + 0|x|^{k-1} \qquad i = 1,2,\ldots p$$

Then when $p \leq k-1$ and

$$\text{rank } (A_{ij}) = k-1$$

there exists a smooth transformation of coordinates

$$\bar{\lambda}_i = h_i(c_1 \ldots c_p) \qquad i = 1,\ldots p$$

$$\bar{x} = h_0(x, c_1 \ldots c_p)$$

such that

$$\bar{f}(\bar{x},\bar{\lambda}) = \bar{x}^k + \bar{\lambda}_1 + \bar{\lambda}_2\bar{x} + \ldots \quad \bar{\lambda}_{k-1}\bar{x}^{k-2}$$

APPLICATION OF CATASTROPHE THEORY TO DISCRETE SYSTEMS WITH ONE STATE VARIABLE

In this section we will concentrate on the simple case of potentials depending upon one state variable and two control parameters; problems of more generality are approached in a similar manner. The physical problems we have studied are traditional in elastic stability: an imperfection-senstive strut and a truss that can experience snap-through. These two problems contain many of the features of more general problems, and the results obtained can be displayed clearly in a graphical form. Similar problems have been treated by Koiter, Thompson and Hunt, Sewell and Ziegler.

Application 1: A Strut With Imperfection Sensitivity

Consider the rigid hinged bar of length 1 that is held in a vertical position by a linear spring, with spring constant k, that is loaded by a vertical force P with an eccentricity $e = \mu\ell$ (see fig. 3). The spring is attached to the strut at a distance h from the base and is supported on its other end so that the spring remains horizontal. The coordinate θ, which is measured between a vertical line and the axis of the bar, specifies the state of the system. The dimensionless parameters $\lambda = \frac{P\ell}{kh^2}$ and μ are the controls.

The force function f is the gradient of the internal and external potentials:

$$f = f(\theta;\lambda,\mu) = \frac{kh^2}{2}\left[\sin\theta\cos\theta - \lambda(\sin\theta + \mu\cos\theta)\right]$$

We begin by finding the surface $f = 0$, which is the catastrophe manifold, and the points of structural instability $f_{,\theta} = 0$. Upon solving these two equations in three unknowns we find

$$\lambda_c = (1 + \mu^{2/3})^{-3/2}$$

$$\theta_c = \tan^{-1}(\mu^{1/3})$$

where the subscript c denotes the critical condition of structural instability.

Next we prepare to use Thom's Theorem. We expand f about the critical value of the state variable and note the leading term. Here we see that in the

case where $\mu \neq 0$, f (expanded as required) is of the order two in the variable $x = \theta - \theta_c$. If $\mu = 0$, f expanded is of order three.

Let us first consider the case where f is of order two. The index k equals 2 and n, the number of control parameters, is also two. Therefore the inequality in the theorem is satisfied. We note also that f evaluated at the critical point vanishes, a further preliminary of the theorem. In order to determine the nature of the catastrophe manifold along this portion of the bifurcation set, we must find the rank of the matrix A which is defined in the theorem. Let f* be f expanded about the critical point in terms of x. Now

$$f^*_\lambda(x;\lambda_c,\mu) = \tfrac{1}{2}kh^2[(\sin\theta_c+\mu\cos\theta_c)+(\cos\theta_c-\mu\sin\theta_c)x + \ldots]$$

$$f^*_\mu(x;\lambda_c,\mu) = \tfrac{1}{2}kh^2[\ \lambda_c\cos\theta_c+\lambda\ \sin\theta_c x + \ldots]$$

and therefore

$$A = \begin{pmatrix} \frac{kh^2}{2}\ [\sin\theta_c+\mu\cos\theta_c] \\ -\frac{kh^2}{2}\ \lambda_c\cos\theta_c \end{pmatrix}$$

The rank of A is one; the conditions of the theorem are satisfied. The singularities are locally equivalent to a fold at points along the bifurcation set away from ($\theta_c=0$; $\lambda_c=1$, $\mu=0$). This behavior is identical to that of the cubic potential discussed earlier.

If we consider this latter case of $\theta_c=0$, we find that the function f is locally equivalent to some form of a cusp, the case where k=3 in Thom's Theorem. In order to identify the normal and splitting factors for the manifold (see fig. 1 for the meaning of these terms), and to display the canonical form of the polynomial, we expand f about the point ($\theta=0$; $\lambda=1$, $\mu=0$). We need only retain terms to the third order since the manifold is a cusp in this neighborhood.

$$f = \frac{kh^2}{4}[-\theta^3 + 2(1-\lambda)\theta + 2\lambda\mu]$$

If we place this expansion in the canonical form

$$\frac{f}{-kh^2/4} = \theta^3 + \bar{\lambda}_2\theta + \bar{\lambda}_1$$

we find that $\bar{\lambda}_1 = -2\lambda\mu$ is the normal factor and $\bar{\lambda}_2 = -2(1-\lambda)$ is the splitting factor. The force function for this example is of the same differential type as a cusp but the negative multiplier causes the loci of maxima and minima for the related potential function to be interchanged. This type of force function is the dual cusp and the behavior of the system on the catastrophe manifold is altogether different from that on the manifold of a regular cusp (fig. 1).

The bifurcation set in the control plane is described by $27\bar{\lambda}_1^2 = 4\bar{\lambda}_2^3$. This relation is an imperfection-sensitivity curve and has the familiar two-thirds power form. The equilibrium surface and the bifurcation set are shown in Figure 1. Notice the effect of the imperfection. It lowers the value of the load at which instability occurs. The area of the catastrophe manifold where $\bar{\lambda}_1 > 0$ is composed entirely of unstable points; it is not accessible to the system. The bifurcation set and a visualization of the equilibrium surface can also be presented as in Figure 4. This presentation is possible because the equilibrium surface is a ruled surface: for each value of the state variable vector, the equilibrium equation is an affine equation in the control parameters. The bifurcation set is the envelope of the projection of these lines onto the control space. The three-dimensionality of these figures can be enhanced by a stereographic technique that is described in Woodcock and Poston (ref. 19).

Application 2: An Essential Modification of the Strut With Imperfection Sensitivity

We will now modify the structure in Figure 3 so that the spring is attached to a fixed point at a distance h from the level of the pivot and is fastened to the rigid bar with a sleeve that allows the spring to remain horizontal. The catastrophe manifold near the structurally unstable point ($\theta=0$; $\lambda=1$, $\mu=0$) has the form

$$\frac{f}{\frac{3}{2}kh^2} = \theta^3 + \frac{2}{3}(1-\lambda)\theta - \frac{2}{3}\lambda\mu$$

In this case the catastrophe manifold is locally equivalent to a cusp with normal factor $\bar{\lambda}_1 = -\frac{2}{3}\lambda\mu$ and splitting factor $\bar{\lambda}_2 = \frac{2}{3}(1-\lambda)$. Note the difference in behavior between trajectories along this cusp and those along the dual cusp.

Application 3: A Symmetric Truss With Moveable Supports

In this example we consider a modification of the well-studied symmetric structure that exhibits snap-buckling (fig. 5). The structure consists of two linear-spring elements of unstretched length ℓ_0 and spring constant k that have a horizontal projection of 2x and that are subjected to a downward load P. The location of the tip of the truss with respect to a horizontal line through its end points is denoted by y. We will analyze the behavior of this structure in much the same manner as we did in example 1.

The force function f is

$$f = f(z;a,b) = z(1 - 1/(z^2+a^2)^{1/2}) + b$$

where $b = P/k\ell_0$
$a = x/\ell_0$
and $z = y/\ell_0$

The solution for the structurally unstable points of the mapping yields the critical set of points whose projection on the control space is the bifurcation set. An investigation of the behavior of the system on the bifurcation set

away from the special point (z=0; a=1, b=0) shows that the singularities are folds locally. A similar investigation in the neighborhood of the special point indicates the expected cusp there.

In order to determine precisely the normal and splitting factors in the neighborhood of the cusp, we expand the force function about the tip of the cusp retaining only terms as high as cubic. We find that the force function can be rewritten in the canonical form

$$2f = \overline{u}^3 + \overline{\lambda}_1 + \overline{\lambda}_2\overline{u}$$

if

$$\overline{u} = \frac{z}{a}$$

$$\overline{\lambda}_1 = 2b$$

$$\overline{\lambda}_2 = 2(a-1)$$

Therefore near the cusp tip ($\overline{\lambda}_1=0$, $\overline{\lambda}_2=0$) $\overline{\lambda}_1 = 2b$ is the normal factor and $\overline{\lambda}_2 = 2(a-1)$ is the splitting factor.

In this example the portion of the equilibrium surface behind the cusp is accessible to the system. Deformations of the system can occur that will take the state variable from values on the top of the cusp surface to values on the bottom without the occurrence of a jump.

CONCLUSION

It is clear from these examples that catastrophe theory and the methods of adjacent equilibrium and energy (given dynamical significance by their embedding in the theory of Lyapunov) lead to similar results and require many of the same calculations. Qualitative features of the singular behavior of systems, including a unique visualization of discontinuous processes, can be gained quickly from the representation of the catastrophe manifold. Catastrophe theory provides an exhaustive classification of structural instabilities in systems with as many as four control variables and clarifies the nature of the controls. A consistent set of controls must satisfy the rank condition of the transversality theorem. This requirement pinpoints controls that are redundant and suggests the need for additional ones; for example, it would have forced the introduction of the imperfection parameter in application 1 had it been omitted. There still remains a good deal of work to be done before a unified theory of bifurcation is developed and Thom's theory provides a useful set of ideas in this direction.

REFERENCES

1. Koiter, W. T.: On the Stability of Elastic Equilibrium. Dissertation, Delft, Holland, 1945 (English Translation: NASA Tech. Trans. F 10, 833, 1967).
2. Thompson, J. M. T. and Hunt, G. W.: A General Theory of Elastic Stability. Wiley, London, 1973.
3. Budiansky, B.: Theory of Buckling and Post-buckling Behavior of Elastic Structures. Advances in Applied Mechanics, Vol. 14, Academic Press, New York, 1974.
4. Chow, S. N.; Hale, J. K.; and Mallet-Paret, John: Applications of Generic Bifurcation. I. Arch. Rat. Mech. Anal., vol. 39, 1975.
5. Thom, R.: Topological Models in Biology. Topology, vol. 8 (1969).
6. Thom, R.: Structural Stability and Morphogenesis, W. A. Benjamin, Inc. Reading, Mass. 1975.
7. Zeeman, E. C.: A Catastrophe Machine. in Towards a Theoretical Biology, Ed. C. H. Waddington, Edinburgh Univ. Press, 1968.
8. Thompson, J. M. T. and Hunt, G. W.: Towards a Unified Bifurcation Theory. J. of Appl. Math. and Phys., vol. 26 (1975).
9. Troger, H.: Ein Beitrag zum Durchschlagen ein facher Strukturen. Acta Mechanica, vol. 23, 1975.
10. Fowler, D. H.: The Riemann-Hugoniot Catastrophe and van der Waal's Equation. in Towards a Theoretical Biology, Ed. C. H. Waddington, Edinburgh Univ. Press, 1968.
11. Chillingworth, D. R. J.: The Catastrophe of a Buckling Beam. in Dynamical Systems-Warwick 1974, ed. A. K. Manning, Springer-Verlag, vol. 468, 1975.
12. Guckenheimer, J.: Caustics and Non-degenerate Hamiltonians. Topology, vol 13, 1974.
13. Schulman, L. S. and Revzen, M.: Phase Transitions as Catastrophes. Collective Phenomena, 1 (1972).
14. Kozak, J. J. and Benham, C. J.: Denaturation; an Example of a Catastrophe. Proc. Nat. Acad. Sci. U.S.A., vol. 71, 1974.
15. Mehra, R. K. and Blum, E. H.: On the Dynamics of the Ignition of Paper and Catastrophe Theory. to appear in Proc. of 1976 Joint Automatic Control Conference.
16. Bibliography on Catastrophe Theory. Dynamical Systems-Warwick 1974, ed. by E. K. Manning, Springer-Verlag, vol. 468, 1975.
17. Poincairé, H.: Les méthodes nouvelles de la mécanique céleste: Vols. I, II, III. reprinted by Dover, New York, 1957.
18. Andronov, A. and Pontryagin, L.: Systémes grossiers. C. R. (Dokl.) Acad. URSS 14 (1937).
19. Woodcock, A. E. R. and Poston, T.: A Geometrical Study of the Elementary Catastrophes. Lect. notes in Mathematics 373, Springer, Berlin, 1974.

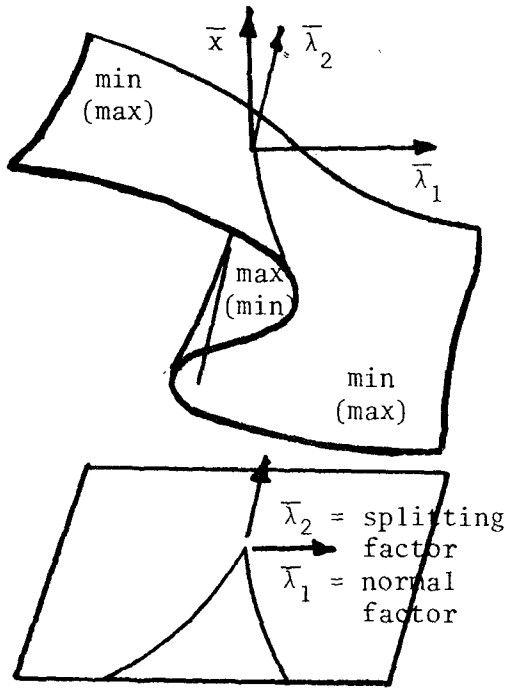

Figure 1.- Quartic potential: cusp (dual cusp).

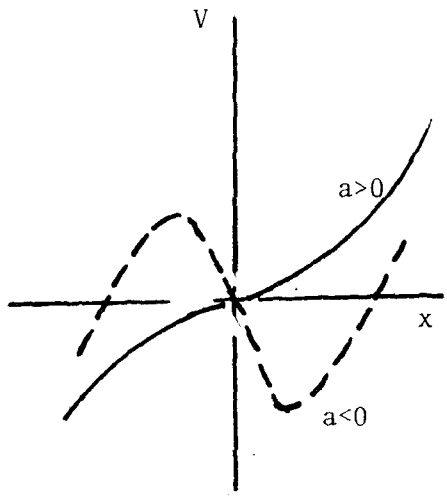

Figure 2.- Cubic potential.

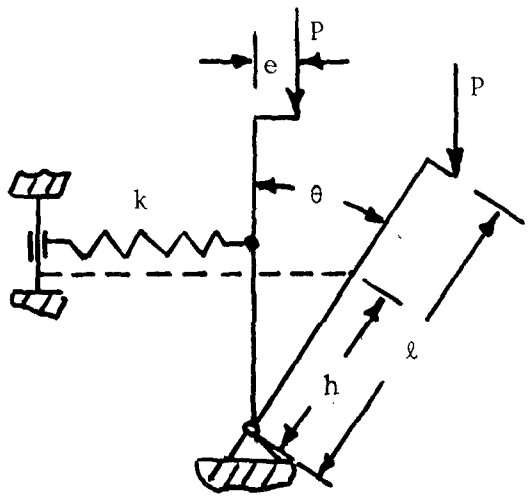

Figure 3.- Imperfection-sensitive bar.

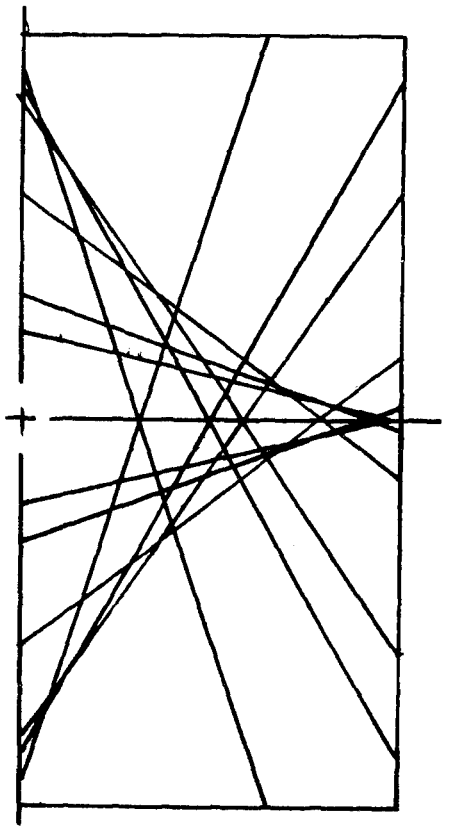

Figure 4.- Ruled surface projections (cusp).

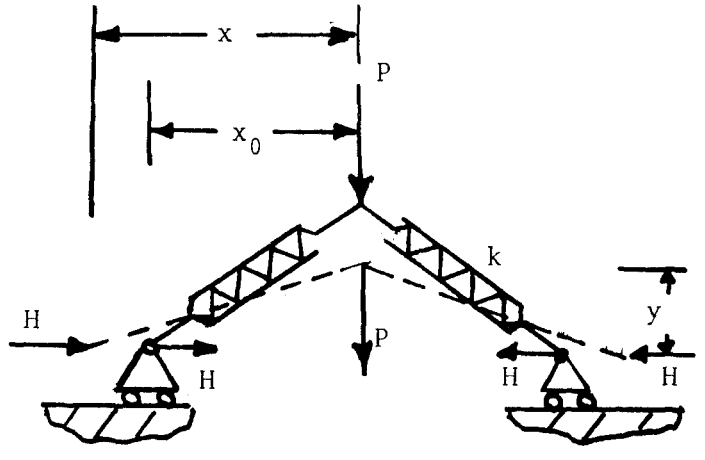

Figure 5.- Snap-through structure (symmetric).

STABILITY OF NEUTRAL EQUATIONS WITH CONSTANT TIME DELAYS

L. Keith Barker
NASA Langley Research Center

John L. Whitesides
Joint Institute for Advancement of Flight Sciences
The George Washington University

SUMMARY

A method has been developed for determining the stability of a scalar neutral equation with constant coefficients and constant time delays. A neutral equation is basically a differential equation in which the highest derivative appears both with and without a time delay. Time delays may appear also in the lower derivatives or the independent variable itself. The method is easily implemented and an illustrative example is presented.

INTRODUCTION

Ordinary differential equations with time delays are called differential-difference equations (ref. 1). Two basic types of differential-difference equations are retarded and neutral equations. The stability of the solutions of these equations is related to the roots of a characteristic equation. Generally this characteristic equation is transcendental and thus has an infinite number of roots.

A convenient method is developed in reference 2 for examining the stability of retarded equations with many time delays (not necessarily distinct) and a scalar neutral equation with one delay. The purpose of the present paper is to develop the basic method of reference 2 for neutral equations with many time delays.

SYMBOLS

a_j, b_j, c, d	real constants
$H_K(s)$	function of s in equation (11)
i	imaginary unit, $\sqrt{-1}$
$J_K(s)$	function of s in equation (12)
j	integer

K	refers to τ_K
$L(s) = 0$	characteristic equation
$L_0(s)$	resulting polynomial with zero delays in $L(s)$
N	highest derivative in neutral equation
$N(\tau_K, -\hat{\mu})$	number of roots of $L(s)$ with $\sigma > -\hat{\mu}$ at τ_K for fixed τ_j, $j \neq K$
$P(s)$	function of s in equation (20)
p	integer
$Q(s)$	function of s in equation (21)
s	complex variable, $\sigma + i\omega$
$\|s\|_m$	an upper bound on magnitude of s which satisfies $L(s) = 0$, where $s = -\hat{\mu} + i\omega$
t	time
$W_K(\sigma, \omega)$	testing function defined in equation (17)
$x(t)$	scalar function of time
α_1, α_2	real numbers
ϵ	small positive number
μ	positive real number
$\hat{\mu}$	specified value of μ
ξ	real gain constant
σ	real part of s
σ_∞	asymptote of real part of large modulus roots
τ, τ_j, τ_K	constant real time delays
$\bar{\tau}_K$	final desired value of τ_K
$\psi(t)$	yaw angle, radians
ω	imaginary part of s
ω_m	an upper bound on ω in $L(s) = 0$, where $s = -\hat{\mu} + i\omega$

Mathematical notations:

$\lvert\ \rvert$	absolute value or magnitude
arg	argument
0^+	arbitrarily small positive values

Dots over a symbol denote derivatives with respect to time.

ANALYSIS

A method is developed herein for determining the stability of the neutral equation

$$\sum_{j=0}^{N} [a_j x^{(j)}(t) + b_j x^{(j)}(t - \tau_j)] = 0 \tag{1}$$

where $a_N \neq 0$, $b_N \neq 0$, $0 < \tau_j \leqq \tau_N$, for $j = 0, 1, \ldots, N - 1$, and $x^{(j)}(t)$ denotes the jth derivative of $x(t)$.

The characteristic equation associated with equation (1) is

$$L(s) = \sum_{j=0}^{N} (a_j + b_j e^{-\tau_j s}) s^j = 0 \tag{2}$$

It has been shown (ref. 3) that if all the roots $s = \sigma + i\omega$ of equation (2) satisfy the property

$$\sigma \leqq -\mu < 0 \tag{3}$$

where μ is a positive constant, then the solution of equation (1) is of exponential order as $t \to \infty$; that is

$$|x(t)| < d\, e^{-c\mu t} \tag{4}$$

where $d > 0$ is a constant real number and c is arbitrary on the

interval (0, 1). Hence, if all the characteristic roots have negative real parts and are not asymptotic to the imaginary axis, then $x(t) \to 0$ as $t \to \infty$ (asymptotically stable).

If there is a root of $L(s)$ with positive real part, then equation (1) has a divergent mode and is said to be unstable.

Relative Stability

If it can be determined that there are no roots of the characteristic equation with real parts greater than a specified negative real number, then the solution to the neutral equation is asymptotically stable.

Relative stability for a specified value $\hat{\mu}$ of μ in equation (3) is indicated herein by the number of roots of the characteristic equation with $\sigma > -\hat{\mu}$. For example, the neutral system is said to be relatively more stable when all the roots satisfy $\sigma < -\hat{\mu} < 0$, than when there is a root with $-\hat{\mu} < \sigma < 0$. Relative stability boundaries in the plane of two system parameters are boundaries corresponding to a root with $\sigma = -\hat{\mu}$.

The stability method to be presented is based on determining the number of roots of the characteristic equation with real parts greater than a specified negative real number $-\hat{\mu}$. The method is convenient for determining the number of roots of the characteristic equation with real parts located between specified negative real numbers. The approach consists of separately examining the arbitrarily large modulus roots and the finite roots. The large modulus roots are examined by using a simple expression for their asymptote; whereas, the finite roots are examined by computing the magnitude of a complex-valued function on a finite interval.

Large Modulus Roots

All roots of equation (2) must satisfy the inequality

$$\left| |a_N| - |b_N| \, e^{-\tau_N \sigma} \right| |s|^N \leq \sum_{j=0}^{N-1} \left(|a_j| + |b_j| \, e^{-\tau_j \sigma} \right) |s|^j \tag{5}$$

obtained from equation (2). It can be shown that since $a_N \neq 0$ and $b_N \neq 0$, the roots have bounded σ. Hence, in order for the large modulus roots ($|s| \to \infty$) to satisfy equation (5)

$$\lim_{|s| \to \infty} \left(|a_N| - |b_N| \, e^{-\tau_N \sigma} \right) = 0 \tag{6}$$

From equation (6), σ becomes arbitrarily close to

$$\sigma_\infty = -\frac{1}{\tau_N} \ln \left| \frac{a_N}{b_N} \right| \tag{7}$$

This relation represents the asymptote of the large modulus roots and is shown graphically in figure 1.

For $\left| \frac{a_N}{b_N} \right| < 1$ in figure 1, $\sigma_\infty > 0$; and equation (3) with $\sigma = \sigma_\infty$ is not satisfied. Now, consider $\left| \frac{a_N}{b_N} \right| > 1$ and let $\sigma_\infty = -\hat{\mu}$ correspond to $\tau_N = \hat{\tau}_N$ in figure 1. Then, $\sigma = \sigma_\infty$ satisfies equation (3) with $\mu = \hat{\mu}$, whenever

$$\tau_N < \hat{\tau}_N = \frac{1}{\hat{\mu}} \ln \left| \frac{a_N}{b_N} \right| \tag{8}$$

There are then no infinitely large modulus roots with $\sigma > -\hat{\mu}$ in the neutral system. It remains to examine the number of finite roots with $\sigma > -\hat{\mu}$.

Finite Roots

For $\tau_j \to 0^+$, L(s) has N roots arbitrarily close to the N roots of the polynomial equation

$$L_0(s) = \sum_{j=0}^{N} (a_j + b_j)s^j = 0 \tag{9}$$

and the remaining roots have arbitrarily large moduli (ref. 2). For $\tau_N \to 0^+$ and $\left| \frac{a_N}{b_N} \right| > 1$ in equation (7), $\sigma_\infty \to -\infty < -\hat{\mu}$. Therefore, L(s) and $L_0(s)$ have the same number of roots with $\sigma > -\hat{\mu}$ (initial relative stability). Since the complex roots occur in complex conjugate pairs, only roots with non-negative imaginary parts ($\omega \geq 0$) are considered.

As one of the time delays, say τ_K, is increased in a continuous manner with the remaining delays held fixed, the finite roots of L(s) move in some continuous manner (ref. 2), generating root locus curves in the complex root plane (s-plane).

Intersection Points $s = -\hat{\mu} + i\omega$ and Corresponding Delays

A root locus curve must intersect the $-\hat{\mu}$-line (dashed line) in figure 2 in order for the number of roots of $L(s)$ with $\sigma > -\hat{\mu}$ to change. These intersection points $(-\hat{\mu}, \omega)$ and the corresponding values of the delay τ_K which result in these intersection points are discussed in this section. The change in the relative stability as a root locus curve crosses an intersection point is presented in the next section.

For a specific time delay τ_K, equation (2) can be written as

$$L(s) = H_K(s) - J_K(s)\, e^{-\tau_K s} = 0 \tag{10}$$

where

$$H_K(s) = \sum_{j=0}^{N} a_j s^j + \sum_{\substack{j=0 \\ j\neq K}}^{N} b_j s^j e^{-\tau_j s} \tag{11}$$

and

$$J_K(s) = -b_K s^K \tag{12}$$

At an intersection point $s = -\hat{\mu} + i\omega$, equation (10) is equivalent to

$$|H_K(-\hat{\mu}, \omega)| = |J_K(-\hat{\mu}, \omega)|\, e^{\hat{\mu}\tau_K} \tag{13}$$

and

$$\tau_K = \frac{1}{\omega} \arg\left[\frac{J_K(-\hat{\mu}, \omega)}{H_K(-\hat{\mu}, \omega)} + 2p\pi\right] \tag{14}$$

where $H_K(-\hat{\mu}, \omega) = H_K(-\hat{\mu} + i\omega)$, $J_K(-\hat{\mu}, \omega) = J_K(-\hat{\mu} + i\omega)$, and

$$-\pi < \arg \frac{J_K(-\hat{\mu}, \omega)}{H_K(-\hat{\mu}, \omega)} \leqq \pi \tag{15}$$

It is assumed that $\omega \neq 0$ and $H_K(-\hat{\mu}, \omega) \neq 0$. To handle these special cases, the approach used in reference 2 may be followed. Only non-negative values of the integer p in equation (14) are of interest because $\tau_K \geqq 0$ and $\omega > 0$.

Equation (13) gives the points $(-\hat{\mu}, \omega)$ where the root locus curves intersect the $-\hat{\mu}$-line in figure 2, and equation (14) gives the corresponding values of τ_K which result in these intersection points. In general, the values of ω at an intersection point must be found by an iteration process. The values of ω which may satisfy equation (14) are restricted to some finite interval $(0, \omega_m]$, where ω_m is an upper bound on ω determined from equation (5). Also, a useful bound on the integer p in equation (14) is obtained as

$$|p| \leqq \frac{1}{2} + \frac{\omega_m \bar{\tau}_K}{2\pi} \tag{16}$$

where $\tau_K \leqq \bar{\tau}_K$ and $\omega \leqq \omega_m$.

Change in Number of Roots With $\sigma > -\hat{\mu}$

Let $N(\tau_K, -\hat{\mu})$ denote the number of roots of $L(s)$ with $\sigma > -\hat{\mu}$ at τ_K for fixed τ_j, $j \neq K$; and define the testing function

$$W_K(\sigma, \omega) = \frac{J_K(\sigma, \omega)}{H_K(\sigma, \omega)} e^{-\sigma\tau_K} \tag{17}$$

Then, the following theorem can be used to determine the change in the number of roots of $L(s)$ with $\sigma > -\hat{\mu}$ as τ_K varies.

Theorem: Let $(-\hat{\mu}, \omega)$ be an intersection point with corresponding delay τ_K. Let $\alpha_1 < \omega$ and $\alpha_2 > \omega$ be real numbers for which $W_K(-\hat{\mu}, \alpha_1)$ and $W_K(-\hat{\mu}, \alpha_2)$ are defined, and such that there are no other intersection points with imaginary parts which lie on the interval $[\alpha_1, \alpha_2]$. Then, for ϵ an arbitrarily small positive number

(1) $N(\tau_K + \epsilon, -\hat{\mu}) = N(\tau_K, -\hat{\mu}) + 1$

if $|W_K(-\hat{\mu}, \alpha_1)| > 1$ and $|W_K(-\hat{\mu}, \alpha_2)| < 1$;

(2) $N(\tau_K + \epsilon, -\hat{\mu}) = N(\tau_K, -\hat{\mu}) - 1$

if $|W_K(-\hat{\mu}, \alpha_1)| < 1$ and $|W_K(-\hat{\mu}, \alpha_2)| > 1$; and

(3) $N(\tau_K + \epsilon, -\hat{\mu}) = N(\tau_K, -\hat{\mu})$ if both

$|W_K(-\hat{\mu}, \alpha_1)|$ and $|W_K(-\hat{\mu}, \alpha_2|$ are greater than 1 or both less than 1.

This theorem is developed in reference 3 by extending the τ-decomposition method, as refined by Lee and Hsu (ref. 4).

The theorem is interpreted as follows: Let $(-\hat{\mu}, \omega)$ be an intersection point, where $\hat{\mu}$ is specified and ω is a root of equation (13). If this is the only value of ω on the interval $\alpha_1 \leqq \omega \leqq \alpha_2$, which satisfies equation (13), then the change in the relative stability at the intersection point is determined by computing $|W_K(-\hat{\mu}, \alpha_1)|$ and $|W_K(-\hat{\mu}, \alpha_2)|$. For example, from condition 1 of the theorem, if $|W_K(-\hat{\mu}, \alpha_1)| > 1$ and $|W_K(-\hat{\mu}, \alpha_2)| < 1$, then the system gains exactly one root with $\sigma > -\hat{\mu}$; that is, $N(\tau_K + \epsilon, -\hat{\mu}) = N(\tau_K, -\hat{\mu}) + 1$.

The values of τ_K at all the intersection points are ordered by increasing magnitude to obtain the change in the relative stability as τ_K increases to its final desired value $\bar{\tau}_K$. As each delay is varied, that delay becomes τ_K in the theorem.

Intersection points $(-\hat{\mu}, \omega)$ satisfy equation (13), or $|W_K(-\hat{\mu}, \omega)| = 1$. In choosing α_1 and α_2 in the theorem, it is expedient to note that $|W_K(-\hat{\mu}, \omega)|$ increases as p increases for each value of $\omega \in (0, \omega_m]$.

APPLICATION

The relative stability of the neutral equation

$$.01024\,\ddot{\psi}(t) + .00704\,\dot{\psi}(t) + .250\,\psi(t) + .163\xi\ddot{\psi}(t - \tau_K) = 0 \tag{18}$$

where ξ is a system gain constant and $\tau_K > 0$ is a constant time delay may now be determined. This equation was used in reference 5 in examining a yaw damper control system for an airplane with rudder deflection made proportional to the yawing acceleration.

The characteristic equation associated with equation (18) can be written as

$$L(s) = P(s) - Q(s)\xi e^{-\tau_K s} = 0 \tag{19}$$

where

$$P(s) = .01024s^2 + .00704s + .250 \tag{20}$$

$$Q(s) = .163s^2 \tag{21}$$

With $s = -\hat{\mu} + i\omega$, equation (19) can be used to write

$$|\xi| = \left| \frac{P(-\hat{\mu}, \omega)}{Q(-\hat{\mu}, \omega)} \right| e^{-\hat{\mu}\tau_K} \tag{22}$$

and

$$\tau_K = \frac{1}{\omega} \left[\arg \frac{Q(-\hat{\mu}, \omega)}{P(-\hat{\mu}, \omega)} + 2p\pi \right] \tag{23}$$

Now, with $\hat{\mu}$ specified, equations (22) and (23) can be used to partition the plane of ξ and τ_K into different regions as $\omega > 0$ is allowed to vary. The solid lines in figure 3 were generated in this manner. Any point on a partitioning line or boundary corresponds to a root locus curve intersecting the $-\hat{\mu}$-line in figure 2.

To examine the stability condition (stable or unstable) or the number of roots with $\sigma > -\hat{\mu}$ in the regions of figure 3, it is useful to write equation (19) in the form

$$L(s) = H_K(s) - J_K(s)e^{-\tau_K s} = 0 \tag{24}$$

where

$$H_K(s) = P(s) \tag{25}$$

and

$$J_K(s) = \xi Q(s) \tag{26}$$

The initial stability of equation (24) along the ξ-axis ($\tau_K \to 0^+$) is evaluated by using equations (7) and (9), which become

$$\sigma_\infty = -\frac{1}{\tau_K} \ln \left| \frac{.01024}{.163\xi} \right| \tag{27}$$

and

$$L_0(s) = (.01024 + .163\xi)s^2 + .00704s + .250 = 0 \tag{28}$$

For $\tau_K \to 0^+$ and $\xi = .04$, there is one root with $\sigma = -.21$ and $\sigma_\infty \to -\infty$. As τ_K increases from 0^+ with $\xi = .04$ in figure 3, the relative stability boundary for $-\hat{\mu} = -.5$ is intersected. For this intersection point, it can be shown that α_1 and α_2 in the theorem can be chosen as $\alpha_1 = 3$ and $\alpha_2 = 4$. Then, since $|W_K(-.5, 3)| < 1$ and $|W_K(-.5, 4)| > 1$, condition 2 of the theorem applies. Thus, the neutral system loses one root with $\sigma > -.5$. (This is the root which originally had $\sigma = -.21$.) Inside the closed region for $-\hat{\mu} = -.5$, there are no roots with $\sigma > -.5$. This same procedure is used to determine which side of the curves in figure 3 should be hatched.

The hatching convention is as follows: Passing from the hatched (unhatched) side of a boundary line corresponding to a particular value of μ to the unhatched (hatched) side of the boundary results in the gain (loss) of exactly one root with $\sigma > -\hat{\mu}$.

At the point $(\xi, \tau_K) = (.04, .2)$, the system has no roots with $\sigma > -.7$. The value of σ_∞ in equation (27) at this point is $\sigma_\infty = -2.257$.

CONCLUDING REMARKS

A method has been developed for determining the stability and relative stability of scalar neutral equations, with constant coefficients and constant time delays. The approach was to determine the number of roots of the characteristic equation with real parts greater than specified negative real numbers. The method consists of separately examining the large modulus roots and finite roots. The large modulus roots are examined by using a simple expression for their asymptote; the finite roots are examined by computing the magnitude of a complex-valued function on a finite interval.

The stability method is convenient for determining the number of roots of the characteristic equation with real parts located between specified negative real numbers. An example which has occurred in practical application has been provided to illustrate the method.

REFERENCES

1. Bellman, Richard; and Cooke, Kenneth L.: Differential-Difference Equations. Academic Press, Inc., 1963.

2. Barker, L. Keith: Stability and Relative Stability of Linear Systems With Many Constant Time Delays. D. Sc. Thesis, George Washington Univ., 1976.

3. Miranker, W. L.: Existence, Uniqueness, and Stability of Solutions of Systems of Nonlinear Difference-Differential Equations. J. Math. Mech., vol. 11, 1962, pp. 101-108.

4. Lee, M. S.; and Hsu, C. S.: On the τ-Decomposition Method of Stability Analysis for Retarded Dynamical Systems. SIAM J. Contr., vol. 7, no. 2, May 1969, pp. 242-250.

5. Beckhardt, Arnold R.: A Theoretical Investigation of the Effect on Lateral Oscillations of an Airplane of an Automatic Control Sensitive to Yawing Accelerations. NACA TN 2006, 1950.

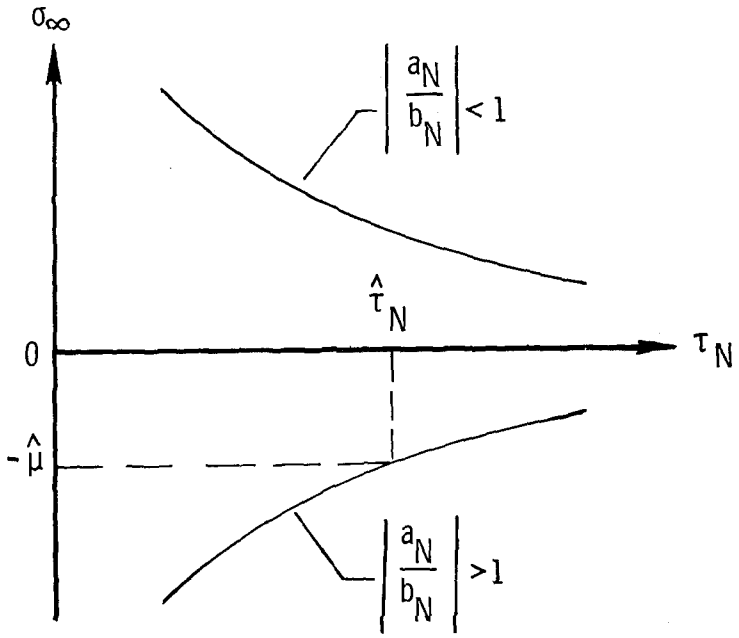

Figure 1.- Real part of large modulus roots.

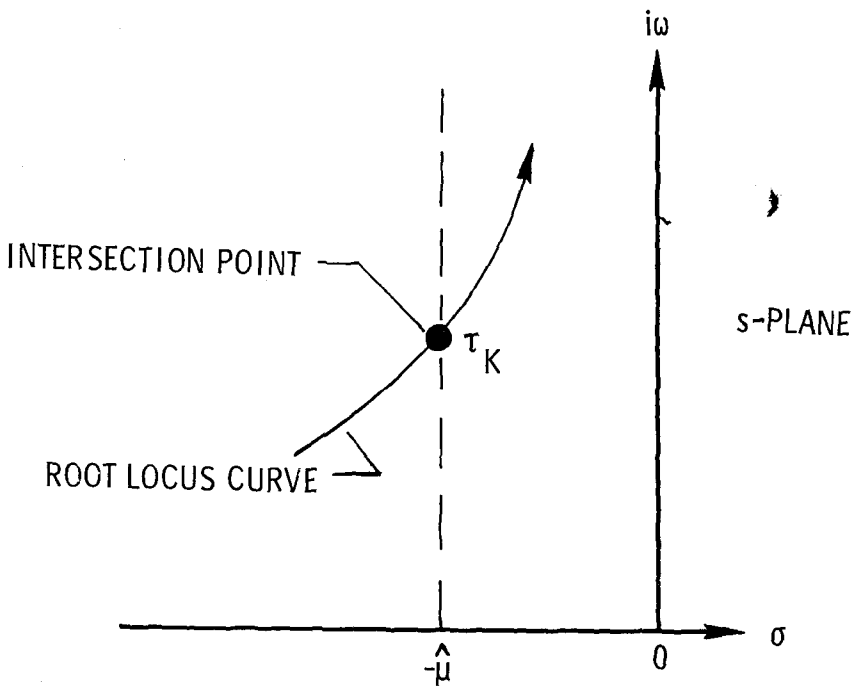

Figure 2.- Illustration of intersection point.

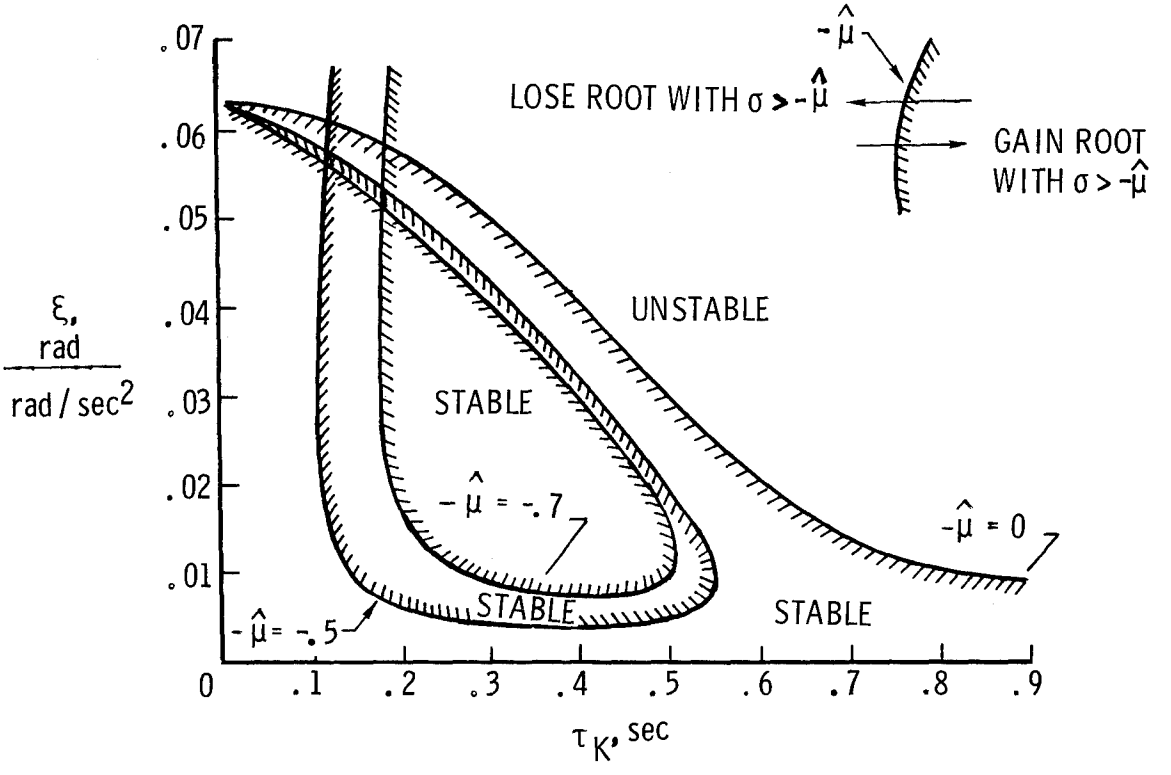

Figure 3.- Relative stability boundaries.

CUBIC SPLINE REFLECTANCE ESTIMATES

USING THE VIKING LANDER CAMERA MULTISPECTRAL DATA

Stephen K. Park and Friedrich O. Huck
NASA Langley Research Center

SUMMARY

A technique was formulated for constructing spectral reflectance estimates from multispectral data obtained with the Viking lander cameras. The output of each channel was expressed as a linear function of the unknown spectral reflectance producing a set of linear equations which were used to determine the coefficients in a representation of the spectral reflectance estimate as a natural cubic spline. The technique was used to produce spectral reflectance estimates for a variety of actual and hypothetical spectral reflectances.

INTRODUCTION

The Viking lander cameras (ref. 1) will return multispectral images of the Martian surface with four orders of magnitude higher resolution than has been previously obtained. It is desired to extract spectral reflectance curves from this data. However, the data are limited to 6 spectral channels and most of these channels exhibit out-of-band response.

It is inappropriate to generate a data point for each channel by associating a reflectance value with a distinct wavelength; this is particularly true for those channels with appreciable out-of-band response. It is unlikely that data points so constructed will lie on the true spectral reflectance curve, and that any method of fitting a curve to these points will adequately approximate the true reflectance.

Instead the output of each channel can be expressed as a linear integral function of the unknown spectral reflectance and the known solar irradiance, atmospheric transmittance, camera optical throughput, and channel responsivity. This produces 6 equations - one per channel - which can be used to determine the coefficients in a representation of the spectral reflectance as a natural cubic spline. In this paper the appropriateness of this technique is demonstrated by using it to produce accurate approximations to the true spectral reflectance of 8 materials felt likely to be present on the Martian surface and 16 hypothetical spectral reflectances chosen for illustrative purposes.

FORMULATION

Let $\rho(\lambda)$ denote the (unknown) spectral reflectance at wavelength λ of the material that is imaged by the Viking lander camera. Knowledge of $\rho(\lambda)$ is limited to 6 spectral samples. Except for a channel-dependent, multiplicative constant, which can be determined by a calibration using as reference a test chart on board the Viking lander (see ref. 2), these 6 spectral samples are given by b_i where

$$b_i = \int_0^\infty T_i(\lambda)\,\rho(\lambda)\,d\lambda \qquad i = 1,2,\ldots,6 \qquad (1)$$

The system transfer functions $T_i(\lambda)$ are given by

$$T_i(\lambda) = \frac{S(\lambda)\,\tau_a(\lambda)\,\tau_c(\lambda)\,R_i(\lambda)}{t_i} \qquad i = 1,2,\ldots,6$$

where $S(\lambda)$ is the solar irradiance, $\tau_a(\lambda)$ the atmospheric transmittance, $\tau_c(\lambda)$ the camera optical throughput, $R_i(\lambda)$ the channel responsivity, and t_i is a constant chosen so that

$$\int_0^\infty T_i(\lambda)\,d\lambda = 1 \qquad i = 1,2,\ldots,6$$

Plots of typical system transfer functions are shown in figure 1. Note specifically the appreciable out-of-band response of the Blue (i=1), IR2 (i=5), and IR3(i=6) channels. Note also that with the possible exception of the Green (i=2) channel, none of the system transfer functions are adequately approximated by an impulse function.

THE REFLECTANCE ESTIMATE AS A NATURAL CUBIC SPLINE

Equations (1) describe the relationship between the 6 multispectral samples $b_1, b_2, \ldots, b_6$ and the unknown reflectance $\rho(\lambda)$. These six equations can be used to produce a natural cubic spline estimate of $\rho(\lambda)$, denoted $\langle \rho(\lambda) \rangle$, where

$$\langle \rho(\lambda) \rangle = \sum_{j=0}^{7} x_j\, C(\lambda - \bar{\lambda}_j) \qquad (2)$$

The 8 knots $\bar{\lambda}_0, \bar{\lambda}_1, \ldots, \bar{\lambda}_7$ are chosen to be equally spaced and located at the wavelengths

$$\bar{\lambda}_j = .33 + j\Delta \qquad j = 0,1,2,\ldots,7$$

where the spacing is $\Delta = .12\ \mu m$. Recall that each cubic spline basis function $C(\lambda - \bar{\lambda}_j)$ is a bell-shaped curve centered at the knot $\bar{\lambda}_j$ and defined by $C(\lambda)$ where

$$C(\lambda) = \begin{cases} 2/3 - \left|\frac{\lambda}{\Delta}\right|^2 + \frac{1}{2}\left|\frac{\lambda}{\Delta}\right|^3 & |\lambda| \leq \Delta \\ \frac{1}{6}\left(2 - \left|\frac{\lambda}{\Delta}\right|\right)^3 & \Delta < |\lambda| < 2\Delta \\ 0 & |\lambda| \geq 2\Delta \end{cases}$$

The coefficients $x_0, x_1, \ldots, x_7$ are to be determined.

It is desirable to impose the natural boundary conditions $\langle \rho(\lambda) \rangle'' = 0$ at the knots $\bar{\lambda}_1$ and $\bar{\lambda}_6$. These two conditions give rise to the equations

$$x_0 - 2x_1 + x_2 = 0 \tag{3a}$$

and

$$x_5 - 2x_6 + x_7 = 0 \tag{3b}$$

The remaining six equations which determine the 8 coefficients are obtained by requiring the estimate $\langle \rho(\lambda) \rangle$ and actual reflectance $\rho(\lambda)$ to have indistinguishable camera multispectral responses (ref. 2), i.e.,

$$\int_0^\infty T_i(\lambda) \langle \rho(\lambda) \rangle \, d\lambda = \int_0^\infty T_i(\lambda) \rho(\lambda) \, d\lambda \qquad i = 1,2,\ldots,6 \tag{4}$$

This produces the six equations

$$\sum_{j=0}^{7} a_{ij}\, x_j = b_i \qquad i = 1,2,\ldots,6 \tag{5}$$

where b_i is given by equation (1) and

$$a_{ij} = \int_0^\infty T_i(\lambda)\, C(\lambda - \bar{\lambda}_j)\, d\lambda \tag{6}$$

To summarize, a natural cubic spline reflectance estimate corresponding to the multispectral sample $b_1, b_2,\ldots,b_6$ can be produced as follows:

(i) evaluate the $6\times8 = 48$ coefficients a_{ij} given by equation (6)

(ii) determine the 8 coefficients x_j by solving equations (3a), (3b), and (5)

(iii) form the estimate $<\rho(\lambda)>$ given by equation (2)

The estimate constructed in this manner reduces to an interpolating spline in the idealized situation where each system transfer function can be represented as an impulse function. To see this suppose that

$$T_i(\lambda) = \delta(\lambda - \lambda_i) \qquad i = 1,2,\ldots,6$$

where the impulse system transfer functions occur at the discrete wavelengths $\lambda_1, \lambda_2,\ldots,\lambda_6$. In this special case

$$b_i = \int_0^\infty \delta(\lambda - \lambda_i)\, \rho(\lambda)\, d\lambda = \rho(\lambda_i) \qquad i = 1,2,\ldots,6$$

and

$$a_{ij} = \int_0^\infty \delta(\lambda - \lambda_i)\, C(\lambda - \bar{\lambda}_j)\, d\lambda = C(\lambda_i - \bar{\lambda}_j)$$

so that $<\rho(\lambda)>$ is the (unique) natural cubic spline which interpolates the spectral reflectances $\rho(\lambda_i), \rho(\lambda_2),\ldots,\rho(\lambda_6)$.

RESULTS

Reflectance estimates were computed for 8 materials felt likely to be present on the Martian surface and for 16 hypothetical spectral reflectances chosen for testing and illustrative purposes. These estimates are presented in figures 2, 3, and 4. In each case the actual spectral reflectance is shown as a sequence of 71 discrete points (circles) in the wavelength range $.4 \leq \lambda \leq 1.1\ \mu m$ and the corresponding estimate is shown as a continuous curve. For each of the spectral reflectances the corresponding multispectral sample $b_1, b_2, \ldots, b_6$ was calculated from equation (1) using a 71 point Simpson's Rule. The coefficients a_{ij} were calculated in the same manner from equation (6) assuming each system transfer function to be zero outside the effective range of the camera photosensor arrays, namely $.4 \leq \lambda \leq 1.1\ \mu m$.

Figure 2 illustrates the reflectance estimates for the 8 materials felt likely to be present on the Martian surface. For those 5 simple reflectances (i.e., pinacetes 5 and 28A, Syrtis Major, augite, and average Mars) the estimates are excellent. For the 3 more complex reflectances (i.e., limonite, hypersthene, and olivine) the estimates are very good. The dominant features are reproduced; however, due to the undersampling inherent with just 6 channels, small period features are lost. Note particularly that the dominant absorption band (at $\lambda \approx .93\ \mu m$) for hypersthene is quite accurately estimated.

Figure 3 illustrates the reflectance estimates for 8 hypothetical spectral reflectances. The first 4 of these spectral reflectances (3a, 3b, 3c, and 3d) are very smooth and the corresponding estimates are almost exact. The next four (3e, 3f, 3g, and 3h) are not smooth but the estimates remain good. Note specifically that the pronounced minima in 3e and 3f are accurately reproduced. Note also in 3g the characteristic oscillation exhibited by the natural cubic spline in the neighborhood of a large slope. In 3h the loss of small period features is again evident.

Figure 4 illustrates the reflectance estimates for 8 additional hypothetical spectral reflectances. All 8 of these are of the form

$$\rho(\lambda) = .25 + .2 \sin \pi \left(\frac{\lambda - \alpha}{\beta} \right) \tag{7}$$

where the parameters α, β have the values:

	figure 4							
	a	b	c	d	e	f	g	h
α	.4	.275	.4	.31	.4	.33	.4	.35
β	.25	.25	.18	.18	.14	.14	.1	.1

As the period becomes shorter (i.e., as β decreases), the quality of the reflectance estimates deteriorates. This is particularly evident in the sequence 4a, 4c, 4e, 4g and less evident in the sequence 4b, 4d, 4f, 4h. It is also true that the quality of the estimate is affected by the location of dominant spectral reflectance features relative to the location of the system transfer functions. This is illustrated by figures 4e and 4f where the spectral reflectances differ only by a shift of .07 μm while the corresponding estimates differ dramatically. Figure 4g is a clear demonstration of aliasing whereby a short period harmonic spectral reflectance curve has a reflectance estimate which is nearly harmonic but with a larger (false) period.

CONCLUDING REMARKS

A technique was formulated for constructing natural cubic spline spectral reflectance estimates from multispectral data obtained with the Viking lander camera. Using this technique it was demonstrated that smooth, simple spectral reflectance curves can be estimated almost exactly. For more complex spectral reflectance curves, large period features can be faithfully reproduced; small period features are lost due to the undersampling inherent with the limited number of spectral channels. The technique completely compensates for system transfer functions with irregular shapes and appreciable out-of-band transmittance. Moreover the technique should be a valuable aid in selecting the number of spectral channels and their responsivity shapes when designing a multispectral imaging system. This design approach would prove to be of value especially if spectral reflectance properties of interest are known a priori and if the transfer function shapes are desired to be broad to obtain good signal-to-noise ratios.

REFERENCES

1. Huck, F. O.; McCall, H. F.; Patterson, W. R.; and Taylor, G. R.: The Viking Mars Lander Camera. Space Science Instrumentation, Vol. 1, 1975, pp. 189-241.

2. Park, S. K.; and Huck, F. O.: A Spectral Reflectance Estimation Technique for the Viking Lander Camera Multispectral Data. NASA TN D-8292, 1976.

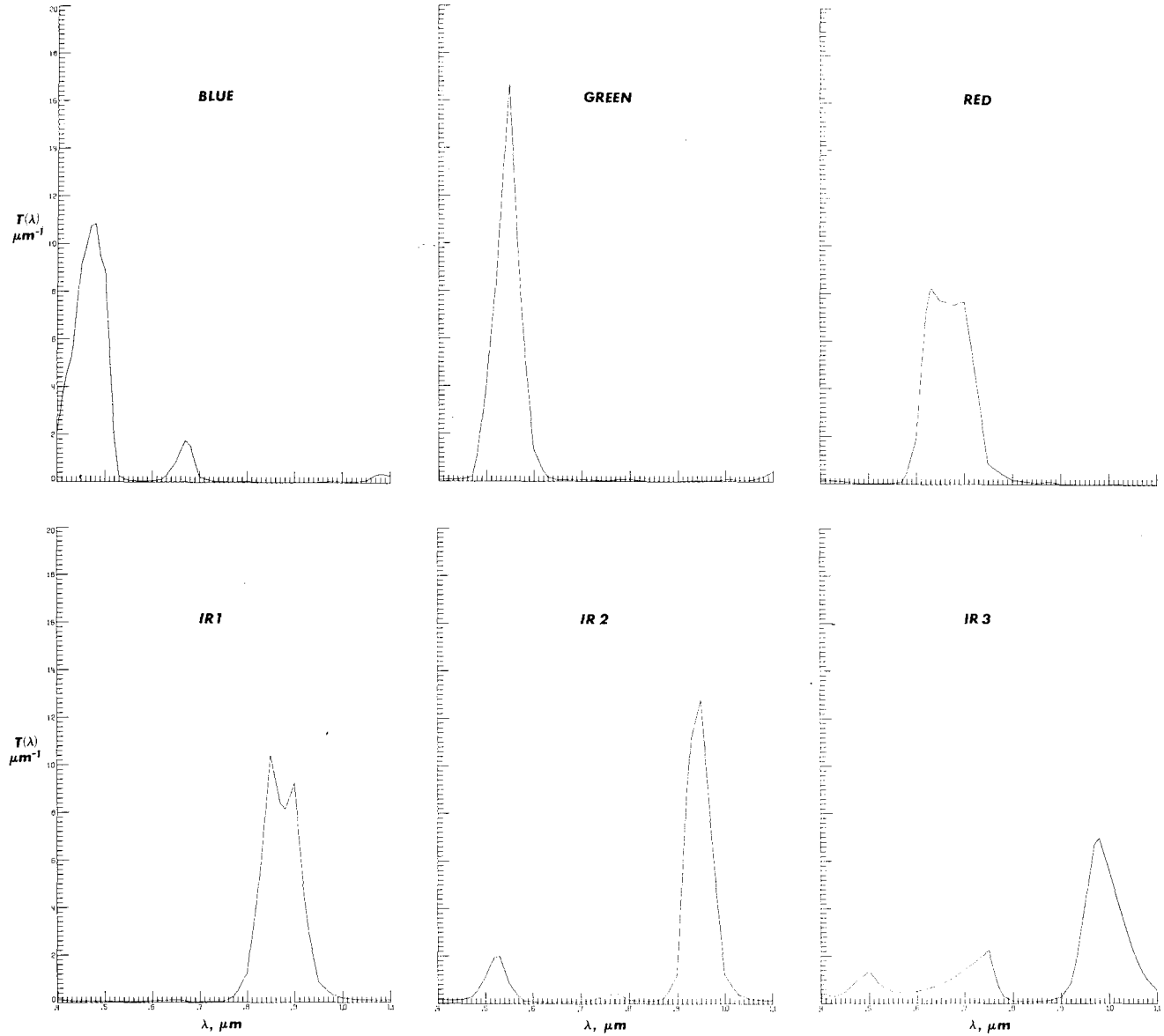

Figure 1.- Typical system transfer functions.

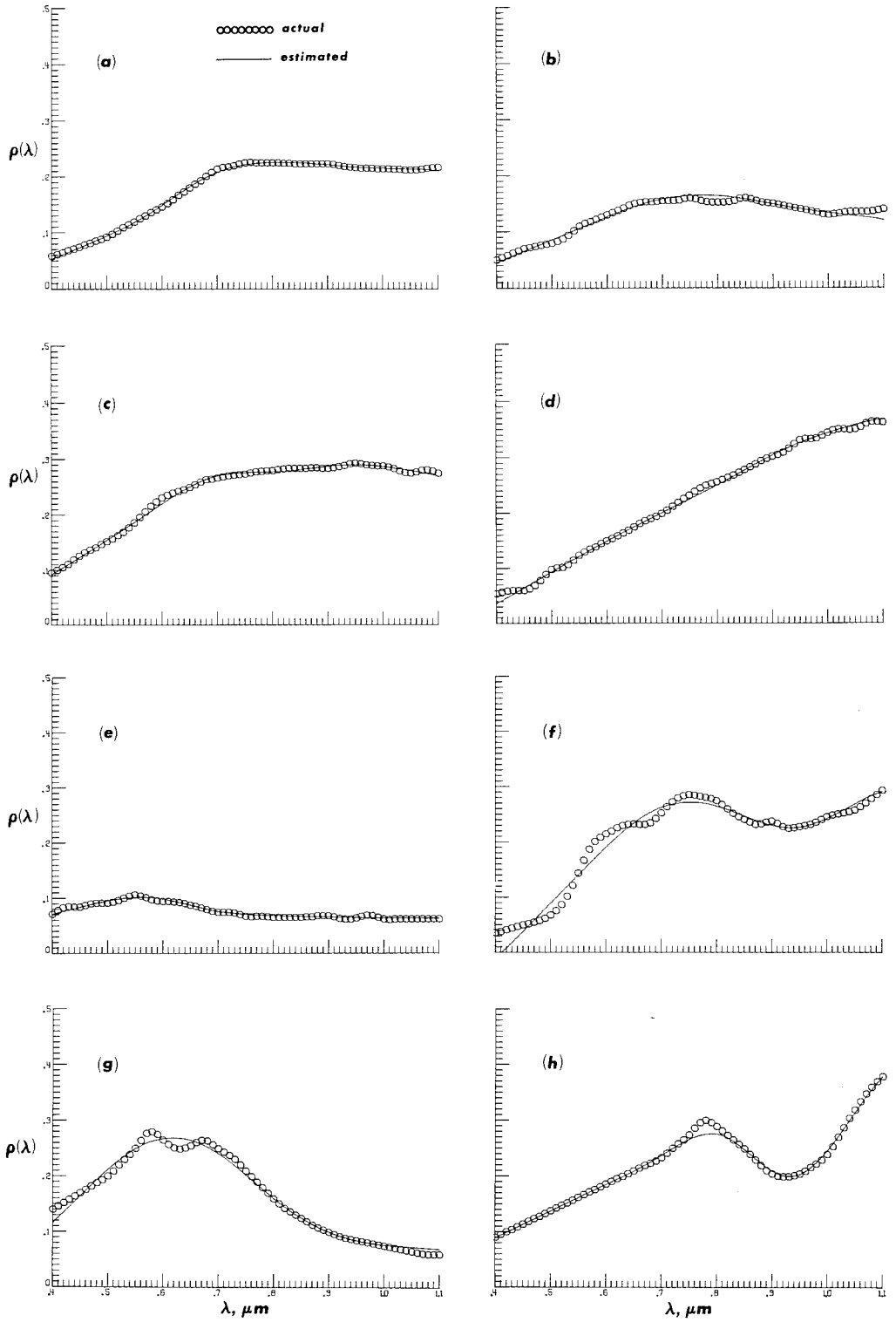

Figure 2.- Spectral reflectance estimates for (a) average Mars, (b) Syrtis Major, (c) pinacetes 5, (d) pinacetes 28A, (e) augite, (f) limonite, (g) olivine, and (h) hypersthene.

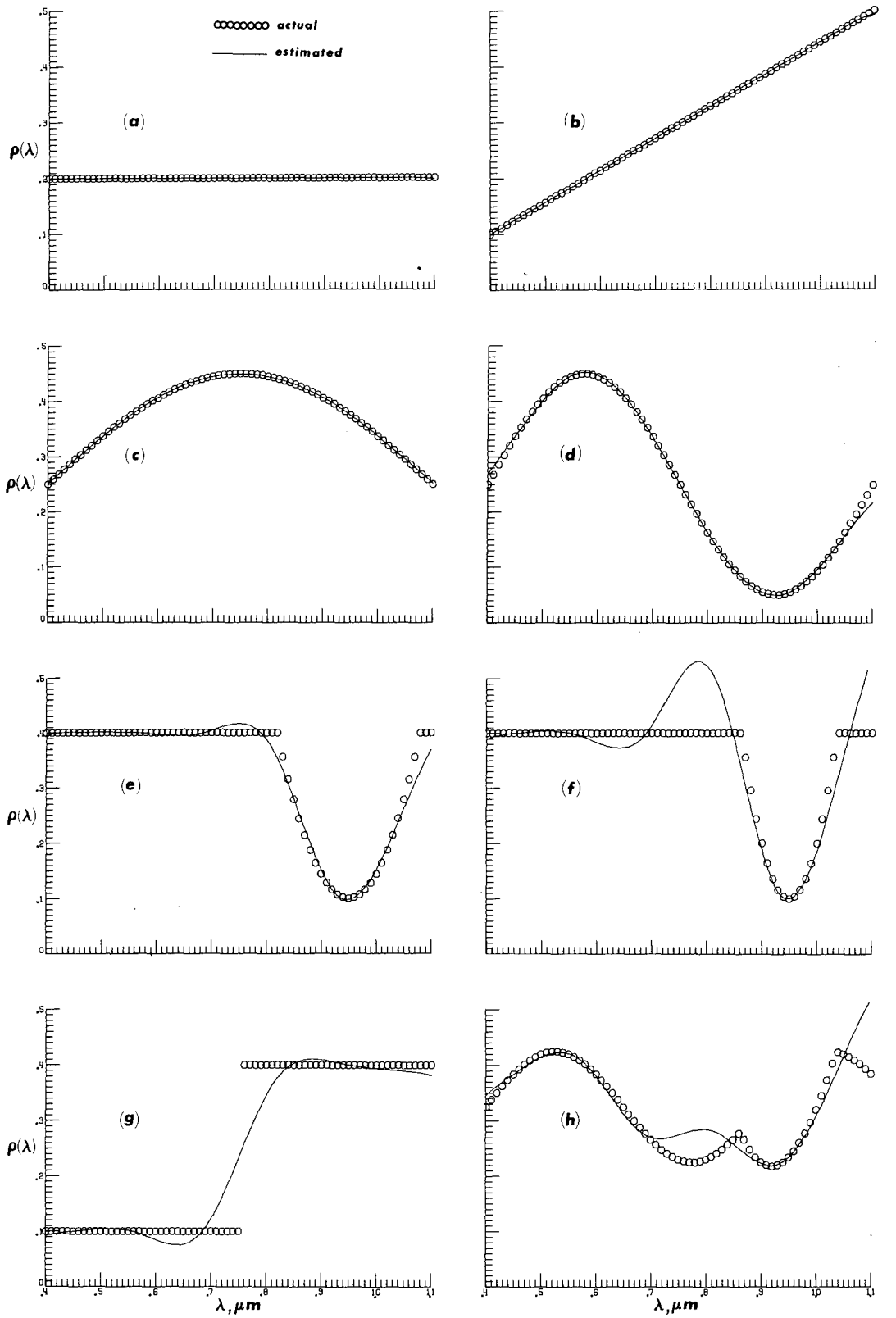

Figure 3.- Estimates for eight hypothetical spectral reflectances.

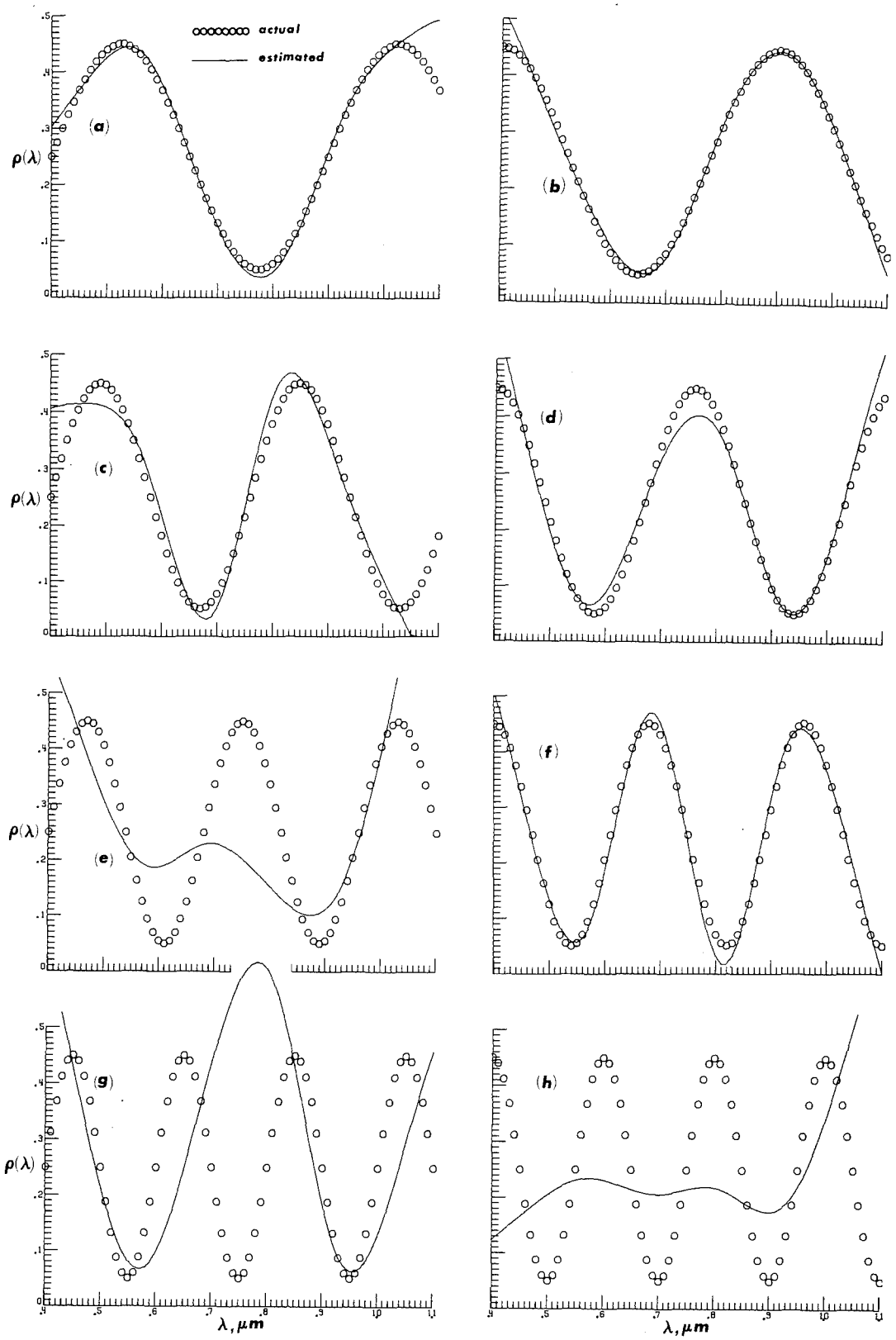

Figure 4.- Estimates for eight hypothetical spectral reflectances of the form given by equation (7).

DATA MANAGEMENT IN ENGINEERING

J.C. Browne
The University of Texas

SUMMARY

Engineering practice is heavily involved with the recording, organization and management of data. This paper is an introduction to computer based data management with an orientation toward the needs of engineering application. The characteristics and structure of data management systems are discussed. A link to familiar engineering applications of computing is established through a discussion of data structure and data access procedures. An example data management system for a hypothetical engineering application is presented.

NEED FOR DATA MANAGEMENT

Formal data management procedures become necessary for a body of information when the information

- has an extended useful lifetime,
- is shared among or used by a substantial group of workers,
- has established relationships among data items.

The use of computer based data management systems is justified by combinations of several circumstances.

- The volume of data outstrips convenient use through traditional media such as handbooks, microfilm, etc.
- The data is produced through computer processing and will perhaps be subjected to further computer processing.
- The data requires frequent revising and updating.
- There is a large and geographically compact group of users.

It is clear that many types of engineering projects meet both sets of criteria. The design of an aircraft or ship makes a cogent example. The design process depends heavily upon the use of computers. The design process may take several years and involve hundreds of engineers. The design data may involve millions of words of specifications and an immense volume of numeric data. 1% or 2% of the data change on a weekly or monthly basis over much of the design cycle.

Engineers have traditionally been heavily involved in the classical forms of data management such as data compilations, design handbooks and system maintenance manuals. Computer based data management has been relatively slow to penetrate standard engineering practice. This may be in part due to the fact that engineering education tends to stress the use of computers as numerical

problem solvers rather than as information managers. It is certainly in part due to the fact that most existing data management systems are oriented towards commercial and business data processing applications.

Engineers have now begun turning to computer based data management for assistance. Since available data management systems are not in general well-suited to engineering applications there is considerable activity in the engineering community towards designing and implementing data base systems which are useable in engineering environments. It is the purpose of this paper to give a perspective on the design and implementation of such data management systems.

Three recent texts, Martin (ref. 1), Date (ref. 2) and Katzan (ref. 3), cover data management systems in readable fashion.

DATA STRUCTURES, DATA REPRESENTATIONS AND STORAGE MAPPING FUNCTION

The basic concepts of data management, data structuring, data representation and storage mapping functions are presented in the familiar context of general purpose programming languages such as FORTRAN or PL/1. Data management systems present and utilize these concepts in more formal and complex forms.

A data structure consists of a conceptual object, i.e., a sparse array, a name or name set for referring to the object and a set of operations on the object.

A realization of a data structure consists of a storage mapping function which maps the name space of the data structure onto a memory structure and the definition of the operations on the structure in terms of primitive operations.

These definitions are completed by defining a storage or memory. A cell is a physical realization which holds a value. Memory consists of an ordered collection of cells. An address is the location in memory for a given cell. A value is an instantiation of a data object or data structure. A storage mapping function accepts a name as input and produces an address of a cell (or cells) in memory as an output.

The definition and realization of a data structure thus consist of a sequence of actions:

- A structure declaration which defines the data type.
- A name assignment which associates the name with a type or structure.
- The definition of the operations on the structure. The only required operations are of course storage and retrieval.
- An allocation of memory to the named instantiation of the data structure.
- The definition of the mapping function which maps the name space onto the allocated memory space.

This sequence of steps is seldom clearly delineated in traditional programming

languages. A FORTRAN DIMENSION or COMMON declaration of a rectangular array executes all of the above steps except the definition of operations upon the array. DIMENSION A (10,10) recognizes the square array as a data structure of the program, associates the name A with the array, assigns 100 contiguous cells of memory each of which will hold a floating point number and assigns the implicit familiar mapping function.

$$\text{Address } [A(I,J)] = A(1,1)+10(I-1) + (J-1) \qquad (1)$$

The definition of operations on an array (except for I/0 operations) must be defined by the programmer in terms of operations on the primitive data objects.

The most complicated data structure definable in FORTRAN is a multidimensional array of identical objects. PL/1 allows arrays whose elements are not identical. Data management systems may allow the definition of considerably more complex structures which include the stipulation of relationships between the data elements in a structure. The aspect of this problem not familiar to the scientist and engineer is the representation of the data structure in the computer memory system and the definition and implementation of storage mapping functions.

The familiar storage mapping function of equation (1) takes the name A(I,J) as input and evaluates the expression on the right hand side for output. This mapping function has the very useful property of mapping names onto addresses in a unique one-to-one fashion. There are other possible mapping functions which do not have this property even for the simple case of square arrays. Consider, for example, the mapping function

$$\text{Address } [A(I,J)] = (I \times J) \text{ MOD } N \qquad (2)$$

with N = 101. It is easily seen to generate identical addresses for many index pairs. It is the general case in data management applications that the magnitude of the name space is much larger than the potentially realizable address spaces. Thus, storage mapping functions which "fold" the name space into a smaller domain and thus lose the one-to-one property are required. Such storage mapping functions typically have several functional phases and are fairly complex. The example data management system which is specified in the last section of this article uses an inverted file or dictionary look-up storage mapping function to locate records and the mapping function defined succeeding to map data elements onto records.

Figure 1 defines a record structure for data relating to the design cycle of the wing section of an aircraft. Figure 2 displays the heirarchical relationships among the data elements. This structure defines the occurence of 40 data records on the design and evaluation of wing sections. The leftmost numbers in Figure 1 define the level in the definition hierarchy as shown in Figure 2. The components at any level with no immediately succeeding components at a lower level are terminal nodes of a tree. The bracketed numbers on the right hand side of the terminating nodes are the number of primitive data objects in each instance of the defined object. The bracketed numbers on the right hand side of the non-terminal nodes in the tree are the number of instances of the structure for which storage is to be allocated.

It is convenient to describe the structure in tabular form. (See Table 1). It is desired to allocate storage for each record in a contiguous block with each terminal node of the tree being stored contiguously for each instance of the structure or sub-structure. Let us define a reference expression ($\exists$name) which orders the names of the structures from left to right by level.

$$A_1(I_1)A_2(I_2)A_3(I_3)$$

$$A_1(I_1)A_2(I_2)A_3$$

The reference expression $WS(I_1)SD(I_2)DH(I_3)$ refers to the I_3^{th} storage element within the I_2^{th} instance of SD within the I_1^{th} instance of WS. $WS(I_1)SD(I_2)$ refers to the I_2^{th} instance of SD within the I_1^{th} instance of WS while $WS(I_1)SD$ refers to all 10 instances of SD within the I_1^{th} instance of WS. A storage mapping function with the one-to-one property for these reference expressions can be derived (ref. 4):

$$\text{address}[A_1(I_1)A_2(I_2)\ldots A_k(I_k)] = \sum_{i=1}^{k} [Q(A_i) + M(A_i)(I_i-1)]$$

where $Q(A_i)$ and $M(A_i)$ are constants for each record element.

The constants Q and M can be defined recursively.

1. If A_i is a terminal node of the structure, then $M(A_i) = 1$.
2. If A_i is a structure or sub-structure with a typical instance $B_1\ldots B_n$
$$M(A_i) = \sum_{i=1}^{n} C(B_i)M(B_i)$$
3. If $B_1\ldots B_n$ is a sub-structure definition, then
$Q(B_1) = 0$
$Q(B_j) = Q(B_{j-1}) + C(B_{j-1})M(B_{j-1})$, $j>1$
$Q(A) = 0$, for root of tree
4. If B_n is the last item in a sub-structure $B_1\ldots B_n$ of A, then
$M(A) = Q(B_n) + C(B_n)M(B_n)$

The last two rows of Table 1 give the results of the calculations for the record structure of Figure 1.

Bertiss (ref.5) and Elson (ref.6) are good general references for further information on data structure. Knuth (ref. 7 and 8) is the most complete source for work prior to publication data in the areas of his coverage.

AN EXAMPLE DATA MANAGEMENT SYSTEM

This section will illustrate the structure of a prototype data management system for engineering data. The example system will be designed to store and retrieve design data on the wing sections of an aircraft.

The components of a data management system are:

1. A data structure definition capability: This includes a set of primitive data objects and a set of composition rules which will enable a user to create a structure which represents the objects of interest. The set of primitive objects and composition rules comprise what is often called the data definition model or data model in the data management system literature. A structure defined by the composition rules will be said to constitute a logical record.
2. A storage mapping function which enables access to the components of a logical data structure or logical record.
3. A representation which packs logical records onto physical records in executable memory.
4. A storage mapping function which determines the address of a logical block and the address of the physical block which contains it.
5. A block transfer function which transmits physical records to and from auxiliary memory.
6. A query language which allows the user to express his storage/retrieval requests in an application-oriented format. Commercial data management systems often have very highly developed query languages. It is often the interface which sells the system more than its internal performance. It is generally the case in scientific/engineering computing that simple or specialized query languages will be all that is required. The users of the system will often by familiar with programming and programming systems.

We proceed by defining for our example system each of the components previously described.

1. Data definition model: The primitive objects which we will need will be character strings, real numbers, integer numbers and real vectors. We will allow the composition of arbitrary tree structures utilizing these primitive data types. Figure 3 defines a logical record for a wing section similiar to the example in the previous section. The record consists of a character string for the aircraft designation, a set of design parameters including thickness, flexibility coefficient and strut spacing, each of which is a real number and a set of stress values which is a vector of length 25 of real numbers. Figure 4 is a tree structure for this data. The [15] following the record declaration declares that a physical record will contain 15 logical records. The primary purpose of this system is to be able to examine the stress values as a function of design parameters. It is anticipated that entire records will be added or deleted from the file but that records will seldom be altered or modified.
2. Storage mapping functions for logical records: We use the storage mapping function defined for hierarchical structures in the previous section.
3. Data representation in physical memory: The logical record will be organized and stored on physical record blocks (PRB) of 512 words in length. Each logical record will require 30 words. Fifteen logical records will be stored on each physical record block. Forty-five of the remaining sixty-two words will be used for the location in the PRB of logical record instantiations which contain a given design parameter value.
4. A storage mapping function for addressing logical records from physical records: The storage mapping function will utilize an inverted file structure (ref. 1). Each design parameter will be represented as an inverted file. An inverted file is a tabulation of record addresses associated with a given name or structure component whereas a normal file contains the values associated

with each name or structure component. Each entry in the inverted files for design parameters will consist of a design parameter, the number (= address) of each physical block which contains a logical record with that design parameter value and a pointer to the address on that physical block of the set of position numbers for logical records containing that particular design parameter value. Each entry in the inverted file on a given design parameter is sorted in ascending order on the design parameter values. The inverted files will also be stored on 512 word PRB's. It will be assumed for simplicity that the set of entries for a given design parameter will always fit on a single physical record block.

There will be a directory to each inverted file which is kept in executable memory. The directory entries for a given inverted file will consist of the largest and smallest value for a design parameter which is stored on a given inverted file PRB together with the number (= address) of the PRB holding those inverted file entries.

5. Physical record transmission: We will assume that the operating system provides a convenient capability for transmitting fixed length blocks to and from disk storage.
6. Query language: The query language consists of a knowledge of the table structures.

A summary of the relationships between the storage mapping function and a given physical record is illustrated in Figure 5.

This data management system structure will support queries for logical records which specify one, two, or three design parameters. To find all records which have a particular design parameter, say thickness = 0.002", the following process would ensue:

- A search would be made on the directory for thickness to locate the inverted file page (PRB containing 0.002" for the thickness design parameter. This PRB would be loaded into executable memory.
- A search of this page of the inverted file for thickness would return the set of physical record blocks containing the logical records with that thickness parameter and the pointer to the physical record block section which holds the positions on the PRB of the logical records containing the given design parameter.
- These physical records could then be read in from the disk. The logical records would be extracted from the PRB's and examined one by one using the hierarchical record addressing scheme.

To obtain all records which have two particular attributes, say a thickness of 0.002" and a strut separation of 0.8", one would carry out an identical search on the inverted files for both thickness and strut separation. The intersection of the two lists of physical record blocks will contain all of the logical records which have the specified value for both parameters.

A simple system such as the one described can be implemented with only a modest amount of effort in FORTRAN under a modern operating system. There are, of course, many other data representations and mapping functions which could be used.

REFERENCES

1. J. Martin, "Computer Data-Base Organization" Prentice-Hall, Inc. Englewood Cliffs, New Jersey, 1975.

2. C.J. Date, "An Introduction to Database Systems" Addison-Wesley Publ. Co., Reading, Mass., 1975.

3. H. Katzan, "Computer Data Management and Data Base Technology" Van Nostrand, Reinhold, New York, 1976.

4. P. Deud, "On a Storage Mapping Function for Data Structures", Communications of ACM, Vol.9, No.5, 1966, pp. 344-347.

5. A.T. Bertiss, "Data Structure: Theory and Practice", Academic Press, New York, 2nd Edition, 1975.

6. M. Elson, "Data Structures" Science Research Associates, Palo Alto, California, 1974.

7. D.E. Knuth "The Art of Computer Programming, Vol. 3, Sorting and Searching" Addison-Wesley, Reading, Mass., 1973.

8. D.E. Knuth "The Art of Computer Programming, Vol. 1, Fundamental Algorithms" Addison-Wesley, Reading, Mass., 1968.

Level	L	1	2	2	3	3	2	3	3
Name	N	WS	SD	DH	DD	PC	ED	TD	PR
Count	C	40	20	10	6	5	10	6	2
	Q	0	0	20	0	6	130	0	6
	M	210	1	11	1	1	8	1	1

Table 1: Tabular Representation of Record Structure

```
1 Wing Section [40]                    1 WS [40]
  2 Surface Description [20]             2 SD [20]
  2 Design History [10]                  2 SD [20]
     3 Design Data [6]                      3 DD [6]
     3 Plant Code  [5]                      3 PC [5]
  2 Evaluation Data      [10]            2 ED [10]
     3 Test Data    [6]                    3 TD [6]
     3 Performance Rating[2]               3 PR [2]
```

Figure 1: Record Definition for Wing Section Data

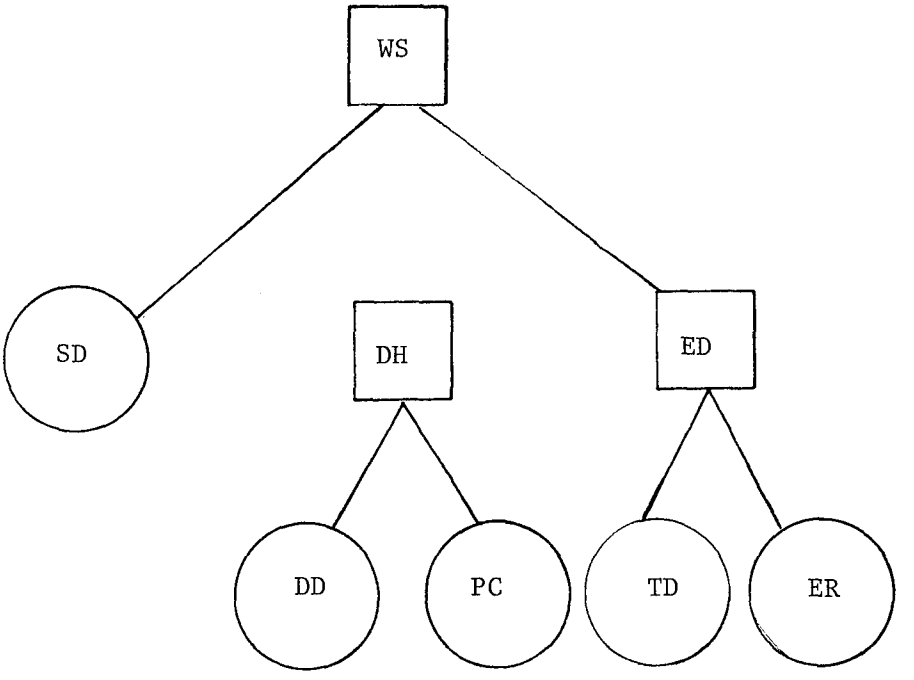

Figure 2: Tree Diagram of Wing Section Data Record

```
1 Wing Section [15]
    2 Aircraft Designation C10
    2 Design Parameters
        3 Thickness R1
        3 Flexibility R1
    2 Stress Values R [25]
```

Figure 3: Logical Record Definition for Wing Section Stress Data

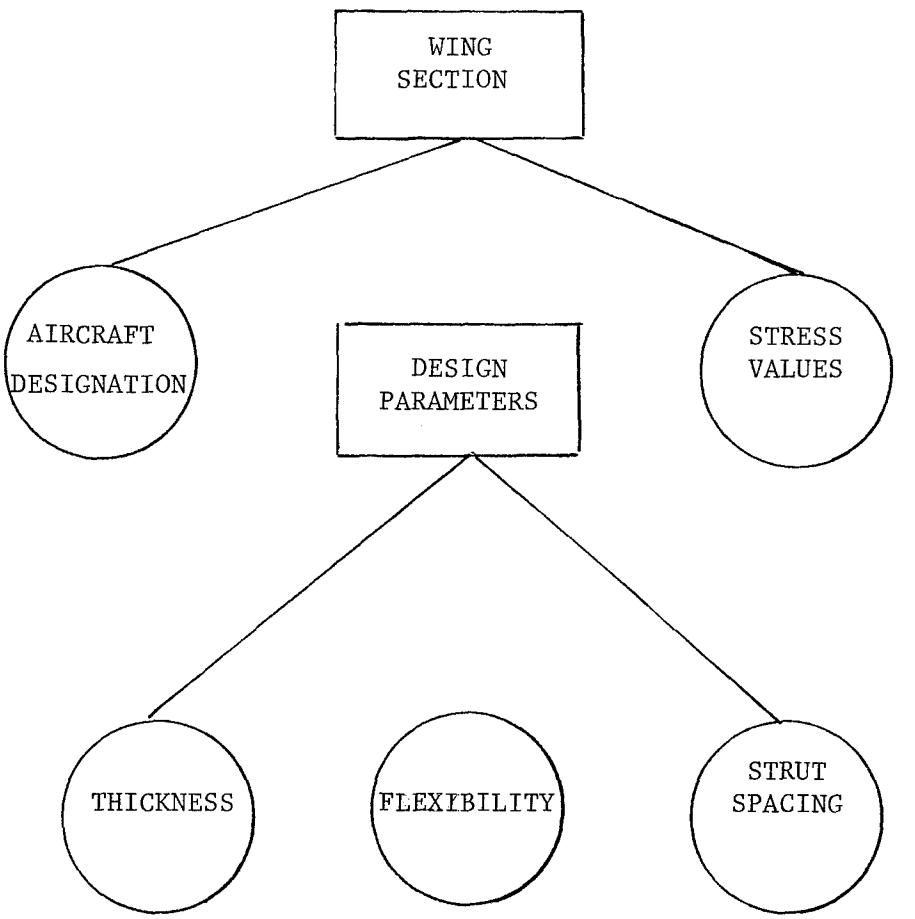

Figure 4: Tree Structure of Wing Section Logical Record

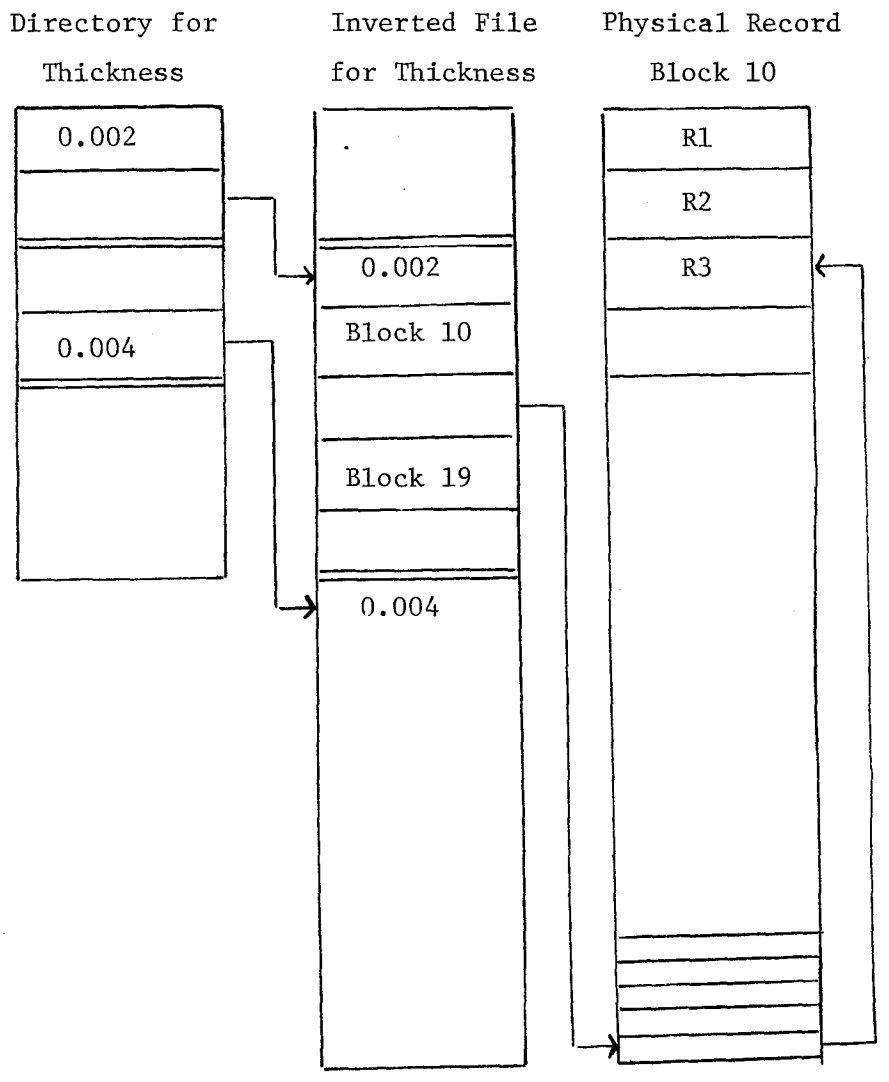

Figure 5: File Structures For Wing Section Data

TOOLS FOR COMPUTER GRAPHICS APPLICATIONS

R.L. Phillips
The University of Michigan

ABSTRACT

Ten years of extensive research in computer graphics has produced a collection of basic algorithms and procedures whose utility spans many disciplines; they can be regarded as tools. These tools are described in terms of their fundamental aspects, implementations, applications, and availability. Programs which are discussed include basic data plotting, curve smoothing, and depiction of 3-dimensional surfaces. As an aid to potential users of these tools, particular attention is given to discussing their availability and, where applicable, their cost.

INTRODUCTION

Direct computer-produced graphical output, once considered a luxury, is becoming relatively commonplace. The availability of low cost plotters and display terminals is largely responsible for the trend. Increased usage of computer graphics has given rise to a need for application-oriented, non-research, graphical software. It is the goal of this paper to point out and discuss such software. The hope is that duplication of effort can be avoided and that the use of non-general, low quality graphic software will be discouraged.

The software to be described here is of such generality, widespread utility and ready availability so as to be classified as a tool—a tool to be employed to the user's advantage and not encumber him in his work. The paper, then, is a survey of sorts, but a rather limited one. We shall not discuss any software in the research stages, nor any software that is not readily available. Moreover, since device and system independence are also valued attributes, vendor supplied packages, no matter how good, will not be discussed. In what follows we shall discuss basic data presentation techniques, both for two and three dimensions. Then certain data processing and enhancement methods will be described (e.g. clipping and shading).

DATA PRESENTATION (2-Dimensional)

Overview

One of the most useful applications of computer graphics is data presentation, or graphing of data on an axis system. The two-dimensional graph is the

most common qualitative and quantitative method of representing relations among data. Several software tools have been developed to facilitate the data presentation process, ranging from automatic axis scale determination to passing smooth curves through the data points.

Automatic Scale Generation

If we impose the reasonable restriction that the scale to be determined is "nice" or readable, the process of automatic scale selection is not at all trivial. A scale obtained by dividing the span of a variable by the corresponding axis length will almost never satisfy this restriction. "Nice" scale intervals will never have values like 0.125 or 1.1 but rather will be more usable values like 0.1 or 2.0. Even where a "nice" interval of, say 5, is used, corresponding axis labels like -1, 4, 9, etc., would not qualify as a readable scale. Tastes may differ on readability but there are some fundamental good practices that should be followed in scale selection.

Several algorithms have been published for automatic production of readable scales. They all produce acceptable results and we shall describe only one in some detail, the algorithm due to Lewart (ref. 1). The rules are simple — the scale intervals must be the product of an integer power of ten and one of a set of "nice" coefficients. Certainly this set should consist of at least 1, 2, and 5 but individual taste may allow perhaps 4 and 8 to be included. The next requirement is that axis labels must be integer multiples of the scale intervals. These requirements result in an axis whose extremes will embrace the data it represents. When the algorithm is applied to each axis, the resulting graph is "efficient" — the data come as close as possible to filling the available plotting area. Figure 1 shows the results of applying this algorithm to a situation where a data zoom is performed on the original graph. The algorithm, being general, can adapt to any situation. Comparable algorithms are described in references 2 and 3.

Labelling with Software Characters

A common goal in the preparation of computer-produced data representations is to make them report-ready, i.e. no subsequent draftsman work should be required. If this goal is to be attained, all text that appears on the graph should be of high quality. The usual stick figure software characters usually will not suffice for this; something more elegant is desired. The nonpareil of all software character fonts are those developed by Hershey (ref. 4). Complete font digitizations as well as several sophisticated typographic subroutines are available for the cost of mailing a tape. A sample of textual output using Hershey's fonts is shown in figure 2; nothing more need be said.

Curve Fitting

We shall make a distinction now between curve fitting, where one attempts to pass a smooth curve through all data points, and curve smoothing, where a smooth curve is passed through a neighborhood of all points according to some least-squares criterion. The latter process is useful where the data is statistical or imprecisely known; this will be discussed in the next section.

In a case where data are precisely known and no smoothing is required, one often wishes to join the data points with a continuous curve. The process is trivial, of course, if many intermediate data points can be calculated so that joining them by a straight line produces a sufficiently smooth curve. This is often not feasible, however. It may be that the data are derived from an expensive computation, as in the solution of a set of nonlinear partial differential equations, or the original computational scheme is not available, such as data obtained from a table of thermophysical properties.

Without benefit of prior experience, one is tempted to try to produce a smooth curve by using either a global high order polynomial fit to all data points or to produce intermediate points by second or higher order interpolation. Neither approach is ever very successful; unwanted oscillations usually result. An excellent overview of these problems is found in Akima's paper (ref. 5) where he proposes a new scheme for curve fitting. His contribution was to devise a new way of locally computing slopes at each data point and using these slopes to construct a series of cubic polynomials, continuous at each join. The program that implements this algorithm appears in reference 6. The author has not been able to find a situation where Akima's method fails. It is inexpensive as well as accurate. Figure 3 demonstrates its capabilities.

In some instances Akima's method produces a curve of greater curvature than may be desired, especially where the original data is sparse. In this case one should consider the tension splines of Cline (ref. 7). Cline develops a rigorous theory for these curves but pragmatically we can imagine them to be flexible wires which are passed through a series of eyelets (the data points) and made as taut as one wishes by pulling on either end. The amount of tension is under control of the user, which is at the same time an advantage and drawback of the approach. It is not clear a priori what value of tension is appropriate. Figure 4 shows Cline's method using different amounts of tension on the same set of data.

Curve Smoothing

For data that is imprecisely known or statistical in nature, a curve-fitting approach as described above would be inappropriate. Rather, we wish to obtain some smooth, mean curve that passes through the neighborhood of the data according to some least-squares criterion. Often, the curve obtained is to be used for further computation such as differentiation or interpolation so it is important to perform the smoothing accurately. Variations that are statistically significant must be accounted for; thus, the method must be capable of recognizing trends. There are, by the way, many nonlinear regression techniques that have been developed in the statistical literature (refs. 8 and 9) that treat this problem, but to use them one must usually make some assumptions about the functional form of the data. The method of smoothing splines, however, requires no such assumptions and it is this technique we discuss. Here a series of spline curves are computed which join continuously at knots. Knots may or may not coincide with data points; the number of them and their position are selected by the program so as to produce a best fit, subject to a least-squares constraint. The user can supply weighting factors to the original data so that outliers can be eliminated from the smoothing process.

Two smoothing spline algorithms have been published in the literature. The method of Powell (ref. 10) requires somewhat more user judgment than one would like but seems to produce good results. Lyche and Schumaker (ref. 11) have described a method that is based upon local procedures, but it is published in Algol and involves a recursive procedure. Thus, the program cannot be easily transliterated into FORTRAN. Results typical of Powell's algorithms are shown in figure 5. Details on a third smoothing spline algorithm have not been published but the routine that implements it is available from Kahaner (ref. 12). This routine is noteworthy because it allows the user to apply certain boundary conditions to the resulting smooth curve. The other algorithms do not allow this, a fact which may sometimes prove objectionable.

DATA PRESENTATION (3-Dimensional)

Overview

Often one wishes to display bivariate data in the form of a surface, a projection of the three-dimensional representation of the data. While this representation is seldom of any quantitative use, it can provide valuable insight into the behavior of complex datasets. Such a representation is shown in figure 6 where the transfer function of an underwater sound signal is represented (ref. 13). The steps required to obtain a plot such as this can be difficult, depending upon the original form of the data. All possibilities will be discussed below.

Interpolation on a Regular Grid

We are imagining a dataset, functional or tabular, Z(X,Y), where Z is some altitude or third dimension associated with every coordinate pair X,Y. If the data happen to have been derived on a regular lattice, that is, Z is known at all points on a specified X-Y array, intermediate points can be obtained fairly easily. It is not even necessary that the lattice spacing be the same in the X and Y directions; it simply must be regular. The production of intermediate points with the aim of plotting a smooth surface can be approached as a simple bivariate interpolation problem. Unless the function Z(X,Y) is very benign, however, straightforward interpolation schemes produce unreal values in the vicinity of strong local variations. The most successful and generally applicable algorithm for regular grid interpolation is due to Akima (ref. 14). The method is, in fact, the bivariate analog of the successful univariate scheme described in reference 6. The program has a simple interpolation entry point for deriving values from a bivariate table, and a smooth surface mode, where a dense array of interpolated points are returned for subsequent plotting. The author has used these routines in many situations, always with good results.

Interpolation from Scattered Observations

A more realistic case than that of the above, is where the dataset consists of a table of Z values known only at irregular and arbitrarily spaced X-Y coordinates. Most spatially distributed geographic data is in this category, as is experimentally derived bivariate data. The process of interpolating from

scattered observations to produce a regular grid is much more challenging than the corresponding problem for regular data; over 100 papers have been published on the subject over the last 20 years. The problem stems from choosing an interpolation function that will not bias the data thus derived. Two interesting and successful solutions to this problem have recently appeared. One is due to Akima (ref. 15), who we have referenced twice already. He again extends his "local procedure" scheme to handle the case of irregularly spaced initial data. The results are in excellent agreement with test data presented in his paper.

Tobler (ref. 16) has recently produced another approach to this problem, which amounts to an iterative solution of the biharmonic equation in the vicinity of each data point. His program produces results equal to those of Akima, using the same data.

Surface Plotting

Once the dataset has been regularized, one can proceed to produce a plot of the surface it describes. Any method that is to be acceptable for our purposes must satisfy three criteria:

a) user-specified perspective projections of the surface must be obtainable,

b) hidden lines, e.g., the back of the surface must be eliminated,

c) one should be able to display the surface as viewed from any orientation, including from below.

There are dozens of surface plotting packages but only a few satisfy all these criteria. One that does is due to Williamson (ref. 17). It is acceptable in all three of the above respects but it might be criticized for its lack of generality. It is very much plotter oriented, expressing size variables in terms of inches rather than abstract user units. Another system which is acceptable in all respects was developed by Wright (ref. 18) and forms part of the impressive NCAR graphics package (ref. 19). Wright's program has many options for representing a surface, including cross-hatching and the production of stereo pairs. Figure 7 is an example of a surface produced by Wright's program.

DATA PROCESSING AND ENHANCEMENT

Shading and Cross-Hatching

It is often the case that one wishes to automatically shade or cross-hatch a general two-dimensional polygon. This capability is frequently required for architectural applications, engineering drawings, and thematic cartography. The task is, given an n-sided simply connected polygon with no restrictions on concavity or convexity, find the intersection of a family of shading lines with

the boundary of the polygon. The lines are then drawn with the proper angle and spacing. For cross-hatching this process is repeated for a different orientation, and perhaps spacing. A general shading routine should also permit variable spacing between shading lines so that arbitrary and unusual patterns can be obtained. Finally, it is desirable to be able to shade a multiply connected region by specifying invisible, coincident cut points that join inner and outer boundaries of a polygon.

All of these desirable properties are displayed in figure 8, which was produced by an algorithm originally suggested by Dwyer (ref. 20) and implemented by Phillips (ref. 21). The algorithm uses vector algebra for the computation of shading line intersections, an operation that is simulated in reference 21 by the complex arithmetic features of FORTRAN. A more elaborate example of shading is shown in figure 9, a thematic map showing the location of water polluting industries in New England. Another shading program has been developed by Ison (ref. 22) which is capable of complex patterns such as bricks, soil patterns, etc. This package, however, seems unnecessarily oriented toward the digital plotter as an output device.

Windowing and Shielding

The process of methodically preventing some part of a graphical display from being plotted is known as clipping. This is often done when the user narrows his field of view in his coordinate space, e.g. zooming in for more detail, and the part of the picture falling outside that area is not to be seen. The boundaries of the narrowed field of view is called a viewport and can generally be formed by any polygon. Usually, however, the viewport is simply a rectangle, making the process of clipping straightforward (refs. 23 and 24). The most general case involves any simply connected polygon, concave or convex. Moreover, the term window implies that the portion of a picture inside the viewport is to be seen, while the viewport acts as a shield if the picture outside it is to be visible. Behler and Zajac (ref. 25) have published an algorithm for treating this general case. The problem differs from the one of general shading in that it does not deal with a family of lines having common characteristics; here every line is a special case. An example of polygonal windowing is shown in figure 10. There the polygon is the lower peninsula of Michigan consisting of 370 points, which windows contour lines that have been computed on a rectangular grid that is much larger than the polygon.

SUMMARY

A reader may find fault with this limited survey for having omitted several of his favorite graphics routines; this is inevitable. I have endeavored to discuss all packages of which I am aware (one could do no more) and with the important stipulations that the software is of proven utility, it can easily be installed on most machines, it is available (from the sources referenced), and the cost, if any, is nominal. Naturally, the author welcomes any revelations of other software that satisfies these constraints.

REFERENCES

1. Lewart, C.R., Algorithm 463: Algorithms SCALE1, SCALE2, and SCALE3 for Determination of Scales on Computer Generated Plots. Comm. Acm, 16, October 1973, pp. 639-640.

2. Thayer, R.P. and Storer, R.F., Algorithm AS21: Scale Selection for Computer Plots. Applied Statistics, 18, 1969, pp. 206-208.

3. Herro, J.J., Program 00546B: Optimum Scale for a Graph. HP-65 User's Library, Hewlett-Packard Co., Cupertino, Cal., 1974.

4. Hershey, A.V.: FORTRAN IV Programming for Cartography and Typography. NWL Technical Report TR-2339, U.S. Naval Weapons Laboratory, Dahlgren, Va., Sept. 1969.

5. Akima, H.: A New Method of Interpolation and Smooth Curve Fitting Based Upon Local Procedures. J. ACM, 17, October 1970, pp. 589-602.

6. Akima, H., Algorithm 433: Interpolation and Smooth Curve Fitting Based on Local Procedures. Comm. ACM, 15, October 1972, pp. 914-918.

7. Cline, A.K.: Scalar- and Planar-Valued Curve Fitting Using Splines under Tension. And Algorithm 476: Six Subprograms for Curve Fitting Using Splines Under Tension. Comm ACM, 17, April 1974, pp. 218-223.

8. Draper, N. and Smith, H.: Applied Regression Analysis. Wiley, New York, 1966.

9. Cuthbert, D. and Wood, F.S.: Fitting Equations to Data. Wiley-Interscience, New York, 1971.

10. Powell, M.J.D., Subroutine VC03A, Harwell Subroutine Library, Atomic Energy Research Establishment, Harwell, Berkshire, England, 1967.

11. Lyche, T. and Schumaker, L.L., Algorithm 480: Procedures for Computing Smoothing and Interpolating Natural Splines. Comm. ACM, 17, August 1974, pp. 463-467.

12. Kahaner, D., Program ISPLIN, Los Alamos Scientific Laboratory, Los Alamos, N.M., 1975.

13. Cederquist, G.N.: The Use of Computer-Generated Pictures to Extract Information from Underwater Acoustic Transfer Function Data. Ph.D. Dissertation, The University of Michigan, 1975.

14. Akima, H., Algorithm 474: Bivariate Interpolation and Smooth Surface Fitting Based on Local Procedures. Comm. ACM, 17, January 1974, pp. 26-27.

15. Akima, H.: A Method of Bivariate Interpolation and Smooth Surface Fitting for Values Given at Irregularly Distributed Points. OT Report 75-70, U.S. Dept. of Commerce/Office of Telecommunications, Boulder, Colo., 1975.

16. Tobler, W.: Tuning an Interpolated Lattice. Dept. of Geography, The University of Michigan, Ann Arbor, Mich., 1976.

17. Williamson, H., Algorithm 420: Hidden Line Plotting Program. Comm. ACM, 15, February 1972, pp. 100-103.

18. Wright, T.J.: A Two-Space Solution to the Hidden Line Problem for Plotting Functions of Two Variables. IEEE Transactions on Computers, C22, January 1973, pp. 28-33.

19. NCAR Software Support Library, Volume 3, NCAR-TN/LA-105, National Center for Atmospheric Research, Boulder, Colo., 1975 (contact T.J. Wright).

20. Dwyer, W.C.: Windows, Shields, and Shading. Proc. 6th UAIDE Meeting, Washington, D.C., 1967.

21. Phillips, R.L.: Subroutine SHADE. Department of Aerospace Engineering, The University of Michigan, Ann Arbor, Mich., 1972.

22. Ison, N.T.: An Algorithm to Shade a Plot. Computer Graphics (SIGGRAPH-ACM Quarterly), 7, 1973, pp. 10-23.

23. Newman, W.M. and Sproull, R.F.: Principles of Interactive Computer Graphics. McGraw-Hill, New York 1973, pp. 121-126.

24. Jarvis, J.F.: Two Simple Windowing Algorithms. Software-Practice and Experience, 5, 1975, pp. 115-122.

25. Behler, B. and Zajac, E.E.: A Generalized Window-Shield Routine. Proc. 8th UAIDE Meeting, Coronado, Cal., 1969.

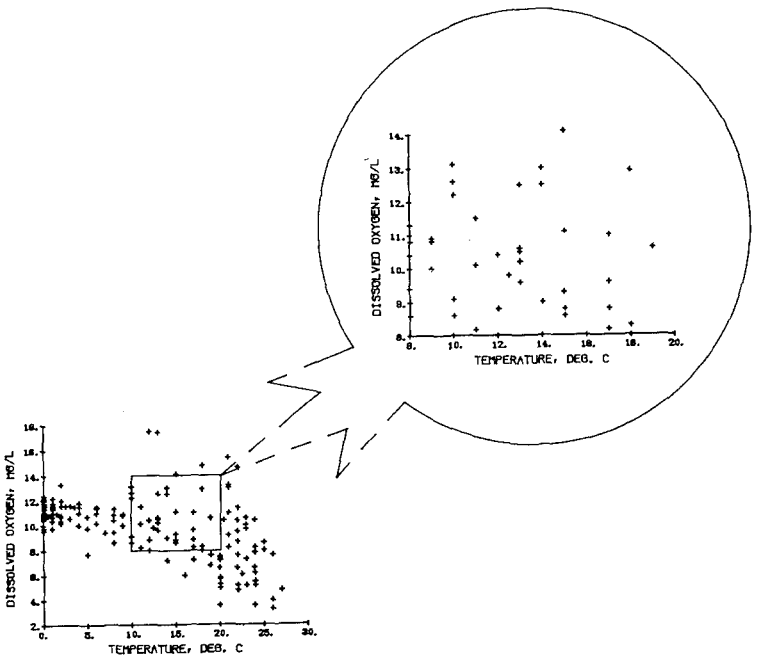

Figure 1.- Automatic scale generation.

Invitation	COMMUNICATION	*Publication*
ECONOMY	*VERSATILITY*	**Quality**
CARTOGRAPHY	Standardization	TYPOGRAPHY
Γραμμα	Συμβολον	Αριθμος
Графика	СЛОЖНОСТЬ	Фонетика
Rotation	EXTENSION CONDENSATION	ROTATION
Syllabary	ΛΕΞΙΚΟΝ	Alphabet
Art	書道	**Music**
Meteorology	**Wiſſenſchaft**	Astronomy
CHEMISTRY	*Electronics*	MATHEMATICS

Figure 2.- Hershey's software character fonts.

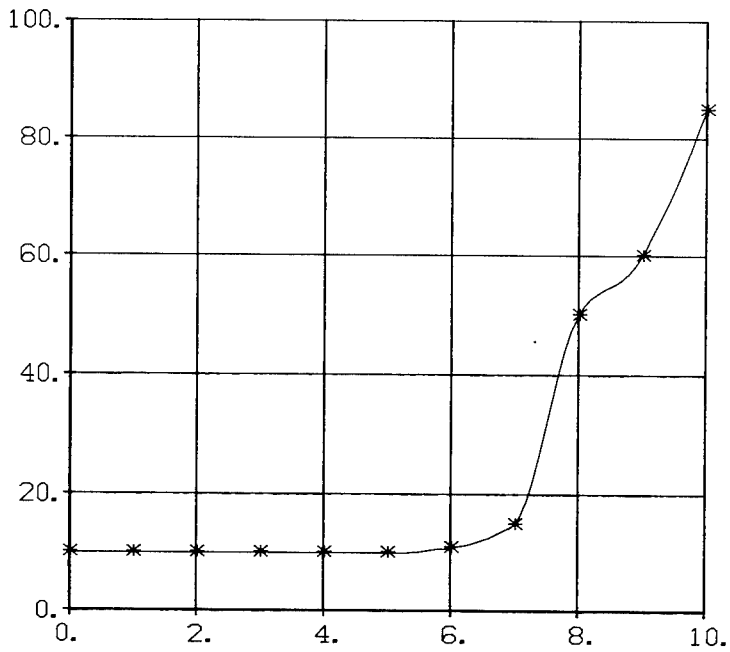

Figure 3.- Curve fitting with Akima's method.

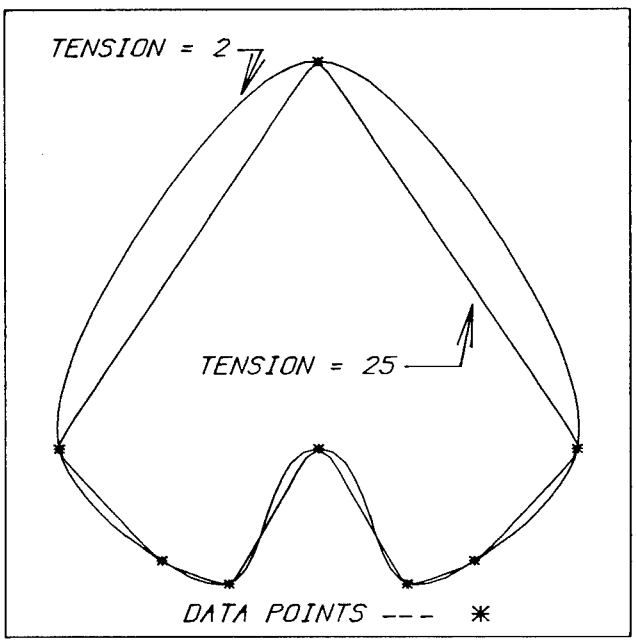

Figure 4.- Application of Cline's tension splines.

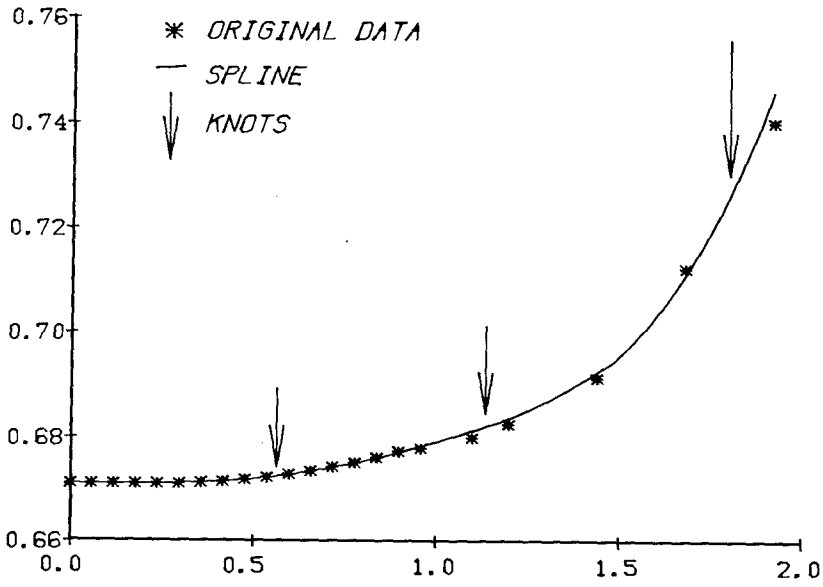

Figure 5.- Application of Powell's smoothing splines.

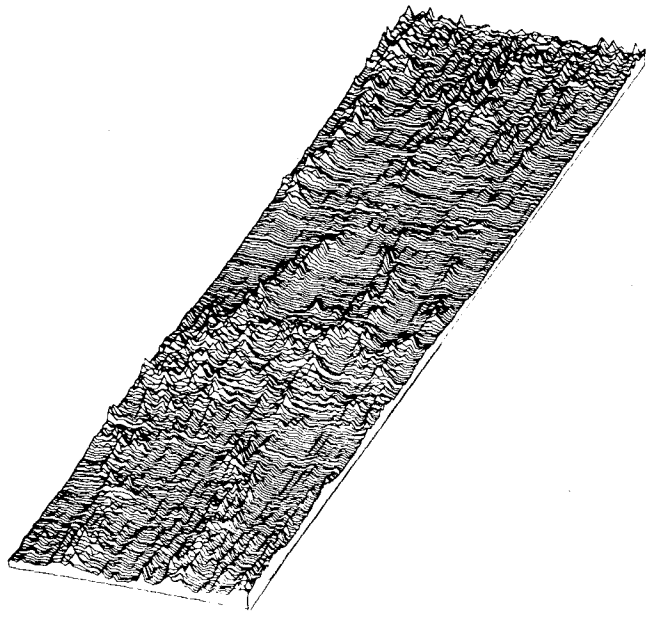

Figure 6.- Representation of a complex dataset as a three-dimensional surface.

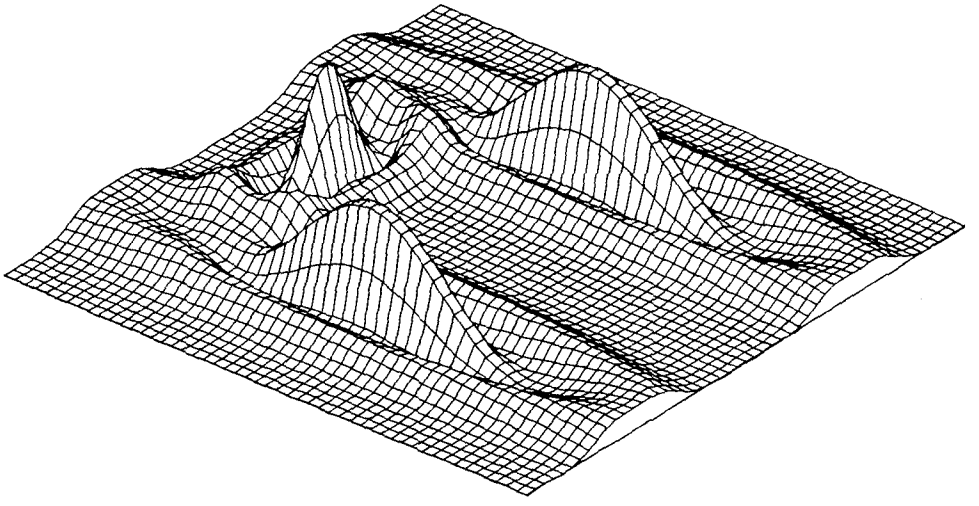

Figure 7.- Three-dimensional representation of a mathematical function.

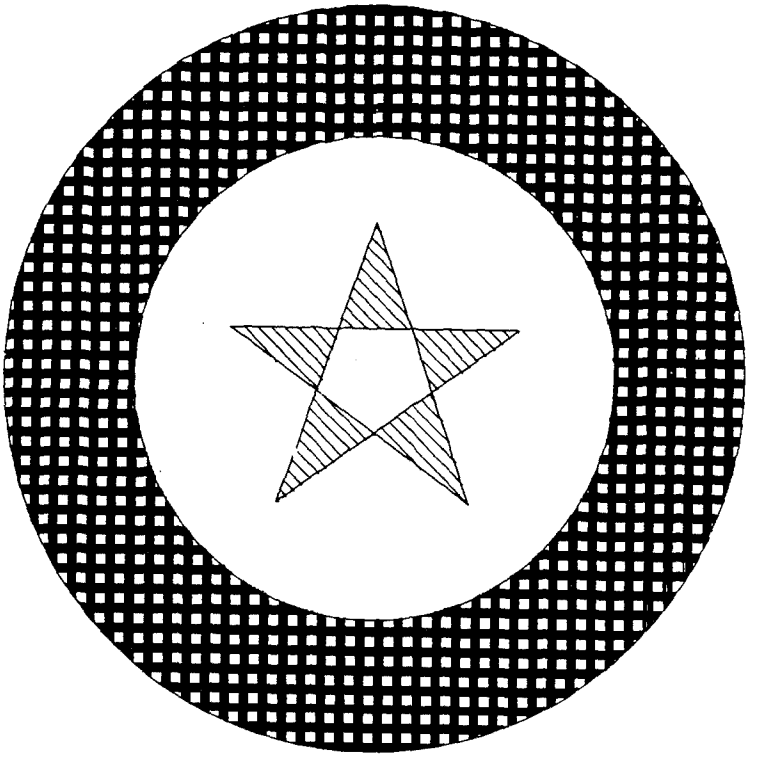

Figure 8.- Shading of compound polygons.

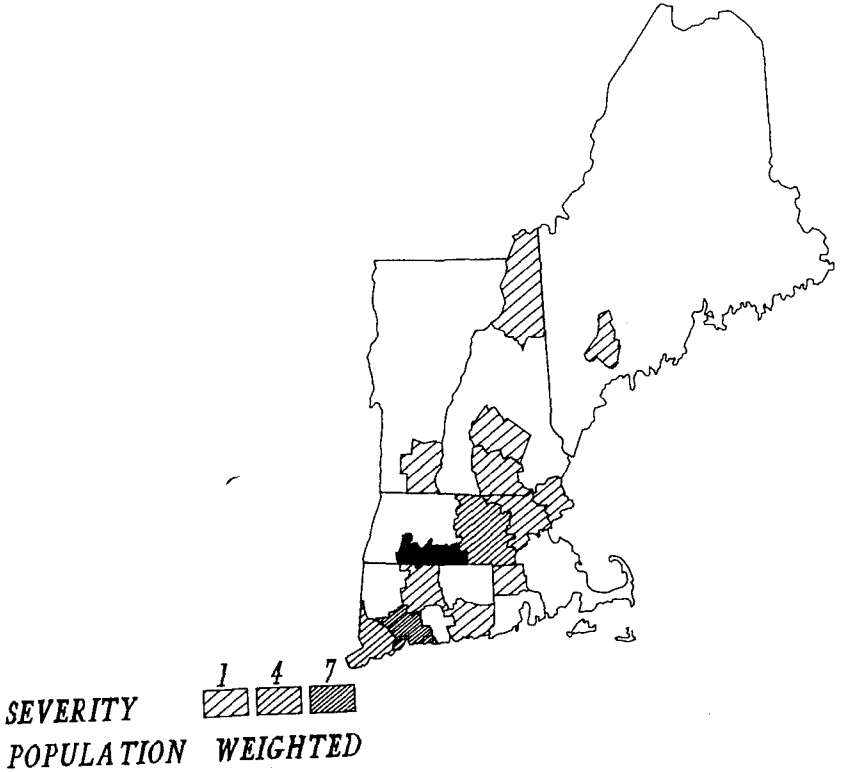

Figure 9.- Use of shading to depict pollution patterns.

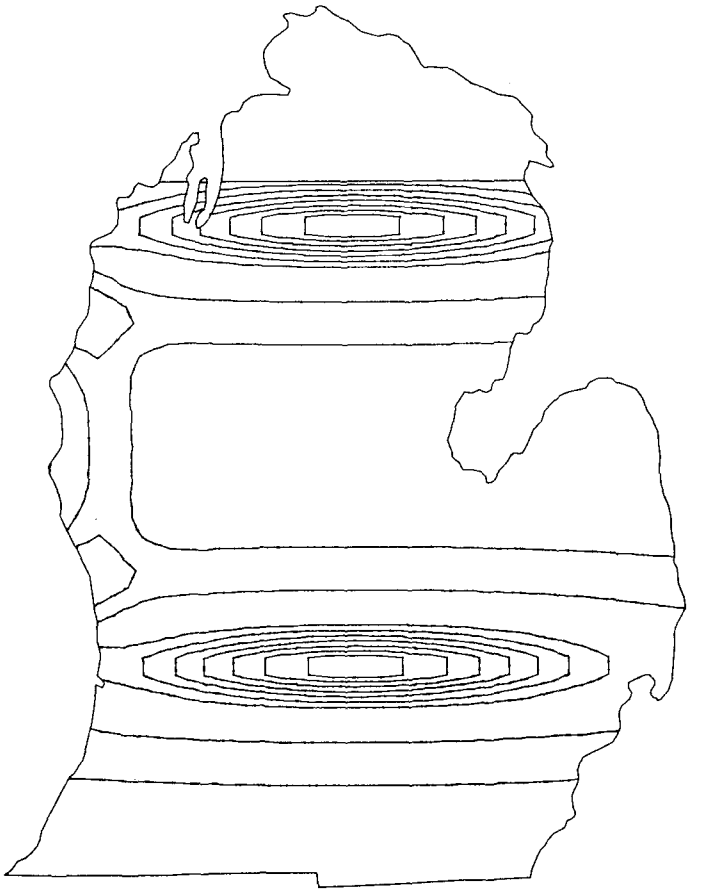

Figure 10.- General polygonal windowing.

COMPUTER SYSTEMS: WHAT THE FUTURE HOLDS*

Harold S. Stone
University of Massachusetts

ABSTRACT

Continuing advances in device technology will result in substantially higher speed devices at rapidly diminishing costs. These changes will in turn have a significant impact on computer architecture in the next decade, and on the wide-scale proliferation of computer systems into new applications.

The microprocessor of today will eventually evolve to a processor with the power of a minicomputer or perhaps a medium-scale computer of today. Non-mechanical auxiliary memories are likely to be available as well. The computational power and low cost of these computer systems will see them used in the home, office and industry for a wide variety of new applications.

Medium-scale systems will tend to be total systems that are service oriented rather than hardware oriented. A major service will be that of the information utility to provide data to a widely distributed pool of on-site computers.

Large-scale computer systems have the potential to achieve two to three orders of magnitude speed improvement over the next decade. A large portion of this may come from the faster devices. Another significant portion will come from higher parallelism. For large numerical computations, the vector processor of today may evolve to a hybrid vector processor-multiprocessor to provide efficient operation on both scalar and vector types of computations.

I. INTRODUCTION

The past two decades have seen truly phenomenal advances in computers, but the potential of computers has barely been realized. The advances in computer technology anticipated in the next decade will be so widespread that computers will directly affect the living habits and quality of life of almost every person in the United States.

Since computer architecture is largely driven by device technology and software interfaces, Section II of this paper is devoted to an analysis of the devices that may be available in the 1980s, and to the smaller end of the computer scale. Here's where growth in the next decade will be most rapid. Medium-scale computers are treated in Section III, where we project that medium-scale computers will tend to be better oriented to the specific needs of the

*This paper is an abbreviated version of the article that appears in Computer Science and Scientific Computing, Academic Press, New York, 1976, edited by J. M. Ortega.

user than their predecessors of today. Finally, for large-scale computers, Section IV indicates that rather few new ideas in high-speed computer architecture are likely to appear in the next decade, but there is room to attain about two to three orders of magnitude increase in speed by perfecting present ideas.

II. ADVANCES IN DEVICE TECHNOLOGIES--THE COMPUTER ON A CHIP

Semiconductor and integrated circuit technologies have consistently achieved advances in density, speed, and power consumption over the history of solid state devices. Figure 1 illustrates some of these trends [Turn^2]. Densities double roughly every two years at the present rate. Assuming that this continues and the 16K bit chip is a standard in 1976, then the megabit memory chip may appear late in the 1980s. To obtain densities leading to megabit chips, it will be necessary to achieve new breakthroughs in the resolution of the etching process by moving from visible light to electron-beam scanning techniques or beyond.

Apart from achieving greater resolution, there are other gains to be made from new processes. In the past decade, processes based on MOS (metal-oxide semiconductor) techniques have been characterized by high density, low power consumption, but low speed. The competing technology is bipolar, with high speed, but roughly one fourth the density and additional complexity in its fabrication. TTL (transistor-transistor logic) has been the favored type of bipolar technology for implementation of reasonably fast logic, and ECL (emitter-coupled logic) is another bipolar technology that attains the fastest logic speed. Unfortunately, the power consumption of ECL is very high, and its density is low, thereby leaving the designer no clearly best choice for a logic family.

Recent changes in technology seem to have pointed bipolar and MOS processes in the same direction. MOS circuits diffused onto a sapphire substrate instead of the traditional silicon substrate attain notably higher speeds than standard MOS circuits, but this technology has not yet overcome some obstacles that have impaired its development. In the bipolar technology, a new offshoot known as I^2L (integrated-injection logic) greatly simplifies the masks for active gates, thus increasing circuit density while retaining speed. I^2L logic has a speed more nearly that of ECL rather than that of the slower T^2L logic. If either I^2L or silicon-on-sapphire technologies succeed in attaining their respective goals, then one may have high speed, high density, and low cost all in one family.

Projecting these developments into architecture has a very interesting impact on the innovation known as the *microprocessor*. A microprocessor is essentially a complete processor compact enough to be constructed on a single chip. Actually, one often finds several chips used to make up a full-fledged computer with one chip consisting of the arithmetic logic and processor registers, another chip holding control memory, and yet another chip used for random-access memory. Input/output interfaces may be on yet other chips. As density of fabrication increases, the chip boundaries will grow larger and the number of different chips will be reduced.

We have three data points on the power of microprocessors. The 4-bit microprocessor was introduced in quantity in 1971, the 8-bit in 1974 and the 16-bit is being shipped in quantity in 1976. This is consistent with the claim that density increases by a factor of two about every two years. The chips themselves are increasing in size, too. Again projecting this forward by several years, we find that the complexity of the arithmetic unit of a microprocessor may attain that of sophisticated medium-scale machines of today by the 1980s. Figure 2 illustrates a speculation on where the trend may lead.

Although microprocessors will have the power of today's minicomputers, or more, in the 1980s, there is a major obstacle that must be crossed before microprocessor based systems can lead to substantial cost reductions in conventional minicomputer systems. The problem is mechanical auxiliary memory.

Fortunately, there are several possible nonmechanical replacements for auxiliary memory in various stages of development. Magnetic bubble memories are nonvolatile magnetic shift-register memories in which storage densities comparable to MOS memories have been achieved. Random-access time may be as low as 20 microseconds, more likely somewhat higher, but still some 100 times faster than access to rotating mechanical devices.

Another attractive storage medium is also shift-register oriented, and known as *charge-coupled device* (CCD) technology. CCD memories are volatile shift registers made up of capacitors. Charge in capacitors must be kept in circulation, unlike bubbles in magnetic bubble memories, but otherwise CCD performance characteristics closely approximate magnetic bubble memory characteristics. The first CCD memory chips for computers announced commercially appeared in 1975 and had 16k bits per chip. This puts CCD technology slightly ahead of magnetic bubbles, since bubbles had not reached the market place by 1975.

One other technology today is a candidate for replacing mechanical auxiliary memory, namely, electron-beam addressable memory (EBAM). This technology uses electron-beam techniques to deposit charges in a small region of a surface, and to read them out at a later time. EBAM is several years behind the development of CCD and bubble memories, but, once perfected, could be a strong contender since access to memory is by random-beam addressing rather than by serial access to shift registers.

III. MEDIUM-SCALE COMPUTERS

Computer manufacturers have to face the 1980s with a mixture of joy and grief. The joy stems from potential unit sales of 100 to 1000 times the present number of systems sold as computers move into every imaginable application. The grief is due to the decreasing cost of the hardware itself so that total sales volume of the hardware may drop precipitously even while unit sales are growing enormously. All the while this is happening, the end-user finds that a paltry sum buys him hardware of incredible potential, but to make

it do his job he has to pour many thousands of dollars into software and program development.

So how will these trends affect medium-scale machines? Medium-scale computers will be designed to use inexpensive additional logic wherever possible to facilitate flexibility, and enhance the range of services that can be done effectively on the machine.

Among the several trends for medium-scale computers that are perceptable are the following:

1. A "rich" instruction set is included that permits many higher level operations to be done efficiently.

2. The use of microprogramming with a writeable control store will be prevalent, so that new instructions can be implemented by the user after physical delivery of the machine. New instructions might be included for each compiler target language to increase efficiency of execution of object code, and emulation of one architecture by another will be commonplace.

3. Large memories, both real and virtual, will simplify problems of writing programs of large size.

4. Executive and control functions will be done by special purpose hardware insofar as is possible to simplify the operating system and control program.

5. Virtual machine architecture will be widely used to aid the writing and debugging of the control software that cannot be implemented in hardware.

Projecting present trends forward to the late 1980s, we see that a device comparable in cost and size to the electric typewriter could be as powerful as a medium-scale computer of 1976. This will have a great effect on decentralizing the computer center as we know it today. What will be the function of shared-resource medium-scale computers then?

In the 1980s there will still be need for central computers for computer users to access. Access will be less for computational power than for information from central data files. The data will be a resource and a commodity of trade by that time if it is not already now. The user will almost certainly use the central data base for numerical data, catalogs, bibliographies, mail, and text, quite apart from uses he makes of programs stored centrally. Since information is created in real time, a computer user must tap that information through access to one or more centralized data bases even when he is able to satisfy his computational needs for that data through the purchase of inexpensive hardware.

IV. LARGE-SCALE SYSTEMS

By early 1976 a number of very high-speed computing systems had been installed and were in operation. Some of the systems use a standard serial instruction set, and use a number of clever design techniques to achieve high speed. For example, the CDC 7600 system uses multiple functional units that can operate simultaneously, and uses an intricate instruction scheduling mechanism to keep these units busy as much as possible, even executing the instructions out of order if that results in a net increase in speed.

One trend that has emerged in recent years is that of using a computer with a vector instruction set. Each vector instruction in such a machine operates on entire vectors instead of single elements. When a vector instruction is issued on a vector computer, that one instruction manipulates all of the elements of the vector operands, and achieves a great deal of parallelism of operation with a large gain in speed.

Two distinct types of computers with vector instructions have been delivered. One type is the *array computer* of the ILLIAC IV class in which each element of the vector is treated by an independent processor. Figure 3 shows a control unit linked to 64 processors in an array by a broadcast bus. Each instruction issued results in 64 responses, each on a different element of a vector of length 64. The other type, the *pipeline computer*, as exemplified by the CDC STAR, has the computational unit partitioned into successive stages, each of which can be busy simultaneously. A vector operation is initiated by placing the first operand pair into the first stage of the computation; as they pass on to the second stage, the next pair is passed into the empty first stage. Thus if there are N stages in the pipeline, N different operations may be in operation simultaneously, each in a different stage. Figure 4 illustrates the structure of a typical pipeline computer. Floating-point operations can be conveniently divided into about eight successive stages, and the pipelines themselves can be replicated to give additional parallelism.

To give some idea of the parallelism achievable on the present machines, ILLIAC IV has 64 processors, but each processor can do two single precision operations simultaneously, so that 128 different computations can be executed at once. The CDC STAR has an effective parallelism of about 32. The parallelism achievable is impressive, but is representative of designs in progress well over five years ago. The ILLIAC IV uses an integrated circuit memory, but no large-scale integration. The CDC STAR uses neither integrated circuit memory nor large-scale integration. It is obvious that technological changes available today can be included in the next generation of these computers to gain a potential speed improvement of approximately another factor of 10 at no increase in cost. If we take into account the advances that are certain to appear in the next five years in integrated circuit technology, then this could contribute a total factor of 50 improvement in speed over machines in operation today.

Unfortunately, a factor of 50 is not enough for the very large-scale problems for which these computer systems are built. Most notable of the

massive calculations are fluid dynamics problems and weather analysis. We will still be a factor of 10^5 too slow to solve these problems in their full detail.

The obvious answer to attain higher speed is to increase the degree of parallelism where possible. When logic costs drop very low, the number of identical units that can be put into a design of marketable cost can increase from 10^2 in 1976 to perhaps 10^3 or 10^4 in the late 1980s. Unfortunately, the speed increases attainable fall short of being equal to the replication factor.

A number of lessons have been learned from experience with vector computers like STAR and ILLIAC. A few of the principal ones are given below:

1. When algorithms can be cast in vector form there are significant advantages due to elimination of unnecessary overhead for individual elements.

2. It is possible to incur substantial overhead in vector algorithms in communicating information among elements of a vector when operations on one element are influenced by the value of another element.

3. There are numerous tricks for casting serial algorithms into vector form. A programmer may have to experiment with various alternatives to obtain the best alternative. The best vector algorithms for particular problems may be quite unconventional and, in fact, may not be very efficient when performed in equivalent serial form.

4. Major bottlenecks occur when sequential scalar operations have to be done in between vector operations. This reduces the effective speed of a highly parallel machine drastically and the effect becomes more pronounced in machines as the parallelism increases.

By all appearances the vector machine is not the final answer, although the range of problems for which vector machines are well-suited has proved to be much larger than anticipated because of innovations in parallel algorithm and architectural features.

T. C. Chen (ref. 1) among others observed the performance deficiences from intermixing parallel and serial processes. Figure 5 illustrates a typical duty cycle for an array processor in which one processor is kept busy initializing a vector process, then all N processors are ganged together performing the vector operation. Chen observed that a pipeline computer duty cycle figure has the form of staircase in figure 6, to show how each successive state initiates activity slightly later than its predecessor stage. The shaded region in dark boundaries is exactly equal to the unshaded region in dark boundaries, so that the shaded area of the pipeline computer duty cycle is exactly equal to the shaded area of an array processor computation as shown in the previous figure. With this observation it is clear that there is a potential performance decrease in a pipeline computer due to a phenomenon very much like the serial overhead prior to a vector computation in an array computer.

The ILLIAC IV is designed to perform the computation shown in figure 5 as shown in figure 7, where the serial computation is done in a single control unit, and is done while the previous vector operation is in progress in the arithmetic processor array. This vastly reduces time lost due to interspersing serial and parallel operations. The equivalent processing duty cycle for the pipeline computer is shown in figure 8, which simply shows one vector operation initiated before the termination of the prior one. The CDC STAR pipeline computer presently does not have the facility to execute in this manner. Thus, the STAR duty cycle is more like that shown in figure 9.

To achieve better total performance than is predicted by Chen's pessimistic analysis, it is clear that the architecture of the 1980s will have a mix of processors, some of which are dedicated to serial types of tasks, and some dedicated to highly parallel or iterative types of tasks. Execution overlap among processing units will have to be significant to attain the speed potential of having many arithmetic units.

With microprocessors so inexpensive, there is an obvious motivation to construct vector or multiprocessor computers from arrays of microprocessors. While the individual speed of any one microprocessor may be moderate, the ability to gather 10^3 or 10^4 processors together in a single computer can lead to a very high-speed computer with tremendous computing power for reasonable cost. Hardware advances have unfortunately, outstripped architectural and algorithmic advances, to the extent that it is now possible to construct arrays with incredible computational power, except that it is not clear what form the arrays should take and how calculations should proceed in them.

To summarize the current trends for high-speed machines, a factor of 50-speed improvement is possible by the end of the 1980s from technological advances in devices, but the demands of very large problems will stimulate evolution of the architecture itself. Vector machines look more promising than multiprocessors for large-scale problems for the long-term future, but some mix of the two may emerge and prove to be the best solution.(See ref. 2.)

V. CONCLUSIONS

With technological advances leading the way as we move into and through the next decade, computer architecture will evolve to enhance the proliferation of the microprocessor, the utility of the medium-scale computer, and the sheer computational power of the large-scale machine. The most dramatic changes will be in new applications brought about because of ever lowering costs, smaller sizes, and faster switching times. There is no evidence at this time that the rate of advance in computer technology will slow significantly in the 1980s. We are truly undergoing a Computer Revolution of the scale of the Industrial Revolution.

REFERENCES

1. Chen, T. C., "Parallelism, pipelining, and computer efficiency," *Computer Design*, pp. 69-74, January 1971.

2. Turn, Rein, *Computers in the 1980s*, Columbia U. Press, New York, 1974.

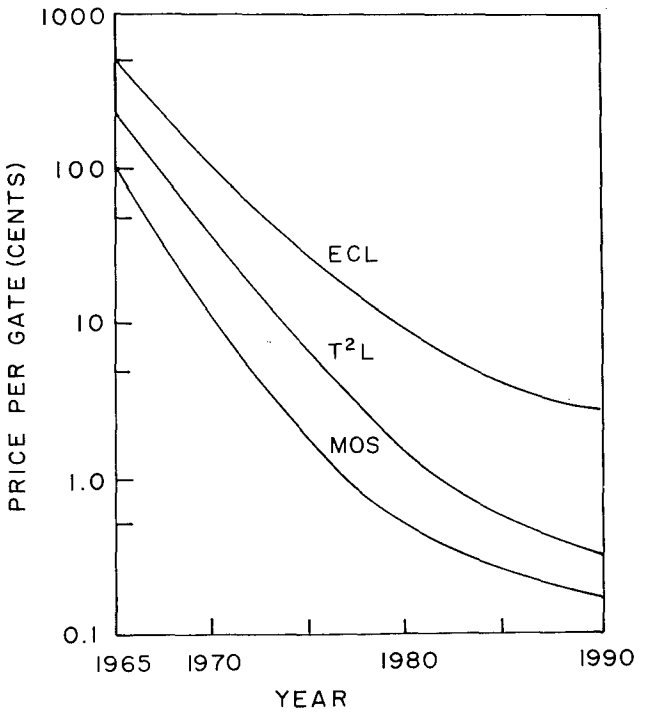

(a) Price trends.

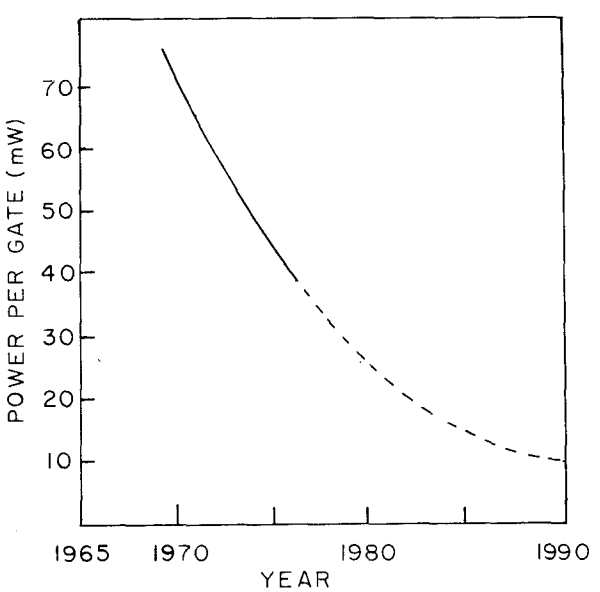

(b) Power consumption trends.

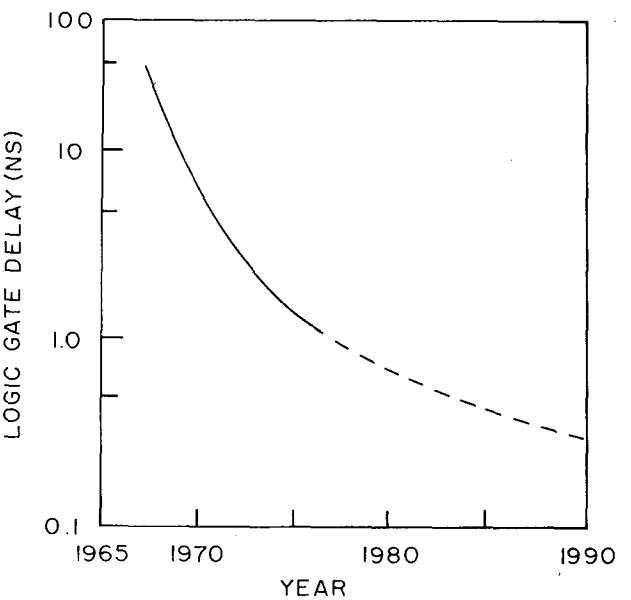

(c) Logic speed trends.

Figure 1.- Trends in device technology.

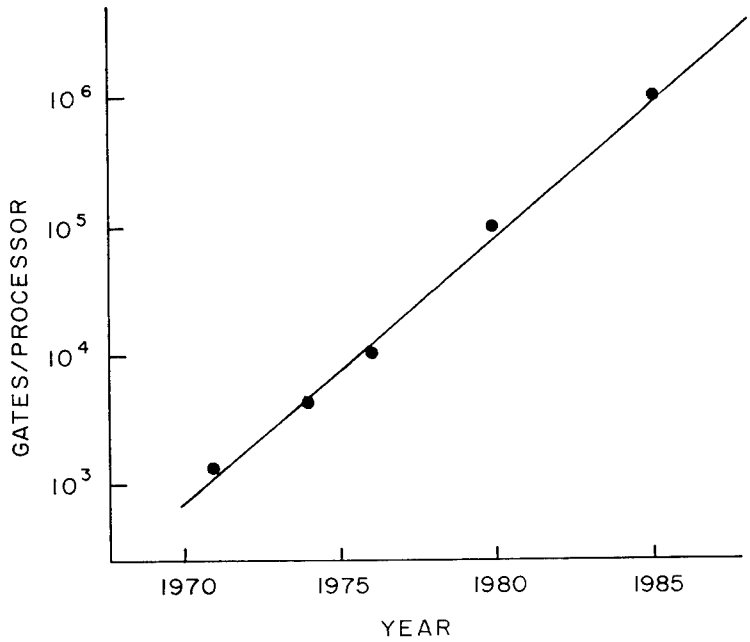

Figure 2.- Microprocessor complexity.

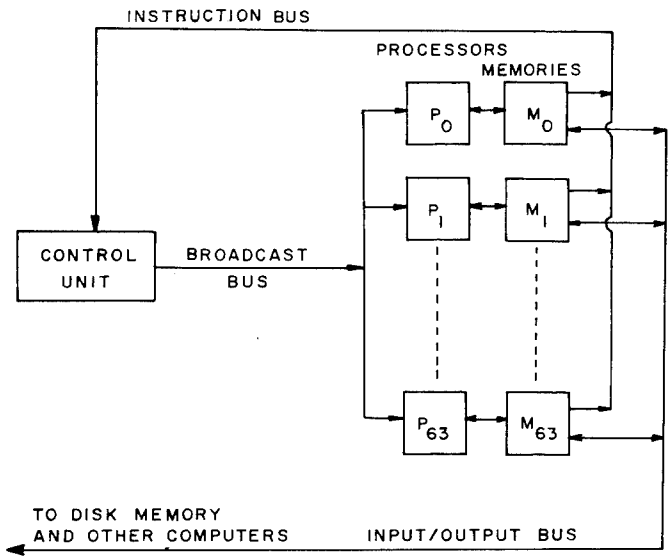

Figure 3.- An array computer (ILLIAC IV).

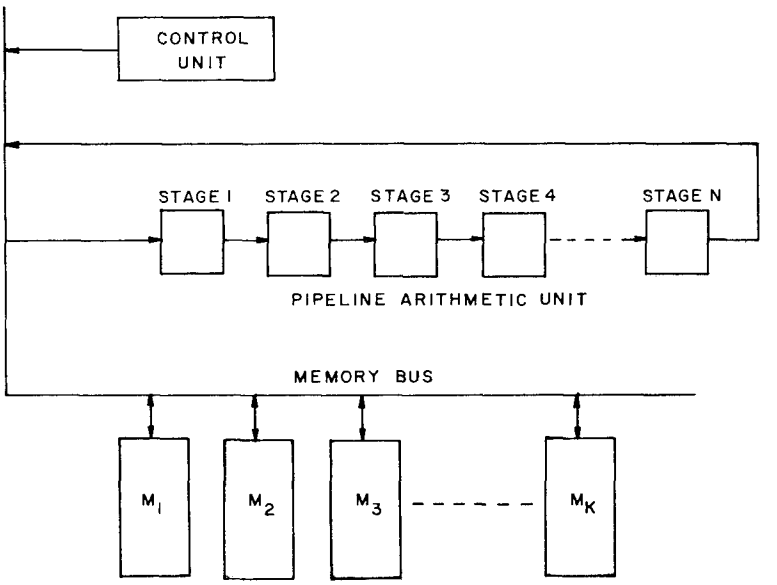

Figure 4.- A pipeline computer.

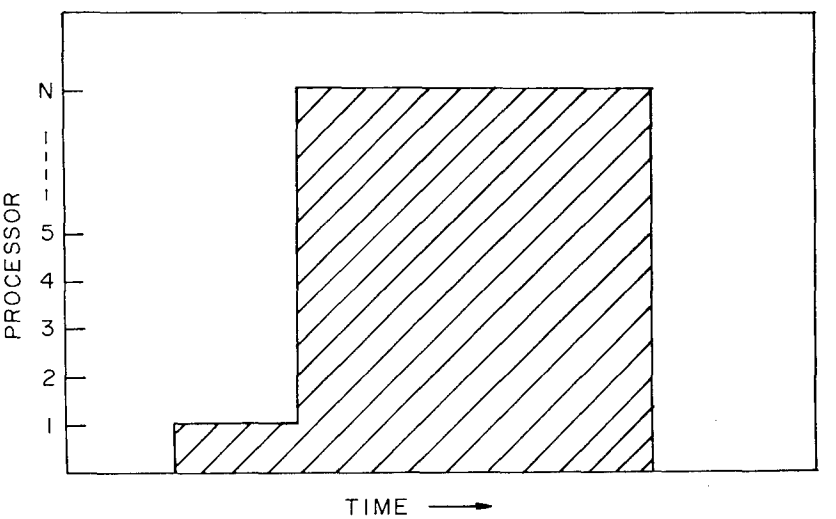

Figure 5. Duty cycle for an array computer.

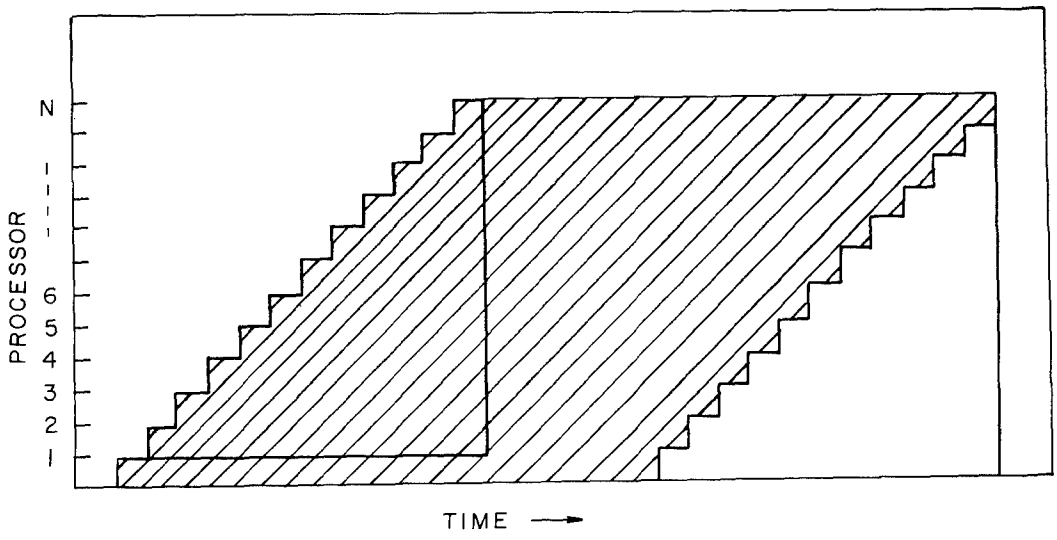

Figure 6.- Duty cycle for a pipeline computer.

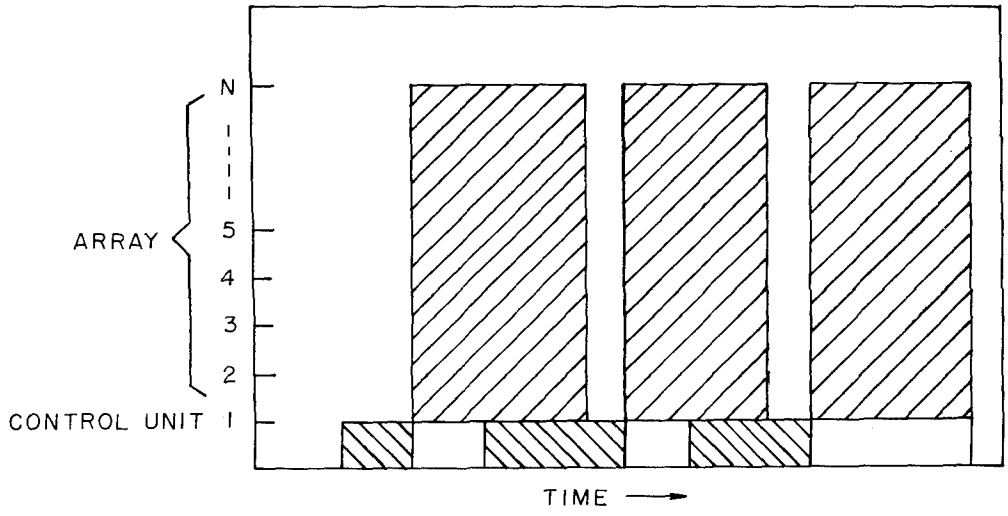

Figure 7.- ILLIAC IV duty cycle.

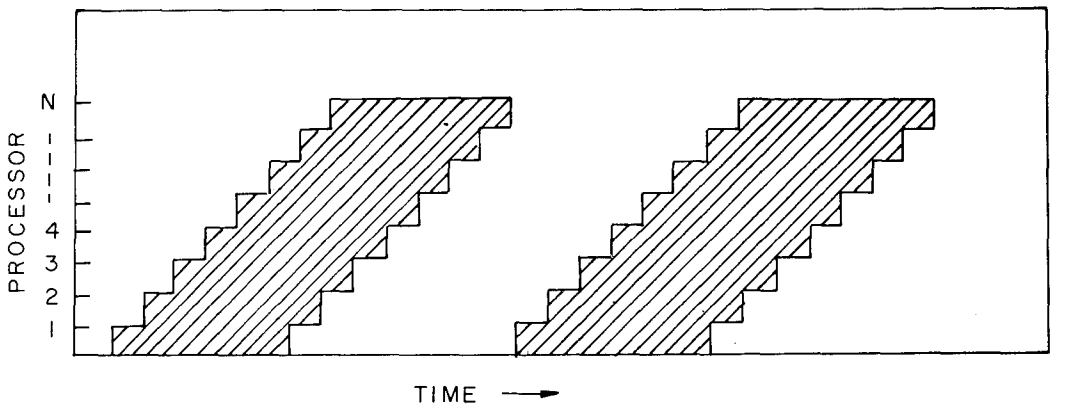

Figure 8.- Duty cycle for pipeline equivalent of ILLIAC IV.

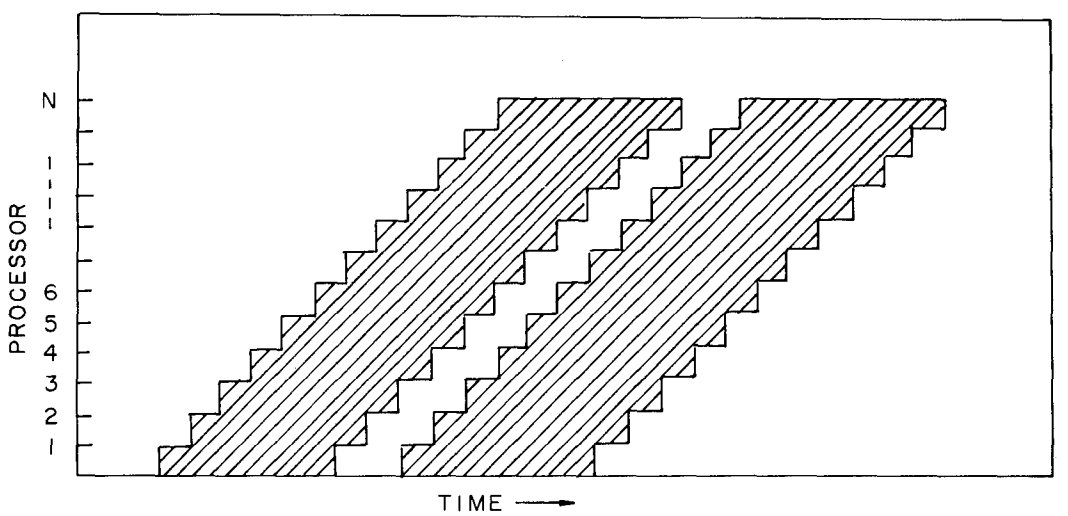

Figure 9.- Duty cycle for STAR.

"The aeronautical and space activities of the United States shall be conducted so as to contribute . . . to the expansion of human knowledge of phenomena in the atmosphere and space. The Administration shall provide for the widest practicable and appropriate dissemination of information concerning its activities and the results thereof."

—NATIONAL AERONAUTICS AND SPACE ACT OF 1958

NASA SCIENTIFIC AND TECHNICAL PUBLICATIONS

TECHNICAL REPORTS: Scientific and technical information considered important, complete, and a lasting contribution to existing knowledge.

TECHNICAL NOTES: Information less broad in scope but nevertheless of importance as a contribution to existing knowledge.

TECHNICAL MEMORANDUMS: Information receiving limited distribution because of preliminary data, security classification, or other reasons. Also includes conference proceedings with either limited or unlimited distribution.

CONTRACTOR REPORTS: Scientific and technical information generated under a NASA contract or grant and considered an important contribution to existing knowledge.

TECHNICAL TRANSLATIONS: Information published in a foreign language considered to merit NASA distribution in English.

SPECIAL PUBLICATIONS: Information derived from or of value to NASA activities. Publications include final reports of major projects, monographs, data compilations, handbooks, sourcebooks, and special bibliographies.

TECHNOLOGY UTILIZATION PUBLICATIONS: Information on technology used by NASA that may be of particular interest in commercial and other non-aerospace applications. Publications include Tech Briefs, Technology Utilization Reports and Technology Surveys.

Details on the availability of these publications may be obtained from:

SCIENTIFIC AND TECHNICAL INFORMATION OFFICE

NATIONAL AERONAUTICS AND SPACE ADMINISTRATION

Washington, D.C. 20546